# Antarctic Meteorites XX

## Papers presented to the Twentieth Symposium on Antarctic Meteorites

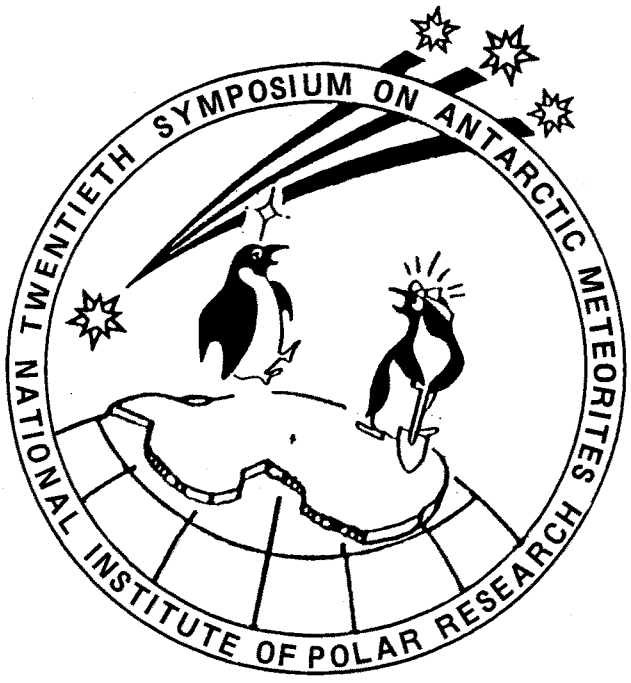


## June 6-8, 1995



NATIONAL INSTITUTE OF POLAR RESEARCH, 国立極地研究所
TOKYO

## Tuesday, June 6, 1995

| | | |
|---|---|---|
| 0900 - 1200 | Registration | Auditorium (6th Floor) |
| 0925 - 0930 | Opening Address | **Takeo Hirasawa**<br>Director-General<br>National Institute of<br>Polar Research |

*Speaker

**Chairmen: Nagahara H. and Kimura M.**

**1** 0930 - 0945 **Funaki M.* and Ishikawa N.**
Collection of Yamato meteorites by the 35th Japanese Antarctic research expedition

**2** 0945 - 1000 **Ishiwatari A.*, Sasatani K., Tazaki K., Sakamoto K., Nakanishi T., Komura K., Tsujimori T., Oura Y., Miyamoto Y., Akahane H., Watanabe M. and Nunomura K.**
A preliminary report on the Neagari meteorite fall on February 18th, 1995

**3** 1000 - 1015 **Yamaguchi A.*, Taylor G.J. and Keil K.**
Eucrites: Global crustal metamorphism by burial on vesta

**4** 1015 - 1030 **Saiki K.* and Takeda H.**
Magma differentiation trend deduced from four polymict eucrites

**5** 1030 - 1045 **Takeda H.*, Otsuki M., Mikouchi T. and Miyamoto M.**
Records of crustal evolution in some Antarctic eucrites

**6** 1045 - 1100 **Ichikawa O.***
Mineralogy of glassy clasts in lunar meteorite Yamato-791197

**7** 1100 - 1115 **Arai T.*, Takeda H. and Warren P.H.**
Chemical variations of spinels in Asuka881757

**8** 1115 - 1130 **Chikami J.*, Mikouchi T., Miyamoto M. and Takeda H.**
Mineralogical comparison of LEW88774 with other ureilites

**9** 1130 - 1145 **Lodders K.***
Experimental partitioning of rare earth elements between sulfides (FeS, CaS) and silicate melt and applications to enstatite achondrites

**10** 1145 - 1200 **Yugami K.*, Takeda H. and Miyamoto M.**
Mineral distribution and the opaque grain shapes of primitive achondrites

1200 - 1300 Lunch Time

**11** 1300 - 1315 **Nagao K.* and Miura Y.N.**
Trapped noble gas component of Brenham pallasite

**12** 1315 - 1330 **Ikeda Y.* and Prinz M.**
Petrology of the Miles IIE iron with silicate inclusions; Relationship to H chondrites and primitive achondrites

**13** 1330 - 1345 **Honda M.* and Nagai H.**
Minor components in Antarctic iron meteorites

-- Special Session: Asuka-881371 angrite --

**Chairman: Warren P.H. and Fujinaki H.**

**14** 1345 - 1415 **Warren P.H.*, Kallemeyn G.W. and Mayeda T.**
Consortium investigation of the Asuka-881371 angrite: Bulk-rock geochemistry and oxygen isotopes

**15** 1415 - 1435 **Warren P.H.* and Davis A.M.**
Consortium investigation of the Asuka-881371 angrite: Petrographic, electron microprobe, and ion microprobe observations

**16** 1435 - 1455 **McKay G.*, Crozaz G., Mikouchi T. and Miyamoto M.**
Petrology of Antarctic Angrites LEW 86010, LEW 87051 and Asuka 881371

1455 - 1520 Tea Time

**17** 1520 - 1540 **Mikouchi T.*, Miyamoto M. and McKay G.A.**
Mineralogical study of angrite Asuka-881371: Its possible relation to angrite LEW87051

**18** 1540 - 1600 **Premo W.R.* and Tatsumoto M.**
Pb isotopic systematics of angrite Asuka-881371

-- Special Lecture (I) --

**19** 1600 - 1700 **Prinz M.* and Weisberg M.K.**
Asuka 881371 and the angrites: Origin in a heterogeneous, CAI-enriched, differentiated, volatile-depleted body

1730 - 1930 Reception Lecture room (2F)

## Wednesday, June 7, 1995

**Chairmen: Tomeoka K. and Nakamura T.**

**20** 0900 - 0915 **Akai J.*, Tari S. and Tanaka H.**
TEM study of Yamato-82042 --- 5th example of thermally metamorphosed Antarctic C1 or C2 Carbonaceous Chondrite

**21** 0915 - 0930 **Matsuoka K.*, Nakamura T., Nakamuta Y. and Takaoka N.**
Yamato-86789: A thermally metamorphosed CM-like carbonaceous chondrite

**22** 0930 - 0945 **Degawa Y.*, Tomeoka K. and Ikeda Y.**
Precursors of PCP in CM carbonaceous chondrites

**23** 0945 - 1000 **Nakamura T.* and Nakamuta Y.**
X-ray study of PCP from the murchison CM carbonaceous chondrites

**24** 1000 - 1015 **Inoue M. and Nakamura N.***
Chemical conditions of aqueous alteration of CM chondrites inferred from REE abundances in chondrules

**25** 1015 - 1030 **Tomeoka K.* and Kojima T.**
Aqueous alteration of the Allende CV3 chondrite: A hydrothermal experiment

**26** 1030 - 1045 **Nomura K.* and Miyamoto M.**
Hydrothermal experiments on refractory minerals related to Ca-Al-rich inclusions (CAIs) in carbonaceous chondrites: Implication for aqueous alteration in parent bodies

**27** 1045 - 1100 **Noguchi T.***
A TEM study of microstructure in silicates in the CK chondrites

**28** 1100 - 1115 **Tanaka H. and Akai J.***
EPMA and TEM study on matrix mineralogy of Allende (CV3)

**29** 1115 - 1130 **Shibata Y.***
Subdivision of metamorphic grade of CO3 chondrites and the occurrence of cohenite in Y-81020, Y-81025 and Y-74135

**30** 1130 - 1145 **Kojima T.* and Tomeoka K.**
Textural variations of dark inclusions in the Allende CV3 chondrite

**31** 1145 - 1200 **Takeda Ha.***
Alteration of coarse grained CAI in Allende meteorite

1200 - 1300 Lunch Time

**Chairmen: Misawa K. and Ebihara M.**

**32** 1300 - 1315 **Fudaki M.* and Kitamura M.**
Finding of sector zoning in isolated olivine grains of ALH-77307 and Murchison

**33** 1315 - 1330 **Kimura M.* and Ikeda Y.**
Anhydrous alteration of Allende chondrules in the solar nebula III: Experimental study of alteration reactions

**34** 1330 - 1345 **Kallemeyn G.W.***
The R chondrite group: Comparisons to other chondrite groups

**35** 1345 - 1400 **Sato T., Matsunami S.* and Ninagawa K.**
Cathodoluminescence of Semarkona chondrules: A classification and the relationships with mesostasis composition

**36** 1400 - 1415 **Sekiya M.* and Nakamura T.**
Which occurred earlier, the settling of dust particles and the formation of chondrules in the solar nebula? - Implication from compound chondrules

**37** 1415 - 1430 **Nakamura T.*, Takaoka N., Nagao K. and Sekine T.**
Shock effects on noble-gas abundance in the experimentally shocked Allende meteorite

**38** 1430 - 1445 **Matsunami S.* and Sato T.**
Re-evaluation of enstatite-oldhamite geothermometer: Formulation and the application to E-chondrites

**39** 1445 - 1500 **Xie X.* and Chen M.**
Occurrences of high-pressure mineral polymorphs in two shocked chondrites

**40** 1500 - 1515 **Kanazawa M., Bridges J.C., Misawa K.*, Nakamura N. and Hutchison R.**
Trace element constraints on origin of $SiO_2$-bearing clasts in ordinary chondrites

1515 - 1545 Tea Time

**41** 1545 - 1600 **Kong P.* and Ebihara M.**
Melting formation of metal phases of ordinary chondrites

**42** 1600 - 1615 **Kong P. and Ebihara M.***
Studies of metallic fractions of L chondrites: Implications to L chondritic parent body

**43** 1615 - 1630 **Bérczi Sz.* and Lukács B.**
A comparison among chondrite compositions

**44** 1630 - 1645 **Ebihara M.*, Shinotsuka K., Shingen T., Togashi S., Kamioka H., Kojima H. and Yanai K.**
An attempt to establish a data base for chemical compositions of Antarctic meteorites

**45** 1645 - 1700 **Sugiura N.*, Kiyota K. and Zashu S.**
Nitrogen isotopic compositions of some gas-rich chondrites

**46** 1700 - 1715 **Bérczi Sz., Holba A. and Lukács B.***
Thermal transformations in the meteorites' parent bodies

**47** 1715 - 1730 **Xie X., Chen M., Zhao B.* and Wang W.**
The behavior of metallic phase in shocked chondrites

## Thursday, June 8, 1995

**Chairmen: Sugiura N. and Hiroi T.**

**48** 0900 - 0915 **Tachibana S.*, Tsuchiyama A. and Kitamura M.**
Incongruent evaporation experiments on troilite (stoichiometric FeS)

**49** 0915 - 0930 **Fegley, Jr.B.*, Lauretta D.S. and Kremser D.T.**
The origin of troilite and pyrrhotite in chondrites: I. Iron sulfide formation kinetics in H2S-H2 gas mixtures

**50** 0930 - 0945 **Lauretta D.S.*, Kremser D.T. and Fegley, Jr.B.**
The origin of troilite and pyrrhotite in chondrites: II. Comparative studies of metal-sulfide assemblages

**51** 0945- 1000 **Hiroi T.*, Pieters C.M., Zolensky M.E. and Lipschutz M.E.**
Thermal metamorphism of the C, G, B, and F asteroids seen from the 3-$\mu$m absorption band in comparison with carbonaceous chondrites

**52** 1000 - 1015 **Bérczi Sz., Holba A. and Lukács B.***
Comparison of spectra of Apollo-Amor, Hungaria, belt and other asteroids in a filter-spanned colour space

**53** 1015 - 1030 **Ninagawa K.*, Hoshikawa Y., Yamamoto I., Wada T., Matsunami S., Takaoka N., Benoit P., Sears D.W.G., Kojima H. and Yanai K.**
Thermoluminescence of Japanese Antarctic meteorites

**54** 1030 - 1045 **Imamura H.* and Ninagawa K.**
Thermoluminescence and cathordoluminescence of eucrites

**55** 1045 - 1100 **Miura Y., Okamoto M.*, Furumoto M. and Fukuchi T.**
Material evidences of Takamatsu impact crater in Japan

**56** 1100 - 1115 **Miura Y. and Okamoto M.***
Shocked calcite and Fe grains from Ries impact crater

**57** 1115 - 1130 **Miura Y.* and Okamoto M.**
New X-ray and compositional data of shocked quartz with high density from Ries impact crater

**58** 1130 - 1145 **Nayak V.K.***
Origin of monomict autochthonous breccia from the lonar impact crater, India

1145 - 1205 Poster Session

1205 - 1300 Lunch Time

**Chairmen: Fukuoka T. and Tsuchiyama A.**

**59** 1300 - 1315 **Tazawa Y.*, Fukuoka T., Yamanouchi E., Miyano Y., Endo K., Kohno M. and Fujii Y.**
Possible cosmic spherules in the Mizuho ice core, Antarctica

**60** 1315 - 1330 **Yada T.*, Nakamura T. and Takaoka N.**
Formation process of magnetic spherules in deep-sea sediments

**61** 1330 - 1345 **Kimura S.*, Kamei K., Tsuda N., Saito Y., Koike C. and Kaito C.**
Electron microscopic and infrared spectral studies on the structure of alumina phases

**62** 1345 - 1400 **Nagahara H.* and Ozawa K.**
Stability of silicate melt in the solar nebula

**63** 1400 - 1415 **Tsuchiyama A.***
Evaporation behavior of mineral dust in the primordial solar nebula

**64** 1415 - 1430 **Bérczi Sz.* and Lukács B.**
Attempt to conjecture the pattern of Alien planetary systems

-- Special Lecture (II) --

**65** 1430 - 1530 **Zinner E.***
Circumstellar grains in meteorites: A new window to the stars

**Poster Session**

**66** **Földi T., Bérczi Sz. and B. Lukács**
Search for icy meteorites on Antarctica

**67** **Lukács B.**
On some ancient meteorite falls

**68** **Kubovics I., Sólymos K.G., Bérczi Sz., Lukács B., Szakmány Gy. and Török K.**
Experimental investigations on ALHA 77005 Shergottite sample from Antarctica

**69** **Kubovics I., Bérczi Sz., Lukács B. and Szakmány Gy.**
The meteorites in the light of the NIPR Japanese Antarctic Meteorite Collection

**Abstract only**

**70** **Bérczi Sz. and Lukács B.**
Why do we not see nitriferous meteorites?

**71** **Birjukov V.V. and Ulyanov A.A.**
Petrological study of new Antarctic carbonaceous chondrites PCA-91082, TIL-91722, and WIS-91600

**72** **Eugster O. and Weigel A.**
Angrite Asuka-881371: Break-up time from parent asteroid and comparison with other angrites

# ABSTRACTS

# TEM study on Yamato-82042 — 5th example of thermally metamorphosed Antarctic C1 or C2 Carbonaceous Chondrite

Akai, J.*, Tari, S.* and Tanaka, H.** : *: Department of Geology , Faculty of Science Niigata University; **: Graduate School of Science, Niigata University

Antaractic carbonaceous chondrites have characteristic features other than non-Antarctic one ( Tomeoka, 1989a,b; Ikeda , 1991; Zolensky, et al,1989). Thermal metamorphism is one of the features( Akai, 1984,1988, 199o) .The causes of this metamorphism have also variously estimated( Kimurta ,1992; Miyamoto ,1990). Some shock effect experiments have been carried out to ascertain this possibility, using shock experiment (Akai and Sekine, 1994).

The Antarctic CM2 chondrite Y-82042 is largely composed of fine grained matrix materials. Few crystals are larger than these matrix materials. The crystals are mostly of olivines and olivine fragments. Olivine crystals are often surrounded by dark brown coronas. Under optical microscope and reflecting microscope, many olivine crystals seems to be suffered alteration (Fig.1). In these grains, olivines do not have brown alteration conronas and are more iron rich than the unaltered olivines(NIPR,1986). Some olivine grains which might be originally chondrule also seem to have suffered alteration (Fig.1a ). Opaque minerals are iron oxide, troilite, pentlandite and metal. Rare round metal grains occur within forsterite crystals.

EPMA analysis of some minerals

Results of EPMA analysis are as follows.

Olivine : -- Fa 0.2 and values rarely to Fa 0.35 or more.

Pentlandite contains up to 3.5 %Co (NIPR, 1986 )

Metal : 7-9 %Ni , 1-1.5%Co. (NIPR, 1986 )

TEM observations

TEM observation indicates matrix texture ( Fig.2). Aggregates of various grains are found. some constituent minerals identified are as follows; "phyllosilicates", "mixed layer mineral of serpentine and tochilinite" , troilite, pentlandite, metal, chromite, calcite . Small olivine grains contain small amount of dislocation.

Pseudomorphs after phyllosilicate : 5th example of thermally metamorphosed C1 or C2 carbonaceous chondrite

Among the mineral grains in the matrix, there are mineral grains whose shape and composition are very similar to phyllosilicate. But they are not phyllosilicate in its structure (Fig.3). The structure

is interpreted to be intermeditate structure in transformation from serpentine to olivine. This is almost the same or similar to those found in Y-793321, Y-82162 and Y-86720; i,e, it is concluded that the Y-82042 is thermally metamorphosed carbonaceous chondrite. So, this meteorite becomes 5th example of thermally metamorphosed C1 or C2 carbonaceous chondrite beside the above three and B-7904. The temperature suffered is roughly estimated based on the degree of transformation in HRTEM image and ED patterns ( Fig. 4) as about 450 -- 650 C.

Mixed layer mineral of serpentine and tochilinite which suffered metamorphism

Fig. 5 shows mineral grain whose compositon is S, Si and Fe ; that is, this mineral might be originally mixed layer mineral of tochilinite and serpentine. But its original structure might not be preserved completely. This grain might have sufferred thermal metamorphism and changed its structure although its structural detail is not clarified yet. Such grains were often found in this Y-82042 although in the other thermally metamorphosed carbonaceous chondrites found hitherto, no or few examples are reported.

References: Akai,J.(1984) Pap.9th NIPR Symp.Ant.Met.59, --- (1988) GCA,52,1593,--- (1990) Proc.NIPR Symp.Ant.Met., 3,55,--- (1992a) Pap.9th NIPR Symp.Ant.Met., --- (1992b) Proc.NIPR Symp. Ant.Met.,5,120; Akai, J. and Sekine, T. (1994) Proc. NIPR Symp. Antarctic meteorites, 7 ,101; Ikeda, Y. (1991) Proc.NIPR Symp.Ant. Met.,4,187; Kimura,M. et al.(1992) Proc.NIPR Symp. Ant.Met.5,74; Miyamoto,M. (1990) Pap.15th NIPR Symp. Ant. Met.89; NIPR (1986) Meteorite News, vol. 5 No.1 ;Tomeoka,K. (1989a) Proc. NIPR Symp.Ant.Met. , 2,36,--- (1989b) Proc.NIPR Symp.Ant.Met.2,55; Zolensky, et al.(1989) Pap.14th NIPR Symp.Ant.Met.24.

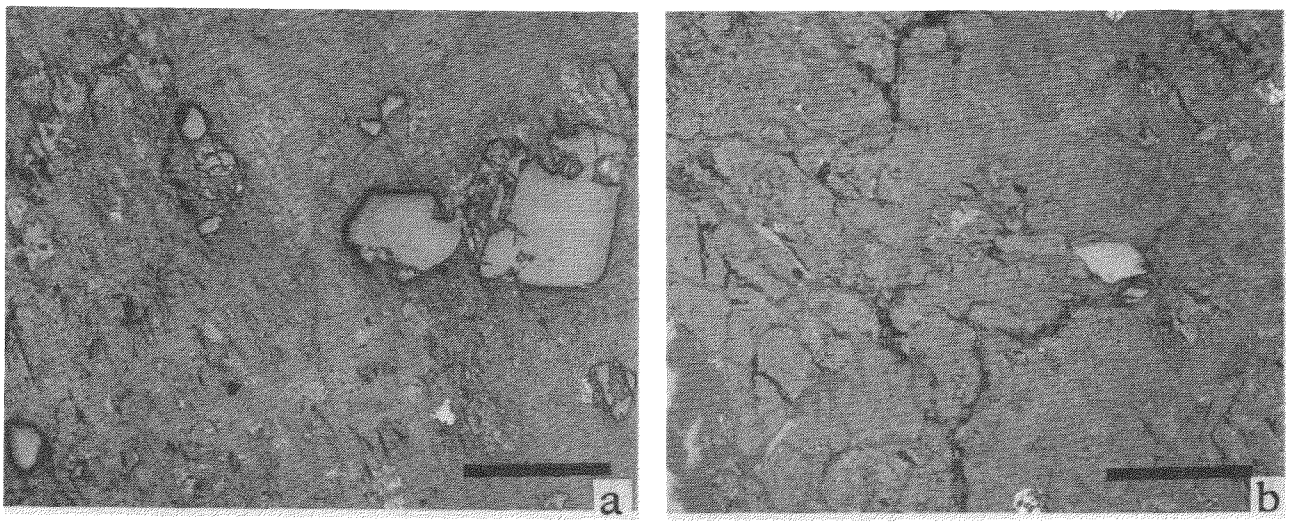


Fig. 1: Photograph of reflecting microscope. Many olivine crystals seems to be suffered alteration. Some olivine grains which might be originally chondrule also seem to have suffered alteration. (Scale bar is 0.5 mm )

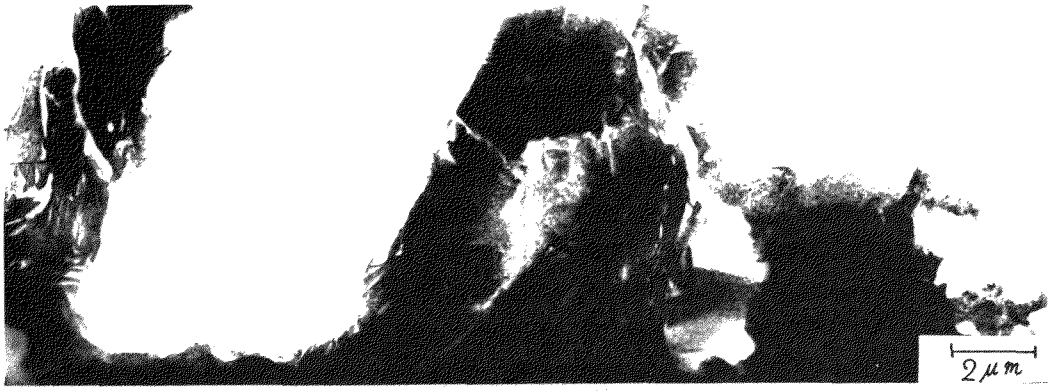


Fig.2: TEM image indicating matrix texture of Y-82042. Aggregates of various grains are found.

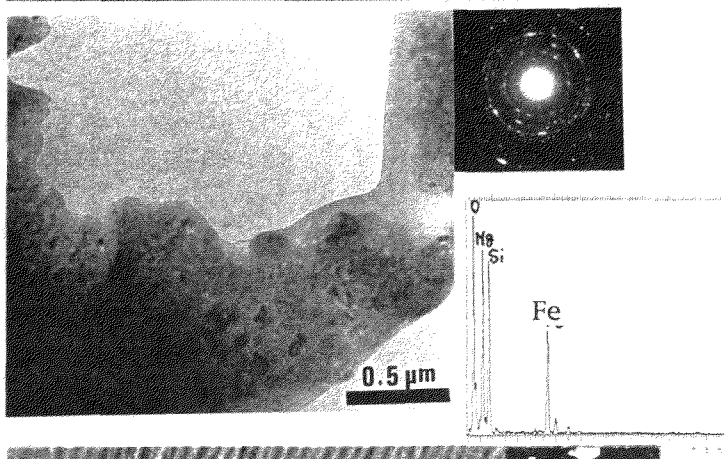


Fig.3 TEM image of mineral grains in Y-82042 whose shape and composition are very similar to phyllosilicate.

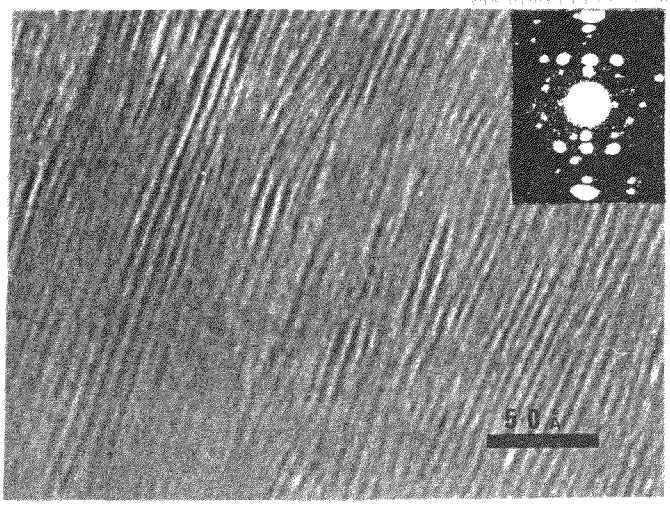


Fig. 4 HRTEM image of the thermally transformed phyllosilicate: intermediate structure in transformation from serpentine to olivine structure.

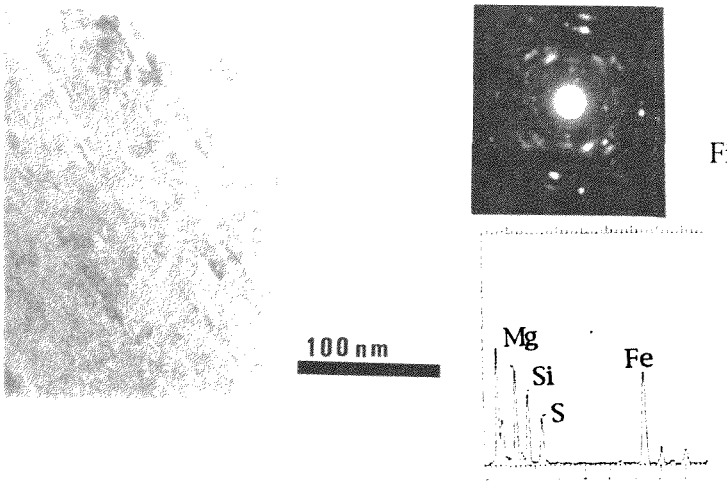


Fig. 5 Mineral grain whose compositon is mainly S, Si and Fe ; that is, this mineral might be originally mixed layer mineral of tochilinite and serpentine. But its structure might have sufferred thermal change although its structural detail is not yet so clear.

# CHEMICAL VARIATIONS OF SPINELS IN ASUKA881757

Tomoko Arai, Hiroshi Takeda and Paul H. Warren
Mineralogical Institute, Graduate School of Science, University of Tokyo,
Hongo, Tokyo 113, Japan.

## INTRODUCTION.

The lunar meteorite Asuka (A)881757 was apparently derived from a mare region of the Moon. Consortium studies [1,2,3,4,5,6] have shown that A881757 is a distinct new type of low-Ti (LT) mare basalt, considerably older than nearly all Apollo and Luna mare basalt samples. Therefore, A881757 may be an product of the earliest mare volcanism. Mineralogy of A881757 has been previously studied [1,7]. It shows gabbroic texture and mainly consists of Fe-rich pyroxene, plagioclase, olivine, ilmenite, Cr-rich spinel and troilite and Fe-Ni. Yanai [1] reported that opaque phases in A881757 mainly consist of ilmenite, and chromian ulvöspinel was a minor opaque phase. But one of the three A881757 polished thin sections (PTSs) of this study contains chromian ulvöspinel as a dominant opaque mineral, and unique spinel crystallization was recognized. Herein, chemical and textural variations of chromian ulvöspinels in A881757 are studied to give constaints on its petrogenesis and cooling history.

## SAMPLES AND METHODS.

We studied polished thin sections (PTS) A881757, 51-4, A881757, 53D-2, and A881757, 53E-2 supplied by the National Institute of Polar Research (NIPR). Especially, we were able to investigate the PTSs of A881757, 53D-2 and A881757, 53E-2 by courtesy of Prof. Yanai. Mineral chemistries and textures were examined by an electron probe microanalyzer (EPMA) and a scanning electron microscope (SEM). Two-dimensional elementary distribution maps of spinels for Ti, Cr, and Al were obtained by EPMA.

## RESULTS.

Spinels found in mare basalts generally have a composition demonstrated by the three components of $Fe_2TiO_4$ (ulvöspinel) - $FeCr_2O_4$ (chromite) - $FeAl_2O_4$ (hercynite) with a small range of Fe-Mg zonation. All spinel compositions from three PTSs nearly fall between chromite-ulvöspinel series. Representative chemical compositions of chromian ulvöspinels in the three PTSs are indicated in Table 1. Their chemical variations are shown in triangular plot Fig.1 where three end members are hercynite (=Her), ulvöspinel (=Ulv), and chromite (=Chr). All spinels in three PTSs we studied are poor in $Al_2O_3$ with only 1.8-2.7 wt% of $Al_2O_3$, and are very Fe-rich with Fe/(Fe+Mg) atomic ratio = 0.99.

In A881757, 51-4, six interstitial spinels, which reach up to 0.6 X 1.2 mm in size, are observed, and their modal abundance is 11%. Four of them appear to have crystallized along with Fe-rich pyroxene and plagioclase. The rest of them crystallized along with ilmenite and fayalite in mesostases. It is striking that chromite component (Chr =100 x Cr/(Cr+2Ti+Al) atomic ratio) and ulvöspinel component (Ulv =100 x 2Ti/(Cr+2Ti+Al) atomic ratio) change from spinel grain to grain with almost the same hercynite component (Her =100 x Al/(Cr+2Ti+Al) atomic ratio). For the four larger chromian ulvöspinels, Chr and Ulv are remarkably zoned, while they are nearly constant for smaller two.

In A881757, 53D-2, two chromian ulvöspinels are found, cocrystallized with ilmenite in mesostases, and their mode is less than 1 %. A main opaque phase is ilmenite, which is consistent with [1]. A little chemical variation is recognized between them and their compositions are nearly homogeneous.

In A881757, 53E-2, two chromian ulvöspinels crystallize with thin rims of ilmenite

and symplectite in mesostases. Thier modal abundances are also less than 1 % and a dominant opaque phase is ilmenite. These two spinels are zoned and their chemical compositions are dissimilar.

**DISCUSSION.**

In chromite-ulvöspinel series, complete solid solution is common [8], and chromite crystallizes at earlier stage and ulvöspinel at later stage as crystallization proceeds. Spinel compositions reported for Apollo12 LT mare basalt, which have similar bulk $TiO_2$ to A881757 ($TiO_2$= 2~3 %), are widely distributed in chromite-ulvöspinel series [9]. Spinels in A881757 are very Ti-rich and show compositions from $Chr_{24}Her_7Ulv_{69}$ to $Chr_4Her_6Ulv_{90}$, which suggests that the spinels possibly crystallized in a melt where chromite had already precipitated. Different spinel populations among three A881757 PTSs suggest imhomogeneity of a coarse-grained rock . Absence of Cr-rich spinel may be due to its imhomogeneity.

Variations of chromite component and ulvöspinel component in spinels for the three PTSs are shown in Fig.2. Differences of chromite component and ulvöspinel component among spinels probably reflect different crystallization stages in a series of crystallization. Because all chromian ulvöspinels are quite Fe-rich and cocrystallized with Fe-rich pyroxene or in mesostases, they apparently precipitated at very last stage of crystallization. Variation of spinel composition between grains may have resulted either because a variety of chromian ulvöspinels probably crystallized one after another from a liquid changing composition successively, or because melt was locally trapped with pyroxene or plagioclase which had already crystallized and thus chromian ulvöspinels possibly crystallized in local melt with different composition.

The fact that some spinel grains are zoned while others are not, is probably due either to unusual growth patterns as the result of rapid crystallization or to geometrical effects as a result of the particular cut in thin section through a zoned grain. Among zoned spinel grains, bigger spinels tend to show wider zoning. Grain size of spinels may roughly reflect the duration each spinel grain grew during igneous crystallization. Assuming that the liquid composition constantly changes as crystallization proceeds, a spinel grain which comparatively is larger and thus took more time to crystallize from the liquid, may show wider variation of its composition.

Yanai [1] suggested that A881757 could be a cumulate because of its coarse-grained texture. Extensive zoning in pyroxene reported by [7], and variations of spinel compositions in the A881757 PTSs don't support a possibility that A881757 is a slowly-cooled cumulate. Assuming A881757 was cooled in relatively thick lava flow, low nucleation rate induced by small degree of supercooling probably resulted in its coarse-grained texture, in spite of rapid cooling rate enough to cause zonings inside spinels, or compositional variations among spinels even in one PTS.

In summary, one of the three A881757 PTSs studied contain chomian ulvöspinel as the dominant opaque, in contrast to [1], and chemical variations of chromian ulvöspinel among three PTSs of A881757 suggest that they may have crystallized one after another from a residue at the last stage of crystallization. These variations indicate that despite its old age [6] and unusually coarse grain sizes, A881757 was cooled only slightly more slowly than typical mare basalts, probably near the base of its parent lava flow.

We thank NIPR for samples, Profs. I. Kushiro and P. H. Warren for discussions, and Mr. H. Yoshida and O. Tachikawa for technical assistances.

**REFERENCES.**
[1] Yanai.K (1991) Gabbroic meteorite Asuka-31: Preliminary examination of a new type of lunar meteorite in the Japanese collection of Antarctic meteorites. *Proc.Lunar Planet. Sci.* **21,** 317-324.
[2] Yanai K., Takeda H., Lindstrom M. M., Tatsumoto M., Torigoye N., Misawa K., Warren P. H., Kallemeyn G. W., Koberl C., Kojima H., Takahashi K., Matsuda A., NishiizumiK, (1993) Consortium reports of lunar meteorites Yamato 793169 and Asuka881757, a new type of mare basalt. In *Lunar and Planetary Science XXIV*, P. 1555-1556.
[3] Lindstrom M. M., Mittlefehldt D. W., and Martinez R. R. (1991) Geochemistry of Asuka-31: Comparison to basaltic lunar meteorites and mare basalts. In *Antarcts, 16th Symp. Antarct. Meteorites,* p. 102-105, Natl. Inst. Polar Res., Tokyo.
[4] Warren P.H. and Lindstrom M. M. (1993) Consortium study of lunar meteorites Yamato-793169 and Asuka-881757: Geochemical evidence of mutual similarity, and dissimilarity vs. other mare basalts. In *Lunar and Planetary Science XXIV*, p. 1483-1484.
[5] Jolliff B. J., Korotev R. L., and Haskin L. A. (1993) Lunar basaltic meteorites Yamato-793169 and Asuka-881757: Samples of the same low-Ti mare-lava? In *Abstract, 18th Symp. Antarctic Meteoritss*, pp. 214-217, Natl. Inst. Polar Res., Tokyo.
[6] Misawa K. Tatsumoto M,m Dalrymple G. B. and Yanai K. (1992) U-Th-Pb, Sm-Nd, and Rb-Sr isotopic systematics and $^{40}Ar/^{39}Ar$ age of lunar meteorite Asuka-881757. In *Abstract, 17th Symp. Antarctic Meteoritss*, pp. 119-121, Natl. Inst. Polar Res., Tokyo.
[7] Takeda H., Arai T., and Saiki K. (1993) Mineraloy of Asuka 881757 lunar meteorite, a new type of mare rock. In *Abstract, 18th Symp. Antarctic Meteorites*, pp. 25-27, Natl. Inst. Polar Res., Tokyo.
[8] Shuart S. and Muan A. (19 ) Equilibrium relations among crystalline phases in the system FeO-$Cr_2O_3$-$TiO_2$ under strongly reducing conditions. (Unpublished data).
[9] Papike J. J., Hodges F. N., Bence A. E., Cameron M., and Rhodes J. M. (1976) Mare basalts; crystal chemistry, mineralogy and petrology. *Rev. Geophys. Space Phys.*, **14**, 475-540.

Table1. Representative analyses of spinels (wt%) in A881757, 51-4, A881757, 53D-2, and A881757, 53E-2.

| | A881757, 51-4 | | | | | | A881757, 53D-2 | | A881757, 53E-2 | |
|---|---|---|---|---|---|---|---|---|---|---|
| | grain1 | grain2 | grain3 | grain4 | grain5 | grain6 | grain1 | grain2 | grain1 | grain2 |
| SiO2 | 0.07 | 0.05 | 0.09 | 0.07 | 0.06 | 0.07 | 0.02 | 0.05 | 0.09 | 0.06 |
| TiO2 | 28.36 | 26.42 | 23.81 | 29.30 | 31.53 | 30.09 | 30.39 | 30.45 | 30.51 | 30.40 |
| Al2O3 | 2.45 | 2.70 | 2.99 | 1.85 | 1.83 | 2.28 | 2.41 | 2.59 | 2.32 | 2.69 |
| FeO | 57.81 | 56.89 | 55.47 | 52.57 | 55.55 | 56.28 | 62.23 | 61.03 | 60.75 | 62.78 |
| MnO | 0.35 | 0.31 | 0.33 | 0.26 | 0.32 | 0.36 | 0.35 | 0.36 | 0.24 | 0.37 |
| MgO | 0.38 | 0.39 | 0.58 | 0.24 | 0.21 | 0.14 | 0.26 | 0.24 | 0.36 | 0.28 |
| CaO | 0.01 | 0.06 | 0.03 | 0.03 | 0.04 | 0.02 | 0.04 | 0.03 | 0.03 | 0.07 |
| Na2O | 0.05 | 0.02 | 0.04 | 0.09 | 0.00 | 0.01 | - | - | 0.01 | 0.02 |
| K2O | 0.03 | 0.02 | 0.01 | 0.04 | - | 0.02 | 0.01 | 0.00 | 0.00 | - |
| Cr2O3 | 9.39 | 12.86 | 16.33 | 11.88 | 6.31 | 8.30 | 3.95 | 4.63 | 4.23 | 3.23 |
| V2O5 | - | 0.34 | 0.34 | 0.16 | 0.20 | - | 0.18 | 0.23 | 2.69 | 0.96 |
| NiO | - | 0.08 | - | 0.02 | - | 0.04 | - | 0.03 | | - |
| total | 98.98 | 100.05 | 100.03 | 98.93 | 98.00 | 100.72 | 99.85 | 99.64 | 101.33 | 100.79 |

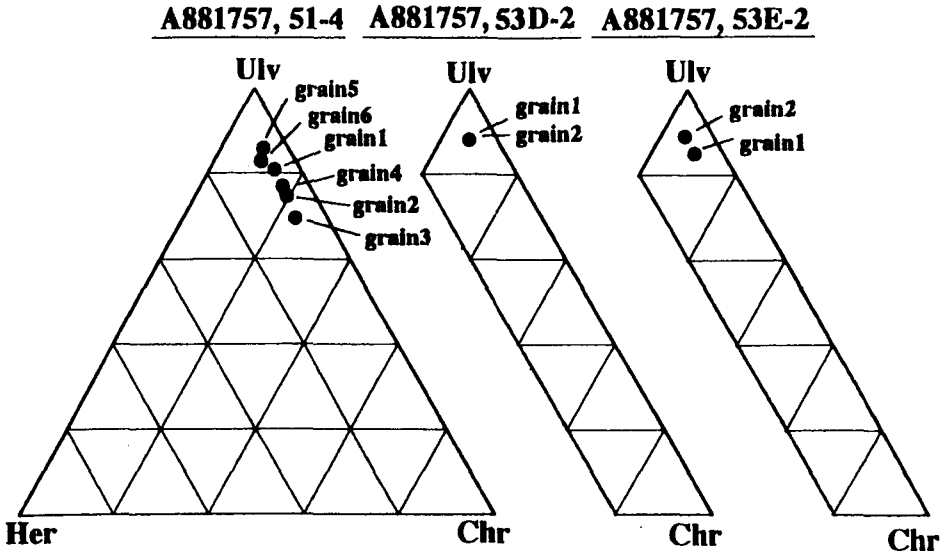


Fig. 1 Variations of spinel compositions in A881757.
Chr: chromite, Ulv: ulvöspinel, Her: hercynite.

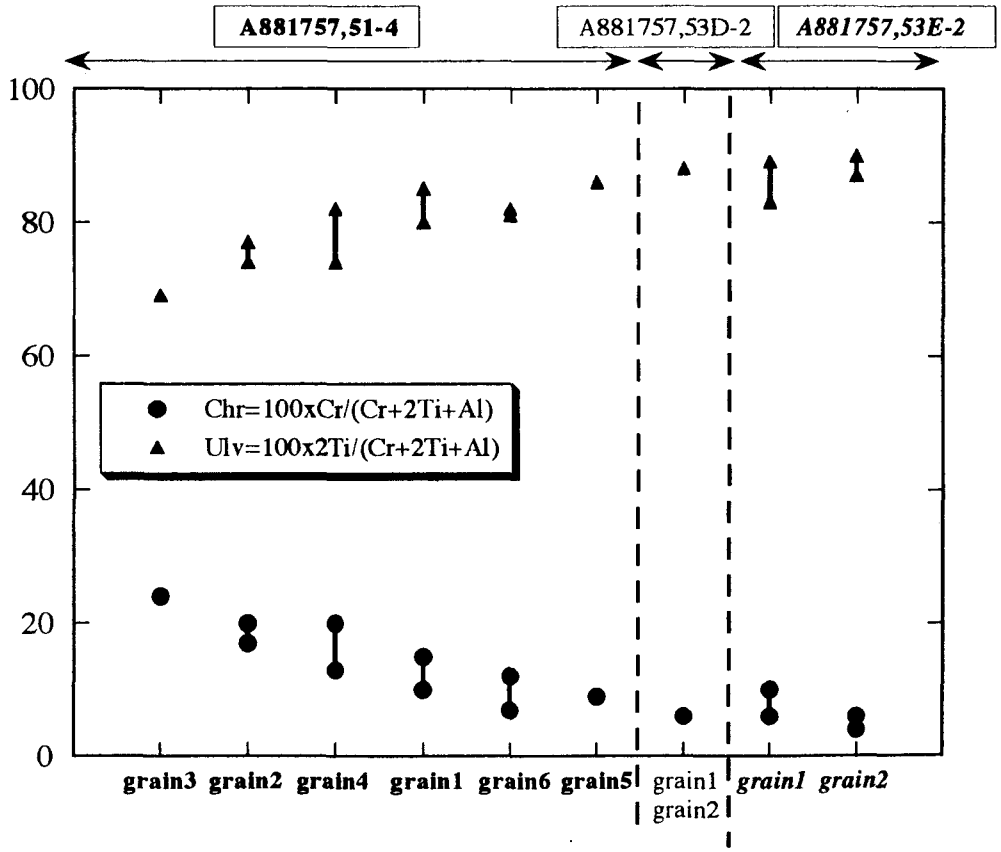


Fig.2 Variations of chromite component and ulvöspinel component in spinel grains from three PTSs of A881757.

# SHOCK EFFECTS IN ANTARCTIC ORDINARY CHONDRITES

I. Souza Azevedo[a], R. B. Scorzelli[a],
T.V.V.Costa[b], V.W.Vieira[b] and M.A.B. de Araújo[b]

[a]Centro Brasileiro de Pesquisas Físicas
Rua Dr.Xavier Sigaud 150, CEP 22290-180,Rio de Janeiro - Brazil
[b]Dep. de Física, Universidade Federal do Ceará , Caixa Postal 6030
60450 Fortaleza - Brazil

We report on the results of Mössbauer spectroscopy measurements on samples of ordinary chondrites recovered from the bare ice fields of the Yamato mountains, in Antarctica, by the Japanese Antarctic Research expeditions .

## 1. Introduction

Mössbauer spectroscopy measurements have been performed on samples of ordinary chondrites recovered from the bare ice fields of the Yamato mountains, in Antarctica, by the Japanese Antarctic Research expeditions [1]. The samples were labelled Yamato (Y) -793464, -793214, -793214, -8435 and classified as L5, LL5, L6 and L6 respectively.

This work is part of a systematic study of thermal and shock history of Antarctic ordinary chondrites, recorded by their metal particles and silicates, using different techniques such as Mössbauer spectroscopy, X-ray diffraction, optical and scanning electron microscopy.

Previous results [2, 3] showed that the tetrataenite (ordered $Fe_{50}Ni_{50}$) present in the metal particles of this type of meteorites, can have different degree of ordering according to their history. This difference is reflected in the Mössbauer hyperfine parameters [2] allowing a correlation between these parameters and the different thermal and shock histories. The study of impact-induced disorder in silicates [4] can also allow us to infer about temperatures and shock pressure suffered by these meteorites.

## 2. Experimental

In this study we investigate four Antarctic chondrites labelled Yamato (Y) -793464 (L5), -793214 (LL5), -793539 (L6) and -8435 (L6).

In order to obtain a broader range of information from the Mössbauer measurements, we prepared three different set of samples from each chondrite: bulk, magnetically separated fraction, and pure extracted metallic particles obtained with HF treatment.

The transmission $^{57}Fe$ Mössbauer spectra were obtained at room temperature using a $^{57}Co/Rh$ source in a conventional Mössbauer spectrometer.

## 3. Results and Discussion

The bulk of all four meteorites was studied by Mössbauer spectrocopy exhibiting a complex superposition of iron silicates, kamacite or martensite and troilite present in different proportions.

The magnetically enriched samples disclosed the presence of FeNi phases overlapping with lines of silicates and troilite that still remain attached to the metal particles.

Only after a complete separation of the metallic particles by treating the magnetic enriched sample with HF it is possible to clearly identify the different FeNi phases. Figure 1 shows the Mössbauer spectra of the extracted metallic particles of the four meteorites.

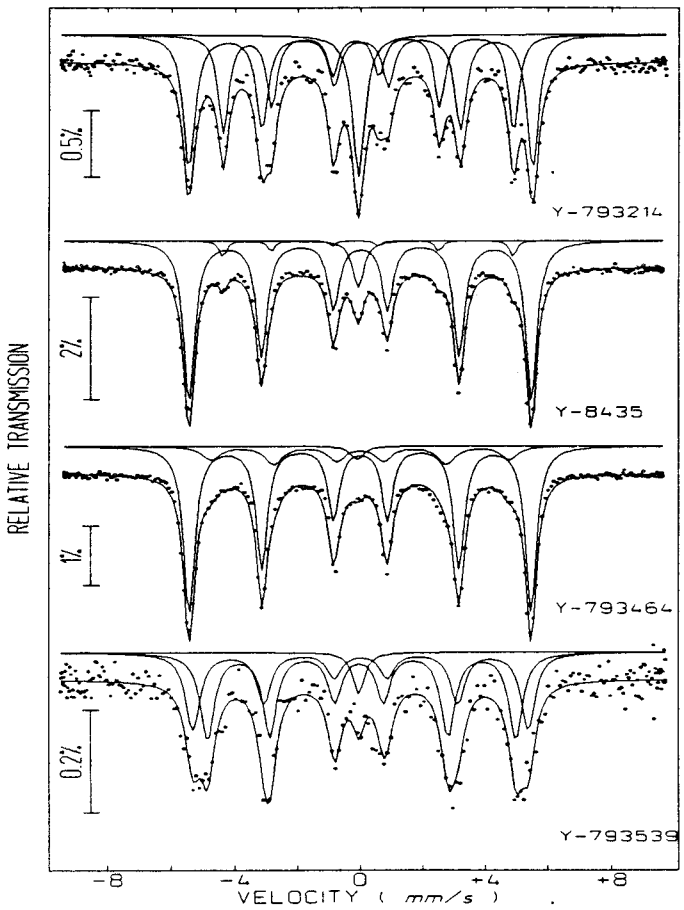


Fig.1 - Mössbauer spectra of the metal fraction from the four Yamato

As an illustration of the different steps of treatment the spectra of Y-793214 is presented in fig.2.

In the spectrum of the extracted metallic particles (fig.2c) we observe an overlapping of two magnetic sextets corresponding to $\alpha$ (kamacite) or $\alpha_2$ (martensite), Ni-rich $\gamma$ -FeNi (tetrataenite) and a Ni-poor $\gamma$ -phase (single line).

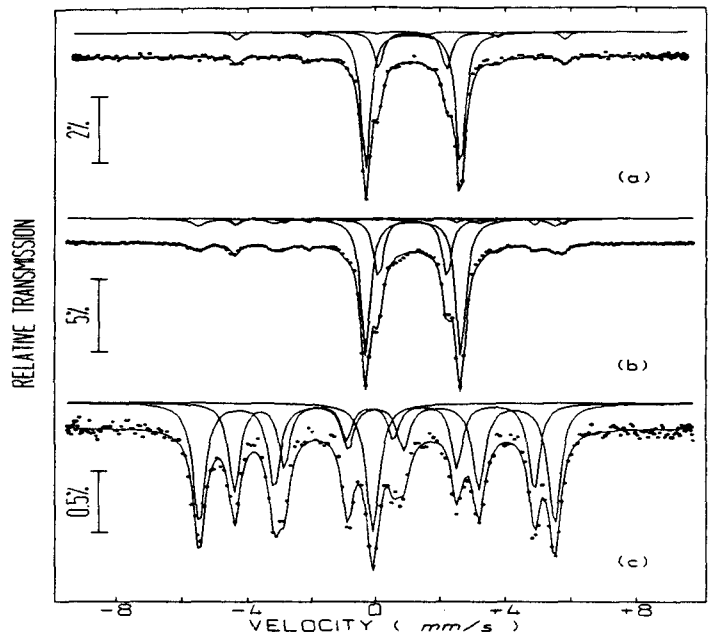


Fig.2- Mössbauer spectra from Y-793214: a) bulk;
b) magnetically separated fraction;
c) extracted metal particles.

Through the corresponding hyperfine parameters of these meteorites (Table 1) it was possible to observe that the Ni-rich phase is present in different degrees of ordering.

The QS and Γ values of Y-793214 and Y-8435 are in the range of the ones already observed for highly ordered tetrataenite [2], while Y-793464 and Y-793539 exhibit values corresponding to a disordered 50/50 alloy, suggesting that in the first case, shock and reheating events did not occurred. The difference in the proportions of tetrataenite between Y-793214 (35%) and Y-8435 (5%) may be due to different cooling rates of these meteorites.

The presence of the disordered 50/50 FeNi alloy is a consequence of the destruction of the ordered superstructure (tetrataenite) by shock and/or reheating. It has been demonstrated that pressure wave from shock induces disordering in ordered alloys[5]. The low order-disorder transition temperature ($T_c$ = 532K) indicates that relatively low energies are required for the phase transformation to occur.

Further evidences of shock effects are given by the isomer shift parameter which is found to be less positive in Y-793214 and Y-8435 as compared to the others.

The increase in the concentration of dislocations as a consequence of the passage of the shock wave in the alloy corresponds to an effective pressure which is known to decrease the value of the IS in $^{57}$Fe [6]. An important question concerns the temporal sequence in which the order-disorder transformation and shock events occurred. One indication is given by the presence of the Ni-poor γ-phase. The presence of this phase (< 30% Ni) in all samples is a confirmation that before any shock or reheating effect happened, segregation and ordering occurred in these meteorites separating γ-FeNi phases with different composition. Then the disordering process occurred as a consequence of shock pressure and/or reheating.

Other evidences of shock events are given by the silicates extracted from these meteorites. The study of impact-induced disorder is in progress and will give us relevant informations about temperature and shock pressures suffered by these chondrites.

**Table 1**

Mössbauer hyperfine parameters of the metal fraction extracted from the Antarctic chondrites, Yamato (Y) -793214, -8435, -793464, 793539; Γ=Linewidth at half height; IS=Isomer Shift relative to $^{57}$Co/Rh source; QS=Quadrupole Splitting; $H_i$=Internal Hyperfine Field; A=Relative Area.

| | α or $\alpha_2$-phase | | | | Ni-rich γ-phase | | | | | Ni-poor γ-phase | | |
|---|---|---|---|---|---|---|---|---|---|---|---|---|
| Y | Γ mm/s (±0.02) | IS mm/s (±0.02) | $H_i$ Tesla (±0.3) | A % (±5) | Γ mm/s (±0.02) | IS mm/s (±0.02) | QS mm/s (±0.02) | $H_i$ Tesla (±0.3) | A % (±5) | Γ mm/s (±0.02) | IS mm/s (±0.02) | A % (±5) |
| -793214 | 0.45 | -0.090 | 34.0 | 51 | 0.40 | -0.067 | 0.201 | 28.8 | 35 | 0.47 | -0.183 | 14 |
| -8435 | 0.43 | -0.100 | 33.8 | 89 | 0.26 | -0.075 | 0.204 | 28.7 | 5 | 0.43 | -0.175 | 6 |
| -793464 | 0.42 | -0.098 | 33.8 | 82 | 0.67 | -0.110 | 0.018 | 29.6 | 16 | 0.55 | -0.200 | 2 |
| -793539 | 0.55 | -0.086 | 33.2 | 40 | 0.53 | -0.099 | 0.042 | 30.5 | 55 | 0.45 | -0.153 | 5 |

**Aknowledgement**

We are grateful to Dr. K. Yanai (National Institute of Polar Research) for supplying us with the samples, and to M. Christophe Michel-Lévy for helpfull discussions.

**References**

[1] K. Yanai, Catalog of Yamato meteorites. Tokyo, Natl. Inst. Polar Res., 188p., (1979).

[2] J. Danon, R. B. Scorzelli, I. Souza Azevedo and M. Christophe Michel-Lévy, Nature 281 (1979) 469.

[3] J. Danon, I. Souza Azevedo and R. B. Scorzelli, Meteoritics 17 (4), 202 (1982).

[4] T.V. V. Costa, V.W.Vieira and M. A B. de Araújo, Hyperfine Int. 67, 46 (1991).

[5] W. C. Leslie, D. W. Stevens and M. Cohen, in "High Strength Materials" (ed. V. F. Zachay) chap.12, Wiles (1965).

[6] D. L. Williamsons, in "Mössbauer Isomer Shifts", p.335 (ed. G. K. Shenoy and F.E.Wagner), North Holland (1978).

**Petrological Study of New Antarctic Carbonaceous Chondrites PCA-91082, TIL-91722, and WIS-91600.**

**Birjukov, V.V., and Ulyanov, A.A.**
*M.V. Lomonosov Moscow State University, Moscow, Russia.*

We report here results of our petrological and mineralogical investigation of 3 antarctic carbonaceous chondrites which were received from Johnson's Space Centre (NASA). Thin polish sections (one from each meteorite) were studied by SEM EDS methods.

PCA-91082 was classified as CR2, TIL-91722 as CV3 and WIS-91600 as CM2 chondrite on the petrological data. We could not determine bulk meteorite composition because we have not enough representative samples. From TIL-91722 to WIS-91600 amount of high-temperature fractions (CAIs and chondrules) decrease. Relative amounts of different petrological fractions reported in Table 1.

| Fraction | TIL-91722 | PCA-91082 | WIS-91600 |
|---|---|---|---|
| CAIs | rare | rare | none |
| chondrules and crystals | abundant | abundant | abundant |
| metal | abundant | abundant | none |
| sulfides | abundant | rare | abundant |

CAIs are represent by typical fine-grained objects (FGIs) and amoeboid olivine aggregates (AOAs). We observed 2 FGIs and 2 AOAs from TIL-91722 and 1 FGI from PCA-91082. FGIs consist of Al-diopside and Mg-spinel (FGI in PCA-91082 also contain melilite (Ak21) and anorthite), main AOAs constituents are forsteritic olivine, Al-diopside and Mg-spinel. Diopside from CAIs does not contain Cr, in contrast to chondrules pyroxene. The absence of Fe-bearing spinel and feldspatoids is the good evidence of small nebular alteration.

Relative amounts of chondrules and their average sizes are similar between TIL-91722 and PCA-91082 but significant less in WIS-91600. Chondrules consist mainly of olivine grains with interstitial material which is mainly pyroxene for TIL-91722, pyroxene and glass for PCA-91082 and glass for WIS-91600. Forsteritic olivines are dominate (see Fig. 1). We study olivines with increasing and decreasing of Fe contents from core to outer part of chondrule. Olivines from all samples contain $Cr_2O_3$, MnO and CaO up to 1.0, 0.6 and 0.8 wt.% respectively. Positive correlation between Fe and Mn contents was detected. We suggest that all Cr is trivalent because there is no deviation between real cation sum and its theoretical mean for Cr-rich olivines.

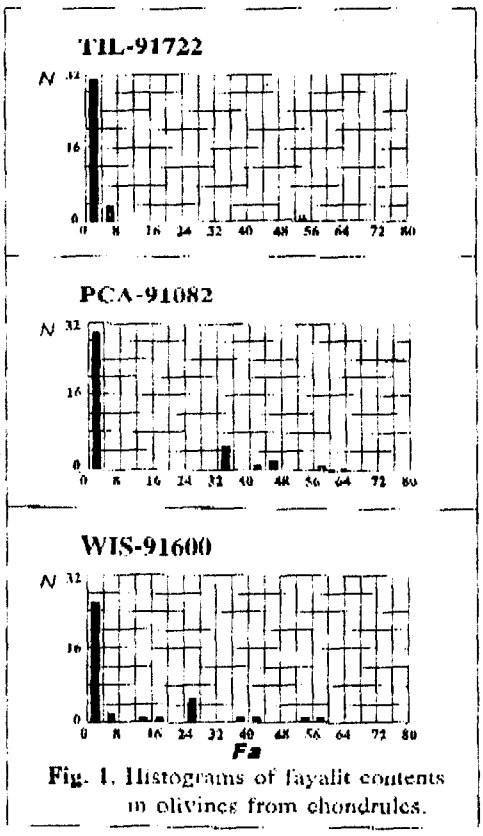

Fig. 1. Histograms of fayalit contents in olivines from chondrules.

Pyroxenes in chondrules are mainly enstatite and Mg-augite; Mg-pigonite and diopside are less abundant. Clinopyroxenes (but not orthopyroxenes) from TIL-91722 and PCA-91082 chondrules probably contain $Ti^{3+}$ and $Cr^{2+}$ with the normal $Ti^{4+}$ and $Cr^{3+}$ that is typically only for CAIs pyroxenes [3]. Maximal concentrations of $Cr_2O_3$ is 3.1 wt.% and MnO - 0.9 wt.%. Orthopyroxenes contain less Cr. All pyroxenes in WIS-91600 chondrules probably are orthoenstatites.

Glass compositions of chondrules are shown in Fig 2, they can be approximately described as a result of mixing of anorthite, diopside, spinel and enstatite in different proportions. PCA-91082 contain Na-Fe-rich glasses which have also acmite and nepheline constituents (Table. 2, an. 6-7) Very unusual glasses were detected in WIS-91600. They have dark-brown color and build interstices between olivine grains and whole glass chondrules. Composition of such glasses is similar with the meteorite matrix but they very enriched in Cr and sometimes in P (Table. 2, an. 8, 10, 11). We does not detect inclusions of chromite grains in these glasses. Ca-carbonate was found as interstitial mass in one chondrule in WIS-91600. It contain up to 14.4 mol.% MgO, 4.0 % MnO and 2.1 % FeO.

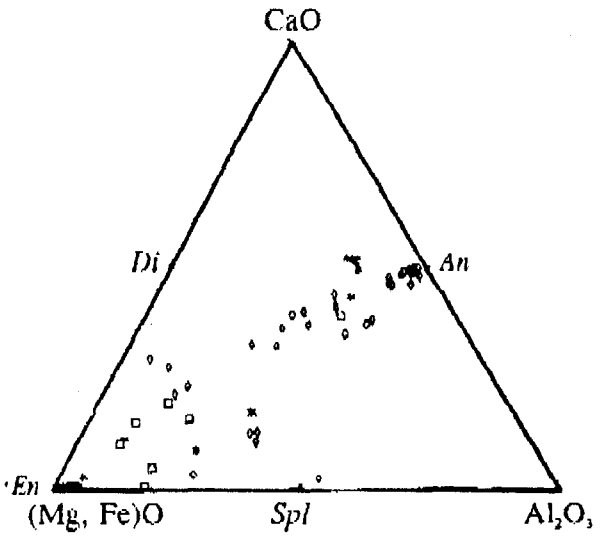


**Fig 2.** Bulk composition of glasses (mol. %)
▫ TIL-91722, ◦ PCA-91082, • WIS 91600
*An-anorthite; Di-diopside; En-enstatite; Spl-spinel*

One unusual radial P-enriched chondrule was described in PCA-91082. It consists of olivine (with 1 wt.% of $P_2O_5$) and Na-Mg-Fe glass (with 2 wt.% $P_2O_5$). Structure of this chondrule can be interpreted as a result of exsolution.

Crystals of olivine and orthopyroxene are relatively abundant in all samples. Large olivine crystals from WIS-91600 contain elliptical inclusions of anorthite-pyroxene glass, sometimes with $P_2O_5$ impurity (up to 6.1 wt.%; Table. 2, an. 13). High contents of $Al_2O_3$ and CaO (up to 0.4 and 0.6 wt.% respectively) in host olivine let us to propose exsolution with the temperature falling. Olivine capture maximal amount of Ca and Al but excess of this elements and P crystallized in glass inclusions. Same minor-elements resemblance between chondrule and intercrystal glasses (high contents of P and Cr) indicate to the formation under the same condition, probably from one precursor.

Opaque phases in studied meteorites are also different. TIL-91722 contains mainly kamasite and pentlandite; taenite and troilite are rare. Some pentlandite grains contain $P_2O_5$ and $Cr_2O_3$ (up to 3.5 and 2.6 wt.%). Kamasite is main opaque phase in PCA-91082, taenite is less abundant and troilite is rare (pentlandite is absent). Mineralogy of WIS-91600 is unusual: it contains only sulfides (troilite and pentlandite in same proportions) and Fe-oxides. Absence of Fe-Ni metal can be connected with the terrestrial alteration process.

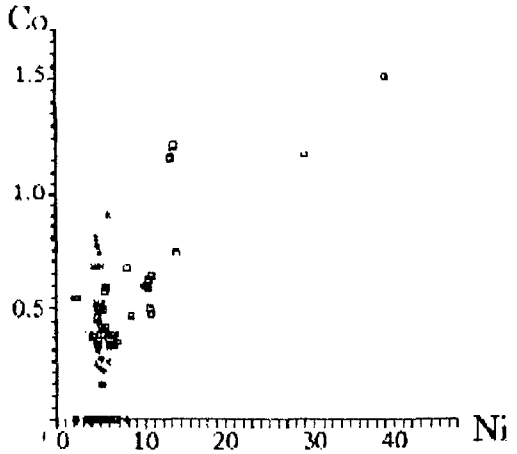


**Fig 3.** Composition of Fe-Ni metal *(at. %)*.
• TIL-91722; ▫ PCA-91082.

Positive trend between Ni and Co contents in kamasite and taenite of PCA-91082 (shown on Fig. 3) is typical for CR-chondrites [4]. According to experimental data [1] enrichment of metal in Co with Ni can be caused by

partial volatilization of kamasite. Also enrichment in Co both Ni can be produced by the process of sulfidization followed by reduction [2] and terrestrial weathering. High concentrations of Cr and P in TIL-91722 sulfides are probably explained by presence of chromite and phosphates but this phases were not detected.

Matrix compositions of studied meteorites are not essentially distinguish from each other and present in Table 2. Mineral composition is usual: Fe-Mg-silicate with small grains of olivine, orthopyroxene and sulfides. Calcite also was detected in TIL-91722 matrix.

Obviously all constituents of studied meteorites have complex history. Bulk compositions of inclusions and chonrules pass along to the equilibrium condensation trend (Fig 4), calculated using PHEQ program [5]. Abundance of glasses and exsolution structures is the evidence of magmatic stage in the history of chondrules evolution. Ni-Co positive correlation in Fe-Ni metal probably is a result of vaporization effect or latest events. Earth weathering alters kamasite to limonite.

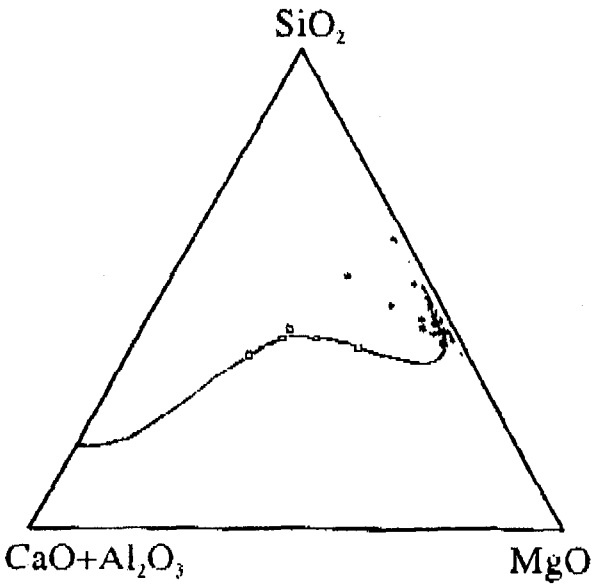


**Fig 4.** Bulk compositions of CAIs and chondrules (mol.%). ▫ CAIs; ▪ chondrules; — condensation trend.

Meteorites described in this publication are distinguished from other carbonaceous chondrites mostly in composition of middle-temperature fraction: chondrules and metal. Usually chondrule pyroxenes do not contain $Ti^{3+}$ and $Cr^{2+}$ (for example Allende) and presence of these valent forms indicate to formation of chondrules under essentially reduction conditions. The second possible explanation is influence of secondary oxidation for series of meteorite like Allende. One of the most interesting questions is way of enrichment of chondrules in two elements: Cr and P, which is very noticeably.

***Acknowledgments:*** The research described in publication was made possible in part by grant No. MPZ300 from the International Science Foundation and Russian Government.

***References:*** 1. Lavruhina, A.K., *et al.* Meteoritika (in Russian), 1979, v. 38, p. 62-64.
2. Lavruhina, A.K., *et. al.* Meteoritika (in Russian), 1989, v. 48, p. 9-17.
3. Ulyanov, A.A., *et al.* Geochimiya (in Russian), 1990, N 5, p.722-730.
4. Weisberg, M.K., *et al.* GCA, 1993, v. 57, p.1567-1586.
5. Wood, J.A., and Hashimoto, A. GCA, 1993, v. 57, 2377-2388.

**Table 2. Bulk composition of glasses (1-13) and meteorite matrix (14-16); normalized to 100 wt. %.**

(TIL - TIL-91722; PCA - PCA-91082; WIS - WIS-91600)

| *meteorite* | *TIL* | *PCA* | *PCA* | *PCA* | *PCA* | *PCA* | *PCA* | *WIS* |
|---|---|---|---|---|---|---|---|---|
| | 1 | 2 | 3 | 4 | 5 | 6 | 7 | 8 |
| $SiO_2$ | 59.07 | 73.54 | 51.88 | 54.27 | 46.75 | 61.85 | 56.89 | 22.62 |
| $TiO_2$ | 0.57 | 0.36 | 0.74 | 0.87 | 0 | 0.72 | 0.52 | 0.1 |
| $Al_2O_3$ | 15.14 | 9.6 | 6.99 | 3.17 | 33.49 | 13.74 | 12.54 | 3.44 |
| FeO | 8.62 | 6.18 | 1.51 | 0.58 | 0 | 12.01 | 11.44 | 33.93 |
| MnO | 0 | 0 | 0 | 0 | 0 | 0 | 0.24 | 0.22 |
| MgO | 0.75 | 1.28 | 21.94 | 20.88 | 0.8 | 0.96 | 0.64 | 14.35 |
| CaO | 8.35 | 5.75 | 15.02 | 19.38 | 18.96 | 2.79 | 2.01 | 0.38 |
| $Na_2O$ | 5.69 | 1.92 | 0 | 0 | 0 | 5.5 | 13.5 | 1.06 |
| $K_2O$ | 0.74 | 0.29 | 0 | 0 | 0 | 1.18 | 1.15 | 0.16 |
| $Cr_2O_3$ | 0 | 0.36 | 1.93 | 0.86 | 0 | 0 | 0 | 2.84 |
| NiO | 0 | 0 | 0 | 0 | 0 | 0 | 0 | 9.32 |
| $P_2O_5$ | 0.94 | 0.61 | 0 | 0 | 0 | 0.89 | 0.89 | 3.02 |
| S | 0.23 | 0.1 | 0 | 0 | 0 | 0.37 | 0.2 | 8.57 |
| *meteorite* | *WIS* | *WIS* | *WIS* | *WIS* | *WIS* | *PCA* | *WIS* | *TIL* |
| | 9 | 10 | 11 | 12 | 13 | 14 | 15 | 16 |
| $SiO_2$ | 45.46 | 21.72 | 39.95 | 45.38 | 23.47 | 38.21 | 39.46 | 32.53 |
| $TiO_2$ | 0.52 | 2.32 | 0.15 | 0.92 | 0.22 | 0 | 0.12 | 0.07 |
| $Al_2O_3$ | 7.17 | 1.83 | 4.09 | 27.32 | 10.22 | 1.8 | 3.59 | 2.74 |
| FeO | 18.37 | 42.56 | 21.48 | 0.74 | 41.03 | 34.04 | 22.06 | 34.62 |
| MnO | 0 | 0.68 | 0.31 | 0 | 0 | 0.37 | 0.21 | 0.35 |
| MgO | 23.19 | 19.81 | 24.31 | 3.52 | 3.6 | 18.02 | 23.2 | 19.7 |
| CaO | 0.25 | 0.57 | 0.13 | 21.52 | 5.5 | 0.88 | 1.53 | 1.07 |
| $Na_2O$ | 2.68 | 0.8 | 0.58 | 0 | 1.78 | 1.8 | 0.61 | 0.77 |
| $K_2O$ | 1.13 | 0.08 | 0.14 | 0 | 0.9 | 0.33 | 0.17 | 0.32 |
| $Cr_2O_3$ | 0.39 | 2.53 | 7.69 | 0.29 | 1.1 | 0.47 | 0.49 | 0.46 |
| NiO | 0 | 1.93 | 0 | 0 | 4.32 | 1.71 | 2.44 | 2.86 |
| $P_2O_5$ | 0.3 | 1.34 | 0.37 | 0.22 | 6.13 | 0.42 | 0.38 | 0.4 |
| S | 0.55 | 3.83 | 0.81 | 0.1 | 1.71 | 1.95 | 5.75 | 4.11 |

# THE INVESTIGATION OF SPHERULES BY ATOMKI SCANNING PROTON MICROPROBE

I. BORBÉLY-KISS[1], I. RAJTA[1], I. BESZEDA[2], Gy. SZÖŐR[2]

[1] Institute of Nuclear Research of the Hungarian Academy of Sciences,
H-4001 Debrecen, Hungary
[2] Kossuth University, H-4010 Debrecen, Hungary

**Abstract:** Scanning proton microprobe, as a complementary technique to electron probe microanalysis has been used for measuring elemental composition of spherules occuring in Upper Pannonian and Quaternary sediments.

## Introduction

Microtektites, cosmic spherules are generally small and rounded glass or magnetic objects. They occur on four widely separated territories of the Earth's surface "strewn fields", and two tektite regions associated with impact craters [Glass, 1990].

By the continuous cores of drillings Miocene, Pliocene and Quaternary sediments were uncovered in the Little Hungarian Plain. We have found sphere and drop like Ca-rich ortho -silicate glasses in the upper Pannonian layers and magnetic spherules in the Quaternary alluvial flat [Szöőr et al. 1994., Gyuricza et al. 1995].

The scanning proton microprobe (SPM) as complementary to electron probe microanalysis (EPMA) is used in geoscience research, especially mineralogy, petrology, geochemistry and cosmochemistry as a suitable method for quantitative, nondestructive microanalysis of minerals, rocks and meteorites [Ryan et al. 1990, Sie 1993, Campbell et al. 1990, Campbell et Teesdale, 1993].

## The scanning proton microprobe

A microprobe system of Oxford Microbeams [Grime, 1991] has been installed in the Institute of Nuclear Research of the Hungarian Academy of Sciences (ATOMKI), on one of the beamlines of the 5 MeV Van de Graaff accelerator.

The 2 MeV proton beam of the accelerator passing through a small object aperture is focused by the quadrupole doublet (comprising two magnetic quadrupole lenses) on the sample under investigation. 1 $\mu m^2$ beam spot size can be achieved with currents sufficient for PIXE analysis.

The microbeam is scanned over the samples in a controlled raster pattern. The maximum scanned area is 2.5 x 2.5 mm. Data pulses from the sample detected by X-ray, electron or particle detector are recorded together with the instantaneous X and Y co-ordinates of the beam in the scan. This can be used to construct elemental maps, to provide on-line energy spectra from each detector. The beam spot can be stopped at any point in the scan.

## Analytical method

As a consequence of charged particle irradiation a number of different types of radiation may be produced. Radiation or particles can be detected to give analytical

information. One of the most important techniques for the scanning proton microprobe is the particle induced X-ray emission (PIXE) [Johansson et Campbell, 1988].

The collision of charged particle and the stationary atoms results in the ejection of an electron from the inner shell of the target atom, leaving a vacancy there. This vacancy is filled by an electron from a higher energy state. Excess of energy is emitted as an X-ray photon. The energy of X-ray is characteristic of the target atom. Detecting the X-ray photons with an energy dispersive detector, elements in a matrix of unknown composition can be identified and quantified. PIXE is providing nondestructive, multielemental in situ analysis of samples offering limits of detection down to a few ppm with 5-10% accuracy.

In our laboratory a Canberra (Lithium-drifted silicon) Si(Li) detector is used for energy dispersive X-ray spectroscopy. To identify and quantify the elements in the sample under investigation the PIXYKLM programme package [Szabó et Borbély-Kiss, 1993.] have been used.

**Samples and analysis**

In the framework of the Little Hungarian Plain mapping project [Scharek (ed) 1993] samples ordered by the Geological Institute of Hungary have been collected from the borehole Nagylózs-1 (geographic coordinates are: 47° 34' 13" N; 16° 48' 04" E).

Three microtektite were collected from Upper Pannonian marly siltstone.

V/b: (in NL-1, 439.7 m): amber, glassy spherule,

VII: (in NL-1, 610.0 m): amber, glassy ellipsoid-like spheroid,

IX : (in NL-1, 787.6 m): amber, glassy double-drop

In the Little Hungarian Plain, surroundings of Gönyü (G) and Győr-Zámoly (GY) villages 36 drillings were ordered by the Geological Institute of Hungary, in a frame research, initiated by U.S. Geological Survey. The depth was 15 m and by continuous cores of drilling Holocene fluvial sands and gravels were uncovered. Magnetic Spherules have been investigated in this program.

G-1: metallic black, drop-like spheroid. Meteoritic dust.

G-2: dull black, ball-like spherule. Volcanic origin (?) or Impactite

G-4: metallic black, ball-like spherule. Meteoritic dust.

G-13: dull black, ball-like spherule. Impactite.

Gy-1: dull black, ball-like spherule. Meteoritic dust.

Gy-2: metallic black, cracked ellipsoid-like spheroid. Meteoritic dust.

The above samples have been analyzed by EPMA (electron probe micro-analysis) and the following four main genetic types were distinguished.

1. Microtektite (glassy spherules)
2. Meteoritic dust (magnetic spherules)
3. Impactite (Iron-silicate spherules)
4. Spheres of uncleared origin (igneous or metamorphic?)

To obtain further microanalytical data, the above samples were selected for parallel scanning proton microprobe ($\mu$-PIXE) studies, too.

In fig. 1. PIXE maps of sample VII. are shown with 1600 $\mu$m scan size, and G-1 sample with 1000 $\mu$m and 250 $\mu$m scan size. In the latter case it is clearly seen, how to find the object in question on the basis of Fe X-ray map decreasing the scan size in a few steps. PIXE spectra were collected with a scan size of less then the size of the spheroid.

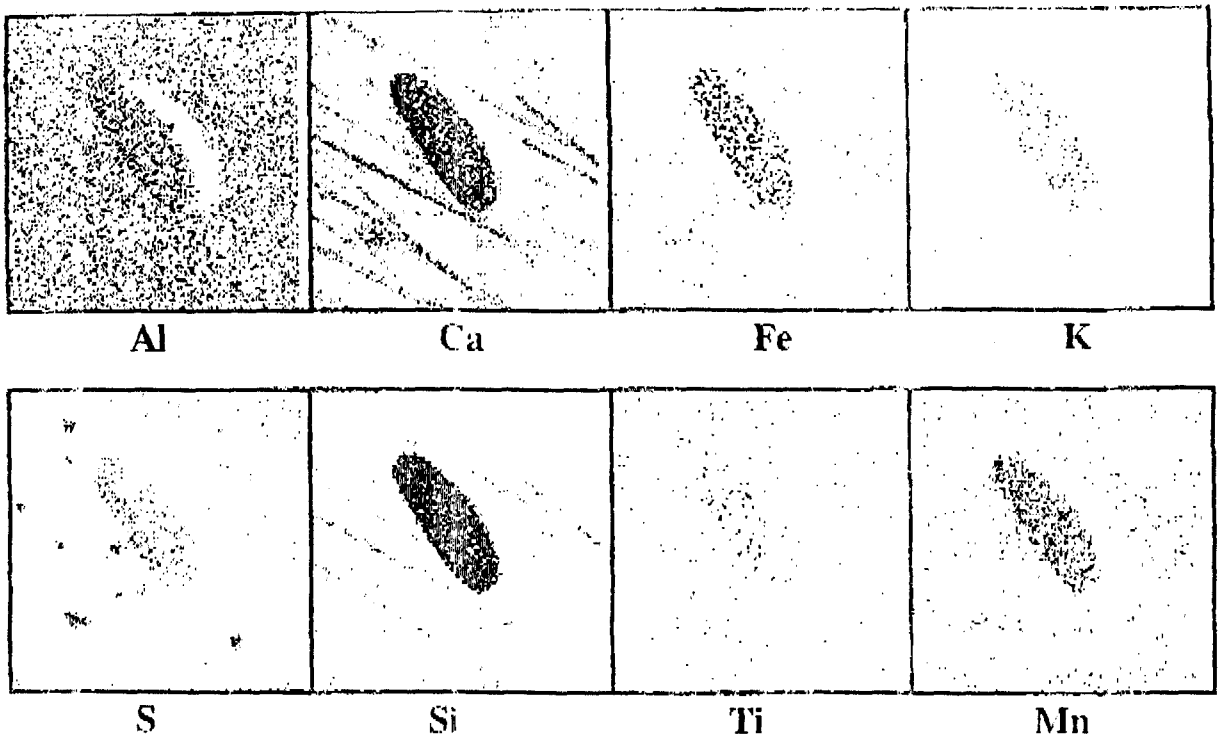


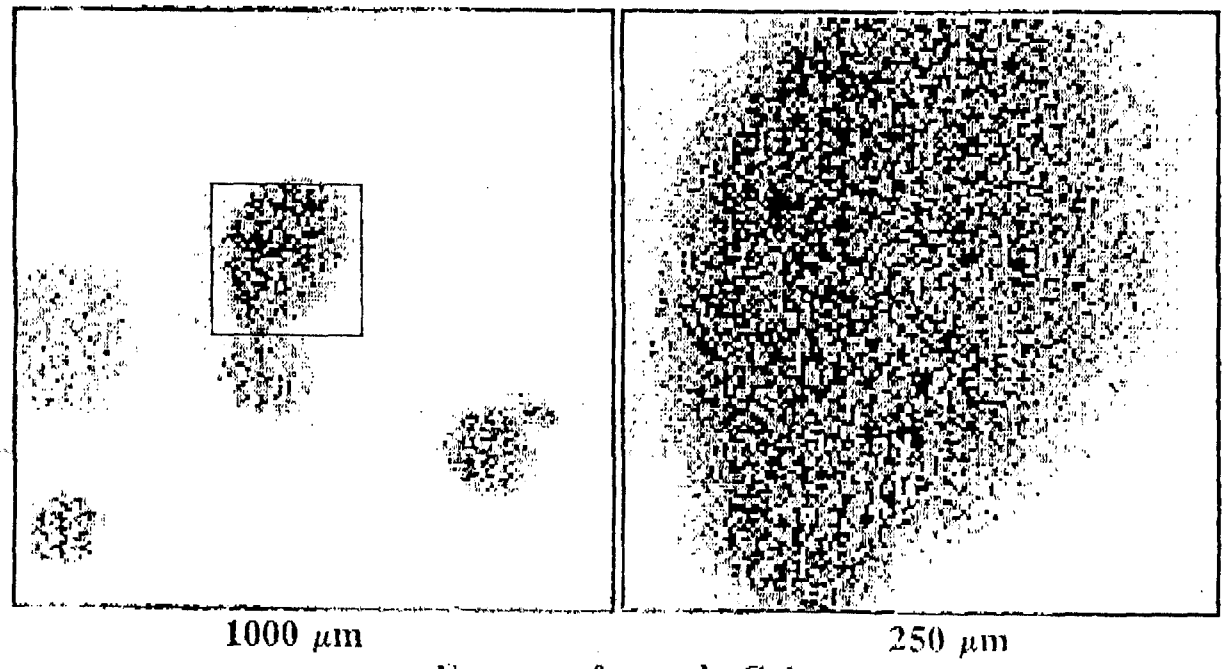


**Figure 1**. X-ray maps of elements on samples VII and G-1

Identification and quantification of elements in the spectra were done by PIXYKLM program. The knowledge of the major element concentrations is required for matrix corrections, both in fitting spectra and calculating trace element concentrations. Major element concentrations obtained by the electron microprobe analysis were used for calculation matrix corrections. (It should be noted that the use of matrix determined by EPMA may result error in concentration calculation. EPMA determines the matrix to depth 1-2 $\mu$m while in $\mu$-PIXE this depth is 10-20 $\mu$m, the sample volume is different.) In case of micrometeorites concentration data were normalized to Ca, in case of magnetic spherules to Fe.

Results of $\mu$-PIXE analysis together with the results of electron probe micro-analysis (EPMA) are shown in the table 1 and table 2. Na and Mg data are missing in $\mu$-PIXE because the X-rays of these elements are absorbed in the 25 $\mu$m thick Be window of the Si(Li) detector.

Table 1. Composition of various micrometeorites collected from Nagylózs-1. borehole. (Concentrations are given in %)

| | V/b | | | VII | | | IX | IX/1 | IX/2 |
|---|---|---|---|---|---|---|---|---|---|
| | EPMA | $\mu$-PIXE | | EPMA | $\mu$-PIXE | | EPMA | $\mu$-PIXE | $\mu$-PIXE |
| Na | 0.535 | | Na | 0.503 | | Na | 0.440 | | |
| Mg | 6.244 | | Mg | 7.057 | | Mg | 6.491 | | |
| Al | 7.828 | 1.014 | Al | 8.357 | 0.956 | Al | 7.796 | 1.011 | 0.936 |
| Si | 29.133 | 37.376 | Si | 31.153 | 35.236 | Si | 29.526 | 43.346 | 40.192 |
| P | | 3.374 | S | 1.383 | 2.275 | P | | 4.100 | 3.531 |
| S | 0.959 | 0.679 | Cl | | 0.462 | S | 1.262 | 1.235 | 1.087 |
| Cl | | 0.245 | K | 1.232 | 1.015 | Cl | | 0.412 | 0.321 |
| K | 1.469 | 1.284 | Ca | 48.085 | 48.085 | K | 1.397 | 1.458 | 1.406 |
| Ca | 51.165 | 51.165 | Ti | 0.362 | 0.386 | Ca | 50.465 | 50.465 | 50.465 |
| Sc | | 0.893 | Mn | 0.877 | 1.116 | Sc | | 0.766 | 0.984 |
| Ti | 0.385 | 0.331 | Fe | 0.345 | 0.497 | Ti | 0.380 | 0.521 | 0.429 |
| Cr | | 0.097 | Nb | | 2.106 | Cr | | 0.147 | 0.089 |
| Mn | 0.933 | 1.181 | Ba | 0.702 | 0.239 | Mn | 0.920 | 1.110 | 1.154 |
| Fe | 0.588 | 0.819 | Zr | | 2.622 | Fe | 0.471 | 0.589 | 0.623 |
| Ni | | 0.179 | | | | Ni | | 0.197 | 0.165 |
| Nb | | 3.801 | | | | Nb | | 4.160 | 3.869 |
| Ba | 0.717 | 0.731 | | | | Ba | 0.677 | 0.743 | 0.871 |

Table 2. Composition of magnetic spherules
(Concentrations are given in %)

| | G-1 | | | G-13 | | | G-2 | | | G-4 | | | GY-1 | | | GY-2 | |
|---|---|---|---|---|---|---|---|---|---|---|---|---|---|---|---|---|---|
| | EPMA | μ-PIXE | | EPMA | μ-PIXE | | EPMA | μ-PIXE | | EPMA | μ-PIXE | | EPMA | μ-PIXE | | EPMA | μ-PIXE |
| Al | 5.49 | 0.225 | Mg | 2.76 | | Mg | 3.30 | | | | | | | | | | |
| Si | 2.08 | 1.169 | Al | 19.51 | 0.134 | Al | 31.46 | 0.611 | Al | 4.49 | 0.181 | Al | 3.29 | 0.078 | Al | 3.29 | 2.467 |
| P | | | Si | 34.86 | 3.853 | Si | 31.49 | 9.670 | Si | 1.40 | 1.276 | Si | 6.15 | 3.314 | Si | 6.15 | 0.545 |
| S | | 0.193 | P | | 0.504 | P | 1.96 | 1.890 | P | | 0.328 | P | | 0.557 | P | | 0.473 |
| Cl | 0.08 | 0.345 | S | 0.65 | 0.098 | S | 1.17 | 0.180 | S | | 0.236 | S | | 0.148 | S | | 0.176 |
| K | | 0.085 | Cl | 0.32 | 0.119 | Cl | 0.62 | 0.355 | Cl | 0.11 | 0.293 | Cl | 0.33 | 0.348 | Cl | 0.33 | 0.275 |
| Ca | 0.09 | 0.071 | K | 0.45 | 0.205 | K | 0.21 | 0.190 | K | | 0.099 | K | | 0.034 | K | | 0.029 |
| Cr | 0.12 | 0.070 | Ca | 14.97 | 5.689 | Ca | 6.47 | 8.967 | Ca | 0.41 | 0.492 | Ca | 0.31 | 0.116 | Ca | 0.31 | 0.046 |
| Mn | 0.63 | 0.405 | Ti | 0.39 | 0.124 | Sc | | 0.081 | Ti | 7.93 | 6.027 | Cr | 0.11 | 0.176 | Fe | 88.37 | 88.370 |
| Fe | 91.34 | 91.340 | Mn | 0.04 | 0.057 | Ti | 0.83 | 0.382 | Cr | 0.01 | 0.064 | Mn | 1.03 | 1.682 | Cu | | 0.096 |
| Ni | | 0.540 | Fe | 25.72 | 25.720 | Fe | 22.70 | 22.700 | Mn | 1.14 | 1.245 | Fe | 88.37 | 88.370 | Nb | | 0.293 |
| Cu | | 0.113 | Cu | | 0.038 | Ni | | 0.129 | Fe | 84.30 | 84.300 | Cu | | 0.117 | Ag | 0.40 | 0.670 |
| Zr | | 0.529 | Nb | | 1.059 | Cu | | 0.054 | Nb | | 0.427 | Nb | | 1.103 | Ba | | 0.064 |
| Nb | | 0.110 | Ag | 0.24 | 0.246 | Zn | 0.05 | 0.035 | Pd | | 0.231 | Ag | 0.40 | 0.938 | Hf | | 4.221 |
| Ag | 0.16 | 0.599 | | | | As | 0.43 | 0.045 | Ag | 0.20 | 0.657 | Cd | | 0.145 | | | |
| Ba | | 0.076 | | | | Sr | | 0.170 | Ba | | 2.693 | Hf | | 1.340 | | | |
| | | | | | | Nb | | 3.174 | | | | | | | | | |
| | | | | | | Ag | 0.12 | 0.403 | | | | | | | | | |

In micrometeorite sample V/b and IX P, Cl, Sc, Cr, Ni and Nb, in sample VII Cl, Ni and Zr elements, not detected by EPMA, have been found by $\mu$-PIXE. The shape of the sample IX is a double-drop. Analysis were made on both drop to get information about the homogeneity of the object.

In case of magnetic spherules similar differences can be seen between the concentration data obtained by EPMA and $\mu$-PIXE .

## Conclusion

We have tried to demonstrate here that $\mu$-PIXE can be a complementary technique to EPMA in spherulites research. The same samples were analyzed on the same position. EPMA provided matrix concentrations, $\mu$-PIXE gave more elements. We will make efforts in the future to get more reliable trace element concentration data determining the matrix by $\mu$-PIXE, too.

## Acknowledgement

This work was supported by the National Research Foundation OTKA No 1742 and OTKA No A 080.

## References

Campbell J.L., Maxwell J.A., Teesdale W.J. and Wang J.-X., 1990, Micro-PIXE as a complement to electron probe microanalysis in mineralogy, Nucl. Instr. Meth. in Phys. Res. B44 pp. 347-356.

Campbell J.L. and Teesdale W.J., 1993, Micro-PIXE analysis of major elements in mineral specimens, Nucl. Instr. Meth. in Phys. Res. B74 pp. 503-510.

Glass B.P., 1990., Tektites and microtektites: key facts and inferences. Tectonophysics 171 pp. 393-404.

Grime G.W., Dawson M., Marsh M., McArthur I.C. and Watt F., 1991., The Oxford submicron nuclear microscopy facility, Nucl.Instr.Meth. in Phys. Res. B54 pp. 52-63.

Gyuricza Gy., Beszeda I. and Szöőr Gy. 1995., Magnetic spherules in the alluvial flat of the Danube, NW Hungary. Abstracts of the Spherulites and Palaeoecology, Int. Meet. Debrecen, Hungary, 2-4 March 1995. p. 13.

Johansson S.A.E. and Campbell J.L. 1988., PIXE: A Novel Technique for Elemental Analysis, John Wiley and Sons,

Ryan C.G., Cousens D.R., Sie S.H. and Griffin W.L., 1990, Quantitative analysis of PIXE in geoscience applications. Nucl. Instr. Meth. in Phys. Res. B49 pp. 271-276.

Scharek P. (editor), 1993., The Geological Map Series of the Little Hungarian Plain, Sopron-Kőszeg Ser. Geol. Inst. of Hungary, Budapest.

Sie S.H., 1993, Progress of quantitative micro-PIXE applications in geology and mineralogy, Nucl. Instr. Meth. in Phys. Res. B75. pp. 403-410.

Szabó Gy. and Borbély-Kiss I. 1993., PIXYKLM computer package for PIXE analysis Nucl. Instr. Meth. in Phys. Res. B75 pp. 123-126.

Szöőr Gy., Korpás-Hódi M., Don Gy., Beszeda I., 1994., Microspherules from the sediments of borehole Nagylózs-1, Hungary. Suppl. of Annales Univ. Sci. Budapest, Sect. Geoph. et Met.(in press)

# COMPARISON OF SPECTRA OF APOLLO-AMOR, HUNGARIA, BELT AND OTHER ASTEROIDS IN A FILTER-SPANNED COLOUR SPACE

Sz. Bérczi[1], Agnes Holba[2] & B. Lukács[2]
1 Dean's Office of R. Eötvös University, H-1088 Rákóczi út 5 and Dept. of Astronomy of R. Eötvös University, H-1083 Ludovika tér 2, Budapest, Hungary
2 Central Research Institute for Physics RMKI, H-155 Bp. 114. Pf. 49., Budapest, Hungary

**ABSTRACT**

We simulate to observe asteroids through 3 specific filters and without them. The filter spectra depend on assumptions of dominant mineral components, 4 selected. We compare the colour coordinates of Apollo-Amors, belt asteroids, and some few other specific bodies. The {C,O,P,I} tetrad, characteristic for meteorites, is insufficient even for Apollo-Amors.

## 1. INTRODUCTION

For 9 months two sets of extraterrestrial materials were available for study at the R. Eötvös University: a lunar rock sample set, by the courtesy of NASA, USA, and an Antarctic meteorite thin section set by the courtesy of the National Institute of Polar Research, Tokyo, Japan. The simultaneous presence and study of these materials, presenting as good a cross section of extraterrestrial solid state matter as possible today, triggered a study of investigating the material constitution of the very diverse asteroid belt via reflected light.

## 2. FILTERING

We observe the asteroids through 3 filters, optimized for discriminating 4 materials, fundamental in meteorites: Iron, Pyroxene, Olivine and Carbonaceous chondrite. The method is described elsewhere (Bérczi, Holba, Lukács 1994)). The optimum must be approximated by existing filters. In the catalog of Spezial Glas Gmbh, Mainz, we found 3 filters approximating optima as

{KG 4, RG 9, BG 7}

## 3. THE INPUT DATA OF THE ANALYSIS

The main target of the present test is the Earth-crossing Apollo-Amor group. We compare them to other important groups too:

*1. Apollo-Amors*

Earth-crossers of serious eccentricity. Their fragments have the biggest chance to collide with Earth, so their composition should be familiar among meteorites. In the data system 6 are given, but one has *two* spectra, quite different: 1566 Icarus (a); 1580 Betulia (b); 1620 Geographos (c); 1685 Toro/1$^{st}$ spectrum (d); 1685 Toro/2$^{nd}$ spectrum (e); 1862 Apollo (f); 2100 Ra-Shalom (g). We are not going to resolve the controversy of Toros.

*2. Mars-crossers*

Best analogons to Apollo-Amors. One of them is well-known, substantial and available among the data: 433 Eros (h).

*3. E-asteroids or "Hungarias"*

At the inner end of the Belt, nearest to Sun, a group is called after 434 Hungaria (Hirayama 1918). Most Hungarias are too small for detailed data. According to the zonal structure of the Solar System (Lewis & Barshay 1975); then Hungarias' compositions should be nearest to those of the inner stony planets. 3 sub-

stantial E-asteroids are often classified together, as aubrites, but two of them are in the main belt, only Hungaria is a true Hungaria. See: 44 Nysa (i); 64 Angelina (k); 434 Hungaria (l).

*4. Metamorphs*

One big asteroid differentiated partially: metamorphised but not completely differentiated into zones: 349 Dembowska (m).

*5. Bigger Belt asteroids*

The first items of asteroid lists are more substantial, than the last ones, and have more chance to belong to the Main Belt. Previously (Bérczi, Holba & Lukács 1994) we studied the first 20. Here we give the points for 8, the first 5 and some important other 3. The remaining 12 can be seen in the previous paper. The list is: 1 Ceres (n); 2 Pallas (o); 3 Juno (p); 4 Vesta (q); 5 Astraea (r); 10 Hygeia (s); 13 Egeria (t); 16 Psyche (u).

*6. Various small objects*

At the end of the database very probably the smallest or farthest objects can be found. They may differ very much even among themselves. We selected 4 of them from the end: 1830 Pogson (w); 2201 Oljato (x); 3102 (y); 5797 (z).

**4. RESULTS**

Let us see Figs. 1-2. We will distinguish two tetrahedrons. The "meteorite" tetrahedron is spanned by {C,O,P,I}, dominant in meteorites. However, this tetrahedron does not contain many asteroids in study; it does not contain the majority of the first 20 (Bérczi, Holba, Lukács 1994). However we found an "asteroid" tetrahedron {C,O,5Astraea,I} containing all the first 20 ones except for 13 Egeria. (Marginal deviations are ignored here and henceforth.) The asteroid tetrahedron contains 23 asteroids of the 24 studied, and the exception is again 13 Egeria.

The Apollo-Amors scatter widely. 4 are in or near the meteorite tetrahedron (1566 Icarus, 1580 Betulia, 1685 Toro 2nd and 2100 Ra-Shalom), 3 more are between 5 Astraea and the OC edge.

433 Eros, is similar to 5 Astraea, not to the Apollo-Amors. The big Belt asteroids occupy a thin region almost on the {C,I,5Astraea} border of the asteroid tetrahedron. The 3 E-s span a small area, partly overlapping with the region of big Belt bodies, shifted to the direction of O. 349 Dembowska deviates from the region of big Belt asteroids, to the direction of O. The small objects scatter in the whole asteroid tetrahedron.

5 Astraea is extremal. As for Apollo-Amors, 1566 Icarus is not too far from 4 Vesta, which is surprising. 1580 Betulia seems quite a C chondrite, 1620 Geographos is unique, but resembles 3 Juno. The two points for 1685 Toro are widely separated. The first Toro could be reproduced from 5 Astraea with some 15% pyroxene added, the second suggests iron+olivine. As told above, we are not in the position to explain the discrepancy. 1862 Apollo is near to 349 Dembowska, but shifted to O+C (or P+C). Finally, 2100 Ra-Shalom is near to I. But in general, the Apollo-Amors are outside of the region of big Belters, to the direction of O (or P). Mars-crosser 433 Eros very much mimics 5 Astraea.

Each E-asteroid shows individual features. 44 Nysa and 64 Angelina lies in the region of big Belt asteroids, but 434 Hungaria is nearer to the O corner.

Finally, among the diverse small bodies 1830 Pogson is on the (5 Astraea,O) edge, 3102 coincides with 1620 Geographos, and 2201 Oljato and 5797 are in the region of big Belters. Specially 2201 Oljato is not unsimilar to 4 Vesta and 1566 Icarus.

## 6. DISCUSSIONS

The meteorite and asteroid tetrahedrons definitely differ, as if one important component of S asteroids is poorly represented (or recognised) in meteorites. Which is this component and why is it poorly represented in meteorites?

The extra component is strongest in 5 Astraea. As for the actual material, the filter method cannot uniquely select it. The most harmless guess is based on the zonal theory. It is known that asteroids' chemical composition tends to change with solar distance, expected as well from the condensation theory.

Pyroxene, olivine and iron all represent the "warm" inner System; in the main belt the temperatures were lower.

Features of 5 Astraea not common with the pyroxene, olivine, metal and carbonaceous chondrite spectra are compatible with antigorite, one variant of serpentine, which has an important role in the Barshay-Lewis condensation (Barshay & Lewis 1975), and according to the Barshay-Lewis prototemperatures its condensation is expected just somewhere in the distance of the asteroid belt (Bérczi & Lukács 1994). An idea that in the asteroid belt low-melting serpentine would replace the crust silicates of higher melting points of the inner System is not a priori impossible, and would fit halway into the sequence between feldspars on Earth, Luna and Mars, and dirty ice on Jovian moons.

*Why* this material (anything it may be) is not familiar in meteorites? To be sure, 4 of the 7 Apollo-Amor points *are* in the meteorite triangle, so they may be source bodies of meteorites, but the other 3 cannot. Various guesses can be tried. It may be weathered away on Earth. But it is hardly reported even in fresh showers. It is possible that "astreait" is a matter unable to survive temperatures above 270 K, lost if perihelia are below 1 AU, and then young Apollo-Amors are evolving towards the meteorite tetrahedron; four already has reached it, and the other 3 represent steps of evolution in the sequence Toro 1, Geographos and finally Apollo. This would be conform with the fact that 433 Eros, just *not* Earth-crossing, is near to the Astraea point.

The general picture is conform with the zonal condensation scheme. There the material composition shows a definite trend when going away from the Sun. And now, "Hungarias", or at least 434 Hungaria, are shifted from the Belt plane {C,I,5Astraea} towards the O point, and Apollo-Amors are shifted even more. Maybe 1566 Icarus is similar to 4 Vesta because is repeatedly being heated up at 0.19 AU.

**ACKNOWLEDGEMENTS**

The use of Planetary Data System, Pasadena, sponsored by NASA is acknowledged. Thanks are given to NIPR Japan for loaning the Antarctic Meteorite Sample and to NASA JSC USA for Lunar sample. Partly supported by OMFB-MEC-94-1613.

**REFERENCES**

Barshay S. S. & Lewis J. S. 1975: The Dusty Universe (Fields G. B. & Cameron A. G. W., Neale Watson Acad. Publ. New York

Bérczi Sz., Holba, Agnes, & Lukács B. 1994: KFKI-1994-22, p. 57

Bérczi Sz. & Lukács B. 1994: KFKI-1994-22, p. 6

Hirayama K. 1918: Astron. J. **31**, 185

Yanai K. & Kojima H. 1987: Photographic Catalogue of Antarctic Meteorites, NIPR, Tokyo

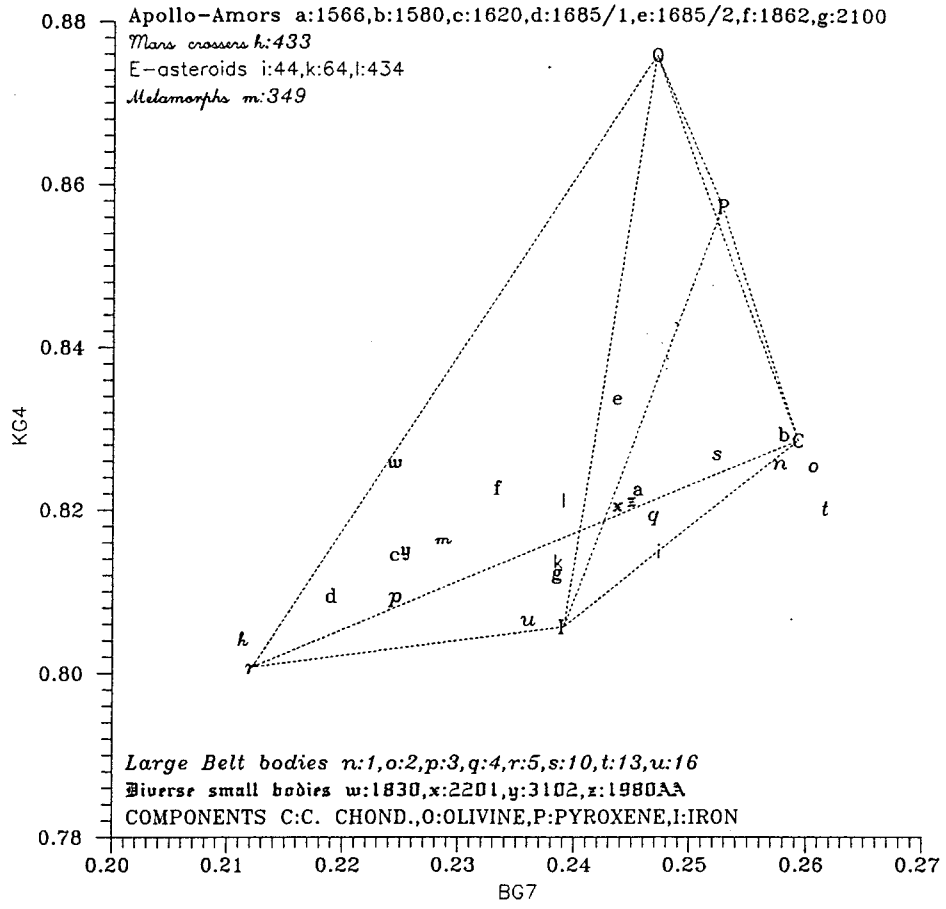


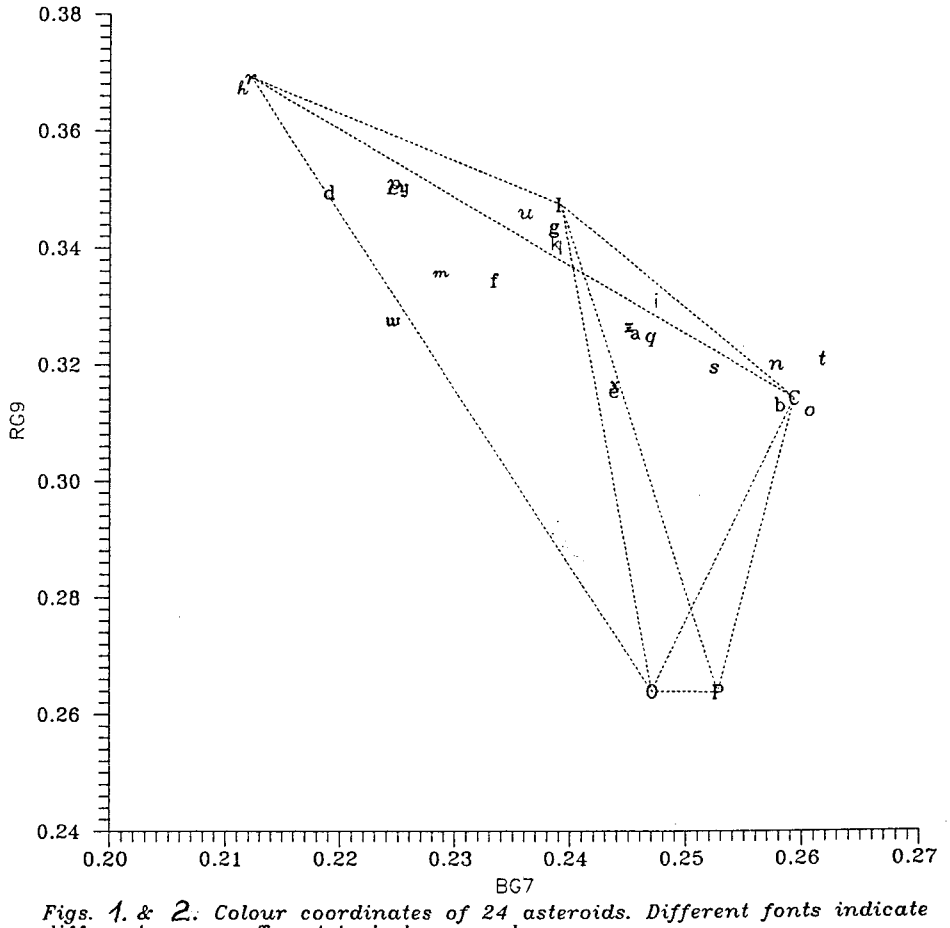


*Figs. 1. & 2. Colour coordinates of 24 asteroids. Different fonts indicate different groups. Two tetrahedra are shown.*

# THERMAL TRANSFORMATIONS IN THE METEORITES' PARENT BODIES

Sz. Bérczi[1], Agnes Holba[2] & B. Lukács[2]

[1] Dean's Office & Astronomy Dept., R. Eötvös University, H-1088 Rákóczi út 5., Budapest, Hungary
[2] Central Research Institute for Physics, H-1525 Bp. 114. Pf. 49., Budapest, Hungary

**ABSTRACT**

The samples of the NIPR Antarctic Meteorite Collection have been arranged in a supposed metamorphosis field spanned by such thermal effects as: diffusion, volatile evaporation, melting and differentiation. The "triangle-field" has been divided by estimated isotherms coming from a model calculation on thermal history of meteoritic parent bodies depending on solar distance and body size.

## 1. INTRODUCTION

Meteorites are i) either the leftover of the planet formation ii) or fragments of composite bodies as comets or iii) chips of asteroids, iv) or, rarely, chips of substantial planets (as Luna or Mars). So they may differ in α) original solar distance (and so in original composition) and ß) thermal history. Here we try to apply an approximate scheme for explaining the samples in the Japanese Antarctic Meteorite Thin Section Set.

## 2. TRIANGLE SCHEMES

Main components of the condensed bodies in the Solar System can be classified as

1) Metal (Mainly FeNi, FeS included), a high temperature component;
2) Stone (silicates, metal oxides, &c.), a middle temperature component,
3) Ices (or bound $H_2O$, $NH_3$, &c.), a low temperature component.

The first part of our composite Figure shows how the meteorites populate the triangle. Interestingly enough, meteorites appear in which all 3 components appear. The I corner is unpopulated in the sample, and extraterrestrial ices are practically absent in the meteorite literature. (Cf. (Bérczi & Lukács 1994; an unconfirmed event was reported from continental China in March).They would survive in the Antarctic interior but hard to detect ice on ice.

The samples are products of a thermal history of 4.5 billion years. This thermal history depended on size and solar distance. But first let us see a phenomenologic classification for thermal history. The second triangle of our Figure has a *primordial* stage on the left corner (PRIM, a C1 or C2 chondrite, supposedly primordial from Venus to the Belt), *differentiated* (DIFF, gravitationally separated) matter on the upper right corner and a *thermally transformed* but not differentiated final stage (EVAP) on the lower right one. So iron--lost basalts and silicate-lost irons are on the upper right edge and carbon- and water-lost materials on the lower right corner. Without differentiation the transforming processes are heating, diffusion and evaporation (of volatiles).

## 3. PROCESSES

Almost all possible processes are driven by heat in the possible parent bodies of meteorites. So from left to right in the second triangle the integrated heat impact is growing, while from down to upwards the gravitation, i.e. the size of the body. They correspond to each other via the approximate formula

$$T(t) \approx T_S + (F(t)/6k)R^2 \quad (1)$$

$$T_S(t) = T_E(t)(r_E/r)^{\frac{1}{2}} \quad (2)$$

where F is the radioactive heat production rate in volume unit, k is the heat conduction coefficient, $T_E$ is the equilibrium temperature at Earth's orbit; r is the solar distance and R is the radius (Holba & Lukács 1994).

Then in a small body far from Sun the original composition remains (left corner), in a small body near to Sun evaporation happens but differentiation does not (lower right corner), while in a large body (at any distance) differentiation is expected (upper right corner).

Heating in small bodies happened in the young Solar System mainly by the short-living radioisotopes, $Al^{26}$ and $Pu^{244}$, extinct for now. So their original concentration is unknown. Astronomers generally believe that $Al^{26}$ was the more important. Now, an estimation is possible for the initial radio-Al concentration, if we assume that k was roughly similar to that of Earth. Then one gets:

$$T = T_E(r_E/r)^{\frac{1}{2}}(1-R/R_{cr})^2 + T_{cr}(R/R_{cr})^2 \quad (3)$$

where $T_{cr}$ is some important temperature and $R_{cr}$ is the radius at which $T=T_{cr}$ in the center. Now, global differentiation starts with melting of iron, because molten iron can flow out from the silicates. The corresponding temperature is cca. 1800 K for FeNi.

Now, observations seem to suggest that the bigger asteroids are differentiated. The picture is not clear because it seems that 349 Dembowska is only partly differentiated, but 44 Nysa is completely such. A possible explanation is that 44 Nysa *was* the mantle of an asteroid, whose iron core might have been 135 Hertha. If so, then differentiation started from $R_{cr} \approx 65$ km; this value may have to be revised in the future but now will do. The third part of our composite Figure is a topographic plot for the central temperature of an asteroid of distance r and size R shortly after formation, and line A there and on the second triangle is the line at which a molten iron core developed. We expect pallasites just the right of this line and mesosiderites just to the left of it. Aubrites and basaltic achondrites must be farther to the right.

Going down in temperature, somewhere a temperature is found where the material of the chondrules could diffuse the chondrule size during the first million years. ($Al^{26}$ has the half life $7*10^5$ y, so heating seriously decreases after a million year.) We do not have olivine diffusion coefficient in olivine at reach, so we guessed this temperature to be at 1200 C°. That is line B separating chondrites fromn achondrites.

The next line, C, is where the C diffusiion during the hot million years is still macroscopic, i.e. cca. 1 cm. At the upper end of this line seems to be the ureilites. On the line

$$D_0 \exp(-Q/T)*t_{hot} \sim 1 \text{ cm}^2 \quad (4)$$

where Q is some characteristic activation energy. Hence obviously $D=3*10^{-14}$ cm²/s. There are measurements for at least some volatile gases in augite, and for them 1000 C° would be needed for this value of D (Fechtig et al. 1960.)

Line D is the temperature where FeO can be reduced to mettalic Fe in a million years. We do not know reaction rates for FeO in silicates. However metallurgic experiments tell us that 1) the reaction FeO+C -> Fe+CO has an energy barrier equivalent to cca. 19400 K (then CO reduces another FeO molecule without energy barrier) and 2) in the Höganäs method of Fe reduction without melting the process needs cca. 10 days at 1100 C°. Then one can extrapolate and gets the surprising result that at 410 C° it takes 1 million years. This temperature is a far-fetched extrapolation, but we have no better, and this is line D. This line separates C3 from C2, and all E, H, L and LKL seem to be right from it.

Line E is the water loss. Serpentine perceptibly loses water at 600 C° (Mason, 1962), but now slower rates will lead to water loss in a million years too. By a sheer guess we again halve the absolute temperature which was good for reduction, and get some 160-200 C°. Maybe this is the dividing line between C1 and C2.

Finally we note that C diffuses in iron very easily. at the melting point of carbonized iron D(T) seems to be 0.001-0.01 $cm^2/s$ (Shewnon, 1963). Therefore if the iron core can be formed, C can diffuse out from km depths, and so one expects only minor C content in iron meteorites or at the surface of iron asteroids (whence the mantle has been peeled off).

## 4. CONCLUSIONS

The second triangular field shows that the NIPR Set well represents all the different major thermal transformations within and outside of the meteorite parent bodies. One sees that the lower half (where solar heat dominates the internal one) is slightly more populated than the upper one, but this is probably a selection effect, because bodies crossing terrestrial orbit have more chance to be meteorites, and such orbits may have quite small perihelion distances.

By comparing the triangle field to the topographic figure one can roughly guees the size and orbit of the parent body of a meteorite. The vertical positions at the upper third of the triangle are somewhat uncertain, and one could improve them by looking at the C concentrations.

## ACKNOWLEDGEMENTS

The investigation has been possible by the courtesy of the NIPR, Dept. of Antarctic Meteorites, loaning the Set to the R. Eötvös University, Budapest. Partly supported by the MEC-94-1613 and the fund "Budapest Bank Budapestért".

## REFERENCES

Bérczi Sz. & Lukács B. 1994: KFKI-1994-11
Holba Agnes & Lukács B. 1994: KFKI-1994-22, p.
Mason B. 1962: Meteorites, J. Wiley & Sons, New York
Shewnon P. G. 1963: Diffusion in Solids, McGraw-Hill, Toronto
Fechtig, H., Gentner, W., Zähringer, J. 1960. Geochim. Cosmochim Acta. 19, 70-79.
Yanai, K., Kojima, H., et al. 1987. Photographic Catalog of the Antarctic Meteorites. National Institute of Polar Research, Tokyo

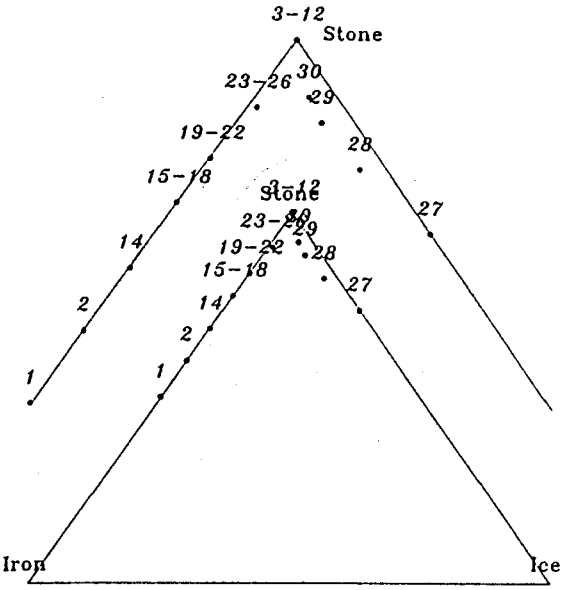


Fig.a. The arrangement of the samples of the NIPR Antarctic Meteorite Thin Section Set in a compositional triangle spanned by the three basic rocky components of the Solar System.

Most of the sample-positions can be found in the vicinity of the upper corner: stone, so this region has been enlarged.

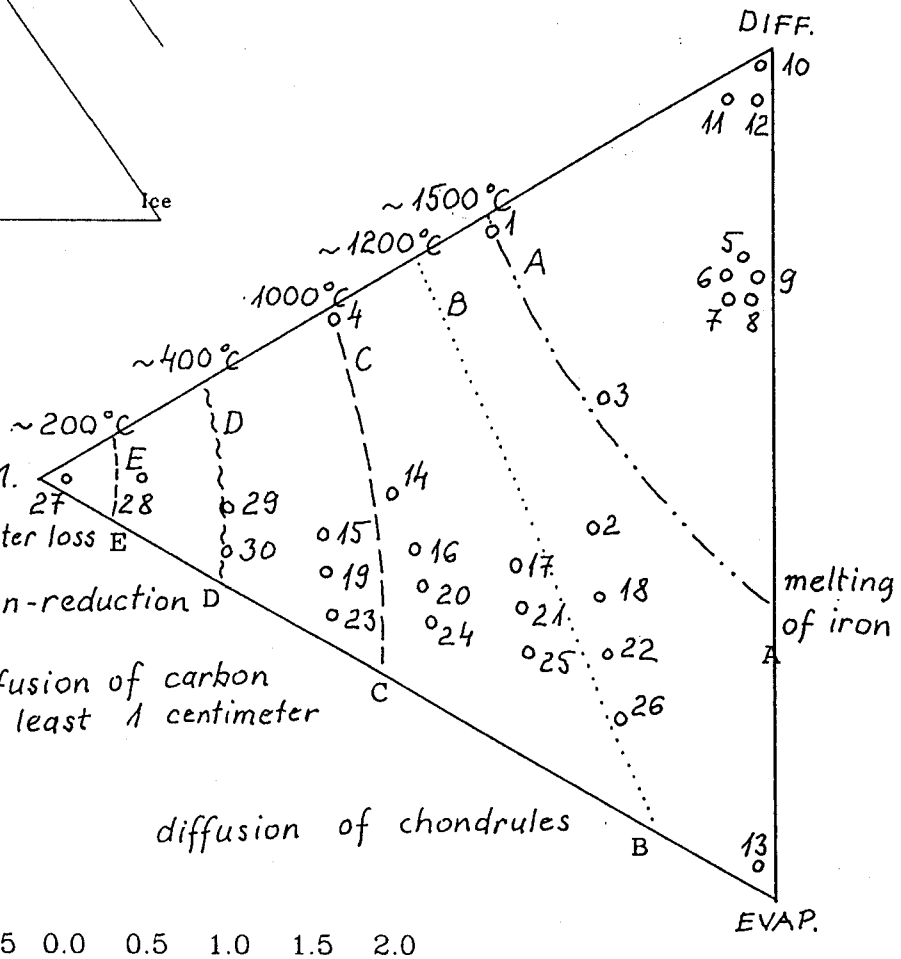


Fig.b. Arrangement of the NIPR Meteorite Collection's samples in a triangle field spanned by thermal effects. The tentative isotherms were estimated on the basis of our model calculations shown on Fig.c. The A, B, C, D, and E lines correspond to the appropriate isotherms in the r-R region of Fig.c.

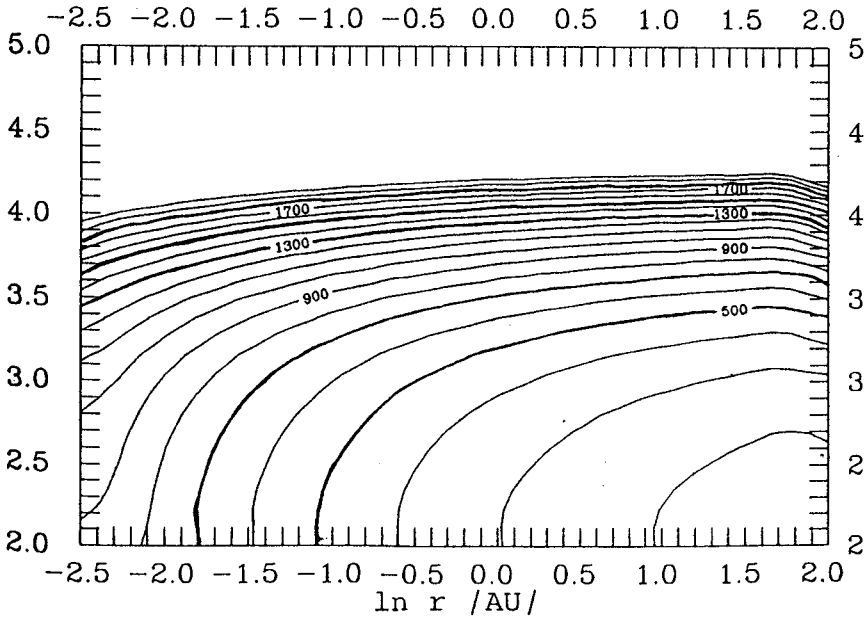


A-1800 K
B-1500 K
C-1300 K
D- 700 K
E- 500 K

Fig.c. Model temperatures /in K/ in the r /solar dist./ and R /body radius/ thermal history field of 1 million yrs. /A, B, C, D, and E correspond to Fig.b. appropriate lines./

# A COMPARISON AMONG CHONDRITE COMPOSITIONS

Sz. Bérczi[1] & B. Lukács[2]

[1] Dean's Office, R. Eötvös University, H-1088 Rákóczi út 5., Budapest, Hungary
[2] Central Research Institute for Physics RMKI, H-1525 Bp. 114. Pf. 49., Budapest, Hungary

**ABSTRACT**

Although chondritic meteorites (without global differentiation) show a large variety in chemistry, structure, &c., not all logical possibilities appear. This suggests the possibility of genetic connections. We concentrate on the dependence of carbon content on petrologic class.

## 1. INTRODUCTION

The Antarctic meteorite collecting project is a great possibility to get a true cross section and statistics about the material composition of the (outer) solar system, because i) survival chances of fragile meteorites are somewhat better than in other terrestrial localities; ii) any stony object is equally conspicious on an ice field. However even before this project it was known that not all logically possible classes are equally abundant; what is more, some classes are absent. This suggests genetic relations among some classes.

In this paper we use a kind of the van Schmus-Wood (1967) classification of chondrites; it is remarkably transparent, using a letter and a number. (For the different C types, see Otting & Zähringer (1967).) The letters refer chemical composition: E (enstatite), H (bronzite), L (hypersthene), LL (amphoterite) and C (carbonaceous), while the number shows the status of chondrules (correlated with carbon and water content): 1 (absent), 2 (sharp) to 6 (very obscure). Now, statistics of falls show moderate correlation between the letter and the number. The composite Figure of this paper contains a graph based on the statistics of Wasson (1974). The diagonal structure of the graph is obvious: e.g. no high numbers are seen for C and no low ones for E.

Long ago Mason (1962) suggested an evolutionary path, starting with C1. Then, with higher and higher heat effects first serpentine loses water (this process is perceptible at 400 C°), and some olivine chondrules crystallize, then the groundmass serpentine decomposes into olivine and pyroxene, finally C starts to reduce the iron oxide in olivine. The scheme is

$$MgFe_2Si_4O_{10}(OH)_8 + 2C + \text{heat} \rightarrow 2(Mg,Fe)_2SiO_4 + 2(Mg,Fe)SiO_3 + 4H_2O$$
$$+ 2C \rightarrow 4MgSiO_3 + 2(Mg,Fe)SiO_3 + 2Fe + 4H_2O + 2CO_2$$

where water and $CO_2$ evaporate. In addition, C as volatile can be lost by diffusion.

One of such schemes may be proven true in the future; indeed it seems as if asteroid 3-filter colors were to suggest an evolution from something exotic in meteorites towards olivine and/or serpentine (Bérczi, Holba, & Lukács 1995). However now we want to use minimal theory. Still, no doubt, C can reduce FeO even well below melting point, and C can be lost by diffusion.

## 2. MODEL EQUATIONS

The above scheme can be represented by 3 toy equations. We consider FeO (mole concentration x), C (y) and Fe (z); the $SiO_2$ content is taken constant. Then in first approximation

$$dx/dt \approx -2A(T)xy \quad (1)$$
$$dy/dt \approx -A(T)xy - R^{-1}B(T)y \quad (2)$$
$$dz/dt \approx -dx/dt \quad (3)$$

The 1/R term takes into account that C loss is through the surface. The temperature-dependent factors have the structure

$$A(T) \approx A_o\exp(-Q_A/T);\ B(T) \approx B_o\exp(-Q_B/T) \quad (4)$$

Early higher temperatures were maintained by the short-living radioisotopes, of which $Al^{26}$ has a half-life 700000 y. The temperature dependence is serious, so in first approximation one can solve the equations until $t=t_c$, somewhere in the order of a million years, and then stop.

The solutions have the form

$$y_f = y_i - x_i + x_f + (B/2AR)\ln(x_f/x_i) \quad (4)$$
$$z_f = z_i + x_i - x_f \quad (5)$$

and $x_f$ is the solution of the implicit equation

$$2At_c = \int_{x_f}^{x_i} w^{-1}(y_i - x_i + w + (B/2AR)\ln(w/x_i))^{-1}dw \quad (6)$$

Therefore the final concentrations depend on the initial ones, on the radius, and on the temperature (which again depends on radius if the heating is internal). Reduction and C loss together goes up with temperature, but C loss is more sensitive on R than reduction.

We will not use explicite solutions. A(T) is fairly calculable from iron productive technics below melting point (mainly belonging to ancient ages, however cf. the Höganäs method), but for free iron oxides, not for silicates; and C diffusion coefficient B(T) is well known in iron (where it is remarkably high, see Kittel (1961)), but not in all meteoritic matrices. However note that during heat impact diffusion goes on too, and for order of magnitude the final diffusion length $a_f$ will be

$$a_f \sim (D(T)t_c)^{\frac{1}{2}};\ D(T) \approx D_o\exp(-Q_D/T) \quad (7)$$

So, with chondrules of radius $a_o$ the petrologic class is 2 if $a_f << a_o$, and 6 if $a_f \geq a_o$. Being $t_c$ fixed, the ratio depends on T, and if A(T), B(T) and D(T) are known, by inverting the formulae A and B will depend on $a_f/a_o$. So concentrations must (more or less) depend on the petrologic class and size.

## 3. OBSERVATIONAL DATA

Let us concentrate first on C content. We used a graph of Otting & Zähringer (1967) giving C content in some chondrites differing both in letter and petrologic class. Since in first approximation C loss is exponential, the vertical axis is logarithmic, and we fitted exponentials in petrologic class number for individual letters. That is the second part of our composite Figure.

E2, H2, L2 and LL2 chondrites are unknown, but they may be visualized as startpoint of chondrule unsharpening with diffusion. The curves extrapolate back there or to an even more hypothetic 1 state. Anyway, the E and H lines are clearly parallel, although mean deviation is substantial for H. The slope is smallest for E and H, then come LL, L and C. It is tempting to conclude that this was the size sequence from upward down for the parent bodies.

The C line meets the E one at 3, and that is the lowest petrological class for E. This fact does not prove the C origin of E-s, but is compatible with such an idea. The original lower C content of H-s is surprising; we do not suggest any reason just

now; an analogy is the difference in x+z between (E,H,C) and (L,LL). The composite Figure contains some remarks. None of them is full-proof at this status of art; however all have some fair probabilities.

**4. OUTLOOK**

Obviously, if all thermodynamical data of a meteorite material are known, the initial compositions can be calculated back in the function of an assumed R; and one can get a rough guess for R by taking $z_i \approx 0$. For a more quantitative analysis, however, individual 3-variable data $\mathbf{x}_\alpha=(x_\alpha,y_\alpha,z_\alpha)$ are needed. In the present moment we mention only one problem suggested by the extrapolation curves.

C5 and C6 chondrites are not known. This is compatible with the idea that E-s (and maybe other types) originate from C-s in thermal evolution. However Otting and Zähringer reported a few C4 and even one E3. Then it is not impossible to follow the C line beyond 4 (if an uncertain idea is needed, by solar heating of small bodies). But then these C5 and C6 chondrites would be characterised by extremely *low* C content, not for high. We do not know of such chondrites, but one cannot too much expect to classify something as C for being free of C.

*Some* achondrites may fit into this scheme. Most so called achondrites have been subjects of iron loss by melting and gravitational segregation; but Mason (1962) reports 3 E "chondrites", Blithfield, Hvittis and Pillistfer) without chondrules. Now, this does not seem to be an anomaly. Extrapolating the diffusion process one may reach $a_f$ values beyond 6. The only question, answerable when the diffusion coefficients in enstatite will be completely known, is if T<1800 K (cca. the melting point of iron) is enough for this or not. The same is true for H, L and LL, for which *undifferentiated* achondrites are not reported at all.

**ACKNOWLEDGEMENT**

Partly supported by OTKA T/014958. and MEC-94-1613 OMFB Founds.

**REFERENCES**

Bérczi Sz., Holba Agnes, & Lukács B. 1995: KFKI-1995-10
Kittel Ch. 1961: Introduction to Solid State Physics. J. Wiley, New York
Mason B. 1962: Meteorites. J. Wiley & Sons, New York
Otting W. & Zähringer J. 1967: Geoch. Cosmoch. Acta **31**, 1949
van Schmus W. R. & Wood J. A. 1967: Geoch. Cosmoch. Acta **31**, 747
Wasson J. T. 1974: Meteorites. Springer, Berlin

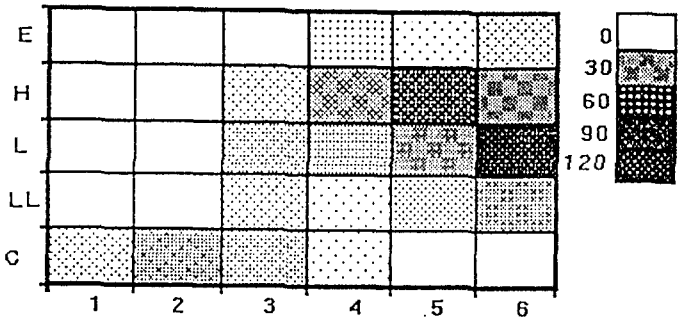


Fig.a. /left/. Frequency of different chondrite types, given here by color grades./Wasson, 1974/
Fig.b. /centre/. Fitting lines for different chondritic types, for their carbon content. The carbon data from Otting and Zähringer /1967/, (the classification of Van Schmus and Wood /1967/) gives ordinata to these grades, which are metamorphic grades, the frequencies of the appropriate types were also given to show bulk iron content as E, H, L, LL, and C chondrite types.

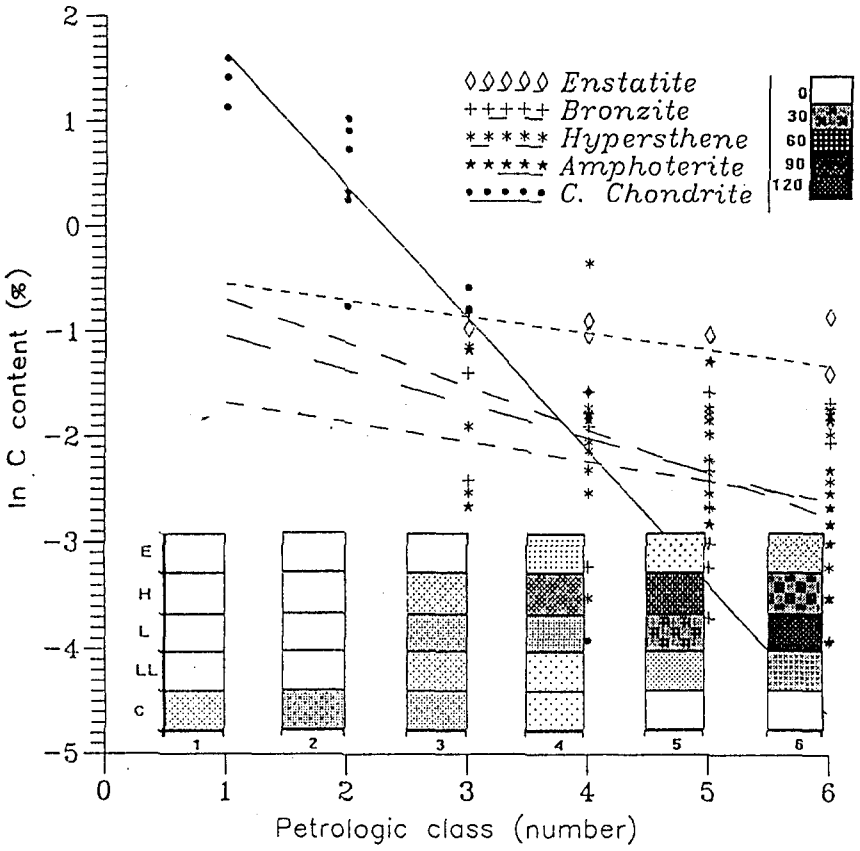


According to Solar Distance

C - far away from the Sun,, they were a number of small bodies or pieces,

E - nearer to the Sun, than C-meteorites; as compared to H and LL they were almost in the same zone, H-meteorites had less carbon then here at E-body

H - less starting carbon, than in E, but they were almost in the same distance from the Sun,

LL - in the same zone as E and H, between them; if a layer in a larger body, they were a deeper layer, than L meteorite layer

L - If many small bodies, then nearer to the Sun, than E,& LL; if in a larger body, they composed the outermost layer.

According to Chondritic types

C - they could be small pieces, so their carbon content quickly evaporated, if they had received any heat; they could come from far

E - they all come from a large body, this large body could transform in its innermost layers to aubritic composition;

H - they mainly come from a large body, as average, but some smaller bodies were also with this composition because of the spreading in carbon content;

L - they are coming from an iron poorer region, and from smaller bodies, as average, but some larger bodies of them were also existing;

LL - they are coming from also an iron poorer region, and also from mainly middle sized bodies with some larger bodies, too.

According to petrologic class

2 - only from small bodies, because no transforming heat effect on them, so they PRESERVE ORIGINAL COMPOSITION

3 - small or middle sized body, which could get a moderate heat effect, therefore it contains some amount of product of reduction; if it were a large body, it could have gone to 6th class;

4 - middle sized body, with moderate transforming heat effect, if small bodies were, they did not go nearer to the Sun;

5,6 - different cases:
LARGE BODY:
it had high heating source inside, therefore the chondrules disappeared, the reduction yielded a large amount of iron, and some carbon also could have remained in it /E,H/;
MIDDLE SIZED BODY:
its carbon did reduction, and some have been evaporated, too, so some FeO remained in it /L/;
SMALL BODY:
it could go nearer to the Sun and it could have less amount of carbon, or carbon had evaporated quickly from it, so no important reduction could happen, more FeO remained /LL/ or C5, C6 could be such type.

# ATTEMPT TO CONJECTURE THE PATTERN OF ALIEN PLANETARY SYSTEMS

Sz. Bérczi[1] & B. Lukács[2]

[1] R. Eötvös University, Dean's Office and Astronomy Dept., H-1088 Rákóczi út 5., Budapest, Hungary
[2] Central Research Institute for Physics RMKI, H-1525 Bp. 114. Pf. 49., Budapest, Hungary

**ABSTRACT**

Meteorites may come from outside of the Solar System; for comets this possibility is often discussed and some orbits suggest this, although with serious uncertainty. If the luminosity of the central body differs from the solar one, or if the chemical abundance of elements is different from that of the solar composition, the condensed bodies will seriously differ from those of our own system. Such systems could have been developed during the condensation of stars of the early Milky Way (I. population stars) with small metal content in elementary abundance, or might have been formed around massive stars with extremal luminosity, and ages may be diverse too.

## 1. INTRODUCTION

Not necessarily all meteorites formed in the Solar System. Many comets come with hyperbolic velocities; this may be a measurement error, but, if the Oort cloud exists, it is sufficiently far from Sun for perturbations by neighbouring stars. These perturbations may send the body into the system but may pull out too. Since, mutatis mutandis, the same is true for neighbouring stars, some small bodies of the Solar System may have started around other stars, and vice versa. Then it is advisable to guess something about condensation in other systems. Of course, extrasolar meteorites are probably exotic rarities.

From the distance of the neighbouring stars a body of usual planetary velocity (~10 km/) travels cca. a million years hither. Since Sun is moving with the same velocity among the local centre of mass, the parent system of the extrasolar meteorite may be well out of sight now, so the parent star may be anything for spectral class and almost anything for age.

## 2. ABOUT ALIEN STELLAR SYSTEMS

We try to give a rough outlook about the general features of planetary systems around stars of Milky Way. Evidences are very scarce but existent. Compositional belts around stars depend on luminosity of the star. If the luminosity of star differs, the planetary system will differ too from our own.

Recently the most accepted class of theories postulate the common origin of star and planets from a galactic nebula via contraction, heating up, differentiation, and finally fusion in the core, crystallization on the periphery. Then change the initial conditions in such a way that the resulting star be something prescribed; and then the planetary system will be automatically obtained. Equilibrium condensation models of the Solar System [1-3] have deduced compositional belts with characteristical mineralogy around the forming Sun. The sequence of belts could be calculated from the intersection of the main gas/crystal phase boundaries by the Cameron-type solar adiabat. Let us try to apply

this scheme on the parent nebulae of other stars. The details are available in [4]. We operate in the following steps:

1) Angular momentum seems too small for stars after A3. The difference from trend is known and may go into planets.

2) Start with a nebula of prescribed mass and average abundances.

3) In Solar System planets seem to have chemical compositions consistent with double temperatures at condensation than now in the specific orbits [3].

4) This means 16-fold protoluminosity, which seems to have happened bw. 4000 and 27000 ys from contraction [5].

5) Take calculated luminosities of protostars at 27000 y.

6) Then temperatures vs. distances are known.

7) Asteroids are expected at the condensation distance of the very fragile hydrated silicate-ice mixtures. Incidentally there also ammoniated silicates can be expected (cf. [6]).

8) The biggest planet is expected at the condensation distance of abundant water ice.

9) Then the available angular momentum sets the mass of the biggest planet(s).

For the details and formulae see Ref. 4. The scheme is shown on the combined Figure. The data are moderately reasonable for the Solar System.

## 3. SPECIALITIES OF AN EXTRASOLAR METEORITE

Although it seems that alien planetary systems are similar to ours except for some scaling, the quantitative data would reveal the alien origin of an extrasolar meteorite. First let us see the ages.

If a meteorite is extrasolar, then

1) its lead isotope age is *not* $4.5*10^9$ y;

2) its cosmic ray age may be anything above $10^6$ y;

3) its terrestrial age may be anything.

Of course, basaltic Solar System meteorites are younger than 4.5 Gy in Vesta or Mars. Ages of chondrites must be cca. the age of the system, and it is indeed so [7].

Now consider an age *greater* than 4.5 Gy. That means that the meteorite has come from a system older than Sun. It is quite possible if the mother star is not brighter than, say, F5. Sun's total age will be 10 Gy. But then at the formation the Galaxy was poorer in heavy elements, possibly even of iron. Therefore then chondrites would be abnormally poor in Fe. To be sure, we do *not* suggest hypersthenes and amphoterites to be extrasolar; they are too numerous for that.

A chondrite with lead age well *below* 4.5 Gy age would be again conspicious to be extrasolar. If so then it may have come from light or massive stars, either. In both cases its Fe content is expected higher than normal, in some proportionality with the age between the formation of the Galaxy and that of the parent system. However our guess is that this is a minor effect. Meteorites from a red dwarf would be richer in volatiles than expected from their overall structure. Namely, condensation age/stationary luminosity ratio is higher for red dwarfs than for G ones [4,5]. So later stellar radiation affects generally less the condensed matter than in the Solar System.

Just the contrary for massive stars. Above cca. 3 solar mass the temperature difference between condensation and latter stationary state is moderate, from 5 solar mass it is negligible. So

condensed bodies of such stars must be continuosly evaporating and therefore strongly being depleted in volatiles, except if expelled to the periphery of the system as conjectured for our meteorites.

## 4. DISCUSSION

We listed some distinctive properties of meteorites coming from outside of the Solar System. As far as we know no such meteorites have been found up to now. Lead isotope ages significantly above 4.6 Gy were not found, and all stones significantly younger than that are basaltic, in which case the age is that of a planetary volcanism as e.g. for shergottites. However anomalous meteorites may turn up in the future.

## ACKNOWLEGDEMENTS

Partly supported by MEC-94-1613.

## REFERENCES

[1] Larimer J. W. 1967: Geochim. Cosmochim. Acta **31**, 1215
[2] Grossmann L. 1972: Geochim. Cosmochim. Acta **36**, 597
[3] Barshay S. S. & Lewis J. S. 1975: In: The Dusty Universe, eds. Field G. B. & Cameron A. G. W., Neale Watson Acad. Publ., New York
[4] Bérczi Sz. & Lukács B., Evolution of Extraterrestrial Materials and Structures, eds. B. Lukács & al., KFKI-1994-22, p. 6.
[5] Novotny, Eva 1973: Introduction to Stellar Atmospheres and Interiors, Oxford Univ. Press New York, and citations therein
[6] King, T.V.V. & al. 1993 (Abstract). Lunar and Planet. Sci. Conf. **XXII**, 717-718.
[7] Mason, B. 1962: Meteorites. J. Wiley & Sons, New York & London

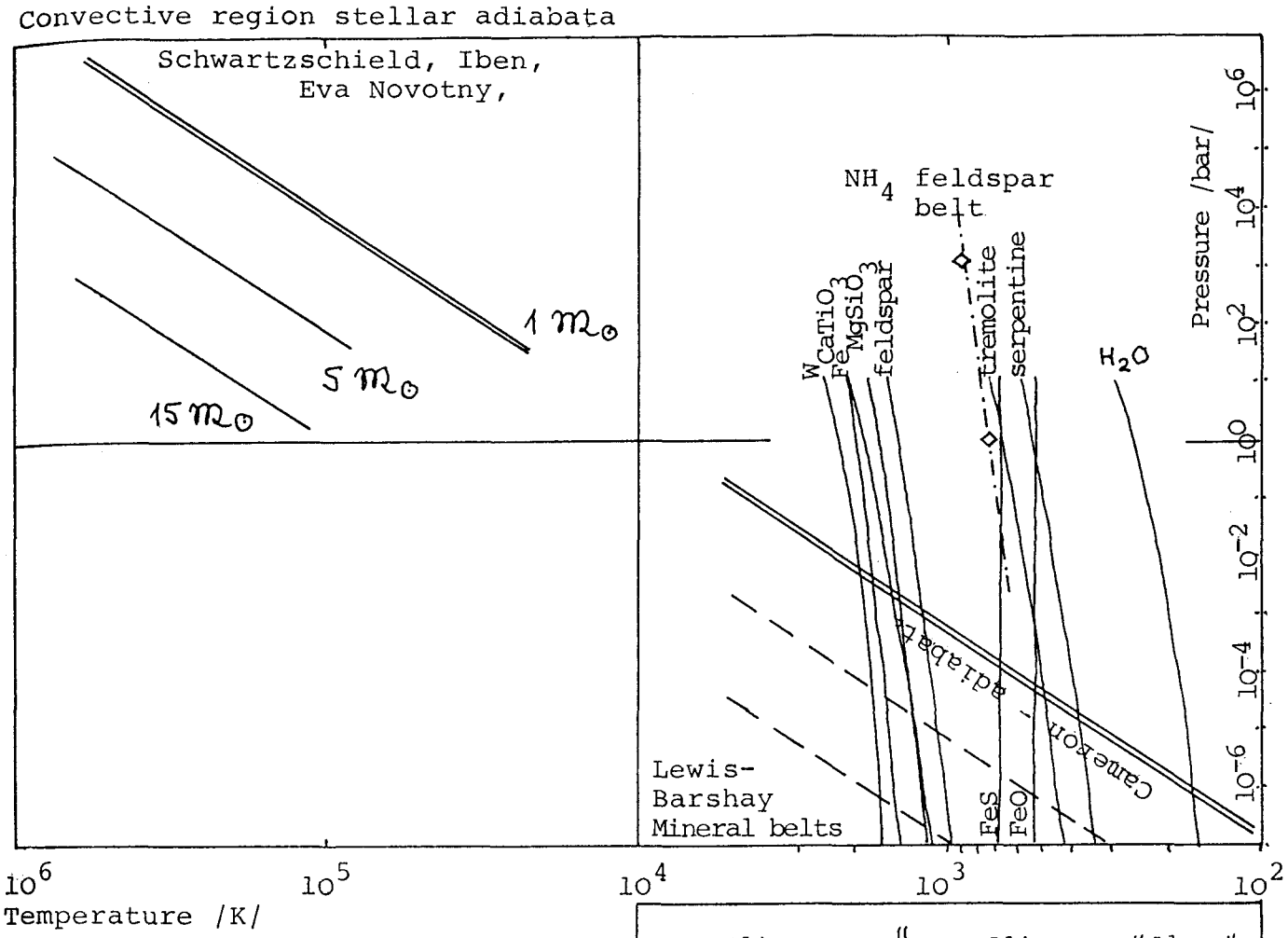


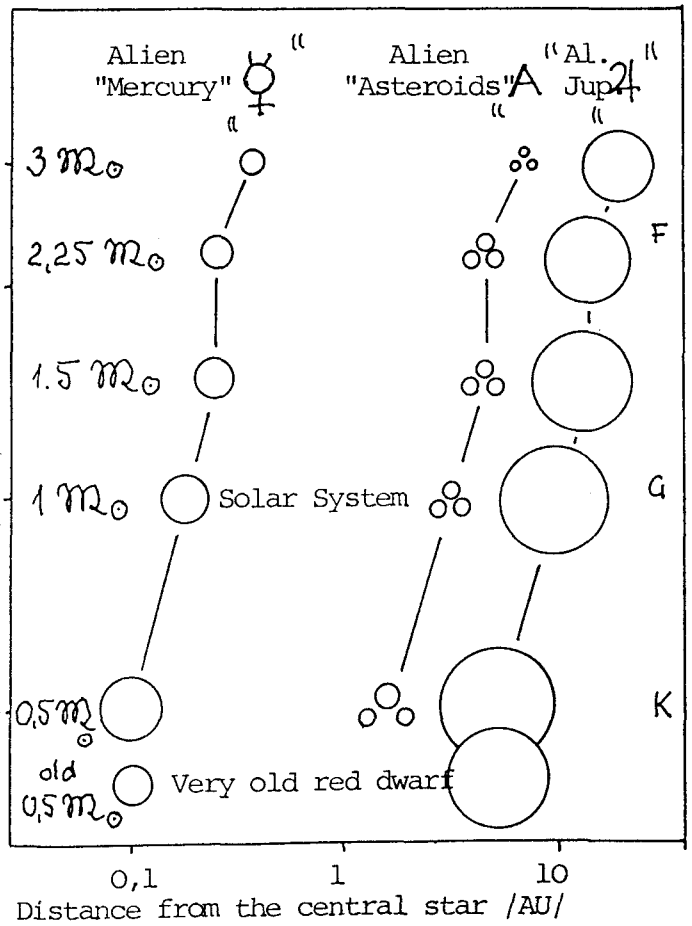


Fig.1. Unification of two different model for calculations of alien planetary systems. Stellar evolutionary models study the inner structure of stars, of which the outer convective region continuously goes into the stellar nebula during the early period of stellar formation. The characteristical function, which connects stellar gas with the surrounding nebula, is the Cameron-type adiabat /for the early Sun/. Solar System condensation models used this adiabat to deduce the sequence of mineral belts around the Sun. Convective outer regions of stars with different other stellar masses can show the position of such adiabat in the p-T diagram. The parallel position of the mineral solid/gas phase boundaries in the p-T diagram, however, will give almost the similar condensational sequence for other type stars, too. But the distance of the mineral belts from the star will be different for stars with different mass. To the Lewis-Barshay mineral belts here we added the $NH_4$-feldspar tentative boundary. "Ammonia-silicates" could contribute to the volatile components of the forming "stone-belt" planets. /Bérczi, Lukács, 1994./

# POSSIBLE METEORITES WITH "HUMAN-TRANSFORMATION": ROYAL SWORDS AND SABRES

Sz. Bérczi and B. Lukács
Eötvös University and Centr. Research Inst. for Physics
RMKI, Hung.Acad.Sci. Budapest
Hungary

Iron age is a historical definition of a period, when communities began use iron instruments, mainly as arms. This period is the first thousand years B.C. but earlier and later occurrence of non-industrial iron/steel/ relics can be found in archaeological literature. Both mythic descriptions and the Ni content of cosmic origin could witness the meteoritic nature of such archaeological finds. Here we offer a program to investigate ancient royal swords and sabres, because of the focused attention of ancient peoples to extraterrestrial events, the results collected for kings and princeps. Royal arms could survive thousands of years human destructions, too. Our exhibition shows possible candidates to such search for royal sabres and swords from famous ancient cultures, which not only used, but considered these objects with cultic, mythic forces, and therefore decorated them. So in our exhibition the ancient possible meteorites with "human-transformation" are shown by their ornamental decoration. But we know, that this transformation of the form, which made usable instruments from the iron/steel/ material, did not transformed their chemical composition. So parallel with this meteoritic search program, a comparison of ancient ornamental art forms can be seen, which hopes to celebrate the 20th Symposium on Antarctic Meteorites, NIPR, Tokyo, Japan.

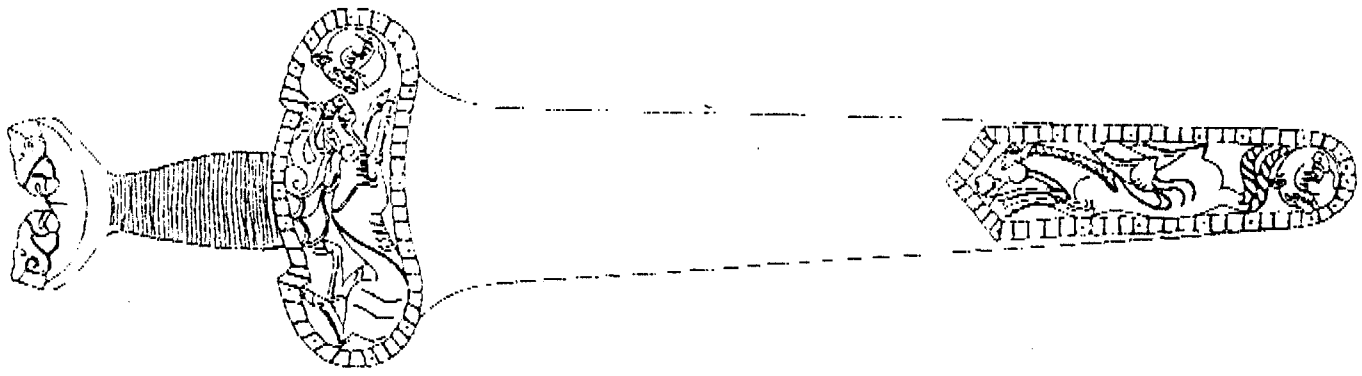

# WHY DO WE NOT SEE NITRIFEROUS METEORITES?

Sz. Bérczi[1] & B. Lukács[2]

[1] Dean's Office, R. Eötvös University, H-1088 Rákóczi út 5, Budapest, Hungary
[2] Central Research Institute for Physics RMKI, H-1525 Bp. 114. Pf. 49., Budapest, Hungary

**ABSTRACT**

Nitriferous meteorites are unknown, although would be expected from the condensation scheme of the System, and ammonium or ammoniated silicates (reported from Ceres) would be needed for explanaining the nitrogen atmospheres and proto-biochemistry.

## 1. INTRODUCTION

The present atmosphere of Earth is not the original, as shown by the free oxygen. The palaeoatmosphere is a matter of speculation. Miller (1953) produced amino acids in an atmosphere with $H_2O$, $CO_2$, $NH_3$ and $H_2$. But $NH_3$ seems to belong to the outer Solar System, and so its original presence is questioned. Indeed Szalay (1975) extracted $H_2$, $H_2O$, $N_2$, $CO_2$ and $CH_4$ from precambrian sediments, but not $NH_3$. Brooks & Shaw (1973) emphasizes that no geologic traces of the "primordial bouillon" have been found. They should be found as carbon layers with high nitrogen abundance; the earliest layers seem poor in nitrogen, the amino acid concentration of such sediments seem to be not higher than $10^{-9}$ (Schöpf, Kwenvolden & Barghoorn, 1968) even in the Fig Tree layer with the oldest fossil microorganisms (3.7-3.0 Gy old).

According to the Barshay-Lewis model (1975) ammonia could have condensated outwards from Saturn. Outgassing from the bulk of Earth may have seriously contributed to the palaeoatmosphere, but the present Earth litosphere seems very poor in ammonia.

Ammoniates (crystals with structural ammonia) may help, if they contributed to primordial Earth, and then lost the ammonia in planetary heating up. Unfortunately the present knowledge about silicates with structural ammonia is next to nothing so they are not included into condensation calculations.

If this is ruled out but there will be evidence for the atmospheric presence of ammonia in the far past, then a possible source would be extraterrestrial, a collision with an ammonia-rich planetesimal during the formation of Earth. A planetesimal of cca. radius of 1000 km from beyond Uranus could have filled up the terrestrial palaeoatmosphere to 1 atm partial pressure.

## 2. AMMONIA AS WATER-ANALOGON

Here we compare the main properties of $H_2O$ and $NH_3$ *as solvents* (cf. e.g. Römpp 1958). They differ only qualitatively.

| Property | Water | Ammonia |
|---|---|---|
| Freezing p. K | 273 | 195 |
| Boiling p., K | 373 | 240 |
| Crit. temperature, K | 647 | 405 |
| Crit. pressure, atm | 218 | 112 |
| Density (liq.), g/cm$^3$ | 1 | 0.65 |
| Dipole moment | 1.85 | 1.47 |
| Dielectric constant | 81 | 22 |
| Spec. heat (l) | 1 | 1.1 |
| Melting heat, cal/g | 80 | 84 |
| Evapor. heat, cal/g | 541 | 327 |

As for solvent of salts, NaCl definitely dissolves worse in $NH_3$ than in $H_2O$ (most chlorides too); the numbers are 2.1 g vs 36 in 100 g solvent. For bromides the solubility is more comparable. Ammonia practically cannot solve chlorides of earths; but can solve some metals in relevant quantities, while water cannot.

Ammonia is nearly as polar as water, so in general solves salts almost as well as water, although differences may be large for individual salts; and ammonia in general is the better solvent of organic compounds. The dielectric constants are comparable and high, although the difference is substantial.

## 3. THE BELTS OF THE SOLAR SYSTEM

Condensation models of the Solar Nebula have deduced the type and sequence of mineral belts which has been formed around the early Sun. (Barshay & Lewis, 1975, Grossman & Larimer, 1974, Grossman, 1972) The sequence of processes seems as

| | |
|---|---|
| ca. 500 K | Formation of **TREMOLITE** (from Ca,Al,Mg,Silicates with $H_2O$) |
| ca. 400 K | Formation of **SERPENTINE** (from Mg(Fe)Silicates with $H_2O$) |
| ca. 170 K | Condensation of **WATER-ICE** (Which exhaust all $H_2O$ gas) |
| ca. 110 K | Formation of **$NH_3.H_2O$ AMMONIA-CLATHRATE** (exhausts all $NH_3$) |
| ca. 60 K | Formation of **$CH_4.8H_2O$ METHANE-CLATHRATE** (exhausts all solid $H_2O$) |

Observe that crystals with structural water are included but those with structural ammonia are not; such crystals are known, e.g. $CaCl_2$ can take up 8 molecule ammonia into its lattice.

Then the most abundant volatile, the $H_2O$ first appears as a component added to the higher temperature condensates to transform (metamorphose) them: forming hydrous silicates of tremolite and serpentine.

There is a wide gap in temperature between these hydrous silicates condensation and ice-condensation. In this region carbonaceous compounds condensate according to the Ryoichy Hayatsu - Anders model (1981).

Tremolite and serpentine are hydrated silicates. If a planet is formed of them, then its body will contain a substantial amount of water. With the heating up of the matter $H_2O$ may go into the atmosphere and this may have happened on Earth.

In the protosolar nebula the temperatures differed from the present. One reason is the different protosolar luminosity. The condensation temperatures are shown by the compositions of the planets (Barshay & Lewis, 1975). The proto-temperatures seem to have been roughly the doubles of the present equilibrium temperatures. Then Earth was just at the inner boundary of the hydrated silicate belt, with a small amount of primordial bulk water. Mars was well inside of the hydrated silicate belt, the bodies of the asteroid belt must have originated with mixtures of $H_2O$ ice and hydrated stones (a fact suggesting internal fragility), and $H_2O$ ice is a main component in the Galilean moons of Jupiter. Outwards from Jupiter ammonia gradually takes over. Unfortunately the papers contributing to the Table did not include stony components with structural ammonia, which may exist, but of course cannot be expected in natural terrestrial environment, where ammonia does not have a chance to replace the dominant water. Still, silicates do exist in which some alkalies are substituted

by ammonium ion, e.g. buddingtonite (Erd & al., 1964). So behind the orbit of Mars the Table cannot be complete in the present state of knowledge. Obviously rough guesses should be done until the ammoniate analogons of hydrated silicates will be known better. We included the best known ammonium silicate, buddingtonite, into the condensation scheme, see the Figure. For the details see Bérczi & Lukács (1994a). Ammoniated silicates are practically unknown. King & al. (1993) reported some ammonium-altered silicate from Ceres.

## 4. RESULTS AND DISCUSSIONS

Now an interesting problem arises. Nitrogen is practically absent in meteorites, except for the organic matter and rare water-soluble (non-silicous) compounds in carbonaceous chondrites (Mason, 1962). In some bronzite and hypersthene chondrites nitrogen was so rare as vanadium or zinc (Mason, 1962). Where are the ammonium and ammoniated silicates which would fit into the condensation scheme and which were reported from Ceres (King & al., 1993)? And if they do not exist, whence has come the terrestrial nitrogen?

It is possible that thermal evolution of chondrites expel the ammonia from such silicates; their decay temperature is not too higher than that of the water loss of serpentine. However up to now no such silicates have been reported even from carbonaceous chondrites. Either we grossly misunderstand something about the Solar System nitrogen, or at least a group of meteorites must contain ammonium or ammoniated silicates.

Finally we note that amino acids are more natural in ammonia than in aquaeous environment, and the peptide link is a direct product of neutralisation processes in ammonia chemistry (Bérczi & Lukács 1994b). Therefore complicated organic matter (in C chondrites) would be compatible with ammonia-altered silicates.

## ACKNOWLEDGEMENTS

Partly supported by MEC-94-1613.

## REFERENCES

Barshay S. S. & Lewis J. S. 1975: Chemistry of Solar Material. In: The Dusty Universe, eds. Field G. B. & Cameron A. G. W., Neale Watson Acad. Publ.

Bérczi Sz. & Lukács B. 1994a: KFKI-1994-22 p. 6

Bérczi Sz. & Lukács B. 1994b: KFKI-1994-22 p. 117

Brooks J., & Shaw G. 1973: Origin and Development of Living Systems. Academic Press, London

Erd R. C. & al. 1964: Amer. Mineral **49**, 831

Grossman L. 1972: Geochim. Cosmochim. Acta **36**, 597

Grossman L. & Larimer J. W. 1974: Rev. Geophys. & Space Phys. **12**, 71

King T. V. V. & al. 1993: Lunar and Planetary Science Conf. **XXII**, 717

Mason, B. 1962: Meteorites. J. Wiley & Sons, New York & London

Miller, S. L., 1953: Science **117**, 528

Römpp H. 1958: Chemielexikon. Franckh'sche Verlagshandlung, Stuttgart

Ryoichy H. & Anders E. 1981: Topics in Current Chemistry **99**, 1

Schöpf, J. P., Kwenvolden, K. A. and Barghoorn, E. S., (1968): Proc. Natl. Acad. Sci. USA **59**, 639

Szalay, S. 1975: Fiz. Szemle 1975/12 (in Hungarian)

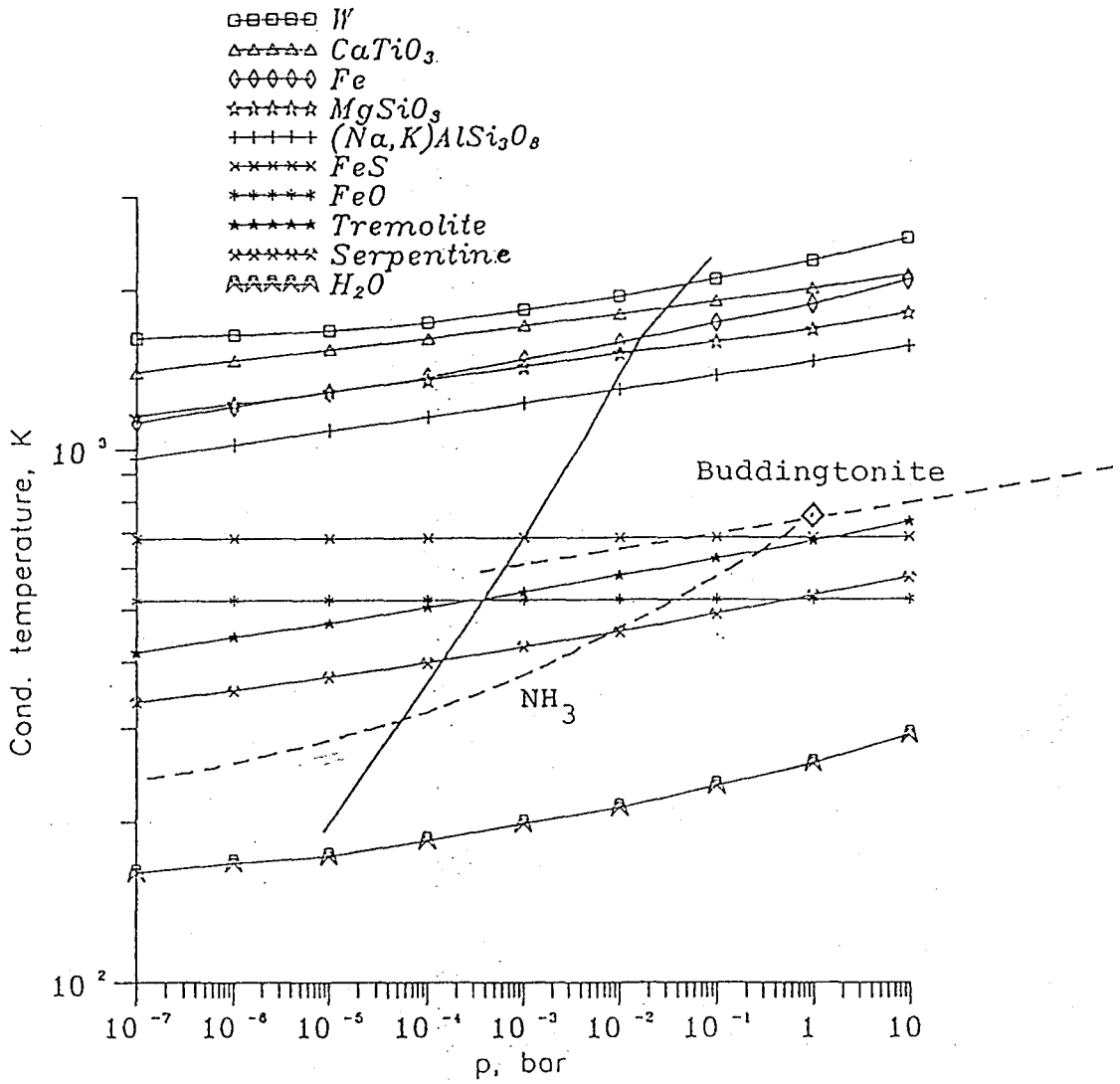


Fig.1.
Sequence of minerals for Solar System

# MINERALOGICAL COMPARISON OF LEW88774 WITH OTHER UREILITES

J. Chikami, T. Mikouchi, M. Miyamoto and H. Takeda

Mineralogical Institute, Graduate School of Science, University of Tokyo, Hongo, Tokyo 113

## INTRODUCTION

Ureilites originally consist of coarse-grained olivine and exsolution-free pyroxene set in a carbonaceous matrix, but preserve O-isotopic anomaly and high noble gas contents known for chondrites. Three major models have been proposed for origin of ureilites, but we have not reached general understanding how the ureilites parent body was formed [1,2,3].

In this study we performed mineralogical investigations for LEW88774,4 and ALH82106,10, which contain pyroxenes with exsolution lamellae of augite. The diffusion profiles of Ca of the exsolved augites will provide us useful information on the cooling history of ureilites.

LEW88774 is a Cr-rich ureilite which is quite different from other ureilites with regard to its mineralogy. For example, LEW88774 includes coarse exsolution lamellae in pyroxene and abundant Cr-rich spinel which has not been found in other ureilites. Satterwhile et al. [4] indicated that it requires slow cooling to form such coarse exsolution lamellae, and Prinz et al.[5] also proposed that it would require extremely slow cooling (millions of years). Warren and Kallemeyn[6] preferred a model of original crystallization deep in the mantle of the ureilite parent body.

ALH82106 is an augite-bearing ureilite [7] which belongs to the high-$^{16}O$ sub group [8]. Augites have been found to coexist with low-Ca pyroxene. The pyroxene in ALH82106 is mostly orthopyroxene (opx), but the crystals exhibit complex textures [7]. No planar exsolution lamellae were observed in pigeonite and the augite inclusions in pigeonite show complex wavy textures [9]. Takeda et al. [10] estimated that the temperature of crystallization was around 1250 °C from coexisting two pyroxenes, using the pyroxene geothermometer of Lindsley and Anderson [11].

Because these two meteorites have exsolution lamellae in pyroxne, their detailed mineralogical comparisons give us better understanding on their formation processes in common. We paid special attention to diffusion profile of exsolved pyroxenes in LEW88774 and ALH82106 and estimated thier cooling rates by the method developed by Miyamoto [12].

## SAMPLE AND EXPERIMENTAL TECHNIQUES

Polished thin sections (PTS) of Lewis Cliff (LEW)88774,4 and Allan Hills (ALH) 82106,10 supplied from the Meteorite Working Group ( NASA/Johnson Space Center ) were examined by an optical microscope, a scanning electron microscope (SEM) (JXA-840A) at the Mineralogical Institute, Univ. of Tokyo and electron probe microanalyzers (JEOL EPMA JCXA-733 at the Ocean Research Institute , Univ. of Tokyo and JEOL EPMA JCXA-733mk II at the Geological Institute, Univ. of Tokyo).

## RESULTS

### *LEW88774*

LEW88774 is composed mainly of pyroxene, olivine, Cr-spinel and several carbon polymorphs. Their rough modal abundances are pyroxene 78 vol. %, olivine 12 vol. %, Cr-spinel 6 vol. %, and other phases 4 vol. %. Our microprobe analysis gave high CaO bulk composition of pyroxene in LEW88774. 100×Ca/(Ca+Mg+Fe) mol% is estimated to be 15-20. Each lamella of the exsolved augite and the low-Ca pyroxene has almost the same width about 50μm and their boundaries are irregular (Fig.1-a). The exsolved augite has composition of $Ca_{33.7}Mg_{2.8}Fe_{13.5}$ and exsolved pigeonite of $Ca_{4.4}Mg_{75}Fe_{20.6}$. Ca diffusion profile intersecting perpendicular to a lamella shows uniform chemical compositions for both augite and low-Ca pyroxene (Fig.2-a). This fact suggests that pyroxene was cooled slowly enough to homogenize the chemical composition of both phases down to 1169°C.

According to the calculation of the cooling rate by a method similar to the developed by Miyamoto [12], we estimated that exsolution lamellae were produced at 1278°C and cooled at 0.01°C/year until 1169°C [11]. The cooling rate corresponds to 1km depth in the ureilite parent body if it was covered by rock-like material.

### *ALH82106*

ALH82106 is mainly composed of olivine and pyroxene. Pigonites have no straight planar exsolution lamellae and the augite shows blebby appearance (Fig.1-b). Microprobe analysis gave CaO bulk composition smaller than that of LEW88774. 100×Ca/(Ca+Mg+Fe) mol% of bulk composition in the pyroxene with exsolution lamellae is estimated to be 9. Exsolved augite is $Ca_{36.75}Mg_{60.50}Fe_{2.73}$ and low-Ca pyroxene is $Ca_{4.81}Mg_{90.87}Fe_{4.31}$. Each lamella has complex blebby shape. Ca diffusion profile shows also uniform chemical composition for each phase (Fig.2-b).

According to the calculation of the cooling rate [12], we calculated that exsolution lamellae were produced at about 1200°C and were preserved at the almost same temperature in more than several hundreds years [11].

## DISCUSSION

Pigeonites in common ureilites have been known to have cooled rapidly by possible destruction of the parent body [13]. From the Ca diffusion profiles of pyroxene lamellae in LEW88774, we found that these pyroxenes do not require extremely slow cooling rate as previously considered, in order to form coarse-exsolution lamellae. Because of high Ca bulk content in pyroxene, the pyroxene composition is located fairly towards the top of solvus with high temperature where fast atomic diffusion rate is expected. The irregular boundary also supports an idea that it required slow cooling rate and annealing. We estimated that these lamellae were formed only in 1km depth. The temperature which is calculated from Ca diffusion profile is found to be consistent with the temperature from coexisting pyroxenes in other ureilites [10]. Therefore, we conclude that although LEW88774 has different texture from any other ureilites, it turned out to be not so unusual ureilite for its peterogenesis.

The temperature calculated from Ca diffusion profile of the ALH82106 augite is also consistent with the temperature given in the previously study and the calculated temperature for the LEW88774 pyroxene, although Fe and Ca contents in pyroxene of LEW88774 is different from that of ALH82106. The cooling rate of ALH82106 is in accordance with that for LEW88774.

The bleby shape of the augites in ALH82106 has been attributed to the decomposition at the pigonite eutectoid reaction line [10]. The lamellae growth of both LEW88774 and ALH82106 pyroxene lamellae terminated at the high temperature. This event is possibly atributed to a collision and destruction of planetasimal resulting in rapid cooling.

**CONCLUSION**

Presence of coarse exsolution lamellae in pyroxene of LEW88774 promoted confusion on peterogenesis of this ureilite by comparing with other ureilites. It will not be surprising that such coarse lamellae were formed from initially Ca-rich pyroxene in a short time. Although LEW88774 has unusual textures unlike other ureilites, we found that cooling history of LEW88774 is not so unusual and that the temperature and the cooling rate of LEW88774 are consistent with those of ALH82106, although Fe and Ca content in pyroxene of LEW88774 is different from that of ALH82106. Both lamellae stopped growing at the high temperature. The rapid cooling might be due to collisions of planetasimal of the ureilite parent body and then the pyroxene were quenched in a small fragment ejected from the body.

**REFERENCES**

[1] Boynton, W. V., Starzyk, P. M., and Schmitt, R. A. (1976) Geochim. Cosmochim. Acta 40, 1439-1447 [2] Berkley, J. L., Taylor, G. J., Keil, K., Harlow, G. E., and Prinz, M. (1980) Geochim. Cosmochim. Acta 44, 1579-1597 [3] Takeda, H. (1987) Earth Planet. Sci. Lett. 81, 358-370 [4] Satterwhile, C. et al. (1993) Antarctic. Meteorite Newsl., 16(1), 15. [5] Prinz, M. et al. (1994) LPSC, XXV, 1107-1108 [6] Warren, P. and Kallemeyn, G. (1994) LPSC, XXV,1465-1466. [7] Ishii, T. and Takeda, H. (1974) Mem. Geol. Soc. Japan 11, 151-162 [8] Clayton, R. N. and Mayeda, T. (1988) Geochim. Cosmochim. Acta 52, 1313-1318 [9] Takeda, H., Mori, H. and Ogata, H. (1988) Proc. NIPR Symp. Antarct. Met. 1, 145-172 [10] Takeda, H., Mori, H. and Ogata, H. (1989) Meteiritics 24, 73-81 [11] Lindsley, D. (1983) American Mineral., 68, 477-493. [12] Miyamoto, M. and Takeda, H. (1994) JGR, 99, 5669-5677 [13] Takeda, H. (1987) Earth Planet. Sci. Lett. 81, 358-370

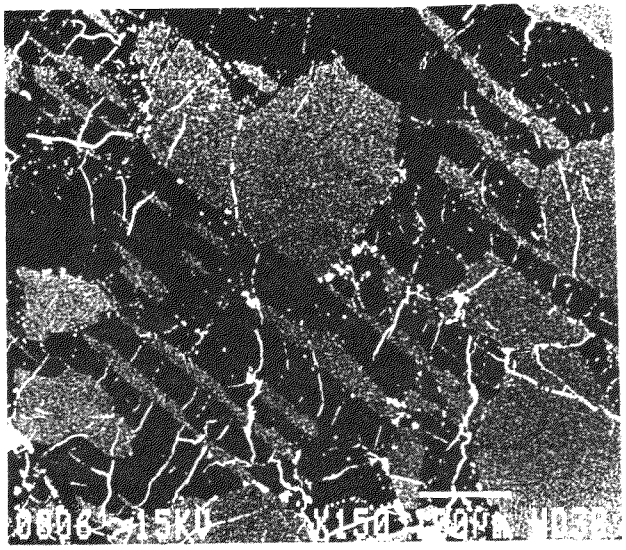

Fig.1-a
Backscattered electron image
of pyroxene exsolution lamellae
in LEW88774

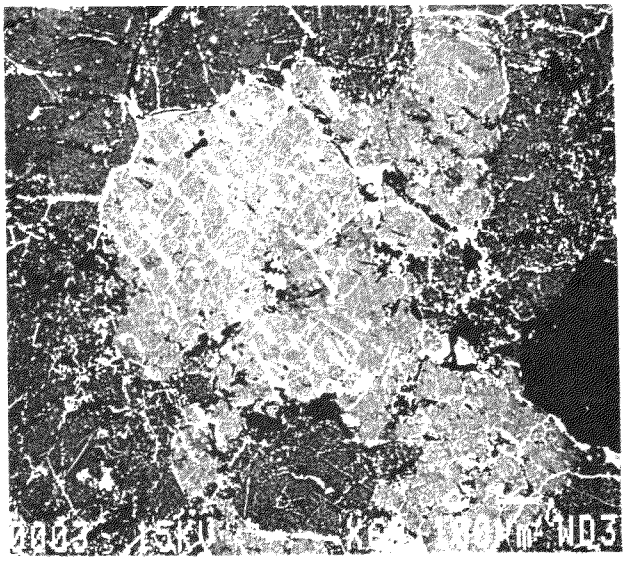

Fig.1-b
Backscattered electron image
of pyroxene exsolution lamellae
in ALH82106

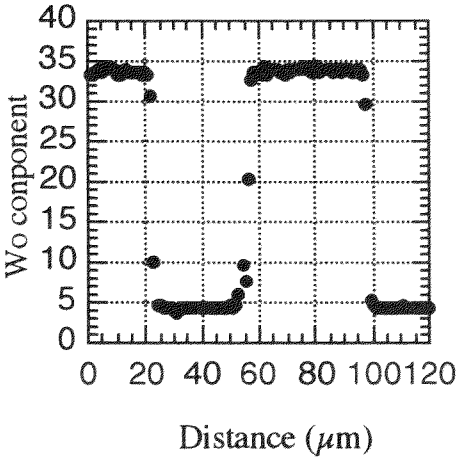


Fig.2-a
Ca diffusion profile intersecting
exsolution lamellae in LEW88774

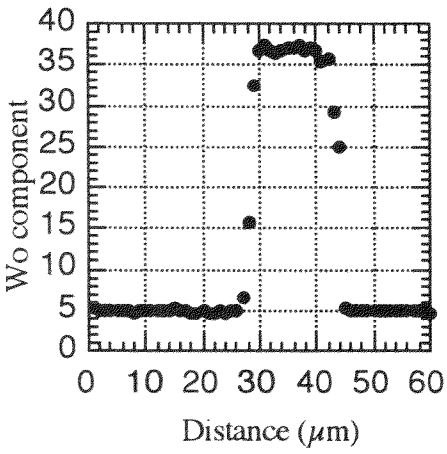


Fig.2-b
Ca diffusion profile intersecting
exsolution lamellae in ALH82106

# Precursors of PCP in CM carbonaceous chondrites

Yoshihiro Degawa[1], Kazushige Tomeoka[1,2] and Yukio Ikeda[3]
[1]The Graduate School of Science and Technology, Kobe University, Nada, Kobe 657.
[2]Department of Earth Sciences, Faculty of Science, Kobe University, Nada, Kobe 657.
[3]Department of Earth Sciences, Ibaraki University, Mito 310.

CM carbonaceous chondrites show abundant evidence that they have experienced aqueous alteration probably on their parent bodies. The most typical and abundant products of alteration are phyllosilicates. Besides them, CM chondrites contain unusual alteration products called "Poorly characterized phase ( PCP )" by Fuchs et al. [1]. PCP is rich in Fe and O and contains variable amounts of S, Si, Mg, Ni, Ca and P. PCP was found to be an intergrowth of an Fe-S-O-Ni phase, cronstedtite and minor amounts of submicron grains of magnetite, chromite, etc. [2, 3]. The Fe-S-O-Ni phase turns out to be tochilinite [4].

PCP occurs in chondrules and aggregatesas rounded inclusions and also abundantly occurs in matrix as aggregates of platelets and acicular fibers. PCPs in these occurrences were classified as Type-I PCP and Type-II PCP, respectively, by Tomeoka and Buseck [3]. Type-I PCP consists largely of tochilinite, and Type-II PCP consists of tochilinite and cronstedtite; the proportion of tochilinite and cronstedtite in Type-II PCP varies in a wide range. Recent petrographic studies showed that Type-II PCP is a predominant component in some CM chondrites [5, 6].

Tomeoka and Buseck [3] showed evidence that Type-I PCP was formed by replacing kamacite. They suggested that, in the progressive alteration process, Type-I PCP grains were separated from chondrules and aggregates and were distributed into matrix, where they were converted to Type-II PCP by reaction with Si produced by decomposition of olivine and pyroxene.

We have studied PCP in Yamato-74662, Yamato-790123, Murray and Murchison CM chondrites by using an SEM and an EPMA. We have found that Type-II PCP contains one or more varieties of phyllosilicates in addition to cronstedtite. Because of the complex intergrown nature, identification of the phyllosilicate phases is difficult, but one is probably Fe-bearing serpentine. We also found evidence that troilite has been partly replaced by PCP in the Murray CM chondrite; this is probably the first petrographic evidence of the formation of PCP from troilite to date. The PCP formed from troilite consists of tochilinite and Fe-bearing serpentine, thus different in composition from Type-I PCP formed from kamacite.

It is now evident that PCP formed from kamacite and troilite. However, it is still uncertain whether all the Type-II PCP in the matrices of CM chondrites have been derived exclusively from kamacite and troilite. Metzler et al. [5] showed that, in the Murchison, Cold Bokkeveld, Yamato-791198 and other many CM chondrites, Type-II PCP constitutes major fractions of bulk meteorites. If kamacite and troilite were the only precursors of Type-II PCP, CM chondrites should have contained much excessive Fe and S compared to normal chondritic abundances before aqueous alteration, and the aqueous alteration should have resulted in the normal chondritic bulk composition. However, Fe and S are not much more mobile in aqueous alteration than elements like Ca, Na, Al, Mg, and it is very unlikely that only Fe and S were selectively removed during aqueous alteration so that the bulk composition became CM-chondritic.

We here propose that the precursors of Type-II PCP are not only kamacite and troilite but also silicates such as olivine, pyroxene and glass. Such silicate precursors may include fragments of chondrules and aggregates. Type-II PCP derived from such silicates are probably much more common than Type-II PCP derived from kamacite and troilite. Because we found CAIs containing PCP in Yamato-790123 and Murray, CAIs may also be among the precursors. The different kinds of precursors and the different degrees of alteration are probably responsible for the observed mineralogical variations of Type-II PCP. For example, some Type-II PCP rich in tochilinite appears to have been formed from kamacite by adding Si, although all Type-II PCP rich in tochilinite may not have been derived from kamacite. On the other hand, Type-II PCP rich in phyllosilicates has been formed from silicates by adding Fe and S. Most of Type-II PCP having intermediate compositions between these two end-members may have resulted from more progressive alteration of either of these end-member PCPs.

References: [1] Fuchs L. H., Olsen E. and Jensen K.J. (1973)Smithon. Contrib. Earth Sci. 10, 1-39. [2] Tomeoka K. and Buseck P. R. (1983) Nature 306, 354-356. [3] Tomeoka K. and Buseck P. R. (1985) Geochim. Cosmochim. Acta 49, 2149-2163. [4] Mackinnon I.D R. and Zolensky M. E. (1984) Nature 309, 240-242. [5] Metzler K., Bishoff A. and Stöffler D. (1992) Geochim. Cosmochim. Acta 56, 2873-2897. [6] Kojima H. and Yanai K. (1993) from Primitive Solar Nebula and Oligin of Planets, 465-477

# EXTRATERRESTRIAL SPHERULES: A NEW TOOL FOR GLOBAL GEOLOGICAL AND PLANETOLOGICAL CORRELATION

*CSABA H. DETRE; GYÖRGY DON*

Geological Institute of Hungary. H-1143 Budapest, Stefánia út 14.

H-1142, P.O. Box 106

In the last hundred years microscopic spheroid or deformed spheroid objects were found in various geological formations by micromineralogists and micropaleontologists. The scientists have given them several names , as "spherules", "microspherules", "spherulites", "spherolites", "micrometeorites", etc. The investigation of these objects is very difficult, because of their very small size (see later). This may be the reason that they were neglected for a long time. The investigations were quite sporadic and no international organization has been established with the aim of their research.

The Carpathian Basin is a favoured region as far as the global occurence of spherules is concerned. They are known from many geological formations there. The Carpathian Basin is one of the deepest sedimentary basins of the world; it is not by chance that it has been nicknamed "Negative Himalaya". The spherules are known to occur in all kinds of sediments, and what is more, probably in all kinds of rocks, even in granite (*see Jakabská,K; Rozloznik,L. 1989*). The high level of sedimentological research in this region may also plays an important role.

The majority of spherules originate from the meteorites exploded in the high atmosphere (cca. 60-120 km from the surface of Earth). It refers to the three main types of spherules; iron-, silicate-, and iron-silicate spherule that are identical with the three main types of meteorites. In this case the surface of the Earth is permanently under a spherule-drizzle, wich has partially been documented in various terrestrial strata.

At the same time, the smaller part of of the spherules may be brough about by impacts of crater-producing meteorites, as dissipated melt (*see Lowe,D.R.-Byerly,R.,1986*). The best documented spherule-producing crater is found in Estonia, the "Kaali " crater (*see Shymankovich,S.-Kolosova,T.-Raukas,A.-Tirmaa,R., 1993*). In some instances terrestrial volcanic (*see Filimonova,L.G. et al.,1981; Filimonova,L.G., 1982*) or industrial origin may be supposed as well (*see Ausset,P. et al.,1994*).

We cannot consider impossible the clouds of spherules to have originated from the active impact activity of the Solar System (*see Hoyle,F.-Wincramansinghe,N.C.,1968*). These clouds were gathered by the planets. It is possible that in the early time of the Solar System more spherules landed on the surface of the Earth than in the recent time spitting through the atmosphere. In early times the meteorite impact activity on the surface of the Earth was stronger, producing more terrestrial impact-originated spherules.

In spite of their different origins the spherules are identical as to their spherical or deformed spherical form. The diameter of the spherules ranges between 1μm-1000μm, with a maximum of about 100μm.

During the history of the Earth the global occurence of spherules seems to have altogether three abundance peaks (by extrapolation of certain sporadic local result) : Permian (*see Hadnagy,Á.,1994*), Upper Cretaceous (*see Xiao Zhifeng et al.,1994*), and Pleistocene (*see Li Chun-Lai-Ouyang Zi-Yuan-Lin Wen-Zhu, 1994*).

Therefore, the comparative studies of the spherules are very important for a global correlation programme.

A very important task of the investigations will be the reambulation of the meteorite fall areas, such as the Kaali crater (Estonia) and the Ries crater area (Germany), accompanied by collection of small fragments of meteorites and spherules. For stratigraphical evaluation the spherule-bearing formations need a "bed by bed" reambulation. Field works of this type were realized in the Apuseni Mts (Rumania) (*see Udubaşa,G.-Arsenescu,V.,1987; Hadnagy,Á.,1995*), East Carpathians (Rumania) (*see Grigorescu,G.-Baltras,A.,1981*), as well as Gemeric granite region (Slovakia) (*see Jakabská,K.-Rozloznik,L.,1989*), and in certain regions of Hungary in the last years. In Hungary the successive collection of spherules from boreholes was started in early 1994 Permian, Triassic, Jurassic, Upper Cretaceous, Miocene, Pliocene, Pleistocene samples from many boreholes in Transdanubia and in the Great Hungarian Plan (*see Detre,Cs.H.,1994; Kákay-Szabó,O.,1994; Gyuricza,Gy.,1994; Rálisch-Felgenhauer,E.,1994; Siegl-Farkas,Á.-Wegreich,M.,1994; Szöőr,Gy.-Korpás-Hódi,M.-Don,Gy.-Beszeda,I.,1994*).

The research of the spherules has involved a lot of interdisciplinary collaborations, including stratigraphy, geochemistry, (micro)mineralogy, paleomagnetic research, planetology, meteoritics, meteorology, glaciology (*see Zbik,M.-Gostin,V.A.,1994*), ocean floor research (*see Glass,B.P.-Zwart,M.J.,1979*), and sedimentology in general.

Radiometric research will certainly gain in importance in the future investigation of spherules. The synchronous occurence of spherules with their host sediment proves their origin from exploding meteorites , while a dischronous situation would support the above mentioned origin from the spherule clouds formed in the early Solar System.

From the point of view of extraterrestrial geology for the time being are the only real tools for interplanetary correlation, since in all likelihood they have to occur on every planet of the Solar System (*see Bérczi,Sz.-Lukács,B.,1994*).

For this purpose a new IGCP project (No.384) is under organization by four proposers: Cs.H.Detre (Hungary), K.Jakabská (Slovakia), A.Raukas (Estonia), G.Uduba şa (Romania), : "Extraterrestrial spherules: a new tool for global correlation". All investigators of spherules are asked kindly reconsider their contacts all over the world and suggest us names and adresses of possible participants. **It is obvious that the investigation of the spherulites has to be global. This project is aimed at developing and organizing these global investigations. By way of this project the first International organization of a new scientific field will be organized.**

Till now two preparatory meetings were organized in Hungary. These were the first international meetings in this theme. 1. "Spherulites (Micrometeorites) in the Carpathian Basin". Budapest, 31 Oct.- 1 Nov. 1994. 2. "Spherulites and (Palaeo)ecology". Debrecen, 2-4 March 1995. Both with Austrian, Chinese, Estonian, Hungarian, Romanian and Slovakian participants. Latter recommended type areas for the world-wide investigations, according to the hitherto informations about the investigations:

1. Baltic and Scandinavian area
2. Central Europe
3. Mediterranean region
4. Central and Southern Africa
5. Central and Eastern Asia
6. North America
7. Caribbean region
8. Australia
9. Antarctica

*References cited*


**Ausset,P.-Lefévre,R.-Philippon,J.-Venet,C. 1994** : Présence constante de cendres volantes industrielles dans le croutes noires d'alteration superficielle de monuments français en calcaire compact. - Comptes Rendus Acad. Sci. Paris, t.318, série II., pp 493-499.

**Bérczi,Sz.-Lukács,B. 1994** : On possible spherulite sources. - Centr.Research Inst. Phys. Report, KFKI-1994-13/C, pp 1-9. Budapest.

**Detre,Cs.H. 1994** : Spherulites - new tool for global geological and planetological correlation. - Abstracts of International Meeting Spherulites (Micrometeorites) in the Carpathian Basin, pp.3-4, Budapest.

**Dosztály,L. 1994** : Glassy spherulites from Hungary. Abstracts of International Meeting Spherulites (Micrometeorites) in the Carpathian Basin, pp.3-4, Budapest.

**Don,Gy. 1994** : Evidences for the cosmic origin of silicat spherulites, and the significance of their investigation. -Abstracts of International Meeting Spherulites (Micrometeorites) in the Carpathian Basin, p.18., Budapest.

**Filimonova,L.G. 1982** : Vulkanogenyje gepoksidy juzhnogo Sichote-Alina kak indikatory glubinnych procesov i rudonosnosti efuzivov. - Doklady AN SSSR 262, 2, pp 447-451, Moskva.

**Filimonova,L.G.-Gorkova,A.I.-Korina,E.A.-Trubkin,N.V. 1981** : O nachodke samorodnych metalov v vulkanitoch juzhnogo Sichote-Alina. - Doklady AN SSSR 256, 4, pp 962-965, Moskva.

**Glass,B.P.-Zwart,M.J. 1979** : North American mikrotektites in Deep Sea Drilling Project cores from the Caribbean Sea and Gulf of Mexico. - Geol.Surv.Amer.Bullet., Part I., v.90., pp 595-602.

**Grigorescu,D.-Baltras,A. 1981** : Magnetic spherules of possibly extraterrestrial origin in Vraconian-Lower Cenomanian Shale (Black Shale Unit, East Carpathians). - Rev. Roum. Géol. Géophys. Géogr. Géologie, 23, pp 117-125.

**Gyuricza,Gy. 1994** : Iron spherulites in unconsolidated sediments in Hungary. -Abstracts of International Meeting Spherulites (Micrometeorites) in the Carpathian Basin, pp.16-17, Budapest.

**Hadnagy,Á. 1995** : Metallic and Glassy Spherules from the Crisu Negru Modern Alluvial Formations. - Abstracts of International Meeting Spherulites (Micrometeorites) in the Carpathian Basin, p.8., Budapest.

**Hoyle,F.-Wickramensinghe,N.C. 1968** : Condensation of the planets. - Nature, 1968, 217, pp 415-418.

**Jakabská,K.-Rozloznik,L. 1989** : Spherical accessories ("Spherules") in Gemeric granites (West Carpathians - Czechoslovakia). - Geologicky Zbornik - Geologica Carpathica, 40. 3, pp 305-322.

**Kákay-Szabó,O. 1994** : The main types of spherulites occuring in the rocks of Hungary. -Abstracts of International Meeting Spherulites (Micrometeorites) in the Carpathian Basin, p.15, Budapest.

**Li Chun-Lai.-Ouyang Zi-Yuan.-Lin Wen-Zhu. 1994** : Microtektites in 0.7 Ma B.P. Loess and Geochemistry of the Microtektite-Bearing Layers. -Abstracts of International Meeting Spherulites (Micrometeorites) in the Carpathian Basin, pp.11-13., Budapest.

**Lowe,D.R.-Byerly,G.R. 1986** : Early Archean silicate spherules of possible impact origin, South Africa and Western Australia. -Geology, v. 14. pp 83-86.

**Rálisch-Felgenhauer,E. 1994** : Extremely small spherulites from the Middle Triassic of Mecsek Mts. (South Hungary). -Abstracts of International Meeting Spherulites (Micrometeorites) in the Carpathian Basin, p.19., Budapest.

**Shymanovich,S., Kolosova,T., Raukas,A., Tirmaa,R. 1993** : Extraterrestrial spherules in the surroundings of Kaali Meteorite Craters (Saaremaa Island, Estonia). - Proc. Estonian Acad. Sci. Geol. 1993. 42, 3, pp 127-133.

**Siegl-Farkas,Á.-Wagreich,M. 1994** : Palynological and nannoplankton correlation of spherulite-bearing Senonian formations in Hungary.-Abstracts of International Meeting Spherulites (Micrometeorites) in the Carpathian Basin, p.23., Budapest.

**Szöör,Gy.-Korpás-Hódi,M.-Don,Gy.-Beszeda,I. 1994** : Micrometeorites from the sediments of Nagylózs-1 borehole. -Abstracts of International Meeting Spherulites (Micrometeorites) in the Carpathian Basin, p.25., Budapest.

**Tiirmaa,R. 1988** : Ploshtshadnoie raspredelenie raspylennogo veshthestva meteorita Kaali. - Izv. AN ESSR. Geol. 37, 1, pp 43-46.

**Udubaşa,G.-Arsenescu,V. 1987** : Greigite in the Gilort and Galbena Rivers Allluvia. Dari de seama Inst. Geol. Geofizica, 72-73/1, pp 61-66.

**Wu Xihao.-Xu Heling.-An Zhisheng.-Zheng Hongbo.-Deng Jiwun.-Yin Weide. 1991** : Records of astrogeologic events in dust deposits of Central China. - Abstracts of XIII. . INQUA International Congress Beijing, 1991, p.393.

**Xiao Zhifeng.-Ouyang Ziyuan.-Lin Wenzhu. 1994** : Simulation of the climatic effect of giant extraterrestrial body impacts on the Earth in Cenozoic.-Abstracts of International Meeting Spherulites (Micrometeorites) in the Carpathian Basin, p.10., Budapest.

**Zbik,M.-Gostin,V.A. 1994** : Morphology of Antarctic Cosmic Dust Spherules and comparison to the spherules from the Tunguska Catastrophe. - Nineteenth Symposium on Antarctic Meteorites, May 30- june 1. 1994; National Institute of Polar Research, Tokyo, pp 169-172.

**An attempt to establish a data base for chemical compositions of Antarctic meteorites.** M. Ebihara[1], K. Shinotsuka[1], T. Shingen[1], S. Togashi[2], H. Kamioka[2], H. Kojima[3] and K. Yanai[3,4]; *[1]Dept. of Chem., Tokyo Metropolitan Univ., Hachioji, Tokyo 192-03, Japan, [2]Geological Survey of Japan, Tsukuba, Ibaraki 305, Japan, [3]Natl. Inst. Polar Res., Itabashi 173, Tokyo, Japan and [4] Dept. of Civil and Environmental Engineer., Iwate Univ., Morioka, Iwate 020, Japan (present address).*

## Introduction

So far, more than ten thousands of meteorites have been collected on Antarctica and, consequently, have greatly extended our knowledge of meteorites. The Antarctic meteorites are first subjected to petrographic and mineralogical examinations. These observations are very useful not only for the identification but also for their classification of meteorites. Degrees of weathering and fracturing also are estimated on these observations. In US, some samples are further examined for their $^{26}Al$ activities and natural thermoluminescence intensities. These informations have been periodically published and distributed among the community of meteorite researchers. The recent publication issued by MWG (US) [1] is very informative and useful. A similar publication will also be issued by NIPR soon.

Major element compositions have been routinely determined and published from time to time. This is, however, not the case for minor and trace elements. These elements are determined by the individual researchers when their data are needed. Considering that minor and trace element contents are equally informative compared with petrologic and mineralogical data, we have attempted to establish a data base for chemical compositions of Antarctic meteorites. Considering the effectiveness in analyses, instrumental neutron activation analysis (INAA) and inductively coupled plasma mass spectrometry (ICP-MS) were used. In ICP-MS, rare earth elements (Y and lanthanoids), Th and U are measured, because these elements are one of the most informative elements for cosmochemical discussion.

## Experimental

In this study, we used aliquants of the meteorite specimens prepared for the determination of major element compositions by wet chemical analysis. Chondritic meteorites were separated into magnetic and non-magnetic fractions by a hand magnet. For the other groups of meteorites, only bulk samples were prepared without magnetic separation. The initial samples were usually more than 5 g, so heterogeneity must be minimized. We started with the specimens already ground and magnetically separated at NIPR.

[INAA] About 5 to 30 mg of each sample was sealed into a quartz tube and irradiated for 6 h at the JRR-4 reactor of the Japan Atomic Energy Research Institute. After irradiation, samples were carried into the radioactivity counting lab. of the Geological Survey of Japan and were subjected to $\gamma$-ray spectrometry.

[ICP-MS] About 10-20 mg of each sample was taken into a teflon vessel and decomposed with mineral acids under high pressure. After decomposition, the residual solution was once evaporated and then dissolved in dil $HNO_3$ solution. The appropriately diluted solution was introduced into an ICP-MS instrument (VG Plasma-Quad $\Omega$, Fissons Instrument). For the quantitative analysis, standard solutions prepared from the appropriate chemical reagents were measured. The detailed procedures will be reported elsewhere.

## Results and Discussions

The feasibility and the usefulness of INAA for multi-element analyses is well recognized. A part of the INAA data in conjunction with this study were reported at this symposium last year [2]. Here, we like to focus on the data obtained by ICP-MS in order to discuss the feasibility of ICP-MS for our study.

The experimental results of ICP-MS for Antarctic eucrite samples are shown in Fig. 1, where elemental abundances are normalized to corresponding CI values [3]. Each

sample was analyzed in duplicate. As easily recognized, duplicate analyses yielded almost identical patterns for lanthanoids. A small discrepancy between two measurements can be found for Th and U, which must have been due to experimental problems. Both positive and negative anomalies of Eu are observed in these eucrites.

Fig. 2 shows CI chondrite-normalized abundance patterns of REE, Th and U for several chondritic meteorites. In this figure, abundances in non-magnetic fractions in place of bulk chondrites are shown, as we haven't analyzed the magnetic fractions for these elements. Since these elements are lithophile and, hence, are essentially located in the non-magnetic fraction, the abundance patterns should be identical for the non-magnetic fractions and the bulk samples of chondrites. All the patterns shown are almost flat and about 1.5 times CI values. Only one sample (Y-791088) shows slight increases of light REE and U. Considering that this meteorite seems to have experienced severe shock, such increases of light REE (La, Ce and Pr) and U may have been caused by shock event for this meteorite.

From Figs. 1 and 2, a common feature can be recognized; a zigzag change for middle and heavy lanthanoids. As we find such a zigzag change commonly in these different groups of meteorites (eucrites and chondrites), the zigzag change is not indigenous in each meteorite but artificial, possibly caused by the improper normalizing values, for which we use the CI values compiled by Anders and Grevesse [3]. This problem has been discussed in details elsewhere [4].

In conclusion, ICP-MS is very useful for the determination of trace lanthanoids and actinoids in meteoritic samples. The combination of INAA and ICP-MS is very effective in obtaining element composition data, which can then serve for a data base for chemical compositions of Antarctic meteorites.

**Reference.** [1] Grossman J. N. (1994) *Meteoritics* 29, 100-143. [2] Togashi S. et al. (1994) *Abstract for the 19th Symp. on Antarctic meteorites, NIPR,* p. 81-83. [3] Anders E. and Grevesse N. (1989) *Geochim. Cosmochim. Acta* 53, 197-214. [4] Shinotsuka K. et al. (1995) (submitted to *Meteoritics*).

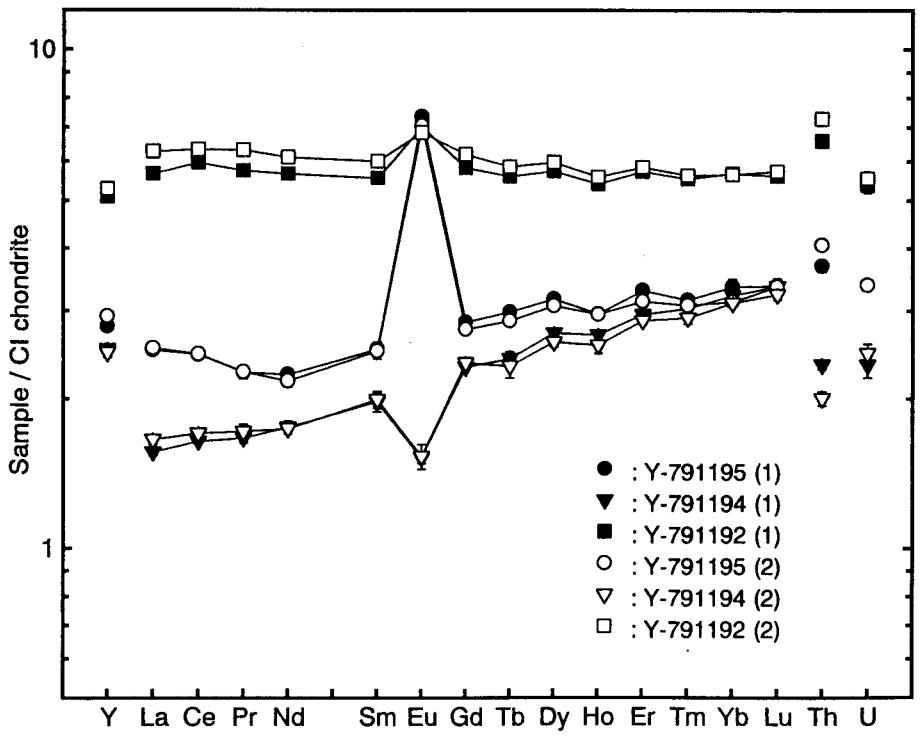


Fig. 1 CI-normalized abundance patterns of rare earths (Y and lanthanoids), Th and U for some Antarctic eucrites. Each samples was analyzed by ICP-MS in duplicate, as shown by numbers 1 and 2.

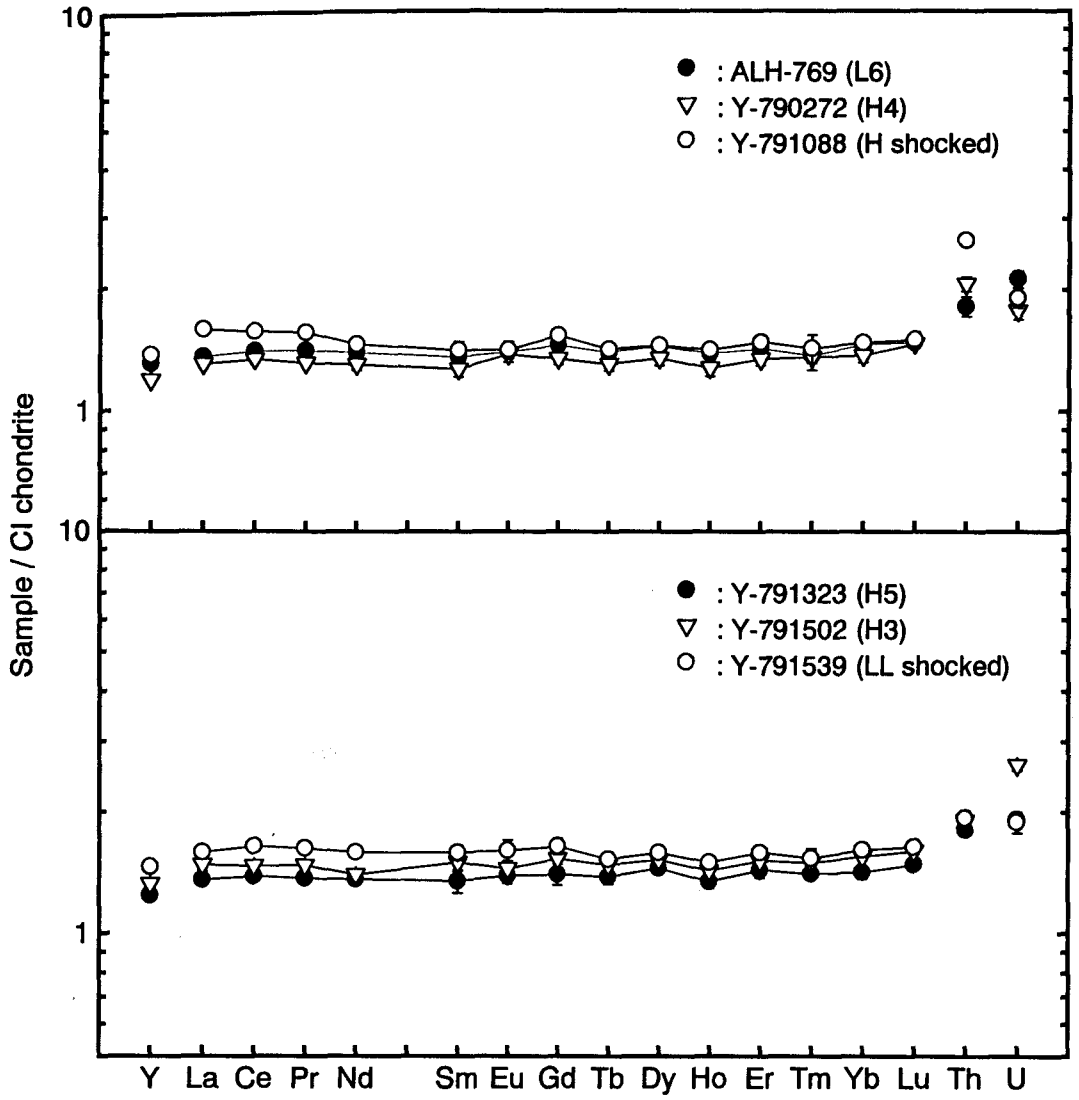


Fig. 2 CI-normalized abundance patterns of rare earths (Y and lanthanoids), Th and U for some Antarctic chondrites. Abundances in non-magnetic fractions are shown. Only one sample (Y-791088) seems to be enriched in light rare (La, Ce and Pr) and U.

# ANGRITE ASUKA-881371: BREAK-UP TIME FROM PARENT ASTEROID AND COMPARISON WITH OTHER ANGRITES

O. Eugster and A. Weigel
Physikalisches Institut, University of Bern,
Sidlerstrasse 5, 3012 Bern, Switzerland

In the framework of a consortium study organized by Paul Warren (UCLA, presently University of Tokyo) we began the analyses of the noble gas isotope abundances of the 11.27 g angrite Asuka-881371 (subsequently named "Asuka"). The total consortium allocation was a single fragment, Asuka-881371,21 with a mass of 1.24 g. Our sample of 35.5 mg consisted of two fragments and some small grains derived from a single 140 mg fragment (field name "A") that appeared to be free to fusion crust. For a general description of this angrite see Yanai (1994).

The objective of our contribution is the determination of the cosmogenic, radiogenic, fissiogenic, and if present, trapped (primordial and solar wind derived) noble gas isotope abundances, calculation of the cosmic-ray exposure ages and of the $^{244}$Pu-fission Xe ages. We performed a first analysis of a 10.2 mg sample for He, Ne, and Ar isotope studies. Here we present preliminary data that will be supplemented later by Kr and Xe and further He, Ne, and Ar analyses.

**1. Cosmic-ray exposure ages.** Based on the concentrations of cosmic-ray produced $^{3}$He, $^{21}$Ne, and $^{38}$Ar cosmic-ray exposure ages $T_3$, $T_{21}$, and $T_{38}$, respectively, were calculated. The target element abundances for Asuka were taken from Yanai (1994). The production rates were derived using the method given by Eugster and Michel (1995), adopting an average shielding dependency for HED's. For Asuka we obtained $T_3$ = 5.0 Ma, $T_{21}$ = 5.5 Ma, and $T_{38}$ = 5.4 Ma. Final ages will be available when the chemical analyses of the consortium sample and our further experiments are completed.

**2. Shielding from cosmic rays.** Cosmogenic $^{22}$Ne/$^{21}$Ne for Asuka is 1.13. This indicates that the meteoroid was much larger than the recovered weight, probably more than 1 kg.

**3. Radiogenic $^{4}$He** = 8600x10$^{-8}$ cm$^3$STP/g. This concentration is relatively high for meteorites and typical for angrites (except for LEW87051, which probably lost $^{4}$He). We conclude, that Asuka contains more than 50 ppb U.

**4. Radiogenic $^{40}Ar = 280x10^{-8}$ cm$^3$STP/g.** The K concentration must be much lower than e.g. in chondrites (which contain about 800 ppm K). This agrees with Yanai's (1994) K content and is also typical for angrites.

**5. No trapped solar gases** were observed in Asuka. This is consistent with the statement by Yanai (1994), that Asuka is an unbrecciated igneous rock. The concentrations of primordial trapped gases are also very low ($^{36}Ar_{tr} \approx 0.6x10^{-8}$ cm$^3$STP/g). These conclusions have also been obtained for the other three angrites.

In the table we compare the results for Asuka with the data for the other angrites (Eugster et al., 1991).

| | Parent body break-up (c.-r. exp. age, Ma) | $(^{22}Ne/^{21}Ne)_c$ | $^4He_r$ | $^{40}Ar_r$ |
|---|---|---|---|---|
| | | | $10^{-8}$ cm$^3$STP/g | |
| A-881371 | 5.3 | 1.13 | 8600 | 276 |
| Angra dos Reis | 55.5 | 1.14 | 41000 | 66 |
| LEW86010 | 17.6 | 1.24 | 15300 | 126 |
| LEW87051 | ≥ 0.2 | 1.37 | 7.9 | 58 |

Inspection of the data in the table shows that Asuka does not originate from the same break-up event as Angra dos Reis or LEW86010. Since LEW87051 lost gases, only a lower limit of its break-up time could be determined.

**Conclusions** obtained from these preliminary data are as follows: (1) In terms of noble gas characteristics Asuka is a typical angrite with high $^4He_r$, low $^{40}Ar_r$, and low trapped gas contents. (2) It appears that each angrite was ejected from the angrite parent asteroid by its own break-up event. This supports the conclusion by Yanai (1994) that Asuka differs in some respects from the other known angrites.

**Acknowledgements:** We thank the National Institute of Polar Research, Tokyo, for the Asuka sample and Paul Warren for organizing the consortium. This work was supported by the Swiss National Science Foundation.

**References**

Eugster O., Th. Michel, and S. Niedermann (1991) *Geochim. Cosmochim. Acta* **55**, 2957-2964.

Eugster O. and Th. Michel (1995) *Geochim. Cosmochim. Acta* **59**, 177-199.

Yanai K. (1994) *Proc. NIPR Symp. Antarctic Meteorites*, No. 7, Natl. Inst. Polar Res., Tokyo, 30-41.

THE ORIGIN OF TROILITE AND PYRRHOTITE IN CHONDRITES: I. IRON SULFIDE FORMATION KINETICS IN $H_2S$-$H_2$ GAS MIXTURES, B. Fegley, Jr.[1,2], D.S. Lauretta[1,2], and D.T. Kremser[1] (1) Dept. of Earth & Planetary Sciences, and (2) McDonnell Center for the Space Sciences, Campus Box 1169, Washington University, One Brookings Drive, St. Louis, MO 63130-4899 USA.

**Introduction.** Troilite (stoichiometric FeS) is the most common sulfide in meteorites. However, pyrrhotite (Fe-deficient $Fe_{1-\delta}S$) is the dominant sulfide in CI chondrites and in chondritic interplanetary dust particles [1-3]. Here we summarize the results of our experimental and theoretical studies of the thermodynamics, kinetics, and mechanism of Fe sulfide formation. Our thermochemical equilibrium calculations describe the stability fields for troilite and pyrrhotite in the solar nebula. Our experimental studies give kinetic data for troilite and pyrrhotite formation via the reaction $H_2S(g) + (1-\delta)Fe(metal) = Fe_{1-\delta}S(sulfide) + H_2(g)$. Our nebular chemistry models utilizing our kinetic data constrain the rate of Fe sulfide formation as a function of temperature, pressure, Fe grain size, and sulfur fugacity. A companion abstract reports our studies of metal-sulfide assemblages in some unequilibrated ordinary chondrites and demonstrates that these assemblages are not pristine nebular condensates, but were altered by post-formation heating events [4].

**Thermochemical Equilibrium Calculations.** We re-examined Fe sulfide condensation for two reasons. In an attempt to explain pyrrhotite in chondrites, [5] claimed that $Fe_{0.875}S$ condensed prior to FeS. However, the Fe-S phase diagram [6] shows this is impossible because only FeS exists in equilibrium with Fe metal. Also, [7] published new thermodynamic data for Fe sulfides (FeS and $Fe_{0.875}S$ to $Fe_{0.98}S$). Figure 1 shows the results of our calculations [8-9]. Troilite (FeS) forms at the pressure independent temperature of 719 K (from pure Fe metal). This is lowered to 716.5 K for a solar $Fe_{0.95}Ni_{0.05}$ alloy. Our results agree with prior calculations by [10-11]. We also used the $Fe_{1-\delta}S$ defect thermodynamics model of [12] to calculate the variation in Fe/S ratios for $Fe_{1-\delta}S$ as a function of temperature and sulfur fugacity in the solar nebula. The results in Figure 2 show that $Fe_{1-\delta}S$ can form by reactions exemplified by $(1-\delta)FeS(troilite) + (\delta)H_2S(g) = H_2(g) + Fe_{1-\delta}S(pyrrhotite)$, in qualitative agreement with suggestions of [3,13]. Reheating of dust-rich regions in the nebula will lead to sulfur fugacities above the "solar" value and to production of more Fe-deficient pyrrhotites, such as those observed in CI chondrites and IDPs.

**Experimental Studies.** Fe sulfide formation was studied by isothermally heating high purity Fe foils of known weight and surface area in $H_2S$-$H_2$ gas mixtures at atmospheric pressure for varying time periods. The nominal $H_2S$ contents of the gas mixtures were 50, 100, 1000, and 10,000 ppm. For reference a solar composition gas has 37 ppm $H_2S$ [14]. About 120 experiments were done to determine the effects of temperature and $H_2S/H_2$ ratio on the reaction [8,9,15,16].

**Chemical Composition of Sulfides.** The reacted samples were chemically analyzed by X-ray diffraction (XRD), electron microprobe (EMP) analysis, and gravimetric analysis by combustion. In many cases, electron microprobe traverses across the sulfide layers were also done. Table 1 summarizes the analytical data for the bulk composition of the sulfide layers. There is good agreement between the results from the three methods. A comparison of the observed Fe/S ratios to those predicted from the defect thermodynamics model of [12] shows that with a few exceptions (e.g., low T runs in 50 ppm $H_2S$), equilibrium was reached. The data in Table 1 show that troilite was formed in the reactions. Also, cracking of layers in some 10,000 ppm runs exposed fresh metal to gas leading to disagreements between predicted and observed Fe/S ratios. The

electron microprobe traverses of many samples show decreases in the Fe/S ratios from the metal/sulfide to sulfide/gas boundaries. Such profiles are expected from Wagner's model for diffusion controlled reactions forming compact scale layers [17].

**Microstructure and Morphology of Sulfide Layers.** The sulfide layers were studied by XRD, optical and scanning electron microscopy. The sulfide layer thickness increased with reaction temperature and time. Initially a compact oriented layer developed on the metal. As the reaction progressed, vertical cracks extending from the sulfide/gas to sulfide/metal interface appeared and the layer pulled away from the metal. Gas penetrated to the metal and a new sulfide layer with small randomly oriented crystals formed. The two distinct layers with different crystal sizes and orientations are commonly observed in sulfide scales formed on Fe metal. We also observed that the growth orientation of the Fe sulfide crystals changed with decreasing temperature and sulfur fugacity. These changes correlate with an increase in the Fe sulfide formation rate (see below).

**Kinetics and Mechanism of FeS Formation.** The weight gain and the fractional thickness change of the Fe foil were used to determine the extent of reaction as a function of time. The two methods show excellent agreement. Experiments at 50 and 100 ppm $H_2S$ followed linear kinetics $\Delta w = k_l t$ or $\Delta x = k_l' t$, where $\Delta w$ is the weight gain, $\Delta x$ is the thickness change, $k_l$ and $k_l'$ are linear rate constants with units of g $s^{-1}$ and cm $s^{-1}$, and t is time. There was a sudden increase in reaction rate between 613 K and 643 K for the 50 ppm $H_2S$ experiments. This correlated with the different growth orientation of the Fe sulfide crystals. Experiments at 1000 ppm $H_2S$ and the 558 K isotherm at 10,000 ppm $H_2S$ initially followed linear kinetics and made a transition to parabolic kinetics $(\Delta w)^2 = k_p t$ or $(\Delta x)^2 = k_p' t$, where $k_p$ and $k_p'$ are parabolic rate constants with units of $g^2\ s^{-1}$, and $cm^2\ s^{-1}$. All experiments at 923 K and 10,000 ppm followed parabolic kinetics, while all the 673 K experiments at 10,000 ppm $H_2S$ displayed linear kinetics. These samples had sulfide layers which did not adhere to the metal and easily lifted off allowing fresh gas to react with the exposed metal surface. Tables 2 and 3 show the linear and parabolic rate constants determined from our experiments. Some of our reaction conditions overlap those employed by prior workers. Our linear and parabolic rate constants for these conditions show good agreement with those reported previously. The following mechanism explains the kinetic data. Initially Fe sulfide formation displays linear kinetics because the chemical reactions at the metal/gas interface are rate limiting. After a thin, coherent sulfide layer has formed, the chemical reactions at the sulfide/gas interface remain rate limiting until the sulfide scale reaches a critical thickness and diffusion through the sulfide layer becomes the rate limiting step. The reaction then displays parabolic kinetics, and as shown by [18], $Fe^{2+}$ diffusion through the sulfide is the rate limiting step.

**Applications to the Solar Nebula.** We used our kinetic data to constrain the rate of Fe sulfide formation in the solar nebula as a function of temperature, pressure, Fe grain size, and sulfur fugacity. First, we graphically determined the critical thickness for transition from linear to parabolic kinetics from the reactions in 1000 ppm and 10,000 ppm $H_2S$ that displayed this transition. Then, as a function of the extent of reaction, we calculated the thickness of sulfide rims on Fe metal grains in the nebula. Our results, which are displayed in Figure 3, show that Fe grains smaller than 20 μm in diameter never reach the critical thickness, while the 20 μm diameter grains only reach the critical thickness after 90% of the Fe has already reacted to form sulfide. Sulfurization of Fe grains larger than 20 μm in diameter will initially follow linear kinetics and later, at different extents of reaction depending on the grain size, follow parabolic kinetics. Table 4 shows the lifetimes for complete sulfurization of spherical Fe metal grains ranging in size from

0.2 μm to 20 μm diameter as a function of temperature along an adiabatic profile in the solar nebula. The grain lifetimes were calculated using the simple collision theory model developed by Fegley [19-22] and an activation energy of 43 kJ $mole^{-1}$ appropriate for the low $H_2S$ concentration in the solar nebula. For reference, we note that grain sizes of ~0.1 μm are found in meteorite matrix, while larger grain sizes of ~10-100 μm are found in chondrules. These results show that Fe sulfurization is a rapid process in the solar nebula and that even ~20 μm diameter grains have lifetimes of only 0.01-1% of the nebular lifetime of $10^5$-$10^7$ years [23]. We also used the simple collision theory (with $E_a$ = 43 kJ $mole^{-1}$) to calculate the chemical lifetime for $H_2S$ depletion via troilite formation. These values, shown in Figure 4, are insignificant compared to the estimated lifetime of the solar nebula [22] and confirm our earlier conclusions that troilite formation was a rapid process that went to completion in a fraction of the nebular lifetime [19-22].

**Acknowledgments.** This work was supported by the NASA Origins of Solar Systems Program (Grant NAGW-3070). We thank K. Lodders for useful discussions.

**References.** [1] J.S. Kerridge 1970 *Meteoritics* **5**, 149-152; [2] J.S. Kerridge et al 1979 *Earth Planet. Sci. Lett.* **43**, 359-367; [3] M.E. Zolensky & K. Thomas 1995 *Lunar Planet. Sci.* **XXVI**, 1567-1568; [4] D.S. Lauretta et al 1995 this volume; [5] J.A. Wood & A. Hashimoto 1993 *Geochim. Cosmochim. Acta* **57**, 2377-2388; [6] M. Hansen & K. Anderko 1959 *Constitution of Binary Alloys*, 2nd ed., McGraw Hill, NY; [7] F. Grønvold & S. Stølen 1992 *J. Chem. Thermo.* **24**, 913-936; [8] D.S. Lauretta & B. Fegley, Jr. 1994 *Lunar Planet. Sci.* **XXV**, 773-774; [9] D.S. Lauretta et al 1995 *Lunar Planet Sci.* **XXVI**, 831-832; [10] J.W. Larimer 1967 *Geochim. Cosmochim. Acta* **31**, 1215-1238; [11] J.S. Lewis 1972 *Earth Planet. Sci. Lett.* **15**, 286-290; [12] G.G. Libowitz 1972 in *Reactions of Solids*, pp. 107-115, Chapman & Hall, London; [13] J.S. Kerridge 1976 *Nature* **259**, 189-190; [14] E. Anders & N. Grevesse 1989 *Geochim. Cosmochim. Acta* **53**, 197-214; [15] D.S. Lauretta & B. Fegley, Jr. 1994 *Meteoritics* **29**, 490; [16] D.S. Lauretta & B. Fegley, Jr. 1994 in abstracts of 19th Symposium on Antarctic Meteorites, pp. 62-65; [17] C. Wagner in *Atom Movements*, pp. 153-173, ASM, Cleveland; [18] R.H. Condit, et al 1974 *Oxid. Met.* **8**, 409-455; [19] B. Fegley, Jr. 1988 in *Workshop on the Origins of Solar Systems*, pp. 51-60, LPI Report No. 88-04; [20] R.G. Prinn & B. Fegley, Jr. 1989 in *Origin and Evolution of Planetary and Satellite Atmospheres*, pp. 171-211, Univ. of AZ Press, Tucson; [21] B. Fegley, Jr. and R.G. Prinn 1989 in *The Formation and Evolution of Planetary Systems*, pp. 171-211, Cambridge Univ. Press, Cambridge; [22] B. Fegley, Jr. 1993 in *The Chemistry of Life's Origins*, pp. 75-147, Kluwer, Dordrecht; [23] F.A. Podosek & P. Cassen 1994 *Meteoritics* **29**, 6-25.

**TABLE I. Effects of temperature and gas composition on Fe/S ratio of iron sulfide layers.**

| Temp (K) | ppm $H_2S$ | Observed Fe/S atomic ratio XRD[a] | Microprobe[a] | Combustion[a] | Mean | Gas-Solid Equilibrium |
|---|---|---|---|---|---|---|
| 558 | 50 | 0.956 | 0.962 | n.a. | 0.959 | 0.994 |
| 613 | 50 | 0.957 | 0.949 | n.a. | 0.953 | 0.997 |
| 673 | 50 | 0.992 | 0.982 | n.a. | 0.987 | 0.998 |
| 558 | 100 | 0.972 | 0.988 | n.a. | 0.980 | 0.991 |
| 658 | 100 | 0.997 | 0.996 | n.a. | 0.997 | 0.996 |
| 723 | 100 | 1.002 | 0.965 | n.a. | 0.983 | 0.998 |
| 673 | 850 | 0.990 | 0.986 | n.a. | 0.988 | 0.987 |
| 778 | 850 | 0.996 | 0.988 | 0.985 | 0.990 | 0.993 |
| 848 | 850 | 0.999 | 0.979 | 0.989 | 0.989 | 0.995 |
| 923 | 850 | 0.990 | 0.989 | 0.992 | 0.990 | 0.997 |
| 558 | 10800 | 0.926 | 0.962 | 0.936 | 0.941 | 0.954 |
| 673 | 10800 | 0.994 | 0.966 | 0.983 | 0.981 | 0.965 |
| 923 | 10800 | 0.987 | 0.979 | 0.988 | 0.984 | 0.988 |
| 1173 | 10800 | 0.991 | 0.983 | 0.991 | 0.988 | 0.992 |

[a]Average uncertainties on XRD, Microprobe and Combustion are ± 1.2%,1.5% and 0.4% respectively.

**Table II**
**Linear Rate Constants**

| T/K | $k_l$ ($10^{-9}$ cm/s) |
|---|---|
| 50 ppm $H_2S$ | |
| 558 | 0.44 ± 0.10 |
| 613 | 0.77 ± 0.08 |
| 643 | 0.05 ± 0.02 |
| 673 | 0.11 ± 0.09 |
| [a]*Activation Energy = 43 ± 19 kJ/mole,* [b]*Activation Energy = 130 ± 56 kJ/mole* | |
| 100 ppm $H_2S$ | |
| 558 | 0.11 ± 0.05 |
| 658 | 0.44 ± 0.03 |
| 723 | 0.86 ± 0.30 |
| [a]*Activation Energy = 61 ± 26 kJ/mole* | |
| 1,000 ppm $H_2S$ | |
| 673 | 9.3 ± 0.1 |
| 778 | 17 ± 1.2 |
| 848 | 21 ± 1.9 |
| 923 | 30 ± 3.2 |
| [a,c]*Activation Energy = 74 ± 32 kJ/mole* | |
| 10,000 ppm $H_2S$ | |
| 558 | 6.6 ± 0.58 |
| 673 | 4.4 ± 0.53 |
| [a,c]*Activation Energy = 92 ± 40 kJ/mole* | |

[a]Growth along a-axis
[b]Growth along c-axis
[c] Value calculated from parabolic rate constants

**Table III**
**Parabolic Rate Constants**

| T/K | $k_p$ ($10^{-11}$ cm²/s) |
|---|---|
| 1,000 ppm $H_2S$ | |
| 673 | 0.31 ± 0.03 |
| 778 | 0.45 ± 0.11 |
| 848 | 2.25 ± 0.25 |
| 923 | 2.99 ± 0.73 |
| [a]*Activation Energy = 74 ± 32 kJ/mole* | |
| 10,000 ppm $H_2S$ | |
| 558 | 0.34 ± 0.02 |
| 923 | 99 ± 25 |
| 1,173 | 414 ± 104 |
| [a]*Activation Energy = 92 ± 40 kJ/mole* | |

[a]Growth along a-axis

**Table IV Grain Lifetimes in the Nebula[a]**

| Radius (μm) | 700 K $10^{-3.77}$ bars | 600 K $10^{-4}$ bars | 500 K $10^{-4.27}$ bars | 400 K $10^{-4.59}$ bars |
|---|---|---|---|---|
| 0.1 | 5.47 | 6.10 | 6.96 | 8.21 |
| 1.0 | 6.47 | 7.10 | 7.96 | 9.21 |
| 10 | 7.47 | 8.10 | 8.96 | 10.21 |

[a]Lifetimes in $\log_{10}$ seconds. $10^{7.50}$ seconds per year.

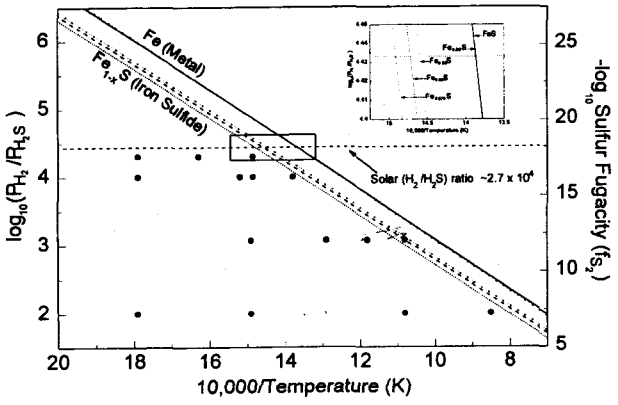


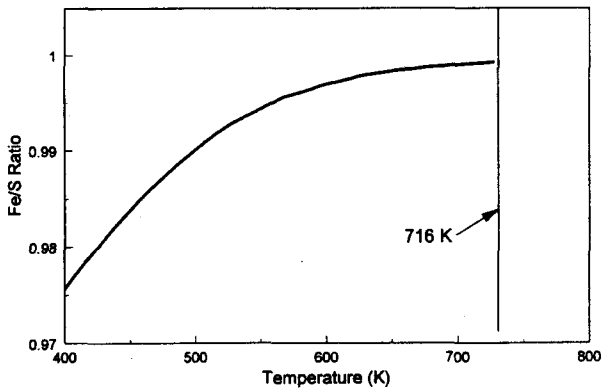


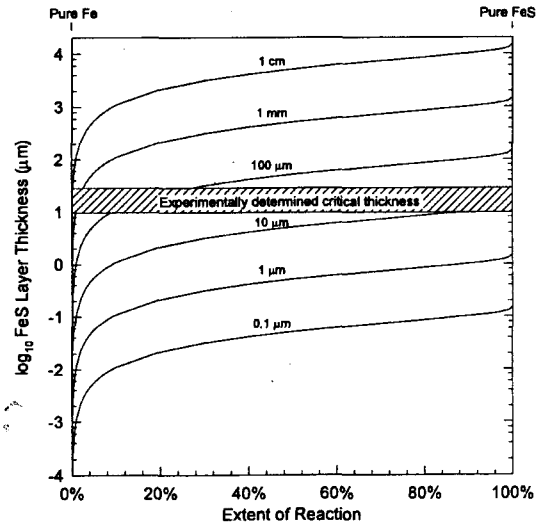


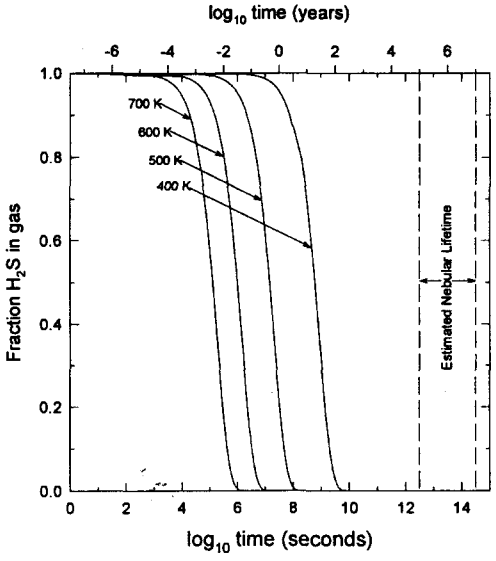


Figure 1 (top left) Fe sulfide condensation calculations and locations of 120 experimental runs (black dots). Figure 2 (top right) Fe sulfide stoichiometry as f(T) in the solar nebula. Figure 3 (bottom left) Thickness of sulfide rims on nebular Fe grains vs. critical rim thickness for parabolic kinetics. Figure 4 (bottom right) $H_2S$ chemical lifetime in the solar nebula.

# Finding of sector zoning in isolated olivine grains of ALH-77307 and Murchison

**Mitsuru FUDAKI and Masao KITAMURA**

Department of Geology and Mineralogy, Faculty of Science, Kyoto University, Sakyo Kyoto 606-01, Japan

Isolated olivine grains are commonly observed in carbonaceous chondrites. They have been considered to have formed by fragmentation of olivine grains in chondrules, because both types of olivine have the similar chemical composition, and because the isolated grains include glass with the composition similar to chondrule mesostasis [1,2]. On the other hand, some of the isolated olivine grain, which are in an euhedral shape and have Fe-poor composition are considered as a direct condensate from the nebula gas [3]. In the present study, we first found sector zoning in two isolated olivine grains in two carbonaceous chondrites (ALH-77307 and Murchison) under a cathodoluminescence (CL) microscope

An isolated olivine grain in the ALH-77307 meteorite (CM-CO) is almost homogeneous in a back-scattered electron image (Fig. 1a) but have sector zoning with different brightness in a CL image (Fig.1b). The zoning consists of two crystallographically different sectors and boundaries between the sectors are sharp and straight. One isolated olivine grain in the Murchison meteorite (CM) also has the same type of the sector zoning as that in ALH-77307 (Fig.2).

Crystallographical orientations of the sectors was estimated from the orientations of optical elastic axes. Since the grains found in thin sections, the orientations could not be determined uniquely. When we assume that these two grains have the faces common to both, the indices of growth surfaces of the sectors were estimated to be {130} and high index faces for the grain of ALH-77307 and {130} and {001} faces for Murchison. The sectors in bright in CL images were then indexed to be {130} sectors in both grains.

These two isolated olivine grains are almost pure forsterite (Fo99), and the compositional difference between the sectors are very small. Electron microprobe analyses with WDX system of the grains show that the {130} sectors are enriched slightly in $Al_2O_3$ than other sectors. The contents of FeO and $Cr_2O_3$ increase gradually from the core to the rim in both the grains. The Ca content in the grain of ALH-77307 decreases from the core to the rim, while that of Murchison

decreases once from the core and then increases to the rim. No differences in the Fe, Cr and Ca contents between the sectors were observed. Therefore, the distribution of $Al_2O_3$ is responsible for the sector zonings and the CL emission of the grains.

The sector zoning suggests the rapid growth of the isolated olivine grains. And straight sector boundaries further indicate no significant change of growth conditions during the formation of the grains. However, it is not conclusive whether these formed from vapor or liquid.

Reference:

[1] Richardson, S. M. and McSween, H. Y. (1978) *Earth. Planet. Sci. Lett.* 37 485-491.

[2] Jones, R. H. (1991) *Geochim. Cosmochim. Acta* 56, 467-482.

[3] Steele, I. M. (1989) *Geochim. Cosmochim. Acta* 53, 2069-2079.

Fig.1
Euhedral isolated olivine grain in ALH-77307 with sector zoning.
(a) Back-scattered electron image.

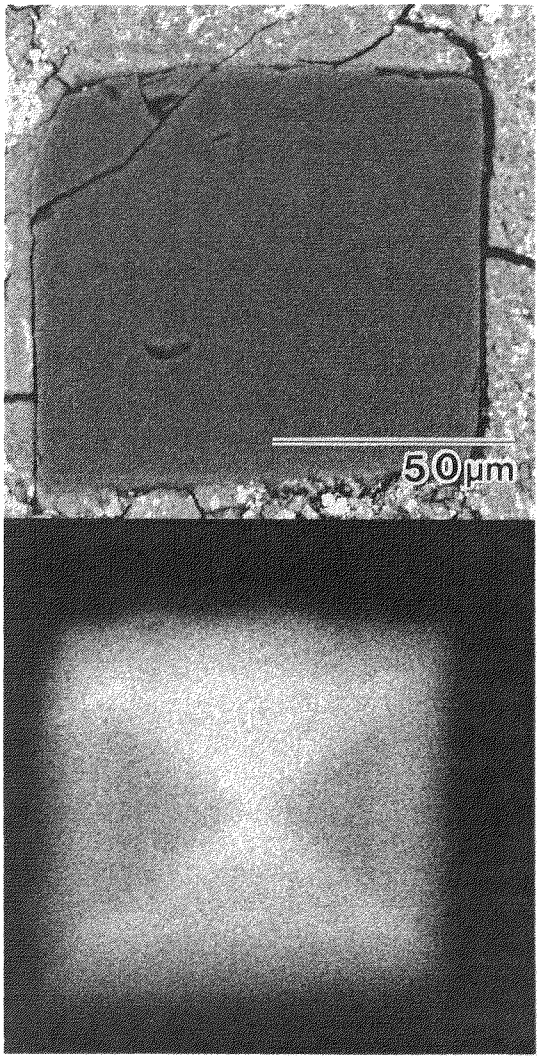


(b) CL image.

Fig.2
CL image of euhedral isolated olivine grain in Murchison with sector zoning.

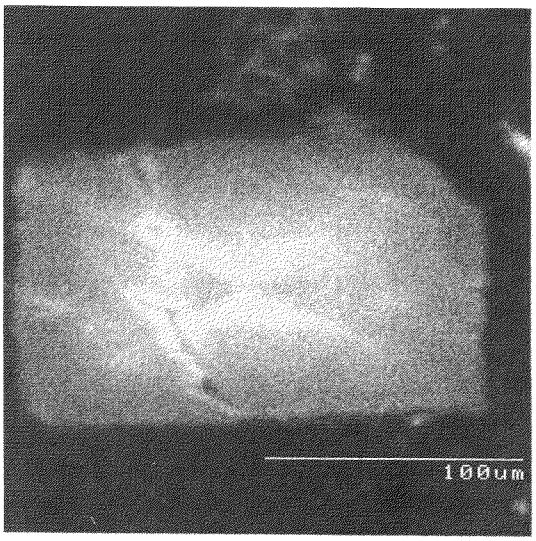

# COLLECTION OF YAMATO METEORITES BY THE 35TH JAPANESE ANTARCTIC RESEARCH EXPEDITION

M. FUNAKI[1] and N. ISHIKAWA[2]

1: *National Institute of Polar Research, 9-10 Kaga 1 Itabashi Tokyo 173*

2: *Kyoto University, Faculty of Integrated Human Studies, School of Earth Sciences, Nihonmatsu Yoshida Sakyou-ku Kyoto 606-01*

Four members of the 35th Japanese Antarctic Research Expedition visited the Yamato Mountains for paleomagnetic sampling from December 11, 1994 to December 24. A search for meteorites was carried out along the route of camp transfering and around the Camps 1 and 3 (Fig. 1). As survey area was located at leeward from a moraine belt and the Mountains, innumerable small terrestrial pebbles from 1 to 2 cm in diameter scattered on the ice field. Nevertheless, we found a total of 16 ordinary chondrites around Camp 1 (latitude 71°32'49"S, longitude 35°24'07"E). The biggest chondrite (Yamato-7403) was 263g in weight, while 13 chondrites were less than 10g in weight, as shown in Table 1. No meteorite was found along the routes and around the Camp 3.

Fusion crust was recognized in a part of the surface on Yamato-7401 to -7404, but it was removed completely from other chondrites. From the feature and color of their surface, these chondrites may be classified into the same group. The classification has been done by meteorite division in NIPR.

*Table 1. Yamato Meteorites collected by the 35th Japanese Antarctic Research Expedition.*

| Sample No. | Field No. | Dimension (cm) | Weight (g) | Remarks |
|---|---|---|---|---|
| Yamato-9401 | 94121901 | 3.3x2.8x2.6 | 42.966 | fusion crust |
| Yamato-9402 | 94122301 | 2.6x1.9x1.6 | 13.890 | fusion crust |
| Yamato-9403 | 94122302-1 | 6.3x5.5x4.3 | 263.13 | same chondrite fusion crust |
| Yamato-9404 | 94122302-2 | 3.0x2.8x1.1 | 6.750 | |
| Yamato-9405 | 94122303 | 2.5x1.7x0.9 | 4.830 | |
| Yamato-9406 | 94122304 | 1.4x1.3x0.9 | 2.546 | |
| Yamato-9407 | 94122305-1 | 2.0x2.0x1.8 | 9.155 | same chondrite |
| Yamato-9408 | 94122305-2 | 2.2x1.7x1.1 | 6.990 | |
| Yamato-9409 | 94122305-3 | 1.9x1.6x0.8 | 2.886 | |
| Yamato-9410 | 941223a-1 | 1.4x0.9x0.8 | 1.534 | same chondrite |
| Yamato-9411 | 941223a-2 | 1.8x0.9x1.0 | 1.840 | |
| Yamato-9412 | 941223a-3 | 1.3x0.9x0.9 | 1.833 | |
| Yamato-9413 | 941223a-4 | 1.2x0.9x0.5 | 0.843 | |
| Yamato-9414 | 941223b-1 | 1.9x1.4x0.9 | 2.939 | same chondrite |
| Yamato-9415 | 941223b-2 | 1.3x0.8x0.6 | 0.749 | |
| Yamato-9416 | 94122401 | 2.0x1.2x0.9 | 2.903 | |

*Fig. 1 Collected area of Yamato meteorites by the 35th Japanese Antarctic Research Expedition*

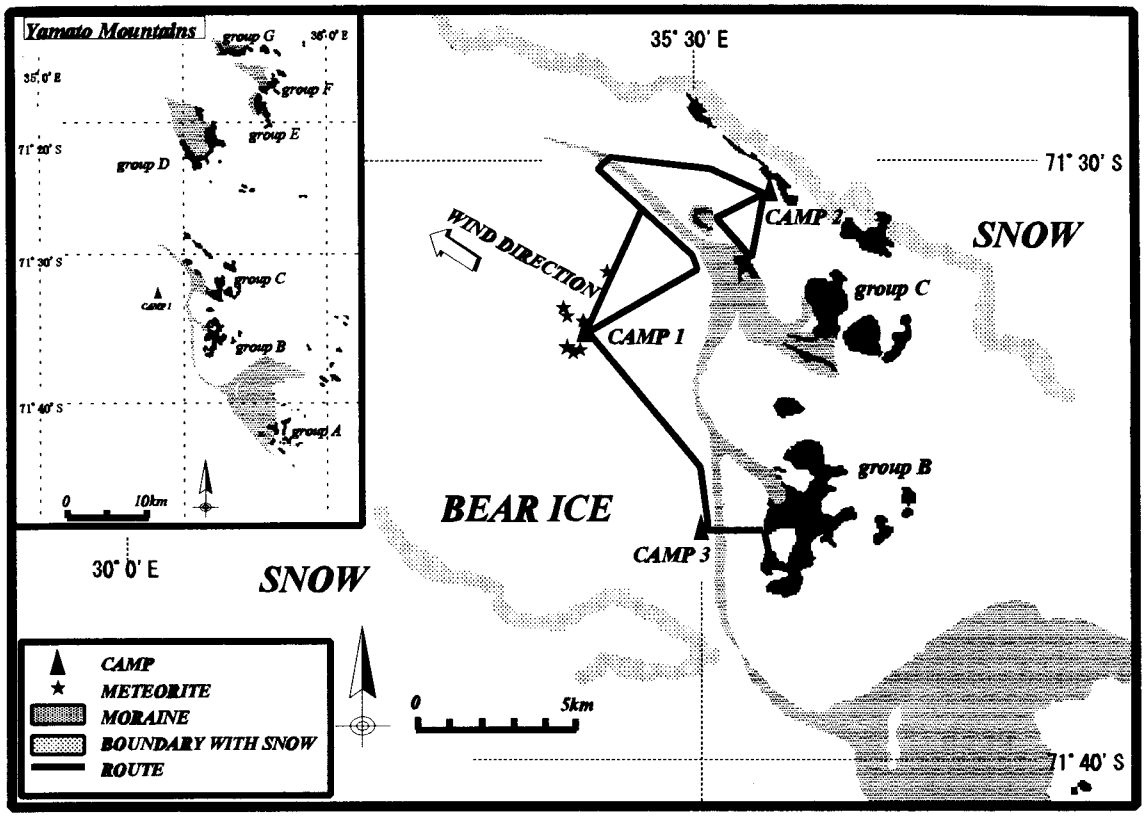

SEARCH FOR ICY METEORITES ON ANTARCTICA; T. Földi, Sz. Bérczi, /Eötvös University, Budapest, Hungary/, B. Lukács, /Central R. Inst. Physics, Hungarian Academy of Sci., Budapest, Hungary/.

Of the pieces from the three strongly different mineral belts / iron, stone, ice / of the Solar System, the third one has not yet been identified on the Earth because of their volatility. The most promisful place to find ice-meteorites would be Antarctica /Bérczi, Lukács, 1994./. To find ice-meteorites we have planned an electronic method. This method uses up the fact, that a considerable amount of ammonia-component should be contained by the ice-meteorite. Our electronic method should identify the ammonia-bearing ice-meteorites inside the ice-fields by frequency slipping.

Let us consider, that an ammonia-bearing ice-meteorite is a discontinuity in the yast ice-field of Antarctica. The complex analysis of the electric and magnetic field makes it possible to measure and determine the spatial and qualitative parameters of the discontinuity.

A practical solution to use up these principles in search of ice-meteorites is the following: we suggest to construct a solenoid /induction coil/ with a few hundred feet diameter. The induction given onto the solenoid would be an alternating current with frequencies between 1 - 1000 Hz. By digital controll an analyser could measure the time-delay of the signal-transitions on the zero electric potential.

By using the frequency method we can determine this time-delay with $10^{-7}$ accuracy. According to our calculations the time-delay by a discontinuity with 1 feet diameter would be $10^{-4}$ unit, so it would be 3 order of magnitude larger, than the estimated accuracy / $10^{-7}$ / of the method.

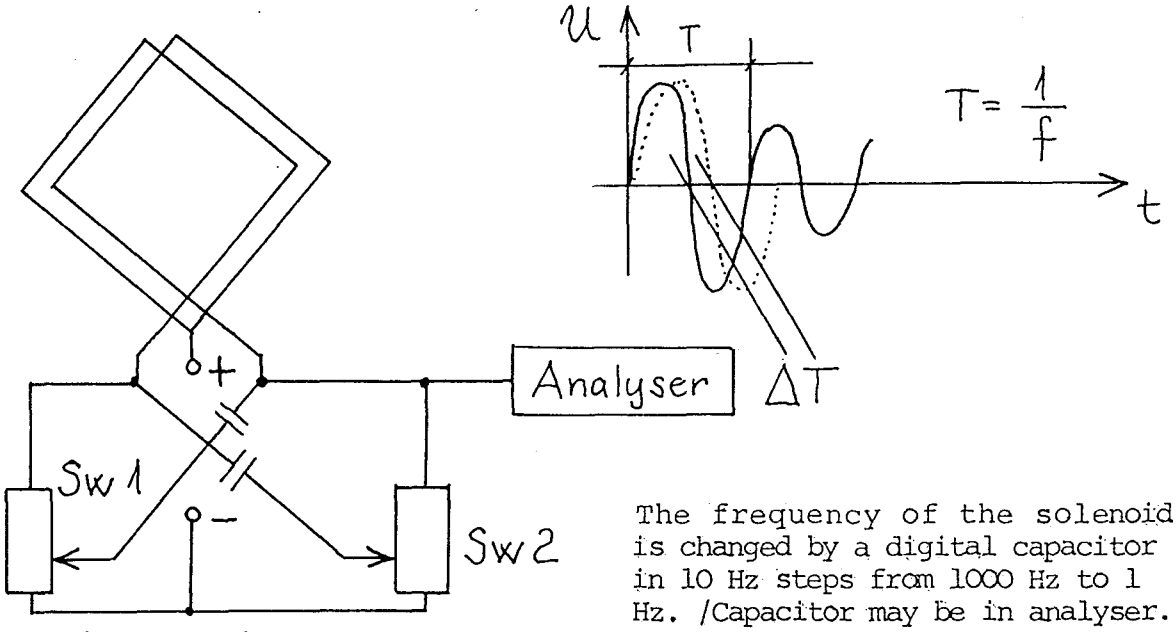


The frequency of the solenoid is changed by a digital capacitor in 10 Hz steps from 1000 Hz to 1 Hz. /Capacitor may be in analyser./

Ref: Bérczi, Lukács,/1994/: Icy Meteorites on Antarctica. 19th Symp. on Antarctic Meteorites. Tokyo, Proc.Vol. K.Yanai, Ed.

# CAN CARBON QUASICRYSTALS OCCUR IN METEORITES?

Gábor Gévay

Bolyai Institute, József Attila University,
Szeged, Aradi vértanúk tere 1, H-6720 Hungary

## 1. Introduction

The idea raised in this contribution stems from three independent sources. First, a series of empirical facts shows that *meteorites* convey information on special formation circumstances of matter. Secondly, the rapidly growing research activity throughout the world in the field of known and less known crystalline modifications of elemental carbon considerably widened our knowledge (for a brief review, cf. Ref. [1]). A natural part of this research is predictive modeling, i. e. constructing models of *hypothetical polymorphs* of carbon. Thirdly, a recently discovered class of solids, the *quasicrystals*, opened new directions of research in several disciplines for which crystallography is accounted a basic or auxiliary science.

In what follows we refer to all these three aspects in a reverse order, and support our suggestion for searching carbon quasicrystals in meteorites by giving a hypothetical structure model.

## 2. Briefly on quasicrystals

Quasicrystals are solids which exhibit long-range translational order and a non-crystallographic rotational symmetry. The translational order is manifested by the sharpness of the diffraction peaks, while the orientational order is manifested by their positions. Non-crystallographic (e. g. icosahedral, octagonal, decagonal and dodecagonal) symmetry can be observed not only in the diffraction pattern, but very often in the external morphologies of these samples studied by electron microscopy as well. (For an overview of the topic see e. g. Ref. [2] and the extensive bibliography therein.)

Quasicrystals are synthetic products prepared in laboratories all over the world, but they are expected to be found sooner or later among naturally occurring minerals as well [3, 6]. Another puzzling aspect, so to say, the absolute dominance of alloys among quasicrystals. Consequently, discovery of naturally occurring and non-metallic quasicrystals would possess twofold scientific value. In what follows a hypothetical model is presented to illustrate what the structure of a carbon quasicrystal would be.

## 3. Sketch of the model

Our model is based on the Penrose-Ammann-Mackay tiling approach to quasicrystals. This approach was applied in one of the first coherent explanation of the structure of quasicrystals by Levine and Steinhardt [2]. The tiling is a space-filling, quasiperiodic packing of two different unit cells, each representing a cluster of atoms. Quasiperiodicity is ensured by local matching rules and results in an orientational order of icosahedral symmetry. The shape of the two unit cells is a prolate and an oblate rhombohedron each bounded by rhombus faces of the same shape. In view from above a wrinkled layer of one unit cell yields the famous two-dimensional Penrose pattern (Fig. 1).

A crucial problem of modeling quasicrystal structures is "decoration" of the tiling, i. e. finding the proper position of atoms in the unit cells. Our decorating motif is a dodecahedrane skeleton, i. e. the carbon skeleton of a recently synthesized, hence existing saturated hydrocarbon $C_{20}H_{20}$ in which the carbon atoms sit in the vertices of a regular pentagonal dodecahedron (Fig. 2). 16 $C_{20}$ dodecahedra form a rhombus as in Fig. 3, which, in turn, form a face of the rhombohedral unit cells (Fig. 4). For further details, see Ref. [**3**]. We note that additional aspects of the model are treated in Ref. [4], where an alternative way of decoration is presented, namely such that yields a (hypothetical) *silicate* quasicrystal.

## 4. On the possibility of carbon quasicrystals in meteorites

It is a common experience that the life history of meteorites is abundant in events producing conditions to matter formation which are strange and unusual in comparison to the terrestrial conditions. One extreme example is the occurrence of stishovite in meteorite impact craters [3, 7], a mineral which is unique with its octahedral $Si - O$ coordination. This sharply contradicts the rule that the only allowed coordination

polyhedron for silicon and oxygen is tetrahedron. To confine to carbon, another surprising occurrence is lonsdaleite, the hexagonal polymorph of diamond, which has been found in meteorites almost simultaneously with its first laboratory production [1].

Study of shocked carbon materials is a current topic of this Symposium, too, cf. e. g. Refs. [7, 8]. In fact, there is a recent report on the occurrence of a quite new crystalline form of carbon obtained in shock compression experiments [9]. There are indications supporting the extraterrestrial occurrence of another exotic carbon modification, the buckminsterfullerene $C_{60}$. Shock experiments show that it tends to produce kerogen-like derivatives similar to those found in carbonaceous condrites [8]. However, it exhibits icosahedral (molecular) symmetry, and this might be a formative factor for spontaneous production of icosahedral carbon quasicrystals in meteorites, in suitable conditions. These few examples (the series of which would have been continued) [1]) show that our suggestion is supplied by a very general methodological principle of science: the analogy. At the time being, since our idea is hypothetical, we cannot put into action stronger principle. As for the instrumental side of searching, we repeatedly stress that the phenomenological characteristics of quasicrystals, the crystallographically forbidden symmetry tends to exhibit not only in the diffraction picture, but morphologically as well. Two of the eight theoretically possible simple "quasicrystal forms" have already been observed, but for a skilful and fortunate observer (electron microscopist) the possibilities (taking into account compound forms as well) are inexhaustible [10].

## References


1. Gévay, G. (1994), pp. 166-173 in: Evolution of extraterrestrial materials and structures , Eds. B. Lukács et al., Report KFKI-1994-22/C.
2. Gévay, G. and Szederkényi, T. (1987-1988) Acta Miner.-Petr. Szeged **29**, 5.
3. Gévay, G. (1990), Acta Miner.-Petr. Szeged **31**, 5.
4. Gévay, G. (1993), Phase Transitions **44**, 47.
5. Loreto, l. and Ronchetti, M. (Eds.) (1990), Topics on Contemporary Crystallography and Quasicrystals, Periodico di Mineralogia, **59** (special issue).
6. Jaric, M. V. (1990), pp. in [5].
7. Miura, T. (1994), Proc. NIPR Symp. Antarct. Meteorites, **19**, 122.
8. Murae et al. (1994), Proc. NIPR Symp. Antarct. Meteorites, **19**, 55.
9. Hirai, H. and Kondo, K. (1991), Proc. Japan Acad. **67**(B), 22.
10. Gévay, G. (1991), Icosahedral Morphology, in: Hargittai, I. (Ed.), Fivefold Symmetry, World Scientific, Singapore.

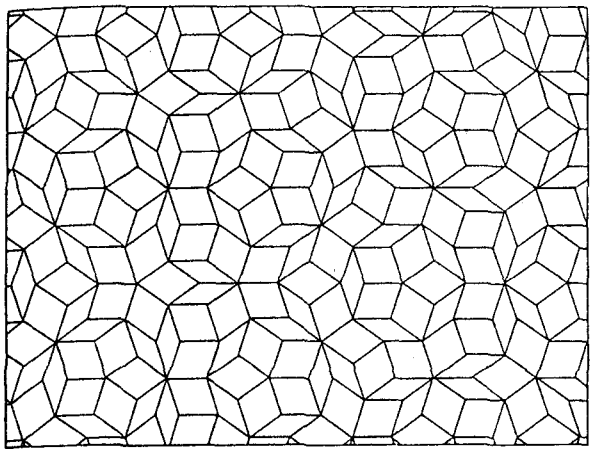

Fig. 1

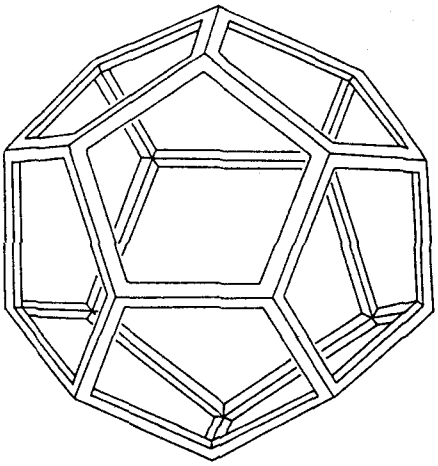

Fig. 2

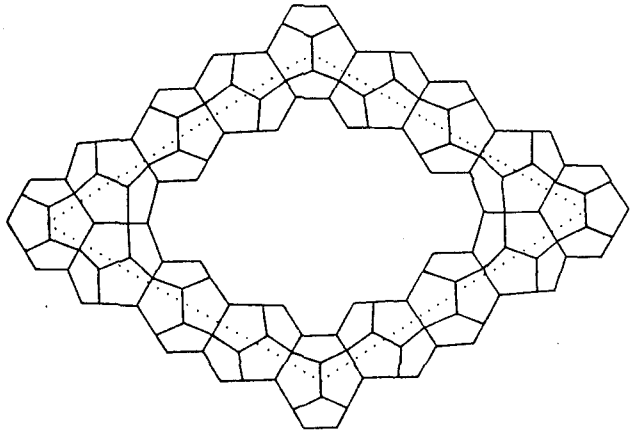

Fig. 3

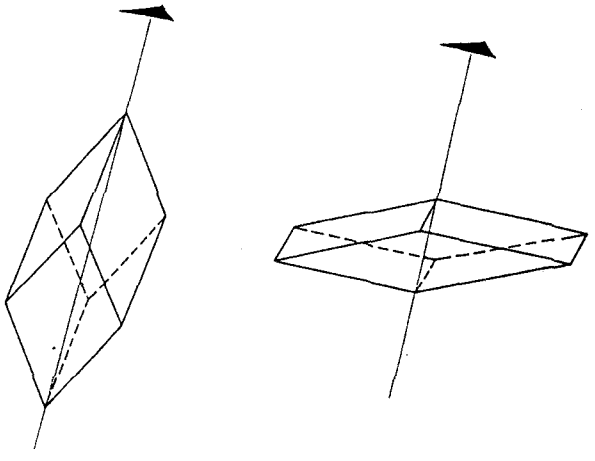


Fig. 4

**THERMAL METAMORPHISM OF THE C, G, B, AND F ASTEROIDS SEEN FROM THE 3-μm ABSORPTION BAND IN COMPARISON WITH CARBONACEOUS CHONDRITES.** Takahiro Hiroi[1], Carlé M. Pieters[1], Michael E. Zolensky[2], and Michael E. Lipschutz[3]. [1]Department of Geological Sciences, Brown University, Providence, RI 02912, USA, [2]SN2, NASA Johnson Space Center, Houston, TX 77058, USA, [3]Department of Chemistry, Purdue University, West Lafayette, IN 47907, USA.

**Introduction:** Possible thermal metamorphism on many of the C, G, B, and F asteroids were suggested by our former studies [1, 2] comparing their UV-Vis-NIR reflectance spectra with those of carbonaceous chondrites including unique CI/CM meteorites and experimentally-heated Murchison samples [3]. Although the UV absorption strength they used to estimate the degree of thermal metamorphism is valid to some extent, the 3-μm hydration band is important to estimate the total hydrogen content [4] which must be deeply related to the thermal history of the asteroids and meteorites. In this paper, we are comparing some of the C, G, B, and F asteroid reflectance spectra (0.3-3.6 μm) with those of carbonaceous chondrites.

**Experimental:** Heating experiment and mineralogy of Murchison samples and preparation of carbonaceous chondrite powders are described in [2, 3]. Bidirectional reflectance spectra (0.3-2.6 μm) of the samples were measured at 30° incidence and 0° emergence angles, and their biconical FT-IR reflectance spectra (1.8-26 μm) were also measured at 30° incidence and 30° emergence angles. These two spectral sets were connected at 2.5 μm. Reflectance spectra of the C, G, B, and F asteroids [5, 6, 7] were combined to cover the wide wavelength range of 0.3-3.6 μm, among which only five spectra were actually used in this study.

**Reflectance Spectra of Carbonaceous Chondrites:** Shown in Fig. 1 are reflectance spectra of selected carbonaceous chondrites. CI1 and CM2 meteorites all have a characteristic 3-μm hydration band at various strengths. Most of CM2 meteorites (Bells is unusual) also have 0.7, 0.9, and 1.1-μm bands due to ferric/ferrous Fe in septechlorites. The unusual CI/CM meteorites that have evidence of thermal metamorphism have no septechlorite feature around 0.7 μm but still have a 3-μm band weaker than those of CM2 meteorites. The shape of their 3-μm band is more round than those of unheated CM2 meteorites that have a steep triangular shape. The unusual CI/CM meteorites also have much weaker UV absorption than other carbonaceous chondrites. CK4 meteorite also have a weaker 3-μm band than those of CM2 meteorites. Allende is an example of meteorites that have little or no hydrated materials detectable from the 3-μm band.

Reflectance spectra of Murchison CM2 meteorite powder (<63 μm) and laboratory-heated ones are shown in Fig. 2. The 3-μm hydration band is gradually weakening up to 500°C and quickly gone around 600°C. Meantime the UV absorption strength continues to decrease toward 700 or 800°C and begins to increase again. The septechlorite bands around 0.7 μm are gone even before 400°C. The above trends of the laboratory-heated Murchison samples are the same as naturally-heated CI/CM meteorites except for their overall spectral profiles.

**Reflectance Spectra of the Selected Asteroids:** Shown in Fig. 3 are telescopic reflectance spectra of seven selected asteroids [5, 6, 7]. The 3-μm band shapes of the largest asteroids Ceres and Pallas are different from the others'. Ceres has a broad round 3-μm band and a sharp 3.1-μm band that can be due to water ice [7]. Pallas has a characteristic 3-μm band shape and a negative spectral inclination from 0.8 to 2.5 μm, which is unlike any carbonaceous chondrite powders. The other asteroids seem to have increasing 3-μm band strength as the IRAS diameter [8]

decreases, although there are many excluded asteroids from this study because of their poor spectral quality.

**Spectral Comparison Between the Asteroids and Meteorites:** As can be seen by comparing Fig. 1 and 3, most CI and CM meteorite powders tend to have too strong 3-μm band except for the thermally metamorphosed ones. None of the selected asteroids have both the 3-μm band strength and overall spectral profile as the common CI and CM meteorites studied here. Among the seven selected asteroids only three have a meteorite counterpart that has similar reflectance spectrum over the wavelength range from 0.3 to 3.6 μm. Their spectral matches are shown in Fig. 4. LEW90500 doesn't have exactly the same 3-μm band strength as 130 Elektra, but if it loses a little hydrated materials in some way, its 3-μm band and UV absorption will become weaker, making the spectrum more similar to the Elektra spectrum. Y82162 has a little different 3-μm band shape from that of 10 Hygiea, but their overall spectral profiles are similar. B7904 and 511 Davida are the closest of all. B7904 seems to have slightly stronger UV absorption and 3-μm band than Davida, but their overall spectral shapes are in an excellent match. Even their brightnesses (Davida 5.3% and B7904 5.1%) are close.

**Origins of CI/CM Meteorites and the C, G, B, and F Asteroids:** The fact that we have some carbonaceous chondrites that went through extensive aqueous alteration and subsequent thermal metamorphism suggests that there were their parent bodies that initially had water ice, were at adequate temperature for long enough a period to induce aqueous alteration, and were heated up to 600°C or so. The increasing 3-μm band strength as the asteroid size decreases for the studied asteroids except for Ceres and Pallas may be due to the more effective heating processes for the larger asteroids, although the differences in their initial water contents may have played an important role in the extent of aqueous alterations. Ceres may have been formed by accreting too much water ice (which may be why it's so big) to become heated enough to cause thermal alteration of hydrous materials and may still have water ice. If most of the larger asteroids were thermally altered, common CI and CM meteorites must have come from different population from the presently observed asteroids. CI/CM meteorites may have come from relatively smaller unobservable parent bodies or outer portions of larger asteroids, which were not heated enough to cause thermal alteration.

**Acknowledgments:** Antarctic meteorites were loaned from National Institute of Polar Research and Meteorite Working Group. Reflectance spectra of carbonaceous chondrites were measured at RELAB in Brown University. We thank S. F. Pratt for the measurements. RELAB is a multiuser facility operated under NASA grant NAGW-748. Asteroidal 3-μm reflectance spectra were taken from SOARD database. T. H. thanks Shane Jensen for assistance with SOARD. This research was supported in part by NASA grant NAG 9-48 to M. L. and the NASA Origins of Solar Systems Program to M. Z.

**References:** [1] Hiroi T. *et al.* (1993) *Science* **261**, 1016-1018. [2] Hiroi T. *et al.* (1994) *Proc. NIPR Symp. Antarct. Meteorites* **7**, 230-243. [3] Matza S. D. and Lipschutz M. E. (1977) *Proc. Lunar Sci. Conf.* **8**, 161-176. [4] Miyamoto M. and Zolensky M. E. (1994) *Meteoritics* **29**, 849-853. [5] Zellner B. *et al.* (1985) *Icarus* **61**, 355-416. [6] Bell J. F. *et al.* (1988) *Lunar Planet. Sci.* **19**, 57-58. [7] Jones T. D. *et al.* (1990) *Icarus* **88**, 172-192; Feierberg M. A. *et al.* (1980) *Icarus* **63**, 183-191; Lebofsky L. A. (1980) *Astron. J.* **85**, 573-585. [8] Tedesco E. F. (1989) *Asteroids II*, 1090-1138. [9] Tholen D. J. (1989) *Asteroids II*, 1139-1150.

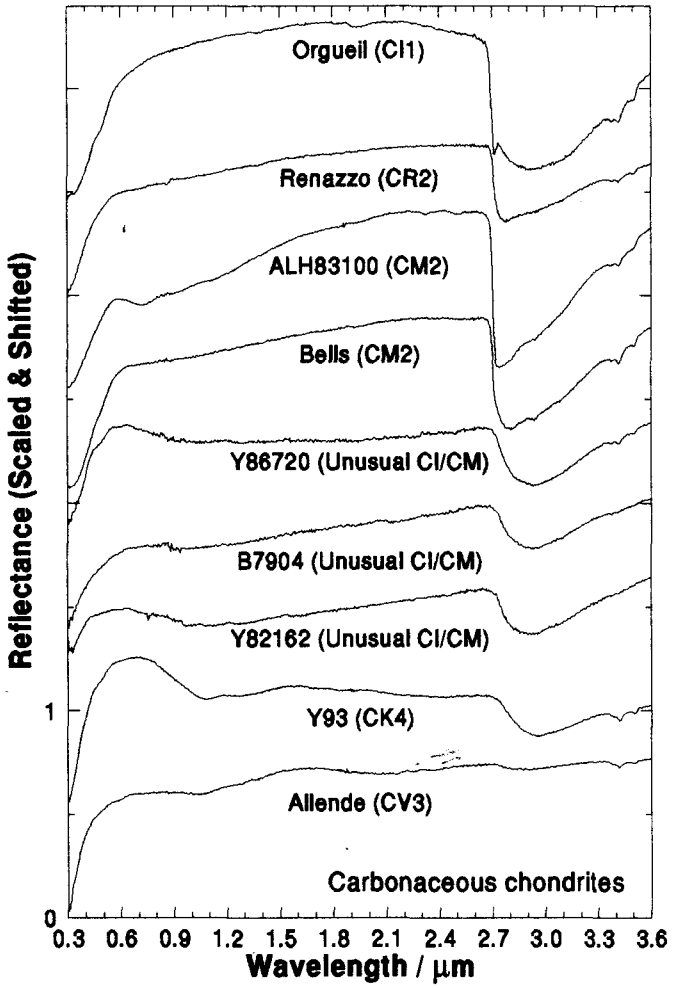


Fig. 1. Reflectance spectra of carbonaceous chondrite powders (<100 or <125 μm) selected from the 21 studied samples [1, 2]. All reflectance spectra are scaled to 1 at 1.95 μm and offset from one another for clarity.

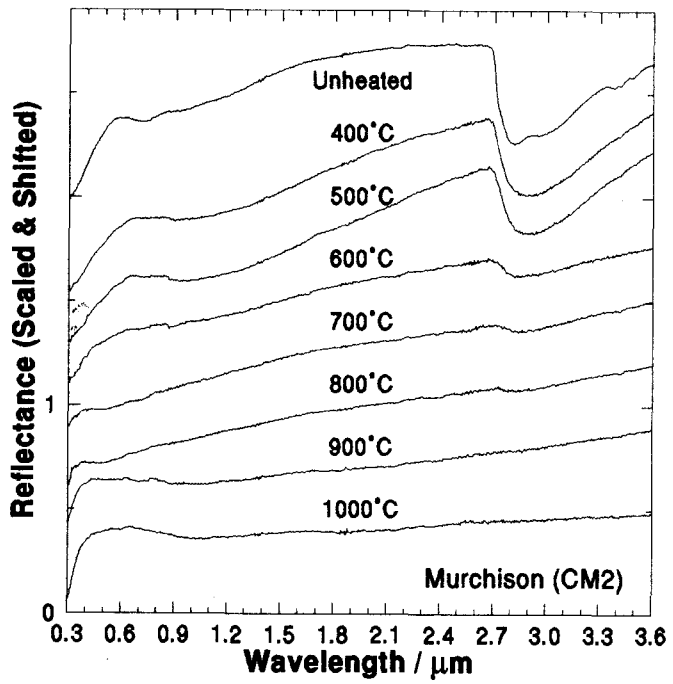


Fig. 2. Reflectance spectra of Murchison CM2 meteorite powder (<63 μm) and the laboratory-heated ones [1, 2, 3]. All the reflectance spectra are scaled to 1 at 1.95 μm and offset for clarity.

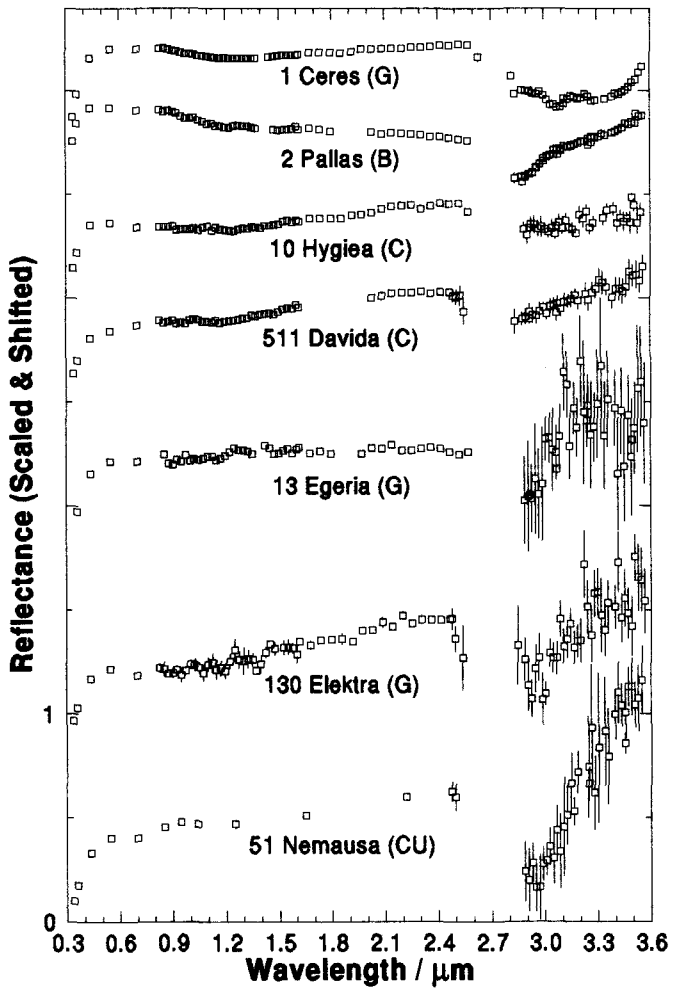


Fig. 3. Telescopic reflectance spectra of seven selected C, G, B, and F asteroids [5, 6, 7]. All reflectance spectra are scaled to 1 at 1.95 μm and offset from one another for clarity. The asteroid classes [9] are given in the parentheses. The asteroids were selected for their relatively high spectral quality around the 3-μm band. The asteroids are arranged in the order of decreasing IRAS diameter [8] from 1 Ceres to 51 Nemausa. Rapidly increasing reflectances beyond 3.4 μm of some asteroids may be due to incomplete removal of the asteroidal thermal emission spectra [7].

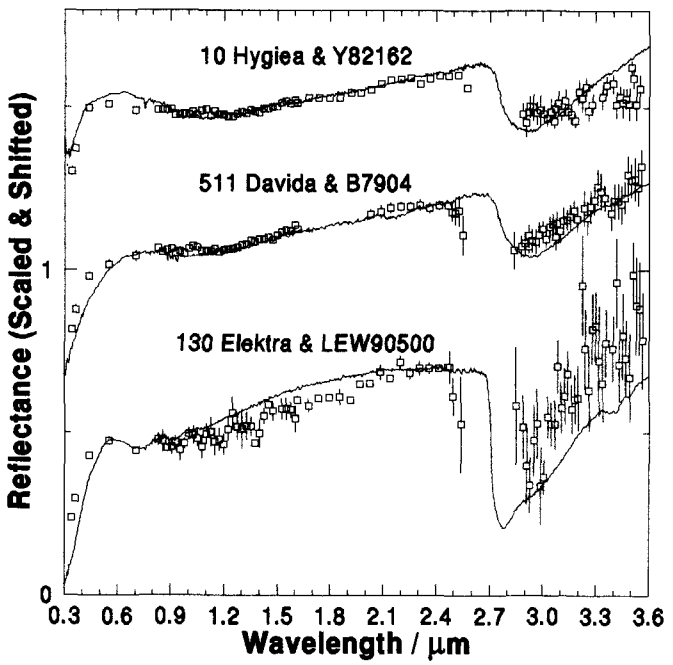


Fig. 4. Asteroid-meteorite counterparts that have similar reflectance spectral shapes. All the reflectance spectra are scaled to 1 at 2.37 μm and offset for clarity.

abstract for Symposium on Antarctic Meteorites, 1995

# MINOR COMPONENTS IN ANTARCTIC IRON METEORITES.

M. HONDA AND H. NAGAI

DEPARTMENT OF CHEMISTRY, COLLEGE OF HUMANITIES AND SCIENCES,
NIHON UNIVERSITY,
Sakura-josui, Setagaya-ku, Tokyo, 156

Some minor components have been determined in antarctic iron meteorites. They are trace elements distributed in the Fe-Ni alloys and cosmogenic stable and radioactive nuclides induced in space. Except for short-lived induced radio activities and terrestrial contaminations or alterations, most of all constituents are identical with non-antarctic irons.[B75,K80,C80,C82,N83,M84,W89] Because of smaller numbers of the population so far collected, any extensive statistcal discussion cannot be made for antarctic irons. A special problem accompanied with antartic meteorites is a judgement for possible pairings. The contents on minor components found in these samples collected will help us to solve the questions for an identification of the fall, or the terrestrial histories after the fall [KN84].

Some siderophile elements among minor elements commonly studied in irons are Ga, Ge and Ir besides Ni. Even for conventional classifications of irons some more extensive searches may be recommended to extend a scope of grouping. Our efforts must be directed to remove labels of so-called "AN" or "ungr" members. In these works various neutron activation methods have been employed conveniently. Based on current status of the achievements it seems necessary to extend our scopes for further developments in classifications of irons and better understanding of the history of irons According to this point of view, other modern techniques should also be employed. Very sensitive and convenient technique for Pb and Pb isotopes, for example, is required in some cases.

Among most refractory siderophile elements, Ir, Os and Re contents have been compared directly. These elements are known to be contained in a wide range, by 4 orders of the magnitudes, from 100ppm to 0.01 ppm for Ir. However their ratios are surprisingly constant throughout the whole range (Fig.1). Furthermore, a proportional relation holds even at primordial solar compositions.That is, solar abundance data provide us with 0.77 for $(Re/Ir)_{atom}$ Fig.1 illustrates a similar relation with a high reproducibility; according to irons data 0.102 , which is a 32% higher value for the same, seems to show a better fitting. Such a direct comparison may also be applied for Os.

Other examples of so-called lithophile elements can be found in Sc, Ti, V, Cr, and Mn, which are located near Fe. A typical example is Sc. Sc-45 is contained in irons as a stable cosmogenic product. Fig.2 illustrates a direct proportionality between Sc-45 and He-4 , just as expected by the nuclear systematics. On the other hand, GDMS, glow discharge mass-spectrometer, was also applied to determine the Sc contents, but with some back-ground. According to this blank, GDMS can only be applicable the contents higher than 0.1 ppbSc, whereas by a radiochemical NAA it seems possible to state that a limit of 0.001ppbSc or even lower blank can be drawn in irons generally.

Y791694 is a unique sample. As it was already reported in this 16th symposium,1991,this meteorite has an outstanding nature; the highest contents of Ni: 36%, Cu:2000ppm, In:140ppb, Sn: 60ppm, Sb: 2ppm, and Pb:0.8ppm , were found in this sample, which are more than 10 times higher relative to other irons in many cases [S93](Fig.3). On the other hand, according to the Sc-45 content, 0.088ppb Sc, and the correspondingly low He-4, 96E-8 cc/g, and higher values for Be-10 and Cl-36 contents, almost the saturated values in a medium size object in space, Y791694 must have the one of the shortest exposure age, 20 my, which is rather common among many L-chondrites but quite rare in irons (Table 1). Many irons are large and heavily shielded inside, the contents of cosmogenic stable products are low but the contents of radio-active nuclides are also correspondingly low, and long irradiation ages, some 100 - 1000my, are quite popular. We feel a serious difficulty to illustrate a whole history of this unique iron.

**Fig.1 relation of Ir and Re in irons.**

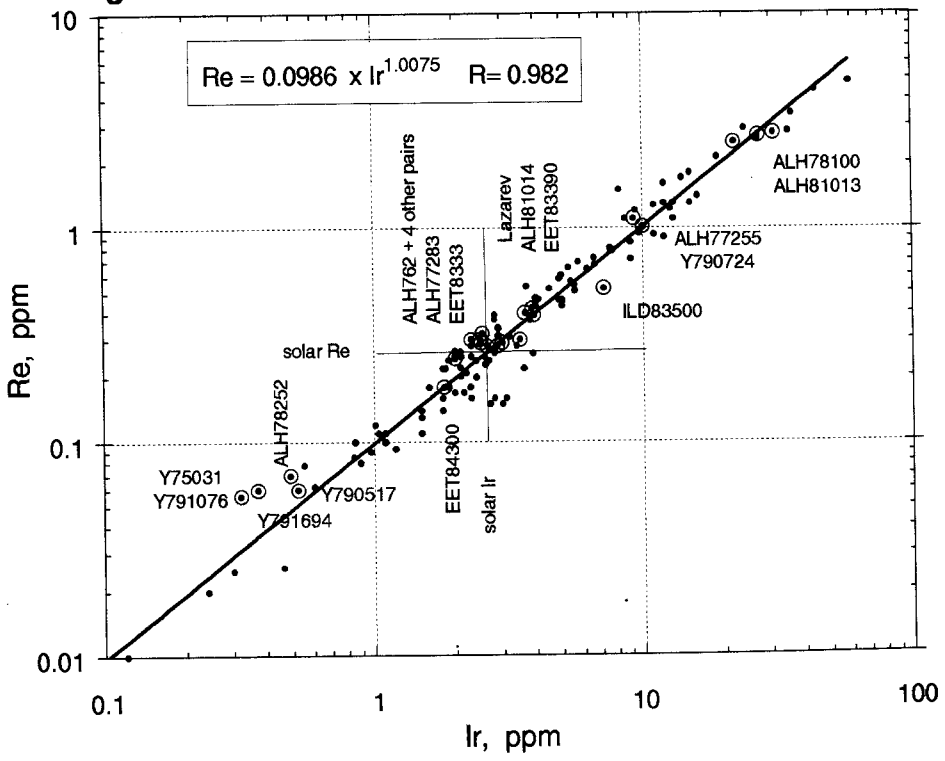

Fig.2. Sc-45 found in iron meteorites

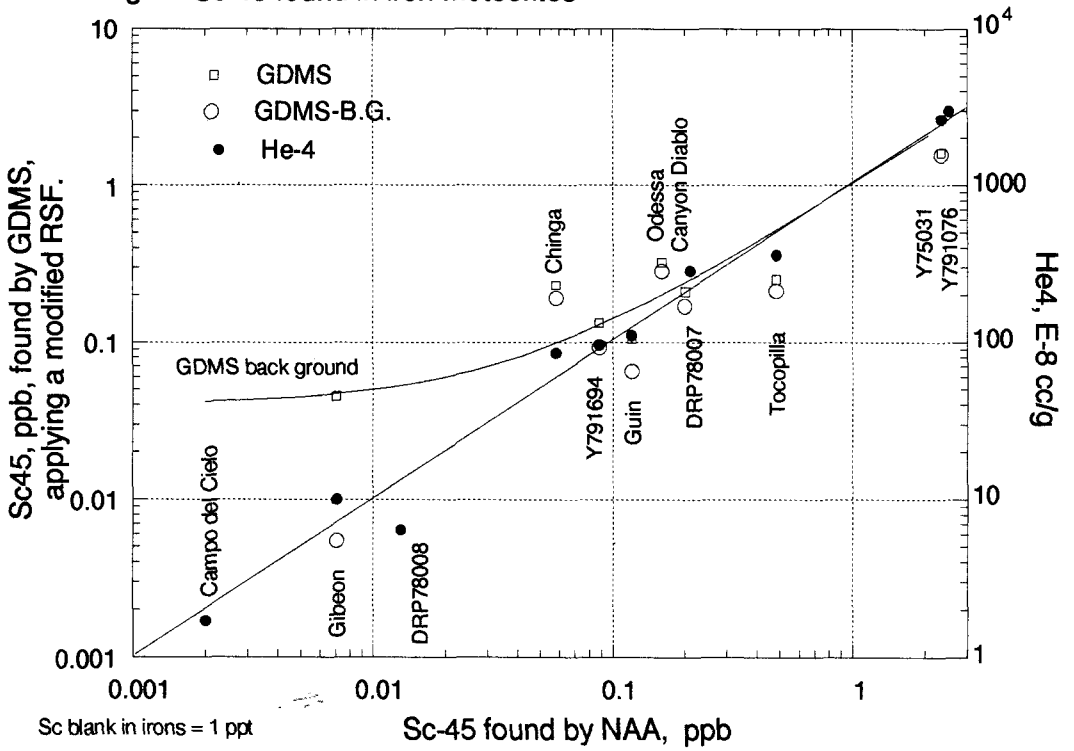


Fig.3. Gamma-ray spectra by INAA. (RSR 5min.in Cd, cool for 20min.)

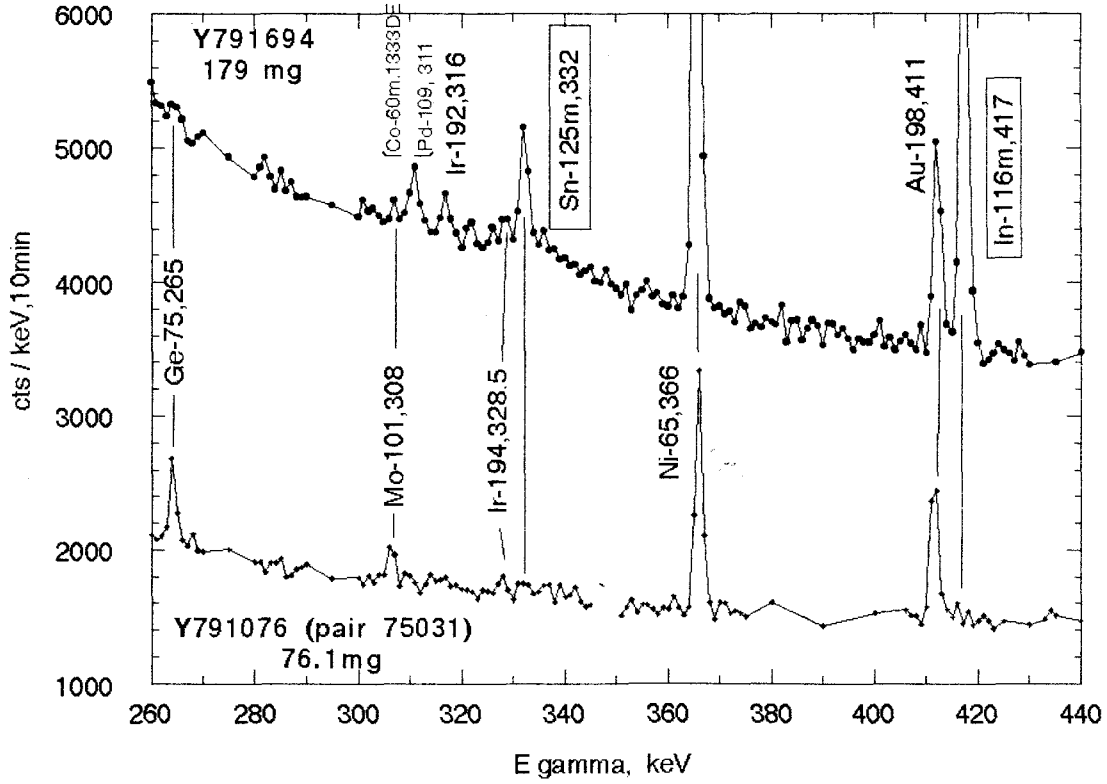

| sample | Sc45 | He4 | He3/ | He4/ | He3/ | Ref. | Mn53 | Cl36 | Al26 | Be10 | k2' | k1' | expos.age | terr.age |
|---|---|---|---|---|---|---|---|---|---|---|---|---|---|---|
| | ppb | E-8cc/g | /He4 | /Ne21 | /Ar38 | | dpm/kg | dpm/kg | dpm/kg | dpm/kg | | atom/m.g | xE8 y. | E3y, KN84 |
| ΔA' | 15, | 14, | 22/14 | 14/39 | 22/22 | | 7, | 24, | 34, | 22, | | | | |
| f | 1 | 18.3, | 16.7/18.3 | 18.3/ 1 | 16.7/ 1 | | 0.78, | 0.64, | 0.23, | 0.11 | | | | |
| Model# | 1.98 | 2157 | 0.28 | 263 | 16.7 | H85;N93 | 570 | 19 | 2.76 | 4.09 | 2.6 | 115 | 5 | |
| Y75031,Opl | 2.34 | 2630 | 0.31 | 258 | 15.1 | Nag83 | 474 | 18 | | 4.1 | 2.6 | 105 | 6.6 | [4.3 by Nag83] |
| Y791076,pair | 2.52 | 2990 | 0.27 | 350 | 24 | T87 | | 18 | | 4.11 | | | 6.9 | <70 |
| Y791694 | 0.088 | 96 | 0.217 | 310 | 18 | T87 | | | | | 2.7 | 130 | 0.25 | |
| Y791694 | | | | | | | | 20.6 | | 5.49 | 2.5 | 110 | 0.18 | <160 |
| ALH762, IA | 1.55 | | | | | | 556 | 14.1 | 2.4 | 3.8 | 2.7 | 122 | 4.3 # | 200 |
| ALH77283,IA | | 800 | 0.301 | 222 | 16.3 | Ott89 | 437 | 17.5 | | | 2.4 | 75 | 1.9 | 110 |
| ALH78100,IIA | 0.66 | | | | | | 437 | 23.2 | 3.98 | 5.31 | 2.2 | | 1.83 | short |
| ALH81013,pair | | | | | | | 488 | 21.4 | 3.61 | 5.09 | 2.4 | | | short |
| DRP78007,IIB | 0.21 | 285 | 0.25 | 490 | 22 | T87 | 143 | 0.486 | 0.229 | 0.597 | 2.9 | 65 | 2.58 | |
| DRP78008,pair | 0.013 | 6.4 | 0.22 | 670 | | T87 | 2.1 | 0.02 | 0.003 | 0.016 | 3.5 | 13 | [1.4] | |
| Ref. | H88 | T87:Takaoka N.,priv.comm.1987 | | | | | KN87; KN91 | | | | | | #: K40:564E10atm/g | |

#: calculated at center in a medium size irons, like Y75031, exposed for 500my. Production rate = f x k1'x (ΔA')^-k2', atom/min.g.


[Ref.]

Buchwald V.F.: Handbook of Iron Meteorites, (1975) pp1418,Univ.Calif.Press.[B75]

Kracher A. et al: Chemical classification of iron meteorites-IX.; Geochim. 44, 773 -787 (1980). [K80]

Clarke R.S. Jr. et al, Meteoritics 15, 273-274 (1980). [C80]; Clarke R.S. Jr. et al,Nature, 291, 396-398 (1981).

Clarke R.S.Jr., Meteoritics, 17, 129-134 (1982). [C82]

Wasson J.T.: The chemical classification of iron meteorites I. Geochim., 31, 161-180 (1967); Malvin D.J. et al., Geochim, 48, 785-804. (1984). [M84]; Wasson J.T. et al, Geochim. 53, 735-744 (1989). [W89]

Shimamura T., Takahashi T., Honda M. and Nagai H., 16th Symp. Antarctic Meteorites, 73-76 (1991).;

Shimamura T. et al.: J.Analyt.Atomic Spectrometry, 8, 453-460 (1993).[S93]

Nishiizumi K., Smithsonian Contributions to the Earth Sciences..No.26,105-109 (1984).[KN84]; Nishiizumi K. Nucl.Tracks Radiat.Meas., 13, No.4, 209-273(1987).[KN87]; Nishiizumi K., priv. commun. (1991-).[KN91]

Nagata T., Masuda A. and Taguchi I., Mem. Natl.Inst.Polar Res., 30, 237 (1983).[N83]; ibid, 41 287 (1986).

Nagao et al : Proc.8th Symp. Antarctic. Meteorites. 83-84 (1983). [Nag83]

Honda M.: EPSL, 75, 77(1985).[H85]; Nagai H.et al,Geochim. 57,3705-3723(1993).[N93]

Honda M. et al: NIPR symp.Antarct. meteor., 1, 197(1988).[H88]

Nitoh O. et al: Cosmogenic K-40 in Antarctic Meteorites.Mem.Natl.Inst.Pol.Res.Sp.Issue, 1, 189-201 (1980).

## A Dicussion on the origin of Antarctic Quasi-C1 chondrites and Their Cosmochemistry Signification

Hou Wei (Institute of Geochemistry, Academia Sinica, Guiyang 550002, PRC)

Through some papers on Antarctic chondrite, a few of Antarctic carbonaceous chondrites draw writers' attention. The common characters of these carbonaceous chondrites are that they all contain phyllosilicate aggregates, and chondrules which to be or not subjected to hydrous effect. The oxygen isotopic compositions of these carbonacous chondrites are similar to that of C1 chondrite. These carbonaceous chondrites are proposed to call as quasi-C1(Q-C1)chondreite by writers.The Table 1 shows the name, type, the forms of their phyllosilicate aggregates and references. The Fig.1 show the oxygen isotopic compositions of these Q-C1 chondrite, and it is seen that the oxygen isotopic compositions of whole rock and matrix of these Q-C1 chondrites are more similar to that of C1 chondrite. The major differences of Q-C1 chondrite from C1 chondrite are that the most Q-C1 chondrite contain some components related to chondrules, for example the chondrules, clasts of chondrule, and high-temperature condensated mineral aggregates(Table 2). The various contents of above components in every Q-C1chondrite, and large range of oxygen fugacity of these chondrules and mineral aggregates indicate that the conditions formed these Q-C1 chondrite were different from the C1 chondrite and other carboneaous chondrites.

Table 1. The Data of Some Antarctic Q-C1 chondrites

| Meteorite | The Forms of phyllosilicate | Type(reference) |
|---|---|---|
| Yamato(Y)-82162 | The matrix; a few of clasts and veins. | C1(1); CY or C1(5) |
| Yamato(Y)-86720 | The matrix; a few of clasts and chondrules. | CM(CY)(2);between the CM and CV(4); CB(6); CM or CI(5) |
| Belgica(B)-7904 | The matrix; some clasts and chondrules. | CM(CY)(3); CB(6);CM or CI(5) |
| PCA(P)-91082 | The clasts; a few of chondrules and matrix | CR(7) |
| Yamato(Y)-793495 | The clasts; a few of chondrules and matrix. | CR(7) |
| Yamato(Y)-8449 | The matrix; the edges of some chondrules | CR(8) |
| CR chondrite | The matrix and dark inclusions | CR(9) |

Table 2. The Chondrules and Other Components related to Chondrule in Q-C1 Chondrite

| Meteorite | Characters of the components related chondrule | Condition formed the chondrite based on oxygen fugacity |
|---|---|---|
| Y-82162 | The olivine aggregate(Fa=16-24%) may be clast of chondrule. | Similar to that of ordinary chondrite(O) |
| Y-86720 | The outlines of chondrules still are discernible, but the mineral in chondrules had become phyllosilicate aggregates. | Similar to that of CM chondrite |
| B-7904 | There are many chondrules in this meteorite. Some chondrules were not subjected to hydrous effect, in which the olivine grains still are fresh. | Similar to that of CM chondrite |
| P-91082<br>Y-793495 | The meteorites possessed chondrule structure, and many chondrules were subjected to hydrous effect and formed phyllosilicate aggregates or clasts. The positive relation between CaO and S in phyllosilicate clast indicates that before the hydrous effect occurred, the chondrules contained CaS. | Similar to that of enstatite chondrite(E) |
| Y-8449 | There are many types of chondrules in the meteorite and the Fa of olivine in chondrules is 2-8%. The enstatite and $SiO_2$ mineral have been observed | Similar to that of enstatite chondrite(E) |
| CR | There are more metal Fe-Ni(7 Vol%) in the chondrule, dark inclusion and matrix in these meteorite. The chondrules were subjected to various degree of hydrous effect, and the olivine and pyroxene prophyritic crystals still are observed. | Similar to that of ordinary chondrite(O) |

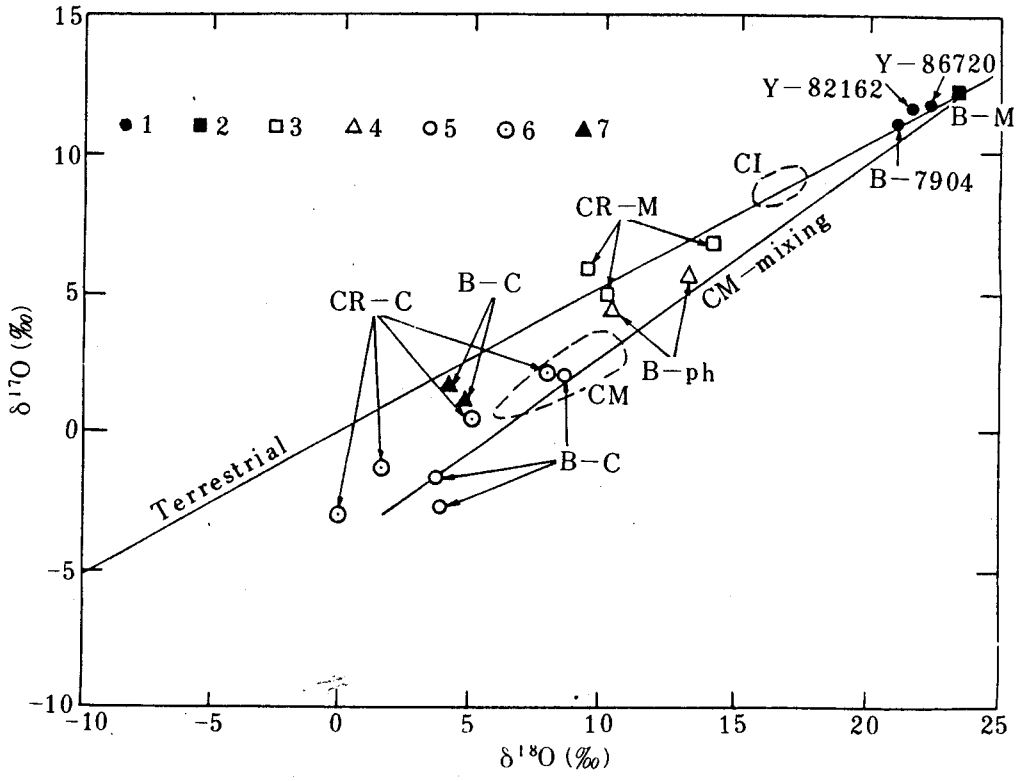


Fig.1 The oxygen isotopic composition of some Q-C1 chondrites (after Tomeoka K.,1990; Weisberg M. 1994)

1. the whole rock of Y-82162, Y-86720, and B-7904
2. B-M: matrix of B-7904
3. CR-M: matrix of CR
4. B-ph: phyllosilicate clasts of B-7904
5. B-C: chondrules of B-7904
6. CR-C: chondrules of CR type chondrites
7. B-O: olivine clasts of B-7904

It is known that the asteroid belt is source region of meteorite, so the chondrites were the results of nebular condensation of asteriod region of solar nebula. Based on above characters of composition and structure of Q-C1 chondrite, we think the Q-C1 chondrites are a new group of chondrite that formed in at the edge of nebular disk of asteriod region far from the equator of

nebular disk, where density of nebular was lower and the accretion process went on slowly, so after melting-drop and dust were subjected hydrous effect, the solidified melting-drops and dust accreted to Q-C1 chondrite bodys.If the asteriod region of solar nebular were divided to E region, O region and C region from near to far for sun, the Q-C1 chondrite must have been formed at in the edges of E,O,C region far from the quartor of nebular disk, but the E, O, C group chondrite formed nearer than Q-C1 chondrite from quartor.

Besides the water sphere on Earth, the track of liquid water had been observed on Mar, and recently scientist of U.S.A. found the ice lake on polar region of the Mercury. Therefore we think some hydrous planetesimals being similar to Q-C1 chondrite would form at the edge of terrestrial region of solar nebular disk during nebular condensation, but the oxygen fugacity of chondrules and other high temperature condensates in these planetsimals was much lower than E group chondrite.

**References:**

(1)Tomeoka K. et al., Proceedings of the NIPR on Antarctic Meteorites, 1989, 2, 36-54.
(2)Tomeoka K.et al., Proceedings of the chondrite NIPR on Antarctic Meteorites, 1989, 2, 55-74.
(3)Tomeoka K., Proceedings of the NIPR on Antarctic Meteorites, 1990, 3, 40-54.
(4)Yamamoto K. and N. Nakamura ,Proceedings of the NIPR on Antarctic Meteorites, 1990, 3, 69-79.
(5)Paul R.L and Lipschutz, Proceedings ofthe NIPR on Antarctic Meteorites, 1990, 3, 80-95.
(6)Prinz M. et al, Abstract of 52th Meeting of the Meteoritical Society,1989, 317-318.
(7)Noguchi T., Papers presented to the nineteenth symposium on Antarctic meteorites, 1994, 16-17.
(8)IchikawaO.andYIkeda, Papers presented to the nineteenth symposium on Antarctic meteorites, 1994, 18-19.
(9)Weisberg M., Papers presented to the nineteenth Symposium on Antarctic meteorites, 1994, 131-133.
(10)"美国天文学家发现水星上存在冰湖", 中国科学报, 国际科技版, 1994.7.15,5.

# URANIUN CONCENTRATION IN TWO H-GROUP CHONDRITES

Hu Ruiying, Xie Xiande and Guo Shilun*

Guangzhou Institute of Geochemistry, Academia Sinica, Guangzhou 510640, China
*China Institute of Atomic Energy, P.O.Box 275(96), Beijing 102413, China

## INTRODUCTION

The studies are focused on two well-known chondrites -the Yanzhuang H6(S6) and the Jilin H5(S3) chondrites. The Yanzhuang meteorite hit the ground at the Yanzhuang village, Wenyuan County of Guangdong Province in China on October 31, 1990. This meteorite is a rare one of its kind due to its heavily shocked features and thick veins made up of black molten materials. The shock pressure and shock-induced temperature are estimated as 80 Gpa and 1500℃. The Jilin chondrite has a thermal metamorphic temperature below or close to 800℃, and it experienced a moderate-grade shock metamorphism, e.g. two collision events at 10 Gpa and 300℃ and 20 Gpa and 500℃ respectively. In order to reveal the behavior of uraniun during shock and thermal metamorphisms of these two meteorites, we investigated the uraniun concentration in both Yanzhuang and Jilin meteorites by using fission track techniques and mapped their microscopic distribution of uraniun. Over 30 polished thin sections were examinated and olivine, pyroxene and other minerals were selected to measure their fission track densities under microscope. A summary of the results is presented in this paper.

## EXPERIMENTAL METHOD

Polished thin sections of the Yanzhuang were prepared and the uraniun concentration has been mapped by the fission track

technique for both the molten materials in shock melt veins and the unmelted chondritic host. For comparison, a Jilin meteorite specimen was split into pieces which weigh around 10g each. Each sample was put into porcelain crucible, and then was heated by thermocouple pyrometric furnace for 60 minutes at the temperature ranging from 700 to 1300℃, and then annealed slowly. Each heated sample was made into more than 2 polished thin sections for the purpose of minimizing statistic derivation. The observed dimension of each polished thin section was about 1 square centimeter. Heated up to 1000℃, chondrule texture in Jilin meteorite become obscured, and at 1280℃ the meteorite become molten. Uranium concentration and microscopic distribution have been obtained by counting tracks of induced fissions of $^{235}U$ in the meteorites. The thermal neutron fluence was $1.14\pm0.06\times10^{8}n\cdot cm^{-2}$, and the standard glass $\rho i$ is $170\pm 4.74\times10^{4}cm^{-2}$.

## RESULTS

The results of measurements for the Yanzhuang and the Jilin chondrites are listed in Table 1 and Table 2.

Table 1 Uranium Concentration of Yanzhuang chondrite

| No. of Samples | Regions | U Concentration(ppb) |
|---|---|---|
| 91-9(1)W | Whole rock | 13.53±0.17 |
| 91-9(1)C | Chondritic host | 12.61±0.29 |
| 91-9(2)C | 〃 | 13.15±0.29 |
| 91-9(3)C | 〃 | 15.78±0.32 |
| 91-9(1)M | Melt Vein | 25.18±0.92 |
| 91-9(2)M | 〃 | 36.59±0.99 |
| 91-9(3)M | 〃 | 28.33±0.87 |

Table 2 Uranium Concentration of Natural and Heated Samples of Jilin Chondrite

| No. of Samples | Heating Temperature (℃) | Heating Time (min) | Features | U Concentration(ppb) | |
|---|---|---|---|---|---|
| | | | | Chondrule | Whole rock |
| 91-7 | Unheated | — | — | 6.74±0.83 | 12.59±0.21 |
| 91-1 | 700 | 60 | no change | 5.52±0.68 | 14.39±0.21 |
| 91-2 | 800 | 60 | 〃 | 4.12±0.65 | 15.18±0.23 |
| 91-3 | 900 | 60 | 〃 | 2.97±0.42 | 13.39±0.28 |
| 91-4 | 1000 | 60 | condrule texture obscured | — | 14.43±0.31 |
| 91-5 | 1100 | 60 | 〃 | — | 12.83±0.18 |
| 91-6 | 1280 | 60 | molten | — | 12.52±0.24 |

## DISCUSSION AND CONCLUSION

(1) Uranium concentration is about 14 ppb for Yanzhuang H6 chondrite and about 13 ppb for Jilin H5 chondrite. This implies that H-group chondrites may have similar uranium concentration.

(2) Uranium concentration of black melt veins in Yanzhuang varies from 25 to 37 ppb while that of grey chondritic host ranges from 13 to 16 ppb, although their bulk chemical compositions are very similar. The fission track density of black melt veins increases greatly compared with that of chondritic host. From this fact we may deduce that shock-induced temperature led the melting of some chondritic mass, and at the same time caused the migration of uranium from chondritic host to the molten materials.

(3) Uranium concentration of Jilin chondrite was determained for both natural and heated samples. It varies within a narrow range, from 12.5 to 15 ppb, eventhough the heating temperature reached as high as 1280℃.

(4) Uranium concentration of chondrules in Jilin chondrite

decreases with the increasing heating temperature, namely from 6.74 ppb for the natural unheated condrule sample to 2.97 ppb for condrule heated at 900℃. The reason is that uranium beingan active element is easy to diffues from inside to outside of chondrules upon hesting. We define this phenomenun as self-purification process. Although the uranium content in condrules decreases with increasing temperature, the total uranium concentration in whole rocks (condrules + matrix) remains unchanged.

## REFERENCE

1. Wang Daode et al., 1993. An introduction to chinese Meteorites. Science Press, Beijing.

2. Hu Ruiying and Klans Thiel, 1986. Chinese Journal of Geochemistry. Vol. 5, No. 4, p. 375-383.

3. Xie Xiande and Huang Wankang, 1991, Chinese Journal of Geochemistry. Vol. 10, No. 2, p. 109-119.

4. Xie Xiande et al., 1994. Chinese Journal of Geochemistry. Vol. 13, No. 1, p. 39-46.

# Mineralogy of glassy clasts in lunar meteorite Yamato-791197

Osamu ICHIKAWA
Department of Polar Science, The Graduate University for Advanced Studies,
National Institute of Polar Research, 1-9-10 Kaga, Itabashiku, Tokyo, 173, Japan

**Introduction** Yamato-791197 (Y-791197) was first studied by YANAI and KOJIMA (1984). The authors concluded that Y-791197 was a regolith breccia from the moon. After the first study, consortium study on the Y-791197 have been conducted, and many results were reported; such as, Y-791197 represents lunar highland crust, Y-791197 are similar to Allan Hills A81005 and both are probably derived from the far-side of the moon. I have done petrographic study of Y-791197 by microscope and an electron microprobe analyzer (EPMA). Some glassy clasts were found in this meteorite. Here I report chemical features of these glassy clasts.

**Glassy clasts in Y-791197** These clasts are classified into three types: brownish glassy clast of which color is brown under the microscope and chemical compositions are similar to those of pyroxene; zoned glassy clast has devitrified mantle; main glassy clasts (including clasts with remaining plagioclase and/or pyroxene crystals) that are glassy clasts except brownish and zoned glassy clast.

The Si-Mg-Fe and Ca-(Mg+Fe)-Al diagrams show that Si and Al contents decrease in the following order; main glassy clasts, zoned glassy clasts, and brownish glassy clast (Fig. 1). All glassy clasts in Y-791197 are different in chemical composition from Apollo 15 and 16 glasses of DELANO J.W. (1980). Brownish glassy clast have similar chemical composition to very low Ti basalt of mare basalt.

The main glassy clasts in Y-791197 coincide in chemical composition with those of the soil samples of Apollo 16 among them of Apollo 14, 15, 16, and 17. This result agrees with other investigations (e.g. OSTERTAG *et al.*, 1986; TAKEDA *et al.*, 1986).

References Yanai K. and Kojima H. (1984). Mem. Nalt Inst. Polar Res., Spec. Issue, 35, 18-34. Delano J.W. (1980). Proc. Lunar Planet. Sci. Conf. 11th, P251-288. Ostertag R. et al. (1986). Mem. Nalt Inst. Polar Res., Spec. Issue, 41, 17-44. Takeda H. et al. (1986). Nalt Inst. Polar Res., Spec. Issue, 41, 45-57.

## *Glass of Yamato-791197*

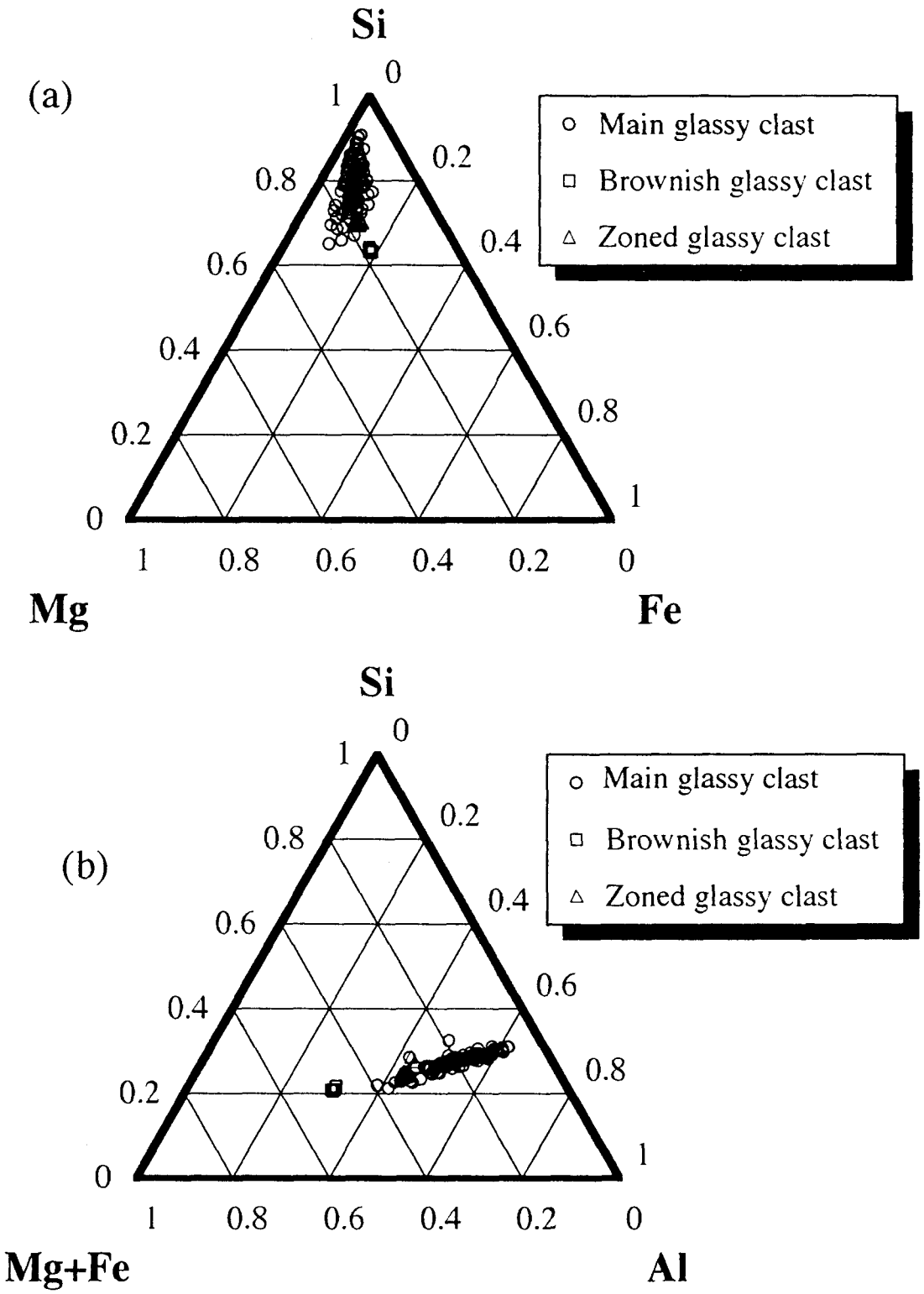


Figure 1. Atomic plot of Si-Mg-Fe ratios (a) and Ca-(Mg+Fe)-Al ratios (b) of Y-791197.

# PETROLOGY OF THE MILES IIE IRON WITH SILICATE INCLUSIONS; RELATIONSHIP TO H CHONDRITES AND PRIMITIVE ACHONDRITES

Yukio IKEDA[1] and Martin PRINZ[2]

[1]Dept. of Earth Sciences, Ibaraki University, Mito 310, Japan

[2]Dept. of Earth and Planetary Sciences, Amer.Mus.Nat.Hist., New York, NY 10024, USA.

Since IIE irons have oxygen isotopic compositions similar to those of H chondrites and H-type primitive achondrites (Y-74359 and Y-74360) (Rubin et al., 1986; Mayeda and Clayton, 1989), they may have an intimate genetic relationship. Miles is a new IIE iron (from Australia) with silicate inclusions, and we carried out a petrologic study on the silicate inclusions in comparison with H-type primitive achondrites (Ikeda et al., 1991) and equilibrated H chondrites.

The Miles inclusions are 2-10 mm in size with round, ellipsoidal, and irregular outlines. Crystallinity of the silicate inclusions is variable; most of them are coarse-grained and gabbroic, but some are cryptocrystalline. The constituent minerals are high-Ca pyroxene, orthopyroxene, inverted pigeonite, plagioclase, antiperthite, K feldspar, tridymite, granitic glass, sodalite, olivine, chromite, rutile, merrillite, Cl-apatite, kamacite, taenite, schreibersite, troilite, and pentlandite. High-Ca pyroxene, orthopyroxene, and plagioclase are the major phases in gabbroic inclusions, and their sizes are 0.5-5 mm across. The modal compositions of clinopyroxene,

orthopyroxene (including inverted pigeonite), and plagioclase are highly variable and average about 34, 17, and 47 vol%, respectively. The other phases are accessory with sizes smaller than 0.5 mm.

High-Ca pyroxene, $En_{45-50}Fs_{8-12}Wo_{40-45}$, is similar in composition to that in H-type chondrites and primitive achondrites, and has fine exsolution lamellae, less than 2 micrometers wide, spaced about 10 micrometers apart. Most of orthopyroxene has a composition of $En_{75-78}Fs_{19-23}Wo_{1-4}$ slightly more ferroan than that of H chondrites and primitive achondrites. Inverted pigeonite grains are sometimes included in large high-Ca pyroxene or orthopyroxene grains, and has a lamellar texture consisting of orthopyroxene host and high-Ca pyroxene lamellae, several microns wide, spaced about 25 micrometers apart. Plagioclase has a wide compositional range, $An_{1-13}Ab_{83-97}Or_{1-5}$, with normal zoning from calcic cores to sodic rims, and spans the whole range of plagioclases in H chondrites and primitive achondrites. Graphic intergrowths of tridymite and antiperthite occurs, and the antiperthite has a bulk composition of $An_{0-1}Ab_{60-74}Or_{25-40}$. K feldspar grains, $An_{0-1}Ab_{5-11}Or_{88-94}$, are intimately associated with the antiperthite. Granitic glass occurs rarely at pyroxene grain boundaries or as small inclusions in apatite, and has a compositional range from 70-80 wt% $SiO_2$, 11-15 wt% $Al_2O_3$, 6-8 wt% $K_2O$, and 1.5-4 wt% $Na_2O$ Chromite is richer in $Cr_2O_3$ and $TiO_2$ than that in H chondrites and primitive achondrites. Sodalite and magnesian olivine ($Fo_{95-96}$) occur as small grains in merrillite-predominant portions of a cryptocrystalline silicate inclusion. Metal is similar in composition to the host metal. Kamacite is predominant and has 3-7 wt% Ni and 0.4-0.7 wt% Co, very similar to that in H chondrites and primitive

achondrites. Taenite is minor and has M-shaped patterns, with Ni-poor cores and Ni-rich rims, ranging from 19-51 wt% Ni and 0.1-0.5 wt% Co. Schreibersite contains 29-40 wt% Ni and 0.25-0.5 wt% Co, and pentlandite has 35 wt% Ni and 0.25 wt% Co.

A shock event is clearly recorded in the Miles silicate inclusions; pyroxene and plagioclase are remarkably fractured, and most of the fractures are filled with limonitic material. However, the dendritic metal-schreibersite melt pockets found in the Watson IIE iron (Olsen et al., 1994) are not observed in the Miles host metal.

The existence of sodalite and magnesian olivine in a cryptocrystalline inclusion and the common occurrence of tridymite in most of gabbroic inclusions indicate that the Miles inclusions were not in equilibrium with each other. However, since the mineral compositions of the Miles silicate inclusions are very similar to those of H chondrites and primitive achondrites, they appear to be cogenetic with them. H-type primitive achondrites are nearly metal-sulfide-free, and were derived from an H chondritic silicate melt (Ikeda et al., 1991). In contrast with them, most of the Miles silicate inclusions are olivine-free, and thus are the result of fractionation from this melt, or formed by crystallization from a feldspar-pyroxene melt produced by a low degree of partial melting of an H chondrite parent. The latter is the more likely scenario.

References: Ikeda Y. et al. (1991) Petrological and geochemical study of the Yamato-74359 and Yamato-74360 achondrites, Proc. NIPR Symp. Antarct. Meteorites, No.4, 131-143. Mayeda T. K. et al. (1989) Oxygen isotopic compositions of unique Antarctic meteorites, 14th NIPR Symp. Antarct. meteorites. Olsen E. et al. (1994) Watson: A new link in the IIE iron chain, Meteoritics 29, 200-213. Rubin A. E. et al. (1986) Properties of the Guin ungrouped iron meteorite: the origin of Guin and of group-IIE irons, Earth Planet. Sci. Lett. 76, 209-226.

# ON TWO DIFFERENT POPULATIONS OF COMETARY SUB-NUCLEI

**E. Illés-Almár**
**Konkoly Observatory, H-1525 Budapest, Box 67, Hungary**

It was supposed earlier that cometary nuclei may essentially be an aggregate of sub-nuclei [1]. Four independent observational facts point to the possibility that there are at least two populations of sub-nuclei, and they are mixed in the nucleus of a comet. One kind may be a loose aggregate of fluffy material (accumulated perhaps in the giant molecular cloud stage of the solar nebula), while the other is more compact and cohesive (accumulated perhaps in a later stage and nearer to the Sun after it had flamed up).

After investigating the comet Halley by an armada of spacecrafts in 1986, the scientific community realised with astonishment that its surface is not uniformly active [2]. There were dust jets originating from rather small parts – not more than 2-3% – of the whole surface. Moreover, "for many comets the morphology of their jets seems to remain similar over several apparitions suggesting that the same active sites are responsible for dust emission over many orbits" [3].

In 1994 awaiting the catastrophic encounter of comet Shoemaker-Levy 9 with Jupiter numerous observations of the chain of cometary nuclei have been carried out. The consecutive HST images demonstrated on the one hand that some of the disintegrated cometary fragments or sub-nuclei drifted off from the main trajectory [4], and interestingly enough later at the impact even those have caused a much smaller effect in the Jovian atmosphere (fragments B,T,F, P2,U); all the others produced more conspicuous effects. On the other hand although the brightness of some of the sub-comets were similar as they approached Jupiter, newertheless, the impact of the corresponding fragments produced very different effects in the Jovian atmosphere. For example the sub-comet of fragment B was as bright as that of A or C, but fragment B has left only an insignificant black spot in Jupiter's atmosphere, on the contrary to A which produced a very large effect [5].

The outgassing of a loose sub-nucleus can be more intense than that of a compact one. In the case of comet Halley the more active parts of the nucleus may be the places where loose sub-nuclei are present on the surface, while the least active parts are those, where the compact ones are exposed to the heating. So the dual character of the surface can be explained by the existence of this two kinds of sub-nuclei.

The same cosmogonical dichotomy can explain the behaviour of comet Shoemaker-Levy 9 as well. After the disintegration of the cometary nucleus a looser sub-nucleus could develop a denser and larger coma than a compact one. So a sub-comet originating from a looser and smaller sub-nucleus can be just as bright as that originating from a larger but more compact fragment. Arriving into the Jovian atmosphere with the same velocity the looser sub-nucleus, however, will disintergrate high in the atmosphere, while the compact one penetrates deep and causes a much larger explosion. On the other hand, as the outgassing of a loose sub-nucleus is more efficient, it can be pushed away by the rocket propulsion of the escaping gases. That can be the reason why those fragments drifted farther from the path of the orbit produced smaller effects plunging into the atmosphere.

**References:**


1. Weissman, P., Nature 370, p. 94, 14. July 1994.
2. Keller, H.U. Paper B.6-M.2.04, XXIX COSPAR, Washington, D.C., Book of Abstracts p.361, 1992.
3. Keller, H.U., Marliewicz, W.J., Knollenberg, J., Paper 38.05, 24th DPS, Munich, 1992, BAAS 24, No 3, p.1018, 1992.
4 Beatty, J.K., Levy, D.H., Sky and Telescope, p. 18, July 1994.
5. Chapman, C.R., Nature 370, p.245, 28. July 1994.

# THERMOLUMINESCENCE AND CATHORDOLUMINESCENCE OF EUCRITES

Hiroo IMAMURA and Kiyotaka NINAGAWA

*Okayama University of Science, 1–1, Ridai–cho, Okayama 700*

INTRODUCTION Eucrite is an achondrite which probably constitutes 4Vesta's crust and is composed of plagioclase, pyroxene and silica phase . Eucrites show thermoluminescence (TL) and cathordoluminescence (CL) mainly from plagioclase as well as ordinary chondrites. In ordinary chondrites blue TL sensitivity correlates to thermal metamorphism and subtypes of them are determined by the blue TL sensitivity. [1] Eucrites are also classified into petrologic types [2] and the blue TL sensitivity of eucrites correlates to thermal metamorphism, too. [3] This time we found in eucrites that plagioclase showed yellow TL with a variety of TL glow curves and silica phases showed blue and purple CL.

SAMPLES AND EXPERIMENTS The TL and CL of several petrologic types of eucrites, Y–75011,106 (type 1), Y–790266,85 (type 2), Y–792510,104 (type 6), Y–791195,101 (cumulate) and Millibillillie (type 4 or 6) were measured. Samples were cut into slices by a wire saw and polished for TL spectra, TL image, CL image measurements and EPMA analysis. The TL spectra and TL images are recorded onto video tape amplified by an image intensifier with a spectroscope and a microscope, respectively, and analyzed by two–dimensional photon counting electronics. Two band pass filters, Andover 450FS80–25 and 600FS80–25, were used for blue and yellow TL measurements, respectively. A mosaic of the CL was measured using a Nuclide Corporation "Luminoscope" operated at 10kV and 1mA. Fujicolor (ASA800) film was used for taking CL photographs. The chemical compositions of minerals were analyzed by electron probe X–ray microanalyzers [EPMA], JXA–8800 and EMAX–2200.

PLAGIOCLASE Figure 1 shows TL emission spectra of eucrite (Millibillillie) and ordinary chondrite (Wickenburg: L6). The TL emission spectrum of ordinary

chondrite consists of a wide band with a maximum at 450nm (blue). On the other hand that of eucrite consists of two wide bands with maximums at 450nm (blue) and 570nm (yellow). It is different from that of ordinary chondrite. The CL spectra of eucrites were also measured and were the same as those of TL. Luminescence center of yellow peak in anorthite is ascribed to $Mn^{2+}$ in $Ca^{2+}$ sites. [4] Yellow CL in anorthite has been reported for lunar materials. [5] Two types of CL colors, yellow and green, are found in anorthite fragments of Y-75011(type 1). But the yellow TLs of these fragments has the same TL glow peak at 180 ℃, as shown Fig.2 (1) and (2). Two types of yellow TL glow curves are found in Y-790266(type 2). One fragment has a glow peak at ~ 120 ℃ as shown in Fig.2 (3). Another fragment has two glow peaks at ~ 110 ℃ and ~ 310 ℃. Normative-anorthite mesostases with ~ 300 ℃ or more higher TL peak temperature have been also found in primitive ordinary chondrites. [6] Y-792510 (type 6) shows yellow CL and ~ 150 ℃ peak [Fig.2 (5)]. Millibillillie(type 4 or 6) shows yellow CL and ~ 130 ℃ peak [Fig.2 (6)]. Y-791195 (cumulate) shows yellow CL and has ~ 150 ℃ TL peak [Fig.2 (7)]. There are a variety type of yellow TL glow curves in eucrites. On the other hand, the blue TL of all the eucrites have the same TL glow peak at 100 ℃ [dashed lines in Fig.2].

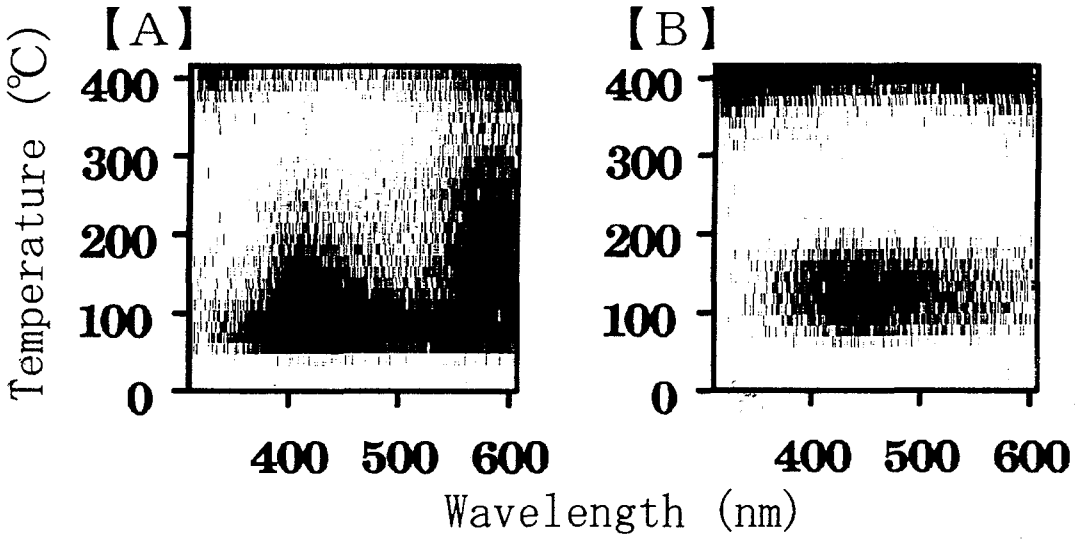


**Fig.1** TL emission spectra. Distribution of the TL intensity as a function of both wavelength and temperature.
【A】 eucrite (Millibillillie) 【B】 ordinary chondrite (Wickenburg)

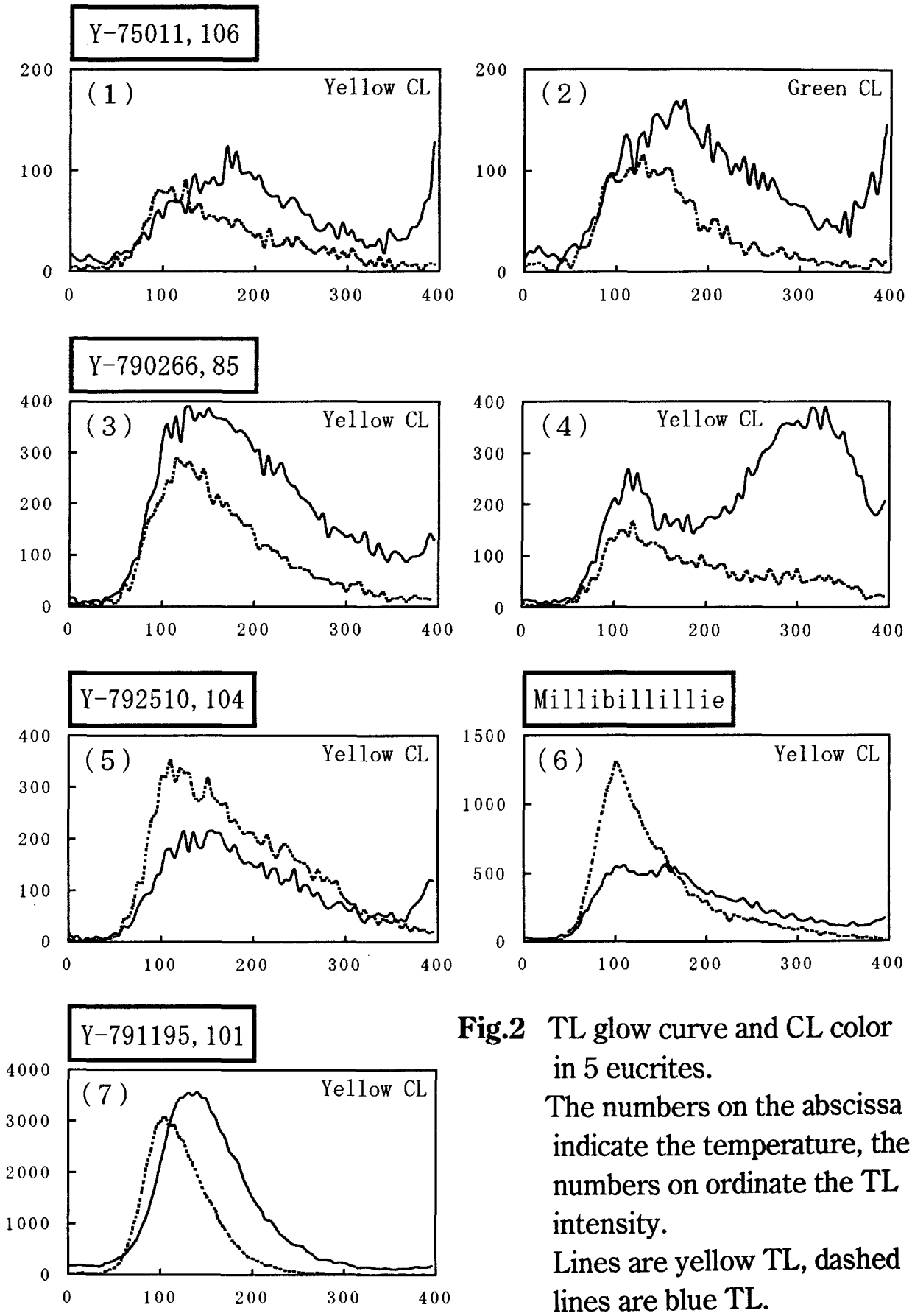


**Fig.2** TL glow curve and CL color in 5 eucrites.
The numbers on the abscissa indicate the temperature, the numbers on ordinate the TL intensity.
Lines are yellow TL, dashed lines are blue TL.

SILICA PHASE Silica phases were found in ordinary eucrites except the cumulate eucrite. These silica phases which cannot be distincted from shape, occurrence and compositions show blue and purple CL. More over blue CL portions have different types of blue TL glow curves as shown in Fig.3. There is a TL glow curve in Millibillillie resembled to TL from cristobalite. [7] Many different colors, ranging from blue, purple and gray to red and brown, are commonly seen in quartz. It is believed that quartz with blue CL is formed at high temperatures whereas red–luminescing quartz is of low temperature origin. [8]

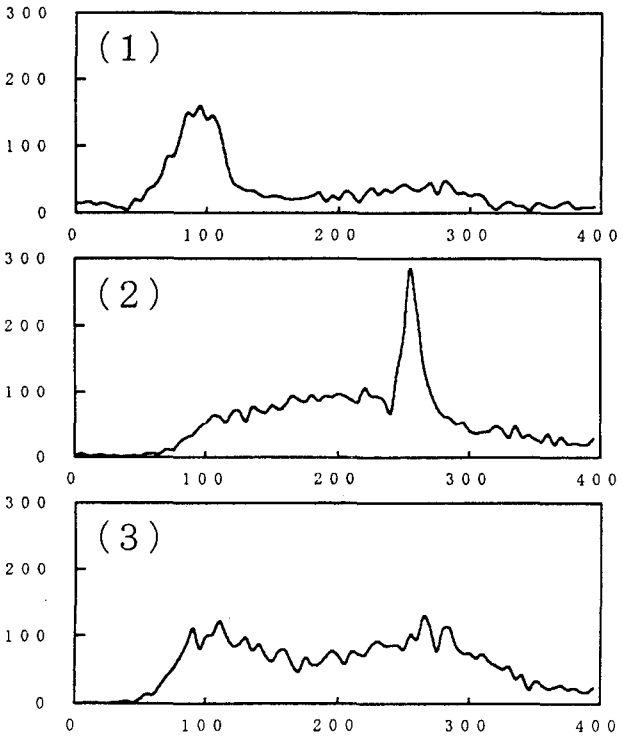


**Fig.3**
TL glow curves of blue CL silica phases in eucrits.
The numbers on the abscissa indicate the temparature, and the numbers on the ordinate indicate the TL intensity.
The silica phases of (1) and (2) are in Y-75011,106, and the silica phases of (3) is in Millibillillie.
Purple CL of silica phases are fine and feeble, so that TL glow curve can not analyzed.

REFERENCES 1) D.W.G.Sears et al. (1980) : Nature, **287**, 791–795. 2) H.Takeda and A.L.Graham (1991): Meteoritics, **26**, 129–134. 3) J.D.Batchelor and D.W.G.Sears (1991): Nature, **349**, 516–519. 4) D.J.Huntley et al. (1988) : J. Lumin. , **39**, 123–136. 5) J.E.Geake et al. (1972): Proc. 3rd lunar Sci. Conf., 2971–2979. 6) K.Ninagawa et al. (1992): Proc. NIPR Symp. Antarct. Meteorites, **5**, 281–289. 7) S.Matsunami et al. (1992): Proc. NIPR Symp. Antarct. Meteorites, **5**, 270–280. 8) D.J.Marshall (1988): Cathodoluminescence of Geological Materials , 67–75, Boston: UNWIN HYMAN

# Chemical conditions of aqueous alteration of CM chondrites inferred from REE abundances in chondrules

M. Inoue and N. Nakamura

Graduate School of Science and Technology, Kobe University, Nada, Kobe 657

We have reported preliminary results of abundances of REE and other lithophile elements in individual chondrules from two CM chondrites, Murchison and Y-793321 [1,2]. It has been found that more than half of CM chondrules analyzed by us indicated light-REE depleted patterns with a large negative Eu anomaly (see Figs. 1a and 1b). Such REE patterns would be the first case for chondrules ever reported and thus be important to understand origin and/or evolution of CM chondrules. In this work, we have re-examined possible implications of the observed REE patterns for aqueous conditions during alteration of the CM meteorites.

In spite of different degree of alteration, barred olivine chondrles indicate no light-REE depletion but show normal or occasionally irregular REE patterns similar to those of CV and CO chondrules [3,4]. On the other hand, altertered porphyritic (PO, POP, PP) chondrules all show light-REE depleted patterns, as typically shown in Fig. 1. The degrees of light-REE depletion, as defined by Sm/La ratio, correlate negatively with Eu anomaly (Fig. 2). Therefore, it is suggested that light-REE depletion occurred during the same processes which caused the Eu depletion. Although the light-REE depleted patterns similar to those in Fig. 1 are commonly found for igneous rocks such as lunar mare basalts, no clear correlations have been identified between light-REE depletion and major chemical changes due to igneous processes for altered chondrules. In addition, it should be pointed out that vapour REE fractionations may be possible only at high temperatures (>1000° C) in the nebular conditions [5] and that light-REE depletion has been found only for altered chondrules among many chondrules reported. Combining these facts with chemical-petrographic features, it may be quite difficult to envision any variety of igneous processes or nebular alteration mechanism in explaining the observed light-REE depletion.

Inspection of extensive studies of aqueously altered terrestrial basalts, hydrothermal fluids and alteration products of water/rock interaction from wide variety of geological environment indicates that light-REEs (and occasionally Eu) have significant mobilities in aqueous systems even at low temperatures and mild pHs. It is also interesting to note that light-REE fractionations and depletion of alkalis occurred in meteorites during burial in Antarctic ice sheets [6,7]. Then gradual enrichment or depletion of light-REE along with anomalies at Eu (and Ce) occurs commonly in altered crustal rocks and meteoritic finds, as well as hydrothermal fluids and sea water [e.g. 8,9].

In view of mineral assemblages of CM chondrites, typically Murchison; calcite, metal/sulfides/pyrrhotite and other $Fe^{+2}/Fe^{+3}$ compounds such as components of PCP, chemical conditions of CM meteorites are considered to be more reducing compared to typical weathering conditions of terrestrial rocks. In view of large negative Eu anomaly of CM chondrules, we suggest that Eu may have act as $Eu^{+2}$ and other REE including Ce as $REE^{+3}$ during alteration. Using the oxidation potential ($E_h$)-pH diagram (Fig. 3) [10], we can estimate possible conditions of aqueous alteration of the CM chondrules. The temperatures of alteration are estimated to be below 20° C [11]. The $E_h$ values are then estimated to be < -0.35 volts at pH of 7~8. In this $E_h$-pH conditions, REE carbonates are stable [10,12]. Therefore, it is considered that during aqueous alteration reaction light-REEs and Eu may have been leached out selectively (together with felsic components) from chondrule-mesostasis (enriched in REE) to the matrix, and incorporated into calcite and other Ca-rich alteration products now in the matrix, yielding depletion of light-REE and Eu for bulk chondrules.

We suggest that, as discussed in current theory, CM chondrules had formed from nebular refractory components, agglomerated into a parent body and suffered low temperature aqueous alteration, resulting in depletion of light-REE and Eu but heavy REE remained unchanged. Marked REE fractionations as found for partially altered CM chondrules would provide a new indicator of chemical conditions of aqueous activities prevailed on the earliest planetary bodies.

**References**: [1] Inoue, Nakamura & Kojima (1994), Mem. Nat. Inst. Polar Res. Spec. Issue **7**, 150-163. [2] Inoue & Nakamura (1995) LPSC **XXVI** 653-654. [3] Misawa & Nakamura (1988) Geochim. Cosmochim. Acta **52**, 1699-1710. [4] Misawa and Nakamura (1988) Nature **334**, 47-50. [5] Boynton (1975) Geochim. Cosmochim. Acta **39**, 585-595. [6] Shimizu & Masuda (1983) Proc. 8th Sympos. Antarct. Meteorites 241-248. [7] Nishikawa et al. (1990) Mass Spectroscopy **38**, 115-123. [8] Pan et al. (1993) Geochim Cosmochim Acta **57**, 355-367. [9] Michard (1989) Geochim. Cosmochim. Acta **53**, 745-750. [10] Brooking (1983) J. Geochem. **17**, 223-229. [11] Clayton & Mayeda (1984), Earth Planet. Sci. Lett. **67**, 151-161. [12] Zhong & Mucci (1995) Geochim. Cosmochim Acta **59**, 443-453.

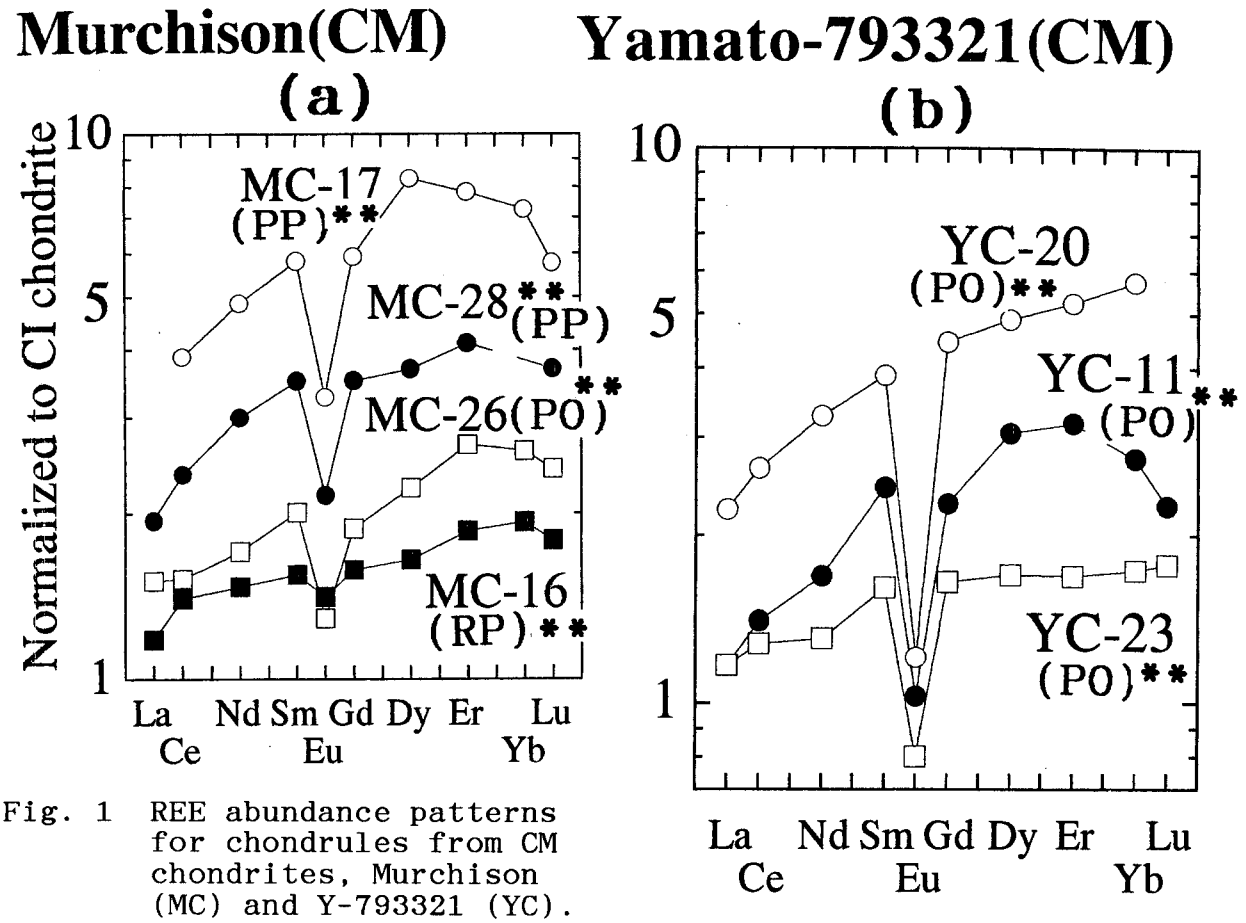


Fig. 1 REE abundance patterns for chondrules from CM chondrites, Murchison (MC) and Y-793321 (YC). (** weakly altered)

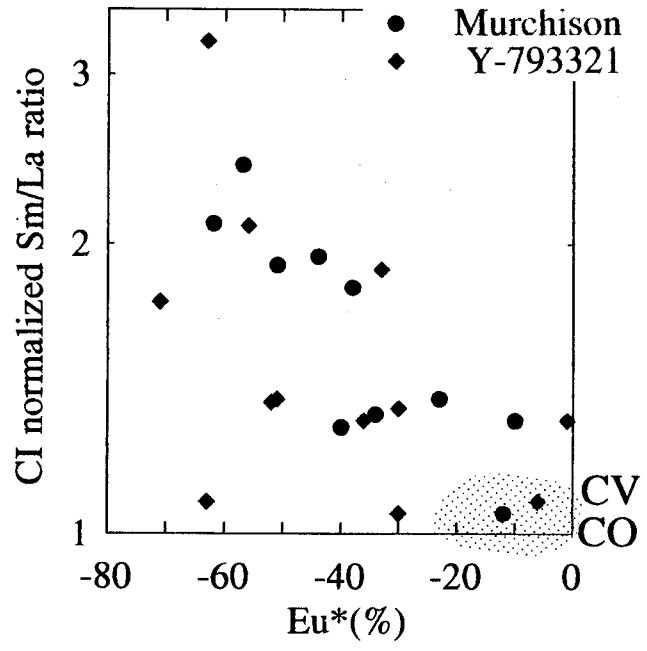


Fig. 2 Correlation between light-REE depletion (Sm/La) and Eu anomaly.

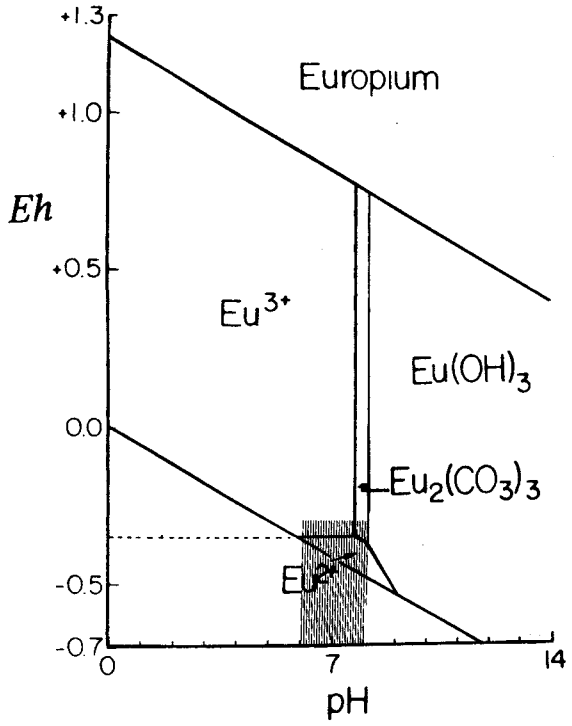


Fig. 3 $E_h$-pH diagram for Eu at 25°C and one bar (Brooking, 1983).

# A preliminary report on the Neagari meteorite fall on February 18th, 1995.

Akira Ishiwatari*, Keiichi Sasatani**, Kazue Tazaki*,
Koh Sakamoto+, Takashi Nakanishi+, Kazuhisa Komura++,
Tatsuki Tsujimori*, Yasuji Oura+, Yutaka Miyamoto+,
Hisatada Akahane#, Makoto Watanabe# and Katsushi Nunomura#

*Department of Earth Sciences, Faculty of Science,
Kanazawa University, Kanazawa 920-11, Japan.
**Ho-4-1, Taisei, Neagari Town, Ishikawa 929-01, Japan
+Department of Chemistry, Faculty of Science, Kanazawa
University, Kanazawa, Ishikawa 920-11, Japan.
++Low Level Radioactivity Laboratory, Faculty of Science,
Kanazawa University, O-24, Wake, Tatsunokuchi Town,
Ishikawa 923-12, Japan.
#Toyama Science Museum, 1-8-31 Nishi-Nakanomachi,
Toyama 939, Japan.

A stone meteorite was found by the second author (Sasatani) in a small town near Kanazawa, central Japan, in the morning of Sunday, February 19th, 1995. Place of finding is Ho-4, Taisei, Neagari (pronounced neh-ah-gari) Town, Nomi County, Ishikawa Prefecture, Japan (N36°26'57", E136°27'55"), and it is named "Neagari Meteorite." The meteorite hit a car parked in the central shopping district of the town. Sasatani started his car which was parked aside his house that morning, and found that the rear trunk cover of his car flapped. He found a black, rounded stone on the trunk cover, which was trapped in a triangular hole at the center of the trunk cover.

The shape of the hole formed on the car indicates that the meteorite came from NNW direction (333°) at an impact angle of 40° from the horizon. Size and weight of the biggest fragment (presumably about 2/3 of the entity) are W6.5 x H4.0 x L6.0 cm (Length may have been 10 cm before crush) and 325 g, respectively. The meteorite is egg-shaped. Black glass crust, 1 mm thick, covers all over the surface. The interior is gray white, fine-grained rock. There were three other major fragments (40, 30 and 18 g) and many tiny fragments in and outside the trunk. Weight of the collected fragments totals 420 g, but the original weight may have been about 500 g before crush. White paint fragments of the car are attached to the glass surface of the meteorite in a circular manner, suggesting that the meteorite rotated around its axis parallel to its flight direction when it hit the car. However, the western side of the impact hole is bounded by a supporting pipe, and the shape of the hole is apparently controlled by this pipe. It is also possible that the meteorite came from the north or northeast. The meteorite may have been prevented to pass through the trunk cover by the pipe and rotated toward northwest.

The precise time of the hit is unknown, but a neighbour heard a big sound at about 22:00 (JST: GMT+9) of Saturday, February 18th, 1995. The discoverer did not notice this sound, though he was in bed in his house at this time. On the other hand, five witnesses are so far available in the Kanazawa-Toyama

area for a fireball which appeared in the northwestern sky, passing to the south (to the left) (Fig. 1, Table 1). Three witnesses correspond with each other in the time of appearance, which may be identified at about 23:55 of February 18th, 1995. The azimuth and elevation of the fireball appearance from each witness site define a point where the radial line reaches the height of 80 km from sea level, an assumed height of fireball ignition. These points are distributed in the area at about 100 km to the northwest of Noto Peninsula, and the flight path of the meteorite restored from the shape of the impact hole passes the area (Fig. 1). This suggests that the fireball has been the Neagari meteorite itself.

The glassy surface is rugged, porous and heterogeneous. Chondrules are not obvious by the naked eyes, but some spherical features, 1 mm in diameter, are visible under the microscope. Tiny iron metal and iron sulfide grains are disseminated.

Mineral composition was determined by the Akashi Alpha-30A SEM - Philips EDAX-9100 system of Kanazawa University (Table 2). A very small fragment (3.5 mm in size) was polished for SEM use. About 70 vol.% of the rock is occupied by olivine ($Fo_{76}$). Other silicate minerals include orthopyroxene (mg=79, Wo=2.0), clinopyroxene (mg=85, Wo=44.7) and plagioclase ($Or_7An_{11}Ab_{82}$). Iron metal with 4-5 wt.% Ni (kamacite) and iron sulfide with some Ni (troilite) occupy only less than 5% of the total volume. These minerals are very homogeneous in their chemistry and distribution. The mineral chemistry clearly corresponds to that of L-chondrite. In view of the obscure chondrules and homogeneous mineral chemistry, this meteorite may be a metamorphosed ordinary chondrite of L6 type.

Gamma-ray spectrometric measurement of the biggest fragment of the meteorite was started about 67 hours after the fall by using a heavily-shielded germanium detector (Ortec HPGe, GEM-10020; low-background type) of Kanazawa University. The biggest fragment (325 g) was used for the measurement. Several radioactive nuclides produced from heavier nuclides through nuclear spallation induced by high-energy cosmic-rays (mainly protons) were identified by their gamma-ray spectrum obtained from 62 hours measurement (Fig. 2). The nuclides includes $^{7}Be$ ($T_{1/2}$=53.3d), $^{22}Na$ (2.60y), $^{26}Al$ ($7.16\times10^{5}$y), $^{44m}Sc$ (2.44d), $^{46}Sc$ (83.8d), $^{48}V$ (15.98d), $^{51}Cr$ (27.7d), $^{52}Mn$ (5.6d), $^{54}Mn$ (312d), $^{58}Co$ (70.8d), etc. The clear peak of $^{40}K$ may be due to radiogenic potassium which has originally been contained in the rock (see plagioclase analysis in Table 2). A further measurement is necessary for a quantitative assay of the cosmic-ray induced radionuclides to depict irradiation history of the meteorite.

The Neagari meteorite is the 7th "fall" in Japan in these 50 years, following the Mihonoseki meteorite fallen in Shimane Prefecture, western Japan, on December 10th, 1992. As described above, the Neagari meteorite is a L6-type ordinary chondrite come from a northern direction most probably at about 23:55 of February 18th, 1995. The radioactive nuclides in this meteorite were measured in the earliest, world-record time (2.7 days) after its fall. Our further research would provide important information on the irradiation history of the meteorite.

Table 1. Detailed witness observations of the fireball possibly related to the Neagari meteorite with new data obtained in March, 1995. Time is in JST (GMT+9). Azimuths of appearance and extinction are measured from the north in a clockwise (eastern) direction.

| Locality | latitude N | longitude E | Time 950218 | App. (Find) | Ext. (Lost) | Elev. (unc.) | Color |
|---|---|---|---|---|---|---|---|
| A Kanazawa Takao (Ishikawa Pref.) | 36°30'41" | 136°38'03" | 23:56 +/- | 318° | 293° | (20°) | Pink |
| B Kanazawa Nakamura (Ishikawa Pref.) | 36°33'26" | 136°38'49" | 23:50-24:00 | 323° | 233° | (20°) | Orange |
| C Kanazawa Fukuhisa (Ishikawa Pref.) | 36°37'00" | 136°41'11" | 24h -25h | (323°) | (293°) | 40° | ? |
| D Shinminato Koshinokata (Toyama Pref.) | 36°46'15" | 137°06'53" | 23:55-56 or 24:15-16 | 320° | 300° | (25° -20°) | Blue-white |
| E Yatsuo Onagatani Higashihara (Toyama Pref.) | 36°26'42" | 137°05'09" | 23h-24h | 323° | 298° | 25° 22° | Blue -red |
| F Neagari Taisei (Ishikawa Pref.) | 36°26'57" | 136°27'55" | 22h? | from 333° | | 40° | Black |
| G Terai Aou (Ishikawa Pref.) | 36°27'22" | 136°30'35" | 23:55+- | 338 | 303 | 15° | ? |
| H Kanazawa Toriki (Ishikawa Pref.) | 36°33'31" | 136°37'42" | 23:45+- | 328 | 278 | 15° | White & Red |

Table 2. Mineral chemistry of the Neagari meteorite. Deficiency of Na in plagioclase may be caused by rugged, deeply etched surface of the mineral.

| wt% | *olivine* | *ortho-pyroxene* | *clino-pyroxene* | *plagioclase* |
|---|---|---|---|---|
| $SiO_2$ | 38.47 | 55.37 | 53.83 | 64.12 |
| $TiO_2$ | 0.00 | 0.18 | 0.53 | 0.07 |
| $Al_2O_3$ | 0.20 | 0.44 | 0.73 | 20.65 |
| $Cr_2O_3$ | 0.00 | 0.56 | 1.00 | 0.19 |
| FeO* | 22.32 | 13.78 | 5.07 | 0.58 |
| MnO | 0.48 | 0.41 | 0.22 | 0.10 |
| MgO | 39.13 | 28.91 | 16.63 | 0.00 |
| CaO | 0.07 | 1.05 | 21.93 | 2.16 |
| $Na_2O$ | 0.00 | 0.03 | 0.03 | 8.66 |
| $K_2O$ | 0.00 | 0.00 | 0.00 | 1.11 |
| Total | 100.67 | 100.73 | 99.97 | 97.64 |
| atomic ratio | | | | |
| *O=* | *4* | *6* | *6* | *8* |
| Si | 0.994 | 1.971 | 1.973 | 2.897 |
| Ti | 0.000 | 0.005 | 0.015 | 0.002 |
| Al | 0.006 | 0.018 | 0.032 | 1.100 |
| Cr | 0.000 | 0.016 | 0.029 | 0.007 |
| Fe* | 0.482 | 0.410 | 0.155 | 0.022 |
| Mn | 0.011 | 0.012 | 0.007 | 0.004 |
| Mg | 1.508 | 1.534 | 0.909 | 0.000 |
| Ca | 0.002 | 0.040 | 0.861 | 0.105 |
| Na | 0.000 | 0.002 | 0.002 | 0.759 |
| K | 0.000 | 0.000 | 0.000 | 0.064 |
| Total | 3.003 | 4.008 | 3.983 | 4.959 |
| *Mg/(Fe+Mg)* | *0.76* | *0.79* | *0.85* | |

* Total Fe as FeO.

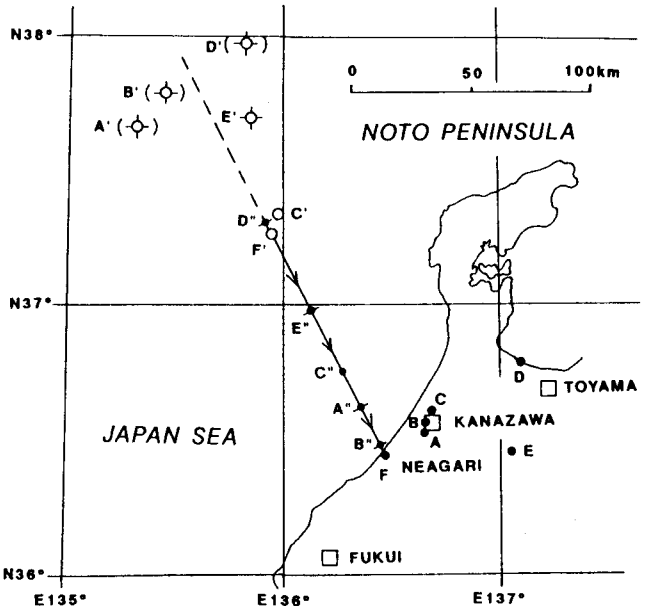


Figure 1. Fall site of the Neagari meteorite (F) and its possible flight path (arrowed) suggested by the shape of the impact hole; coming from azimuth 333°, elevation 40°. The point where the path reaches 80 km altitude is indicated by a circle (F'). Witness sites of the fireball (A-E) are plotted with big dots. Appearing (with bars) or finding (without bars) azimuth of the fireball at each site is represented by a numbered circle (A' to E'), where the elevation reaches 80 km altitude; an assumed firing level. Elevation of 25° is assumed for A', B', D' and E', while 40° is certain for C'. The azimuths with uncertain elevations are in parentheses. Extinction (with bars) or lost (without bars) azimuth of the fireball at each site is represented by a numbered small dot, which is projected on the possible flight path (A"-E"). Open squares stand for large cities. See Table 1 for detailed data.

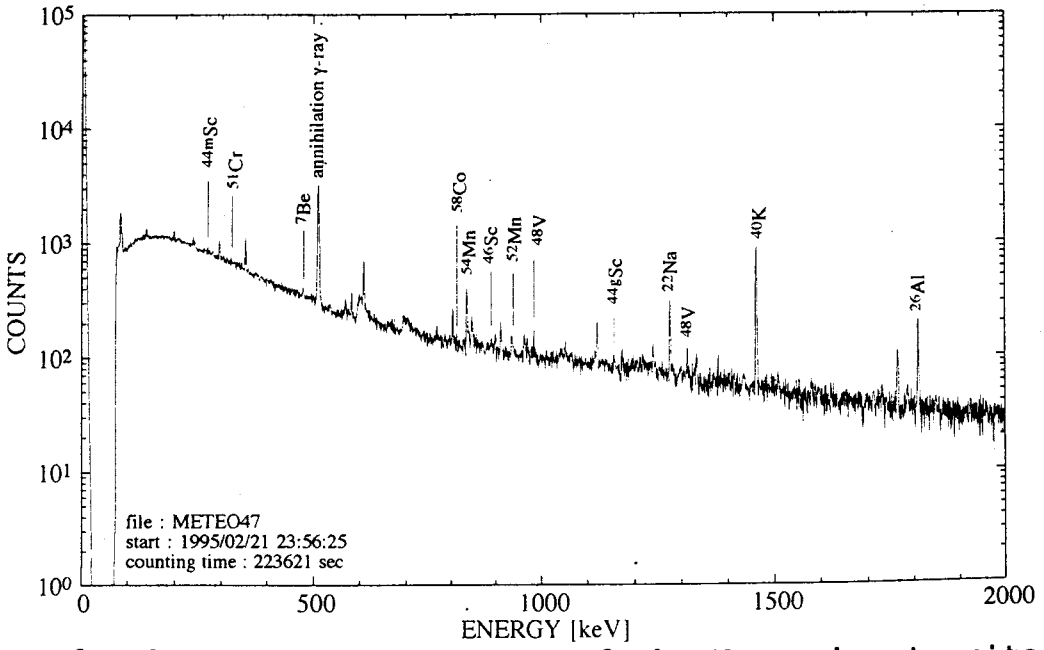


Figure 2. The gamma-ray spectrum of the Neagari meteorite. The biggest fragment (325 g) was placed at 1 cm from the detector window (Ortec HPGe, XLB-GEM-10020). Measurement started at ca. 2.7 days after the inferred impact time, and continued for 2.6 days.

THE R CHONDRITE GROUP: COMPARISONS TO OTHER CHONDRITE GROUPS Gregory W. Kallemeyn, Institute of Geophysics and Planetary Physics, University of California, Los Angeles, CA 90024 USA.

There are currently nine R chondrites, representing at least eight separate falls: Acfer 217, Allan Hills 85151, Carlisle Lakes, Pecora Escarpment 91002, Pecora Escarpment 91241 (likely paired with PCA91002), Rumuruti (the only observed fall), Yamato 75302, Yamato 793575, and Yamato 82002. With the addition of the R chondrite group, there are now 12 well-established chondrite groups with ≥5 members: CI CK, CM, CO, CR, CV, EH, EL, H, L, LL and R.

Primary petrographic characteristics of the R chondrites include small chondrules (~400 μm) and abundant matrix. Secondary characteristics include moderate metamorphic recrystallization, and with the exception of Carlisle Lakes, extensive brecciation. Brecciated samples have a typical light/dark structure. All of the R chondrites, except Carlisle Lakes, contain solar gases (L. Schulz and H. Weber, priv. comm.) and are therefore regolith breccias. The R chondrites have a higher degree of Fe oxidation than ordinary chondrites, with olivine compositions peaking at $Fa_{38-40}$. (Rubin and Kallemeyn, 1994)

The compositions of seven R chondrites (Acfer 217, Allan Hills 85151, Carlisle Lakes, Pecora Escarpment 91002, Pecora Escarpment 91241, Rumuruti, Yamato 793575) were studied by instrumental neuton activation analysis. The average CI,Mg-normalized lithophile abundances for the R chondrites are ~0.95× CI. This is lower than all of the carbonaceous chondrites which have average values ≥1.0× CI, and slightly higher than ordinary chondrites (H,L,LL all ~0.9× CI). Refractory siderophile abundances are similar to refractory lithophiles. Abundances of Se and Zn are much higher than those in ordinary chondrites. Elemental ratios such as Zn/Mn and Al/Mn are very useful in deliniating the various chondrite groups. Plotting these ratios in Fig. 1, one sees that the R chondrites fall in an area distinct from all other chondrite groups.

Noble gas data (L. Schulz and H. Weber, priv. comm.) indicate cosmic ray exposure ages for the R chondrites as follows: ~38 Ma for Acfer 217, ALH85151, PCA91002, PCA91241; ~18 Ma for Rumuruti; ~7 Ma for Carlisle Lakes. The oxygen isotope compositions of the R chondrites are distinct from the other chondrite groups and well about the terrestrial fractionation line ($\Delta^{17}O$ ~+2.7‰; Schulze et al., 1994). One model for the formation of the R chondrites is that the precursors of these meteorites were similar to those of ordinary chondrites, but agglomerated abundant magnetite-laden matrix-like dust enriched in $\Delta^{17}O$.

REFERENCES:
Rubin A. E. and Kallemeyn G.W.(1994) *Meteoritics* **29**, 255.
Schulze H., Bischoff A., Palme H., Spettel B., Dreibus G. and Otto J. (1994) *Meteoritics* **29**, 275.

# TRACE ELEMENT CONSTRAINTS ON ORIGIN OF $SiO_2$-BEARING CLASTS IN ORDINARY CHONDRITES

M. Kanazawa[1], J.C. Bridges[2], K. Misawa[1,3], N. Nakamura[1,3], and R. Hutchison[2]
[1] Dept. of Earth & Planet. Sci., Kobe Univ., Nada, Kobe 657, Japan
[2] Dept. of Mineralogy, Natural History Museum, Cromwell Road, London SW7 5BD, UK.
[3] Dept. of Nature of the Earth, Graduate School of Sci. & Tech., Kobe Univ., Nada, Kobe 657, Japan

Silica-rich igneous-textured clasts are found in ordinary chondrites (OC) [1-6]. Brigham *et al.* [2] have described two distinct types: silica, low-Ca pyroxene assemblages, and silica-fayalite ± low-Ca pyroxene clasts in OC. The $SiO_2$-bearing clasts found in the Parnallee (LL3.6) and Farmington (L5) chondrites may be belong to the former types and are chemically and isotopically unique [4, 5]. As shown in the oxygen three isotope diagram (Fig. 1), they plot on a mixing line defined between unequilibrated ordinary chondrite (UOC) chondrules and an $^{16}O$-depleted end member of CB1 [4, 5].

We analyzed trace elements including REE by isotope dilution mass spectrometry for $SiO_2$-bearing clasts (CB4, CB7, and CB8) along with a barred olivine-pyroxene chondrule (P22) and a macrochondrule (MC) previously described in [7] from Parnallee. Part of results were presented at Prague Meeting [5]. Some major and minor elements of CB8 and macrochondrule were determined by atomic absorption or ICP atomic emission spectrometry. The CI-chondrite normalized REE patterns of the clasts, chondrule and macrochondrule are shown in Fig. 2.

CB8 is a large tridymite-bearing clast, ~1.6 cm in size and clearly a fragment of a larger object. The mineralogy, major element chemistry and oxygen isotopic compositions of the clast were already presented in [4, 5]. CB8 has a high Si/Mg ratio (2.49), although its bulk Mg/(Mg + Fe) and Fe/Mn ratios (0.79 and 51.2, respectively) are within chondritic. Refractory elements Ca and Al are highly fractionated in CB8; the clast is enriched in Ca (3 x CI) but depleted in Al (0.7 x CI). CB4 and CB7 consist of enstatite + cristobalite. They also show Ca enrichment (3-7 x CI). CB8 is depleted in moderately volatile lithophiles Mn, Na, K, and Rb (0.18-0.71 x CI), siderophile elements Fe, Co, and Ni (0.0041-0.39 x CI), and chalcophile element Zn (0.076 x CI). The $SiO_2$-bearing clasts analyzed in this study exhibit a gradual depletion from light to heavy REE and a large positive Eu anomaly possibly along with a positive Ce anomaly, or a depletion of La (see Fig. 2a). This REE pattern is quite different from those of typical ferromagnesian chondrules in UOCs, $SiO_2$-bearing pyroxene-rich clast in Hedjaz (L3.7) [3], and silica-rich orthopyroxenite Bo-1 in Bovedy (L3) [6].

P22 shows a flat REE pattern (2.2 x CI) with a negative Eu anomaly. P22 is depleted in K, Rb, and Fe (0.5 x CI). MC also shows a flat REE pattern (1.6 x CI) with no specific anomaly. Enrichment factors of alkaline earths, Al, Mn, and Cr are comparable to those of REE. Na, K, and Rb are enriched (2-5 x CI), but siderophile elements Fe, Co, Ni, (0.26-0.84 x CI) and chalcophile element Zn (0.094 x CI) are depleted in this object.

Absence of metal and sulfide, low abundances of siderophile and chalcophile elements in the clasts imply that metal and sulfide removed from precursor material before or during clast formation. General REE patterns of $SiO_2$-bearing clasts from Parnallee suggest that they are from igneous fractionation controlled by the plagioclase component. Partial melting model is compatible with trace element signature of the clasts. However, a simple extraction of partial melting liquid from a chondritic source could produce neither large fractionation of Ca/Al nor enrichment of Si relative to Mg. Moreover, oxygen isotopic compositions of the clasts do not support this model.

As discussed by [2], $SiO_2$-rich clasts could have formed by disequilibrium condensation in the nebula. Precursor materials of the clasts were intermediate temperature condensates after refractory condensates removed from the nebular gas. They separated from ambient gas before condensation of moderately volatile elements. Refractory lithophile components must have incorporated into precursors as an additional nebular component. Large Ca/Al fractionations are the results of nebular condensation combined with aggregation [8]. Alternatively, loss of liquid by means such as ablation, and/or evaporation from partially molten high-temperature condensates could be responsible for refractory element fractionations [9]. The $SiO_2$-rich clasts produced by melting of these precursor materials. During the clast crystallization, solid/liquid fractionation mainly controlled by plagioclase occurred. The clasts reacted with an ambient $^{16}O$-poor nebular gas. After fragmentation of the clasts they were incorporated into an LL chondrite parent body.

**REFERENCES:** [1] E.J. Olsen *et al.*, *EPSL* **56**, 82-88 (1981). [2] C.A. Brigham *et al.*, *GCA* **50**, 1665-1666 (1986). [3] N. Nakamura *et al.*, *EPSL* **99**, 290-302 (1990). [4] J.C. Bridges *et al.*, *Meteoritics* **28**, 329-330. (1993). [5] J.C. Bridges *et al.*, *Meteoritics* **29**, 448-449. (1994). [6] A. Ruzicka *et al.*, *Meteoritics* **30**, 57-70 (1995). [7] R.T. Dodd *Mineralog. Mag.* **37**, 230-237 (1969). [8] G.J. MacPherson & A.M. Davis *GCA* **58**, 5599-5625 (1994). [9] A.S. Kornacki & B. Fegley *Proc. 14th LPSC* B588-B596 (1984).

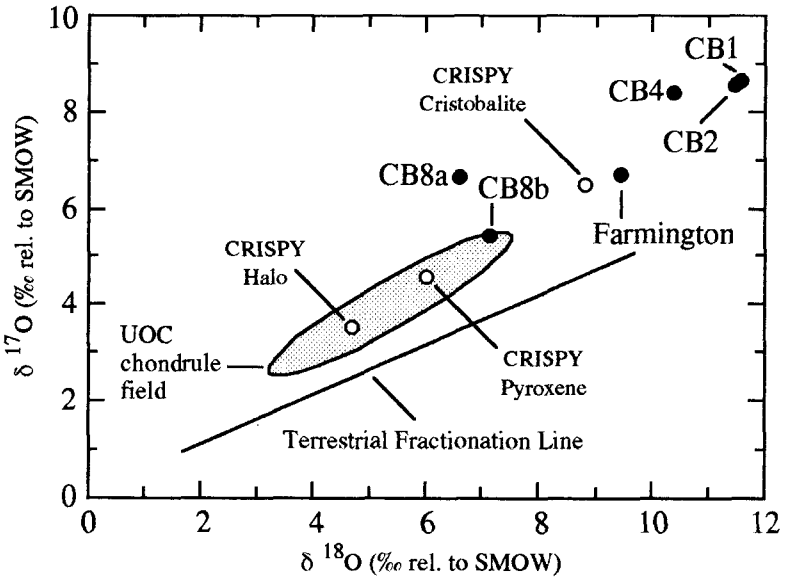


**Fig. 1.**
Three isotope oxygen plot showing the composition of $SiO_2$-rich clasts from ordinary chondrites. CRISPY (a cristobalite-pyroxene assemblage in the L6 chondrite ALHA76003) data are from [1]. Parnallee (CBs) and Farmington data are from [4, 5].

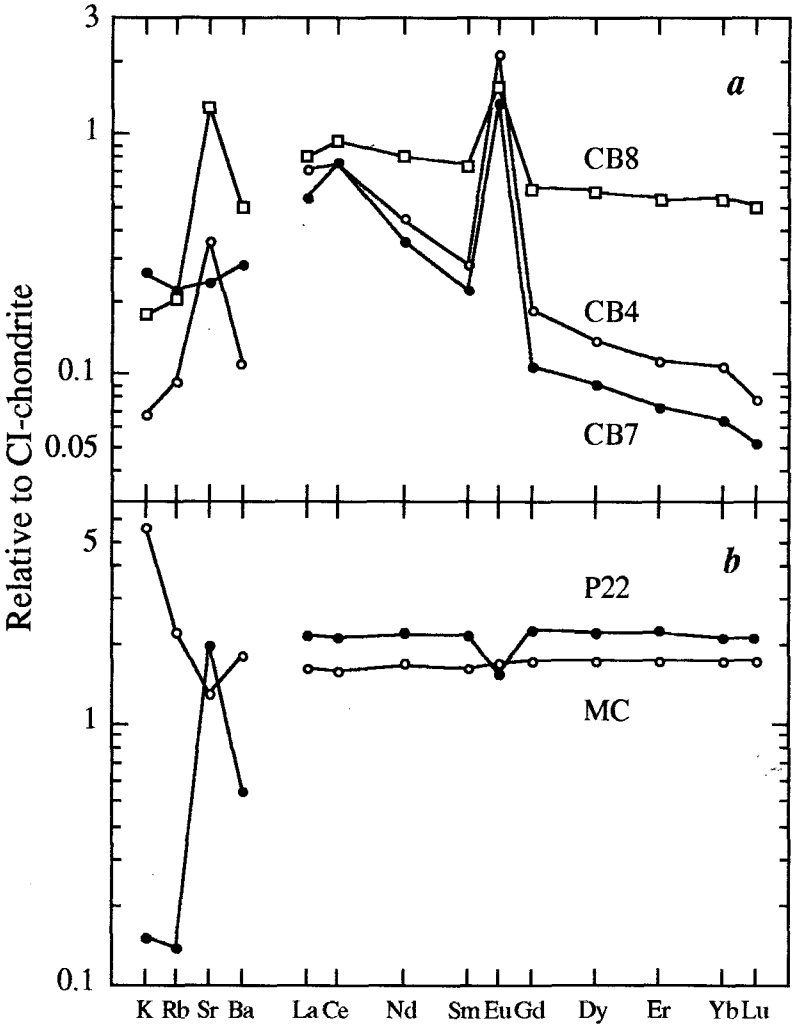


**Fig. 2.**
The CI-chondrite normalized elemental abundances of $SiO_2$-rich clasts (CB4, CB7, CB8), barred olivine-pyroxene chondrule (P22), and macrochondrule (MC) [7] from the Parnallee (LL3.6) chondrite.

# Anhydrous alteration of Allende chondrules in the solar nebula III: Experimental study of alteration reactions.

KIMURA Makoto and IKEDA Yukio
Ibaraki University, Bunkyo 2-1-1, Mito 310

Ikeda [1], and Ikeda and Kimura [2] notified that some chondrules in the ALH-77003 (CO3) and Allende (CV3) were subjected to secondary reaction to form $Na_2O$-rich groundmass in peripheral parts of the chondrules. Recently, Ikeda and Kimura [3], and Kimura and Ikeda [4] studied 69 chondrules in Allende, and they concluded as follows; 1) All of these chondrules have experienced anhydrous alteration and contain nepheline abundantly with sodalite in the devitrified groundmass. These nepheline and sodalite formed secondarily by an alkali-Ca exchange reaction: Na, K and Cl were introduced from outside of chondrules, and Ca was released by breakdown of the anorthite component of chondrule groundmass. 2) Hedenbergite, wollastonite, kirschsteinite, grossular and andradite secondarily formed together with nepheline and sodalite. 3) The alteration reaction includes other two processes: secondary olivine zonation and replacement of enstatite by ferroan olivine.

Ikeda and Kimura [2] performed heating experiments to reproduce the secondary reaction in chondrules. Following their preliminary work, we conducted heating experiments in order to estimate the conditions of the alkali-Ca exchange reaction. The starting materials were single plagioclase crystal ($An_{97}$) and synthetic glass bead whose chemical composition is a mixture of normative anorthite and diopside in equal amounts. They were held within NaCl powder, and were heated under atmospheric conditions. Temperatures were 700 and 800°C, and the heating durations ranged from 20 to 670 hours.

The peripheral portion of the starting material reacts with the surrounding NaCl to produce reaction rims ranging from a few to several tens of microns in width (Fig. 1). The texture of the reaction rims resembles that of the altered groundmass in Allende chondrules. The predominant phases in the rims are also nepheline in the heated plagioclase, and nepheline and diopside in the glass. Within these rims, we observed some minor phases, probably such as gehlenite,

wollastonite and forsterite, mixed with nepheline.

It seems that the width of the reaction rims increases linearly with the experimental duration. Thus, we calculated that the durations to produce nepheline rims with 10 microns width were about 100 hours for glass and 140 hours for plagioclase at 900°C. On the other hand, Housley [5] produced ferroan olivine from low-Ca pyroxene for 100 hours at 900°C. Such a replacement of enstatite is commonly encountered in altered groundmass of Allende chondrules. From experimental works of Housley [5] and ours, the alkali-Ca exchange reaction took place along with the replacement of enstatite by ferroan olivine.

References: [1] Ikeda Y. (1982) Mem. Natl. Inst. Polar Res., 25, 34-65. [2] Ikeda Y. and Kimura M. (1985) Meteoritics, 20, 670. [3] Ikeda Y. and Kimura M. (1995) Proc. NIPR Symp. Antarctic Meteorites (in press). [4] Kimura M. and Ikeda Y. (1995) Proc. NIPR Symp. Antarctic Meteorites (in press). [5] Housley R.M. (1986) Lunar Planet. Sci. XVII, 364-365.

Fig. 1. A synthetic glass bead was heated at a temperature of 800°C for 670 hours. The peripheral portions of the bead reacted with the surrounding NaCl to produce rim consisting of nepheline and diopside often with minor Ca-rich phases. The width is about 160 microns.

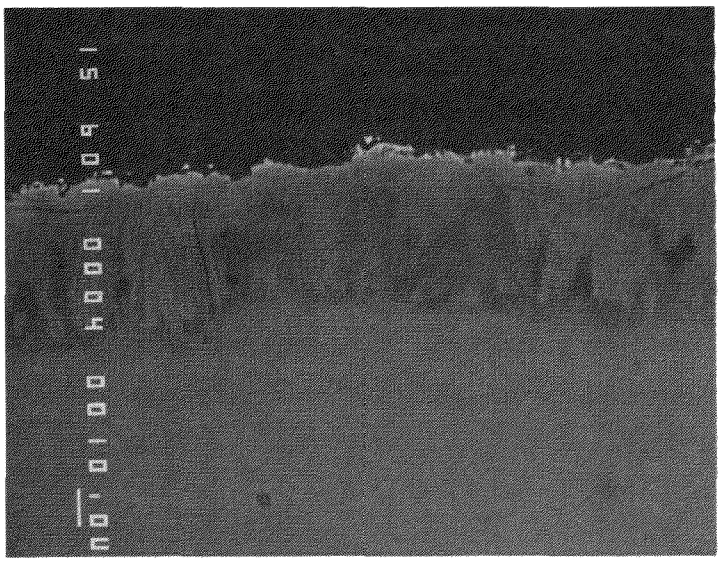

# Electron microscopic and infrared spectral studies on the structure of alumina phases

°Seiji Kimura, Kazuhiko Kamei, Noritoshi Tsuda, Yoshio Saito[1], Chiyoe Koike[2] and Chihiro Kaito

Department of Physics, Ritsumeikan University, Kusatsu, Shiga, 525, Japan.

[1]Department of Electronics and Information Science, Kyoto Institute of Technology, Sakyoku, Kyoto, 606, Japan.

[2]Department of Physics, Kyoto Pharmaceutical University, Yamashina, Kyoto, 607, Japan.

Introduction Corundum is the refractory phase predicted to condense first from a cooling gas of solar composition [1], but corundum has been found to be an exceeding rare phase in meteorites. The main reason is that corundum disappears at 1240°C due to the formation of spinel ($MgAl_2O_4$)[1]. Recently, however, numerous corundum grains were found in the Murchison C2 chondrites [2]. The analysis of grains by ion microprobe mass spectrometry indicated the existence of $^{26}Al$ and $^{16}O$ in the early solar system [2]. Corundum grains in meteorites are the good tracer for studying the early solar system.

The presence of corundum grains in space is also suggested from astronomical observations [3~5]. For example, the broad 12 $\mu$m feature observed in spectra of Mira variables is identified as a characteristic band of alumina grains [4]. It is suggested theoretically that corundum grains may condense in the ejecta of SN 1987A [5]. But it is not obvious at present that alumina grains in the ejecta of SN 1987A are amorphous or crystalline, or whether they are $\alpha$-alumina or $\gamma$-alumina. In spite of increasing interests for alumina grains, the spectral studies of alumina grains are hardly done up to the present, except for those of bulk $\gamma$-alumina [6] and $\alpha$-alumina [7]. In this paper, various alumina particles and alumina films have been studied by infrared spectrum and electron microscopy. The relationship between the crystal structure of alumina particles and/or alumina films and infrared spectrum was discussed.

Samples and experimental method Alumina which was produced by oxidation of metallic particle and film have been studied. Al particles were produced by evaporating metallic aluminium in Ar gas pressure of about 13kPa. Al particles were oxidized by heating in air at 400 ~ 1100°C for 20 hours. Al film was produced by evaporating metallic aluminium in vacuum of $10^{-3}$Pa on KBr substrate. The vacuum-evaporated film on KBr substrate was oxidized by heating in air at 550°C. In addition to those samples, two types of

commercial alumina particles were prepared. One is $\gamma$-$Al_2O_3$ particles from Nippon Aerosil Co., LtD., and the other is $\alpha$-$Al_2O_3$ particles using as a standard for checking the intensity of X-ray diffraction pattern. Those particles were embedded in KBr pellets. The transmittance of KBr pellets was measured with a Fourier transform infrared spectrometer (FTIR) (Horiba Inc., FT-210). Electron microscopic observation was carried out by using Hitachi H-7100R electron microscope.

Results and discussion Figure 1 shows infrared spectra of alumina films after heat treatment and aerosil $\gamma$-$Al_2O_3$ particles. The solid curve shows the spectrum of alumina film heated at 550°C for 1 hour, the dotted curve the spectrum of alumina film heated at 550°C for 5 hours, and the dashed curve the spectrum of aerosil $\gamma$-$Al_2O_3$ particles. The infrared spectrum of the $\gamma$-$Al_2O_3$ particles showed very broad peaks at about 13$\mu$m. The feature agreed very well with those of the spectrum [8] calculated using bulk data of amorphous $\gamma$-alumina film [6]. On the other hand, the infrared spectrum of alumina film oxidized in air at 550°C for 1 and 5 hours showed the peak at 10.8$\mu$m. The as-deposited Al film was completely oxidized by heating at 550°C for 1 or 5 hours, which were confirmed by electron diffraction (ED) pattern. In general, alumina produced by the oxidation has been considered as $\gamma$-alumina. Diffraction patterns of $\gamma$-alumina and $\eta$-alumina phases were very similar, because the same cubic structure with nearly same lattice constant. The difference of structure may be due to the position of Al atoms, thougth the structure of $\eta$-phase was not clear. Moreover, in addition to the absorption peak of 10.8$\mu$m, the absorption peaks of alumina film oxidized in air at 550°C for 5 hours were observed at 16, 21 $\mu$m. From the theory of Pearce and Evans [9], it was found that the absorption peaks of 16 and 21 $\mu$m correapond to those of $\alpha$-$Al_2O_3$. Appearence of $\alpha$-$Al_2O_3$ phase by heating at 5 hours also was confirmed by ED pattern. Though the $\alpha$-$Al_2O_3$ was considered to be a stable phase above 1500°C, it turns out that a part of $\eta$-$Al_2O_3$ film changes to $\alpha$-$Al_2O_3$ phase even the heating at 550°C.

Figure 2 shows infrared spectrum of Al particles heated in air at 400°C for 20 hours. IR spectra of both alumina particles and films produced by the oxidation of metal showed the same absorption position(10.8$\mu$m). Intensity of the ED pattern of the collected samples of alumina particles produced by the oxidation of Al particles fitted well to the $\eta$-$Al_2O_3$ data. Therefore it was concluded that oxides produced by oxidation of the metal in air was not $\gamma$-$Al_2O_3$ but $\eta$-$Al_2O_3$. In order to confirm the structural difference of the

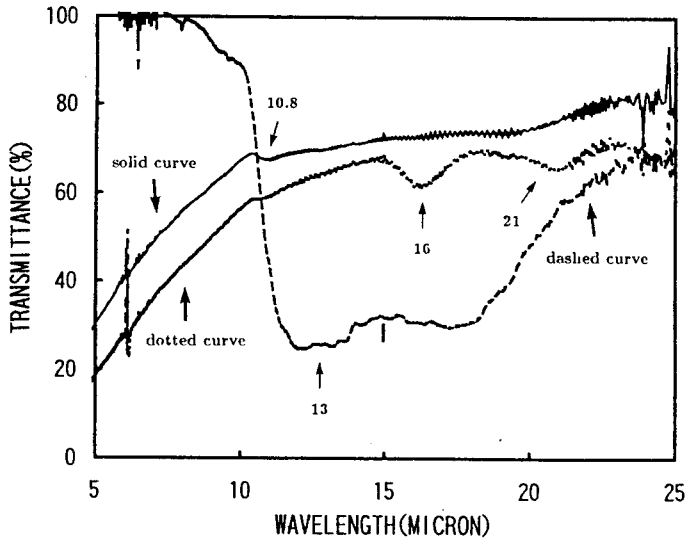


Fig.1. Infrared spectra of alumina films oxidized in air and aerosil $\gamma$-$Al_2O_3$ particles.

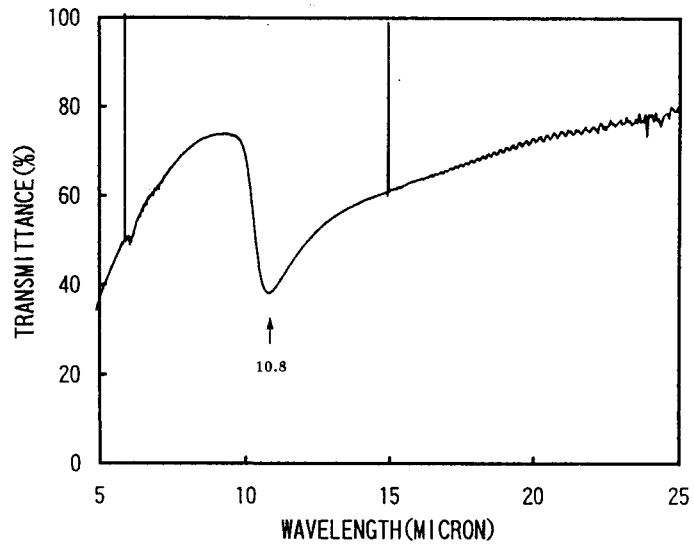


Fig.2. Infrared spectra of Al particles heated in air at 400°C.

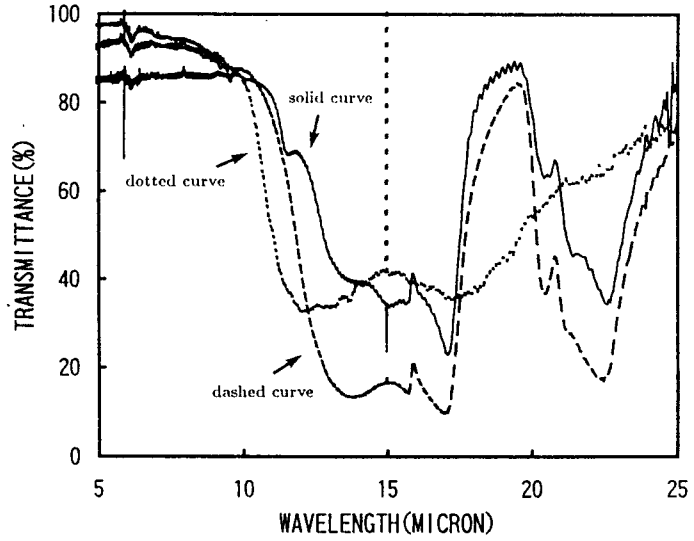


Fig.3. Infrared spectra of alumina particles and aerosil particles heated in air at 1100°C and a standard $\alpha$-$Al_2O_3$ particles .

oxidized film ($\eta$-phase) and aerosil samples ($\gamma$-$Al_2O_3$), the phase transition temperature of these samples to $\alpha$-phases were examined. Since the phase transition temperature of $\eta$ and $\gamma$ to $\alpha$-phase is different, the present oxidized particles and/or films and the aerosil samples was heated. Figure 3 shows infrared spectra of those samples and standard $\alpha$-$Al_2O_3$ particles. The solid curve shows the spectrum of alumina particles heated in air at 1100°C for 20 hours, the dotted curve the specrtum of aerosil particles ($\gamma$-$Al_2O_3$) heated in air at 1100°C for 20 hours, and dashed curve correspond to the standard $\alpha$-$Al_2O_3$. Figure 3 suggests that the structure of aerosil particles heated in air at 1100°C is different from the structure of alumina particles oxidized in air at 1100°C. Therefore it became evident that the phase transition temperature of $\eta$-$Al_2O_3$ was 1100°C. The phase transition temperature of $\gamma$-$Al_2O_3$ is above this, because the $\gamma$-$Al_2O_3$ absorption peaks was only seen in the dashed curve in Fig.3. The phase transition temperature of the present $\gamma$-phase particles was about 1500°C. The structure and IR spectrum details on these particles will be shown in OHP.

References


1) L. Grossman: Geochim. Acta., 36, 567-619, 1972.
2) E. Anders, A. Virag, E. Zinner and R.S. Lewis: Appl. Phys. J., 373, 77-80, 1991.
3) M.S. Vardya, T.De Jong and F.J. Willens: Appl. Phys. J., 304, 29-32, 1986.
4) T. Onaka, T.De Jong and F.J. Willens: Astron. Astrophys., 218, 169-179, 1989.
5) T. Kozasa, H. Hasegawa and K. Nomoto: Appl. Phys. J., 344, 325-331, 1989.
6) T.S. Eriksson, A. Hjorsberg, G.A. Niklasson and C.G. Granqvist: Appl. Opt., 20, 2742-2746, 1981.
7) A.S. Barker Jr: Phys. Rev., 132, 1474-1481, 1963.
8) C. Koike, C. Kaito, S. Kimura, T. Yamamoto, H. Shibai and H. Suto: ICARUS, 1995, in press.
9) G. Pearce and A. Evans: Astron. Astrophys., 136, 306-312, 1984.

# TEXTURAL VARIATIONS OF DARK INCLUSIONS IN THE ALLENDE CV3 CHONDRITE

Tomoko Kojima[1),2)] and Kazushige Tomeoka[1)]

1) Department of Earth and Planetary Sciences, Faculty of Science, Kobe University, Nada, Kobe 657

2) Mineralogical Institute, Faculty of Science, University of Tokyo, Hongo, Tokyo 113

## INTRODUCTION

A variety of dark lithic clasts have been reported from Allende and other CV3 chondrites, and are called "dark inclusions (DIs)" [e. g., 1-3]. They widely range in texture from chondritic one with chondrules and CAIs embedded in a fine-grained matrix, to the aggregates of fine grains of Fe-rich olivine free of coarse-grained components [1, 3]. We recently studied two DIs in Vigarano [4] and one DI (named All-AF) in Allende [5]; All-AF has been previously investigated by KURAT *et al.* [6] and PALME *et al.* [7]. All of these DIs are classified as the fine-grained variety of DIs. Our studies [4, 5] revealed abundant evidence that the DIs have experienced intense aqueous alteration and subsequent thermal metamorphism on the meteorite parent body. However, it still remains to be known whether our interpretation can be applied to other DIs, or is only unique to the DIs we studied.

We present the results of petrographic and scanning electron microscope studies of two other DIs in Allende. One of the two DIs (16-S-1) was previously studied by FRULAND *et al.* [1] and ZOLENSKY AND BUCHANAN [8], and the other DI (DN1) was newly sectioned for this study. These two DIs are very different in mineralogy and texture from each other, but both show evidence suggesting that they were affected by secondary processes similar to those experienced by the Vigarano DIs and All-AF.

## RESULTS AND DISCUSSION

16-S-1 contains abundant, relatively large (<0.1~ 1.6 mm in diameter) chondrules that are composed mainly of Mg-rich olivine and pyroxene, embedded in a fine-grained matrix. The general petrographic feature differs from that of the Vigarano DIs and All-AF, and appears to be common to the CV3 chondrites. However, this DI also shows mineralogy and texture indicative of secondary alteration. Mesostasis of chondrules are filled with porous aggregates of fine grains (<1~10 $\mu$m in diameter) of Si-, Al-, Ca-rich phases and Fe-rich olivine ($Fo_{55}$); they commonly show characteristic, fibrous to acicular morphologies, being reminiscent of phyllosilicate. In addition, most of Mg-rich olivine and pyroxene in chondrules have Fe-rich (25~35 wt.% FeO) rims, indicating that they were altered at their edges. We would like to point out that the mineralogy and texture of the chondrules closely resemble the

products formed by experimental hydrothermal alteration of the Allende chondrite [9]. The matrix of 16-S-1 is composed mostly of Fe-rich olivine ($Fo_{50\sim55}$) and minor amounts of tiny grains (<5 $\mu$m in diameter) of Fe-Ni sulfide. It has much more compacted appearance than the Allende matrix, so grain boundaries are hardly discernible by the SEM. The textures suggest that 16-S-1 was affected by minor aqueous alteration, so only chondrule mesostasis and edges of Mg-rich olivine and pyroxene were affected. Probably, part of the matrix was also replaced by phyllosilicate. The phyllosilicates in chondrules and matrix were later transformed to Fe-rich olivine by thermal heating. These interpretations agree with the results of ZOLENSKY AND BUCHANAN [8].

DN1 has mineralogy and texture closely similar to All-AF. It consists of densely packed, rounded to oval-shaped inclusions that appear brownish translucent in transmitted light, embedded in a dark matrix. The inclusions are composed mostly of fine grains (<1~20 $\mu$m in diameter) of homogeneous Fe-rich olivine ($Fo_{65\sim68}$) like those in All-AF, but are much smaller (< 600 $\mu$m, mostly ~150 $\mu$m in diameter) in size. Olivine grains in the inclusions commonly show fibrous morphology, suggesting pseudomorphs after phyllosilicate. Matrix is also composed mostly of Fe-rich olivine, but the grains are smaller (<1~5 $\mu$m in diameter) than those in the inclusions, and show lath-like morphology somewhat similar to olivine in matrix of host Allende. In both inclusions and matrix, a Na-Al-Si-rich phase (3~5 wt.% $Na_2O$, ~30 wt.% $Al_2O_3$, ~45 wt.% $SiO_2$) abundantly occurs in the interstices between olivine grains. The phase may be related to nepheline. Another feature common to All-AF is the abundance of veins around relatively large inclusions. The veins in DN1 have layered structure similar to the veins in All-AF [5]; the central portions are pore space sandwiched by two continuous, thin plates (<5 $\mu$m in thickness) of salitic pyroxene. In relatively thick veins (~40 $\mu$m in width) the pore space is partly filled with grains (~10 $\mu$m in diameter) of andradite. The mineralogical and textural features suggest that DN1 was involved in intense aqueous alteration, and was subsequently dehydrated by mild heating; the extent of aqueous alteration was probably similar to that of All-AF. However, the precursor of DN1 appears to be different from that of All-AF, because sizes of inclusions, which are probably pseudomorphs after chondrules, are much smaller than those in All-AF.

The present study shows that the secondary processes experienced by the Vigarano DIs and All-AF are probably not unique to them but appear to be common to other DIs including the chondritic type of DIs containing chondrules and CAIs. The differences in mineralogy and texture are probably related to different degrees of alteration in which each DI was involved; DIs of the chondritic type were affected by minor aqueous alteration so that only mesostasis and edges of olivine and pyroxene in chondrules were altered, while DIs of the fine-grained type were so strongly altered that chondrules and CAIs in them were almost

completely replaced by phyllosilicates. The sequence of alteration, i. e., aqueous alteration and subsequent thermal metamorphism, was probably a common event that occurred near the surfaces of meteorite parent bodies. We believe that systematic studies of DIs would provide a more precise view regarding the evolution of carbonaceous chondrite parent bodies.

ACKNOWLEDGMENT

We thank Dr. M.E. Zolensky and Dr. P.C. Buchanan for providing the 16-S-1 sample and also for helpful discussion.

REFERENCES

[1] FRULAND R.M., KING E.A. AND MCKAY D.S. (1978) Proc. Lunar Planet. Sci. Conf. 9th, 1305-1329.

[2] BISCHOFF A., PALME H., SPETTEL B., CLAYTON R.N. AND MAYEDA T.K. (1988) Lunar Planet. Sci. XIX (Abstr.), 88-89.

[3] JOHNSON C.A., PRINZ M., WEISBERG M.K., CLAYTON R.N. AND MAYEDA T.K. (1989) Geochim. Cosmochim. Acta 54, 819-830.

[4] KOJIMA T. TOMEOKA K. AND TAKEDA H. (1993) Meteoritics 28, 649-658.

[5] KOJIMA T. AND TOMEOKA K. (1994) Meteoritics 29 (Abstr.), 484 .

[6] KURAT G., PALME H., BRANDSTÄTTER F. AND HUTH J. (1989) Z. Naturforsch. 44a, 988-1004.

[7] PALME H., KURAT G., SPETTEL B. AND BURGHELE A. (1989) Z. Naturforsch. 44a, 1005-1014.

[8] ZOLENSKY M.E. AND BUCHANAN P.C. (1995) Lunar Planet. Sci. XXVI (Abstr.), 1565-1566.

[9] TOMEOKA K. AND KOJIMA T. (1995) 20th Symp. Antarct. Meteorites (Abstr.), this volume.

# Melting formation of metal phases of ordinary chondrites

Ping Kong and Mitsuru Ebihara
*Department of Chemistry, Faculty of Science, Tokyo Metropolitan University, Hachioji, Tokyo 192-03, Japan*

## Introduction

Ordinary chondrites constitute about 80% of all meteorites observed to fall on the earth. Although bulk compositions of ordinary chondrites are similar to that of the Sun, implying that ordinary chondrites have not experienced melting fractionation, the characteristics of chondrules do suggest that chondrules have been melted at high temperature and then cooled rapidly at the early history of the solar system. Siderophile elements are depleted in chondrules and, instead, are highly enriched in the metal phases. Here, we may have a clue to find the relationship of chondrules and the metal phases of chondritic meteorites. Although redistributions of Ni and Fe among metal phases occurred for all ordinary chondrites, it seems that element diffusions were restricted only to the metal phases in low petrographic type 3 chondrites, and redistributions of elements between metal and other phases were very limited. Thus, study of bulk metal compositions of petrographic type 3 chondrites and comparison of their compositions with those of equilibrated chondrites may help to specify the chemical characteristics of the UOC metals and subsequently to consider the formation conditions of metals before their accretion into the parent bodies.

## Experimental

Bulk metal phases of 10 H, 6 L and 7 LL chondrites were analyzed by INAA. Magnetic fractions were first separated by a hand magnet, and then were treated by boiling in conc. HF for 2 min. for the removal of attached silicates or sulfides. Our preliminary experiments showed that boiling in conc. HF for 2 min can effectively remove silicates from the magnetic fraction, while not attack kamacite or taenite [1].

## Results and discussions

Mean element abundances for the metallic fractions of both equilibrated and unequilibrated chondrites are normalized to the average chondritic compositions of the corresponding chemical groups and shown in Fig. 1a. Their CI-normalized abundances are also shown in Fig. 1b.

Significant difference in the metallic compositions between the EOCs and the UOCs is the systemic variations of the abundances of three lithophile elements, Cr, Mn and V, and three weakly siderophile elements, W, Mo and Ga. This can be observed clearly in Fig. 2, where the relative abundances of these six elements in the bulk metals of five L chondrites were plotted. It is obvious that the abundances are well correlated with the petrographic types of the meteorites; the abundances of W, Mo and Ga are increased and those of Cr, Mn and V are decreased with increase of petrographic type. In the equilibrated chondrites, Ga, Mo and W are enriched in the metals in an increasing order, while in the unequilibrated chondrites, the order changes to Ga, W and Mo.

Before accreting into chondritic parent bodies, metal grains were either interstellar grains, condensates from the solar nebula or melted droplets from a primary body. Let us first examine the possibility that the UOC metals are the direct condensates from the canonical solar nebula. According to condensation sequence [2], Fe was condensed into a metal phase at high temperature. With temperature falling, Fe was partly entered into silicates and partly transferred into troilite during equilibrium with the solar nebula. If Fe could equilibrate with the solar nebula, why could V, Cr and Si partly remain in the metal phases since they should be oxidized at higher temperatures? Rapid formation of silicates around metal grains might preserve these elements but would keep W and Mo quantitatively present in the metals. Our results showed that compared with Ir and Os, W and Mo were both depleted in the UOC metals to some extents, implying that portions of W and Mo were present in the non-metal phases. The depletion of W and Mo in the metals cannot be explained in terms of the condensation of

W and Mo being involved in a highly oxidizing condition, since in that case, Mo should be depleted in the metals to a higher extent than W [3]. In contrast, our results showed that W was more depleted than Mo in the UOC metals. Depletion of Mo and W hence must have occurred after the condensation of W and Mo. It is difficult to envision that the "being reduced" Si, Cr and V could coexist with the "being oxidized" W, Mo and Ga in the metallic fractions if the metallic fractions were nebula condensates.

W, Mo and Ga are enriched in the metallic fractions of the EOCs in order of: W >Mo >Ga, while in those of the UOCs the order changes to: Mo >W >Ga. We believe that the truly equilibrated distribution tendency of W and Mo among different phases should be preserved in the equilibrated chondrites because the redox states of the elements would be readjusted to reach equilibrium or near to equilibrium during the thermal metamorphism. So, if the UOC metallic fractions were equilibrated condensates, the distributions of W and Mo in the UOC metals should exhibit the same tendency as those in the EOC metals. Apparently, this is not the case.

If the metals were interstellar grains and have not changed their characteristics before accreted into chondrites, the compositions of the metals should be uniform for all the ordinary chondrites of different groups. Actually they have changed however. If the compositions of the metals were adjusted according to the redox condition in places where chondrites formed, the contradictory states of "being reduced" V, C, Cr and Si and "being oxidized" W, Mo and Ga preserved in the UOC metals should be erased. Thus, it seems that the metals of ordinary chondrites were not the interstellar grains before they were accreted into chondrites.

Formation of chondritic metals seems to be attributable only to the remaining melting mechanism. Experimental results showed that the metal/silicate partition coefficients of W were always lower than those of Mo at the temperature of 1300°C and oxygen fugacities between $10^{-13}$ to $10^{-11}$ [4]. Experimental partitions of Cr, V and Mn [5] exhibit a similar alteration trend as we have found in the UOC metals. Co is enriched in the UOC metals to a lower degree compared with Ni and, instead, the Co/Ni abundance ratios are higher in the corresponding non-magnetic fractions. At 1300°C and oxygen fugacity of $10^{-11}$, the partition coefficients for Co and Ni are 81 and 1380, respectively [4], indicating that a portion of Co may enter the silicate phase while Ni is quantitatively concentrated in the metal phase when melting occurred on this condition. We compared the partition coefficients for some elements between metal and silicate phases obtained by experiments and from our work in Table 1. Our results for UOC metals are highly consistent with a melting hypothesis.

In summary, we conclude that the metals of ordinary chondrites were the melting remnants before they were accreted into chondritic parent bodies.

**References** [1]. Kong P., Ebihara M., Endo K. and Nakahara H. (1995) Proc. NIPR 8, in press. [2]. Wasson J. T. (1985) In Meteorites: Their Record of Early Solar-System History. W.H. Freeman, New York. [3]. Fegley B. and Palme H. (1985) EPSL 72, 311-326. [4]. Schmitt W., Palme H. and Wanke H. (1989) GCA 53, 173-185. [5]. Drake M. J., Newsom H. E. and Caplbianco C. J. (1989) GCA 53, 2101-2111.

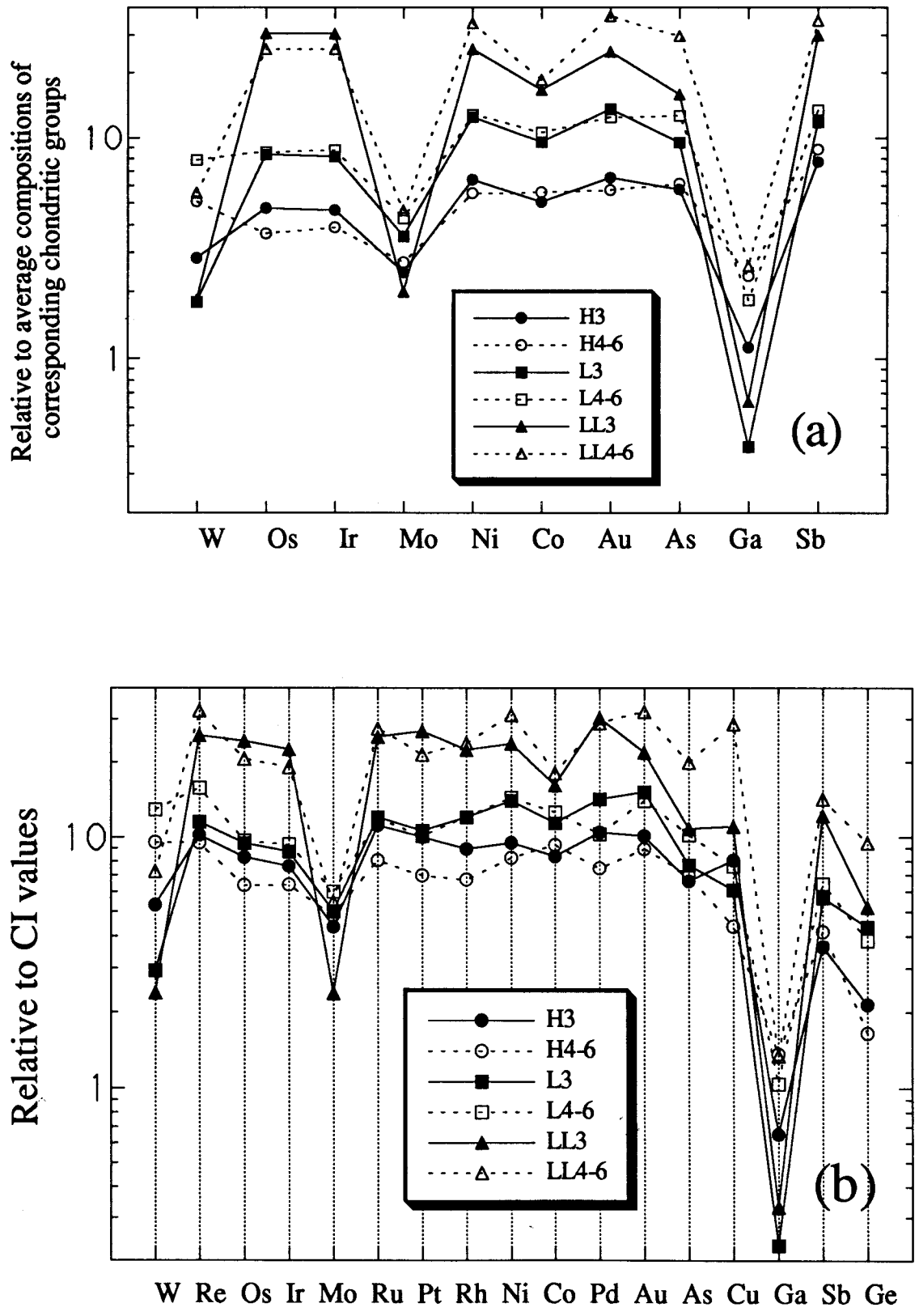


Fig. 1. Siderophile element abundances in bulk metals of chondrites

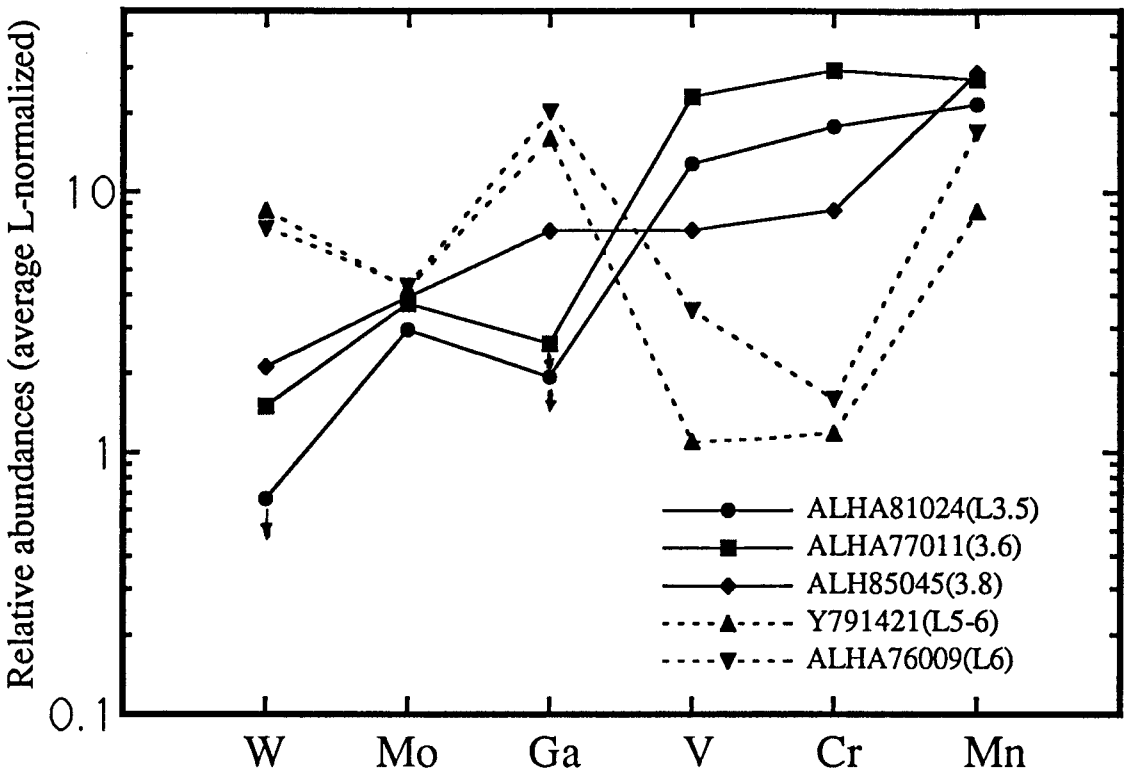


Figure 2. Varitions of some element abundaces in the bulk metals of different petrographic type L chondrites. Scales are: x1 for W and Mo, x10 for Ga, x100 for V and Cr, x1000 for Mn.

**Table 1. Comparation of metal/silicate partition coefficients of some elements obtained by partition experiments and from this work**

| 1300°C* 1260°C# | W | Mo | Ga | Co | Ni | Fe | Cr | V | Mn |
|---|---|---|---|---|---|---|---|---|---|
| Experimnetal | | | | | | | | | |
| $fO_2=10^{-12}$ | 19 | 155 | 10 | 135 | 2239 | 7.1 | 0.50 | 0.063 | 0.022 |
| $fO_2=10^{-11}$ | 0.44 | 5.6 | 1.8 | 81 | 1380 | 2.6 | | | |
| This work | 5.0 | 9.8 | 0.55 | 63 | | 7.0 | 0.24 | 0.20 | 0.024 |

* Schmitt et al. [4]; # Drake et al. [5].

# Studies of metallic fractions of L chondrites: implications to L chondritic parent body

Ping Kong and Mitsuru Ebihara

*Department of Chemistry, Faculty of Science, Tokyo Metropolitan University, Hachioji, Tokyo 192-03, Japan*

## Introduction

All the metallic fractions in ordinary chondrites have been developed into kamacite and taenite, the intergrown iron-nickel alloys with different compositions and crystal structures. Ordinary chondrites contain 3-20 wt.% of metallic fractions and the metallic fractions have average Ni contents in range of 8-35 wt.%. Investigations on binary Fe-Ni system (e.g., [1]) demonstrated that metals having Ni contents in this range would develop into kamacite and taenite when temperature fell below 700°C. Because the compositions of kamacite and taenite are sensitive to the changes of temperatures and especially the cooling rates, it is expected that the thermal histories of chondrites can be deduced from the compositional alterations and internal heterogeneity of the kamacite and taenite grains. Our goals of this work are: (1) to determine siderophile element distributions between taenite and kamacite and to specify the formation of the taenite and the kamacite from their distributional trends, and (2) to identify the metallic components of different petrographic types of chondrites and to infer the physical conditions when thermal metamorphism occurred.

## Experimental

Bulk metal and taenite fractions were separated using the scheme shown in Fig. 1. Three EOCs and three UOCs of L chondrites were studied in this work. Our previous results showed that the treatment of chondritic metals in conc. HF could selectively dissolve kamacite, with taenite and tetrataenite not being substantially affected, and that trace elements were not reprecipitated during leaching in conc. HF for up to 60 min [2]. The bulk metal and taenite fractions were studied by INAA and the taenite fractions of three EOCs were analyzed by Mössbauer spectroscopy.

## Results and discussions

Mean abundance ratios of siderophile elements between taenites and bulk metals for three UOCs and three UOCs are shown in Fig. 2. The distributions demonstrate that siderophile elements, except Co, and maybe As and Mo, are more enriched in taenite fraction with different abundance ratios between taenite and kamacite. Thus, kamacite has neither been produced by reducing non-metallic Fe on primary metals having a taenitic composition, nor has taenite been produced by oxidizing metallic Fe in the primary metals having a kamacitic composition, otherwise trace siderophile elements would be enriched in taenite to the same extent as Ni. Not only refractory siderophile elements but also less refractory siderophiles such as Cu, Sb and Ga, which are more volatile than Ni, are enriched in taenite, suggesting that kamacite and taenite were not produced by condensation fractionation. If kamacite and taenite formed during the melt-solid fractionation, Ir, Os, Re, and Ga should be enriched in Ni-poor kamacite, while Cu and Au should be enriched in Ni-rich taenite, as is observed in iron meteorites. Thus it seems that kamacite and taenite can only be the equilibrated products of low temperature diffusion following the Fe-Ni diagram. Positive correlation of Co and Ni in carbonaceous chondritic metals and the existence of a high Co and low Ni metal phase suggest that chondritic kamacite and taenite can not be developed in the nebula. Rather, it seems that kamacite and taenite can only be produced through solid diffusion in the chondritic parent bodies.

The difference in the development of kamacite and taenite in the equilibrated and the unequilibrated L chondrites is found: the taenite phase of the unequilibrated L

chondrites is mostly or totally developed into tetrataenite while low-Ni paramagnetic taenite is still present abundantly in the equilibrated L chondrites. The low-Ni paramagnetic taenite is believed to be an unequilibrated phase of either an incompletely transformed phase during fast cooling [3] or metastable taenite located out of the miscibility gap on the Fe-Ni phase diagram [4]. The former is related to a reheating event whereas the later is related to the diffusion status during the metamorphism.

If the low-Ni paramagnetic taenite was formed by incomplete transformation of taenite during fast cooling after reheating the preexisted kamacite and taenite, UOCs need to be more deeply buried than EOCs, considering a reheating must derive from outer rather than inner heat source for the preservation of the low-Ni paramagnetic taenite. This is opposite to the normal onion shell model [5]. If the low-Ni paramagnetic taenite was a metastable phase which was not developed into tetrataenite due to a relative faster cooling, the cooling rates for the UOCs should be slower than those for the EOCs. Chondrites having slow cooling rates must be deeply buried when an intrinsic metamorphism occurred. It seems impossible that an external heating could be maintained long enough to develop taenite into tetrataenite. Thus, the unequilibrated chondrites were also needed to be deeply buried compared to the equilibrated ones. In both cases, the arrangement of the EOCs and the UOCs in the parent body was the same; the EOCs located near the surface of the parent body, with the UOCs being near the center, if they were derived from the common parent body. An intrinsic thermal activity in the parent body would produce a temperature gradient decreased from the center to the surface, whereas an external heating would exhibit a inverse gradient. If a "reverse" onion shell structure is invoked, the generally accepted metamorphic temperatures of the equilibrated chondrites must be connected with an external heating event rather than the intrinsic activity.

The taenite fractions of the unequilibrated chondrites have been developed into tetrataenite, suggesting that a cooling rate corresponding to the development of kamacite and taenite was quite slow. The energy yielding such a slow cooling must have derived from intrinsic heat source which heated the parent body to a temperature high enough for the development of kamacite and taenite, but too low to recrystallize silicates. During or after this "metamorphism", an external heating took place on the chondritic parent body, which recrystallized the silicates and modified the structure of kamacite and taenite. This external heating was more violent than the intrinsic one and the early activities of the Sun may be a possible source. The duration of this heating on the chondritic parent body was short, so the cooling followed was relatively rapid; a long-time heating would erase the existence of kamacite and a slow cooling would redevelop taenite into tetrataenite. The highest temperature of the external heating was imprinted in the type 6 chondrites located near the surface of the parent body, being in range of 800°C-950°C [6], and the temperature decreased gradually from the surface to the center of the body. If the reheating event occurred at the late stage of the intrinsic "metamorphism", it would change the structures of the metal phases and any cooling rates deduced from those structures might be less meaningful.

**References** [1]. Goldstein J. I. and Ogilvie R. E. (1965) Trans. TIME 233, 2083-2087. [2]. Kong P., Ebihara M., Endo K. and Nakahara H. (1995) Proc. NIPR 8, in press. [3]. Gutlich P. Link R. and Trautwein A. (1978) In Mössbauer Spectroscopy and Transition of Metal Chemistry. Springer-Verlag, Berlin-Heidelberg-New York. [4]. Reuter K. B., Williams D. B. and Goldstein J. I. (1989) Metall. Trans. 20A, 719-725. [5]. Miyamoto M., Fujii N. and Takeda H. (1981) Conf. LPS 12, 1145-1152. [6]. Dodd R. T. (1981) In Meteorites: A petrologic-chemical synthesis. Cambridge Univ. Press, London.

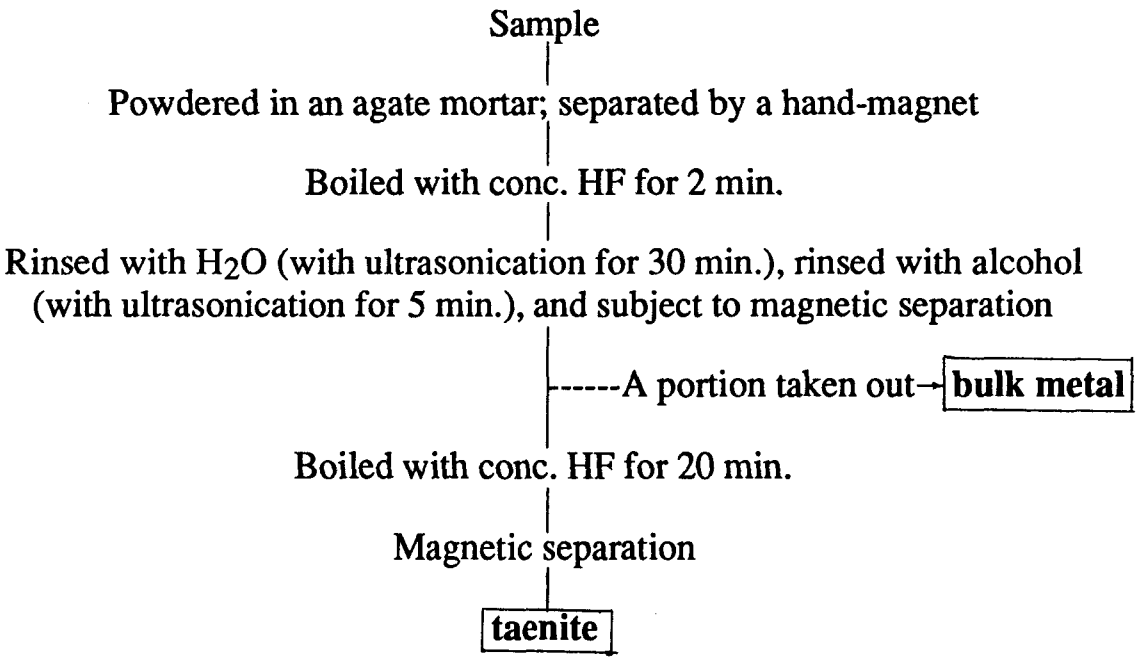


Fig. 1. Scheme for the separation of kamacite and taenite from ordinary chondrites

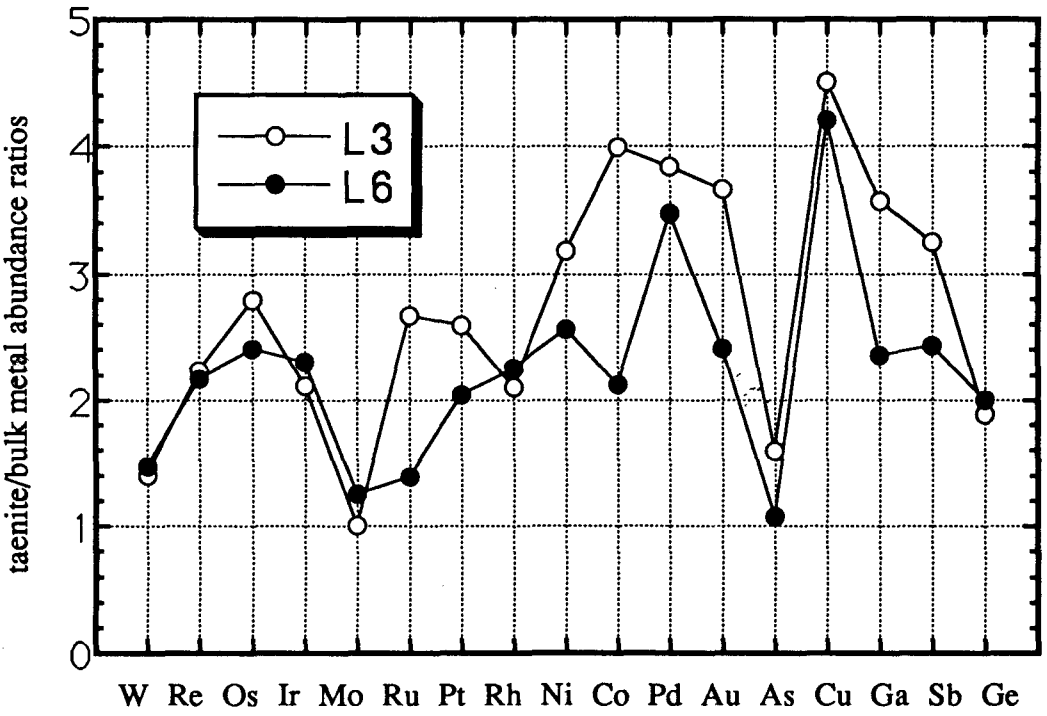


Fig. 2. Siderophile element distributions between taenite and bulk metal. Only Co is plotted inversely, i. e., as bulk metal/taenite.

# THE METEORITES IN THE LIGHT OF THE NIPR JAPANESE ANTARCTIC METEORITE COLLECTION

I. Kubovics[1], Sz. Bérczi[1,2], B. Lukács[3] & Gy. Szakmány[1]
[1] Dept. of Petrology & Geochemistry, R. Eötvös University, H-1088 Múzeum krt. 4a, Budapest, Hungary
[2] Dean's Office, R. Eötvös University, H-1088 Rákóczi út 5
[3] CRIP RMKI, H-1525 Bp. 114. Pf. 49, Budapest, Hungary

**ABSTRACT**

In 1993 an extraordinary Antarctic Meteorite Thin Section Educational Set was made in 20 copies by the National Institute of Polar Research (NIPR), Tokyo, Japan, an excellent cross section of the rocky materials of the Solar System. Our paper gives short overview of this collection, loaned to the R. Eötvös University, Dept. of Petrology and Geochemistry, for one year.

## 1. INTRODUCTION

From the end of 60's first Japanese, then also American expeditions hunted meteorites on Antarctica. Meteorite search became annual in Japan and USA and after a quarter century this competition resulted in cca. 15000 **Antarctic Meteorites**. Half of them is stored at the National Institute of Polar Research (NIPR), Tokyo, Japan, and half at the Planetary Materials Laboratory, NASA Johnson Space Center (JSC), Houston, Texas, USA.

Contrary to the classical collections Antarctic collections are free some of the selection effects. The great number of irons in finds is a result of the good chance of survival + difference from soil, helping the finding. The small number of falls of carbonaceous chondrites is also enhanced by their fragility. But the ice cover is a good preserver. Both great Antarctic Meteorite Collections are the best available sources for investigations.

The Antarctic Meteorite Collections made it possible to prepare an almost full set of representative types of meteorites. This full set was completed in 1993 June at the NIPR, Dept. of Antarctic Meteorites, by Keizo Yanai, principal investigator and curator of these meteorites. One copy of this set was given as loan for Hungarian universities, on the 19$^{th}$ Symposium on Antarctic Meteorites in June, 1993, another in December, 1994.

## 2. OUR TENTATIVE CLASSIFICATION

We chose two tripolar tentative classifications for the Antarctic Meteorite Educational Thin Section Set of NIPR. First there are three main material types, namely iron, stone, and ice. Second, the primordial matter may have been preserved; may have been gradually transformed by solar heat; and may have been intensely transformed inside a planetary body. (See the Figure.)

Mixing is suppressed between iron and ice due to the great difference of condensational temperatures. Nevertheless, their simultanaeous presence can occur in CIII chondrites if hydrated silicates are considered the "containers" of structural water.

The primordial matter is represented by C1 or C2 chondrites. External heating is shown, perhaps, by primitive achondrites, while differentiation is seen best on a shergottite, a Martian basalt. Half-points of edges may be: ureilites on the CC -- basalt edge; chondrites on the CC -- primitive achondrite edge; eucrites on the primitive achondrite -- basalt edge. The NIPR Antarctic Meteorite Thin Sections contain representatives for all.

One may choose the Van Schmus-Wood classification table for chondrites. There are 18 chondrites in the set, arranged now in a Van Schmus-Wood type table with their numbers. (See the Figure.) This Table can serve later as frame of reference, for any such chondrite collection, like to the planned Hungarian collection, too. On these backgrounds now we shortly describe all the 30 thin sections of the Japanese NIPR Antarctic Meteorite Collection.

## 3. A SHORT DESCRIPTION OF THE THIN SECTIONS IN THE SET

The set contains 30 samples, The numbered as here.

**N° 1. Pallasite - Yamato 8451.**

Large spherulic olivine grains are embedded in the opaque metal phase (nickel-iron).

**N° 2. Mesosiderite - Allan Hills 77219.**

Large orthopyroxene grains, opaque metal phase and smaller orthopyroxenes and olivines in the groundmass of the texture.

**N° 3. Aubrite (Enstatite achondrite) - Allan Hills 78113.**

Slightly brecciated texture, mainly large enstatite grains. Some regions contain olivine, too.

**N° 4. Ureilite - Allan Hills 77257.**

Large, clear olivine, pyroxene and less plagioclase grains and opaque phase. All the mineral grains have opaque edges, which is very characteristic to the ureilitic texture.

**N° 5. Diogenite A - Yamato 74097.**

Monomineralic crystalline texture of orthopyroxene.

**N° 6. Diogenite B - Allan Hills 77256.**

Monomineralic brecciated texture of orthopyroxene.

**N° 7. Howardite - Yamato 7308.**

Brecciated basaltic achondrite with plagioclase, orthopyroxene and less olivine, and clinopyroxene in the texture.

**N° 8. Eucrite A - Yamato 791195.**

Basaltic achondritic meteorite, crystalline texture similar to that of a microgabbro with clinopyroxene (also with twin-lamellae) and plagioclase (in subhedral grains).

**N° 9. Eucrite B - Yamato 74450.**

Basaltic achondrite, brecciated (polymict) and plagioclase +pyroxene basaltic clasts; mineral clasts of these minerals, too.

**N° 10. Shergottite - Allan Hills 77005.**

Brown pyroxene and mainly glassy plagioclase (maskelynite) + some plagioclase, and opaque component (chromite?) in this basaltic achondritic texture supposedly from Mars. At the edge of one plagioclase grain fine grained plagioclase crystals with glass between them with variolitic texture. Both diaplectic glass (maskelynite) and this region of melting and recrystallization refers to the impact event which delivered the sample to Earth.

**N° 11. Lunar Meteorite A (regolith breccia) - Yamato 86032.**

Large plagioclase-rich clasts embedded in a darker matrix, with small olivine grains, too.

**N° 12. Lunar Met. B (norite) - Asuka 881757 (earlier Asuka 31).**

The gabbroic texture of this lunar meteorite sample consists of orthopyroxene and glassy plagioclase (maskelynite). In many respects the sample is very similar to the NASA Lunar Sample N° 78235, except that there brown glass veins can also be found in the texture. In maskelynite, the Lunar Meteorite B - Asuka 881757 is also similar to the N° 10. Shergottite - Allan Hills 77005 sample; similarity might have resulted from excavation from the surface of a planetary body with greater than asteroidal mass.

**N° 13. Primitive achondrite - Yamato 794046.**

Equigranular texture, olivines, pale brown pyroxenes embedded into a large, long plagioclase grain Few opaque minerals (troilite) and brown, almost isotropic glass, interstitially.

**N° 14. EH3 chondrite - Yamato 691.**

Well developed chondrules mainly consisting of olivine and pyroxene. It contains opaque phases (metal + troilite) too.

**N° 15. H3 chondrite - Yamato 791428.**

Well developed chondritic texture. The chondrules are both from olivine, plagioclase and pyroxene + opaque component. There are chondrules mixed from these three main mineral phases, too.

**N° 16. H4 chondrite - Allan Hills 77233.**

Rather well defined chondritic texture, chondrules mainly from clinopyroxenes, and in less number from olivine.

**N° 17. H5 chondrite - Yamato 74079.**

Less well developed chondritic texture with chondrules of olivine and pyroxene. (Among meteorites from Hungary *Zsadány*, *Ohaba*, and *Nagy-Dévény* are similar chondrite types.)

**N° 18. H6 chondrite - Yamato 74014.**

Slightly discernible chondrules. Chondrules of skeletal olivine. By this chondrule there are also olivine crystals.

**N° 19. L3 chondrite - Yamato 74191.**

Well developed chondritic texture. Mainly chondrules from olivine and pyroxene + devitrified brown glass. (Among meteorites from Hungary: *Mezö-Madaras* is similar, although brecciated.)

**N° 20. L4 chondrite - Yamato 74355.**

Well developed chondrules of olivine and pyroxene.

**N° 21. L5 chondrite - Yamato 790957.**

Less well defined chondrules, mainly pyroxenes. (Among meteorites from Hungary see: *Borkút*, *Knyahinya*, *Nagy-Borove*.)

**N° 22. L6 chondrite - Allan Hills 769.**

Chondritic texture with poorly defined chondrules. In a large pyroxene grain olivine inclusions can be found, and the pyroxene grain itself is also surrounded by olivine grains. (Among meteorites from Hungary *Mócs* and *Kakova* are of this type.)

**N° 23. LL3 chondrite - Yamato 790448.**

Dense with chondrules and fragments, mainly clinopyroxenes (some twinned). Cellular olivine containing fine fibre of glass. Also lamellar clinopyroxene with fine devitrifying glass fibres. Between chondrules sulfide type opaque patches.

**N° 24. LL4 chondrite - Yamato 74442.**

A rather well defined chondritic texture with a little bit brecciated character also with olivine and pyroxene grains.

**N° 25. LL5 chondrite - Allan Hills 78109.**

Poorly defined chondrules. Chondrules consisting of barred olivines grown together with lamellae with different directions. Also olivine chondrules+opaque minerals+olivine crystals together. (Among meteorites from Hungary cf. *Nyírábrány*.)

**N° 26. LL6 chondrite - Yamato 75258.**

Poorly defined chondrules, mainly of olivine. In a chondrule olivines radiate from an opaque core. Also olivine grains in the fine grained groundmass.

**N° 27. CI carbonaceous chondrite - Yamato 82162.**

Irregular chondrulic grains in dark carbonaceous groundmass. Fine fibrous material in one grain - devitrifying glass?

**N° 28. CM2 carbonaceous chondrite - Yamato 74662.**

In the dark carbonaceous matrix mainly olivine (clear, transparent) and pyroxene (less clear) chondrules occur.

**N° 29. CO3 carbonaceous chondrite - Yamato 791717.**

Well developed chondrules in a fine grained groundmass seeming fresh. Spheroidal olivine chondrules. In a chondrule olivine, metal and haematite together. A chondrule with skeletal olivine between glass, forming a spinifex textural character, all surrounded with olivine grains.

**N° 30. CV3 carbonaceous chondrite - Yamato 86751.**

Well defined chondrules in fine grained matrix. A chondrule with many small olivine and twinned clinopyroxene surrounded with glassy material. (Among meteorites from Hungary cf. *Kaba*.)

## 4. SUMMARY

The Japanese NIPR Antarctic Meteorite Educational Thin Section Set loan to Hungary was an excellent occasion to get an overview on the materials of the Solar System. It was edifying to compare the Antarctic meteorites to the NASA Lunar Sample. At the same time the Collection triggered to reinvestigate Hungarian meteorites fallen mainly in the last century. The Antarctic Meteorite Collection gave a reference and background.

## ACKNOWLEDGEMENTS

The authors highly appreciate getting the NIPR Antarctic Meteorite Collection for studies and thank the National Institute of Polar Research, Japan, specially to Dr. Keizo Yanai, curator of Antarctic Meteorites. Partly supported by OTKA 014958.

## REFERENCE

Yanai K. & Kojima H.: Photographic Catalog of the Antarctic Meteorites. NIPR. Tokyo, 1987.

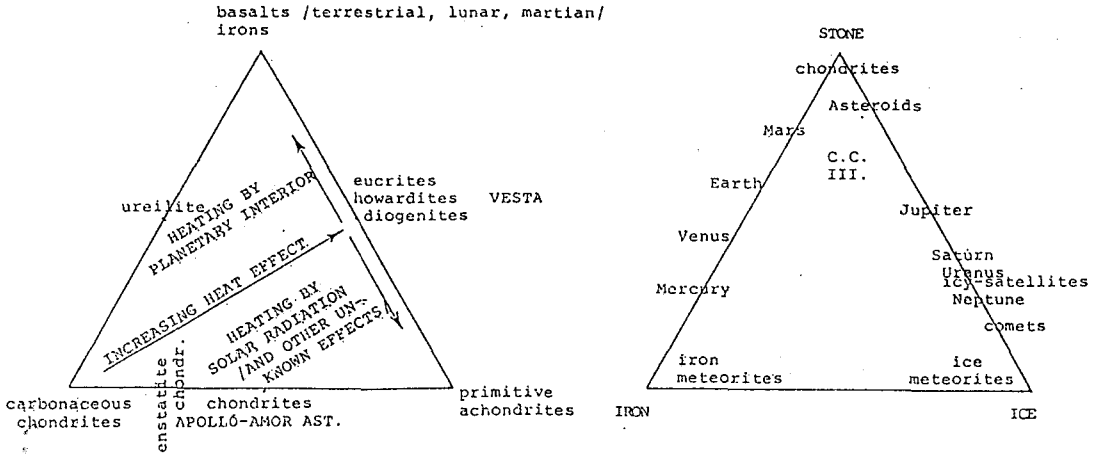


Fig. Two tentative classifications of meteorites according to their mixing with increasing solar distances and according to the heat effects suffered at different solar distances or inside planetary bodies.

| | 3 | 4 | 5 | 6 |
|---|---|---|---|---|
| E | EH3 chondrite Yamato-691 14 | | | |
| H | Yamato-791428 15 | Allan Hills-77233 16 | Yamato-74079 17 | Yamato-74014 18 |
| L | Yamato-74191 19 | Yamato-74355 20 | Yamato-790957 21 | Allan Hills-769 22 |
| LL | Yamato-790448 23 | Yamato-74442 24 | Allan Hills-78109 25 | Yamato-75258 26 |
| C | O Yamato-791717 29<br>V Yamato-86751 30 | | | |

27 CI Ch. Yamato-82162, and CM2 Ch. Yamato-74662 28

Fig. Chondrites of the Japanese Antarctic Meteorite Thin Section Set, arranged according to the Van Schmus and Wood system of chondrite petrologic types table.

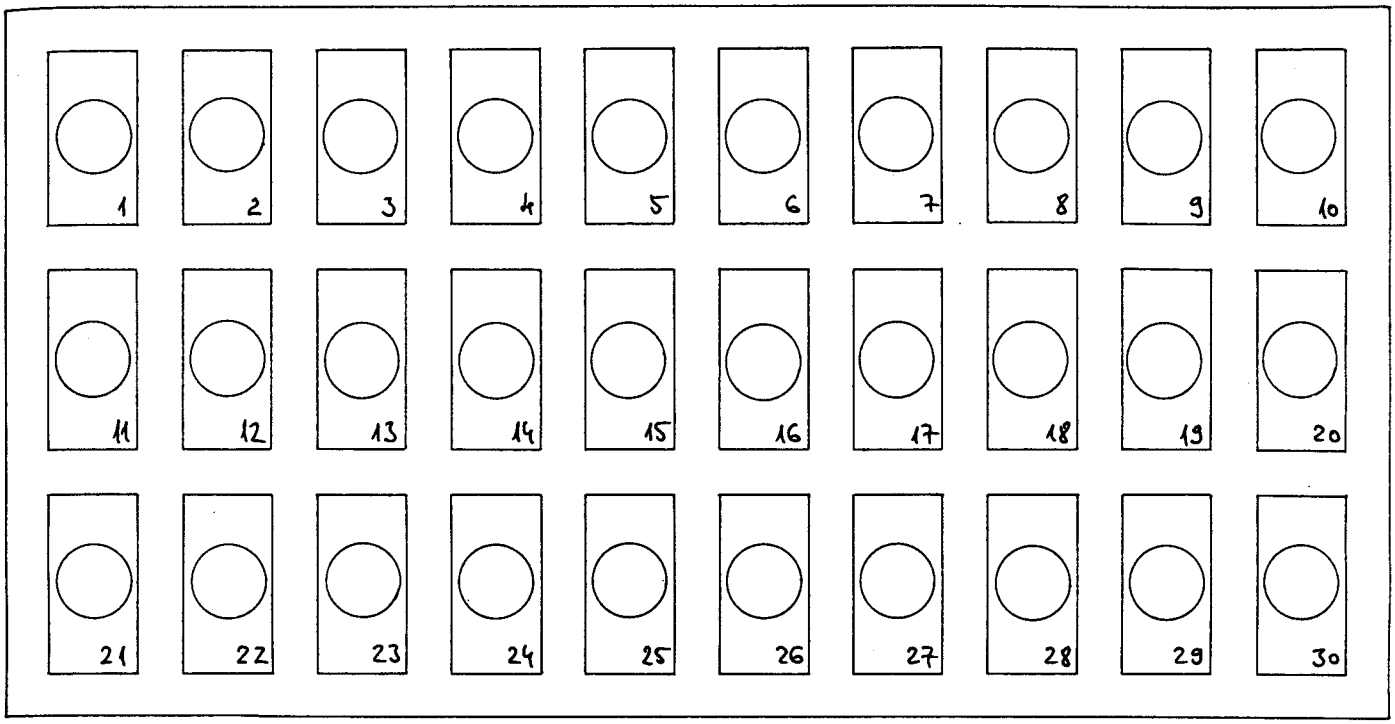


教育用南極隕石研磨薄片セット No. 2　　1993.6

| No. | Type | Meteorite Name | Sub Number | Remarks |
|---|---|---|---|---|
| 1 | Pallasite | Yamato-8451 | 50A-3 | Pyroxene Bearing, Fa9-11, Fs8-9 |
| 2 | Mesosiderite | Allan Hills-77219 | 74-5 | Fs19-31, An90-96 |
| 3 | Aubrite | Allan Hills-78113 | 82-1 | Monomict Breccia, Fs0-0.1, An25 |
| 4 | Ureilite | Allan Hills-77257 | 64-5 | Fa11-14, Fs11-13 |
| 5 | Diogenite A | Yamato-74097 | 64-4 | Crystalline(Recrystallized), Fs23-26 |
| 6 | Diogenite B | Allan Hills-77256 | 71-4 | Monomict Breccia, Fs22-25 |
| 7 | Howardite | Yamato-7308 | 77-3 | Polymict Breccia, Fa15-33, Fs21-57, An85-96 |
| 8 | Eucrite A | Yamato-791195 | 61A-3 | Crystalline, Fs54-57, An89-92 |
| 9 | Eucrite B | Yamato-74450 | 74-4 | Polymict Breccia, Fa72, Fs26-31, An78-93 |
| 10 | Shergottite | Allan Hills-77005 | 93-4 | Crystalline, Fa25-31, Fs20-21, An49-56 |
| 11 | Lunar Meteorite A | Yamato-86032 | 51-6 | Regolith Breccia, Fa63-93, Fs17-41, An91-97 |
| 12 | Lunar Meteorite B | Asuka-881757 | 228-2 | Mare Gabbro, Fa87-95, Px(wide range), An74-96 |
| 13 | "Primitive Achondrite" | Yamato-794046 | 53-6 | Fa18-20, Fs13-16 |
| 14 | EH3 Chondrite | Yamato-691 | 53A-3 | Fa0.1-2.5, Fs0.3-20 |
| 15 | H3 Chondrite | Yamato-791428 | 74-4 | Fa16-18, Fs5-26 |
| 16 | H4 Chondrite | Allan Hills-77233 | 82-4 | Fa16-18, Fs14-16 |
| 17 | H5 Chondrite | Yamato-74079 | 51-3 | Fa16-19, Fs15-17 |
| 18 | H6 Chondrite | Yamato-74014 | 70-3 | Fa18-20, Fs16-17, An11-12 |
| 19 | L3 Chondrite | Yamato-74191 | 58-3 | Fa12-25, Fs4-25 |
| 20 | L4 Chondrite | Yamato-74355 | 84-1 | Fa23-26, Fs20-21 |
| 21 | L5 Chondrite | Yamato-790957 | 72-5 | Fa23-25, Fs19-21 |
| 22 | L6 Chondrite | Allan Hills-769 | 75-6 | Fa23-25, Fs18-21, An11 |
| 23 | LL3 Chondrite | Yamato-790448 | 64-3 | Fa0.2-22, Fs1-30 |
| 24 | LL4 Chondrite | Yamato-74442 | 62-3 | Fa28-30, Fs7-24 |
| 25 | LL5 Chondrite | Allan Hills-78109 | 83-4 | Fa28, Fs23 |
| 26 | LL6 Chondrite | Yamato-75258 | 74-3 | Fa31-33, Fs24-25, An9 |
| 27 | CI Meteorite | Yamato-82162 | 4-7 | |
| 28 | CM2 Chondrite | Yamato-74662 | 50-7 | Fa0.2-53, Fs0.5-45 |
| 29 | CO3 Chondrite | Yamato-791717 | 66-1 | Ornans Type, Fa0.2-66, Fs0.6-14, An79 |
| 30 | CV3 Chondrite | Yamato-86751 | 52-3 | Vigarano Type, Fa0.1-45, Fs0.4-10, An46 |

# EXPERIMENTAL INVESTIGATIONS ON ALHA 77005 SHERGOTTITE SAMPLE FROM ANTARCTICA

I. Kubovics[1], Kamilla G. Sólymos[1], Sz. Bérczi[1,2], B. Lukács[3], Gy. Szakmány[1], K. Török[1]

[1] Dept. of Petrology & Geochemistry, R. Eötvös University, H-1088 Múzeum krt. 4a, Budapest, Hungary
[2] Dean's Office, R. Eötvös University, H-1088 Rákóczi út 5
[3] CRIP RMKI, H-1525 Bp. 114. Pf. 49, Budapest, Hungary

**ABSTRACT**

We have measured mineral compositions in ALHA 77005 Antarctic Shergottite sample from the NIPR Tokyo Collection. This paper is a preliminary report. Olivine and pyroxene content shows its basaltic/lherzolithic nature, maskelynite presence keeps the memory of the original shock to throw the rock into spatial orbit, while the sulphide composition suggests extraterrestrial origin.

## 1. INTRODUCTION

ALHA 77005 was the first shergottite meteorite collected on Antarctica (Yanai & Kojima 1987). Mittlefehldt & Lindström (1994) classified it into a clan of Martian Meteorites. We have got a small chip of ALHA 77005 on loan from NIPR, Japan, for studying local chemical compositions. These investigations corroborate the extraterrestrial origin and point strongly towards Mars.

## 2. OVERALL COMPOSITION

A thin section of ALHA 77005 can be found in the Antarctic Meteorite Thin Section Educational Set made in 1993 by the National Institute of Polar Research (NIPR), Tokyo, Japan, on loan in Budapest. We performed microscopic investigations on that thin section. The results are as follows.

Under microscope ALHA 77005 thin section from the NIPR collection shows brown pyroxene and glassy plagioclase (maskelynite), with some non-glassy plagioclase, and an opaque component (chromite?), texture is igneous. At the edge of one plagioclase grain fine grained plagioclase crystals can be seen, with glass between them.

In microscope the microprobe sample seems more lehrzolithic (in accord with Mittlefehldt & Lindström (1994)); both the diaplectic glass (maskelynite) and the region of melting and recrystallization refer to an impact dislodging the sample from its original site. Such glass formation is conform with impacts able to hurtle pieces onto orbit from smaller planetary bodies.

Generally, compared to lunar basalts of the NIPR and NASA Lunar Petrographic Thin Section Sets, and eucrites of the NIPR Thin Section Set, ALHA 77005 thin section seems less caleidoscopic under the microscope, so suggesting higher orientating effects (higher gravity?) and slower crystallisation.

However even these facts together do not prove Martian origin. Venus is out of question, since her atmosphere would stop a fragment before getting to solar orbit. However, as McSween & Stolper (1980) states, maskelynite does *not* rule out terrestrial origin, by a mechanism analogous to that of tektite formation: an impact may have formed the maskelynite, thrown the fragment up above the atmosphere, whence it returned later. (All of known tektites are non-basaltic, but the mechanism would work too with impact on basaltic surface.) So a detailed analysis is needed.

## 3. CHEMICAL ANALYSIS

We started with a microsonde investigation of the ALHA 77005 chip at some characteristic spots. The work is going on; this is a preliminary report. The full chip is shown by Fig. 1. Observe a "flag-like" shape at the top, slightly to the left. The major components are olivine, pyroxene, and two amorphous phases. One of them is of diaplectic glass origin, the other seems to have originated in melting; the compositions differ. The first one has plagioclase composition, so must be maskelynite, the second is a more basic silicate. In the specific chip olivine and pyroxene dominate. Fig. 2 shows the upper left part; Spot 1 is olivine, Spot 2 is pyroxene and Spot 3 (the "flag") has plagioclase composition, so it is maskelynite. In specific scattered places iron sulphide, chromite and pentlandite are identified, the latter with 2:3 Ni:Fe ratio. Fig. 3 shows a chromite spot near the "flag" as 1; 2 is olivine and 3 is pyroxene. Fig. 4 displays the immediate neighbourhood of the "flag". The numbers show the identified minerals as 1: iron sulfide, 2: plagioclase (i.e. maskelynite, being glass), 3: orthopyroxene, 4: olivine and 5: apatite.

So far nothing is contrary to terrestrial origin, more details are needed. Thus we have analysed the iron sulphide in one specific spot. The results in atomic numbers: Fe 49.2 %, S 50.3 %, others 0.5%. (Mean errors are not given in the present status of study.) This resembles terrestrial pyrrhotine, inclusion in basalts. But pyrrhotine has always $\geq 3$ % S excess. In the spot the sulphide is nearer to troilite than to pyrrhotine.

Troilite is usual in meteorites. In the Barshay-Lewis (1975) scheme it condensed at cca. 700 K. This temperature is higher than the condensation temperature of Venus, but troilite is guessed to be abundant in Earth, Mars and some asteroids. Theory suggests that the "iron core" of Mars is troilite.

## 4. CONCLUSION

It seems that the FeS composition in the studied spot of ALHA 77005 is not pyrrhotine but something between terrestrial pyrrhotine and meteorite troilite, nearer to the latter. This composition (to be checked in other spots), separates the sample from terrestrial basalts. Then, by exclusion, remains only Mars in System as source region. Of course, we have no direct information about the composition of Martian iron sulphides at the present status of art. Similarly, theoretical chemical studies may reveal the origin of the S excess in pyrrhotine; then one could predict degrees of excess in various environments.

## ACKNOWLEDGEMENT

The NIPR Dept. of Antarctic Meteorites, Tokyo, Japan is thanked for loaning the sample.

## REFERENCES

Barshay S. S. & Lewis J. S. 1975: in The Dusty Universe, eds. Field G. B. & Cameron A. G. W., Neale Watson New York

McSween H. J. & Stolper E. M. (1980): Sci. Amer. **242**, 54

Mittlefehldt D. W. & Lindström M. M. 1994: Abstacts of 19th Symp. Antarctic Meteorites. Tokyo, 1994, p. 59

Yanai K. & Kojima H.: Photographic Catalog of the Antarctic Meteorites. NIPR. Tokyo, 1987.

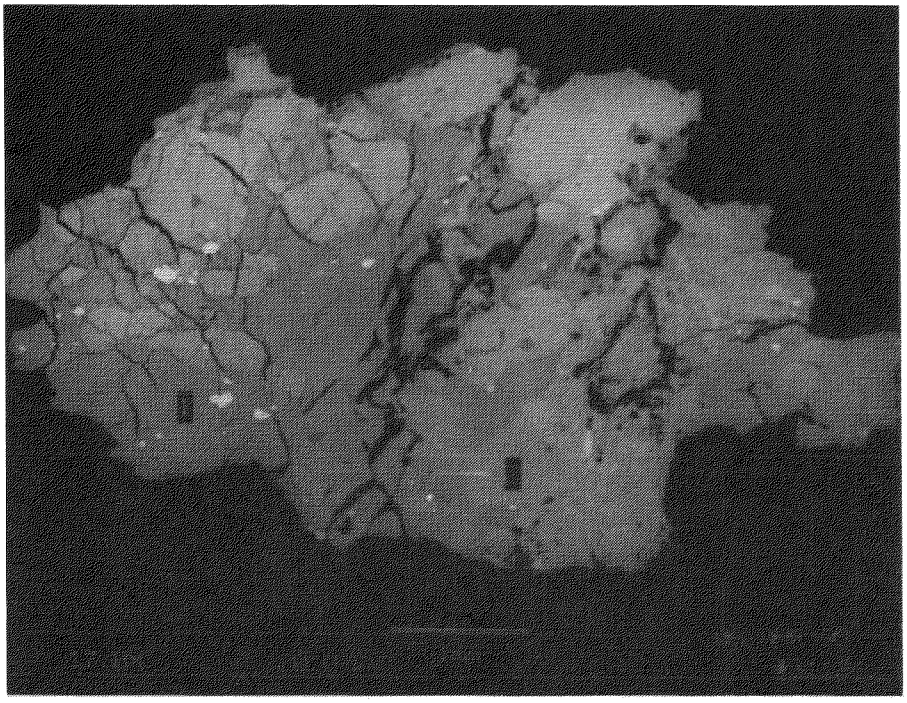

Fig.1.

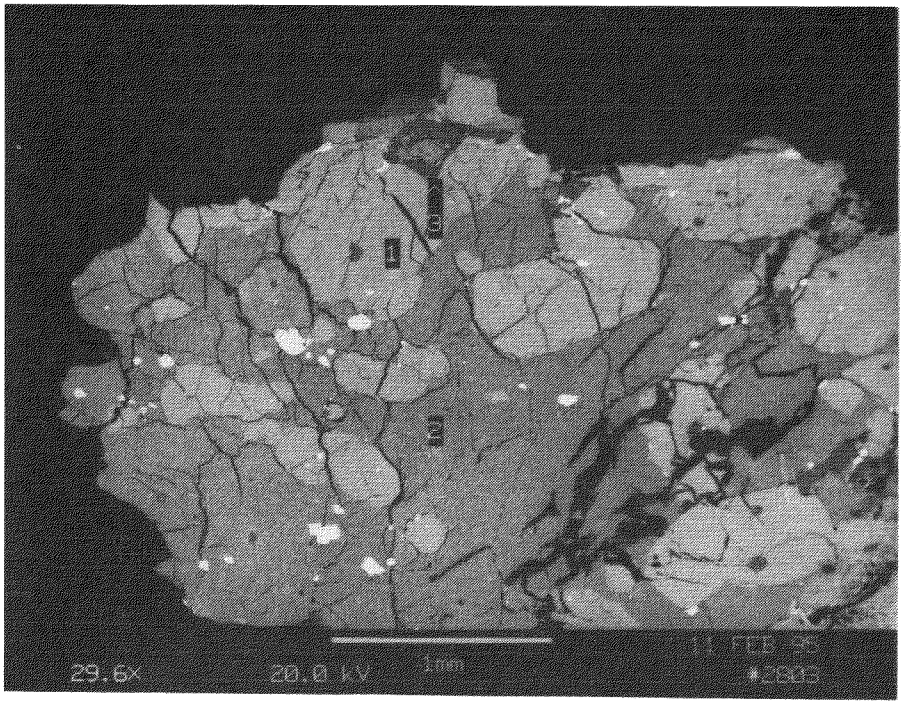


Fig.2.

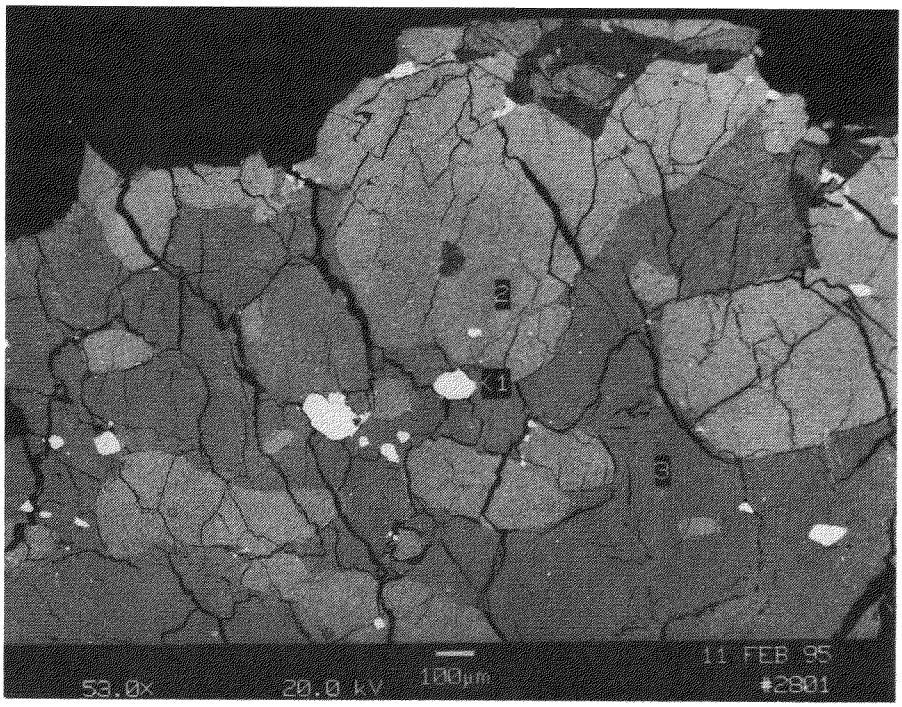
2
1
3
53.0x
20.0 kV
100µm
11 FEB 95
#2801

Fig.3.

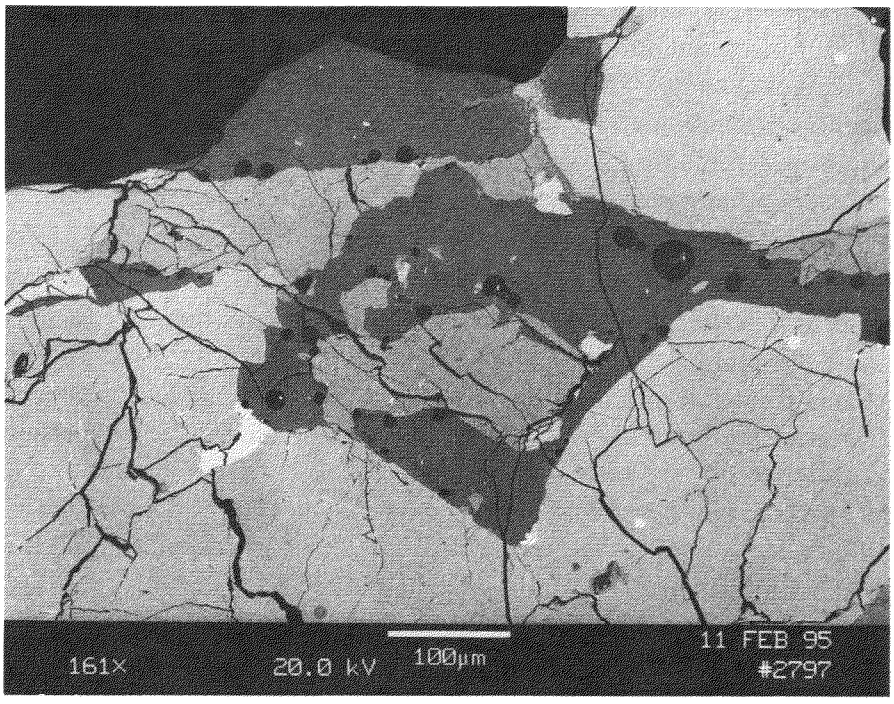
161x
20.0 kV
100µm
11 FEB 95
#2797

Fig.4.

THE ORIGIN OF TROILITE AND PYRRHOTITE IN CHONDRITES: II. COMPARATIVE STUDIES OF METAL-SULFIDE ASSEMBLAGES, D. S. Lauretta[1,2], D. T. Kremser[1], and B. Fegley, Jr.[1,2] (1) Dept. of Earth and Planetary Sciences, and (2) McDonnell Center for the Space Sciences, Campus Box 1169, Washington University, One Brookings Drive, St. Louis, MO 63130-4899 USA.

**Introduction.** Identification of pristine nebular condensates is of prime importance for determining the conditions of the early solar system. Chemical fractionation patterns that result from nebular processes provide an important constraint in the identification of such condensates. Here we present a summary of elemental fractionation observed during sulfide formation via a gas-solid reaction with an iron-nickel alloy. The resulting fractionation is distinctive of sulfurization processes and establishes a set of criteria to identify sulfide assemblages formed by such a process. The absence of these patterns in metal-sulfide assemblages in the LL3 chondrite ALH-764 indicate that these grains are not pristine nebular condensates but are the products of post formation heating events.

**Experimental Studies.** Sulfurization experiments were performed on pieces of the Sikhote Alin iron meteorite ($Fe_{0.95}Ni_{0.05}$) to study the microstructure and chemical fractionation that occurs during sulfurization. The details of the experimental and analytical procedures are discussed in [1]. Figure 1 shows a microprobe traverse across a sulfide layer formed at 923 K in 1% $H_2S$-$H_2$ gas mixtures. The total metal/sulfur ratio and the nickel mole fraction are plotted versus distance from the metal-sulfide interface. The metal to sulfur ratio is the deviation from stoichiometry (1-δ) in the mono-sulfide solid solution $(Fe,Ni)_{1-\delta}S$. At the metal-sulfide interface the sulfide is very nearly stoichiometric (δ~0). The value of δ increases with distance from the reaction interface, reaching a maximum value of 0.05 at the outer edge of the sulfide crystal. This pattern has also been reported by [2,3] and is indicative of sulfide formation via a gas-solid reaction [4].

We found significant amounts of nickel in the sulfide layer. Close examination revealed a sharp gradient in the nickel content of the metal at the reaction interface with values ranging from the initial composition of 5 atomic % to 18.5 atomic % nickel over a distance of 10μm. We also found small blebs of metal in an inner sulfide layer that contain as much as 37 atomic % nickel. The sulfide in this region contains ~2% NiS, as expected for a sulfide in equilibrium with the small metal blebs. The nickel content increases with distance from the metal interface, reaching a maximum value of ~6% NiS at the outer edge of the crystal. The gradient in the nickel content of the sulfide is the result of equilibrium of the sulfide at the two interfaces. The activity of NiS in equilibrium with the gas phase is higher than that in equilibrium with the metal. Increasing nickel content with distance from the interface was also observed by [3]. The enrichment of nickel in the metal is the result of preferential formation of iron sulfide during the early stages of reaction. The increased nickel content (and activity) of the metal causes larger amounts of nickel to enter the sulfide in order to maintain chemical equilibrium at the metal-sulfide interface.

These experiments demonstrate several key chemical fractionation patterns that can be used to identify sulfides formed via a gas-solid reaction with an iron-nickel alloy containing a small fraction of nickel. One is the variation in the stoichiometry of the sulfide caused by an increase in the sulfur content with distance from the metal interface. Another is the thin band of nickel enriched metal at the metal-sulfide interface. The presence of measurable amounts of nickel in the sulfide with nickel content increasing away from the metal interface is also suggestive of formation by this process.

**Analysis of Sulfides in ALH-764.** We counted a total of 66 metal-sulfide assemblages in the thin section ALH-764-71-4 (NIPR, Tokyo). A large number (33) of these assemblages occur in rims surrounding larger silicate chondrules. Twelve of the other metal-sulfide assemblages appear as anhedral blebs in the matrix and 7 are contained within other chondrules. Eight of the assemblages occur as intergrowths of metal or metal-silicate and sulfide. Only 6 of the assemblages display troilite rims surrounding metal grains. [5] uses the criteria of a two layer structure which many previous investigators [eg. 6,7], including ourselves [8,9], have found to be a common product of a gas-solid reaction. [5] claims that this morphology is a common occurrence in this chondrite, but we were only able to locate one grain with such a morphology, shown in Figure 2. This assemblage has a central core of iron-nickel metal, the majority of which is kamacite (5.4-6.2% nickel). Two small grains of taenite, both with average composition of ~47% nickel are also contained within the metal. The metal is surrounded in part by a two layer rim of troilite. The dark grain at the left edge of the metal has been semi-quantitatively identified as magnetite containing a small amount of sulfur (1.5-2.5%).

We performed extensive electron microprobe analyses in this region to look for the fractionation patterns indicative of formation via a gas-solid reaction. The locations of the analyses are shown in Figure 3. The sulfide composition was analyzed in three traverses, which are displayed in Figure 4. Several features of these traverses are noteworthy. First the sulfide composition at the metal-sulfide interface is not always that in equilibrium with the metal ($\frac{Fe+Ni}{S}$ = 1). Also, the layers do not show any sign of sulfur enrichment at the outer crystal edges. In fact, traverse 3 appears to be enriched in metal away from the interface. These profiles are not at all similar to those observed in the products of iron-nickel metal sulfurization. The nickel content of the sulfide is also plotted in Figure 4. All three traverses show very low nickel sulfide concentrations (less than 0.3% in all cases). There is no trend in nickel content in the sulfide with distance from the metal, and instead the values scatter randomly.

We also performed traverses across the metal. The results of these are presented in Figure 5. Traverses 4 and 5 were done across the large kamacite grain while traverse 6 was done on a taenite grain. Traverses 4 and 5 show increasing nickel content towards the center, a common feature of kamacite grains in ordinary chondrites [10,11]. We found no evidence of an enriched band of Ni at the outer edge of the metal grains. The traverse of the taenite grain contains two distinct regions, one having a composition of 50% nickel, the other with 40% nickel. We also analyzed the composition of the troilite in contact with the taenite. [12] presented formulas for calculating the equilibrium temperature from metal-sulfide assemblages. We have revised the formulas and calculate a temperature of 818K for the kamacite-troilite assemblage and a temperature of 983K for the taenite-troilite contact. Both of these are well above the calculated troilite condensation temperature of 716.5 K [1].

**Possible Sulfide Formation Scenarios.** The metal-sulfide rims surrounding the silicate chondrules are similar to those described by [13] for the Semarkona chondrite (LL3). [13] suggest that these rims formed during chondrule formation, when metal/sulfide melts migrated to the exterior of the chondrule and that later reheating caused the material to spread out into a fine grained rim material. A later reheating event could also explain the origin of the troilite rimmed metal grains. Experiments done by [10] show that heating of carbonaceous chondrite-like material produces significant sulfur mobilization even in solid phases. In these experiments troilite rims containing very little Ni (~0.5%) formed around pure Fe metal in a period of 20

hours. Ni was also extremely mobile and virtually all of it moved from the matrix material into the metal phase.

**Conclusions.** Chemical analyses of a two-layer troilite rimmed metal grain in ALH-764 does not show any evidence of formation via a gas-solid reaction. Key patterns include an outer nickel enriched band in the metal, an increase in the sulfur content of the sulfide towards the outer edge of the crystal, and significant amounts of nickel in the sulfide layer. We feel that these criterion are necessary to establish the origin of such mineral assemblages and that textural arguments are insufficient for identifying nebular condensates. A more probable explanation for the origin of these rims is sulfur mobilization during a later reheating event. There are many possibilities for the formation of the two layer structure including multi-stage sulfur mobilization, disruption of the initial sulfide layer during formation and chance contact between two or more sulfide rimmed grains. It is absolutely necessary to perform detailed chemical analyses when attempting to identify pristine nebular condensates.

**References.** [1] D. S. Lauretta, D. T. Kremser and B. Fegley Jr. 1995 LPSC XXVI. [2] T. Narita and K. Nishida 1973 Trans. Japan Inst. Met. 14, 447-456. [3] J. P. Orchard and D. J. Young 1989 J. Electrochem. Soc. 136, 545-550. [4] C. Wagner in Atom Movements, 153-173, ASM Cleveland. [5] N. Imae 1994 Proc. Japan Acad. 70, Ser. B 133-137. [6] E. M. Fryt, W. W. Smeltzer and J. S. Kirkaldy 1979 J. Electrochem. Soc. 126, 673-683. [7] W. L. Worrel and E. T. Turkdogan 1968 Trans. AIME 242, 1673-1678. [8] D. S. Lauretta and B. Fegley, Jr. 1994 Meteoritics 29, 490. [9] D. S. Lauretta and B. Fegley, Jr. 1994 in Abstracts of the 19th Symposium on Antarctic Meteorites, 62-65. [10] H. Nagahara 1979 Proc. of the Fourth Symposium on Antarctic Meteorites 111-122. [11] J. A. Wood 1967 Icarus 6, 1-49. [12] N. I. Bezmen, V. S. Lotov and Ye. G. Osadchiy 1978 Geokhimiya 10, 1466-1473. [13] J. N. Grossman and J. T. Wasson 1987 Geochim. Cosmochim. Acta 51, 3003-3011.

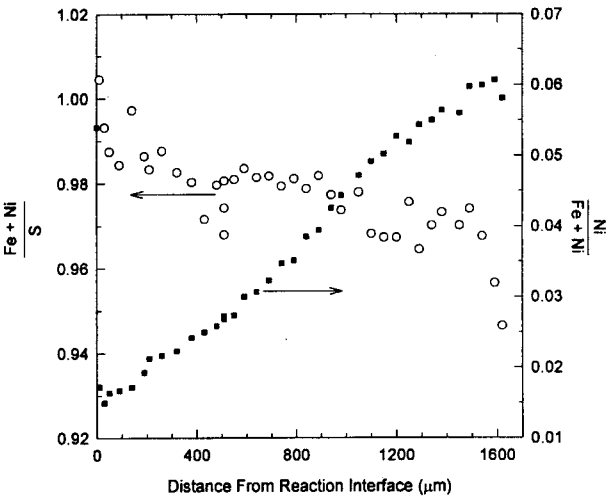


Figure 1. Elemental composition of experimentally produced sulfide layer. Open circles correspond to the y-axis on the left, closed to the y-axis on the right.

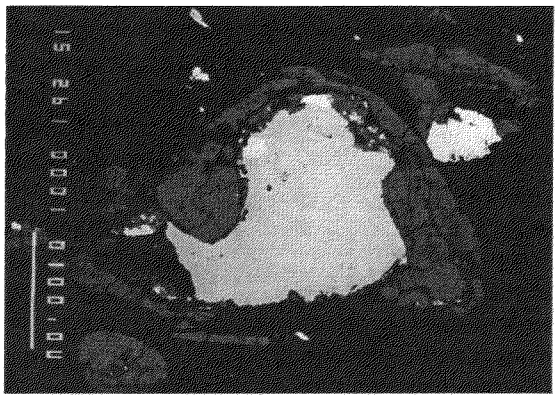

Figure 2. Metal-sulfide assemblage showing two layer structure. Scale bar corresponds to 100 microns.

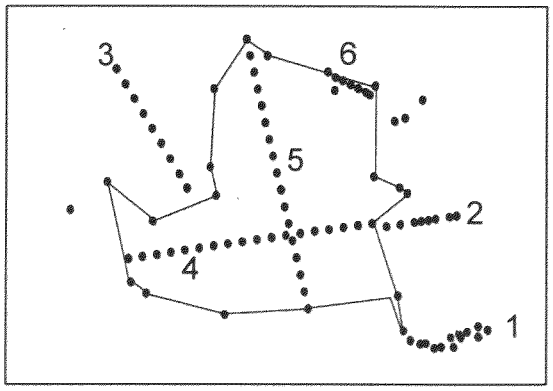


Figure 3. Locations of microprobe spot analyses. Outline shows metal-sulfide interface.

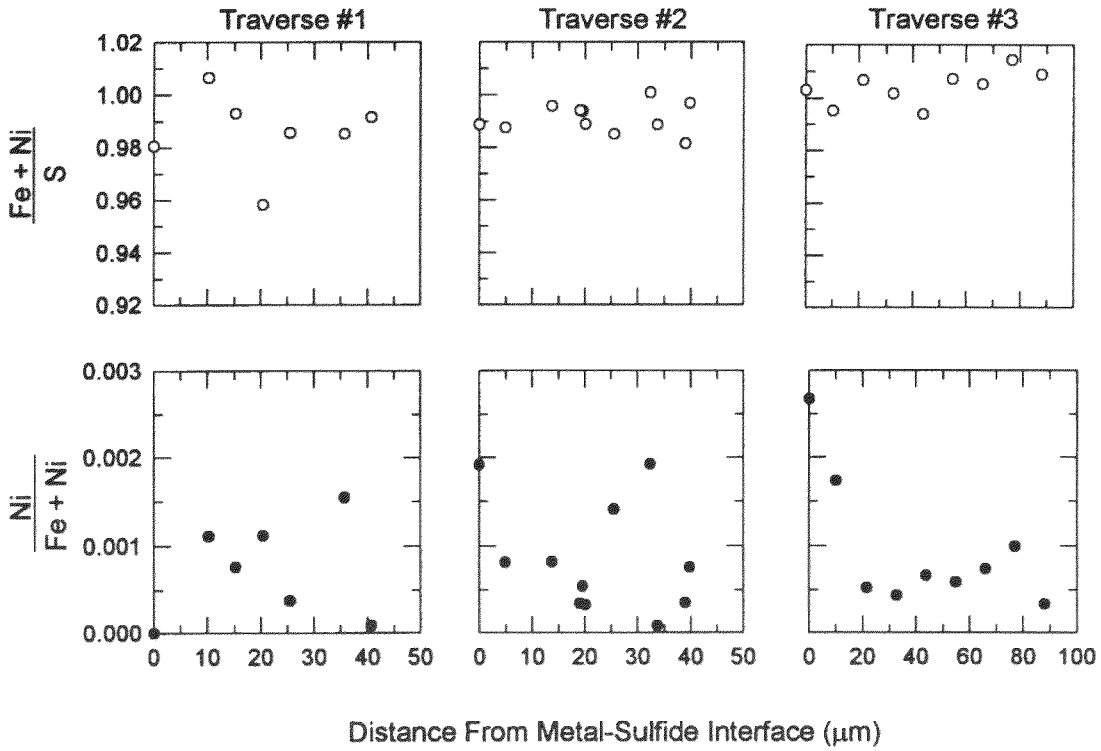


Figure 4. Elemental composition of sulfide layers.

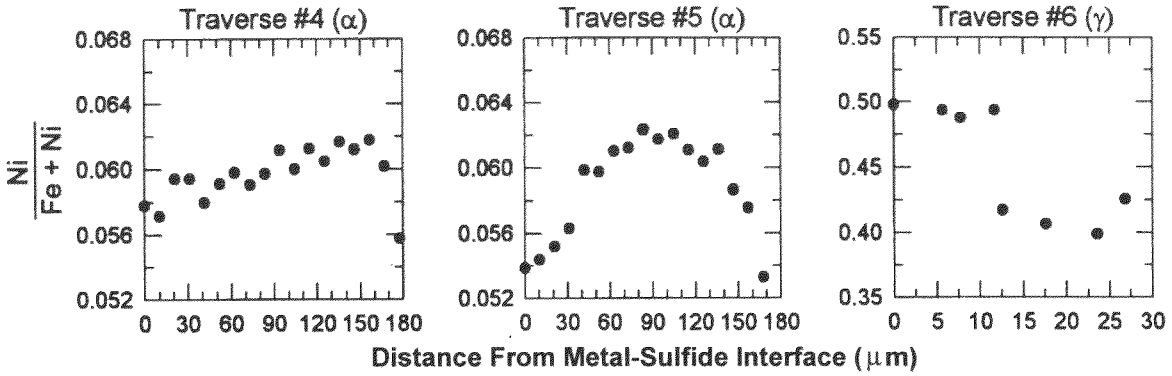


Figure 5. Elemental composition of metal grains.

# Comet Impact As a Cause of The Origin of Tektites

Lin Wenzhu
(Institute of Geochemistry, Chinese Academy of Sciences)

Most investigators believe that tektite are impact-produced glasses, but some conclusion until now are still unclear. Firstly, in the four tektite strewnfields, only Ivory Coast and Czechoslovakia tektite strewnfields are proved to have its own primary impact craters, but the primary craters of both North America and Australia tektite strewnfields are not found until now. That's a real puzzle! It is also pointed out that only using a single impact event to explain the width of distribution area of tektites is difficult according to the principle of aerodynamics; Secondly, many impact craters, more specially Cenozoic impact craters, do not have tektites existed in or around craters, and only have melt rock sheet-impactite existed; Thirdly, at least three different microtektite/ microspherule layers have been recognized in late Eocene sediments, recently Hazal(1990) suggested that as many as seven stratigraphical distinct layers of late Eocene impact ejecta may existed. The hypothesis of single impact event is also hard to explain this tektite distribution phenomenon; Finally, most tektites do not contain anomaly siderophile elements.

Comet are caused by perturbation of the Oort cloud due to close passage of neighboring stars. The comet may be disrupted to be highly fragmented. The fragment each other can be apart from very long distance, but lie along a line and travel on the same trajectory. Comet consists of hydrocarbons, volatile ices and silicates, so its bulk density is small. When comet colloids with Earth at supervelocity 60Km/s, if comet explodes at Earth's atmosphere or hits the solid earth surface, impacting would heat and melt large area material near surface, then eject and condense melt to produce tektites, just as the phenomenon observed in explosion of nuclear bomb laid at tower or nuclear explosion happened at earth surface respectively, if during its journey to Earth the comet has been fragmented, just as presently observed Shoemaker-Levy 9, it would yield multiple impact cratering to make tektite distributed in wide areas, maybe it is the real reason for the origin of the tektite strewnfields.

A lot of explosion experiments suggested that ejecta deposit was thickest at the rim of crater and thins with increasing distance from the rim. Thus, Falling back to Earth surface tektites (melt glasses) should distribute around the crater, maybe in some distance but no far away from the crater. However, we have not observed this phenomenon for most known impact craters. From viewpoint of cratering author suggests that at the instant of impacting explosion temperature in the cavity was high enough to vaporize most melt rocks formed by pressure above 55GPa again, only

a few melt and debris mixtures can be remained to form impactite sheets and there is not too much melt to eject to form tektites during the process of impact cratering. So, energy released from impacting is key factor to distinguish comet impact from asteroid impact. Compared with asteroid impact energy released by comet impact or nuclear explosion is too small to make melt rocks vaporized again and to form the deeper craters, maybe this is one reason why few comet impact craters have been recognized. Moreover, explosion experiments and the field evidences show that the low-energy impact cratering could produce concentric ring faults in base rocks. Based on this reason author considers that Chesapeake Bay crater, which was manifested to exist concentric ring faults from the study of the seismic reflection by Poag et al(1994), probably is the source crater of North America tektite strewnfield.

Reference: Lin wenzhu and Ouyang Ziyuan, Scientia Geologica Sinica 1991 2, 148-157. Hazel,J.E. Palaios 1990 4, 318-329. Crieve,R.A.F.,Meteoritics 1990 26, 175-194. Takata,T.,et. al. ICARUS 1994 109.3-19. Poag,C.W. et. al. Geology 1994 22, 691-694. Polanskey,C.A. and T.J. Ahrens ICARUS 1990 87, 140-155.

**EXPERIMENTAL PARTITIONING OF RARE EARTH ELEMENTS BETWEEN SULFIDES (FeS, CaS) AND SILICATE MELT AND APPLICATIONS TO ENSTATITE ACHONDRITES** K. Lodders, Washington University, Department of Earth and Planetary Sciences, Campus Box 1169, St. Louis, MO 63130-4899, U.S.A.

**Synopsis:** Partition coefficients of the rare earth elements (REE) between sulfides (FeS or CaS) and silicate melt were determined experimentally at 1200-1300°C. The REE sulfide/silicate partition coefficients (D) are $\leq 1$ under the experimental oxygen and sulfur fugacities. REE partition coefficients in the FeS/silicate system decrease from light to heavy REE, while the opposite behavior is found for the CaS/silicate system. In both sulfide systems Eu is preferentially incorporated into the sulfide phases. The Eu sulfide/silicate partition coefficient is about a factor of ten higher than that of neighboring Sm and Gd, in accordance with thermodynamic predictions of REE sulfide/silicate partition coefficients. The low sulfide/silicate partition coefficients indicate that CaS (oldhamite) in enstatite achondrites (aubrites) cannot have gained its high REE concentrations during igneous differentiation processes. The high REE concentrations and the REE patterns in oldhamite can be explained by REE condensation into refractory CaS. The refractory nature of CaS prevented major exchange reactions of the oldhamite with other aubritic minerals during the short differentiation and metamorphism period on the aubrite parent body. Thus, oldhamite in aubrites is probably a slightly metamorphosed relict condensate, as suggested earlier.

**Introduction:** The distribution of the REE among minerals in the highly reduced enstatite achondrites may provide information about the differentiation process on the aubrite parent body (APB). In order to model crystallization processes the REE distribution in aubritic minerals and the partition coefficients for the relevant mineral/melt systems need to be known. Several measurements of REE abundances in bulk aubrites and in their individual mineral phases are available (e.g., Schmitt *et al.*, 1963; Masuda, 1967; Wolf *et al.*, 1983; Graham and Henderson, 1985; Floss and Crozaz 1993, Lodders *et al.*, 1993; Wheelock *et al.*, 1994). Likewise, the REE mineral/melt partition coefficients for silicates (e.g., pyroxene, olivine, diopside, plagioclase) found in aubrites are available (Kennedy *et al.*, 1993; Grutzeck *et al.*, 1974; Drake and Weill, 1975). However, oldhamite is the main REE carrier in enstatite meteorites (e.g., Larimer and Ganapathy, 1987; Lundberg and Crozaz, 1988; Floss *et al.*, 1990; Lodders and Palme, 1991). Several bulk aubrite analyses show relative Eu-depletions (e.g., Wolf *et al.*, 1983), and because the REE show chalcophile behavior in aubrites, some Eu may have been removed by an Fe-FeS melt during formation of the metal-sulfide core in the APB (Lodders and Palme, 1989,1990). Thus, the REE sulfide/silicate partition coefficients for CaS and FeS must be known for modeling the igneous differentiation history of the APB. This paper gives an overview and more discussion about experimental procedures and updates implications described earlier (Lodders and Palme, 1989, 1990; Lodders *et al.*, 1990; Lodders, 1991).

**Experimental:** Charges in the **FeS/silicate** system were made of about 200 mg of a tholeiitic basalt, 200 mg Fe powder, and 60-150 mg sulfur. The powdered basalt was mixed with REE-oxides at the ppm level for instrumental neutron activation analyses (INAA) or with a selected set of three REE-oxides at the one percent level for electron microprobe (EMP) analyses. Charges for **CaS/silicate** partitioning experiments consisted of 200 mg silicate similar in composition to the silicate portion of enstatite chondrites and 200 mg synthetic CaS. The starting silicate was fused from $SiO_2$, $Al_2O_3$, MgO, $TiO_2$, $Na_2CO_3$, $K_2CO_3$ and a set of three REE-oxides (La, Yb, Lu or Sm, Eu, Gd) in the percent level range suitable for EMP.

The powdered starting materials were equilibrated at 1200-1300°C in evacuated quartz tubes. More reducing conditions were produced by placing some samples in corundum or mullite crucibles, which were surrounded by Al-foil and then heated in evacuated quartz tubes. All CaS/silicate experiments were done by placing the charge into mullite crucibles, which were heated in evacuated quartz tubes. The duration of the experiments was limited by the stability of the quartz tubes at 1200 or 1300°C, especially under more reducing conditions, where the tubes tended to implode during quenching in air. The FeS and CaS-bearing charges were sectioned and polished in oil for EMP analyses. The sulfide and silicate in the FeS-bearing charges were also separated for INAA. The INA analyses were done by irradiating samples at the TRIGA Mark II reactor of the Johannes Gutenberg-Universität Mainz, Germany. Gamma ray counting procedures and evaluation of spectra were done by using the standard methods of the Mainz cosmochemistry group. EMP-analyses were done with the CAMECA SX50 electron microprobe at the Lunar and Planetary Laboratory in Tucson, Arizona. The REE were analyzed using ZAF correction procedures and the REE standards of Drake and Weill (1972).

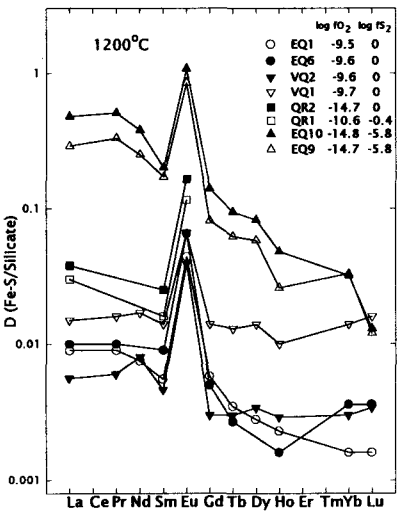


Figure 1:
REE FeS/silicate partition coefficients

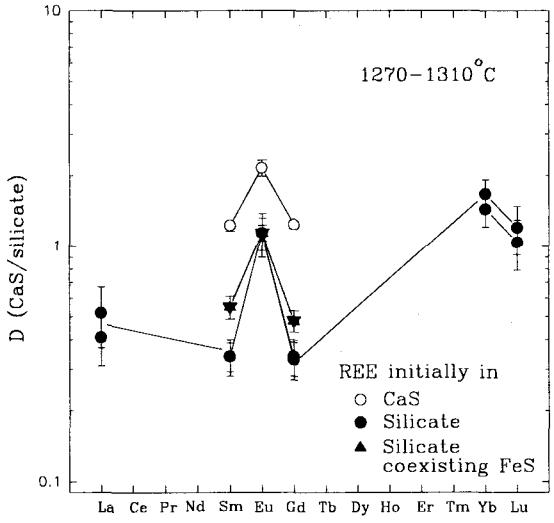


Figure 2:
REE CaS/silicate partition coefficients

**Results:** Results are shown in Figure 1 and 2. The partition coefficients (D) are expressed as weight ratios of concentration in sulfide over concentration in silicate matrix.

The charges from the **FeS/silicate** experiments resulted in FeS spherules and silicate. REE FeS/silicate partition coefficients decrease from light to heavy REE, except for Eu, which partitions about ten times stronger into the sulfide than neighboring Sm or Gd. Experiments conducted under more oxidizing conditions show lower REE FeS/silicate partition coefficients than in reducing experiments where Al-foil was present as an oxygen getter. The oxygen and sulfur fugacities in the FeS bearing experiments were calculated from the phase assemblage after the experiment (see Lodders and Palme, 1991).

In all experiments in the **CaS/silicate** system, small CaS grains are surrounded by silicate melt. Larger CaS aggregates probably formed during sintering. A CaS melt is not expected at T = 1200-1300°C because of the high melting point of CaS (2450±50°C). After the experiment, CaS contained up to 5 wt% Mg from exchange reactions with the silicate. Although the starting silicates are essentially CaO-free, the matrix can contain up to 15 wt% CaO after equilibration with CaS. REE partition coefficients at temperatures between 1270-1310°C show an increase from light to heavy REE (DLa ~ 0.5 to DLu ~ 1.1), with the exception of Eu (Figure 2). Europium shows a preferential incorporation into CaS (DEu ~ 1.2), relative to neighboring Sm and Gd. The partitioning behavior of Eu between CaS and silicate is similar to its partitioning between FeS and silicate. However, the overall trend for REE partitioning into CaS is a decrease in D values from LREE to HREE. This trend is opposite to that found for REE partitioning between FeS and silicate. Reversal experiments, which used REE-spiked CaS and initially REE-free silicate yield somewhat higher CaS/silicate partition coefficients (about a factor of 2 for Eu and ~4 for Sm and Gd). This indicates that equilibrium was not reached within the duration of the experiments. Thus, results of the reversal experiments represent upper limits for REE partitioning between CaS and silicate melt.

**Comparison of REE Sulfide/Silicate Partition Coefficients with Other Data:** The overall trend that REE FeS/silicate partition coefficients decrease from La to Lu and REE CaS/ silicate partition coefficients increase from La to Lu was also found by Jones and Boynton (1983) and Dickinson *et al.* (1990a,b, 1991). However, absolute D values are up to ten times higher for FeS/silicate and up to 20 times higher for the CaS/silicate partition coefficients than values found here. These differences may be due to the different composition of the sulfide and silicate phases and are also due to different $fO_2$ and $fS_2$ conditions. The major difference in partitioning behavior was found for Eu. Dickinson *et al.* (1990a,b) found that DEu for (Ca,Mg)S/basaltic liquid was smaller than D values for neighboring Sm and Gd. This behavior of Eu is opposite to that found in the experiments here, where DEu > DSm~DGd. The chemical behavior of $Eu^{2+}$ is similar to that of $Ca^{2+}$ and Eu may be preferentially incorporated into Ca-rich, Mg-poor sulfides over Mg-rich, Ca-poor sulfides. The CaS in the experiments here contains about 48-50 wt% Ca and up to 5 wt% Mg while the CaS in experiments by Dickinson *et al.* contains about 30 wt% Ca and is thus more Mg-rich. Other

results by Dickinson *et al.* (1991) indicated that the partitioning of Eu may depend on the oxygen fugacity. Thermodynamic calculations of partition coefficients can show that this is indeed the most likely explanation for the apparent discrepancies between the two different experimental results.

**Application to Enstatite Achondrites:** To test if aubrites formed by crystallization from a single parent melt the REE concentration ratios in the mineral phases are compared to the respective partition coefficient ratios. A comparison of observed and predicted ratios shows that these ratios disagree and indicates that the REE bearing minerals are not in equilibrium. Co-crystallization from a parent melt can be excluded as also discussed by Graham and Henderson (1985). The other possible crystallization process is fractional crystallization and subsequent removal of crystallized phases from the melt (Okada *et al.* 1988). Graham and Henderson (1985) concluded that a late crystallization of plagioclase in a fractional crystallization sequence is consistent with the REE distributions in the Mayo Belwa aubrite. However, the high REE concentrations in oldhamite are not explained by any of these crystallization processes.

In any crystallization sequence, the refractory oldhamite is expected to be among the first phases to crystallize (although it is not clear how CaS can crystallize from a Mg-rich melt). Partition coefficients of about 100-200 are necessary to extract all REE from a melt into the small amount (~1 wt%) of CaS found in aubrites. However, the measured partition coefficients are about $\leq 1$. If we assume that enstatite and olivine crystallize and CaS continues to equilibrate with the remaining melt, REE partitioning into CaS is more efficient. However, even in this case, neither the observed REE abundances in CaS nor the abundance patterns can be explained by partitioning. One could argue that the experimentally determined partition coefficients are too small because equilibrium was not reached between the CaS and silicate melt. However, the reversal experiments gave D values within a factor of 2-4 of the D values obtained from experiments with REE-doped silicate. Furthermore the independent work by Jones and Boynton (1983) and Dickinson *et al.* (1990a,b, 1991) also gave partition coefficients << 100. Thus, models postulating the efficient incorporation of REE into oldhamite from silicate magma are not supported by the available experimental data and appear extremely unlikely.

Another problem with crystallization processes is that they cannot explain the different REE patterns in oldhamite or diopside. At least 12 different types of patterns have been observed for oldhamite and at least three different patterns have been reported for diopside (Floss and Crozaz, 1993). Lodders and Palme (1990) proposed that oldhamite in aubrites is a relict phase from the solar nebula. The diversity of REE patterns in aubritic oldhamite was also seen as an indicator of relict origin of oldhamite (Floss *et al.*, 1990, Kurat *et al.*, 1992; Floss and Crozaz, 1993). The REE abundances and REE patterns in oldhamite from aubrites are similar to those in enstatite chondrites, which can be explained by REE condensation into oldhamite from a highly reduced nebular gas (Lodders and Fegley, 1993). Other indicators of the condensation origin of aubritic oldhamite are the mass independent sulfur isotopic anomalies observed by Thiemens *et al.* (1994).

Wheelock *et al.* (1994) proposed that oldhamite in a oldhamite-dominated clast in Norton County crystallized from a melt and that the high REE abundances in the CaS resulted from equilibration with the aubritic melt. This suggestion is favored by the large (up to 2 cm) crystal size, which cannot have formed by condensation processes. They postulated the presence of a liquid CaS phase because forsterite grains are surrounded by oldhamite, and because rounded sulfide blebs occur in oldhamite. However, for *liquid* CaS temperatures of about 2450°C are required and even if melting point depression of CaS due to dissolved MnS, FeS, or MgS is considered, it is doubtful if these temperatures were reached on the APB (Lodders *et al.*, 1993). High temperatures would also lead to substantial vaporization of e.g., Na, K, Si, and Mg (Fegley and Cameron, 1987). However, evaporative loss did not occur because aubrites still contain moderately volatile elements such as Na and K.

**Preferred differentiation model of the aubrite parent body and the origin of oldhamite**: The aubrite parent body assembled from material compositionally similar to EH-chondrites (Fogel *etal.*, 1988; Lodders *et al.*, 1993). The REE are mainly located in oldhamite, which gained REE during condensation, as reflected by the diversity of its REE patterns and the high REE abundances. Impact melting leads to heating and differentiation of the APB. Once temperatures reach ~1000°C, the Fe-FeS eutectic started segregating to form a core. Since oldhamite contains the REE and is not expected to be involved in major exchange reactions at these temperatures, the segregating FeS cannot take up any significant amounts of REE. The low density of CaS (2.5 g/cm$^3$) allowed floatation and accumulation of small CaS grains once the silicates started melting.

The collection of CaS by a silicate melt may be the reason for the CaS-rich 1.6 cm long impact produced melt vein in the Jajh deh Kot Lalu (EL6)- enstatite chondrite (Rubin *et al.*, 1995). Once larger concentrations of CaS are produced, sintering can occur leading to larger CaS aggregates. However, not all oldhamite inherited from the enstatite chondrite-like precursor may come in contact with melt and accumulate. Most oldhamite in aubrites is small and comparable in grain size with that in enstatite chondrites (30-200 μm; Larimer and Ganapathy, 1987).

Lodders *et al.* (1993) previously proposed that the different REE patterns in diopside can be understood if diopside was formed from oldhamite. Fogel *et al.* (1988) suggested the reaction of oldhamite with enstatite to form diopside and forsterite. In that case, the diopside would inherit the REE inventory of the oldhamite. If diopside formed solely by crystallization from a melt, only the REE pattern expected from diopside/melt partitioning should be observed, instead of the different types of patterns which are actually found. Crystallization processes also cannot explain the observed plagioclase zoning with anorthite at the rim and albite in the center, which was described by Wheelock *et al.* (1994) for an oldhamite dominated clast in the Norton County aubrite. Anorthite is more refractory than albite and crystallizes first. Thus a crystallization process predicts an anorthite rich interior and albitic rim instead.

It appears that the oldhamite from the precursor material of aubrites underwent different degrees of exchange reactions with its surrounding minerals but that these exchange reactions never reached equilibrium. These exchange process should also lead to zoning profiles in the REE distributions among minerals coexisting with CaS. Further REE measurements on such mineral assemblages may reveal that the REE underwent metamorphic redistribution. For example, preliminary ion probe investigations of enstatite in contact with oldhamite from the Pena Blanca Spring aubrite (Fahey *et al.*, 1995) show a falling concentration gradient of the REE from the oldhamite-enstatite interface towards the enstatite interior. Clearly more analytical work on aubrites and experimental work for modeling the behavior of REE among aubritic minerals is needed to understand the differentiation history of the APB.

*Acknowledgments*: Experimental work on REE partitioning was performed at the Max-Planck Institut für Chemie, Mainz, Germany. Experiments on the CaS/silicate system were performed at the Lunar and Planetary Laboratory in Tucson, Arizona. The data analysis and preparation were supported by NASA grant NAGW-2861.

**References:** Dickinson T. L., Lofgren G. E., and McKay G. A. (1990a) *Lunar Planet. Sci.* **21**, 284-285. Dickinson T. L., Lofgren G. E., and McKay G. A. (1990b) *Meteoritics* **25**, 358. Dickinson T. L., Lofgren G. E., and McKay G. A. (1991) *Lunar Planet. Sci.* **22**, 319-320. Drake M. J. and Weill D. F. (1972) *Chem. Geol.* **10**, 179-181. Drake M. J. and Weill D. F. (1975) *Geochim. Cosmochim. Acta* **39**, 689-712. Fahey A., Huss G., Wasserburg G. J. and Lodders K (1995) *Lunar Planet. Sci.* **26**, 385-386. Fegley B. and Cameron A. G. W. (1987) *Earth Planet. Sci. Lett.* **82**, 207-222. Floss C., Strait M. M., and Crozaz G. (1990) *Geochim. Cosmochim. Acta* **54**, 3553-3558. Floss C. and Crozaz G. (1993) *Geochim. Cosmochim. Acta* **57**, 4039-4057. Fogel R. A. Hess P. C. and Rutherford M. J. (1988) *Lunar Planet Sci.* **19**, 342-343. Graham A. L. and Henderson P. (1985) *Meteoritics* **20**, 141-149. Grutzeck M., Kridelbaugh S., and Weill D. (1974) *Geophys. Res. Lett.* **1**, 273-275. Jones J. H. and Boynton W. V. (1983) *Lunar Planet. Sci.* **14**, 353-354. Kennedy A. K., Lofgren G. E., and Wasserburg G. J. (1993) *Earth Planet. Sci. Lett.* **115**, 177-195. Kurat G., Zinner E. and Brandstätter F. (1992) *Meteoritics* **27**, 246-247 .Larimer J. W. and Ganapathy R. (1987) *Earth Planet. Sci. Lett.* **15**, 123-134. Lodders K. and Palme H. (1989) *Meteoritics* **24**, 293-294. Lodders K. and Palme H. (1990) *Lunar Planet. Sci.* **21**, 710-711. Lodders K. (1991) Ph. D. thesis, Univ. Mainz, Germany. Lodders K. and Palme H. (1991) *Earth Planet. Sci. Lett.* **103**, 311-324. Lodders K., Palme H., and Drake M. J. (1990) *EOS Trans. AGU* **71**, 1434. Lodders K. and Fegley B. (1993) *Earth Planet. Sci. Lett.* **117**, 125-145. Lodders K., Palme H. and Wlotzka F. (1993) *Meteoritics* **28**, 538-551. Lundberg L. L. and Crozaz G. (1988) Meteoritics **23**, 285-286. Masuda M. (1967) *Geochem. J.* **2**, 111-135. Okada A., Keil K., Taylor G. J. and Newsom H. (1988) *Meteoritics* **23**, 59-74. Rubin A. E., Scott E. R. D. and Keil K. (1995) *Lunar Planet. Sci.* **26**, 1197-1198. Schmitt R. A, Smith R. H. Lach J. E., Mosen A. W., Olehey D. A. and Vasilevskis J. (1963) *Geochim. Cosmochim. Acta* **27**, 577-622. Thiemens M. H., Brearley A., Jackson T., and Bobias G. (1994) *Meteoritics* **29**, 540-541. Wheelock M. M., Keil K., Floss C. Taylor G. J. and Crozaz G. (1994) *Geochim. Cosmochim. Acta* **58**, 449-458. Wolf R., Ebihara M., Richter G. R. and Anders E. (1983) *Geochim. Cosmochim. Acta* **47**, 2257-2270.

# ON SOME ANCIENT METEORITE FALLS

B. Lukács
Central Research Institute for Physics RMKI, H-1525 Bp. 114. Pf. 49., Budapest, Hungary

**ABSTRACT**

We list four historically important meteorite falls between 1500 BC and 450 AD. Up to now in none of them has the meteorite been identified and investigated.

## 1. INTRODUCTION

Going back in time meteorite events become more and more hazy. However some meteorite falls were reported in history, and behind some events there *may* have been meteorite falls. In the followings we mention 4 examples.

First observe that iron was not produced artificially anywhere up to the second half of the 2nd millenium BC, since the Fe-O binding is rather strong. The first community producing iron is mentioned by ancient Greeks as Khalybs, somewhere in the southeastern corner of Black Sea, just south of modern Georgia. Previously iron came from iron meteorites, in Egypt as far back as 3500 BC, and was used for jewellery, amulets, &c. Meteorite iron can be distinguished from terrestrial one by its nickel content always absent in old industrial irons. Ancient terrestrial iron was nickel-free, often contaminated by carbon.

At the beginning of iron industry (bw. 1500-1200 BC) the Hittite Empire still monopolized iron as military hi-tech (until its collapse in 1190 BC in the Bronze Age Migration), so only small amounts of ornamental weapons left Hatti as diplomatic gifts. Thus iron objects from before 1500 BC are almost certainly of meteoritic origin, even if chemical analysis is not at reach.

Such objects have been found, so there is no doubt that people knew the extraterrestrial origin. Indeed, Old Egyptians knew about the celestial origin of meteorite iron called "sky metal" [1]. Similarly, in Sumer (so before 2000 BC) it was called the "gift of sky" [2], indicating observed falls.

## 2. METEORITES AS SAFETY HAZARDS IN EGYPT

In the era of the Late Empire Egyptians felt meteorite falls real hazards. Bw. 10th and 8th centuries BC magic papyri contain decrees of gods for the benefit of men. One of them promises to defend men from stars falling from the sky and striking down men [3]. This is strange because nowadays meteorites are ignored as hazards and no documented case is known from the last centuries for anybody seriously harmed by a meteorite. This fear is old in Egypt. An insription of Thotmes III of New Empire mentions a meteorite ("star") falling to the enemy's camp from southern direction, laying down everybody [4]. According to the text this happened somewhere in Syria, "in the second hour" of the night. The Pharaoh claims this a unique event, never happened before.

However an earlier short fiction, the Shipwrecked's Story from Middle Empire mentions an analogous event. The narrator is cast ashore on an island of a lone giant serpent who tells him that his people have been killed by a fallen star [5].

So the fear from meteorites was persistent in Old Egypt during the 2nd millenium BC. Hence Kákosy conjectures higher fall rate in Early Ancient Ages [6]. As an analogy, Mesopotamian omen texts also suggest meteorites as hazards [7].

This fear may have been superstition, and royal war reports are not always genuine. However Thotmes may have emphasized his own abilities instead of the destructive intervention of a star.

**3. THE METEORITE AT AIGOSPOTAMOI**

The last, and decisive, (naval) battle of the Pelloponesian War was fought at Aigospotamoi (Goat River) on Chersonesos, Sep. 405 BC. The Spartans were the absolute winners, and the battle was so decisive that Plutarch was not surprised that some authors believed in divine influence [8]. He quotes a belief that a meteorite fall predicted the event; he calls it "stone", and. cites some Damiakhos (On Religion) having reported the event. The report is strange, telling that for 75 days a fiery body had been being seen on the sky, on irregular path, casting away fragments shining as shooting stars. Finally the body fell, causing a great terror, and then the observers saw that it was quite big, still negligible if compared to the celestial object seen previously. Plutarch is cautious to take Damiakhos' details in face value. It seems that the meteorite was a stone one, not iron.

**4. THE CELESTIAL STATUE OF ARTEMIS IN EPHESOS**

During classical Greek times something of celestial origin was continuously kept in the Holy of Holies of the Temple of Artemis in Ephesos (Little Asia). Some authors call it a great black stone from the skies, maybe the arrowhead of Artemis the Huntress [12]. A different description is given by the New Testament, when, in 56 AD Saul of Tarsos, on Roman name Paul the Apostle, met with a revolt against him. The revolt was triggered by some Demetrios, the silversmith, who manufactured miniature silver replicas of the Temple for pilgrims and naturally did not like a new religion in which Artemis is irrelevant. After 2 hours of shouting the Mayor soothed the mob by declaring that of course nobody questions that Ephesos keeps the statue of Artemis, descended from the skies. So the celestial object was in the temple in 56 AD, and was said to be a statue, not an arrowhead. This suggests rather a stone meteorite than an iron one.

**5. ATILLA'S SABRE**

In 448 AD Emperor Theodosius II of Byzance sent envoys to Attila, Great King of Huns, whose capitol was then somewhere near to the modern New Szeged (at the confluence of Tisa and Maros Rivers of the Great Hungarian Plains, on the eastern bank of Tisa). One of the delegates, Rhetor Priscos, reports a story of common knowledge about the sabre of the ruler [9], [10]. According to the story the ruler possesses the sabre of the War God, so he is invincible. The sabre was hidden for ages, and then found by a herdsman, who observed that one of his cows had a hurt foot. After some investigation he found that the cow stepped on a sabre buried almost completely into the soil, point upwards. He believed that the sabre was unique and carried to the King.

It is tempting to interpret the "sabre" its material, i.e. an iron meteorite found on the meadows, from which then the sacred sabre became made. Sky iron was not only sacred; it was superior to irons of Ancient Ages, being nickel-iron alloy.

There is another explanation not involving meteorites. Ammianus Marcellinus mentions that Alans bury swords soil vertically, for cultic reasons [11]. It is possible that the cow stepped on such cultic object. But i) an old iron sabre, buried for decades

(Huns settled the Plains 40 years earlier) would be rusty and decaying, for which there is no mention; ii) ifburied sabres were commonplace why to believe a regular one divine?

**6. DATING THE EVENTS**

Thotmes III's meteorite (if existed) can be dated to the first half of the XV$^{th}$ century, BC, since the Pharaoh ruled bw. cca. 1502-1448 BC. The locality is somewhere in "Syria", which is probably the later Palestine, or Kanaan.

For the Aigospotamoi meteorite one guessses 405 BC, or just before, because the Battle of Aigospotamoi was in Sep. 405. However Strabo mentions a "stone shower" in the time of the Persian War [13], so in cca. 480 BC. This statement directly contradicts to Plutarch, who tells that Anaxagoras "predicted" the event in the sense that *previously* said that a celestial body may drop out of its position. But Anaxagoras worked in the time of Pericles, and propagated his astronomical ideas about 430 BC. So either Plutarch is wrong and Anaxagoras did not predict but explained the event, or Strabo is wrong and it happened not during the Persian War (480 BC) but during the Pelloponesian War, so in cca. 405 BC. My guess is that the second mistake is easier to explain, since Persia was involved into the final struggles of the Peloponesian War; one may consult further with Refs. 14 and 15. As for the location the village of Aigospotamoi had vanished before the age of Strabo, but archeologists can locate the place. It is almost exactly west from Gelibolu, Turkey.

The time of the fall of the celestial object in Ephesos is unknown. It can be much older than the time of St. Paul. Ephesos, on the name Apasas, seems to have been capitol of the Western Anatolian kingdom Arzawa [16]. Greeks reached Ephesos in the Ionian migration, traditionally put to and after 1077 BC, and, according to Pausanias, ousted the local Karians and Lelegs, but made an agreement with the natives around the temple of the local goddess. She may have been the Karian fertility goddess, because in the classical times virgin Artemis had fertility aspects in Ephesos. If so, then cult and cultic objects were continuous at the conquest. We know of two complete renovation (Metagenes about 550 BC and Deinocrates in 334 BC, but they did not have reasons to influence the cultic objects. Herostratos in 357 BC burnt the temple, but big meteorites do not burn. The cult was, therefore, continuous at least from the end of the 2$^{nd}$ millenium BC, and the object may have been put into the temple in any time (most probably before the classical Greek ages).

Attila's sabre must have been found between 445 and 448 AD, most probably somewhere on the Great Hungarian Plains. Before 445 Attila's brother, Buda, was Great King, so the celesrtial sword would have gone to *him*.

**7. THE FATES OF THE OBJECTS**

Most probably Thotmes III's meteorite was never collected. If it existed, it must have been large for size, so excavations may unearth it together with the military camp; the material would be unique enough to recognise it.

As for the Aigospotamoi meteorite, Plutarchos tells that it had been preserved to his years (end of 1$^{st}$ century AD) and was being displayed "on Chersonesos". Nothing more is known.

Nothing is known about the extraterrestrial Artemis statue in Ephesos, but it was in the Artemision. Well after the episode

of St. Paul the city and the temple was damaged by an earthquake, and later Emperor Theodosius forbad its use in 389 AD. Afterwards some of the ruins were used in the Hagia Sophia. Wood found the ruins in 1869 AD, and excavations started there. It seems that no extraterrestrial matter has been found up to now, but the site is exactly located. It is, of course, quite possible that the last priestess carried away the holy relic.

Atilla's sabre, as we saw, may have been either an old, buried sabre or a new one from sky-metal. Chemical analysis of the sabre could be decisive. The sabre may have been buried with the King; his grave has not yet been found, which is an old and great task of Hungarian archaeology. However 6 centuries later a sabre appeared in Hungary which was regarded as Attila's one by the Hungarian Royal Court. The widow of Andrew I, Anastasia, daughter of Yaroslav I of Kiev gave it in 1063 as a gift to Otto von Nordheim, Duke of Bavaria. Hence it went to Leopold von Merseburg, whom the sabre killed accidentally in 1071 as reported in the Annalen of Lambert of Hersfeld [17]: "Notatum autem est hunc ipsum gladium, quo famosissimus quondam rex Hunorum Attila in necem christianorum atque in excidium Galliarum hostiliter debachatus fuerat...Legitur autem de hoc gladio in Gestis Getarum, qui et Gothi dicuntur, quod Martis quondam fuerit,...". Hungarian archaeology identified the object [18]: it is a sabre, not a sword, in the Schatzkammer, Vienna, sometimes believed to come from Harun al Rasid. Hungarian historians doubt that it really comes from Attila. To my knowledge no chemical analysis happened on it, therefore up to now nothing is known about its nickel content.

So no successful identification of these meteorites exists. Still all the events are of historic interest.

**REFERENCES**


[1] L. Kákosy: Természettudományi Közlöny **XCV**, 373 (1964)
[2] J. Klíma: Lidé Mezopotámie. Orbis, Praha, 1976
[3] I. E. S. Edwards: Hieratic Papyri of the British Museum. IV. Oracular and Amuletic Decrees of the Late New Kingdom I-II London, 1960. (I. 2 II. 1., British Museum 10083 14-16)
[4] K. Sethe: Urkunden der ägyptischen Altertums IV, 1238, Leipzig, 1905-08
[5] A. Erman: Z. Aegypt. Sprache u. Altert. **XLIII**, 1 (1906)
[6] L. Kákosy: Egyiptomi és antik csillaghit. Akadémiai Kiadó, Budapest, 1978.
[7] J. Kingston Bjorkman: Meteoritics **8**, 91 (1973)
[8] Plutarchi vitae parallelae (Lys. 12). Teubner, Leipzig, 1892
[9] Priscos Rehetor: Fragm. 8. in C. Müller, Fragmenta Historicorum Graecorum IV, Paris, 1851
[10] Jordanes: Getica XXXV, 183 in Monumenta Germaniae Historica (ed. Th. Mommsen) V. 1
[11] Ammianus Marcellinus, Res gestae (XXXI, 2, 23), ed. by C. U. Clarck, Berlin, 1910-15
[12] C. Sagan: Broca's Brain. Ballantine Books, New York, 198
[13] H. L. Jones: Geography of Strabo, London 1917 VII Frag. 56
[14] Aristotle: Meteorologica, **1**, 7
[15] Pliny: Naturalis Historia **2**, 58-59
[16] A. Goetze: Die Annalen des Mursilis. Mitt. Vorderasiat-Aegipt. Gesell. **38**, 1 (1933)
[17] Lampertus Hersfeldensis: Annalen. See the next reference.
[18] Z. Tóth: Attila's Schwert. Akad. Wiss. Budapest, 1930

# GENESIS OF DIAMONDIFEROUS MINERALIZATION IN METEORITES

**Alexey A. Marakushev, Olga B. Mitreikina, Nina G. Zinovieva, and Lev B. Granovsky**
Department of Petrology, Faculty of Geology, Moscow State University, Lenin Gory, Moscow 119899, Russia

Detection of microcrystalline aggregates of diamonds in different types of chondrules has been a considerable achievement in studies of meteoritic materials. Until then, diamond has been found only in iron meteorites and ureilites (pyroxene-olivine primitive achondrites). Noteworthy are the genetic relationships between diamond-bearing carbonaceous chondrites (C3) and ureilites (with high diamond contents) in the context of the diamond genesis problem.

Comparison of the diamondiferous mineralization of both meteorite types shows their similarity in many respects. Chondrite diamonds are characterized by high concentration of such gases as hydrogen, nitrogen, helium, and other noble gases. It is necessary to note that these gases are anomalous in the isotopic compositions. Fluids occur as numerous microinclusions in the diamond grains, so that the volume density of the diamond is reduced to 2.2 $g/cm^3$, whereas the usual diamond density is 3.5 $g/cm^3$. The ureilite diamond also carries abundant fluid microinclusions. The fluid phases of the C3-chondrite and ureilite diamonds are approximately the same in the concentrations and composition of noble gases. This similarity is likely to extend to other gases, such as hydrogen and hydrocarbon. This similarity is also apparent from the influence of fluid on the olivine and pyroxene of ureilite, which causes the origin of their diamondiferous mineralization in the form of veinlets containing, in addition to diamond, lonsdaleite, graphite, kamacite, daubreelite, troilite, cohenite, perryite, and moissanite.

Their formation was accompanied by the recrystallization of olivine and pyroxene under the influence of hydrogen fluids, which had been produced by iron-carbon-hydrocarbon melts intruding the ureilite along the fractures and grain boundaries. Thus, process was accompanied by magmatic replacement [1, 2]. The olivine recrystallization is described by the reaction:

$$2Mg_{1.5}Fe_{0.5}SiO_4 + H_2 = Mg_2SiO_4 + MgSiO_3 + Fe \text{ (native iron)} + H_2O$$

Newly formed native iron contains no nickel, by contrast to kamacite from diamond bearing veins.

The kamacite sometimes dominate over graphite phase, but usually the graphite phase dominates. Systematic occurrence of drop-like kamacite separations in graphite, and sometimes, in the diamond proves their magmatic genesis and reflects the liquid immiscibility of the melts. The diamond is the first phase to crystallize. It forms euhedral crystals on vein boundaries. Graphite occurs in the central parts of the veins and bears captured kamacite drops (sometimes dumbbell-shaped) with fine inclusions of cohenite. The kamacite drops are surrounded by daubreelite

and perryite rims. The examined meteorites Novo-Urei, Dyalpur, Havero, Kenna, and Y-74659 carry no mutual replacement textures of diamond and graphite. These minerals sequentially crystallized from a carboniferous melt. This predetermined the crystallization conditions, which were close to the diamond-graphite P-T curve. The high-pressure conditions of the origin of ureilites is evident from tiny pyrope grains. We were the first to discover this mineral in meteorites.

Hence, studies of meteorites have revealed complex nature of their diamondiferous mineralization, which is typical of ureilites the carbon-kamacite fluid-melt phase. The latter probably concentrated in the internal parts of the parental planets during their immiscible splitting. Later, the melt intruded, under the effect of the high ambient pressure, into the external (ureilitic) planetary envelopes. These specific features further accentuate the similarity between diamond in ureilites and chondrites, which is restricted not to silicate chondrules but rather to carbon- and nickel-iron-rich (kamacite) groundmass. The pervasive assemblage of carbon and kamacite emphasizes the similar nature of diamond in chondrites and ureilites, on the one hand, and iron meteorites, on the other.

Substantiated was the two-stage (I and II) evolution model of the parental planets of meteorites: I - under a high pressure of the hydrogen envelopes in progressively more reduced environment and II - after migration of these envelopes under increasingly oxidized conditions. The model accounts for the relict nature of the diamondiferous mineralization of chondrites, which is related exclusively to the earlier (I) stage of the planetary evolution. The increasing hydrogen influence on the molten meteorite material during this stage explains the simultaneous occurrence of the diamondiferous mineralization and isotope anomalies in chondrites. This parallelism relates the origin of chemical compounds with anomalously low oxidation grades of metals (SiO, $SiH_2$, $SiCl_2$, etc.) to reactions like $SiO_2 + H_2 = SiO + H_2O$ and the like. These reactions result in the origin, together with diamond, of silicates anomalously enriched in isotopically light oxygen, for example

$$2MgO + 2SiO + CH_2 + CO = Mg_2SiO_4 + SiC \text{ (moissanite)} + \\ + C \text{ (diamond)} + H_2O$$

The assemblage of diamond and moissanite (SiC) in chondrites, along with the occurrence of native silicon, provides evidence for the participation of such reactions in diamond-forming processes.

**ACKNOWLEDGMENTS:** This research described in this contribution was made possible in part by Grant MU8300 from the International Science Foundation and Russian Government, and by Grant 93-05-8566 from Russian Foundation for Fundamental Researches.

**REFERENCES:** [1] Marakushev A.A., Mitreikina O.B., Zinovieva N.G., and Granovsky L.B. (1995) Origin of diamonds in meteorites. *Doklady RAN*, v. 341, N 1, 1-4; [2] Mitreikina O.B., Zinovieva N.G., and Granovsky L.B. (1995) Magmatic replacement processes in ureilites. *Proc. NIRP Symp. Antarct Meteorites* 8, (in press).

# Re-evaluation of Enstatite-Oldhamite Geothermometer: Formulation and the Application to E-chondrites

**Satoshi MATSUNAMI and Takako SATO**

Department of Earth Sciences, Miyagi University of Education, Aramaki-Aoba, Sendai 980, Japan

Enstatite chondrites give clues to understanding an environment of the primitive solar nebula that is distinct from that where ordinary and carbonaceous chondrites were formed. The Enstatite-Oldhamite Geothermometer (EOG) proposed by Larimer and Buseck (1974) is a useful tool to determine their formation conditions (T, $PO_2$ and $PS_2$), showing that they are the products of extreme reducing conditions during metamorphic equilibration (T=640-840°C; $PO_2=10^{-28}$-$10^{-37}$atm). However, in the model of Larimer and Buseck (1974), uncertainties of activity coefficients of Si in kamacite and $CaSiO_3$ (Wo) component in enstatite lead to an uncertainty of +-150°C in the calculated equilibrium temperatures.

Fogel *et al.* (1989) conducted a re-evaluation of thermodynamic foundation of the EOG in detail. They revised activity coefficient of Si in kamacite using thermochemical data of Sakao and Elliott (1975). And they formulated the model using $CaMgSi_2O_6$ as the Ca-rich component in enstatite: [$2CaMgSi_2O_6$ (en) + $S_2$ = 2CaS + $2MgSiO_3$ + $2SiO_2$(qtz) + $O_2$], assuming that it behaves as a symmetric regular Margules solution. With an appropriate constraint of the Margules interaction parameter ($W_G$ = 52 kJ/mol), they obtained metamorphic temperatures of EL6 chondrites greater than about 1000°C, ranging from 981°C for Yilmia to 1068°C for Blithfield. However, their assumption that the value of $W_G$ is approximately constant in the range of the metamorphic temperatures is not reasonable.

In the present study, we revise the EOG based on the basically similar considerations to Fogel *et al.* (1989), except for treatment of Ca-rich component in enstatite. We use $CaSiO_3$ as Ca-rich component in enstatite, as originally selected in the model of Larimer and Buseck. Although they used thermodynamic data of $CaSiO_3$ (triclinic) to evaluate equilibrium constant of the reaction: [$2CaSiO_3$ (opx) + $S_2$ = 2CaS + $2SiO_2$ + $O_2$], we estimate the equilibrium constant using the following additional reaction: [$CaSiO_3$(opx) = $CaSiO_3$(cpx)]. The thermodynamic data of the reaction and activity coefficient of $CaSiO_3$ in enstatite are obtained from experimental data for opx/cpx phase equilibria in the (Mg, Fe, Ca)$SiO_3$ system. We adopt the ternary solution model derived by Grafchikov and Fonarev (1988). They presented empirical equations for mixing properties of En, Fs, and Wo components

in coexisting opx-cpx pair and the standard Gibbs free-energy change for the above reaction. In addition, their equations were corrected to fit recent experimental data for the En-Di system at 1 atm (Carlson, 1988). Final expression for equilibrium temperature in the modified EOG is as follows:

$$T\,[K] = \frac{8454 + 18300X_{Si} + 173.56(X_{Mg}^{opx})^2 + 7184X_{Mg}^{opx}X_{Fe}^{opx}}{1.84 + 2\log X_{Fe} + 6.30X_{Si} - \log X_{Si} - 2\log X_{Ca}^{opx} - 0.26(X_{Mg}^{opx})^2 + 6.30X_{Mg}^{opx}X_{Fe}^{opx}}$$

where $X_{Fe}$ and $X_{Si}$ are mole fractions of Fe and Si in kamacite, respectively; $X_{Mg}^{opx}$, $X_{Fe}^{opx}$, and $X_{Ca}^{opx}$ are mole fractions of En, Fs, and Wo components in enstatite (opx), respectively.

Using this equation, we estimate equilibration temperatures for 15 enstatite chondrites. Mean chemical compositions of enstatite and kamacite used in the calculation were adopted from Keil (1968), except for Eagle (EL6). The compositional data for Eagle were determined using the SEM-EDS system of Miyagi University of Education.

The calculated results are quite in good agreement with those of Fogel *et al.* (1989). Equilibrium temperatures for EL6 chondrites determined via the present method range from 1006°C for Eagle to 1067°C for Blithfield, indicating that EL6 chondrites experienced metamorphic temperatures of greater than 1000°C. This means the formation of a metal-sulfide liquid during metamorphism in the parent body of EL chondrites.

References: Carlson W.D. (1988): *Am. Mineral.* **73**, 232-241./ Fogel R.A. *et al.* (1989): *GCA* **53**, 2735-2746./ Grafchikov A.A. and Fonarev V.I. (1988): *Geochemistry Int.* **24**, 89-99./ Keil K. (1968): *JGR* **73**, 6945-6976./ Larimer J.W. and Buseck P.R. (1974): *GCA* **38**, 471-477./ Sakao H. and Elliott J.F. (1975): *Metall. Trans.* **A 6A**, 1849-1851.

Table 1. Metamorphic temperatures of 15 enstatite chondrites determined via the modified enstatite-oldhamite geothermometer

| Meteorite | Type | Temperature [°C] |
|---|---|---|
| Adhi Kot | EH4 | 881 |
| Indarch | EH4 | 1029 |
| Kota-Kota | EH4 | 983 |
| Abee | EH4 | 820 |
| St. Sauveur | EH5 | 819 |
| St. Mark's | EH5 | 828 |
| Eagle | EL6 | 1006 |
| Ufana | EL6 | 1025 |
| Atlanta | EL6 | 1014 |
| Jajh deh Kot Lalu | EL6 | 1019 |
| Khairpur | EL6 | 1020 |
| Daniel's Kuil | EL6 | 1023 |
| Hvittis | EL6 | 1019 |
| Pillistfer | EL6 | 1025 |
| Blithfield | EL6 | 1067 |

# YAMATO-86789: A THERMALLY METAMORPHOSED CM-LIKE CARBONACEOUS CHONDRITE

Matsuoka,K., Nakamura,T., Nakamuta,Y. and Takaoka,N.
Department of Earth and Planetary Sciences, Facuity of Scence, Kyushu University, Hakozaki, Fukuoka 812-81

## INTRODUCTION

CI and CM carbonaceous chondrites are primitive meteorites but are known to be affected by secondary aqueous alteration [1]. Recently, several Antarctic carbonaceous chondrites with CI-CM affinities were revealed to have experienced mild thermal metamorphism after aqueous alteration. They include Bergica(B)-7904, Yamato(Y)-793321, Y-82162 and Y-86720 [e.g. 2-6]. They are very important samples to carry distinct imformation about more advanced material evolution processes than usual CI-CM chondrites in the early solar system. We here present results of our electron microscope and X-ray study of the Y-86789 meteorite, which has been classified as carbonaceous chondrite [7]. We found that the meteorite predominantly comprises of dehydrated phyllosilicate, thus we concluded that it is a new member of thermally metamorphosed carbonaceous chondrites with CI-CM affinities.

## ANALYTICAL METHODS

We made a polished thin section and a polished section from a chip of the Y-86789 meteorite, and studied them with an optical microscope and an EPMA. A portion of matrix ($\sim$ 100$\mu$m X 100$\mu$m X 100$\mu$m) was removed from a meteorite chip and X-ray diffraction was measured with a Gandolfi X-ray camera.

## GENERAL PETROGRAPHY

Y-86789 consists in major part of dark brownish to black, fine-grained matrix, but there are also considerable amounts of non-matrix objects; translucent replaced chondrules and opaque isolated minerals.

Replaced chondrules show subrounded or irregular outlines, and range in size from a few tens of microns to a few millimeters. They exhibit well-preserved accretionary dust mantles similar to those observed in CM chondrites. The modal proportion of the replaced chondrules is 13.8 vol%. This value is apparently higher than that of CI chondrites and is in the range of CM chondrites [8].

Isolated minerals are mainly Fe-sulfide (troilite) and Fe-Ni metal (taenite and kamacite), and disperse throughout the matrix. Some Fe-sulfide grains have an euhedral lath-like morphology, which are sometimes up to several hundreds of microns in length. While others are irregularly shaped grains, which are smaller than a few tens of microns.

## REPLACED CHONDRULES

Replaced chondrules consist mainly of brownish, translucent materials with variable amounts of opaque minerals. The translucent minerals show fibrous texture which is reminiscent of phyllosilicates. The opaque minerals are mainly Fe-sulfide (troilite) and Fe-Ni metal (taenite and kamacite), and the minor mineral is ilmenite. Some of replaced chondrules preserve their original shapes and texture including porphyritic and barred texture, although no anhydrous silicate minerals such as olivine or pyroxene of optically visible size are observed, suggesting that primary olivine in chondrules has been completely altered to phyllosilicates by extensive aqueous alteration. The phyllosilicate-like replacement products are rich in Si, Mg, Fe and Al and contain minor Na. Chemical compositions of the phyllosilicate-like materials mainly fall between the serpentine and saponite solid solution lines in a Fe-Si-Mg ternary diagram (Fig. 1-a), suggesting that the phyllosilicate-like materials may be a mixture of serpentine- and saponite-type phyllosilicates. However, analytical totals of phyllosilicate-like materials tend to be considerably higher than phyllosilicates, suggesting that they were dehydrated and partially altered to anhydrous phases by mild thermal metamorphism

Some replaced chondrules showing irregular outline are rich in Ca and thier chemical conpositions show mixture of phyllosilicate and Ca-carbonate. this implies that small particles of Ca-carbonate exist in them.

## MATRIX

Matrix also consists of phyllolicate-like materials which are dehydrated. Chemical compositions of the phyllosilicate-like materials mainly fall between the serpentine and saponite solid solution lines in a Fe-Si-Mg ternary diagram (Fig. 1-b), although parts of them concentrate on the serpentine solid solution line, suggesting that the phyllosilicate-like materials in matrix originally comprised major serpentine and minor saponite components. Portions surrounding isolated Fe-sulfide grains become more or less Fe-rich without variation in Mg/Si ratios, suggesting that they resulted from diffusion of the tiny Fe-bearing phases (Fig. 1-b). These Fe-rich halos are several to a few tens of microns wide.

X-ray measurement reveals that matrix consists mainly of olivine and troilite, and minor amounts of taenite and kamacite. Basal reflections of olivine, however, show unusual broadening. No refrection of phyllosilicate mineral is recognized. This broadening probably results from reflections of imcompletely transformed phyllosilicates. All these results suggest that almost all phyllosilicate materials are metamorphosed to secondary olivine by thermal metamorphism.

## SIMILARITY TO Y-86720

B-7904, Y-793321, Y-82162 and Y-86720 are known as unusual Antarctic carbonaceous chondrites [e.g. 2-6], since they show many characteristics indicating that they underwent metamorphic heating after aqueous alteration on thier parent bodies. We recognized the same characteristics in Y-86789 in this study. Y-86789 is most similar to Y-86720 in the four meteorites on petrographical, mineralogical and compositional details: existence of replaced chondrules, accretionary dust mantles, euhedral sulfide laths, Ca-carbonate and secondary olivine, opaque mineral compositions and the absence of primary olivine, These similarities suggest that Y-86789 and Y-86720 are a pair.

## REFERENCES


[1] McSween Jr.,H.Y., (1987) Geochim. Cosmochim. Acta 51, 2469.

[2] Akai,J. (1992) Proc. NIPR Symp. Antarct. Meteorites, 5, 120.

[3] Bischoff,A. and Metzler,K. (1991) Proc. NIPR Symp. Antarct. Meteorites, 4, 226.

[4] Ikeda,Y. (1992) Proc. NIPR Symp. Antarct. Meteorites, 5, 49.

[5] Miyamoto,M. (1991) Meteoritics, 26, 111.

[6] Tomeoka,K., Kojima,H. and Yanai,K. (1989b) Proc. NIPR Symp. Antarct. Meteorites, 2, 55.

[7] Yanai,K. and Kojima,H., comp. (1987) Photographic Catalog of the Antarctic Meteorites. Tokyo, Natl Inst. Polar Res., 297p.

[8] McSween Jr.,H.Y.,Jr. (1979) Geochim. Cosmochim. Acta 43, 1761.


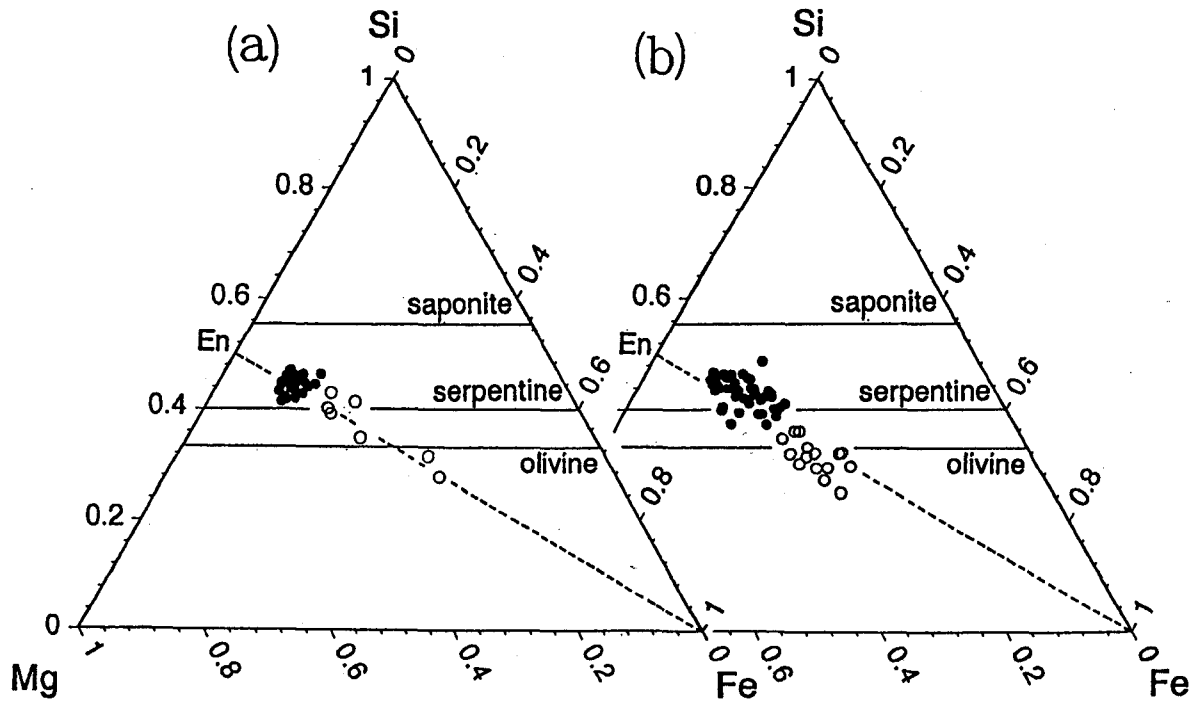


Fig. 1. Fe-Si-Mg ternary diagrams of phyllosilicate-like materials in replaced chondrules (a) and matrix (b). Solid circles are normal Fe-poor portions and open circles are Fe-rich halos surrounding Fe-sulfide grains.

# Petrology of Antarctic Angrites LEW 86010, LEW 87051, and Asuka 881371.

G. McKay[1], G. Crozaz[2], T. Mikouchi[3], and M. Miyamoto[3]

[1]*Mail Code SN4, NASA-Johnson Space Center, Houston, TX, 77058, USA.*
[2]*Department of Earth and Planetary Sciences and McDonnell Center for the Space Sciences, Washington University, St. Louis, MO, 63130, USA.*
[3]*Mineralogical Institute, Graduate School of Science, University of Tokyo, Hongo, Tokyo 113 Japan*

**Introduction.**

Angrites are a group of basaltic meteorites distinguished by very early formation ages (e.g., Nyquist et al., 1994), strong depletion in volatile elements (e.g., Mittlefehldt and Lindstrom, 1990), an unusual mineral assemblage (including fassaitic pyroxene, Ca-rich olivine, and anorthite that is nearly Na-free, e.g., McKay et al., 1988a, 1990) and formation under oxidizing conditions (McKay et al., 1994). The group consists of four meteorites, one from Brazil (Angra dos Reis), and three from Antarctica (LEW 86010, LEW 87051, and Asuka 881371). Because these samples record magmatic activity from the earliest history of the solar system (e.g., Nyquist et al., 1994), it is important to learn as much about their formation as possible.

Angra dos Reis was the first angrite to be recognized, but it is in may ways atypical. It is dominated by coarse-grained fassaitic pyroxene, and has generally been interpreted as a pyroxene cumulate (*e.g.*, Prinz *et al.*, 1977, but see Treiman, 1989, for another interpretation). Its minerals are quite homogeneous, suggesting extensive subsolidus equilibration. In this respect, it has a significantly different petrogenetic history from the Antarctic angrites, and is difficult to relate to the other samples except in the broadest terms. Hence we will not consider it further in this abstract.

In contrast, the Antarctic angrites clearly represent crystallized melts with only a limited amount of crystal accumulation. Moreover, they have been subjected to much less subsolidus equilibration than Angra dos Reis. LEW 86010 is a coarse-grained granular aggregate of fassaitic pyroxene, olivine, and anorthite, with crystals ranging up to ~6 mm in size (*e.g.*, McKay *et al.*, 1988a). Its olivine has been strongly affected by subsolidus processes, including complete homogenization of primary igneous zoning and exsolution of kirschsteinite lamellae (*e.g.*, Mikouchi *et al.*, 1995b). However, its pyroxene retains primary zoning (Crozaz and McKay, 1994). LEW 87051 is porphyritic in texture, with olivine phenocrysts up to 0.5 mm set in a fine-grained intergranular groundmass of elongate euhedral anorthite and interstitial fassaitic pyroxene, Fe-rich olivine, kirschsteinite, and accessory phases (*e.g.*, McKay *et al.*, 1990). Asuka 881371 is ophitic in texture, with large olivines distributed in a groundmass very similar in mineralogy to LEW 87051 (Yanai, 1994). Neither Asuka 881371 nor LEW 87051 have undergone significant subsolidus equilibration.

In this abstract, we present new data on mineral compositions in Asuka 881371, including minor and trace elements, compare these data with similar data for LEW 87051, and use results of our experimental crystallization studies of analog angrite compositions (McKay *et al.* 1988b, 1991) to develop a petrogenetic framework for these samples.

**Samples and Analytical Technique.**

Petrographic observations of Asuka 881371 were made on a polished thin section supplied by the curatorial laboratory of the NASA Johnson Space Center as part of a consortium study organized by the National Institute of Polar Research, Japan, and lead by P. Warren. Samples of LEW 86010 and LEW 87051 were provided by the Meteorite Working Group as part of consortium studies led by G. McKay.

Backscattered electron images, elemental maps, and quantitative wavelength dispersive analyses were performed on a JEOL JXA840 scanning electron microscope (Mineralogical Inst., Univ. of Tokyo), JEOL 733 electron probe (Ocean Research Inst., Univ. of Tokyo), JEOL 8600 Super Probe (Geol. Inst., Univ. of Tokyo), Cameca Camebax electron microprobe (NASA Johnson Space Center), and Cameca SX-100 electron microprobe (NASA Johnson Space Center) using standard techniques. SIMS analyses were performed on a Cameca IMS-3f ion microprobe, using experimental procedures similar to those given by Zinner and Crozaz (1986).

**Mineralogy and Petrology.**

Asuka 881371 was initially described by Yanai (1994). Additional details of the petrography of this sample are given by Mikouchi *et al.* elsewhere in this volume. Here we focus mainly on mineral cores that might contain information about the melt composition at the beginning of crystallization of each mineral.

**Olivine.** As reported by Yanai (1994), olivine in Asuka 881371 occurs in three textural types: Large porphyritic grains, euhedral groundmass grains, and interstitial groundmass grains. Our section of Asuka 881371 contains seven large (up to ~2 mm across) porphyritic olivine crystals that we interpret as xenocrysts. Analytical data for these olivines are shown in Fig. 1. These crystals are remarkably different in composition from the cores of euhedral groundmass olivines (also shown in Fig. 1). Moreover, the large olivines are very homogeneous within each individual crystal, except for distinct rims that are enriched in Fe and appear to be in a reaction relationship with the surrounding melt. In addition, there are distinct differences in composition from one crystal to another. We believe that the clear reaction relationship with the surrounding melt, the homogeneous nature of each crystal, and the large differences in composition between crystals provide strong support for the xenocrystic origin of these olivines. The source of these xenocrysts is an important clue to the petrogenesis of this sample that remains to be deciphered.

Fig. 1 also shows the cores of the porphyritic olivine crystals from LEW 87051. These are all richer in Mg than the groundmass olivines from Asuka 881371. Although we believe that most of the porphyritic LEW 87051 olivines crystallized from the groundmass melt, a few of them contain cores that are more Mg- and Cr-rich, and less Ca-rich than the majority of the porphyritic olivine cores. We had previously suggested that these cores are xenocrysts (*e.g.*, Jurewicz and McKay, 1993; Mikouchi *et al.*, 1994, 1995a). The clear xenocrystic nature of the large olivines in Asuka 881371 supports this conclusion. The olivines in

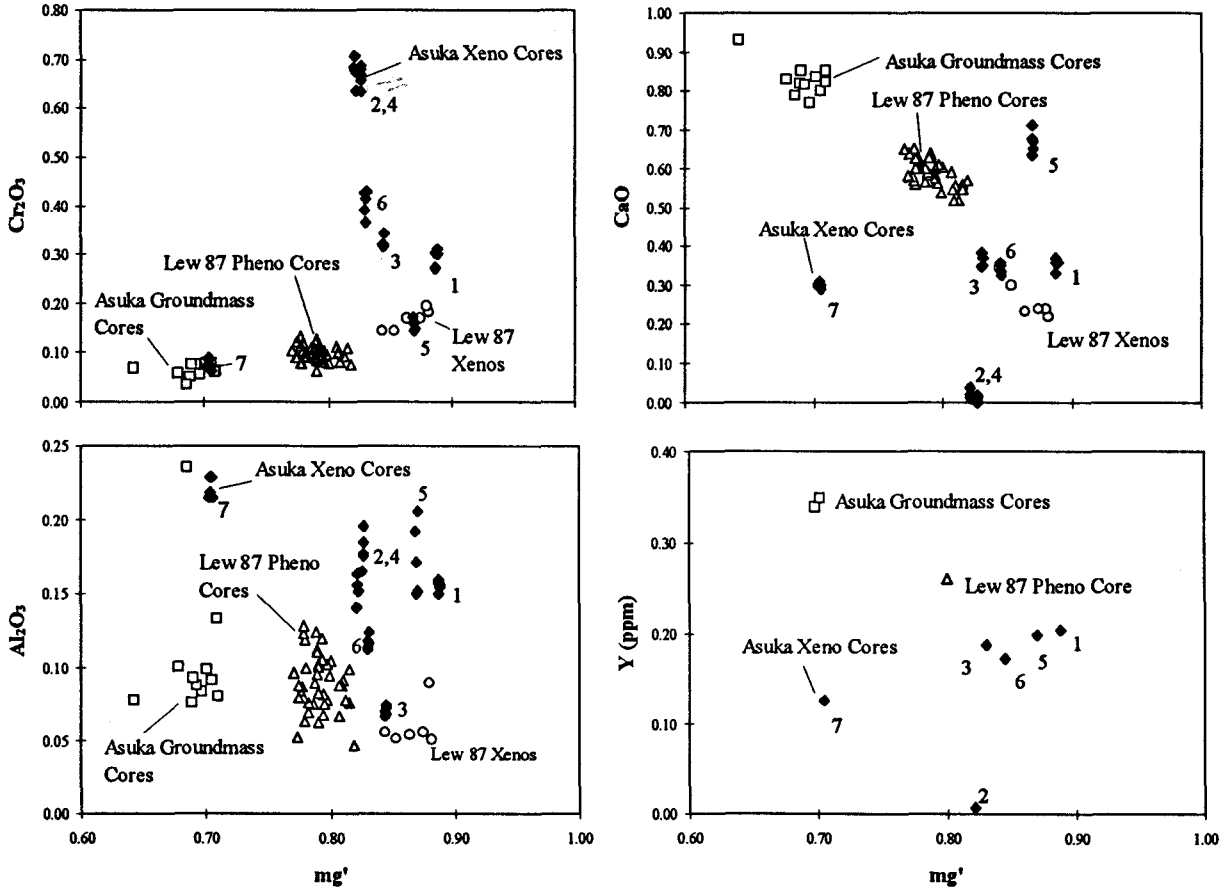


Fig. 1. Cr, Ca, Al, and Y vs mg' (= molar Mg/Mg+Fe) for olivines in Asuka 881371 and LEW 87051. Xenocrysts from Asuka 881371 are very homogeneous within individual grains, but show large variations from grain to grain. We also interpret the most Mg-rich olivines in LEW 87051 as xenocrysts. In both samples, the xenocrysts tend to be much richer in Mg and Cr and poorer in Ca and Y than the olivines that grew from the melt. Ca and Y are strongly correlated in all the olivines. Numbers beside diamonds indicate which of the 7 xenocrysts analyses they are from.

LEW 87051 and Asuka 881371 are discussed in greater detail by Mikouchi *et al.* elsewhere in this volume.

**Pyroxene.** Pyroxene occurs as anhedral grains interstitial to plagioclase in both Asuka 881371 and LEW 87051. Pyroxenes are strongly zoned from core to rim, with Fe and Ti increasing, and Mg and Cr decreasing towards the rims (Fig. 2). These trends are as expected because pyroxene/melt partition coefficients for Cr in our angrite analog experiments are ~ 10, while those for Ti are ~ 0.6. In both samples, Al shows a slight initial decrease followed by a slight increase from core to rim, but these trends are very subtle. Elemental mapping was used to locate the highest Mg and Cr contents in Asuka 881371 pyroxenes, and thus the earliest crystallizing pyroxenes. These are virtually identical in Fe/Mg to the most Mg-rich pyroxenes found in a ~700 point survey of LEW 87051.

SIMS analyses reveal strong correlations of Y and Zr with Ti in pyroxenes from both meteorites. Sc and V are correlated with Cr, and are strongly depleted in the rim of Asuka 881371 pyroxene.

**REE Abundances.** REE abundances in LEW 87051 and Asuka 881371 pyroxene and plagioclase are shown in Fig. 3. Abundances in Asuka 881371 pyroxene core and rim bracket the average value for LEW 87051 pyroxene, while those in Asuka 881371 plagioclase are nearly a factor of 10 lower than in LEW 87051 plagioclase. Although both plagioclase analyses were of spots near the center of an exposed crystal, we cannot verify that both represent crystal cores, because the plane of the section might have cut the crystal near its rim. Lacking any major or minor element variation in the plagioclase to help locate early-formed regions, we suspect that the higher abundance of trivalent REE in LEW 87051 plagioclase results from analysis of a region formed at a later stage of crystallization. The smaller Eu anomaly in LEW 87051 plagioclase is consistent with this hypothesis.

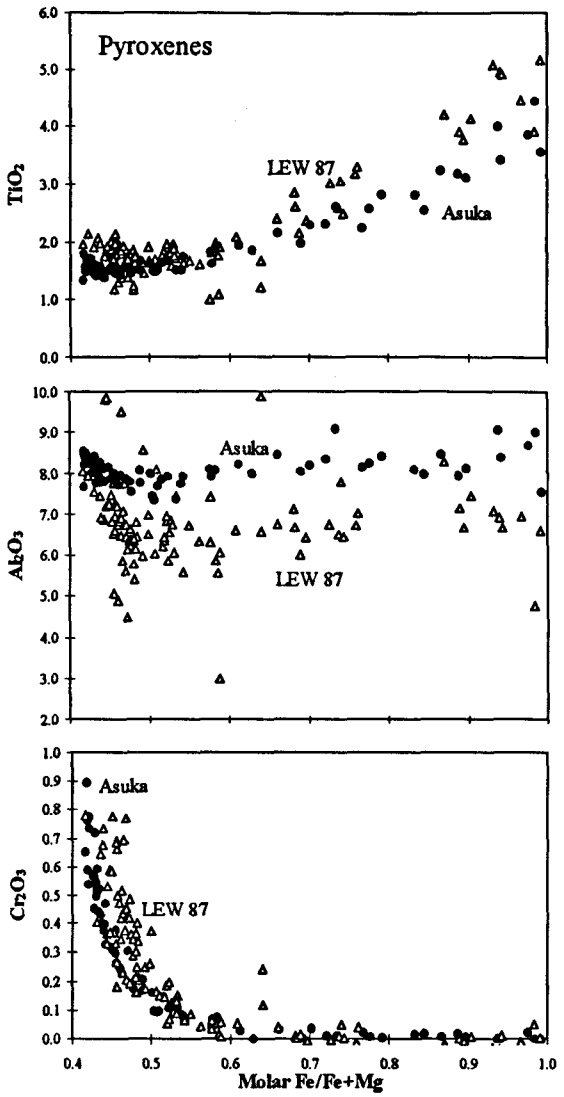


Fig. 2. Minor element variations in pyroxene from Asuka 881371 and LEW 87051.

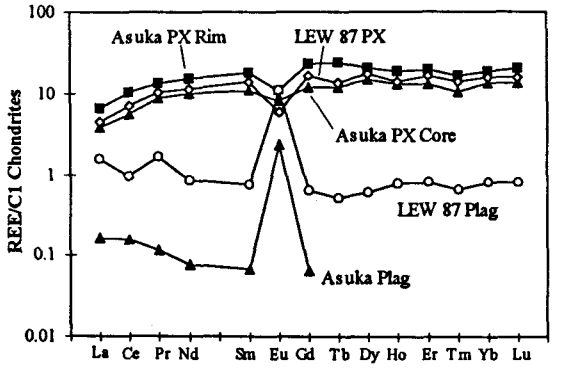


Fig. 3. REE abundance patterns in pyroxene and plagioclase from LEW 87051 and Asuka 881371.

## Experimental Crystallization Studies

Synthetic compositions resembling LEW 86010 and LEW 87051 were equilibrated over a range of temperatures under controlled oxygen fugacities (McKay *et al.*, 1988b, 1991). Charges were quenched and analyzed to obtain mineral and glass compositions, and resulting major and minor element partition coefficients. Glass compositions were projected onto the pseudoternary system Ol-Pl-Qtz-Wo, and used to define the position of cosaturation curves.

Cosaturation curves for 1200°C experiments are shown in Fig. 4, together with the bulk compositions of LEW 86010, LEW 87051, and Asuka 881371. Because the latter two samples might contain excess cumulus or xenocrystic olivine, their bulk compositions

do not necessarily represent melt compositions. Thus, using the ol/liq $K_{D(Fe/Mg)}$ value of 0.29 from our angrite experiments, we calculated melt compositions for these samples by subtracting sufficient olivine from the reported bulk compositions so that Fe/Mg of the resulting melt would be in equilibrium with the cores of phenocryst or euhedral groundmass olivine. The resulting compositions are shown in Fig. 4. The LEW 87051 melt calculated from the bulk composition of Mittlefehldt and Lindstrom agrees closely with the bulk composition reported by Warren and Kallemeyn (1990) (Fig. 4), suggesting that the latter sample did not contain significant excess porphyritic olivine.

Calculated melts for Asuka 881371 and LEW 87051 are far from the cosaturation curves, well within the olivine field. Thus, if these samples were formed by partial melting in a parent body mantle, olivine (± spinel) was the only phase left in the residuum. These melts must have formed at rather high temperatures. McKay *et al.* (1991) estimated that the LEW 87051 melt formed at around 1320°C. The Asuka 881371 melt would have formed at slightly lower temperature. The heat source for such extensive and high temperature melting is not known.

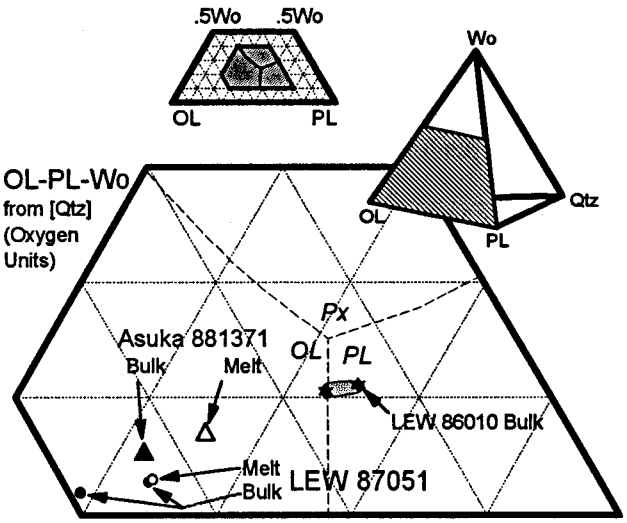


Fig. 4. LEW 86010, LEW 87051, and Asuka 881371 compositions projected onto the face of the Ol-Pl-Qtz-Wo pseudoternary system. Shaded region in small quadrilateral indicates location of the enlargement. Dashed lines are 1200°C cosaturation curves from experimental crystallization studies. Bulk compositions for LEW 86010 and 87051 are from Mittlefehldt and Lindstrom (1990) and Warren and Kallemeyn (1990). Bulk composition for Asuka 881371 is from Yanai (1994). Melt compositions are computed as described in text.

In contrast, the bulk composition of LEW 86010 has a liquidus temperature near 1200°C, plots near the Ol-Pl cosaturation curve, and is only slightly enriched in plagioclase relative to the point of cosaturation with pyroxene, plagioclase, and olivine. Thus, this sample could be a low-pressure partial melt of an Ol-Pl-Px assemblage, with a slight amount of excess accumulated plagioclase. Alternatively, it could be produced by fractional crystallization of an olivine normative melt such as LEW 87051 or Asuka 881371. These alternatives remain to be explored in detail.

According to the px/liq $K_{D(Fe/Mg)}$ value of ~0.2 from our angrite experiments, even the most Mg-rich pyroxene in LEW 87051 and Asuka 881371 is far too Fe-rich to have crystallized from the calculated melt compositions. Thus, pyroxene crystallization can only have begun after crystallization of a large amount of olivine from the initial melt. The lack of Al enrichment towards pyroxene rims (Fig. 2) suggests that the melt was at an invariant point while pyroxene was crystallizing, and hence that crystallization of pyroxene followed that of plagioclase. Moreover, the location of the melt compositions relative to the cosaturation curves in Fig. 4 suggests that pyroxene would follow plagioclase. This sequence also appears consistent with the groundmass texture. Thus, we infer the crystallization sequence for these two angrites to be olivine, followed by plagioclase, followed by pyroxene.

**References:**

**Crozaz** G. and McKay G. (1990) Earth Planet. Sci. Lett. 97, 369-381. **Jurewicz** A. and McKay G. (1993) Lunar Planet. Sci. XXIII, 643-644. **McKay** G., Lindstrom D., Yang S.-R., and Wagstaff J. (1988a) Lunar Planet. Sci. XIX, 762-763. **McKay** G., Lindstrom D., Le L., and Yang S.-R. (1988b) Lunar Planet. Sci. XIX, 760-761. **McKay** G., Crozaz G., Wagstaff J., Yang S.-R. and Lundberg L. (1990) Lunar Planet. Sci. XXI, 771-772. **McKay** G., Le L., and Wagstaff J. (1991) Meteoritics 26, 370. **McKay** G., Le L., Wagstaff J., and Crozaz G. (1994) Geochim. Cosmochim. Acta 58, 2911-2919. **Mikouchi** T., McKay G., and Le L. (1994) Lunar Planet. Sci. XXV, 907-908. **Mikouchi** T., Miyamoto M., and McKay G. (1995a) Lunar Planet. Sci. XXVI, 973-974. **Mikouchi** T., Takeda H., Miyamoto M., and McKay G (1995b) Amer. Mineralogist, in press. **Mittlefehldt** D. and Lindstrom M. (1990) Geochim. Cosmochim. Acta 54, 3209-3218. **Nyquist** L, Bansal B., Wiesmann H., and Shih C.-Y. (1994) Meteoritics 29, 872-885. **Prinz** M., Keil K., Hlava P., Berkley J., Gomes C., and Curvello W. (1977) Earth Planet Sci. Lett. 35, 317-330. **Treiman** A. (1989) Proc. 19th Lunar Planet. Sci. Conf., 443-450. **Warren** P. & Kallemeyn G. (1990) Lunar Planet. Sci. XXI, 1295-1296. **Yanai** K. (1994) Proc. NIPR Symposium on Antarctic Meteorites, No. 7, 30-41. **Zinner** E. and Crozaz G. (1986) Int. J. Mass Spectr. Ion Processes 69, 17-38.

# Mineralogical Study of Angrite Asuka-881371: Its Possible Relation to Angrite LEW87051

Takashi Mikouchi[1], Masamichi Miyamoto[1], Gordon A. McKay[2]

[1]*Mineralogical Institute, Graduate School of Science, University of Tokyo, Hongo, Tokyo 113, Japan*
[2]*Mail Code SN4, NASA/Johnson Space Center, Houston, TX 77058, USA*

## Introduction

Angrite is a unique class of achondrite with an ancient crystallization age (4.56 b.y.) (*e.g.* Nyquist *et al.*, 1994) and characteristic mineral assemblages (*e.g.* Prinz *et al.*, 1977; McKay *et al.*, 1988; McKay *et al.*, 1990; Yanai, 1994). Although Angra dos Reis had been the only known angrite as one of its kind for more than one century, three angrites were discovered recently in the Antarctica (Mason, 1987; Mason 1989; Yanai, 1991), and they have offered an opportunity to revaluate their unusual properties. Most recently identified angrite Asuka-881371 is 11 g discovered mass (Yanai, 1991) and shows ophitic texture. Large olivine crystals (> 2 x 2 mm in size) are set in a fine-grained groundmass mainly composed of fassaitic clinopyroxene, olivine, kirschsteinite, and anorthite. Olivines and fassaites are extensively zoned and their zoning profiles show distinctive features which indicate their complicated formation process. In this abstract we analyzed these zoned olivines and fassaites, especially xenocrystic olivines to compare Asuka-881371 mineralogy with other angrites in the light of olivine crystallization and found the possibility that Asuka-881371 experienced similar crystallization process to angrite LEW87051.

## Sample and Analytical Technique

Petrographic observations were made on two polished thin sections (PTS) of Asuka-881371 supplied from the Meteorite Working Group (NASA/Johnson Space Center) as a consortium study organized by National Institute of Polar Research (NIPR), Japan. The consortium leader of Asuka angrite is Prof. P. Warren.

Backscattered electron images and quantitative wavelength dispersive analyses were performed on a JEOL JXA840 scanning electron microscope (Mineralogical Inst., Univ. of Tokyo), JEOL 733 electron probe (Ocean Research Inst., Univ. of Tokyo), JEOL 8600 Super Probe (Geological Inst., Univ. of Tokyo) and Cameca SX-100 Automated Electron Microprobe (NASA/Johnson Space Center).

## Petrography and Mineral Compositions

Asuka-881371 (A8) is an unbrecciated igneous rock partially covered with fusion crust. A8 is ophitic in texture, consisting mainly of large olivines distributed in the groundmass of olivine, fassaite, kirschsteinite, and anorthite with minor spinel, ilmenite, and troilite (Fig. 1).

**Olivine** is one of the most dominant phase in the PTS and both PTS that we studied have large olivine grains (> up to 2 x 2 mm in size) which seem to be xenocrystic origin. These olivine xenocrysts are the most Mg-rich in the PTS and their Fo component reaches $Fo_{89}$. Almost all part of the crystal is homogeneous in composition except remarkably zoned rim. Some olivine xenocrysts show wavy extinction. Although these large olivines are most conspicuous in both PTS, there are another Mg-rich olivines whose core composition ranges from $Fo_{85}$ to $Fo_{70}$. These olivines are a little smaller than large olivine xenocrysts. They have unique zoning profiles, and most of them are similar to those in LEW87051 (L7) porphyritic olivines (Fig. 2). The core is rich in Cr and poor in Ca. Groundmass olivine is the third type and also widely zoned. The core is ~ $Fo_{70}$ and the most Mg-poor of the three. The rim is very Fe, Ca-rich and almost pure kirschsteinite. Linear texture possibly due to fine exsolution lamellae of kirschsteinite and fayalite can be observed in the rim. **Fassaites** are euhedral to subhedral and show zoning from pale-colored core to reddish brown rim. $Al_2O_3$ ranges from 5-10 wt%, $TiO_2$ 1-6 wt%, and $Cr_2O_3$ 0.8-0.0 wt%. CaO is almost constant like other angrite fassaites, but $P_2O_5$ increases a little towards the rim (0.3-0.5 wt%). Cr and V are positively correlated. **Plagioclase** is homogeneous and nearly pure anorthite ($An_{>99.5}$). In a few areas of the PTS, radiating plagioclase can be observed. FeO (0.4 wt%) and MgO (0.2 wt%) are not as rich as those in LEW87051 anorthite. Minor phases are mainly opaque minerals. They are **troilite**, **ilmenite**, and **spinel**. Ilmenite includes more than 2 wt% $Al_2O_3$. These chemical compositions are listed in Table 1.

**Olivine Mineralogy**

As stated before, it is notable that extremely large olivine is included in the PTS (Fig. 1), and thus seems to be xenocryst. The zoning profile of this olivine shows almost homogeneous chemical composition except the rim part of about 100 $\mu$m. This is the most Mg-rich in the PTS ($Fo_{89}$) and also rich in Cr and Al. $Cr_2O_3$ and $Al_2O_3$ in the core is 0.3 wt% and 0.15 wt%, respectively. CaO is 0.3 wt%. A few large olivine grains are also observed in the other PTS. Except these large olivine xenocrysts, several Mg-rich core olivines can be detected. Their Fo components are $Fo_{85\text{-}70}$, and $Cr_2O_3$ and $Al_2O_3$ range from 0.1-0.7 wt% and 0.05-0.25 wt% in the core. CaO also shows variation from nearly free to 0.7 wt%. CaO and $Cr_2O_3$ are negatively correlated. It is notable that these olivines show unique zoning profile with two stage as seen in some L7 olivines (e.g. McKay *et al.*, 1991; Mikouchi *et al.*, 1994a, b, 1995) (Fig. 2). Previously, we proposed a relict core model for L7 olivines using experimental data measuring Cr and Mn partition coefficients for olivine (Mikouchi *et al.*, 1994a, b) . We also pointed out that the rim of these Cr-rich core olivine show similar chemical compositions and zoning patterns to normal porphyritic olivines, and concluded that these two types co-crystallized (Mikouchi *et al*, 1995). The same situation can be observed for A8 olivines. The rim of some two-stage zoning olivines in A8 has similar composition to the core of groundmass olivines ($Fo_{70}$, CaO 0.7-0.8 wt%, $Cr_2O_3$ 0.05 wt%).

## Relation to LEW87051 Olivine

It is remarkable that both L7 and A8 have similar Cr-rich core olivines. As we suggested that Cr-rich core of L7 olivine is relict (Mikouchi *et al*. 1994a, b, 1995), it can be considered that Mg-rich olivines in A8 also include relict core. The large olivine xenocrysts and the core of two-stage zoning olivines in A8 will be relict grains. However, unlike L7 relict olivines, A8 relict olivines show a little variation of chemical composition from one grain to another. This will be because A8 includes more xenocrysts than L7. Although these two can be suggested to have similar origin, there are a little difference. The model we prefer to explain these angrite formation is as follows. First, olivine crystallized from primary magma. Then, some event which partially melted these olivines occurred. To melt the rim of these pre-existed olivines, impact heating will be the best candidate. Thus, the relict cores of L7 and A8 seem to have the same origin. After impact, the second stage of olivine crystallized possibly with the groundmass. The difference of the grain size between L7 and A8 will be due to the difference of burial depth. We estimated the burial depth of L7 olivine using chemical zoning of olivine (Mikouchi *et al*., 1995). According to our results, 2 m or shallower depth is enough to retain olivine zoning. This result indicates the formation in a shallow lava flow. Namely, A8 with larger grain size would crystallize deeper position than L7 in the same or similar lava flow containing relict olivine. Deeper area where A8 crystallized might include more olivine xenocrysts with a little wider chemical compositions.

**Acknowledgment**

We thank National Institute of Polar Research for the sample and the Meteorite Working Group (NASA/Johnson Space Center) for sample processing. Discussion with Prof. P. Warren of Univ. of Tokyo was very much helpful. This work was supported by JSPS Research Fellowships for Young Scientists (T.M.).

**References**

Mason, B. (1987) *Antarct. Meteorite Newsletter*, ***10-2***, 32.

Mason, B. (1989) *Antarct. Meteorite Newsletter*, ***12-1***, 15.

McKay, G., Lindstrom, D., Yang, S.-R., Wagstaff, J. (1988) *Lunar Planet. Sci.*, ***XIX***, 762-763.

McKay, G., Crozaz, G., Wagstaff, Yang, S.-R., Lundberg, L. (1990) *Lunar Planet. Sci.*, ***XXI***, 771-772.

McKay, G., Le, L., Wagstaff, J. (1991) *Meteoritics*, ***26***, 370.

Mikouchi, T., McKay, G., Le, L. (1994a) *Lunar Planet. Sci.*, ***XXV***, 907-908.

Mikouchi, T., McKay, G., Miyamoto, M., Takeda, H. (1994b) *Meteoritics*, ***29***, 503-504.

Mikouchi, T., Miyamoto, M., McKay, G. (1995) *Lunar Planet. Sci.*, ***XXVI***, 973-974.

Mittlefehldt, D.W. and Lindstrom, M.M. (1990) *Geochim. Cosmochim. Acta*, ***54***, 3209-3218.

Nyquist, L.E., Bansal, B., Wiesmann, H., Shih, C.-Y. (1994) *Meteoritics*, ***29***, 872-885.

Prinz, M., Keil, K., Hlava, P.F., Berkley, J.L., Gomes, C.B., Curvello, W.S. (1977) *Earth Planet. Sci. Let.*, ***35***, 317-330.

Prinz, M., Weisberg, M.K., Nehru, C.E. (1990) *Lunar Planet. Sci.*, ***XXI***, 979-980.

Prinz, M., Weisberg, M.K., Nehru, C.E. (1988) *Lunar Planet. Sci.*, ***XIX***, 949-950.

Yanai, K. (1991) *Lunar Planet Sci.*, ***XXII***, 1539-1540.

Yanai, K. (1994) *Proc. NIPR Symp. on Antarctic Meteorites*, 7, 30-41.

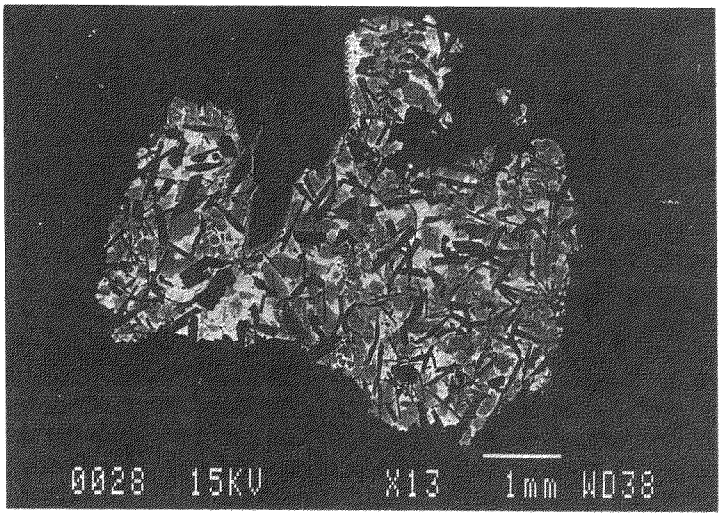


Fig. 1: Backscattered electron image of Asuka-881371. One large olivine crystal (> 2 x 2 mm) with zoned rim is included. Gray-colored minerals are zoned olivines and fassaites. White-colored areas are mainly Fe-rich olivine (kirschsteinite) and Fe-rich fassaite. Black elongated crystals are anorthites. Scale bar is 1 mm.

Table 1: Chemical compositions of each phase of Asuka-881371 (Wt%)

| | Olivine (Xenocryst) | | Olivine (Groundmass) | | Fassaite | | Plagioclase | Ilmenite | Spinel |
|---|---|---|---|---|---|---|---|---|---|
| | Core | Rim | Core | Rim | Core | Rim | | | |
| $SiO_2$ | 39.63 | 34.22 | 37.55 | 30.58 | 46.54 | 41.48 | 43.84 | 0.10 | 0.25 |
| $TiO_2$ | 0.05 | 0.04 | 0.04 | 0.10 | 1.78 | 3.90 | 0.03 | 27.33 | 1.48 |
| $Al_2O_3$ | 0.06 | 0.06 | 0.04 | 0.04 | 7.82 | 6.63 | 35.36 | 2.42 | 37.75 |
| FeO | 13.54 | 43.54 | 28.57 | 53.38 | 12.14 | 26.07 | 0.37 | 68.43 | 31.42 |
| MnO | 0.16 | 0.50 | 0.34 | 0.77 | 0.17 | 0.16 | 0.01 | 0.22 | 0.26 |
| MgO | 45.42 | 19.63 | 32.82 | 0.35 | 8.19 | 0.05 | 0.19 | 0.02 | 6.98 |
| CaO | 0.28 | 1.89 | 0.85 | 13.49 | 23.08 | 21.46 | 20.20 | 0.09 | 0.13 |
| $Na_2O$ | 0.01 | | | 0.01 | | 0.04 | 0.04 | 0.01 | 0.01 |
| $K_2O$ | 0.01 | | | 0.01 | 0.00 | 0.02 | 0.01 | 0.01 | |
| $Cr_2O_3$ | 0.34 | 0.08 | 0.07 | | 0.38 | 0.00 | 0.01 | 0.01 | 20.93 |
| $V_2O_3$ | 0.04 | 0.01 | 0.01 | | 0.11 | | 0.01 | 0.08 | 0.60 |
| NiO | | 0.03 | 0.02 | | | 0.03 | 0.00 | 0.03 | 0.05 |
| $P_2O_5$ | | | 0.04 | 0.03 | | 0.25 | 0.01 | 0.08 | |
| Total | 99.52 | 100.00 | 100.36 | 98.75 | 100.21 | 100.09 | 100.06 | 98.78 | 99.85 |
| *Fe* | 14.3 | 53.8 | 32.4 | 74.9 | 21.6 | 48.6 | | | |
| *Mg* | 85.3 | 43.2 | 66.4 | 0.9 | 25.9 | 0.2 | | | |
| *Ca* | 0.4 | 3.0 | 1.2 | 24.2 | 52.5 | 51.2 | | | |

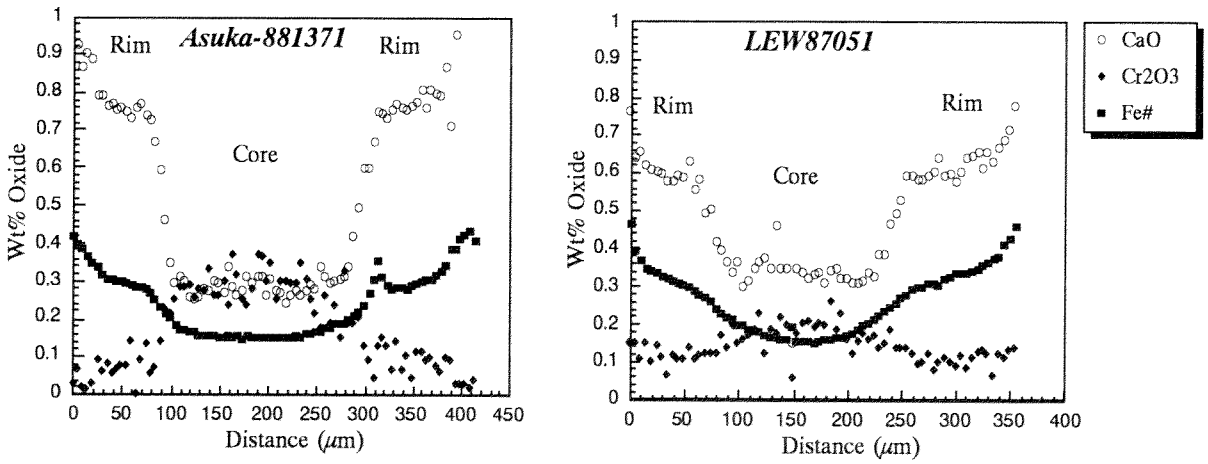


Fig. 2: CaO, $Cr_2O_3$, and Fe# (Atomic Fe/(Fe+Mg)) zoning profiles of Asuka-881371 olivine (left) and LEW87051 olivine (right). It is apparent that both olivines have Cr-rich and Ca-poor cores, and show two-stage zoning profiles from Mg-rich core to Mg-poor rim. Ca and Cr are negatively correlated.

# Material Evidences of Takamatsu Impact Crater in Japan

Yasunori Miura[1], Makoto Okamoto[1,2]
Muneyoshi Furumoto[3] and Tatsuro Fukuchi[1]

[1] Faculty of Science, Yamaguchi University, Yamaguchi, 753, Japan.
[2] Faculty of Science, Okayama University, Okayama, 700, Japan.
[3] Faculty of Science, Kanazawa University, Kanazawa, Ishikawa, 921, Japan.

## 1. Introduction

Anomalously low value of Bouguer gravity anomaly in systematic gravimetric survey of the Japanese islands is incidentally found in the southern part of Takamatsu City, northeast Shikoku, Japan. Kono et al. [1] showed that the crater is ca. 4km in diameter with -10 mgal of gravity anomaly from surrounding granitic region. Two boring cores of 300m deep near small mountains could not reach the bottom of the crater so far. We hereafter call this circular crater structure as 'Takamatsu crater' in this paper.

The surface area of the Takamatsu crater structure is partly covered by Mitoyo-Group sediments of Plio-Pleistocene Epoch (up to 150m deep), which are intruded by Sanuki-Group rocks of small biotite-andesites (Hiyama, Umayama, and Jissojiyama) and brecciated rocks of Hiyama and Jissojiyama breccias. The small volcanic intrusions inside the crater are not related with origin of large circular structure, because the small volcanic mountains of Hiyama and Jissojiyama inside the Takamatsu crater are the same volcanic activities of the Goshikidai and Yashima intrusions. There are no large pyroclastic flow deposits and progressive volcanic activities on the surface of the surrounding area [2], though the Goshikidai and Yashima show high plateau topography with volcanic intrusions. These geological and geophysical data cannot be explained by volcanic cauldron origin of the Takamatsu crater. No active large fault activities near the crater can be observed as fault origin of the crater. Shallow boring core of 300m deep at the Funaokaike (No.B-1) in the western part of the crater is composed of upper 70m of intruded biotite-andesite, and lower brecciated flow deposits including anomalous quartz and feldspar grains which cannot be found other andesitic intrusions outside the crater.

The brecciated flow deposits including anomalous mineral grains can be found only on the surroundings of the small intruded biotite-andesites, though the brecciated rocks around Hiyama, Jissojiyama and Umayama inside the Takamatsu crater are partly altered by hydrothermal activity after volcanic intrusions [4,5,6,7,8].

## 2. Analyses of anomalous materials

The detailed examinations of the anomalous minerals of the brecciated flow mixed rocks which are found at the surrounding rim of andesitic intrusions, are clue to origin of the Takamatsu crater. The materials from brecciated rocks are divided into the following four major mineral materials:

(a) pebble fragments from the Rhyoke granitic basement (Sampking No.15),
(b) rock fragments from intruded biotite andesites (Nos.2,15,20),
(c) impact-induced fragments of shocked quartz (Nos.2,3,6,15,18), diaplectic feldspars (Nos.2,3,6,11,15), silica glasses (Nos.2,15) and small Fe-Ni metallic grains (No.15), and
(d) small fragment of halite (No.2) or such zeolites as mordenite (Nos.6,20) or stilbite (No.15).

Table 1. Characterization of surface samples on the Takamatsu crater [4,5,6,7,8].

| Sample No. | Location | Rock Name | Anomalous materials in Xenoliths |
|---|---|---|---|
| 2 | Hiyama-1(E)* | Mixed Breccia | Shocked quartz, diaplectic feldspar, glass, halite, and mordenite. |
| 3 | Hiyama-2(E) | Mixed breccia | Shocked quartz (lamellae), diaplectic feldspar, glass & mordenite. |
| 6 | Hiyama-3(E) | Mixed breccia | Shocked quartz, mordenite and glass. |
| 10 | Mae-Ike (N) | Altered andesite | Ellipsoidal quartz with crack. |
| 11 | Hira-Ike(W) | Altered andesite | Diaplectic glass. |
| 15 | Jissojiyama(S) | Mixed breccia | Fe-Ni grains, glass, feldspar spherule breccias, and stilbite. |
| 17 | Umayama (S) | Mixed breccia | Shocked quartz and glass; zeolite. |
| 12(Out) | Asano (S) | Granite | Shocked feature |
| 21(Out) | Tohridani(S) | Granite | Shocked feature |

* Direction in the Takamatsu crater. S:South, W:West, N:North, E:East.

These impact-induced grains of shocked minerals and Fe-Ni grains (c) could not be obtained at similar whitish sediments of rhyolitic intrusions on the surrounding rims of the Goshikidai and Yashima outside the crater(with mainly as FeS grains). These material evidences are the main reason why the Takamatsu crater is considered to be formed by meteoritic impact.

Although there are no many boring-core samples, tiny grains of halite in glassy rocks are evidences of lake-

sediments of original Takamatsu crater after impact. This is the same analytical scanning electron microscopic (AEM) data of tiny halite grains in shocked limestone from the Ries crater, Germany, taken in this study, which are considered to be relicts of the crater-lake sediments after impact. These impact-induced fragments are examined by polarized and reflected microscopes, powder and single-crystal X-ray diffracto-meters, analytical scanning electron microscope (AEM) as follows [3,4]:

1) **Fe-Ni graines**: Black glassy rocks at Jissojiyama (No.15) contain irregularly Fe-Ni grains of 10 to 100 $\mu$m in diameter (Fig.1). Chemical composition of the small grains of Fe+Ni varies from ca. 18~90 atom.% mixed with the major granitic components (cf.Table 2). Atomic ratios of Fe/Ni are 3.4 to 68.7 which are the similar those of kamacite in Antarctic meteorites, but differ from those of awaruite (Fe/Ni<0.5) from the deep seated rock of the interior of the Earth [5]. The same tiny Fe grains can be found on the Wolf Creek meteorite crater and the Ries impact crater.

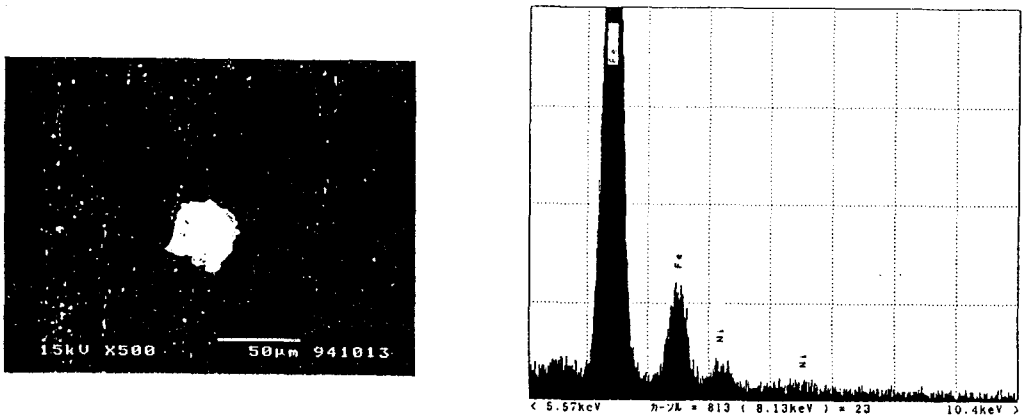


Fig. 1. Fe-Ni mixed grain involved in black glassy rock (No.15) in the Takamatsu crater [3,4]. Composition of the grain is that of sample No. 151G-15 in Table 2.

Table 2. Representative chemical compositions of impact-generated materials (shocked quartz, Fe-Ni grains, and glasses) and of halite in the Takamatsu crater [3]

| Sample Oxides | Takamatsu 3B-SQ1 | Takamatsu 3B-SQ2 | Takamatsu 15-GL2 flow | Takamatsu T3-4-1 | Sample Oxides | Takamatsu 151G-15 | Takamatsu 15-FE5 |
|---|---|---|---|---|---|---|---|
| $SiO_2$ | 99.9 | 92.7 | 83.1 | 2.5 | Fe | 89.3 | 12.2 |
| FeO | 0.0 | 0.6 | 1.1 | 0.0 | Ni | 1.3 | 1.3 |
| $Al_2O_3$ | 0.0 | 6.4 | 8.7 | 1.8 | $SiO_2$ | 8.0 | 49.5 |
| $Na_2O$ | 0.1 | 0.2 | 3.4 | 20.7 | $Al_2O_3$ | 1.4 | 21.9 |
| CaO | 0.0 | 0.0 | 0.0 | 0.0 | $K_2O$ | 0.0 | 12.8 |
| $K_2O$ | 0.0 | 0.2 | 3.8 | 0.0 | $Cr_2O_3$ | 0.0 | 2.4 |
| MgO | 0.0 | 0.0 | 0.0 | 0.0 | | | |
| Cl | 0.0 | 0.0 | 0.0 | 75.0 | (Fe/Ni) | (68.7) | (9.4) |
| Total | 100.0 | 100.1 | 100.1 | 100.0 | Total | 100.0 | 100.1 |

2) **Shocked quartz with high-density and shock lamellae**: Anomalous quartz grains with undulatory extinction and shock lamellae are found at Hiyama (Nos.2,3,6 in whitish fine rocks) and Jissojiyama (No.15 in black glass) as brecciated xenolith from the interior of crater sediments. There are two types of shocked quartz:
   (a) glassy fragments of lamellar texture of crystalline quartz (3B-SQ1 in Table 2) and glassy silica (3B-SQ2 in Table 2) checked by the AEM which are considered to be formed during brecciation after impact.
   (b) Typical shocked quartz grain with two sets of shock lamellae along $\pi$ (102) crystallographic planes [6]. The shocked quartz grains with undulatory anomalous extinction and with a few shock lamellar texture are selected for X-ray single diffraction analysis.

The main X-ray diffraction peaks of each plane in shocked quartz of meteoritic impact crater and geological boundary (K-T etc.) always show high Bragg angle and high X-ray density which are considered to be relict of high-pressure silica phases with high density [7,8,9]. Anomalous quartz grains of the Takamatsu crater (Nos. 3,6,15) reveal high density ($\Delta\rho$=+0.9±0.3%) as listed in Table 3, and lower values (ca.- 0.4%) of each plane-distance of all shock-generated plane deformation features (PDFs). These structural data of high density are the same of shocked quartz grains in terrestrial impact craters (10,11).

3) **Diaplectic feldspars** : Shock-generated diaplectic feldspars with compositions of albite plagioclases with undulatory extinction [9] are observed with dark or partly dark (i.e. diaplectic) glassy materials under cross polarized microscope (Nos.2,3,6,11,15). Crushed plagioclase with circular or ellipsoidal shape are also found at Hiyama (No.6) and Hiraike (No.11). Diffuse and irregular textures of feldspar fragments are different with other localities outside the crater.

Table 3. X-ray data of single grains of shocked quartz (with high density) in the Takamatsu crater. Sample No.3 at Hiyama [3,5,7,8].

| Sample | Peak No. | a(A) | c(A) | V($A^3$) | $\rho$ ($g/cm^3$) | $\Delta\rho$ (%) |
|---|---|---|---|---|---|---|
| T3-1 | 14 | 4.902(4)* | 5.392(9) | 112.2(3) | 2.667(6) | +0.9(3) |
| T3-2 | 13 | 4.905(4) | 5.396(9) | 112.4(3) | 2.661(6) | +0.6(4) |

* Standard deviation is shown at the last decimal place by round parentheses, and are obtained from least square calculation of the highest X-ray peak values which reveal average structure of shocked quartz with high-density [6].

4) **Glasses of potassium feldspar compositions**: Many glassy fragments with flow texture are observed from fine-grained sediments around Hiyama (Nos.2,3,6), which have compositions of potassium feldspars. The main mass of the glasses are found irregularly at outcrop of the largest intrusions in Jissojiyama (No.15), which the sizes of blocks are irregularly up to a few ten cm in diameter. Some brecciated rocks with the black and white texture of the outcrop (No.15) contain slightly birefringent white shocked quartz silica with flow texture and are similar with suevite in the Ries crater, though the Takamatsu crater has also mixed outcrop with red colour by the hydrothermal alteration which feldspar grains are completely replaced by zeolite as stilbite. The dense (without bubble) and circular quenched textures of the glasses which can be found also in the Ries impact crater, are similar to obsidian or perlite volcanic glasses. Compositions of the glasses can be distinguished with impact or volcanic glasses. Compositions of the glasses by the AEM are high-silica ($SiO_2$=78~85wt.%) without MgO (cf. Table 3) which are not typical glassy volcanic rocks (in Gosikidai or Yashima), but impact-generated mixed glasses [3].

3. Discusssion

K-Ar dating of the white fine-grained breccias of Hiyama (No.3) (analyzed by Teledyne Isotopes) is 14.2±0.7 (Ma), which is the same age of the Goshikidai or Yashima activities outside of the crater. This suggests that fine-grained breccias mixed with crater products are formed with Hiyama andesitic intrusion, and that impact of the Takamatsu crater is older than small and many volcanic intrusions [3,4].

The Takamatsu crater is considered to be formed by meteoritic impact on the granite (before ca. 14 Ma), followed by filling with brecciated rocks to form crater lake, and penetrating small biotite-andesite magma through cracks of the bottom of the crater (ca.14 Ma ago) to form the small volcanic mountains and whitish surrounding breccias mixed with the crater sediments and hyrothermal alteration [3,4].

Among 22 buried impact craters from 141 impact craters reported on the stable continents of the Earth [2,10], four impact craters of the Manson, Vredefort, Sythylemenkat Lake and Sudbury are intruded by volcanic or plutonic rocks along the cracks after impact. However, there are few meteoritic impact craters on active volcanic islands or coasts, because original meteoritic impact craters are completely broken by crustal evolution by volcanism or earthquake, where impact-generated materials formed by the original impact can be found finally in volcanic crater. Even there exist volcanic rocks in impact crater, this is called as impact crater, which is the same case on the lunar crater.

Therefore, the Takamatsu crater is considered to be the similar type of crater as impact crater followed by volcanic intrusions [3,6]. The Takamatsu crater seems to be the first impact crater in Japan or active orogenic areas on the Earth. The buried impact crater can remain in active volcanic islands, because this crater is surrounded with wide (ca. 100km size), rigid and stable granite of the Cretaceous Rhyoke-granitic basement.

**References:**


[1] Y. Kono et al. (1994): ISAS Lunar and Planetary Symp. (Japan), 27, 67-70.
[2] H. Sato (1982): Sci. Rep. Kanazawa Univ. (Japan), 27, 13-70.
[3] Y. Miura et al. (1995): Lunar. Planet. Sci. (USA), XXVI, 987-988.
[4] Y. Miura et al. (1995): Shock Waves Japan-1994, 613-616.
[5] Y. Miura et al. (1981): Contrib. Mineral. Petrol., 76, 17-23.
[6] R.A.F.Grieve et al. (1988): LPI Technical Report (USA), No.88-03, 89 pp.
[7] Y. Miura (1991): Shock Waves (Springer-Verlag), 1, 35-41.
[8] Y. Miura et al. (1992): Celestial Mechanics, 54, 249-253.
[9] Y. Miura et al. (1992): Shock Wave Proc. (Springer-Verlag), 18, 403-407.
[10] P. Hodge (1994): Meteorite Craters and Impact craters of the Earth (Cambridge Univ.), 124 pp.

# New X-ray and Compositional Data of Shocked Quartz with High Density from Ries Impact Crater

Yasunori Miura[1] and Makoto Okamoto[1,2]

1 Faculty of Science, Yamaguchi University, Yamaguchi, 753, Japan
2 Graduate school of Natural Sciences, Okayama University, Okayama, 700, Japan

## 1. Introduction

One of the major factor of material evidence for impact metamorphism is high density of average structure of shocked quartz [1,2,3,4,5]. Optical data of refractive indices cannot discuss in the detail about crystalline individuals of shocked materials because of (a) mixing with both crystalline and amorphous phases, and of (b) tiny grains less than 1 $\mu$m. Thus X-ray diffraction data of crystalline parts of shocked grains are important to discuss impact process.

There are two ways for discussion of high density of shocked materials as follows:

(a) The previous shocked materials reveal decrease of X-ray intensity and high-density. High-density of shocked quartz is obtained and calculated from the highest peak of each crystalline plane among splitted peaks. Thus high density obtained from the highest X-ray peaks suggests an average crystal structure. But low value of the highest X-ray intensity can be only obtained with computer-controlled X-ray diffractometer which requires the same experimental method for many measurements [1,2,3,4,5].

(b) New type of shocked quartz which is recrystallized by evolution of shock metamorphism [2], reveal high value of X-ray intensity, compared with the above (a) type of normal shocked quartz. Such anomalous shocked quartz can be found from only sandstone target-rock of Wolf Creek meteorite crater, Australia [6].

The main purpose of this study is to discuss on new type of shocked quartz with clear high Bragg angle shift and high-density.

## 2. Samples and textures

Shocked quartz samples used in this study are collected by the senior author from Nos.1(red color, East rim of the crater), 2(white, Northeast rim), 3(red, North rim), 4(red, North rim), 5(white, West rim), 6(brown, West rim), 7(Center), 8(Center) and 9(red, East rim). These samples are almost silica with foreign elements and amorphous materials [6].

There are various kinds of texture of shocked quartz which is formed by shock metamorphism through gas and melt conditin from solid state as follows [6]:

a) Minor content of Fe-Ni in shocked quartz: Shocked quartz (No.3) contains Fe and Ni from iron meteorite (Table 1).

b) Flow and mantle texture: Shocked quartz with rounded shape (No.4) are contained in glassy flow texture or mantle texture of shocked quartz or high pressure-type silica (core) and Fe-Ni (mantle). Size of rounded shocked quartz are from 0.03 to 0.3 mm in size (Nos.1,2,3,4,5,9)

c) Gas (or bubble)-contained wormy texture: Various sizes of gas (or bubble)-included wormy texture are found many shocked quartz grains (Nos.3, 5, 9).

d) Primary gaseous shape of shock lamellae in shoched quartz: A few vein of shock lamellae with gas-bubble formation are found in shocked quartz (Nos. 1, 2). This suggests that shock lamellae are formed initially from gas-bubble-shaped glasses to form vein-like lamellae. But there are few multi-vein type of shock lamellae in the Wolf Creek meteorite crater.

## 3. X-ray and compositional data

Chemical compositions of shocked quartz are listed in Table 1, where ther are no 100% quartz. X-ray diffraction pattern of powdered shocked quartz shows high Bragg-angle and high density in No.3 shocked quartz in the Wolf Creek meteorite crater, as shown in Fig.1 and Table 2 [6].

## 4. Long-range periodic structure of shocked quartz

Shocked quartz with high density reveals the following characteristics:

a) Chemical composition of shocked quartz (Table 1) are not pure silica but mixed with Fe·Ni·Ti·Al, which is explained as chemical relict in vapor plume [6,7]. But the X-ray calculated density corrected inclusion in molecular weight (MW) is still high density of about 1% (than rock-crystal) as listed in Table 2. Thus high density of shocked quartz is confirmed in this samples.

Table 1. Compositions of shocked quartz from the Wolf Creek meteorite crater, Australia. There are few pure silica (100%). All shocked quartz grains are mixed with Fe.

| Sample<br>Oxides | WC3-1<br>FNT-1 | WC3-2<br>FNT-1 | WC3-3<br>FT | WC3-4<br>FNT-2 | WC2-1<br>(impact site) | WC4-1<br>(SB) |
|---|---|---|---|---|---|---|
| $SiO_2$ | 97.3 | 99.9 | 99.7 | 98.9 | 99.3 | 94.6 |
| FeO | 0.90 | 0.1 | 0.1 | 0.1 | 0.3 | 0.2 |
| NiO | 0.06 | - | - | 0.8 | 0.4 | 0.1 |
| $TiO_2$ | 1.74 | - | 0.2 | 0.2 | - | - |
| $Al_2O_3$ | - | - | | - | - | 5.1 |

WC: Wolf Creek meteorite crater.

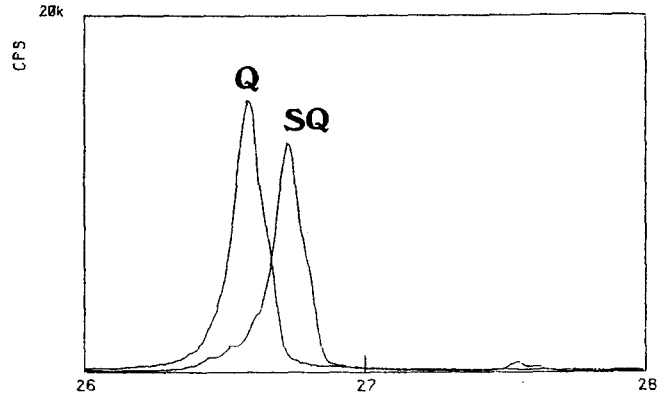


Fig. 1. X-ray profile of powdered No. 3 shocked quartz (SQ) from the Wolf Creek crater. High Bragg angle shift means high X-ray density, compared with standard rock-crystal (Q). This anomalous data are explained by following crystalline evolution of shock metamorphic quartz.

Table 2. X-ray calculated density of WC-No. 3 and WC-No. 4 shocked quartz from the Wolf Creek crater. Single grain data.

| Data | WC-3-1HA | WC-4-1HA |
|---|---|---|
| a (A) | 4.916 (4) | 4.89 (1) |
| c (A) | 5.409 (6) | 5.42 (1) |
| V ($A^3$) | 113.2 (2) | 112.0 (6) |
| Mole. Weigh (MW) | 28.716 | 28.040 |
| $\rho$ ($g/cm^3$) * | 2.671 (7) | 2.663 (7) |
| $\Delta\rho$ (%) | +1.0 (3) | +0.6 (3) |

* Density ($\rho$) = MW x 3 x 1.6602 / V. Standard pure MW ($SiO_2$) = 28.086

b) Original X-ray data of shocked quartz is not typical hexagonal (rhombohedral) cell of a=b axes. All X-ray data of $a \neq b$ suggest that shocked quartz contains of structure relict of high-pressure type silica (coesite or stishovite) [1, 3, 5, 6].

c) Structural distortion of shocked quartz is larger data in low Bragg angle than in high Bragg angle, as listed in Table 3. This suggests that shocked quartz has long-range periodic structure (than short-range one beyond the measurement precision) [6].

Table 3. X-ray data and unit-cell parameters of shocked quartz with high density from the Wolf Creek meteorite crater. Single grains.

| Sample<br>Cell | WC3-1LA*<br>(low angle) | WC3-1HA *<br>(high angle) | WC4-1LA<br>(low angle) | WC4-1HA<br>(high Bragg angle) |
|---|---|---|---|---|
| a(A) | 4.88(4) | 4.916(4) | 4.896(5) | 4.89(1) |
| c(A) | 5.37(9) | 5.409(6) | 5.405(9) | 5.42(1) |
| V($A^3$) | 111.0(3) | 113.2(2) | 112.2(3) | 112.0(6) |

* LA: low Bragg angle (from 9 to 16 degree of Mo target).
* HA: high Bragg angle(from 20 to 35 degree of Mo target).

## 5. Formation process of shocked quartz

The following experimental data are obatined in shocked quartz [6]:

(a) Density of shocked quartz is not the same of standard rock-crystal or normal quartz, but high density (ca. 1% higher than standard).

(b) Shocked quartz contains gas or bubble inclusion of silica glass, which suggests that shocked quartz is formed not from solid-state but from mixture with melt or gas state silica.

(c) Shocked quartz contains with minor amounts of Fe-Ni of iron meteorite components, or Ti·Al of meteorite and/or target rock inclusions, which suggests that shocked quartz is not formed from solid-state but from mixture of imapct materials.

(d) Gas and melt reaction can be also confirmed experimentally from the result that gas-bubble-like inclusion glasses to form shock lamellar vein in shocked quartz are found in shocked quartz of Wolf Creek crater (Nos.1,2).

(e) Transmitted electron micrograph shows bubble-texture with stacking fault of quartz lattice, which indicates that bubble-like silica glass crystallizes to quartz after impact to form shocked quartz structure.

(f) $^{29}Si$ NMR spectra of typical shocked quartz indicates that shocked quartz is (i) quartz with coesite, (ii) mixture of quartz, coesite and stishovite. Tentative inclusions of dense amorphous silica or stishovite on the Si NMR spectra cannot explained high-density quartz data of X-ray diffraction data of single grain.

From the above data, shocked quartz with high-density is explained by average structure of quartz that its remains on atomic scale of Si-O arrangements of coesite, stishovite or high dense glassy silica. But, it is not the large-scale mixture of high-density silica, because X-ray peaks were selected only from each crystal plane of quartz (no possibility to mix X-ray peaks of other silica materials which have different Bragg angles).

In any case, shocked quartz with clear high shift of Bragg angle, and high X-ray intensity in the Wolf Creek meteorite crater is the first case from the previous natural and artificial impact craters. This anomalous shocked quartz can be explained by recrystallization of glassy shocked quartz after impact (i.e. shock metamorphic evolution) [3].

Therefore, high-density of shocked quartz as average structure of impact indicator is confirmed on clear shocked quartz crystal in this study .

## 6. Summary

The experimental results in this study are summarized as follows [6]:

1) Shocked quartz (No.3) from the Wolf Creek meteorite crater, Australia, shows strong X-ray peaks with high density, though normal shocked quartz with high density has small X-ray peaks.
2) X-ray structural analyses by the single grain indicate that No.3 shocked quartz with high density shows distorted unit-cell dimensitions and short atomic distances compared with rock crystal.
3) New shocked quartz in the Wolf Creek crater confirms impact indicator of high density.
4) From the detailed study of the formation process on the Wolf Creek crater, the No.3 shocked quartz was formed by recrystallization during impact (i.e. shock metamorphic evolution) after mixing in vapor plume of impact event.

**References**

[1] Miura Y. (1991): Shock Waves, 1, 135-141.
[2] Miura Y. et al. (1992a): Shock Waves (Springer-Verlag), 18, 403-408; 19, 4pp.
[3] Miura Y. et al. (1992b): Celestial Mechanics, 54, 249-253.
[4] Miura Y. (1994): Proc. ISAS Lunar & Planet. Sci. (ISAS, Japan), 27, 204-207.
[5] Miura Y. (1994): Astron.Soc.Pac.Conf.Series, 63, 286-288.
[6] Miura Y. et al. (1995): Shock Waves, Japan- H6FY, 621-624.
[7] Melosh H. (1989): Impact cratering (Oxford University Press), 245pp.

# Shocked calcite and Fe grains from Ries impact crater

Yasunori Miura[1] and Makoto Okamoto[1,2]
1 Faculty of Science, Yamaguchi University, Yamaguchi, 753, Japan
2 Graduate School of Natural Sciences, Okayama University, Okayama, 700, Japan

## 1. Introduction

Shocked minerals with simple chemical composition are reported on quartz silica, graphite carbon, and iron materials. But calcite has no shocked phases, because the soft crystal structure of calcite with low hardness is considered to destroy immediately its structure by impact. Miura et al. (1994) reported that some shocked phases are formed from high-pressure phase surrounded by stopper (i.e. quenching) materials of gas-melt phases [1,2,3,4,5]. Thus calcite mineral reveals shocked phase, because it has high-pressure type phase of aragonite.

The main purposes of this study are (1) to discuss the new shocked materials of calcite found in Ries crater, Germany and artificial impact phases, and (2) to show new findings of Fe-grains and halite grain, and anomlaous feldspar in Ries impact crater for discussion of impact crater formation and meteorite materials in the Ries crater.

## 2. Texture, X-ray data and compositions of shocked calcite

### 2-1. Texture:

Limestone with shocked calcite shows wormy or bubble-included texture. The single grains show the following two-types of anomalous calcite phases in Buschelberg, Ries crater (sample R-8) [6]:

(a) fine-grained aggregates (including amorphous materials),

(b) Lamellar texture with dark amorphous materials.

The (a) type calcites can get the cell-dimensions only from powdered samples, though the (b) type calcites shows two data of the cell-dimensions from powdered and single grain samples.

### 2-2. X-ray data:

Powdered samples of anomalous calcites shows low X-ray intensity, and High Bragg angle shift, compared with standard calcite of Akiyoshi limestone as listed in Fig. 1 and Table 1 [8].

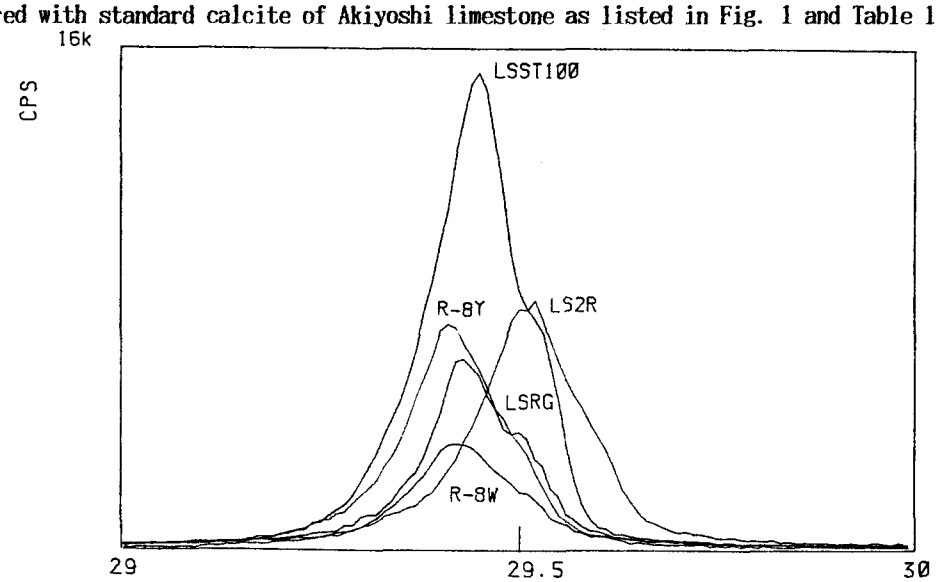


Fig.1. X-ray profiles of shocked calcites of standard limestone (LSST), yellow limestone (R8Y) and white limestone (R8W) from Noerdlingen-Ries, Germany, artificial shocked limestones of oxidation (LSRG) and reduction (LSR1) conditions of railgun apparatus, ISAS.

Single grains of anomalous calcite (sample R8) were selected for single-crystal four-axes X-ray diffractometer (Rigaku AFC, Yamaguchi University). The unit cell-dimensions were determined by the least square calculation from the highest X-ray intensity peak of each crystal plane which is the same data of the powdered X-ray diffraction sample as an average structure. Both powdered and single grains data reveal high density 2.76 g/cm$^3$ (between aragonite, density: $\rho$=2.8g/cm$^3$, and normal calcite, $\rho$=2.71g/cm$^3$) of the calcite sample which is the same characters of shocked phases [1,6] as listed in Table 1.

## 3. Fe-grain in Ries crater

Suevite sample of Otting (R-5) of the Ries impact crater includes various shapes (sperule, wormy or bubble-like texture) of Fe-Ni (Fe-ich) grains with 0.2 mm to 0.4 mm in size. There are no possibility of awaruite ($FeNi_3$) from deep-seated rocks. Thus these Fe-Ni grains are from impacted meteorite of iron which were melted and mixed with suevite to ejected out of the crater near the crater rim [6] (Fig.2).

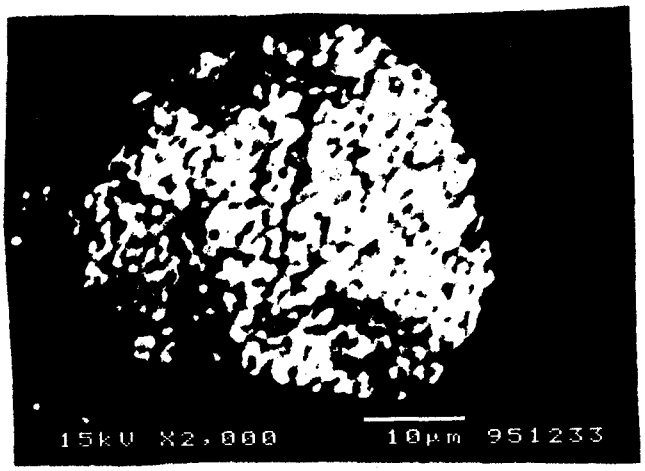


Fig.2. Fe-Ni grain with wormy texture on the Ries impact crater, Germany.

## 4. Halite grain in Ries crater

Limestone of Ronheim (R-13) of crater rim in Ries crater contains halite grain with 0.2 mm to 0.3 mm in size. This grains are considered to be relict of crater-lake materials after impact event [6].

## 5. Anomalous shocked plagioclase

There found anomalous plagioclases in suevite from Otting (R-5) of the Ries impact crater. The following two different data are obtained [6]:

(a) Compositions of R-5 plagiocalse are Ca-plagioclase of anorthite.
(b) Structure of R-5 anorthite grain shows low X-ray intensity. The highest X-ray peak of each plane reveals albite cell by the least square calculation. The anomalous low density of the R-5 plagioclase of 2.48 ($g/cm^3$) indicates that shocked plagioclase of albite structure from granitic target rocks are evaporated or melted by impact and recrystallized to shocked Ca-albite mainly mixed from Ca source from limestone.

## 6. Glassy flow texture

Typical glassy flow texture are found as pseudotachylite (i.e. pseudo-basaltic glass) from the suevite in Otting (R-5) of the Ries crater. Chomposition of the pseudotacylite formed by impact are similar to alkali-feldspar which contains Ca from limestone target rock.

The glassy flow-texture contains shocked quartz, Fe-grains, shocked feldspars, and shocked calcite as xenolith-like inclusion during impact process [6].

## 7. Summary

The results in this study are summarized as follows:

1) Shocked calcites of fine-grained wormy texture and high density are obtained on the Ries impact crater.
2) Shocked calcites of the Ries impact crater are consitent with reduction formation with cabon materials.
3) The similar shocked calcites with high dennsity can be obtained both oxidation state and reduction state at fine-grained ejecta of artificial impact materials.
4) Fe-Ni grains are found in this study fromthe Ries crater, which indicates iron-meteorite origin.
5) Halite grains are found in limestone of the Ries crater.
6) Anomalous shocked plagioclases from the suevite are found as Ca-albite-like phase.

## References

[1] Miura Y. (1991): Shock Waves, 1, 135-141.
[2] Miura Y. et al. (1992a): Shock Waves (Springer-Verlag), 18, 403-408; 19, 4pp.
[3] Miura Y. et al. (1992b): Celestial Mechanics, 54, 249-253.
[4] Miura Y. (1994): Proc. ISAS Lunar & Planet. Sci. (ISAS, Japan), 27, 204-207.
[5] Miura Y. (1994): Astron.Soc.Pac.Conf.Series, 63, 286-288.
[6] Miura Y. et al. (1995): Shock Waves, Japan, 617-620.621-624.613-616.
[7] Melosh H. (1989): Impact cratering (Oxford University Press), 245pp.

2-3. Chemical composition:

Anomalous calcite contains minor amount of Si·Fe·Ti, though major cation is Ca of 99.4 % in cation content. These foreign elements are mixed with during the formation in vapor plume. In this sense, calcite grain in meteorite should be checked whether it is impact-generated or not [8].

Table 1. X-ray density and unit-cell parameters of anomalous shocked calcite with high density from Ries and artificial impact craters. Impact velocity is 7km/s (railgun of ISAS) [8].

| Sample | | Powdered sample | | data | | Single grain data |
|---|---|---|---|---|---|---|
| Unit-Cell | Standard calcite LSST (Akiyoshi) | R-8Y1 (Ries) | R-8W1 (Ries) | LSRG1 (Oxidation) | LS2R1 (Reduction) | R-8Y |
| a(A) | 4.991(1) | 4.976(1) | 4.982(1) | 4.972(1) | 4.979(1) | 4.953(4) |
| c(A) | 16.994(5) | 16.990(1) | 16.994(4) | 16.990(6) | 17.018(1) | 16.956(12) |
| V($A^3$) | 366.6(2) | 364.2(3) | 365.3(2) | 363.8(2) | 365.4(1) | 360.8(6) |
| $\rho$ ($g/cm^3$) * | 2.720(1) | 2.738(3) | 2.730(1) | 2.741(1) | 2.729(1) | 2.763(4) |
| $\Delta\rho$ (%) | (std.) | +0.7(1) | +0.4(1) | +0.8(1) | +0.3(1) | +1.9(2) |
| I(104) | 11772 | 4830 | 2697 | 6162 | 5662 | (1067) |

2-4. Formation process of shocked calcites:

The following two types of shocked calcites are found in artificial imapct experiments (cf. Fig.1)

(a) Shocked calcite formed on oxidation condition (near the rim of vapor plume of impact [7]).

(b) Shocked calcite formed on reduction condition (interior of vapor plume of impact [7]).

The shocked calcites of the Buschelberg (R-8) in side the crater are corresponded to shocked calcite with reduction state, which suggests recrystallization inside the crater. The detailed experiments of the R-8 samples are done on yellow (Fe-rich) colored sample of R-8Y and white colored sample (R-8W). From the X-ray diffraction data of Bragg angle shift, the R-8W is more close to reduction state during impact.

The shocked calcites under oxidation state are formed as non-stoichiometric (n.s.) compound (and high density) after gas of $CO_2$ formation mainly near rim of vapor plume, which is the same data of artificial impact experiments of oxidation condition (i.e. sample No. LSST100).

The shocked calcite under reduction state are formed as normal calcite (with normal or a little high density) and carbon after formation of gaseous materials of CO, $O_2$ and Ca. Thus cabon source from target rock of limestone can be explained as reduction formation of impact, as listed in Tables 2 and 3.

Table 2. Formation process of shocked calcites materials by shock impact.

| Condition | Reaction | Main product |
|---|---|---|
| 1) **Oxidation state** (near rim of vapor plume or jetting stream) | $2CaCO_3 \rightarrow CaCO_3$(fine) $+CaO+CO_2$(gas) $\rightarrow Ca_{(1+x)}CO_3$(fine) | Fine-grained n.s. shocked calcites |
| 2) **Reduction state** (inside of vapor plume or jetting stream) | $2CaCO_3 \rightarrow 2Ca+2C+3O_2$(gas) $\rightarrow CaCO_3$(f) + C | Fine-grained n.s. shocked calcites, Carbon materials |

Table 3. Relation of carbon-materials and target rocks of natural impact craters.

| Craters | Target rock | Shocked materials | Example of Crater |
|---|---|---|---|
| 1) Carbon-bearing impact craters | Limestone & others | Shocked carbon materials, Shocked quartz & feldspars. | Barringer & Ries |
| 2) Carbon-free impact craters | Sandstone, Granite & Gneiss | Shocked quartz & feldspars. | Wolfe-Creek, Canadian, and American craters |

**Stability of silicate melt in the solar nebula.** H. Nagahara and K. Ozawa, Geol. Inst., Univ. Tokyo, Hongo, Tokyo 113, Japan. *e-mail*: hiroko@geol.s.u-tokyo.ac.jp

Origin of chondrules has been one of the most debated problems in the planetary sciences, which has not yet been reached to a consensus among researchers. One extreme model suggest their origin during the accretion of the solar nebula, that is, at the earliest stage of the solar nebula. Another extreme suggests the formation on the surface of planetesimals, that is, at the latest stage or even after dissipation of the solar nebula. Those models are constructed on the basis of constraints for temperature and cooling rates obtained mostly from experimental reproduction of texture and mineralogy of various chondrules, which are about 1600-2000°C and "flash-heating" to several hundreds degrees per hour during crystallization. Although temperature regime has been intensively considered, pressure regime for formation of silicate melt has not been fully considered. Silicate melt is generally unstable in most part of the solar nebula; the total pressure of the solar nebula, which is mainly of $P_{H2}$, is thought to have been $10^{-4}$ to $10^{-5}$ bar at the midplane at 1-2 AU where most meteorites might have formed. At that pressure conditions, solid materials should have directly without passing the molten state evaporated when heated to high temperature. In order to generate silicate melt in the solar nebula, enrichment of dust component relative to hydrogen gas has been proposed. The degree of dust enrichment for the formation of silicate melt in the solar nebula, however, has not been quantitatively studied. In the present study, formation of silicate melt in the solar nebula has been studied by thermochemical equilibrium calculations.

Calculations were made by the energy minimization technique; at equilibrium, the change in the Gibbs free energy should be zero, and therefore the total Gibbs free energy of the system should be minimized with as many constraints on $\Delta G$ as there are independent reactions. We have developed a new code; it examines the stability of all the condensed phases considered, obtains the stable mineral assemblages, then determines the composition and abundance of phases by minimizing the free energy of the system. We have considered 76 gaseous species, 47 condensed phases, and silicate melt. Due to lack of thermochemical data for non-ideality of silicate melt with chondritic composition, which is more magnesian and less aluminous and calcic compared to terrestrial basaltic melt, silicate melt was assumed to be an ideal solution. This assumption, however, should be incorrect because of non-ideality of silicate melt. The results of calculations, thus, contains considerable uncertainty that should be corrected by introduction of regular solution model. All the thermochemical data are taken from JANAF.

Calculations were made at temperatures from 1750 to 1900 K with 50° interval, where chondritic materials are partially to almost totally melt; total pressures from $10^{-7}$ to $10^{-2}$ bar with 4 steps in one order of pressure which are plausible for the most area of the solar nebula from 1 to several AU, and dust enrichment factor from 1 to $10^5$ with 4 steps for one order of enrichment compared to the abundance of metallic elements relative to hydrogen of the solar system elemental abundance. Enrichment of dust includes silicate and metallic dust, dust plus ice, and dust plus ice plus "tar", of which compositions follow [1]. Silicates, ice and "tar" are enriched simultaneously with the same degree.

The results for 1900K are shown in Fig. 1, where phase boundary between gas and solid plus gas and that between solid plus gas and liquid plus solid plus gas regions are shown 3 dust compositions. The as and solid plus gas boundary is the condition where condensation of silicates in temperature decreasing nebula or total evaporation of silicate dust in temperature rising nebula takes place. Liquid is stable at the upper right portion of the solid plus gas and liquid plus solid plus gas boundary. The boundary has a negative slope, where increase in total pressure requires smaller degree of dust enrichment and increase in dust enrichment requires lower total pressure for the stability of silicate melt in the solar nebula. At 1900K, which is the temperature widely suggested for formation of chondrules, about 4 orders of enrichment is required at the total pressure of $10^{-4}$ bar which is the pressure proposed for the midplane pressure at about 2 AU. At that temperature, at least 3 orders of enrichment is required regardless of the total pressure. Although at lower temperatures the boundary shifts to smaller enrichment, at least 3 to 4 orders of dust enrichment is necessary to stabilize silicate melt.

Solids coexisting with the melt include aluminous minerals, Ca-Al-rich minerals, forsterite, diopside and metallic Ni-Fe. The ratio of melt to silicates increases toward upper right.

The effect of ice and "tar" is also shown in Fig. 1, where liquid-free and liquid bearing boundaries for three different compositions are shown by different curves. In the presence of ice, the boundary moves to lower left; that is, silicate melt tends to be stable at lower pressures with the same degree of dust enrichment or smaller degree of enrichment at the same total pressure. Presence of "tar" along with ice appear to have a similar effect on the stability of silicate melt in the solar nebula; the liquid-fre and liquid-bearing boundary moves to lower dust enrichment portion. Silicate melt is stabilized in the coexisting of ice and "tar". This may be due to fairly oxygen rich composition of "tar" by [2]. If the tar is of pure carbon, the boundary is effectively moved toward upper right portion of the figure, although it is not shown here.

In the coexistence of ice with silicate dusts, melt is stable in the enrichment of dusts by 3 orders at $10^{-4}$ bar total pressure, which is one order smaller than the case without ice. Simultaneous enrichment of silicate dusts and ice could be the case when silicates for chondrule precursor were mantled by ice.

In summary, silicate melt is stable when dust is enriched by 3 to 4 orders with or without coexisting of ice or carbonaceous material at the total pressure above $10^{-4}$ bar. Melt is, however, unstable at total pressure below $10^{-5}$ to $10^{-4}$ bar depending on the composition of dust. Present conclusion favors formation of chondrules in dust enrich midplane or dust convergent zone by turbulent nebula by [2].

References [1] Wood, J. A. and Hashimoto, A. (1993) *GCA* **57**, 2377-2388, [2] Cuzzi, J. N., Dobrovolskis, A. R., and Hogan, R. C. (1994) Paper presented to the Conference on Chondrules and the Protoplanetary Disk.

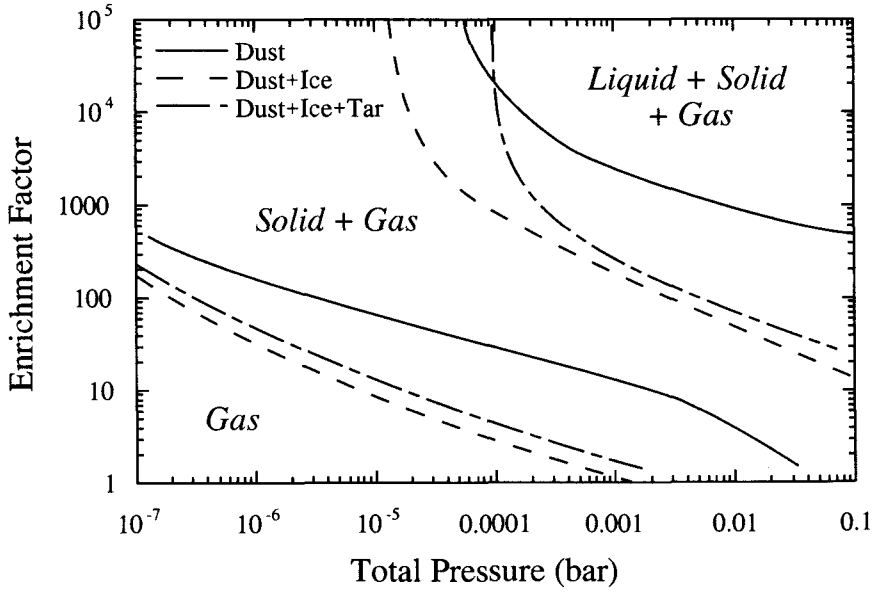


Fig. 1 Phase boundaries between gas and gas plus solid and gas plus solid and gas plus solid plus liquid at 1900 K for enrichmentof dust with three different compositions.
plus ice plus "tar".

# TRAPPED NOBLE GAS COMPONENT OF BRENHAM PALLASITE

Keisuke NAGAO[1] and Yayoi N. MIURA[2]
1) Institute for Study of the Earth's Interior, Okayama University, Misasa, Tottori 682-01, Japan.
2) Earthquake Research Institute, University of Tokyo, Bunkyo-ku, Tokyo 113, Japan.

**Introduction**

Trapped noble gas components of meteorites are regarded to be closely related to their origin of their parent body. Heavy noble gases in most chondrites have isotopic compositions of AVCC, and some chondrites and achondrites have noble gases which probably representative of solar noble gases. Since the trapped noble gas concentrations in howardites, eucrites, and diogenites (HED) are generally too low to perform precise measurement, their trapped component is not conclusive yet. Recently, trapped xenon isotopic compositions similar to those of U-Xe have been reported for a diogenite (Tatahouine) and the Lodran (Eugster and Michel, 1994), which are different from both AVCC and solar Xe. This result may indicate that some achondrites formed from materials and in circumstances different from those for most chondrites.

We have measured noble gas isotopic compositions in silicate samples from the Brenham pallasite on a modified VG5400 noble gas mass spectrometer to clarify the trapped noble gas component in this meteorite and to investigate relationship between the pallasite and other types of meteorites such as HED and chondrites.

**Results and discussion**

Concentrations of cosmogenic He, Ne, and Ar isotopes in these samples showed wide variations, more than two orders of magnitude, corresponding to variable shielding depths against to cosmic-ray irradiation. Isotopic compositions of He and Ne indicate that they are mostly cosmogenic. Ar isotopic ratios are interpreted as a mixture of cosmogenic Ar and an atmospheric Ar contamination, though a small amount of radiogenic $^{40}Ar$ was observed in some samples. No trapped Ar component with low $^{40}Ar/^{36}Ar$ ratio was observed in these samples. These results suggest that this meteorite has been well degassed during its formation, which is supported by the low concentrations of Kr and Xe, $<10^{-10}cm^3STP/g$, observed in this meteorite. The low concentrations of Kr and Xe

make it difficult to identify trapped component owing to the atmospheric contamination as well as the cosmogenic component.

$^{130}Xe/^{132}Xe$ vs. $^{136}Xe/^{132}Xe$ ratios are shown in Fig. 1. Xe with isotopic ratios plotted around the earth atmospheric Xe is probably due to the contamination. Many data points are, however, plotted along the mixing lines between Earth-Solar or Earth-U, which indicates that the trapped Xe in this meteorite is not AVCC-Xe but Solar or U-Xe. Kr isotopic composition also supports that the trapped Kr is not AVCC.

If the trapped noble gas component is not AVCC, which is commonly observed in most chondrites, the Brenham pallasite must have been formed from materials different from those for chondrites. Hence, trapped noble gases in achondrites such as HED, stony-iron, and iron should be determined to investigate the origin and relationship between these meteorites.

Fig. 1

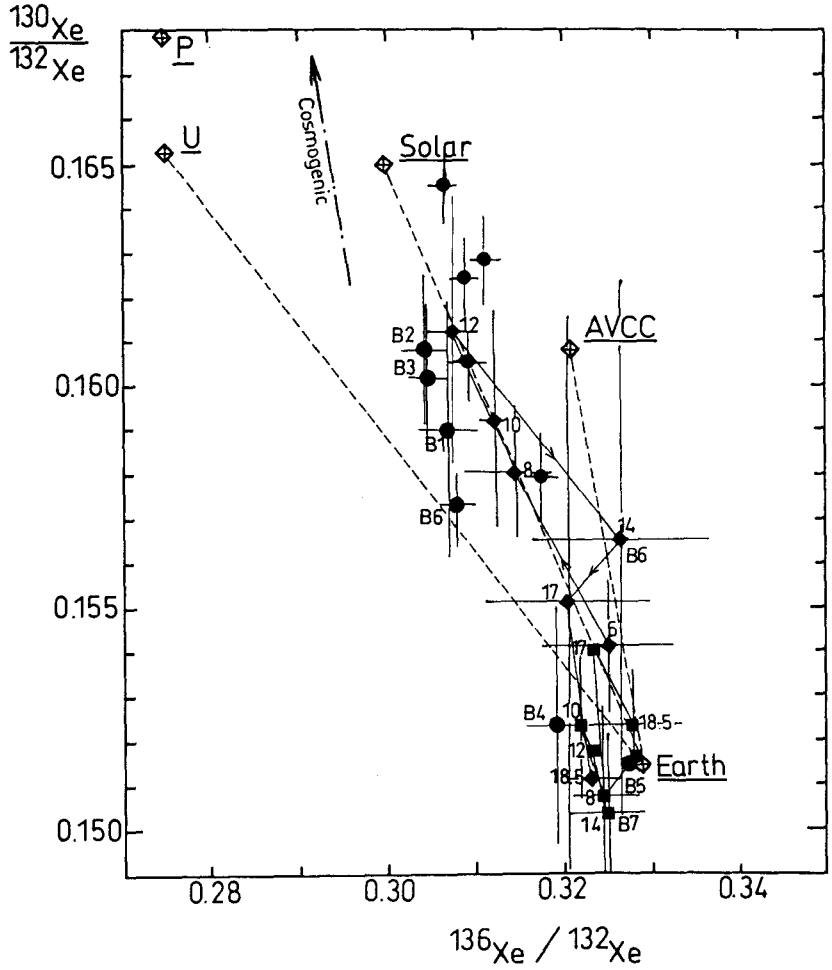

# X-RAY STUDY OF PCP FROM THE MURCHISON CM CARBONACEOUS CHONDRITES

Tomoki Nakamura and Yoshihiro Nakamuta

Dept. of Earth and Planet. Sci., Fac. of Sci., Kyushu univ. 33, Hakozaki, Fukuoka 812-81

## Introduction

Poorly-characterized phases (PCP; defined by Fuchs et al., 1973) are major constituent of CM carbonaceous chondrites. They range typically 20-200 $\mu$m in diameter and mainly occur in matrix as rounded to subrounded, massive forms (type I) and fibrous needle-like aggregates (type II) and amount up to 30 vol. % of matrix (Bunch and Chang, 1980; Barber, 1985). They commonly replace Fe, Ni-metal grains thus are thought to be secondary products of aqueous alteration (Fuchs et al., 1973). Despite their original definition, their characteristics become partly evident by transmission electron microscope (TEM) studies (e. g., Akai, 1980; Tomeoka and Buseck, 1983; Barber et al., 1983; MacKinnon and Zolensky, 1984; Tomeoka and Buseck, 1985); generally they consist of two major phases, tochilinite and various serpentine. Tomeoka and Buseck (1985) proposed a model explaining alteration sequence of PCP, in that PCP are primarily dominated by tochilinite and, as alteration proceeds, the tochilinite changes to cronstedtite (Fe-serpentine) and intergrowth of tochilinite and cronstedtite.

In this study, we performed X-ray experiments of PCP and rim around chondrules in the Murchison CM chondrites by using a gandolfi X-ray camera which enables to obtain a X-ray powder pattern from a small particle approximately 50 $\mu$m in size. Portions of interest in PCP are removed for X-ray study from a thin section of ~100 $\mu$m thick after petrographic and electron microscope observation. Our goal is to estimate relative abundance of phases comprising PCP of various types and to see how the abundance changes in the course of alteration.

## Results

The X-ray pattern of type I PCP which has ~70 wt.% FeO in composition shows a very strong 5.4 Å reflection. It is assigned to 002 reflection of tochilinite, since tochilinite has 10.8 Å interlayer spacings along *c*-axis (Organova at al., 1974). But, in the X-ray pattern, the 001 reflection of 10.8 Å basal spacing is not recognized. This might be explained by that mackinawite and brucite layers of tochilinite are predominantly occupied by Fe in their cation sites, thus the 001 reflection is weakened due to 5-Å periodicity of Fe-rich layers in the structure. X-ray intensity calculations using a structure model of tochilinite (Organova at al., 1974) confirm this interpretation.

Type II PCP show a very strong 7.1~7.2 Å, strong 3.6 Å and variable

intensities of 6.0 Å and 5.4 Å refractions. The 7.1~7.2 Å and 3.6 Å reflections are identified as cronstedtite (JCPDS 17-140). Cronstedtite may be disordered, since the prism reflection is observed around 4.5 Å. The 5.4 Å reflection shows presence of tochilinite. The 6.0 Å reflection may be 003 basal reflection of tochilinite-cronstedtite mixed layered mineral (Fig. 1). This identification is verified by following evidence. (1) The 6.0 Å reflection accompanies a weak reflection at 18 Å (tochilinite 10.8 Å plus cronstedtite 7.2 Å). (2) The 6.0 Å reflection is very strong relative to the 18 Å reflection, being resulted from interstratified Fe-rich layers with roughly 6 Å spacing in the tochilinite-cronstedtite mixed layer structure (Mackinnon and Zolensky, 1984). Relative abundance of tochilinite, cronstedtite and mixed layered mineral significantly varies among type II PCP (Fig. 2).

Rim around chondrules commonly contains many small PCP particles (< 10 $\mu$m in diametar) embedded in fine grained serpentine groundmass. The X-ray pattern of the rim shows the presence large amounts of serpentine and tochilinite and minor amounts of olivine but shows the absence of mixed layered mineral.

## Discussion

X-ray study reveals that the mixed layered mineral which is intergrowth of tochilinite and cronstedtite comprises variable fraction of PCP. The amount of mixed layered mineral increases with decreasing amounts of tochilinite (Fig. 2), suggesting that the mixed layered mineral is produced by replacing tochilinite. Thus the presence of the mixed layered mineral strongly indicates *in situ.* alteration from tochilinite to cronstedtite. The inverse reaction from cronstedtite to tochilinite must be ruled out, since primary PCP which forms at the expense of kamacite are dominated by tochilinite (Tomeoka and Buseck., 1985). The mixed layered mineral in PCP contains various amounts of Si in the cronstedtite layers, whereas tochilinite generally lacks Si. Hence, to form the mixed layered mineral from tochilinite, Si cation needs to be continuously supplied from exterior of PCP.

Rim around chondrules contains PCP which comprises mainly tochilinite, but lacks mixed layered minerals. This indicates that PCP in the rim are not subjected to progressive aqueous alteration, in contrast to PCP in the matrix. PCP in the rim are smaller thus higher surface / volume ratio than those in matrix. Therefore, PCP in the rim should be intensely affected by the aqueous alteration, but again our results do not support this. Further X-ray study of rim around chondrules is needed to clarify this point.

## References

Akai J. (1985) Men. Nat. Inst. Polar Res., Special Issue No. 17, 299-310.
Barber D. J., Bourdillon A. and Freeman L. A. (1983) Nature 305, 295-297.
Barber D. J. (1985) Clay Miner. 20, 415-454.
Bunch T. E. and Chang S. (1980) Geochim. Cosmochim. Acta 44, 1543-1577.

Fuchs L. H., Olsen E. and Jensen K. J. (1973) Smithson. Contrib. Earth Sci. 10, 1-39.
MacKinnon I. D. R. and Zolensky M. (1984) Nature 309, 240-242.
Organova N. I., Drits V. A. and Dmitrik A. L. (1974) Am. Miner. 59, 190-200.
Tomeoka K. and Buseck P. R. (1983) Nature 306, 354-356.
Tomeoka K. and Buseck P. R. (1985) Geochim. Cosmochim. Acta. 49, 2149-2163.

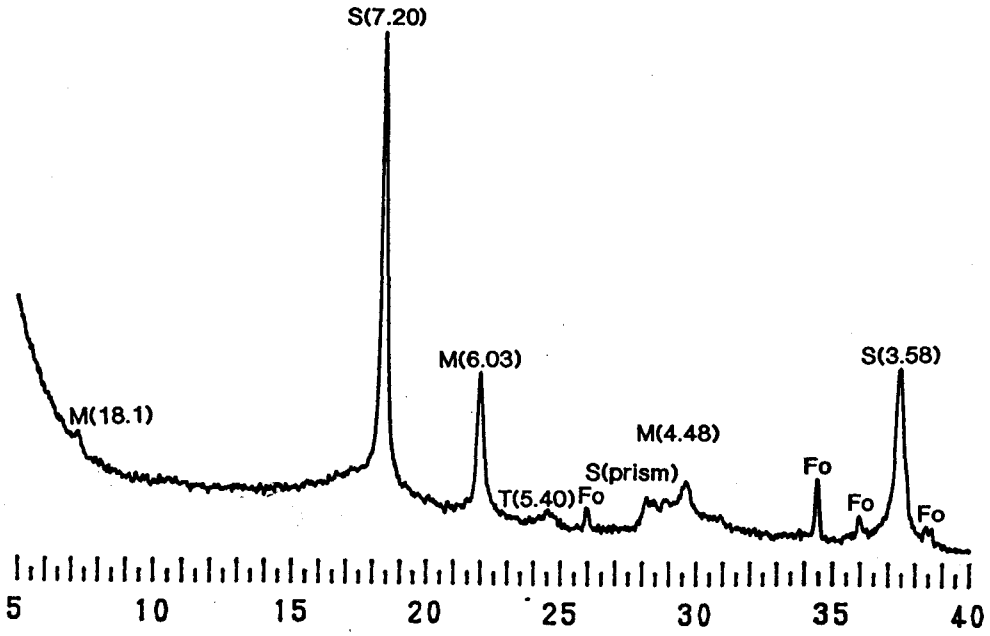


(Fig. 1) A X-ray pattern of type-II PCP in Murchison matrix showing that cronstedtite (S) and mixed layered mineral (M) are major constituents of the PCP. A prism reflection is observed at 28-30 degrees. Minor amounts of forsterite are also contained. Vertical sacale is X-ray intensity and horizontal one is $2\theta$ angle (degree).

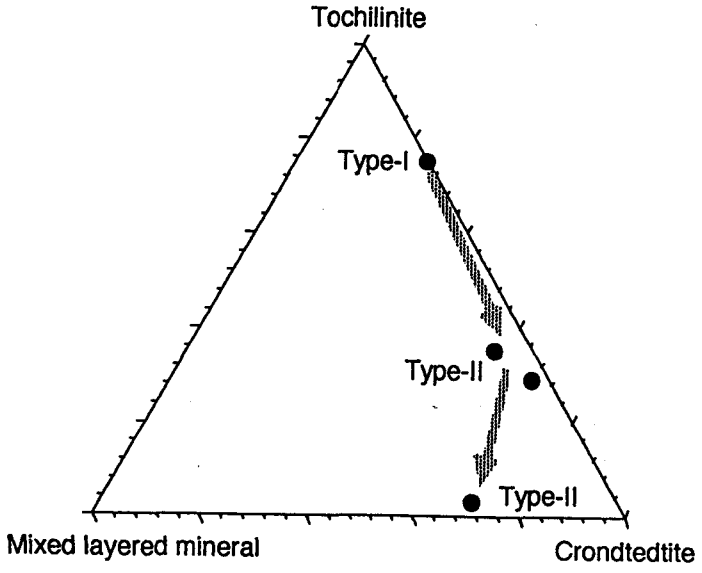


(Fig. 2) A ternary diagram (in terms of X-ray intensity ratio) showing alteration sequence of PCP in the Murchison matrix. Relative abundance of the three minerals in PCP changes along the arrow as the alteration proceeds.

# COMPOUND CHONDRULES FROM ANTARCTIC CARBONACEOUS AND UNEQUILIBRATED ORDINARY CHONDRITES

Tomoki Nakamura, Minoru Sekiya, Kenji Matuoka,
and Hideyasu Kojima*

Dept. of Earth and Planet. Sci., Fac. of Sci., Kyushu univ. 33, Hakozaki, Fukuoka 812-81 *Dept. of Antarc. Met., Natl. Inst. of Polar Res., 9-10, Kaga 1-chome, Itabashi-ku, Tokyo 173

## Introduction

Compound chondrules are those being comprised of two or more chondrules that are partially or completely embedded in one another (e.g., McSween, 1977). Their texture strongly suggests that they formed by collisions between chondrules which were plastic at the time of mutual counter (Gooding and Keil, 1981). The collisions between chondrules occur more frequently when chondrules disperse in the nebula with high space density and high inter chondrule velocity. Therefore, compound chondrules are of interest as indicators of physical conditions in the early solar nebula, and they should be extensively studied to obtain enough data for statistics.

Some unique features of compound chondrules are reported by previous works. High proportion (~28%) of nonporphyritic chondrules are compound (Gooding and Keil, 1981). Most compound chondrules consist of components having similar bulk compositions and textures (McSween, 1977; Lux et al., 1981; Wasson, 1993), while some are not (Scott and Taylor, 1983; Wasson, 1993). Lee et al., (1991) intensively studied a L3.5 chondrite, ALH77011 and reached to similar conclusions. Compound chondrules are found both in carbonaceous and ordinary chondrites, but abundances of compound chondrules in individual chondrite group (H, L, LL and C) are poorly known. We here present the results of our optical and electron microscope study of compound chondrules in 50 thin sections involving eleven H3, twenty-four L3, six LL3 and nine C2~3 chondrites.

## Definition and classification of compound chondrules

We have defined and classified compound chondrules manly based on the scheme proposed by Wasson (1993). According to the scheme, compound chondrules are divided into three classes; (1) enveloping type in which secondary chondrule encloses primary one (Fig. 1a), (2) adhering type in which small secondary is superimposed on the primary (Fig. 1b), and (3) consorting type in which secondary attaches to primary and both are comparable in size (Fig. 1c). In the course of observation of chondrules, we come to realize that it is difficult to distinguish compound chondrules of enveloping type from chondrules with a relict core and those with coarse-grained rim. We count chondrules as enclosing type only in case the chondrules having principally rounded, non-dusty chondrule-like

core for eliminating relict-bearing chondrules. Also, for eliminating chondrules with coarse grained rim, we do not count chondrules as enveloping when they have no mesostasis glass in their outer portions. Adhering and consorting morphology could be made from nearby sited chondrules by compression of the meteorite parent body, as pointed out by Wasson (1993). Thus we do not count a set of chondrules as compound if a thin rind of matrix material is observed between chondrules.

## Results and discussion

65 compound chondrules are identified through the inspection of ~6500 chondrules in H, L, LL and C chondrites and they include 14 enclosing, 29 adhering and 22 consorting type. 37 compound chondrules show similar texture and mineral assemblage between primary and secondary chondrules, involving 14 BO-BO, 12 RP-RP, 5 POP-POP, 4 PO-PO and 2 C-C combinations. 30 compound chondrules contain at least one BO chondrules in their constituent chondrules. Contrast to low abundance of BO in non-compound chondrules (~5 %), the BO-bearing compound chondrules are significantly abundant. RP chondrules show the same tendency. Exceptionally large abundances of BO and RP in compound chondrules might couple with the fact that both chondrules were totally molten when they formed, because molten droplets easily stick to each other or to another objects.

Abundances of compound chondrules in H, L, LL and C chondrites are rather constant; these are ~0.8 %, ~1.2 %, ~1.4 % and ~0.9 %, respectively. Relative abundances of enclosing, adhering and consorting type are roughly similar among each chondrite group. These results might imply that chondrules in each chondrite group formed in nebula subregions of similar physical conditions. Alternatively, chondrules were well mixed in the nebula, after chondrules that have similar texture and composition formed independently in the local nebula (Wasson, 1993).

## References

Gooding J. L. and Keil K. (1981) Meteoritics 16, 17-43.
Lee M. S., Rubin A. E., and Wasson J. T. (1991) Meteoritics 26, 362.
Lux G., Keil K. and Taylor J. (1981) Geochim. Cosmochim. Acta 45, 675-685.
McSween H. Y. (1977) Geochim. Cosmochim. Acta 41, 1777-1790.
Scott E. R. D. and Taylor G. J. (1983) Proc. Lunar Planet Sci. Conf. 14, B275-286.
Wasson J. T. (1993) Meteoritics 28, 14-28.

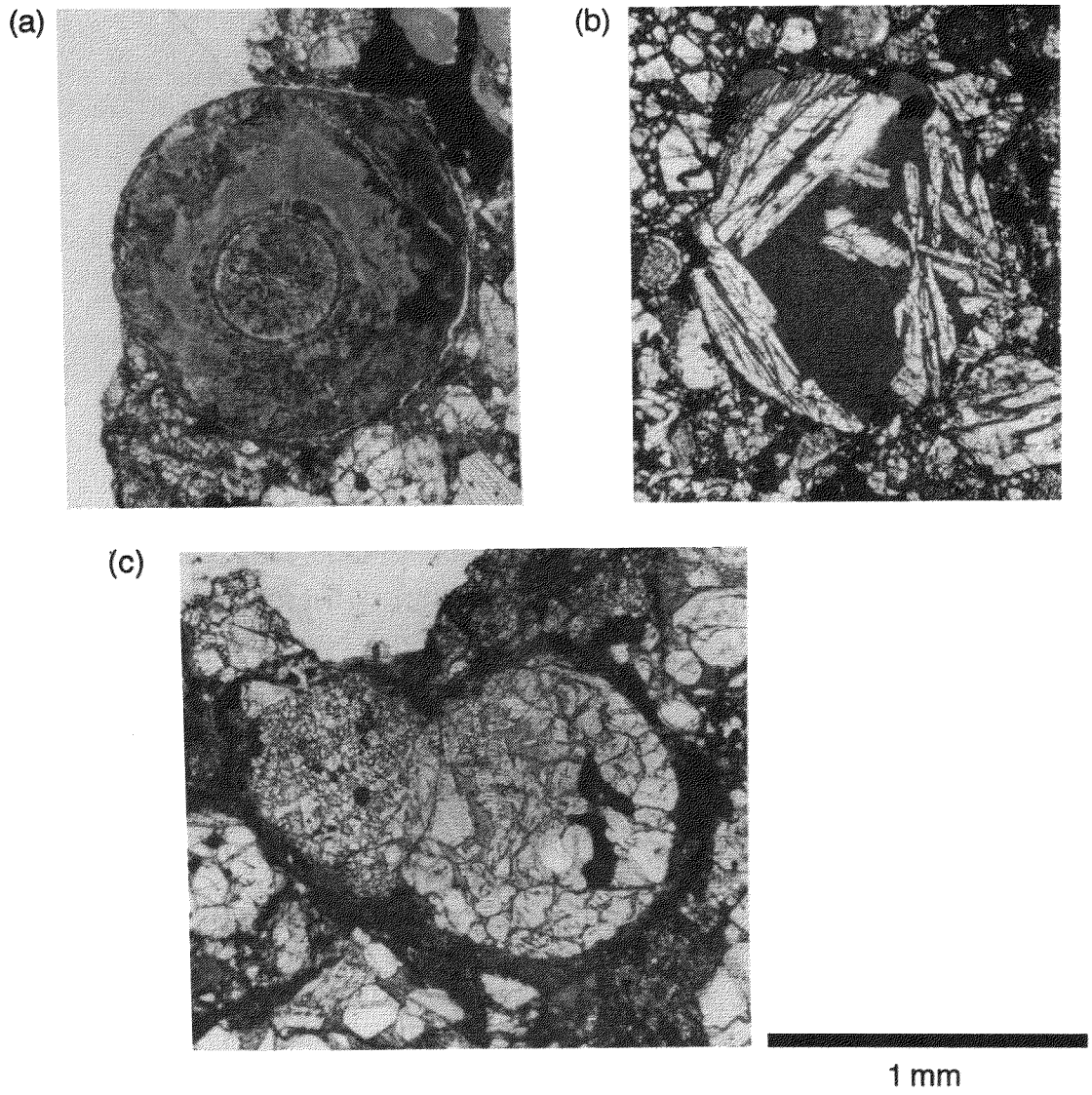


(Fig. 1) Optical photomicrographs showing variations of compound chondrules.
(a) An enveloping type with C (cryptocrystalline chondrule)- C combination.
(b) An adhering type with BO-RP combination. Note that on the secondary chondrule (upper left of the primary), two more small chondrules are imposed.
(c) A consorting type with POP-PO combination.

# SHOCK EFFECTS ON NOBLE-GAS ABUNDANCE IN THE EXPERIMENTALLY SHOCKED ALLENDE METEORITE

Tomoki Nakamura, Nobuo Takaoka, Keisuke Nagao*, and Toshimori Sekine**

Dept. of Earth and Planet. Sci., Fac. of Sci., Kyushu univ. 33, Hakozaki, Fukuoka 812-81 *Inst. of Study for Earth's Interior, Okayama univ., Misasa, Tottori 682-01 ** National Institute for Research in Inorganic Materials, 1-1 Namiki, Tsukuba 305

Carbonaceous chondrites contain large amounts of noble gases and these gases are mainly incorporated during formation of meteorite parent bodies. Recently, it comes to be known that shock effects are recorded in many carbonaceous chondrites (e. g. Nakamura et al., 1992; Scott et al., 1992), suggesting that impact events are a common process in the early solar system. However, it is poorly known how shock effects change noble-gas abundance in carbonaceous chondrites.

We have carried out shock experiments on the Allende CV3 chondrites and measured noble gas composition of both unshocked and shock-loaded samples by stepped heating. Allende samples were shocked to 23 GPa at different temperature conditions, room temperature and preheated to 600 °c. In the latter experiment, approximately 2 hours are needed to heat the sample to 600 °c, thus most of noble gases that are usually extracted at 600 °c fraction in the stepwise heating might disappear prior to shock loading. The Allende sample was encapsuled in a steinless holder that has a through hole 3 mm in diameter and shock loading was conducted in vacuum at ~1 torr for ambient air pressure. The shock duration is approximately 4-5 micro seconds, which is determined by rarefaction catch-up from the back of the stainless plate of the projectile (Fowles, 1960). Details of shock-experimental procedures are described elsewhere (Nakamura et al., 1995).

Noble gas composition of the unshocked Allende sample shows initial characteristics before shock experiments, including (1) He is dominated by planetary-type trapped components and is mainly released between 600-1000 °c temperature steps, (2) Ne is composed of spallogenic and planetary-type trapped components and, at 1200 °c or higher temperature fractions, spallogenic components become predominant, (3) Ar is mostly extracted at two temperature steps, 600 and 1200 °c and the former step is dominated by ragiogenic $^{40}$Ar whereas the latter step is overwhelmed by trapped component, and (4) Kr and Xe comprise trapped components, approximately 98 % Q-gas and 2 % HL-gas, and the Q-gas is released in larger part in 1200 and 1400 °c fractions and the HL-gas is released in 900-1200 °c fractions.

Noble gas composition and release patterns of the shock-loaded Allende samples both of room-temperature and preheated experiment are similar to those of the unshocked Allende sample especially in the middle to high temperature fractions (>900 °c). This indicates that spallogenic and trapped components are generally unaffected by shock wave propagation and subsequent residual heating generated by experimental shock loading. This appears to be consistent with that the spallogenic and trapped components in the shocked CV3 chondrites such as Leoville and Efremovka are not affected by shock effects (Mazor et al., 1970; Huss et al., 1995).

Lower temperature steps are remarkably different between unshocked and shocked Allende samples. Ar 600 °c fraction is a typical example (Fig. 1). The fraction of the unshocked Allende has high $^{40}Ar/^{36}Ar$ ratio of 847, indicating that ragiogenic $^{40}Ar$ is dominant. Whereas $^{40}Ar/^{36}Ar$ ratio of the fraction of the shocked Allende at room temperature is 270, close to and smaller than the air value. This suggests that gas exchange might occur upon impact between indigenous meteorite Ar and air Ar, i. e., shock-induced gas implantation and degassing occur simultaneously. If this is a case, 20-30 % of total meteorite $^{40}Ar$ was lost due to experimental shock effects.

Electron microscope observation shows that the shock-loaded Allende at high temperature is partially molten to form FeS veins and Ca-, Si-rich glassy grains in the matrix, indicating that the temperature concentration beyond 1000 °c occurred in the matrix due to high porosity. It is thus expected that significant loss of noble gases would occur. However, noble gas analysis reveals that major portions of ragiogenic and spallogenic components are not affected by the high-temperature shock effects. This might indicates that the high-temperature duration after shock is very short for diffusive loss of the noble gases.

References

Fowles G. R., (1960) J. Appl. Phys. 31, 655-661.
Mazor E., Heymann D. and Anders E., (1970) Geochim. Cosmochim. Acta. 34, 781-824.
Nakamura T., Tomeoka K., Sekine T. and Takeda H., (1992) Earth Planet Sci. Lett. 114, 159-170.
Nakamura T., Tomeoka K., Sekine T. and Takeda H., (1995) Meteoritics, in press.
Scott E. R. D., Keil K. and Stöffler D., (1992) Geochim. Cosmochim. Acta. 56, 4281-4293.
Huss G. R. and Lewis R. S. (1994) Meteoritics 29, 811-829.

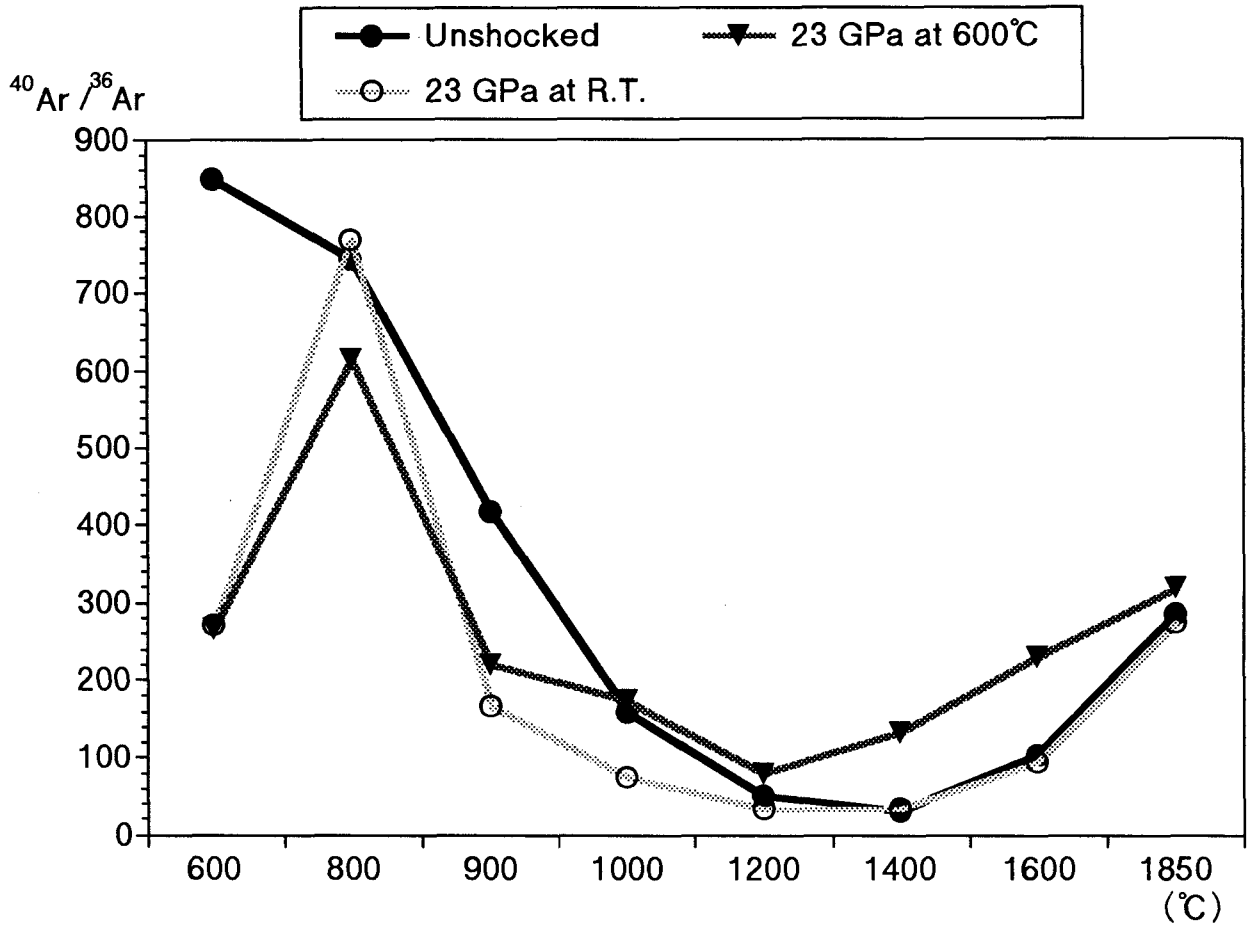


(Fig. 1) A noble gas release pattern showing variation of Ar isotopic ratio among unshocked Allende sample and shocked ones at room temperature and 600°c.

## Chemical compositions, Rb-Sr isotopic systematics and K-Ar age of the shocked H chondrite Y-790746

T. Nakashima[1], K. Nagao[2], T. Fujiwara[1], K. Misawa[1], N. Nakamura[1], H. Kagami[2], K. Yanai[3] and H. Kojima[3]

[1]Graduate school of Science and Technology, Kobe University, Nada, Kobe 657, [2]Institute for Study of the Earth's Interior, Okayama University, Misasa, Tottori 682-01, [3]National Institute of Polar Research, Kaga, Itabashi, Tokyo 173

Shocked meteorites are key materials for study of impact evolutionary history of asteroids. Although many age data by K-Ar and/or Ar-Ar methods have been accumulated, young ages determined by less susceptible clocks such as Rb-Sr isotopes, are still limited [e.g. 1,2,3]. Particularly, young ages obtained by Rb-Sr for H-chondrites are rarely reported [4]. Shock effects on chondrites are normally quite heterogeneous [3]. In order to clarify chemical effect, intensity as well as age of shock event, it is important to examine combined multi-chronological and chemical features for shocked materials. In this work, we have carried out analyses of Rb-Sr and rare gas isotopes along with trace elements for the shock-melted H chondrite, Y-790746.

Under binocular microscopes, the Y-790746 specimen studied here appeared mostly shock melted [5]. After gentle crushing, a part of sieved fraction (100~150 mesh) were used for whole rock analyses and other part was further crushed, sieved and subjected to mineral separation by Franz isodynamic separator (specimens; C1, C2, M1, M2, F1 and F2). For comparison, an unshocked H6 chondrite, Allegan, was also analyzed for rare gases in this work.

Results of trace element and rare gas analyses are presented in Table 1. Abundances of K, Rb, Sr and Ba in whole rock are typical for H-chondrites. Allegan shows an age of 4.68 $\pm$ 0.24 Ga which is in agreement with the typical formation age of meteorites. On the other hand, the whole rock of Y-790746 indicates a significantly young age of 2.66 $\pm$ 0.20 Ga. The age is in complete agreement with those of mineral separates. Therefore, we suggest that the age represents a date of shock event. In this work, we employed the mineral sepration technique similar to that of Nakamura et al. (1990). Neverthless, the $^{87}Rb/^{86}Sr$ spread among different mineral separates are quite small. Then, a precise Rb-Sr internal isochron can not be obtainable for these specimens, though Sr isotopic analyses are now in progress. To clarify if the K-Ar age represent an impact-melting event, it is required to obtain more refined mineral separates.

**References:** [1] Nakamura & Okano (1985), Nature 315, 563-566. [2] Nakamura, Fujiwara & Nohda (1990), Nature 315, 51-52. [3] Okano, Nakamura & Nagao (1990), Geochim. Cosmochim Acta 54, 3509-3523. [4] Fujimaki et al. (1993) Proc. NIPR Sympos. Antarct. Meteorites No. 6, 364-373. [5] Yanai (1981) In Photographic Catalog of

Selected Antarc-tic Meteorites 98, [6] Nishikawa et al. (1990) Mass Spectrometry 38, 115-123.

Table 1 Results for Y-790746 and Allegan

| | Whole rock | Mineral separates C1 | C2 | Allegan |
|---|---|---|---|---|
| K (ppm) | 861 | 972 | 998 | 817* |
| Rb (ppm) | 3.16 | 3.56 | 3.65 | 1.6* |
| Sr (ppm) | 11.23 | 11.7 | 12.0 | 9.30* |
| Ba (ppm) | 3.96 | 4.57 | 5.13 | 2.96* |
| $^{40}Ar$ ($10^{-8}cm^3STP/g$) | 2030 | 2100 | 2050 | 7100 |
| K-Ar age (Ga) | 2.66 ±0.20 | 2.54 ±0.19 | 2.47 | 4.68 ±0.24 |
| $^{87}Rb/^{86}Sr$ | 0.814 | 0.881 | 0.880 | |

*Data from Y.Nishikawa et al. (1990). [6]

# ORIGIN OF MONOMICT AUTOCHTHONOUS BRECCIA FROM THE LONAR IMPACT CRATER, INDIA

V. K. NAYAK
Department of Applied Geology, Indian School of Mines, Dhanbad, India

Lonar ($19^{\circ}58'N$ : $76^{\circ}31'E$) is an authentic meteorite impact crater in India (Nayak, 1972; Fredriksson et al. 1973; Kieffer et al. 1976). The Indian crater is unique because it is probably the only terrestrial crater in basaltic terrain and is recognized as the closest analog with the Moon's craters (Fredriksson et al. 1979). The geoscientific significance of the Lonar impact event was highlighted by Nayak (1989).

Five Deccan Trap basalt flows of tholeiitic nature of Cretaceous-Eocene age are exposed within the depression. They are of variable thickness, massive, hard, resistant, fine to medium grained and sometimes vesicular with or without zeolite, quartz and other secondary minerals.

The monomict autochthonous breccia occurs 50 to 60 feet southwest of Sita-ki-nahani Temple which is located midway along the northeast breach in the crater. The autochthonous breccia consists of various basalt fragments (Photograph 1). A large subangular shape (4 ft. X 3 ft. 10") ash-grey coloured fine grained basalt with a few empty vesicles, is surrounded by fine grained ashy somewhat pulverized like material which is embeded with small fragments of dark-grey vesicular basalt. Also associated is violet-reddish basalt which is profused with altered zeolite. The field relations, lithological composition, matrix and textures of various basalt components of the autochthonous breccia are described in detail. Megascopic and microscopic characteristics of basalt fragments are furnished. It is observed that most of the basalt fragments have a uniform composition but heavily oxidised and appears almost opaque in thin sections in some areas.

The location of the autochthonous breccia along the northeast breach strongly indicates it to be related with the NE-SW trajectory of the impacting projectile on the target basalts. A possible relation of the origin of autochthonous breccia with the crater formation is emphasized. It is realised that more field work is imperative to search for such autochthonous breccia in other parts of the Indian crater and work in this direction is in progress.

REFERENCES

Fredriksson, K., Dube, A., Milton, D.J. and Balasundaram, M.S. 1973. Lonar Lake, India - An Impact Crater in basalt: Science, Vol. 180, pp. 862-864.

Fredriksson, K., Brenner, P., Dube, A., Milton, D.J., Mooring, C. and Nelen, J.A. 1979. Petrology, Mineralogy and distribution of Lonar (India) and Lunar impact breccias and glasses: Smithosonian Contribution, Earth Science, No. 22, pp. 1-13.

Kieffer, S.W., Schaal, R., Gibbons, R.V., Horz, F., Milton, D.J. and Dube, A. 1976. Shocked basalt from Lonar Impact Crater, India and experimental analogues: 7th Proc. Lunar Sci. Conf., pp. 1391-1412.

Nayak, V. K. 1972. Glassy objects (Impactite Glasses?) A possible new evidence for meteoritic origin of the Lonar Crater, Maharashtra State, India: Earth and Planetary Science Letters, Vol. 14, No. 1, pp. 1-6.

Nayak, V. K. 1989. Geoscientific significance of the Lonar Impact Event, India: 14th Symposium on Antarctic Meteorites, National Institute of Polar Research (NIPR), Tokyo, Japan, p. 74.

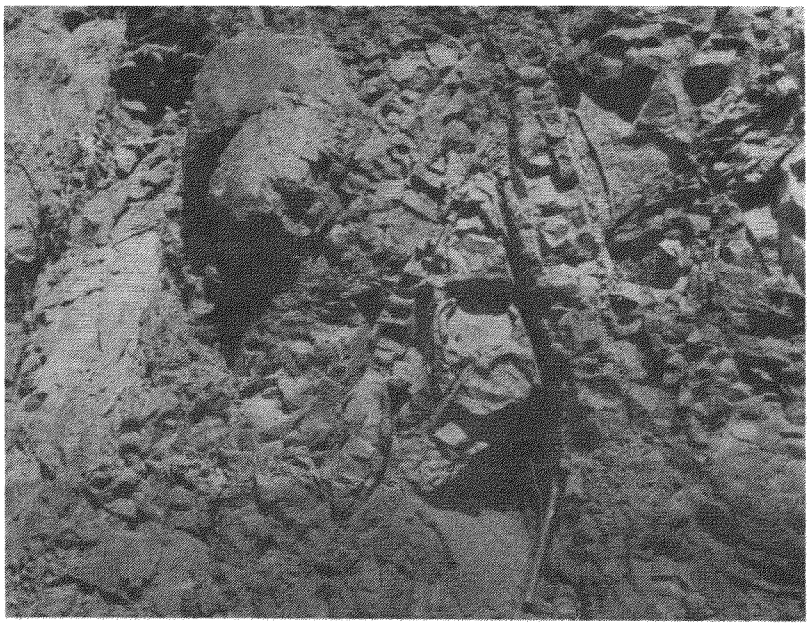

A field photograph showing monomict autochthonous breccia located midway along the NE-SW breach of the Indian Lonar Impact Crater.

# Thermoluminescence of Japanese Antarctic Meteorites

K. NINAGAWA[1], Y. HOSHIKAWA[1], I. YAMAMOTO[1], T. WADA[2], S. MATSUNAMI[3]
N. TAKAOKA[4], P. BENOIT[5], D.W.G. SEARS[5], H. KOJIMA[6] and K. YANAI[7]

[1]*Okayama University of Science, 1-1, Ridai-cho, Okayama 700*
[2]*Okayama University, 1-1, Tsushimanaka 3-chome, Okayama 700*
[3]*Miyagi University of Education, Aramaki-Aoba, Sendai 980*
[4]*Kyushu University, 10-1, Hakozaki 6-chome, Higashi-ku, Fukuoka 812*
[5]*University of Arkansas, Fayetteville, Arkansas 72701, USA*
[6]*National Institute of Polar Research, 9-10, Kaga 1-chome, Itabashi-ku, Tokyo 173*
[7]*Iwate University, 3-5, Ueda 4-chome, Morioka 020*

**Introduction** The thermoluminescence [TL] of meteorites is a useful tool with which to study meteorite history. Induced TL, the response of a luminescent phosphor to a laboratory dose of radiation, reflects the mineralogy and structure of the phosphor, and thus bears valuable information on metamorphic and later thermal history. The natural TL, the luminescence of a sample which has received no irradiation in the laboratory, reflects radiation history of the meteorite in space and the thermal history of the meteorite in space and on Earth. Natural TL data thus provide insights into such topics as the orbits of meteoroids, the effects of shock heating, and the terrestrial history of meteorites. For several years natural TL data have been routinely reported in the U.S. Antarctic Meteorite Newsletter and these data, along with induced TL data and cosmogenic radionuclide (*e.g.*, $^{26}$Al) and noble gas abundance data have been used to identify potentially paired fragments of Antarctic meteorites. We have started to measure the TL properties of meteorites from the Japanese Antarctic collection. In this paper we report our initial results for a suite of these meteorites.

**Samples and TL measurements** The induced and natural TL of three groups of ordinary chondrites were measured. Group 1, MBR a and b [H6] were paired on the basis of exposure age and cosmogenic nuclide ($^{53}$Mn) data[1]. Group 2, consisting of Y-74190, Y-75097, Y-75102, Y-75108 and Y-75271 [L6], were paired on the basis of noble gas and cosmogenic nuclide ($^{53}$Mn) data.[1,2] Group 3 includes the remaining samples considered in this study, consisting of Y-74115, Y-74371 and Y-74418 [H6]. The original find weights of these meteorites were all>20 g, so that it was possible to avoid material which may have suffered heating during atmospheric passage and wind-blown transport on the ice. With the exception of the MBR samples, Y-75097 and Y-75271, these meteorites were found over 1.5 km apart each other; the MBR samples were 700m apart; Y-75097 and Y-75271 were 800m apart. Cosmogenic isotope and exposure age data are listed in Table 1.

The samples were gently ground with a mortar and pestle and magnetic materials removed with a hand magnet. The TL of 8 mg samples was measured in a nitrogen atmosphere with a heating rate of 0.5 °C/sec. Corning 4-69 and 7-59 filters were used to suppress black-body radiation and a photomultipulier with bialkali photocathode (R762: Hamamatsu Photonics Co.) and photon-counting electronics were used. After measurement of the natural TL, samples were irradiated to a dose of 25 krad by Co-60 $\gamma$-rays and the induced TL measured.

Natural TL data is usually reported in terms of "equivalent dose", which is obtained by dividing the intensity of natural TL at a given glow curve temperature by the intensity of the TL in the induced glow curve (normalized to a unit laboratory dose) at the same temperature. For

ordinary chondrites, natural TL levels can also be determined using the ratio of the intensity of the low temperature and the high temperature peaks (LT/HT) in the natural TL glow curve only. This ratio can be calibrated to true equivalent dose, the calibration being laboratory specific due to differences in irradiation sources and geometries and measurement apparatus. It has been previously observed that the LT/HT ratio has much lower uncertainties than true equivalent dose in routine measurements and thus the LT/HT ratio is often used rather than equivalent dose for measurements on ordinary chondrites. In the present paper we present our natural TL data in terms of LT/HT ratio, pending completion of our laboratory calibration to equivalent dose.

**Results** The natural and induced TL glow curves of the samples are shown in Fig.1. These data are summarized in Table 2. We report the maximum induced TL intensity (sensitivity) for these samples relative to the meteorite Dhajala, using ALH-77304 [L3.7] as a standard, which TL sensitivity to Dhajala is $0.60 \pm 0.03$.

Previously natural and induced TL data have been used to identify potential pairing groups in Antarctic meteorite collections.[3] The criteria used to test potential pairing of meteorite fragments include petrological classification, and coincidence of induced TL peak temperature (within 10%), peak width (within 20%) and TL sensitivity (within a factor of 3 for weathered finds), and natural TL (within 25%). In our analysis of the three groups we find that, in general, our data support the pairings suggested by cosmogenic nuclide data. MBR a and MBR b have very similar natural TL levels, but their induced TL sensitivities are significantly different, although still well within the factor of three variation observed in weathered meteorites. Among the meteorites of Group 2, most exhibit very similar induced and natural TL data, with the exception of Y-75271. This meteorite exhibits relatively high TL sensitivity (although still within the factor of three) but has a very low natural TL level compared to the others. It is therefore likely that Y-75271 is not a member of this pairing group. Among the meteorites of Group 3, Y-74115 and Y-74418 have very similar induced and natural TL properties and thus are probably paired. The remaining meteorite of this group, Y-74371, however, has a much higher natural TL level than the others and should not considered a member of this pairing group.

The TL sensitivities of all these meteorites are significantly less than those of equilibrated ordinary chondrites among the modern falls (typically 4-10 relatively to Dhajala). Much of this difference between these meteorites and modern falls can be attributed to weathering.[4] Even taking weathering into consideration, however, the low TL sensitivities of the meteorites in the Y-74190 pairing group are very low, especially since the hand specimens of these meteorites generally exhibit the lowest degree of weathering observed in Antarctic meteorites (Table 1). It is likely that these meteorites have been subjected to high degrees of shock, such that a significant portion of crystalline feldspar in these meteorites was converted to non-luminescent glass. Maskelynite has been found in all members of Group 2. The large induced TL peak widths of these meteorites compared to meteorites in the other two groups may also reflect this shock processing, with some ordered feldspar in these meteorites being converted to disordered feldspar either during recrystallization of shock glass or by solid-state transitions.

There is no evidence in our present data that any of the meteorites considered here had unusual thermal histories, either in space or during metamorphism, aside from the shock processing experienced by the Y-74190 group. Meteorites with very low natural TL levels (LT/HT ratios $<0.5$) may have been heated prior to reaching Earth, probably while in orbits with small perihelia.[5] It appears that all the meteorites considered here were in orbits with perihelia $\geq 0.8$ AU prior to reaching Earth.

**Conclusions** We have measured the natural and induced thermoluminescence

of meteorites from three proposed pairing groups. We find that the TL results generally confirm the pairing of the meteorites in these groups, although a few meteorites previously thought to be paired appear not to be paired accordingly to the present data, and our data indicate shock processing for one of the pairing groups, namely the Y-74190 group.

Table 1. Samples

| Samples | Weight [kg] | Weathering | $^3He/^{21}Ne$ [2] | $^{22}Ne/^{21}Ne$ [2] | $^{53}Mn$ [1] [dpm/kgFe] | Exposure age $T_{21}$ [Ma] [2] | Terrestrial age [ka] [6] |
|---|---|---|---|---|---|---|---|
| MBR a [H6] | 4.108 | ≥b | 3.5[7] | 1.078[7] | 394 | 4.9[1] | >39[8] |
| MBR b [H6] | 13.782 | ≥b | 3.9[7] | 1.083[7] | 355 | 4.3[1] | |
| Y-74190 [L6] | 3.236 | a | 2.2 | 1.053[9] | 441±16 | 22[1] | 74 |
| Y-75097 [L6] | 2.570 | a | 4.6 | 1.087±5 | 424±18 | 17.8 | 40 |
| Y-75102 [L6] | 11.000 | a | 4.8 | 1.079±8 | 452±19 | 17.1 | 3.4, 3±1[8] |
| Y-75108 [L6] | 0.591 | b | 4.0 | 1.089±7 | 407±17 | 18.8 | |
| Y-75271 [L6] | 1.798 | a | 4.7 | 1.095±7 | 424±8 | 19.7 | 1.2, 2[10] |
| Y-74115 [H6] | 1.045 | b | 6.2 | 1.142±11 | 335±14 | 8.10 | 6 |
| Y-74371 [H6] | 5.067 | a | 7.0 | 1.188±35 | 309±12 | 8.02 | 6 |
| Y-74418 [H6] | 0.567 | c | 7.5 | 1.183±10 | 275±11 | 7.05 | |

Table 2. TL Characteristics

| | Induced TL | | | Natural TL |
|---|---|---|---|---|
| Samples | Sensitivity* | Peak Temp. [°C] | FWHM [°C] | LT/HT |
| MBR a [H6] | 0.45±0.04 | 153±1 | 118±2 | 1.11±0.01 |
| MBR b [H6] | 0.79±0.06 | 156 | 127 | 1.28±0.02 |
| Y-74190 [L6] | 0.14±0.01 | 156±2 | 146±1 | 1.78±0.02 |
| Y-75097 [L6] | 0.16±0.02 | 161±7 | 160±3 | 1.61±0.02 |
| Y-75102 [L6] | 0.22±0.02 | 159±3 | 146±1 | 1.37±0.06 |
| Y-75108 [L6] | 0.23±0.02 | 156 | 141 | 1.53±0.03 |
| Y-75271 [L6] | 0.34±0.03 | 160±3 | 143±1 | 0.76±0.07 |
| Y-74115 [H6] | 0.58±0.05 | 155±2 | 121±1 | 2.39±0.01 |
| Y-74371 [H6] | 1.22±0.10 | 158±2 | 124 | 4.12±0.10 |
| Y-74418 [H6] | 0.43±0.04 | 153 | 123±1 | 2.86±0.02 |

*: ALH-77304 [L3.7], which TL sensitivity is 0.60±0.03, is used as a standard.

References: 1) M.Honda (1981): Geochemical Journal, **15**, 163-181. 2) N.Takaoka *et al.* (1981): Mem. Natl. Inst. Polar Res., Spec. Issue, **12**, 207-222. 3) P.H.Benoit *et al.* (1994): J. Geophysical Research, **97**, 4629-4547. 4) P.H.Benoit *et al.* (1991): Meteoritics, **26**, 157-160. 5) P.H.Benoit *et al.* (1991b): Icarus, **94**, 311-325. 6) S.Miono and A.Nakanishi (1994): Proc. NIPR Symp. Antarct. Meteorites, **7**, 225-229. 7) N.Takaoka (1987): Science in Antarctica, 6 Antarctic Meteorites, 228-242 (Japanese). 8) A. J. T. Jull *et al.* (1984): Proc. 15th Lunar Planet. Sci. Conf., J. Geophys. Res., **89**, C329-C335. 9) K.Nagao and J.Matsuda (1986): Papers presented to the 11th symposium on antarctic meteorites, 131-132. 10) R.P.Beukens *et al.* (1988): Proc. NIPR Symp. Antarct. Meteorites, **1**, 224-230.

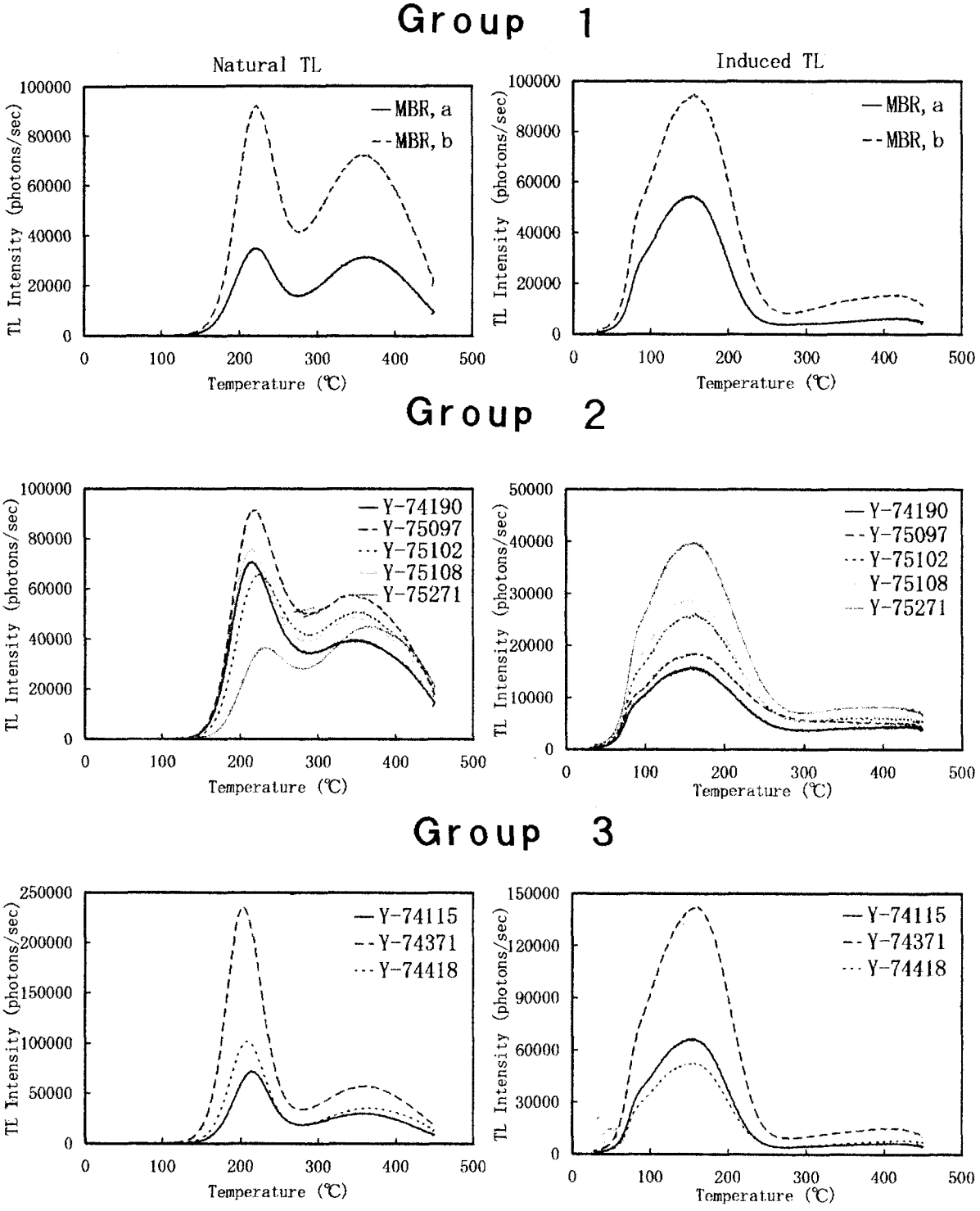


Fig.1 The natural and induced TL glow curves

# Matrix of Colony (CO3) chondrite

Takaaki Noguchi and Kei-ichi Ishikawa
Department of Earth Sciences, Ibaraki University, Bunkyo 2-1-1, Mito 310, Japan

**Introduction** Petrological studies of CO chondrites show that CO chondrites experienced metamorphism (*e. g.*, Jones and Rubie, 1990; Scott and Jones, 1990; Sears et al., 1991). Among CO chondrites, type 3.0-3.1 CO chondrites have some features which are rare in the higher types; mesostases in type I chondrites and very fine-grained matrix produce yellow and red CL, respectively (Sears et al., 1991). Sears et al. (1991) shows that Colony (CO 3.0), ALHA77307 (CO 3.1), and LEW85332 (CO 3.0) are also compositionally anomalous. We investigate the matrix of Colony meteorite which is one of the least metamorphosed CO chondrites, using SEM, EPMA, and TEM. We will show characteristics of the matrix and compare the matrix with the matrices of ALHA77307 (CO 3.1) and Lancé (CO 3.4) that were investigated using TEM by Brearley (1993) and Keller and Buseck (1991).

**Results** SEM observation shows that matrix of Colony is composed mainly of very fine-grained (probably sub-μm) groundmass. Some olivine crystals which are about 10 μm or less across are also observed among the groundmass. Back-scattered electron images (BEIs) of the matrix display that the fine-grained groundmass is composed of areas which have different brightness. The scale of each area is about 50 μm or less. Thin weathering veins with about 5 μm or less thick (bright veins in BEIs) are often observed.

The matrix compositions were studied by focused (beam diameter: 1μm) and broad beam (beam diameter: 20 μm) analyses. Both of analyses give comparable results. But total weight % of focused analyses (average 90 wt %) are higher than that of broad beam analyses (average 84 wt %). Intraelemental correlations of analyzed elements between focused and broad beam analyses show that focused analyses tend to be higher wt % than broad beam analyses. Similar tendency was reported from ALHA77307 (Brearley, 1993).

Focused beam analyses of the fine-grained groundmass and the weathering veins are plotted on a ternary (Si+Al)-Mg-Fe diagram (Fig. 1). The fine-grained groundmass is temporarily divided into three based on the brightness in BEI photographs. Because the each area changes gradually each other and because there is a possibility that other areas which have different brightness are within an X-ray emission area, individual analyses of each areas overlap each other. But there is a tendency that dark areas tend to have higher (Si+Al)/(Si+Al+Mg+Fe) ratios than other areas and that bright areas are plotted near the analyses of the weathering veins. Compositions of the weathering veins suggests that the they are composed of mixture of limonite and $SiO_2$ bearing materials ( 6.8 $SiO_2$ wt % on average).

Preliminary TEM observation of matrix was performed. Sub-μm olivine, pyroxene,

and chromite crystals are observed. Olivine is the most abundant among them. Among these crystals fills the interstitial material which is composed of poorly crystalline materials. High-resolution TEM micrographs of the interstitial material indicate that there are ultrafine crystalline phases which have 0.7, 0.9, and 1.4-1.5 nm diffuse lattice fringes. Their microstructure suggest that they may be ultrafine phyllosilicates. They may be serpentine, smectite, and chlorite.

**Discussion** Figure 1 suggests that fine-grained groundmass of matrix is interpreted as mixtures of three components. Component A is probably olivine. Component C is probably the same material which constitutes the weathering veins. Component B is the main constituent material of the darkest areas in the fine-grained groundmass of matrix. It may be composed mainly of smectite based on this diagram.

Figure 1 is similar to the results of analytical electron microscope analyses of constituent components of the matrix of ALHA77307 (Brearley, 1993). In ALHA77307, component C situates near the Fe apex. In Colony, Fe-Ni metal grains in matrix are replaced by mixture of limonite and $SiO_2$ bearing material, and only Fe-Ni metal grains within olivine crystals in chondrules are preserved. On the other hand, sub-μm Fe-Ni metal grains were observed in matrix in ALHA77307 (Brearley, 1993). Therefore, this difference between Colony and ALHA77307 probably results from the different degrees of terrestrial weathering, although both meteorites are badly weathered (Rubin et al., 1985). Sears et al. (1991) shows that average Fe/(Fe+Mg) ratios in Colony (CO 3.0; 0.8) and ALHA77307 (CO 3.1; 0.71) are higher than those in Lancé (CO 3.4; 0.63) and Warrenton (CO 3.6; 0.54). This fact can be also interpreted as the different degrees of terrestrial weathering. In badly weathered Colony and ALHA77307, $Fe^{3+}$ cations which were formed by weathering of Fe-Ni metal probably precipitated in fine-grained groundmass of their matrices. Therefore, the precipitation of $Fe^{3+}$ cations resulted in the highter Fe/(Fe+Mg) ratios of matrices in Colony and ALHA77307 than those in Lancé and Warrenton. Figure 1 also indicates that component A (probably olivine) is not greatly affected by terrestrial weathering even in the case of Colony.

Matrix of Lancé is mainly comprised of fine-grained (<0.1 to 10 μm) olivine ($Fa_{40-50}$) with variable amounts of phyllosilicate and other poorly crystalline materials (Keller and Buseck, 1990). Different from the case of ALHA77307 and Colony, fine-grained olivine and alteration material in matrix in Lancé are plotted between component A and component C in a ternary (Si+Al)-Mg-Fe diagram. Component B is characteristic of the matrices of ALHA77307 and Colony. However, it is not clear whether this component is primary or secondary.

**References** Brearley (1993) Geochim. Cosmochim. Acta, 57, 1521-1550. Keller and Buseck (1990) Geochim. Cosmochim. Acta, 54, 1155-1163. Rubin et al. (1985) Meteoritics, 20, 175-195. Sears et al. (1991) Proc. NIPR Symp. Antarct. Meteorites, 4, 319-343.

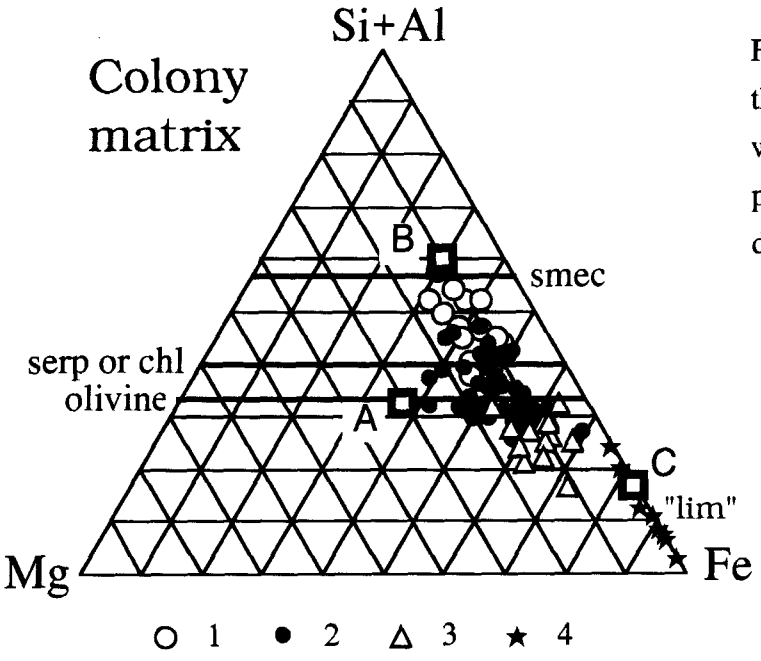


Figure 1 Focused beam anayses of the fine-grained groundmass and the weathering veins in matrix of Colony plotted on a ternary (Si+Al)-Mg-Fe diagram.

# A TEM study of microstructure in silicates in the CK chondrites

Takaaki Noguchi

Department of Earth Sciences, Ibaraki University, Bunkyo 2-1-1, Mito 310, Japan

**Introduction** Silicates in the CK chondrites show blackening. The blackening is due to tiny ( < a few μm across) magnetites inclusions dispersed in silicates (Rubin, 1992). In Ordinary chondrites, the heavily shocked chondrites typically show the blackening of silicates (e. g. Stöffler et al., 1991). However, only two CK chondrites, EET83311 and LEW87009, experienced relatively heavy shock among the CK chondrites. Shock stages of EET83311 and LEW87009 are S4 and S3, respectively (Scott et al., 1992). There are no remarkable differences of the extent of the blackening among the weakly shocked (S1-S2) and heavily shocked (S3-S4) CK chondrites, except for inside and neighbor of the shock veins. Therefore, there is a question whether nearly all CK chondrites experienced intense shock and then annealed to remove these shock effects (Scott et al. 1992; Rubin, 1992). If this is the case, the shock features that are currently recorded in the silicates were formed after shock events which caused blackening had been removed by annealing. Scott et al. (1992) pointed out that thermal metamorphism that is characteristic of petrologic type 6 is required in order to wipe out shock features in olivine such as planar fractures and deformation features and that pervasive shock blackening is relatively rare in ordinary chondrites. On the other hand, TEM study of matrix olivine in Y693, high dislocation density was reported (Nakamura et al., 1993). To investigate the relation between shock features and blackening, I am investigating the microstructure of olivine, pyroxene, and plagioclase. Karoonda, Maralinga, and EET87507 were investigated by TEM as well as SEM and EPMA. Y693, ALH85002, EET9007, and LEW87009 were investigated by SEM and EPMA.

**Results** *(1) Optically brown olivine* Under optical microscope, olivine in chondrules and isolated olivine grains in the CK chondrites have brown cores and colorless rims. Along with fine-grained magnetite dispersed throughout these meteorites, brown color of olivine crystals is one of the cause of blackening of CK chondrites. TEM observation of olivine in Karoonda, Maralinga, and EET87507 reveals that such cores contain abundant minute precipitates. Most of the precipitates are 10-30 nm across. Number densities of the olivine cores in Karoonda, Maralinga, and EET87507 are 1-2 x $10^{10}$, 1-2 x $10^{10}$, and 2 x $10^{10}$ $cm^{-2}$, respectively. Those of the olivine rims in Karoonda, Maralinga, and EET87507 are <1 x $10^{8}$, <1-6 x $10^{8}$, and <3 x $10^{8}$ $cm^{-2}$, respectively. In the rims, coarser magnetite (>100 nm across) were observed. It is very difficult to recognize lattice fringes of these precipitates even in high resolution photomicrographs. But moire fringes are often observed in the precipitates. When host olivine crystals are observed along the direction perpendicular to c* direction, moire fringes in the

precipitates are almost parallel to the lattice fringes of (100) of host olivine. Because these precipitates are too fine-grained to analyze their own composition even by the microbeam analysis (about 30-50 nm in a diameter) of AEM, the obtained data show the mixed compositions of host olivine and the precipitates. The data sometimes display Ti and/or Cr peaks and suggest that the precipitates contain higher amounts of Fe and often Ti and Cr than the host olivine.

*(2) Dislocation in olivine* Dislocation microstructure and dislocation densities in olivine are various among Karoonda, Maralinga, and EET87507. In olivine in Karoonda, short dislocations are often observed. The dislocations do not have elongated segments. Their density varies from 2 x $10^7$ to 1-4 x $10^8$ $cm^{-2}$ among grain by grain. Olivine in Maralinga has the lowest dislocation density among these three meteorites. The highest density of free dislocations was 2 x $10^7$ $cm^{-2}$. They also do not have elongated shapes. It is interesting that in this meteorites, dislocation networks are often observed. It means that olivine in Maralinga often contains subgrains. Olivine in EET87507 has the highest value, 1-2 x $10^9$ $cm^{-2}$. In EET87507, dislocations often have long straight segments parallel to their Burgers vector [001]. Other dislocations in EET87507 tangle complicatedly.

*(3) Microstructure in pyroxene* Some stacking faults parallel to (100) are observed in augite in Karoonda. Augite in Karoonda often shows mottled texture. Low-Ca pyroxene in Karoonda has a pigeonite structure (clinoenstatite). Lamellae having orthopyroxene structure are rare. Mottled texture is also observed in low-Ca pyroxene. Microstructure of augite in Maralinga is various among grain by grain. Some augite crystals have stacking faults parallel to (100). Their spacing is narrower than that in Karoonda. In augite which are dark brown under optical microscope, free dislocations and elongated magnetite inclusions are observed. Density of such dislocations is 2-7 x $10^8$ $cm^{-2}$. Most magnetite inclusions have elongated shapes, 40-70 x 50-300 nm. Precipitation density of magnetite inclusions in augite is 1 x $10^8$ $cm^{-2}$. Low-Ca pyroxene in Maralinga consists of unit cell-scale intergrowths of clinopyroxene with pigeonite structure and orthopyroxene slabs. Augite in EET87507 contains abundant faults parallel to (100). Low-Ca pyroxene in EET87507 consists of unit cell-scale intergrowths of orthopyroxene and clinopyroxene with pigeonite structure slabs. Abundant stacking faults are observed in it. Due to these planar defects, electron diffraction patterns of such pyroxene display streaking parallel to a*.

*(4) Mineralogy and microstructure of plagioclase and K-rich feldspar*

SEM observation of feldspars in the CK chondrites is mentioned mainly and TEM observation is only briefly mentioned here. Among the plagioclase in various occurrences, plagioclase in matrices has An-rich rims and An-poor cores (Noguchi, 1993; Keller, 1993). This reverse zoning is conspicuous in Maralinga. However, it is observed in the other CK

chondrites which are more recrystallized than Maralinga. In them, the aggregates of plagioclase (100-500 μm in diameters) have An-poor cores and An-rich rims. Plagioclase in LEW87009 which experienced stronger shock (shock stage, S3) than the other CK chondrites also has a wide compositional range, $An_{93.4-31.4}$. However, the texture of plagioclase in this meteorite is different from the other CK chondrites. The aggregates of plagioclase in LEW87009 heterogeneously contain An-rich regions. The boundaries between An-rich regions and An-poor host are sharp in BEI photographs. The composition of an aggregate of plagioclase in LEW87009 changes from $An_{40.5}$ to $An_{92.2}$ within the interval of < 10 μm. The reverse zoning of plagioclase was rarely observed in LEW87009.

K-rich feldspar is observed sporadically in all the CK chondrites investigated except for Y693 (thin section of this meteorite is too small to search K-rich feldspar). Its modal abundance is <0.1 %. Many K-rich feldspar contains $An_{10}$ mol %. It appears in the rims of matrix plagioclase aggregates, and plagioclase-rich clast in the case of Karoonda. Typical morphology of the such K-rich feldspar is acicular or lamella-like shapes. K-rich feldspar in chondrules in Maralinga and ALH85002 has anhedral shape and $<Ab_2$. On the other hand, K-rich feldspar in LEW87009 has different morphology from that in other CK chondrites. It occurs as fine-grained ( <5 μm across) anhedral inclusions in host plagioclase aggregates. The most Or-rich one is $An_{12.1}Ab_{15.1}Or_{72.8}$. K-rich feldspar in EET87507 was observed by TEM. The feldspar contains contain relatively high Ab component and very unstable under irradiation of electron beam.

Discussion Microstructure of olivine in Karoonda, Maralinga, and EET87507 clearly shows that CK chondrites experienced various degrees of shock. High dislocation density EET87507 (1-2 x $10^9$ $cm^{-2}$) and Y693 (0.8-5 x $10^9$ $cm^{-2}$; Nakamura et al., 1993) and microstructure of dislocation in olivine indicates that these two meteorites experienced moderately to heavy shock. Shock stage was not assigned to Y693 in Scott et al. (1992). Shock stage of EET87507 has greater uncertainty because of small thin sections (Scott et al., 1992). Under optical microscope, both meteorites contain dark pockets which are similar to shock-darkened pockets in ordinary chondrites. Probably these meteorites experienced heavier shock (S3?) than other CK chondrites. Microstructure of olivine in Maralinga suggests that olivine in Maralinga experienced recovery. Recovery experiments of olivine in Kyushu L6 chondrite (Ashworth and Mallinson, 1985) shows that nearly 1000 °C annealing is required in order to recover olivine with the formation subgrain boundaries within a short timescale. If Maralinga had experienced such high temperature, all sulfides and most feldspar would have melted. However, there is no clue that the meteorite experienced pervasive melting. Therefore, it is likely that it experienced slow cooling from temperature rather lower than 1000 °C. If true, slow cooling after a shock event accomplished by blanketing of thick hot deposits, or a high temperature

shock event (a shock event during thermal metamorphism). Olivine microstructure in Karoonda shows that this meteorite do not show heavy shock as stated by Scott et al. (1992). As estimated from microstructure of olivine and pyroxene, the three CK chondrites experienced different shock histories. However, there is no remarkable difference in the extent of blackening among them except for areas similar to shock-darkened pockets in EET87507. Therefore, it is supported that shock events themselves were not responsible for blackening of CK chondrites. Number density of the minute precipitates in olivine does not greatly changed among three chondrites investigated, although dislocation density changes greatly among them. This fact also supports that shock events themselves were not responsible for blackening of CK chondrites.

At present, mineral species of the precipitates have not been identified yet. Chemical compositions of the precipitates only show that they are enriched in Ti and/or Cr and Fe, although spinel-group minerals such as titanomagnetite and chromite are plausible. If they are spinel-group minerals, it is not clear whether only the self-oxidation under the oxidized conditions in the parent body could form the precipitates in the host silicates without the slight shock or not. The texture and composition of the rare K-rich feldspar suggest that small extent of melting occurred in their parent body. It may support the possibility of slight shock. The scarcity of the minute precipitates in the olivine rims were probably due to the segregation of them to the grain boundaries of the host silicates during annealing.

References Ashworth, J. R. and Mallinson, L. G. (1985) EPSL., **73**, 33-40. Bischoff, A., Rubin, A. E., Keil, K., and Stöffler, D. (1983) EPSL., **66**, 1-10. Brearley, A. J. and Scott, E. R. D. (1987) Meteoritics, **22**, 339-340. Geiger, T. and Bischoff, A. (1989) Meteoritics, **24**, 269-270. Geiger, T. and Bischoff, A. (1991) Meteoritics, **26**, 337. Keller, L. P. (1993) LPSC, **XXIV**, 783-784. Keller, L. P., Clark, J, C., Lewis, C. F., and Moore, C. B. (1992) Meteoritics, **27**, 87-91. Nakamura, T., Tomeoka, K., and Takeda, H. (1993) Proc. NIPR Symp. Antarct. Meteorites, **6**, 171-185. Noguchi, T. (1993) Proc. NIPR Symp. Antarct. Meteorites, **6**, 204-233. Rubin, A. E. (1992) GCA., **56**, 1705-1714. Scott, E. R. D. and Taylor, G. J. (1985) Proc. 15th LPSC, pt. 2, JGR., **90**, Suppl., C699-709. Scott, E. R. D., Keil, K., and Stöffler, D. (1992) GCA., **56**, 4281-4293. Stöffler, D., Keil, K., and Scott, E. R. D. (1991) GCA., **55**, 3845-3867. Takeda, H., Huston, T. J., and Lipschutz, M. E. (1984) EPSL., **71**, 329-339.

# Hydrothermal Experiments on Refractory Minerals Related to Ca-Al- rich Inclusions (CAIs) in Carbonaceous Chondrites: Implication for Aqueous Alteration in Parent Bodies

**Koji Nomura and Masamichi Miyamoto**

Mineralogical Institute, Graduate School of Science, University of Tokyo, Hongo, Tokyo 113, Japan

## Introduction

Ca-Al-rich inclusions (CAIs ) in carbonaceous chondrites are objects composed of refractory minerals such as gehlenite, spinel and diopside which have high condensation temperatures. CAIs were believed to be the most pristine materials and have in general not been affected by significant alteration. However, many of CAIs in carbonaceous chondrites do contain secondary minerals such as nepheline, calcite and phyllosilicates as reviewed by Lee and Greenwood [1]. The problem of how these secondary minerals were produced is controversial. There is no consensus on whether secondary minerals were produced by reaction with a solar nebular gas [2, 3] or by aqueous alteration in parent bodies [4]. Few experimantal studies have ever tried to solve this problem in spite of a large number of observations.

We performed hydrothermal experiments on several minerals common in CAIs under various conditions to study aqueous alteration in parent bodies. We also performed vapor deposition experiments on gehlenite to study reactions with solar nebular gas.

## Experiments

Hydrothermal experiments in this study were divided into two categories. The first category was the experiments with three refractory minerals, gehlenite ($Ca_2Al_2SiO_7$), diopside ($CaMgSi_2O_6$) and spinel ($MgAl_2O_4$) as starting materials. The second one was the experiments done on assumption of further alteration of gehlenite from the first experiments with amorphous Al-Si ( decomposed gehlenite with a 1N HCl solution ) as starting materials and the mixtures of $Al_2O_3$ and $SiO_2$ for comparison.

Gehlenite and diopside were synthesized from mixtures of $CaCO_3$, $Al_2O_3$ , $SiO_2$ and MgO reagents in our laboratory. Spinel that is commercially produced was used for this study. A mixture of $Al_2O_3$ and $SiO_2$ (mole ratio is 1:1) was prepared for comparison.

Each of the hydrothermal experiments was done with a teflon reaction cell loaded into a stainless steel vessel. A sample was placed at the bottom of a vessel and a solution was added. Each of vessels was heated at 200℃ for 2 or 7 days. We used both powder samples for characterization by X-ray diffraction (XRD) and pellets (about 1 cm in diameter) for observation by a scanning electron microscope. The volume of solution in each cell was 14 ml. The weight of each powder sample was 0.3 g.

In vapor deposition experiments, $Na_2O_2$ was evaporated in a silica tube at 1000 ℃ with a total pressure of about $10^{-3}$ atm. Na was transported to the surface of the gehlenite substrate and deposited on it.

**Results**

Tables 1 and 2 list the products and all run conditions of hydrothermal experiments. Gehlenite was decomposed to hydrogrossular and acicular Ca-Si material ( probably Ca-Si-hydrate but not identified in the XRD powder pattern ) in a 1N NaOH solution (Table 1). Hydrogrossular and Ca-Si material may be converted into grossular and wollastonite with elevated temperature. In a 1N $Na_2CO_3$ solution, gehlenite was decomposed to calcite and sodalite (Table 1). These secondary minerals were probably produced by reaction of

$$\text{Gehlenite} + Na_2CO_3 \text{ solution} \rightarrow \text{Calcite} + \text{(Hydro) Sodalite.}$$

Calcite was euhedral and surrounded by sodalite matrix. Calcite and feldspathoid rich in sodium coexist in CAIs in the Murchison CM chondrite [5]. The result of this run is consistent with the textures of the CAIs.

Gehlenite was decomposed to amorphous Al-Si probably by leaching of Ca in a 1N HCl solution (Table 1). This may be related to formation of phyllosilicates in CAIs.

Analcime was produced easily both in a 1N NaOH solution and a 1N $Na_2CO_3$ solution, but was not produced in a 0.01N NaOH solution (Table 2). In a 2N $Na_2CO_3$ solution, (hydro)sodalite was produced from the mixture of $Al_2O_3$-$SiO_2$ (Table 2).

Diopside and spinel were not affected in all run conditions (Table 1).

Table 3 summarizes the change in pH in solutions. Elevation of pH was probably due to leaching of Ca from the surfaces of gehelnite grains.

In vapor deposition experiments, Na-Ca-Al-Si and/or Na-Ca-Al phases were observed on the surface of the gehlenite substrate with a scanning electron microscope equipped with energy-dispersive X-ray spectrometer (EDS). These phases were probably produced by reaction of gehlenite with transported Na. However, we could find neither nepheline nor sodalite on the surface of the substrate.

**Discussion**

Comparison to CAIs

Secondary minerals in CAIs include nepheline, sodalite, calcite, grossular, monticellite, zeolite, fine-grained anorthite, wollastonite and Fe-bearing phyllosilicates [6]. Many previous workers interpreted them to have resulted from reaction of primary phases with the solar nebular gas. However, we propose from this work that secondary minerals in CAIs were produced by aqueous alteration in parent bodies only from gehlenite.

The redox condition of fluids in a parent body seems to have affected alteration of CAIs. Because C reacts with $O_2$ in a fluid under oxidizing condition, a fluid initially containing Na probably became a fluid with $Na_2CO_3$. We consider that the difference of the experimental conditions between a NaOH solution and $Na_2CO_3$ corresponds to those of redox condition in fluids in parent bodies. There was a difference in products between runs with a NaOH solution and $Na_2CO_3$ (Table 1). Thus, it seems reasonable to suppose that the difference in redox condition in a fluid affected mineral assemblages of products.

Durability against hydrothermal alteration of minerals in this study suggests a similar trend to susceptibility to alteration of primary minerals included in CAIs [6]. In a 1N HCl solution, only gehlenite was decomposed to amorphous Al-Si. However, spinel and diopside survived alteration. These results are consistent with

those of observations that gehlenite seems to be the most susceptible to alteration as reviewed by MacPherson et al. [6].

From the results of further alteration of amorphous Al-Si (decomposed gehlenite) and of the $Al_2O_3$-$SiO_2$ mixture (Table 2), we found that the Na concentration of a solution affects the products. Analcime was produced under lower Na concentration than that of sodalite.

Alteration model of Yamato791717

We attempt to extend these results into how gehlenite in CAIs was converted into nepheline and/or sodalite. Here we limit the discussion on CAIs in Yamato(Y) 791717 CO3 chondrite which is marked by containing the most nepheline- rich CAIs ever known. Most CAIs in Y791717 are single concentric objects. Each has a core of gehlenite and spinel, mantled by nepheline, fassaite and diopside. These textures suggest that nepheline formed by replacing mainly gehlenite [7].

In our experiments, gehlenite in a $Na_2CO_3$ solution was converted into calcite and sodalite. In CAIs in Y791717, however, neither nepheline nor sodalite coexist with calcite. The most likely explanation is that nepheline and/or sodalite in CAIs in Y791717 were produced by two stage aqueous alteration mainly from gehlenite in the parent body. In the first stage of aqueous alteration, gehlenite was decomposed to Al-Si material by leaching of Ca. At this stage, this leaching of Ca and that of Na from matrix glassy materials elevated the pH of the fluid (Table 3). At a later stage, Al-Si material reacted with Na in the fluid and converted into nepheline and/or sodalite under higher pH condition. Spinel and diopside did not react with Na in the fluid at this later stage. The texture in CAIs that spinel and diopside were hardly affected by alteration corresponds to the results of experiments that these minerals escaped alteration [7] under both alkaline and acidic conditions (Table 2).

**Conclusion**

(1) Gehlenite is the weakest mineral among the refractory minerals used in hydrothermal experiments against alteration both under alkaline and acidic conditions. Our results suggest secondary minerals in CAIs were produced by aqueous alteration of gehlenite in parent bodies.

(2) The results of our hydrothermal experiments suggest that many of the secondary minerals in CAIs in carbonaceous chondrites were produced from gehlenite by aqueous alteration in each parent body. The variety of secondary minerals reflects the conditions of a fluid ( pH, Na concentration and redox ) in parent bodies.

(3) Gehlenite was decomposed to Al-Si material by leaching of Ca. This leaching of Ca and that of Na from matrix glassy materials elevated the pH of a fluid. Subsequently, Al-Si material reacted with Na in the fluid and converted into nepheline and/or sodalite.

**Acknowledgments**

We thank H. Yoshida for assistance with microprobe analysis, H. Horiuchi for X-ray powder diffraction, K. Toyoda for experiments, K. Tomeoka of Kobe University for helpful suggestion and discussion, and M. E. Zolensky for suggestion.

**Reference**

[1] Lee M. R. and Greenwood R. C. (1994) Meteoritics 29, 780-790

[2] Grossman L. and Steele I. M. (1976) Geochim. Cosmochim. Acta. 40, 149-155

[3] Ikeda Y. (1982) Proc. 7th Symp. Antarct. Meteorite 34-65

[4] Greenwood R. C., Lee M. R., Hutchison R. and Barber D. J. (1994) Geochim. Cosmochim. Acta. 58, 1913-1935

[5] MacPherson G. J., Bar-Matthews M., Tanaka T., Olsen E. and Grossman L. (1983) Geochim. Cosmochim. Acta. 47, 823-839

[6] MacPherson G.J., Wark D.A., and Armstrong J.T. (1988) In *Meteorites and the Early Solar System* (eds. J. F. Kerridge and M. S. Matthews) 746-807

[7] Tomeoka K, Nomura K and Takeda H. (1992) Meteoritics 27, 136-143

**Table 1. Results of Hydrothermal Experiments of Refractory Minerals**

| Starting Material | Solution | Time (hours) | Temperature (℃) | Product |
|---|---|---|---|---|
| Gehlenite | NaOH 1N | 168 | 200 | Hydrogrossular, Ca-Si-(hydrate) $[Ca_3Al_2(SiO_4,OH)_3]$ |
| Gehlenite | $Na_2CO_3$ 1N | 168 | 200 | Calcite, Sodalite |
| Gehlenite | HCl 1N | 48 | 200 | Amorphous Al-Si |
| Diopside | NaOH 1N | 168 | 200 | No product |
| Diopside | $Na_2CO_3$ 1N | 168 | 200 | No product |
| Diopside | HCl 1N | 48 | 200 | No product |
| Spinel | NaOH 1N | 168 | 200 | No product |
| Spinel | $Na_2CO_3$ 1N | 168 | 200 | No product |
| Spinel | HCl 1N | 48 | 200 | No product |

**Table 2. Results of Hydrothermal Experiments of Amorphous-Al-Si and Mixture of $Al_2O_3$ and $SiO_2$**

| Starting Material | Solution | Time (hours) | Temperature (℃) | Product |
|---|---|---|---|---|
| Amorphous | NaOH 2N | 168 | 200 | Analcime+Sodalite |
| Amorphous | NaOH 1N | 168 | 200 | Analcime |
| Amorphous | NaOH 0.01N | 168 | 200 | No product |
| Amorphous | $Na_2CO_3$ 2N | 168 | 200 | Analcime |
| Amorphous | $Na_2CO_3$ 1N | 168 | 200 | Analcime |
| Mixture | NaOH 2N | 168 | 200 | Analcime |
| Mixture | NaOH 1N | 168 | 200 | Analcime |
| Mixture | NaOH 0.01N | 168 | 200 | No product |
| Mixture | $Na_2CO_3$ 2N | 168 | 200 | Sodalite $[Na_8Al_6Si_6O_{24}(OH)_2 \cdot 2H_2O]$ |
| Mixture | $Na_2CO_3$ 1N | 168 | 200 | Analcime $[NaAlSi_2O_6 \cdot H_2O]$ |

**Table 3. Change in pH in Solutions**

| Starting Material | Solution | Time(hours) | Temperature (℃) | Initial pH | Final pH |
|---|---|---|---|---|---|
| Gehlenite | HCl 0.1N | 168 | 200 | 0.97 | 3.95 |
| Gehlenite | HCl 0.01N | 168 | 200 | 2.15 | 11.00 |

# Pb Isotopic Systematics of Angrite Asuka-881371

Wayne R. Premo and M. Tatsumoto
U.S. Geological Survey, MS 963, Box 25046,
Federal Center, Denver, CO 80225

## Abstract

Preliminary Pb isotopic results on three separates from the unusual angrite, Asuka-881371 (formerly A-9) indicate that it is very old at 4.56 Ga, similar to previous age results for other angrites. As part of the present consortium study of Asuka-881371, U-Th-Pb concentrations and isotopic compositions were and are continuing to be measured in an attempt to determine its age and petrogenetic history. Our allocation was initially separated into fragments containing evidence of a dull black fusion crust (FC) and one fragment that did not (N-FC). These two groups were processed separately and further separated into several fractions, including olivine, pyroxene, and plagioclase. Large phenocrysts of olivine from both N-FC and FC were hand-picked into two fractions depending on the degree of clarity. The separates were then washed and leached, the U-Th-Pb extracted, and their isotopic ratios measured. At present, preliminary Pb isotopic results have been obtained on only two of the residues and three of the leachs from the two olivine phenocryst fractions and a separate of fusion crust fragments. These data do yield a quasi-linear array even though the Pb data from one of the olivine residues was not high quality. A preliminary Pb-Pb age for Asuka 881371 based on the "best" of these first results is 4567 ±1.8 Ma; an age using all five analyses is 4566 ±24 Ma, indicating that this proposed angrite is essentially the same age as the others. More fractions are presently being analyzed to refine this age and will be presented at a later time.

## Introduction

This "new angrite-type" achondrite, Asuka-881371, has been described by Yanai (1994) and is presently the subject of a consortium study headed by Paul Warren, of which our work on the U-Th-Pb concentrations and isotopic compositions is of course only a small part. Although unique, this meteorite was classified as an angrite largely because of its mineral assemblage, texture, and compositional similarities to the three previously classified angrites, Angra dos Reis (ADOR), LEW86010, and LEW87051. All of these are ophitic-textured, mafic plutonic rocks with varying amounts of fassaitic pyroxene, plagioclase (anorthite), and olivine (which some proportion is kirschsteinite; Ca-rich). Radiometric isotopic work (including U-Th-Pb) has been performed on two of the angrites, ADOR and LEW86010 (Tatsumoto et al., 1973; Wasserburg et al., 1977; Lugmair and Marti, 1977; Chen and Wasserburg, 1981; Jacobsen and Wasserburg, 1984; Lugmair and Galer, 1992; Nyquist et al., 1994). Their results showed that these angrites are very old (~4.55 Ga), characterized by near-primordial compositions for initial Pb with a common initial $^{87}Sr/^{86}Sr$ value of ~0.69897 from a reservoir with chondritic Sm/Nd, and certainly may be related despite the differences in bulk chemistries (Yanai, 1994; Lugmair and Galer, 1992) and mineralogical abundances (Nyquist et al., 1994). Because Pb among other isotopic characterisites of angrites are relatively distinct, analyzing Asuka 881371 by this method offers an excellent test as to its age and meteoritic affinity.

## Sampling and Methods

Our consortium allocation of 327 mg was initially separated into fragments containing evidence of a dull black fusion crust (FC) and one fragment that did not (N-FC). These two groups were processed separately. The N-FC fragment that was marred with a sawed face was first lightly leached to remove any contaminants from the sawed edge, then crushed, sieved, and separated into several fractions. Medium-size grains (~100 to 250 micron-size) of interstitial and groundmass olivine, pyroxene, and plagioclase were handpicked into monomineralic separates. Fine-grain (<100 micron-size) and medium-grain polymineralic magnetic separates serve as pseudo-whole-rock separates. Unfused porphyritic-textured portions of FC (FC-R) were removed from the blackened, fused portions (FCP) using an electric micro-drill. FC-R was processed similarly to N-FC. Large phenocrysts of olivine (up to 1.5 mm in length) from both N-FC and FC were hand-picked into two fractions depending on the degree of preservation (clarity ?). All of the fractions were then washed with ultrapure water and leached in three steps using first 0.01N HBr, then 0.1N HBr, and finally 1N $HNO_3$. U, Th, and Pb were extracted using conventional methods and their isotopic ratios measured on thermal ionization mass spectrometers. The Pb isotopic data was reduced using the methods of Ludwig (1985) and the age regressions using the methods of Ludwig (1986).

## Pb Isotopic Results

Preliminary Pb isotopic results were obtained on three separates including both olivine phenocryst fractions (Ol-Ph-1 and Ol-Ph-2) and a separate comprising fusion crust pieces (FCP), and are shown in Figure 1 below. Ol-Ph-1 is composed of the "best" olivine phenocrysts handpicked from the others because of their clarity and lustrous nature. Unfortunately, this separate yielded very low Pb contents (~7.5 ppb), resulting in a very low ion beam intensity and consequently rather imprecise measurements. Ol-Ph-2 is composed of translucent to opaque grains with varying amounts of interstitial and intragranular inclusions of unknown mineralogy. The FCP was composed of blackened and fused mineral assemblages of all known compositions, and therefore approximates a whole-rock separate.

The Asuka 881371 data yield a quasi-linear array despite the imprecise results from fraction Ol-Ph-1. The linear array is composed of residue data from FCP and Ol-Ph-2 and leach data from all three separates, and yields an isochron age of 4566 ±24 Ma. The Ol-Ph-2 leach deviates significantly from the isochron and if excluded, results in an isochron age of 4567 ±1.8 Ma, using only data from the "best" analyses. In either case, these preliminary Pb results indicate that this proposed angrite is essentially the same age as other angrites that have

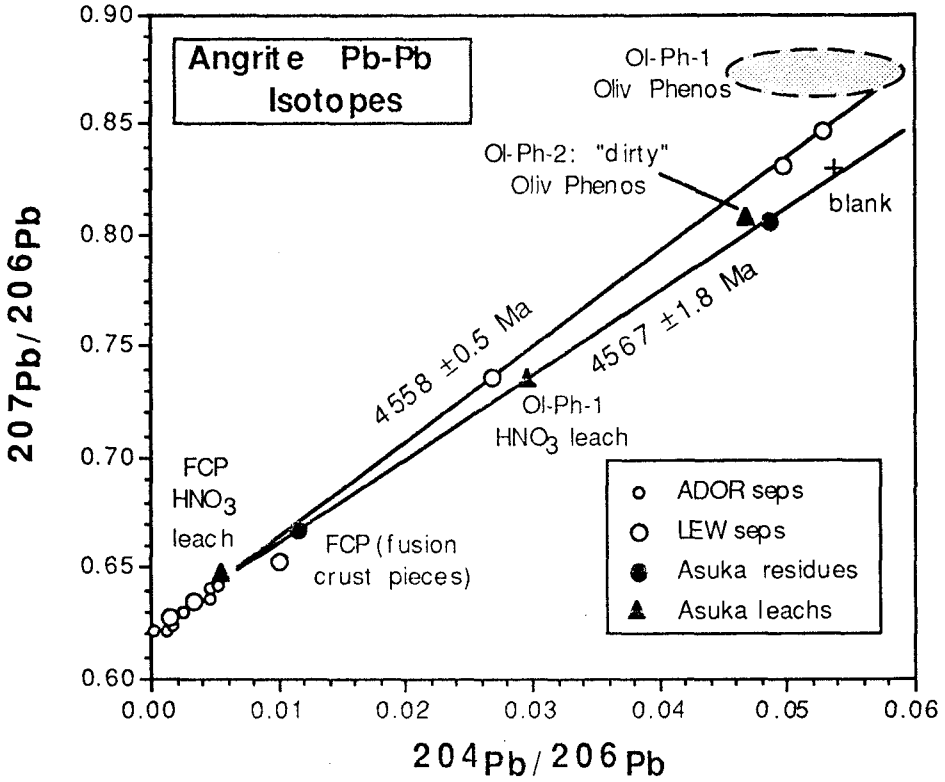


**Figure 1:** Pb-Pb correlation diagram of all available angrite isotopic data (Tatsumoto et al., 1973; Wasserburg et al., 1977; Chen and Wasserburg, 1981; Lugmair and Galer, 1992; this study).

been recently dated at 4558 Ma using the Pb-Pb method (Lugmair and Galer, 1992) and 4553 ±34 and 4530 ±40 Ma using the conventional Sm-Nd method (Lugmair and Galer, 1992; Nyquist et al, 1994. The Pb-Pb isochron for Asuka-881371 is very similar to that for ADOR, indicating near primordial initial Pb compositions. More fractions are presently being analyzed to refine this age and will be presented at a later time.

## References


Chen J.H. and Wasserburg G.J. (1981) The isotopic composition of uranium and lead in Allende inclusions and meteoritic phosphates. EPSL 52, 1-15.

Jacobsen S.B. and Wasserburg G.J. (1984) Sm-Nd isotopic evolution of chondrites and achondrites, II. EPSL 67, 137-150.

Ludwig K.L. (1985) PBDAT: A Computer Program for Processing Pb-U-Th Isotope Data. USGS Open-File Report 88-542, 34 pp.

Ludwig K.L. (1991) ISOPLOT: A Plotting and Regression Program for Radiogenic-Isotope Data. USGS Open-File Report 91-445, 39 pp.

Lugmair G.W. and Galer S.J.G. (1992) Age and isotopic relationships among the angrites Lewis Cliff 86010 and Angra dos Reis. GCA 56, 1673-1694.

Lugmair G.W. and Marti K. (1977) Sm-Nd-Pu timepieces in the Angra dos Reis meteorite. EPSL 35, 273-284.

Nyquist L.E., Bansal B., Wiesman H., and Shih C.-Y. (1994) Neodymium, strontium, and chromium isotopic studies of the LEW86010 and Angra dos Reis meteorites and the chronology of the angrite parent body. Meteoritics 29, 872-885.

Tatsumoto M., Knight R.J., and Allegre C.J. (1973) Time differences in the formation of meteorites as determined from the ratio of Lead-207 to Lead-206. Science 180, 1279-1283.

Wasserburg G.J., Tera F., Papanastassiou D.A., and Huneke J.C. (1977) Isotopic and chemical investigations on Angra dos Reis. EPSL 35, 294-316.

Yanai K. (1994) Angrite Asuka-881371: Preliminary Examination of a Unique Meteorite in the Japanese Collection of Antarctic Meteorites. Proc NIPR Symp. Antarct. Meteorites, 7, 30-41.

**ASUKA 881371 AND THE ANGRITES: ORIGIN IN A HETEROGENEOUS, CAI-ENRICHED, DIFFERENTIATED, VOLATILE-DEPLETED BODY.** Martin Prinz and Michael K. Weisberg. Department of Earth and Planetary Sciences, American Museum of Natural History, New York, NY 10024, USA

Asuka 881371, an 11.27g meteorite from Antarctica, was found in 1988 and is the fourth known angrite. It was described in a preliminary study by Yanai [1], and this report presents a more detailed petrologic study of the meteorite. The other angrites are Angra dos Reis (ADOR), LEW 86010 and LEW 87051. In addition, angrite-like clasts have been found in the N. Haig and Nilpena polymict ureilites [2-4]. The angrites have highly unusual petrologic, geochemical and isotopic characteristics which present a challenge in terms of interpreting their origin and history. The petrologic data from this new angrite, in conjunction with previous data, allows us an opportunity to reassess the origin and significance of this meteorite group.

TEXTURE AND MODE. Asuka 881371 is a fine-grained igneous rock, with low-Ca high-Cr olivine xenocrysts, texturally similar to LEW 87051, but slightly coarser-grained; it is intermediate between LEW 86010 and LEW 87051. The melt rock portion has an ophitic texture consisting of laths of anorthite (up to 800μm) intergrown with highly zoned euhedral to subhedral high-Ca low-Cr olivine and fassaite, of similar size, all of which crystallized rapidly. The three major phases crystallized near-simultaneously, perhaps with fassaite slightly later, thus indicating a multiply saturated melt. The euhedral high-Ca olivine is sharply zoned to higher-Ca fayalitic rims (generally ~20μm thick), and is bounded by zones of high-Ca and low-Ca kirschteinite ($CaFeSiO_4$)(Ki), which constitutes the groundmass between the olivine and fassaite crystals. The two Ki phases are intimately intermixed along some portions of the olivine rims, and are clearly separated along other portions of the same olivine crystals, with the high-Ca Ki being the innner zone. The Ki phases are larger and more clearly separated than in LEW 87051 (because it is coarser-grained) and they are in exsolution relationship (Fig. 1).

The olivine xenocrysts are large (up to 1.5mm), more magnesian than the euhedral olivines, and the texture is analogous to LEW 87051. The xenocrysts contain trails of micron-sized FeCr-rich chromites that differ from the FeAl-rich spinels in the melt rock portion; they have sharp contacts with the melt rock, which crystallized fine grained high-Ca olivine on their margins. The melt rock spinels (up to 40μm) are zoned, not found in other angrites, and are mainly included in the euhedral olivine. Irregularly-shaped grains of two silicophosphate phases (up to 40μm), not found in other angrites, are present in the outer margins of fassaite grains. Late-crystallizing Ti-magnetite crystals (up to 40μm) are also zoned, not found in other angrites, and on the outer portions of the two-Ki zones surrounding euhedral olivines. Minor troilite is present, but no FeNi metal was observed (minor amounts are found in the other angrites).

The modal abundances in the melt rock portion (exclusive of xenocrysts) are difficult to determine because the samples we studied are very small and may not be representative. Nevertheless, a first approximation is (vol %): 31 olivine and Ki, 35 fassaite, 33 anorthite, 1 Ti-magnetite and trace amounts of spinel, phosphate and magnetite.

MINERAL CHEMISTRY. Mineral data (in wt %) representative of the major phases in Asuka 881371 are presented in Table 1 and Figs. 1,2. Olivine xenocrysts range from $La_{0.5}Fo_{81-89}$ (La is the larnite component in olivine, $Ca_2SiO_4$), with 0.3 CaO and 0.3 $Cr_2O_3$, whereas euhedral olivines range from $La_{1-11}Fo_{14-67}$, with 0.8-6 CaO and <0.05 $Cr_2O_3$. Ca-rich olivine is bounded by high-Ca Ki ($La_{30-35}Fo_{1-7}$, with 17-20% CaO) and low-Ca Ki ($La_{12-18}Fo_{2-14}$, with 7-10 CaO). The Ki is in exsolution relationship, indicating a temperature of ~1000°C (Fig. 1). Fassaite is highly zoned, with 1-4.5 $TiO_2$, 5.5-9 $Al_2O_3$, 0-0.7 $Cr_2O_3$, 12-27 FeO, 0.2-9.3 MgO and 21-23 CaO. Anorthite is $An_{100}$. Spinels are often zoned, with 48-52% $Al_2O_3$, 11-15% $Cr_2O_3$ and FeO (23) and MgO (12) constant, while some smaller crystals have higher FeO (29) and lower MgO (9). Zoned Ti-

magnetite has 22-28 $TiO_2$ and 1.5-6 $Al_2O_3$. One silicophosphate phase has: 13 $SiO_2$, 1.7 $TiO_2$, 5 FeO, 48 CaO, 2 F, 0.3 Cl, 0.3 S and 29 $P_2O_5$, whereas the other has: 2 $SiO_2$, 6.5 FeO, 46.5 CaO, 0.6 $Na_2O$, 3.3 F and 40.5 $P_2O_5$.

BULK COMPOSITION. The melt rock portion of Asuka 881371 was analyzed by broad beam electron microprobe analysis, and the results are given in Table 2. The analysis excludes xenocrysts, as was done for LEW 87051[5], and thus the melt portions of these two rocks can be directly compared with LEW 86010 (all melt). The results (wt %) show that the three melts are highly fractionated and characterized by (1) very high CaO (15-18), $Al_2O_3$ (14-20) and $TiO_2$ (0.8-1.2), (2) high FeO (14-21) and low MgO (5-8), and (3) near-absent alkalies. The comparison of these melts reduces some of the variability between angrites, although ADOR (which may be a melt) differs.

DISCUSSION AND CONCLUSIONS. The origin of the angrites has been controversial because of their highly unusual petrologic, geochemical and isotopic characteristics. There is uncertainty as to whether they are direct melts of fractionated, or unfractionated, nebular components, or are fractionated planetary melts, or both. The following are some conclusions and speculations derived from Asuka 881371, as well as from earlier studies of other angrites: **(1)** It has been suggested that angrites and HED meteorites may be related because their oxygen isotopic compositions overlap, as do some other isotopic characteristics [6,7]. However, howardites contain no angrite clasts and the oxygen isotopes of brachinites also overlap these groups. Thus, we find little support for the concept that HED meteorites and angrites have an intimate relationship. **(2)** Recent studies [8,9] indicate that ADOR need not be a cumulate rock, as previously suggested [10], and may be a fassaitic melt. This melt is not directly related to the other angrite melts, indicating significant inhomogeneity in the major and trace element-bearing constituents [11]. This may be due to heterogenous nebular components, and perhaps planetary fractionation as well. **(3)** Olivine xenocrysts in LEW 87051 indicate two-stage cooling and closed-system fractional crystallization from an earlier event [12]; the data indicate a cooling rate of >1000°C/year at a depth of ~2m of solid rock. LEW 86010 cooled more slowly and formed at a depth of ~15-170m [13]. Asuka 881371 should be intermediate in cooling rate and depth, and ADOR probably also cooled rapidly [9]. Thus all angrites appear to be near-surface melts. **(4)** Jones et al. [14] noted that siderophile element depletions in angrites mimic those of eucrites and the Moon, but that it is unlikely that they are solely due to the core-forming process. Thus, there are no constraints on the size of the angrite body, and the presence of near-surface melts and extreme volatile depletion may be indicative of a very small body. **(5)** Experimental partial melting of the Allende and Murchison chondrites to produce angritic melts showed that while IW+2 oxidizing conditions resulted in melts that were somewhat similar to angrites, there were important differences [15]. Only minor pyroxene was produced, none of which was fassaitic. These oxidizing conditions also produced magnetite and not metal, as needed for core formation. Experimental analogs of LEW 86010 did, however, produce the appropriate multiply saturated melt at ~1170°C [16]. The lack of formation of angrites from Allende resulted in speculation that angritic melts may be from "nonchondritic" material (unspecified) or were impact-produced, although there is no evidence to support this concept and CAI-enriched target material would be required. We suggest that the multiply saturated nature of angritic melts argues against an impact origin, and the evidence favors melting of chondritic material-enriched in the CAI component, as suggested earlier [5, 17]. This will clearly enrich subsequent melts in the refractory (Ca, Al, Ti) elements so prominent in these melts. This type of material is not "nonchondritic", but is chondritic material enriched in one component in an amount beyond our present sampling of chondrites. CV chondrites are already enriched in CAI's beyond other chondrites, and we propose a further enrichment. **(6)** It has been argued [6] that if the parental material of angrites were CAI-enriched the isotopic signatures of elements such as $^{48}Ca$ or $^{50}Ti$ would have survived. We argue that since the angrites may be evolved melts with complex fractionation histories (e.g., ADOR

vs. the other angrites), there is no necessity to expect isotopic signatures after intense processing. (7) The extreme volatile depletion of the angrites is a remarkable feature for a body which formed from chondritic precursors, and could not be the result of any common fractionation process. We suggest that this may be a clear indication of the small size of the angrite body, perhaps on the order of a few hundreds of meters. It may be analogous to volatile loss in chondrules during the chondrule-forming process, except that angrites did not form by flash heating. The angrite body may have been devolatilized as a result of rapid and complete planetary melting as a result of its enriched CAI component, combined with its small size. The diversity of rock types may be due to its heterogeneous chondritic character, rapid heating, fractionation and devolatilization.

References. [1] Yanai, K. (1994) Proc. NIPR Symp., Ant. Meteorites No. 7, 30-41. [2] Prinz, M. et al. (1986) LPSC XVII, 681-682. [3] Davis, A.M. et al., (1988) LPSC XIX, 251-252. [4] Jaques, A.L. and Fitzgerald, M.J. (1982) GCA 46,893-900. [5] Prinz, M. et al. (1990) LPSC XXI, 979-980.[6] Lugmair, G.W. and Galer, S.J.G. (1992) GCA 56, 1673-1694. [7] Nyquist, L.E. et al. (1994) Meteoritics 29, 872-885 [8] Treiman, A.H. (1989) Proc. 19th LPSC, 443-450. [9] Lofgren, G. and Lanier, A.B. (1991) EPSL 111,455-466.[10] Prinz, M. et al. (1977) EPSL 35,317-330. [11] Mittlefehldt, DW. and Lindstrom, M.M. (1990) GCA 54, 3209-3218. [12] Mikouchi, T. et al. (1995) LPSC XXVI, 973-974. [13] McKay, G. et al. (1993) LPSC XXIV, 967-968. [14] Jones, J. H. et al. (1988) Meteoritics 23, 276-277. [15] Jurewicz, A.J.G. et al. (193) GCA 57, 2123-2139. [16] McKay, G. et al. (1988) LPSC XIX, 760-761. [17] Prinz, M. et al. (1988) LPSC XIX, 949-950. [17] Davidson, P.M. and Mukhopadhyay, D.K. (1984) Cont. Min. Pet. 86, 256-263.

Table 1. Textures, modes and mineral data of Asuka 881371 and other angrites.

| | ADOR | LEW 86010 | LEW 87051 | Asuka 881371 | N.Haig Clast |
|---|---|---|---|---|---|
| Texture | Rextal | Coarse | Fine | Intermed | Rextal |
| Xenocrysts | None | None | 25% | 5% | None |
| Modes | | | | | |
| Ol + Ki | 5 | 24 | 13 | 31 | 10 |
| Fassaite | 95 | 43 | 45 | 35 | 70 |
| Anorthite | tr | 32 | 42 | 33 | 20 |
| Spinel | tr | 0.1 | tr | tr | - |
| Phosphate | tr | 0.3 | tr | tr | - |
| Ti-magnetite | tr | tr | tr | tr | - |
| FeNi metal | tr | tr | tr | - | - |
| Troilite | tr | 0.7 | tr | tr | - |
| Min. Comp. | | | | | |
| Olivine (xeno) | | | | | |
| % Fo cores | - | - | 73 - 90 | 81 - 89 | - |
| Olivine (melt) | | | | | |
| % Fo | 53 | 33 | 55 - 10 | 67 - 14 | 48-61 |
| % CaO | 1.3 | 1.5 -2 | 0.5 - 2 | 0.3 - ~6 | 1.2 - 1.8 |
| Fassaite | | | | | |
| FeO | 6.7 | 7 - 11 | 11 - 26 | 10 - 27 | 8 - 11 |
| $TiO_2$ | 2.2 | 1 - 3 | 1 - 5.5 | 1 - 4.5 | 1.3 - 2.5 |
| $Al_2O_3$ | 10.0 | 6 - 12 | 4 - 8 | 3.5 - 9.8 | 5.5 - 7.7 |
| % An | 86 | 100 | 100 | 100 | 98 |
| Ti in mt. | 22 | 22 | 30 | 22-28 | - |
| % Ni, metal | 2 - 4 | 4.5 - 6.5 | 6 | - | - |

tr, present in trace amounts. -, not found.

Table 2. Bulk Compositions of Angrites (recalculated to 100 wt. %).

| | +LEW 86010 | +LEW 87051 | *LEW 87051 Melt Rock | #Asuka 881371 | *Asuka 881371 Melt Rock |
|---|---|---|---|---|---|
| $SiO_2$ | 40.2 | 40.4 | 42.1 | 37.3 | 39.2 |
| $TiO_2$ | 1.2 | 0.7 | 0.8 | 0.9 | 1.0 |
| $Al_2O_3$ | 14.3 | 9.2 | 20.4 | 10.1 | 15.5 |
| $Cr_2O_3$ | 0.21 | 0.11 | 0.14 | 0.17 | 0.21 |
| FeO | 18.8 | 19.0 | 14.2 | 23.8 | 21.1 |
| MnO | 0.20 | 0.24 | 0.31 | 0.20 | 0.23 |
| MgO | 7.1 | 19.4 | 4.6 | 14.8 | 7.9 |
| CaO | 17.8 | 10.8 | 17.6 | 12.5 | 14.9 |
| $Na_2O$ | - | - | - | 0.03 | - |
| $K_2O$ | - | - | - | 0.02 | - |
| $P_2O_5$ | 0.13 | 0.08 | 0.31 | 0.17 | - |
| Total | 99.94 | 99.93 | 99.98 | 99.99 | 99.92 |

---

+ Fused bead electron microprobe analysis, Mittlefehldt and Lindstrom (1990).
* Broad beam analysis of melt rock portion [5].
# Recalculated from analysis by H. Haramura in [1].

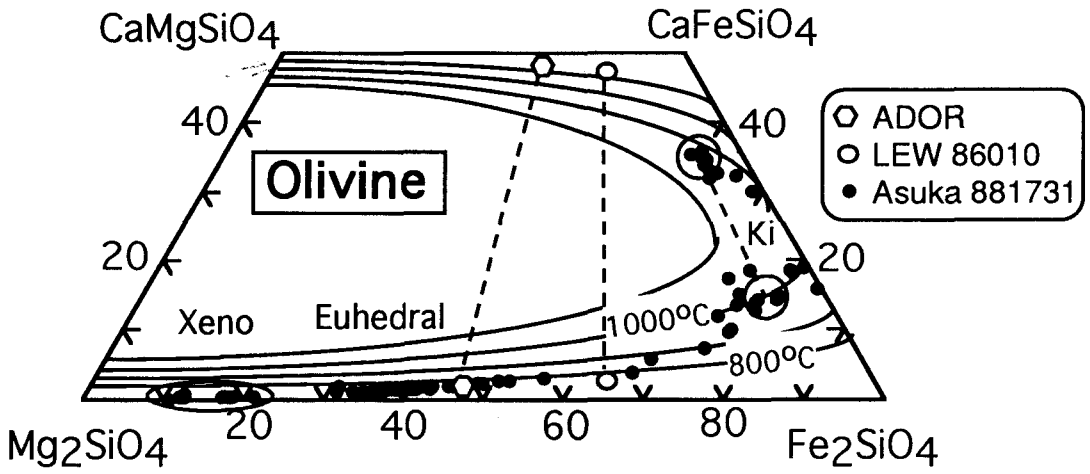


Fig. 1. Olivine compositions for Asuka 881371 and other angrites. Phase relations from [17].

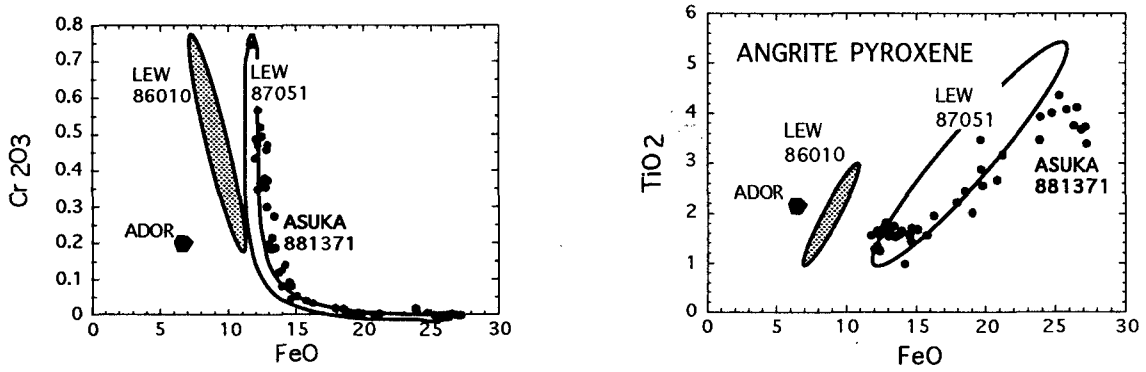


Fig. 2. Variation diagrams for fassaites in Asuka 881371 and other angrites.

# GEOCHEMICAL AND PETROGENETIC EVALUATION OF THE GLASSY MICROSPHERULES FROM UPPER PANNONIAN LAYERS OF BOREHOLE NAGYLÓZS 1, NW HUNGARY

Rózsa, P. - M. Braun - Gy. Szöőr
Department of Mineralogy and Geology, Kossuth University
H-4010 Debrecen, P.O.Box 4, Hungary

**Abstract:** Glassy spherules and spheroids of 300-1600 μm from Upper Pannonian sediments transversed by borehole Nagylózs 1 were investigated. Statistical and petrochemical comparative analyses were performed to answer the question of their possible genesis. On the basis of the performed investigation none of the possible ways of origin can be rejected, however, their extraterrestrial origin seems to be more possible because some lunar glasses and achondritic meteorites show similar petrochemical character to that of the Nagylózs microspherules.

By continuous cores of the borehole Nagylózs 1 Miocene, Pliocene and Quaternary sediments were uncovered in the Little Hungarian Plain (Boldizsár et al., 1993). In the Upper Pannonian sediments (marly siltstone) glassy spherules and spheroids were found which are amber to light brown objects of 300-1600 μm. The most important morphological groups are the following :

- acicular, vesicular decorated sphere
- acicular, vesicular decorated tear-drop
- crystals decorated sphere
- filamental fragment
- acicular, vesicular decorated double-drop.

Their terrestrial (magmatic, metamorphic) or extraterrestrial (microtektite, impactite) origin was raised in a preliminary report (Szöőr et al., 1994). On the basis of the major elements composition, using statistical and petrochemical methods our purpose was to determine their likeliest origin by comparing them with terrestrial and extraterrestrial objects (uncompahgrite, pyroxenite, microtektites, tektites, impactites, lunar basalt, lunar glasses, achondrites).

The major element composition of the samples from Nagylózs 1 borehole was determined by microprobe analyses with SEM-EDAX. In spite of their morphological variability their major element compositions are very similar to each other and differ from those of the comparative terrestrial and extraterrestrial objects (Table 1).

Table 1. Major element components of the comparative samples

| Code | Name | $SiO_2$ | $Al_2O_3$ | FeO | MgO | CaO | $Na_2O$ | $K_2O$ | $TiO_2$ | Reference |
|---|---|---|---|---|---|---|---|---|---|---|
| a | Lunar glass (an. comp.) | 45.40 | 34.50 | 0.30 | 0.20 | 19.00 | 0.80 | 0.10 | 0.10 | Chao et al., 1970 |
| a | Lunar glass (py comp.) | 55.40 | 1.40 | 10.40 | 16.70 | 20.10 | 0.00 | 0.00 | 0.90 | Duke et al., 1970 |
| a | Lunar glass (ol comp.) | 43.50 | 6.90 | 22.10 | 17.40 | 8.40 | 0.20 | 0.10 | 0.40 | Chao et al., 1970 |
| a | Lunar glass (titaniferous) | 41.10 | 10.30 | 18.90 | 6.80 | 10.50 | 0.50 | 0.20 | 9.20 | Chao et al., 1970 |
| a | Lunar glass (color) | 40.00 | 11.00 | 19.00 | 10.00 | 11.00 | 0.50 | 0.10 | 9.00 | Von Engelhardt et al., 1970 |
| a | Lunar glass (feldspathic) | 46.00 | 24.60 | 5.90 | 8.00 | 15.10 | 0.20 | 0.10 | 0.40 | Chao et al., 1970 |
| a | Lunar glass (colorless) | 46.00 | 24.60 | 7.00 | 8.00 | 13.00 | 0.60 | 0.10 | 0.80 | Von Engelhardt et al., 1970 |
| b | Shergottite, achondrite | 50.40 | 7.00 | 19.30 | 9.30 | 9.60 | 0.00 | 0.20 | 0.90 | Bunch, 1974 |
| b | Nakhlite, achondrite | 48.96 | 1.74 | 19.63 | 12.01 | 15.17 | 0.41 | 0.14 | 0.38 | Bunch, 1974 |
| b | Eucrite, achondrite | 48.16 | 15.57 | 15.69 | 8.41 | 11.08 | 0.45 | 0.09 | 0.32 | Bunch, 1974 |
| b | Howardite, achondrite | 48.47 | 9.46 | 17.16 | 12.00 | 8.08 | 0.46 | 0.05 | 0.37 | Mason & Wiik, 1966 |
| b | Angrite, achondrite | 44.58 | 8.86 | 8.50 | 10.05 | 24.51 | 0.19 | 0.26 | 2.39 | Bunch, 1974 |
| * | Nagylózs spherule | 39.76 | 9.22 | 0.38 | 0.66 | 40.57 | 0.00 | 1.05 | 0.29 | Szöör et al., 1994 |
| * | Nagylózs spherule | 40.50 | 9.08 | 0.36 | 6.01 | 38.91 | 2.01 | 1.02 | 0.21 | Szöör et al., 1994 |
| * | Nagylózs spherule | 37.70 | 8.89 | 0.49 | 6.72 | 42.59 | 0.15 | 1.06 | 0.38 | Szöör et al., 1994 |
| * | Nagylózs spherule | 37.83 | 8.95 | 0.45 | 5.89 | 42.71 | 0.80 | 1.06 | 0.30 | Szöör et al., 1994 |
| * | Nagylózs spherule | 38.12 | 9.33 | 0.30 | 6.33 | 42.14 | 0.40 | 0.97 | 0.33 | Szöör et al., 1994 |
| * | Nagylózs spherule | 38.98 | 8.92 | 0.42 | 6.56 | 41.88 | 0.49 | 0.85 | 0.29 | Szöör et al., 1994 |
| * | Nagylózs spherule | 37.57 | 8.90 | 0.47 | 6.25 | 43.13 | 0.45 | 1.07 | 0.39 | Szöör et al., 1994 |
| * | Nagylózs spherule | 41.40 | 10.24 | 0.38 | 5.77 | 39.39 | 0.05 | 0.85 | 0.48 | Szöör et al., 1994 |
| * | Nagylózs spherule | 43.57 | 9.79 | 0.10 | 6.98 | 36.49 | 0.00 | 0.80 | 0.42 | Szöör et al., 1994 |
| * | Nagylózs spherule | 41.83 | 9.79 | 0.40 | 5.28 | 39.65 | 0.00 | 0.92 | 0.34 | Szöör et al., 1994 |
| * | Nagylózs spherule | 39.71 | 9.38 | 0.25 | 6.99 | 40.09 | 0.40 | 0.88 | 0.34 | Szöör et al., 1994 |
| * | Nagylózs spherule | 38.16 | 8.85 | 0.36 | 6.45 | 42.45 | 0.37 | 1.03 | 0.42 | Szöör et al., 1994 |
| d | Australasian bottle green microtektites | 57.00 | 12.00 | 7.00 | 18.00 | 4.00 | 0.80 | 0.40 | 0.60 | Glass, 1969 |
| e | Australasian yellowish green microtektirtes | 65.80 | 15.20 | 5.40 | 6.10 | 3.90 | 1.10 | 1.00 | 0.70 | Glass, 1969 |
| f | Australasian normal microtektites | 69.20 | 14.90 | 5.30 | 3.20 | 3.10 | 1.10 | 2.30 | 0.80 | Glass, 1969 |
| g | Ivory Cost bottle green microtektites | 51.30 | 16.00 | 8.50 | 17.80 | 4.20 | 0.40 | 0.20 | 0.80 | Glass, 1969 |
| h | Ivory Cost normal microtektites | 65.60 | 15.60 | 6.90 | 4.60 | 1.40 | 1.90 | 1.80 | 0.70 | Glass, 1969 |
| i | Lunar basalt | 49.31 | 13.41 | 12.26 | 9.48 | 12.49 | 0.67 | 0.40 | 1.12 | Mason & Melson, 1970 |
| k | Ries Crater impactite | 61.04 | 17.26 | 5.99 | 3.39 | 4.59 | 5.54 | 1.44 | 0.93 | Graup, 1981 |
| k | Ries Crater impactite | 62.59 | 16.71 | 5.14 | 2.79 | 4.29 | 5.18 | 2.12 | 0.64 | Graup, 1981 |
| k | Ries Crater impactite | 64.97 | 15.70 | 4.36 | 2.53 | 2.89 | 5.10 | 2.74 | 0.81 | Graup, 1981 |
| k | Ries Crater impactite | 59.33 | 17.01 | 5.29 | 3.23 | 3.96 | 3.47 | 4.57 | 1.04 | Graup, 1981 |
| k | Ries Crater impactite | 61.09 | 17.97 | 5.15 | 3.35 | 4.93 | 5.63 | 1.42 | 0.84 | Graup, 1981 |
| k | Ries Crater impactite | 60.36 | 17.75 | 5.89 | 3.64 | 5.39 | 5.39 | 1.22 | 0.84 | Graup, 1981 |
| k | Ries Crater impactite | 63.80 | 15.22 | 5.32 | 3.09 | 3.90 | 3.02 | 4.09 | 0.80 | Graup, 1981 |
| m | Australites, tektites | 73.45 | 11.53 | 4.57[+] | 2.03 | 3.50 | 1.28 | 2.28 | 0.69 | Glass, 1990 |
| n | Indochinites, tektites | 73.00 | 12.83 | 4.95[+] | 2.48 | 1.91 | 1.45 | 2.40 | 0.73 | Glass, 1990 |
| o | Philippinites, tektites | 70.80 | 13.85 | 4.93[+] | 2.60 | 3.09 | 1.18 | 2.40 | 0.79 | Glass, 1990 |
| p | Javanites, tektites | 72.32 | 11.68 | 5.57[+] | 2.75 | 2.89 | 1.78 | 2.35 | 0.75 | Glass, 1990 |
| r | Muong Nong-type, tektites | 78.30 | 10.18 | 3.75 | 1.43 | 1.21 | 0.92 | 2.41 | 0.63 | Glass, 1990 |
| s | Ivory Cost tektites | 68.00 | 16.30 | 6.50[+] | 3.32 | 1.12 | 2.06 | 1.89 | 0.57 | Glass, 1990 |
| t | Bohemian tektites | 78.82 | 10.62 | 1.83[+] | 1.84 | 2.08 | 0.56 | 2.61 | 0.35 | Glass, 1990 |
| u | Bediasites, tektites | 76.37 | 13.78 | 3.98[+] | 0.63 | 0.65 | 1.54 | 2.08 | 0.76 | Glass, 1990 |
| v | Georgiaites, tektites | 81.30 | 10.80 | 2.56[+] | 0.53 | 0.51 | 1.24 | 2.37 | 0.50 | Glass, 1990 |
| c | Irghizite, impactite | 54.27 | 19.47 | 7.67 | 2.64 | 8.85 | 3.51 | 1.39 | 0.81 | Shaw & Wasserburg, 1982 |
| c | Irghizite, impactite | 75.11 | 9.32 | 5.34 | 2.65 | 2.30 | 0.81 | 1.96 | 0.76 | Shaw & Wasserburg, 1982 |
| c | Irghizite, impactite | 74.46 | 9.54 | 5.50 | 2.77 | 2.43 | 0.86 | 1.96 | 0.76 | Shaw & Wasserburg, 1982 |
| c | Irghizite, impactite | 74.28 | 10.16 | 5.60 | 2.93 | 2.36 | 0.97 | 2.00 | 0.78 | Taylor & McLennan, 1979 |
| c | Irghizite, impactite | 73.32 | 9.99 | 6.49 | 3.69 | 2.43 | 0.85 | 1.74 | 0.72 | Taylor & McLennan, 1979 |
| x | Average pyroxenite | 50.50 | 4.10 | 9.57[+] | 21.71 | 12.00 | 0.45 | 0.21 | 0.53 | Nockolds, 1954 |
| x | Average alkali pyroxenite | 41.55 | 7.25 | 13.90[+] | 13.02 | 16.93 | 1.38 | 0.70 | 3.31 | Nockolds, 1954 |
| y | Zhamanshinite, impactite | 72.01 | 15.55 | 5.50 | 1.11 | 0.55 | 1.10 | 2.83 | 0.78 | Taylor & McLennan, 1979 |
| z | Average uncommalgnite | 38.34 | 6.07 | 10.86[+] | 8.12 | 28.98 | 2.25 | 0.27 | 1.85 | Nockolds, 1954 |

[+] total iron content calculated as FeO

Major element composition of the spherules from borehole Nagylózs 1 are characterized by extremely high CaO content, relatively high MgO content, relatively low $Al_2O_3$ and alkali contents, and extremely low FeO content.

To demonstrate the similarities and differences these data are figured in a $SiO_2$ versus other oxides variation diagram (Figure 1). On the basis of distribution of the different formations five distinct and characteristic fields can be marked in the variation diagram:

- Nagylózs microspherules,
- lunar glasses,
- achondrites,
- tektites and microtektites,
- Ries Crater impactites.

As it can be seen in figure 1, fields of lunar glasses and achondrites as well as points of pyroxenites and uncompahgrite have similar position to the field of Nagylózs microspherules in the case of every major element.

For a more accurate evaluation of the major element composition a mathematical evaluation was used. After the log-ratio transformation of the compositional data statistical measures were performed on the independent principal components. For the Cluster-analysis the squared Euclidean distances measurements and the Ward-method computed by SPSS/PC+ were used. On the basis of the dendogram of the Cluster-analysis (Figure 2) the samples can be divided into two main groups: the first one includes all samples of lunar glasses, Nagylózs microspherules and achondrites, while the second one is formed by most of the other samples. It has to be noted that samples of Nagylózs form a distinct group, and the lunar glasses are closest to them.

In petrographical point of view it seems to be useful to calculate the CIPW-norms of samples listed in Table1. For the sake of the comparison we try to figure the comparative data together with a simple diagram. For this reason a double triangle diagram was constructed to figure and compare normative quartz (Q), the normative olivine + calcium orthosilicate ($Ol+Ca_2SiO_4$), the normative feldspars (Or+Ab+An) and the normative pyroxenes (Cpx+Opx) of the samples (Figure 3). It was a criterion that sum of these norms had to be more than 70 % of the total sum of the norms of the given sample. By using this new diagram we try to point out similarities rather than differences between the different formations.

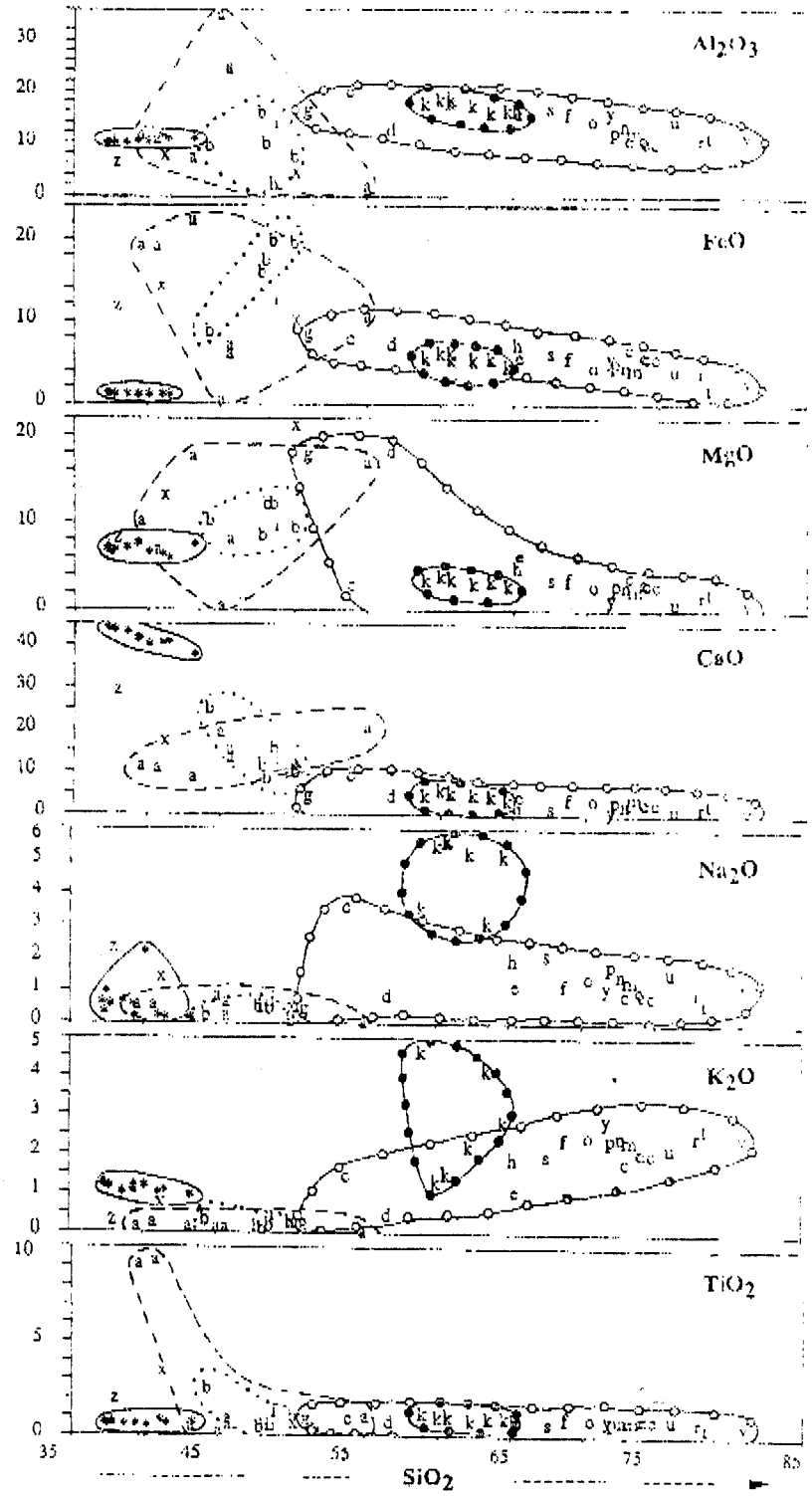


**Figure 1**. Variation diagram for major element compositions of the Nagylózs microspherules and those of the comparative formations. (Symbols see in Table 1)

Legend:

—— Field of the Nagylózs 1 spherulites
– – – Field of the Lunar glasses
····· Field of the Ca-rich achondrites
—●—● Field of the Ries Crater impactites
—○—○ Field of the other impactites, tektites, microtektites

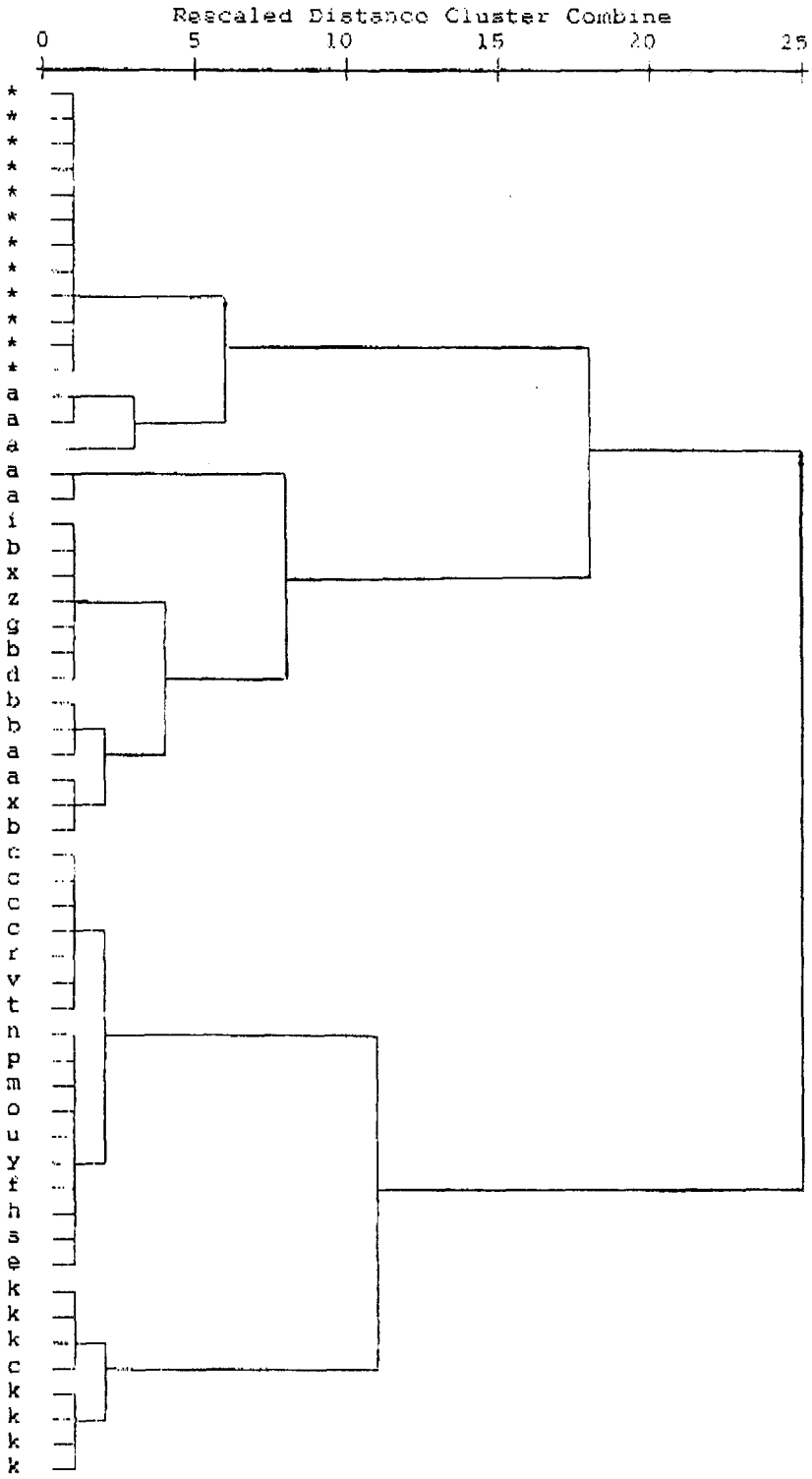


**Figure 2.** Dendogram of the Cluster-analysis of major element data of the Nagylózs microspherules and those of the comparative formations. (Symbols see in Table 1)

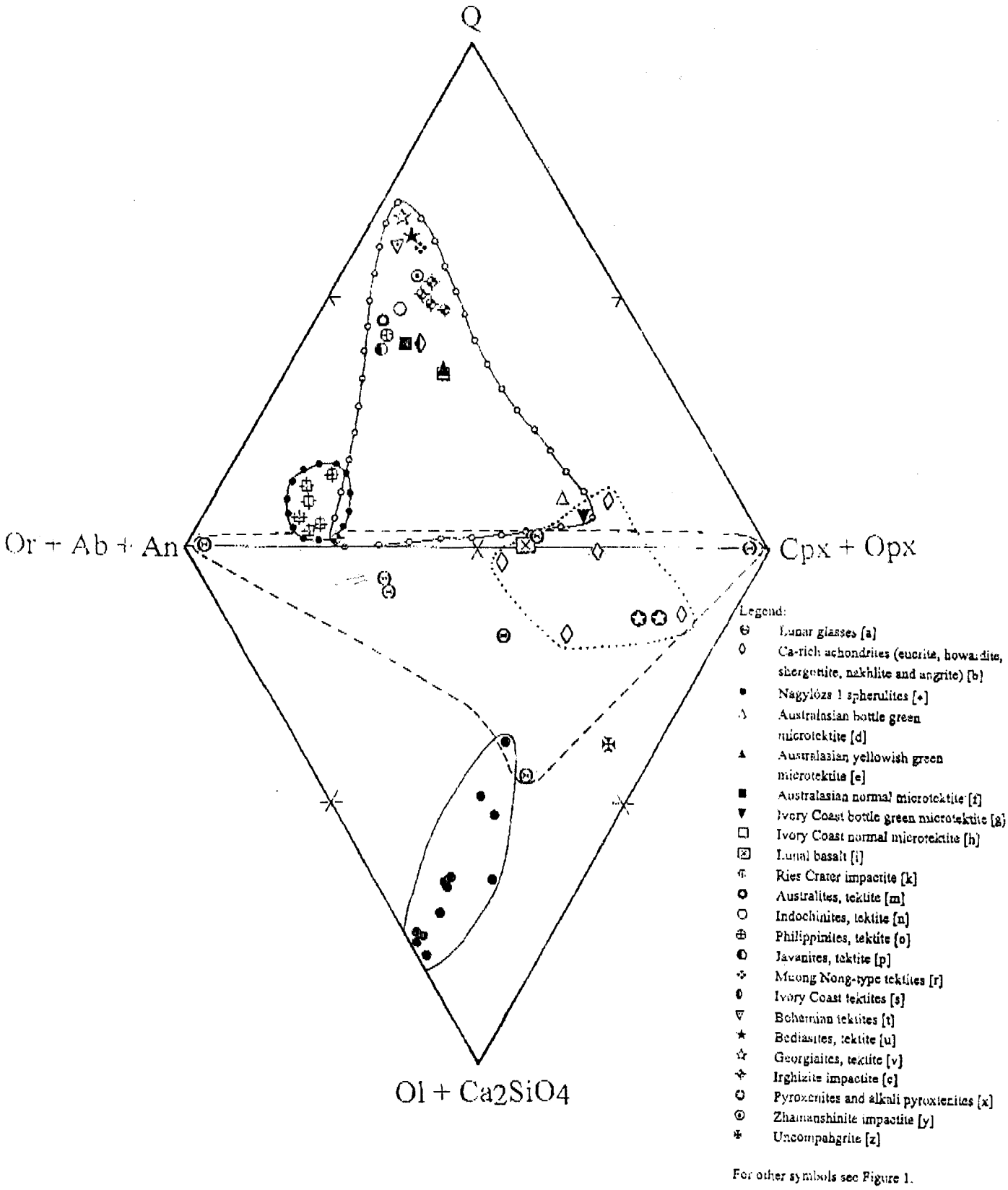


**Figure 3.** Q-(Ol+$Ca_2SiO_4$)-(Cpx+Opx)-(Or+Ab+An) double triangle diagram for the representation of the CIPW norms of Nagylózs microspherules and the comparative formations.

In the diagram characteristic fields marked in Figure 1 can also be indicated. As the Figure 3 shows, our findings well separated from tektites and microtektites, and the Ries Crater impactites. Only some points of lunar glasses and Ca-rich achondrites as well as those of the uncompahgrite and pyroxenites are relatively close to the field of the Nagylózs microspherules.

It can be said as a summary that after these petrochemical and statistical analyses none of the possible ways of the origin can be rejected. Morphology and certain REE contents of these findings as well as conditions of their occurrences seem to suggest an extraterrestrial origin, but their major element contents and CIPW norms (especially the high normative calcium orthosilicate in accordance with the low silica and the extremely high CaO content) could be brought into connection with contact metamorphic processes, too (Williams et al., 1982). These microspherules could be formed by "shock metamorphosis" of carbonate rocks caused by a hypothetical meteorite impact. Although points of pyroxenites and uncompaghrite are relatively close to those of Nagylózs microspherules, magmatic origin of them may hardly be supposed because such kinds of magmatic rocks have not been known in this area. It seems to be sure that the Nagylózs microspherules belong to neither microtektites nor tektites because tektite and microtektites are much more siliceous. Among the extraterrestrial formations some Ca-rich achondrites and lunar glasses have similar major elements composition and, consequently, similar CIPW norms to those of our findings. In our opinion, however, their extraterrestrial origin (achondritic microtektite? micrometeorite of lunar origin?) seems to be more possible.

**Acknowledgement**

A grant obtained from the OTKA Bureau, Hungary (No. 1742) supported this work.

**References**

Boldizsár I., Don Gy., Erhardt Gy., Hobot J., Ivancsics J., Kaiser M., Marsi I., Scharek P., Szeiler R., Szurkos G., Tullner T., Zsámbok I. 1993., The Geological Map Series of the Little Hungarian Plain, Sopron-Kőszeg. Manuscript. Geological Institute of Hungary. ed. by P. Scharek.

Szöőr Gy., Korpás-Hódi M., Don Gy. and Beszeda I. 1994., Suppl. of Annales Univ. Sci. Budapest, Sect. Geoph. et Met. (in press)

Williams, H., Turner, F.J. and Gilbert C.M. 1982., Petrography. Freeman and Co.

Nockolds, S.R., 1954., Average chemical composition of some igneous rocks. Geol. Soc. Am. Bull. 65. 1007-1032.
Bunch, T.E., 1974., Meteorites: Clues to the origin of the solar system. In: A Primer in Lunar Geology (eds: Greely, R. and Schultz, P.). NASA, pp.69-88.
Mason, B. and W.G. Melson, 1970., The Lunar Rocks. Wiley and Sons.
Chao, E.C.T., O.B. James, J.A. Minkin, J.A. Boreman, E.D. Jackson, and C.B. Raleigh, 1970., Petrology of unshocked crystalline rocks and shock effects in lunar rocks and minerals. Science, 167, 644-647.
Von Engelhardt, W., J. Arndt, W.F. Muller and D. Stoffler, 1970., Shock metamorphism in lunar samples. Science, 167, 669-670.
Duke, M.B., C.C. Woo, M.L. Bird, G.A. Sellers andR.B. Finkelman, 1970., Lunar soil: size distribution and mineralogical constituent. Science, 167, 648-650.
Mason, B. andH.B. Wiik, 1966., The composition of the Barratta, Carraweena, Kapoeta, Moresport, and Ngasir meteorites. Am. Mus. Novatites, 2273, 1-20.
Graup, G., 1981., Terrestrial chondrules, glass spherules and accretionary lapilli from suevite, Ries Crater, Germany. Earth and Planet. Sci. Let., 55, 407-418.
Shaw, H.F. and G.J. Wasserburg, 1982., Age provenance of the target materials for tektites and possible impactites as inferred from Sm-Nd and Rb-Sr systematics. Earth and Planet. Sci. Let., 60, 155-177.
Glass, B.P., 1969., Chemical composition of Ivory Coast mictektites. Geochim. Cosmochim. Acta, 33, 1135-1147.
Glass, B.P., 1990., Tektites and microtektites: key facts and inferences. Tectonophysics, 171, 393-404.
Taylor, S.R. and S.M. McLennan, 1979., Chemical realtionship among irghizites, zhamanshinites, Australasian tektites and Henbury impact glasses. Geochim. Cosmochim. Acta, 43, 1551-1565.

# MAGMA DIFFERENTIATION TREND DEDUCED FROM FOUR POLYMICT EUCRITES.

Kazuto Saiki * and Hiroshi Takeda **

* Geological Institute, Faculty of Science, University of Tokyo, Hongo, Tokyo 113, Japan.

** Mineralogical Institute, Faculty of Science, University of Tokyo, Hongo, Tokyo 113, Japan.

**Introduction** All the polymict breccias: howardites, polymict eucrites and polymict diogenites are considered to be members of a mineralogical and compositional continuum with several lithic components (eucirtes and diogenites) mixed in varying proportions [1]. The breccias are named after the most abundant component type. If more than 90% of a component is present, then the meteorite is named after such dominant component [2]. The polymict achondritic breccias containing less than 10% of diogenitic material are polymict eucrites. The howardites are defined as polymict achondritic breccias containing more than 10% of diogenitic component. In order to gain a better understanding of evolutional trend of the HED parent body, we reinvestigated four polymict breccias Y791439, Y791192, Y82009 and Y82049. They are polymict breccias mainly composed of cumulate eucrites with minor diogenitic and ordinary eucrite components.

**Samples and analytical methods** Polished thin sections (PTSs) of Y791439,51-2, Y791192,91-2, Y791192,99-2, Y82009,51-2 and Y82049,61-2 were supplied from the National Institute of Polar Research (NIPR). Y791439, Y791192, and Y782009 are Y75032-type polymict breccias and, Y82049 is a howardite. These samples were investigated by SEM (JEOL840A) at Mineralogical Inst., Univ. of Tokyo, equipped with a new chemical mapping system named "PXQUAD system" [3] which is capable of identifying pyroxene phases, and plots an elemental distribution map and the Ca-Mg-Fe trends in a pyroxene quadrilateral with the same color scale simultaneously. The chemical compositions of particular minerals on the above PTSs were analyzed by electron probe microanalyser (EPMA) JEOL 733 Mark II at Geological Inst., Univ. of Tokyo. The bulk compositions of pyroxenes are average compositions obtained by EPMA line analyses.

**Results** We investigated an entire surface of the PTSs by the PXQUAD system and classified all pyroxenes in them. These polymict breccias are found out to be composed of abundant cumulate eucrites and minor non-cumulate eucrites without other components such as remnant of primitive materials. Close association of non-cumulate and cumulate eucrites can be explained by a model in that they are located adjacent to each other in the parent body crust, and that there are variety of cumulate eucrites existed at one region.

The outline of our samples are summarized as follows. Y791439 was classified as a polymict cumulate eucrite with small diogenitic and rare non-cumulate eucrite components [4]. It contains more clasts of cumulate eucrite than Y75032, which was classified as diogenite. Six cumulate eucrite clasts up to 2.8 x 2.3 mm with large amount of plagioclase have been found in the PTS. Pyroxene chemical compositions of Y791439 are divided into four types. Y791192 is a polymict cumulate eucrite with large non-cumulate eucrite component and a small diogenitic component. One large ordinary eucrite clast 1.5 x 2.0 mm in size with plagioclase laths has been found in the PTS. Pyroxene chemical compositions of Y791192 are divided into six types. Y82009 was classified as a polymict eucrite [5]. The Y82009 PTS has large non-cumulate eucrite clasts up to 2.0 x1.5 mm. Pyroxene chemical

compositions of Y82009 are divided into five types. Y82049 was classified as a polymict eucrite [5]. The Y82049 PTS has two large clasts 1.1 x 2.0 mm and 5.0 x 1.0 mm. These clasts contains the Juvinas type pyroxenes. Pyroxene chemical compositions of Y82049 are divided into seven types. Because the range of chemical compositions of seven types of pyroxenes in Y82049 is very wide (mg# =26 - 77) and this sample includes olivines of $Fa_{50}$ and $Fa_{36}$, it is more likely to be a howardite.

The remarkable textures of polymict eucrites: Many pyroxenes in polymict breccias in this study show chemical zoning. Most of zonal structures of pyroxenes must be originally produced in crystallization process, because there is Ca heterogeneity. In this study, we show the first evidence that there is a zonal structure produced by secondary diffusion after breccia formation. That is one of pyroxenes in Y82009 (Fig.1). This pyroxene has both chemical zoning and exsolution lamellae 10μm in width. Because the diffusion coefficient of Fe is about hundred times larger than that of Ca [6], this zonal structure must have been produced after the formation of the augite lamellae. This zoning profile may be formed by a secondary heating event.

Another unique texture found in pyroxene of Y791192, is the presence of second generation lamellae in the host and lamellae (Fig.2). It may indicate two stages cooling. In the pyroxene of the same type there is a pyroxene aggregate (Fig.3). This texture suggests that there was a high temperature reheating event after the crystallization or brecciation of pyroxenes.

Magma differentiation trend of the HED parent body: In these PTSs, there are many clasts including both pyroxene and plagioclase. We divided these clasts into two types. One is the clast including Ca-rich pyroxenes and another is the clast including Ca-poor pyroxenes. The threshold between Ca-rich and Ca-poor is defined Ca/(Ca+Fe+Mg) (mol ratio) = 0.1.

Anorthite (An) mol % of plagioclases are plotted against fe number (Fe/(Fe+Mg) mol ratio) coexisting low-Ca pyroxene (solid line) and high-Ca pyroxene (shaded line).

In 1985, Ikeda and Takeda [7] studied details of lithic clasts and mineral fragments in an Antarctic howardite Y7308. They plotted En mol % of low-Ca pyroxenes against An mol % of coexisting plagioclases and showed the continuum of chemical composition of minerals in lithic clasts and fragments. That trend was named Na-poor trend (trend A). For explaining the trend, they proposed a model on the evolutional process of magma ocean on the parent body and introduced Na-rich trend (trend B) as the source of cumulate eucrites.

In our work, the clasts of four kinds of polymict breccias are plotted on the An vs. fe number diagram. The remarkable point is that all clasts including Ca-poor pyroxene are located along the trend A. But there is no Na-rich plagioclase coexisting with Mg-rich and Ca-poor pyroxene. All Na-rich plagioclase are zoned one coexisting with Ca-rich pyroxene or are in the clast which crystallized at the end of magma differentiation.

**Discussion** The polymict breccias in this study include many kinds of cumulate eucrites and non-cumulate eucrites. The fact that cumulate eucrites and non-cumulate eucrites are coexisting in the same PTS suggests that non-cumulate eucrites and cumulate eucrites existed in almost the same region of the HED parent body. In addition, many kinds of cumulate eucrites may have existed together in a close region. The surface of the HED parent body must be differentiated by magmatic process all over the body, because there is no chondritic clast nor fragments of the primitive crust in these PTSs.

The mechanisms for origin of the remarkable textures shown in this work are not clear. It can

be, however, concluded that there are many local variations in thermal history on the HED parent body. The fact that many equilibrated Mg-rich pyroxenes are coexisting with pyroxenes of the remarkable textures, show that a mixing event such as an impact mixing occurred in the course of crustal formation when the crust was still hot.

The result of our study for the magma trend on the HED parent body suggest that there is no trend B magma. If the trend B magma should exist, it must be solidified as major components in polymict breccias. Fe rich clasts on trend B are, however, present. For example, in the Y791192 Fe-rich pyroxene coexists with an Na-rich plagioclase ($An_{80}$-$An_{88}$). In the last stage of fractional crystallization, Na-rich liquid may be accumulated and Na-rich plagioclase crystallized. Na-rich plagioclases often coexist with Ca-rich pyroxenes. In this case, such clasts must be crystallized as mesostasis, because their pyroxenes are Ca-rich and zoned. Considering the fact that such clasts have variation in their Fe number, we believed that some event such as an impact may bring a part of solidifying liquid near the surface and cooled rapidly.

**Summary** In this work, four polymict breccias have been investigated to check the systematic variation of pyroxenes in eucrites by employing chemical mapping system constructed by the author. The results are summarized as follows:

(1) The existence of mixtures of non-cumulate eucrite and cumulate eucrites in polymict breccias Y791439, Y791192, Y82009 and Y82049 indicates that non-cumulate eucrite and several kinds of cumulate eucrites existed together in a close region of the HED parent body.

(2) There are local variations in the thermal history in the pyroxenes in cumulate eucrite clasts. Especially, one pyroxene in Y82009, with Fe/Mg zoning at the rims despite augite exsolution lamellae, is the first evidence for secondary diffusion after lamellae formation.

(3) The plot of chemical compositions (An vs. fe) of clasts in polymict breccias suggest that there is certainly a magma differentiation trend A. But trend B is not likely present. In the last stage of fractional crystallization, or in rapid cooling conditions, Na-rich liquid may be accumulated and Na-rich plagioclase crystallized.

(4) All the above evidences suggest that a mixing event such as an impact mixing occurred in the course of crustal formation when the crust was still hot.

**Acknowledgments:** We thank the staff of the National Institute of Polar Research for providing us with meteorite samples. We are indebted to Mr. O. Tachikawa for his assistance during the SEM, EDS, and CMA work, Mr. H. Yoshida and Prof. M. Miyamoto for his assistance during the EPMA work. This work is supported by Fellowships of the Japanese Society for the Promotion of Science for Japanese Junior Scientists and a Scientific Grand of Ministry of Education.

**References:** [1] Dreibus G. and Wänke H. (1979) Proc. Lunar Sci. Conf. 8th, 211-227. [2] Delaney J. S., Prinz M. and Takeda H. (1984) Proc. Lunar Planet. Sci. Conf. 15th, C251-C288. [3] Saiki K., Yamaguchi A., and Takeda H.(1992) Lunar Planet. Sci. XXIII . pp.1201-1202. [4] Takeda H. and Hidaka O.(1989) Meteoritics, 24, p.331 [5] Yanai K. and Kojima H.,comp. (1987): Photographic Catalog of Antarctic Meteorites. Tokyo, Natl. Inst. Polar Res., 298p. [6] Miyamoto M. and Takeda H. (1994) Journal of Geophys. Res., 99, 5669-5677. [7] Ikeda Y. and Takeda H. (1985) Proc. Lunar Planet. Sci. Conf. 15th, in J. Geophys. Res., 90, C649-C663.

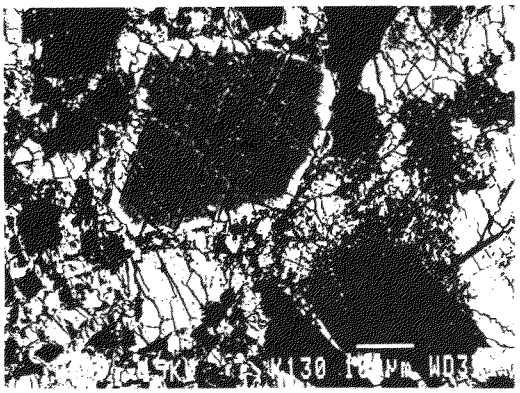

Fig.1 Backscatterd electron image (BSI) of pyroxene in Y82009. This pyroxene has both chemical zoning and exsolution lamellae 10μm in width. This zonal structure must have been produced after the formation of the augite lamellae.

Fig.2 BSI of pyroxene in Y791192 including second generation lamellae in the host and lamellae.

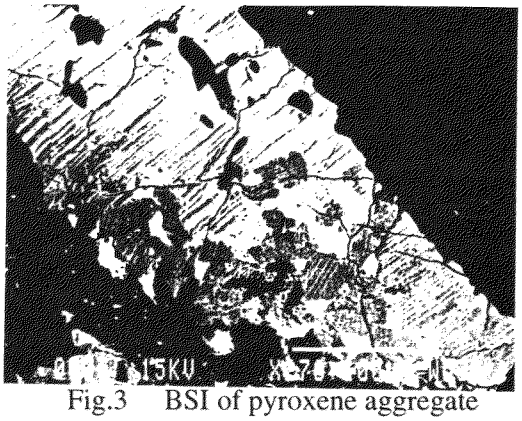

Fig.3 BSI of pyroxene aggregate in Y791192.

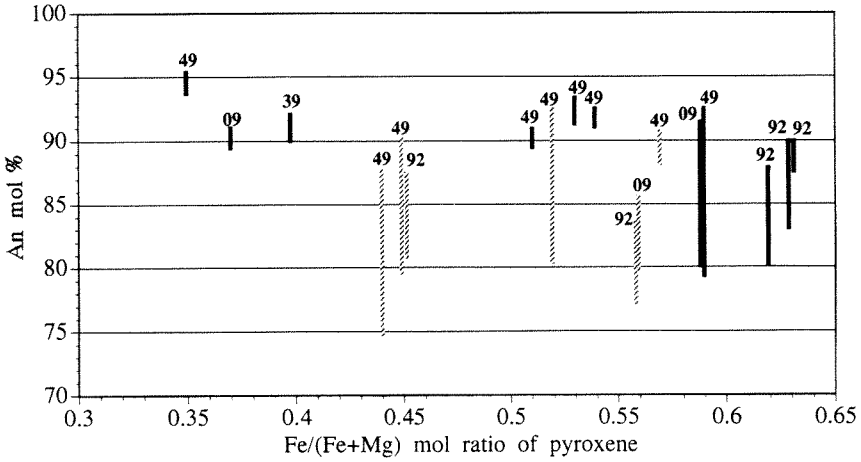


Fig.4. Anorthite (An) mol % of plagioclases are plotted against fe number (Fe/(Fe+Mg) mol ratio) coexisting low-Ca pyroxene (solid bar) and high-Ca pyroxene (shaded bar). The chemical compositions of plagioclases are shown as range and the chemical compositions of pyroxenes are shown as average. The numbers plotted above the bar indicate its sample number (last two digits). The threshold between high-Ca and Low-Ca is Ca/(Ca+Fe+Mg) (mol ratio) = 0.1.

# Cathodoluminescence of Semarkona Chondrules: A Classification and the Relationships with Mesostasis Composition

Takuya SATO[1], Satoshi MATSUNAMI[1] and Kiyotaka NINAGAWA[2]

1) Department of Earth Sciences, Miyagi University of Education, Aramaki-Aoba, Sendai 980, Japan

2) Department of Applied Physics, Okayama University of Science, Ridai-cho 1-1, Okayama 700, Japan

Cathodoluminescence (CL) is the process that visible radiation is emitted, when energetic electron bombared the surface of certain materials (Marshall, 1988), and is closely related to the presence of lattice defects and impurities generated in the crystals during their formation. CL observation under optical microscope and/or SEM is a technique which is now widely used for the petrographic examination of meteorites (Steele, 1986; Sears *et al.*, 1992; DeHart *et al.*, 1992). We recently began detailed studies on TL and CL characteristics of chondrules in type-3 chondrites (Matsunami *et al.*, 1993; Ninagawa *et al.*, 1994) in order to clarify chondrule-forming processes in the early solar system.

In this study, we petrographically examine chondrules in detail based on CL properties of mesostasis and phenocrysts in six type-3 ordinary chondrites (Semarkona, Krymka, Chainpur, Sharps, ALH-77214, ALH-77216). CL of chondrules were observed using Luminoscope ELM-3 attached to an optical microscope and recorded as a series of color photomicrographs at Okayama Univ. of Science. Using the SEM-EDS system of Miyagi Univ. of Education, we analyzed chemical compositions of phenocrysts and mesostases in 22 chondrules of the Semarkona (LL3.0) meteorite with special attention to variety of CL colors observed in chondrules.

The results of the present study are summarized as follows:

(1) Colors of CL emitted from chondrules in six samples studied here revealed to show a wider variability than that previously observed by Sears *et al.* (1992). In addition to CL colors described by Sears *et al.* (yellow, blue, red, and none), we newly observed CL emissions with greenish, whitish-brown, or reddish-brown colors. Especially in many chondrules, CL color in the mesostasis is heterogeneous on photomicrographs, indicating that the CL emissions are mixtures composed of lights from several ranges of wavelength. From our CL observations, we partly modify the classification of chondrules presented by Sears *et al.* (1992) and propose eight groups of chondrules mainly based on CL colors of mesostasis: groups ①-⑧ (Table 1).

(2) CL colors of phenocrysts and mesostasis in chondrules sensitively reflect the chemical compositions. As already shown by Sears *et al.* (1992), CL colors of mesostases in chondrules are closely related to relative proportions of contents of normative quartz (Q), albite (Ab), and anorthite (An). In Semarkona, the CL colors are related to Ab mole % (Fig. 1): yellow for mesostases with 0-30% Ab, heterogeneous greenish color for mesostases with 30-55% Ab, and non-luminescent for mesostases with Q more than 70 mole %. Phenocrysts of chondrules (olivine and low-Ca pyroxene) containing FeO less than 2 wt% show red CL.

References: DeHart J.M. *et al.* (1992): *GCA* **56**, 3791-3807. / Marshall D.J. (1988): *Cathodoluminescence of geological materials*, Unwin Hyman. / Matsunami S. *et al.* (1993): *GCA* **57**, 2101-2110. / Ninagawa K. *et al.* (1994): *Proc. NIPR Symp. Antarct. Meteorites* **7**, 217-224. / Sears D.W.G. *et al.* (1992): *Nature* **357**, 207-210. / Steele I.M. (1986): *GCA* **50**, 1379-1395.

Table 1. A classification of chondrules in type-3 ordinary chondrites based on CL colors of mesostasis

| group | mesostasis | phenocrysts |
|---|---|---|
| ① | bright yellow | red |
| ② | bright yellow | none |
| ③ | heterogeneous greenish | none |
| ④ | none | none/red |
| ⑤ | dark blue-green | none |
| ⑥ | bright light blue | none |
| ⑦ | heterogeneous whitish brown | none |
| ⑧ | dark reddish brown | none |

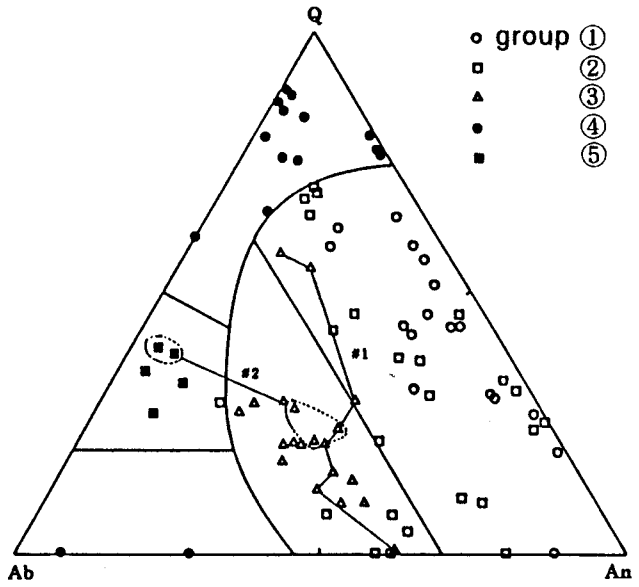


Figure 1. Molar ratios of normative Q, Ab, and An contents in the mesostases of 22 Semarkona chondrules, obtained by the SEM-EDS method. Solid lines are boundaries showing regions of five chondrule groups (①-⑤).

# Which occurred earlier, the settling of dust particles and the formation of chondrules in the solar nebula? - Implication from compound chondrules.

Minoru SEKIYA and Tomoki NAKAMURA
Department of Earth and Planetary Sciences,
Kyushu University, Hakozaki, Fukuoka 812-81

## Introduction

The standard scenario of the formation of the planetary system is as follows (Hayashi et al., 1985): (1) The Sun and the solar nebula are formed after the collapse of a molecular cloud core. (2) Solid dust particles coagulate each other and settle towards the midplane of the solar nebula. (3) The thin dust layer fragments owing to gravitational instability and planetesimals with radii on the order of 10 km are formed. (4) The terrestrial planets and cores of the giant planets are formed by collisional coagulation of planetesimals.

In which stage of the above scenario, the chondrules are formed? To answer the question, we consider the condition for the formation of the compound chondrules. We assume that the compound chondrules are formed by collisions of pre-chondrule particles which are hot enough to be partially melted. We shall estimate the number densities and velocities of the particles to form the observed ratio of the compound chondrules.

## Observed ratio of the compound chondrules

The ratio of the compound chondrules were determined by microscope observation on the thin sections of 50 unequilibrated ordinary and carbonaceous chondrites from Antarctica (Nakamura et al., 1995). 65 compound chondrules were identified through the inspection of $\sim$ 6500 chondrules, suggesting that the ratio of the compound chondrules is around $10^{-2}$. All chondrite types (H, L, LL and C) show similar abundances of compound chondrules, thus we regard the ratio of $10^{-2}$ as being representative in the early solar nebula at the time of chondrule formation.

## Condition for the formation of the compound chondrules

We here consider the condition for the formation of compound

chondrules using a simple model. We do not specify mechanisms of chondrule formation, which may be heating by gravitational instability or magnetic reconnection in the solar nebula. We only use the facts that the chondrules have the following characteristics: the typical radius is $10^{-1}$ cm, the typical cooling time is $10^{3}$ sec (Tsuchiyama et al., 1980), and the ratio of the compound chondrule is about $10^{-2}$. The notations and representative values of the model are listed in Table 1.

Table 1. The notations and representative values.

| | |
|---|---|
| $a$ : the typical radius of pre-chondrule particles. | $10^{-1}$ cm |
| $v$ : the typical velocity of pre-chondrule particles. | $10^{3}$ cm s$^{-1}$ |
| $n$ : the number density of pre-chondrule particles. | $3.2\times10^{-7}$ cm$^{-3}$ |
| $\Delta t$ : time duration of partial melting. | $10^{3}$ sec |
| $f$ : the probability of formation of a compound chondrule per a collision of pre-chondrule particles. | 0.5 |
| $p$ : the ratio of compound chondrules. | $10^{-2}$ |
| $R$ : the orbital radius from the sun. | 3 AU |
| $n_d$ : the number density of dust particles at the midplane before the settling. | $2.2\times10^{-11}$ cm$^{-3}$ |
| $\rho_s$ : the solid density of dust particles. | 3 g / cm$^{3}$ |

The probability of a pre-chondrule particles to collide with another particle and to form a compound chondrule before solidification is given by

$$4\pi a^2 f n v \Delta t = 2p. \qquad (1)$$

Thus we have

$$n = \frac{p}{2\pi a^2 f v \Delta t}$$

$$= 3.2\times10^{-7}\left(\frac{p}{10^{-2}}\right)\left(\frac{a}{10^{-1}\,\mathrm{cm}}\right)^{-2}\left(\frac{f}{0.5}\right)^{-1}\left(\frac{v}{10^{3}\,\mathrm{cm\,s^{-1}}}\right)^{-1}\left(\frac{\Delta t}{10^{3}\,\mathrm{s}}\right)^{-1}\ [\mathrm{cm^{-3}}]. \qquad (2)$$

On the other hand, the dust number densities $n_d$ at the midplane of the solar nebula before the settling are given by (Hayashi, 1981)

$$n_d = 2.2\times10^{-11}\left(\frac{\rho_s}{3\,\mathrm{g\,cm^{-3}}}\right)^{-1}\left(\frac{a}{10^{-1}\,\mathrm{cm}}\right)^{-3}\left(\frac{R}{3\,\mathrm{AU}}\right)^{-11/4}\ [\mathrm{cm^{-3}}]. \quad (3)$$

Since $n >> n_d$, it is concluded that the chondrule formation occurred after the settling of dust particles.

Next, we examine the condition for the gravitational stability (Sekiya, 1983):

$$\frac{4\pi}{3}a^3\rho_s n \le \frac{7.617M_\odot}{4\pi R^3}, \quad (4)$$

where $M_\odot$ is the solar mass. This equation is rewritten

$$n \le 1.1\times10^{-6}\left(\frac{\rho_s}{3\,\mathrm{g\,cm^{-3}}}\right)^{-1}\left(\frac{a}{10^{-1}\,\mathrm{cm}}\right)^{-3}\left(\frac{R}{3\,\mathrm{AU}}\right)^{-3}\ [\mathrm{cm^{-3}}]. \quad (5)$$

Substituting Eq. (2) to Eq. (5), we have

$$v \ge 3.0\times10^{2}\left(\frac{R}{3\,\mathrm{AU}}\right)^{3}\left(\frac{a}{10^{-1}\,\mathrm{cm}}\right)\left(\frac{\rho_s}{3\,\mathrm{g\,cm^{-3}}}\right)\left(\frac{p}{10^{-2}}\right)\left(\frac{f}{0.5}\right)^{-1}\left(\frac{\Delta t}{10^{3}\,\mathrm{s}}\right)^{-1}\ [\mathrm{cm\,s^{-1}}]. \quad (6)$$

This value of the collision velocity is rather large. We are now intend to examine whether the collisional coagulation is possible with such a large velocity. If the coagulation is impossible, it is concluded that the chondrule formation did not occur in the stage where dust particles floating in the solar nebula; we have to consider the chondrule formation during the stage of the planetesimal collisions.

References

Hayashi, C. (1981) Progr. Theor. Phys. Suppl. 70, 35-53.

Hayashi, C., Nakazawa, K. and Nakagawa, Y. (1985) In "Protostars and Planets II" (Black, D.C., and Mathews, M.S., Eds.) pp1100-1153, Univ. Arizona Press.

Nakamura, T., Sekiya, M., Matsuoka, K. and Kojima, H. (1995) in this volume.

Sekiya, M. (1983) Progr. Theor. Phys. 69, 1116-1130.

Tsuchiyama, A., Nagahara, H. and Kushiro, I. (1980) Earth Planet. Sci. Lett. 48, 155-165.

# Subdivision of metamorphic grade of CO3 chondrites and the occurrence of cohenite in Y-81020, Y-81025 and Y-74135.

Yasuhiro Shibata

Department of Earth and Planetary Sciences, Hokkaido University, Sapporo 060, Japan.

## Introduction

It is believed that the primitive CO3 chondrite (e.g., Colony meteorite, ALH-77307) share several characteristics, TL properties, olivine composition, metal composition etc.. Existence of carbide, cohenite ($Fe_3C$) and haxonite, is also one of them[1], however, carbide do not exist necessarily in the least unequilibrated CO3 chondrite (e.g., Colony meteorite)[2]. I determined metamorphic grade of CO3 chondrites (Y-74135, Y-81020, Y-81025 (Y-81020 and Y-81025 are paired samples[3]), Y-82050, Y-790992, Y-791717 and ALH-77307) on the basis of silicate and oxide compositions and investigated opaque minerals in low metamorphic grade CO3 chondrites by EPMA.

## Result

Samples studied here were investigated by some available methods in order to determine metamorphic grade. Results of analyses of mean fayalite compositions are as follows: Fa 5.3 in Y-81020, Fa 5.2 in Y-81025, Fa 7.4 in Y-74135, Fa 12.5 in ALH-77307, Fa 12.7 in Y-82050, Fa 15.6 in Y-790992 and Fa 16.8 in Y-791717. Fig. 1 shows zoning profiles for FeO, $Cr_2O_3$, MnO and CaO taken from core to rim of olivine grains in type IA chondrules in Y-81025, Y-74135, ALH-77307 and Y-791717. Zoning profiles for $Cr_2O_3$ of Y-81025, Y-74135 are very similar to that of ALH-77307 and those three samples are richer in $Cr_2O_3$ than Y-791717. Moreover, temperature suggested by Fe-Mg partition between olivine and chromite in type II chondrules were investigated. The obtained data from Y-81020, Y-81025, Y-74135 and ALH-77307 are high (approximately 1400 ℃), while those from Y-790992, Y-791717 and Y-82050 are relatively low (approximately 600 ℃).

Cohenite grains exist abundantly in Y-81020, Y-81025 and Y-74135. Table 1 shows the average compositions of cohenite. Cohenite grains are typically from several to 100 micron, often reach 500 micron in diameter. Cohenite grains generally coexist with tetrataenite and/or troilite and exist in both chondrule and matrix. The occurrence of cohenite does not seem to be replacement texture (e.g., Fe-Ni metal surrounded by cohenite rims or cohenite surrounded by Fe-Ni metal rims). Major Fe-Ni metal are kamacite and tetrataenite. Kamacite grains often have very fine-grained phosphate and silicate inclusions. Kamacite grains in chondrules have fine-grained phosphide and silicide (probably schreibersite and perryite). Kamacite grains generally have below 0.1 wt.% Si and P except for those bearing phosphide and silicide inclusions.

## Discussion

Y-81020, Y-81025 and Y-74135 have very low mean fayalite compositions resulting of analyses of randomly selected olivine. Olivine grains in type IA chondrules in low metamorphic grade CO3 chondrites have low-Fa and relatively high $Cr_2O_3$ content (e.g., ALH-77307)[4]. The data from Y-81020, Y-81025 and Y-74135 show the same properties. Moreover, high temperatures suggested by Fe-Mg partition between olivine and chromite in type II chondrules in above three samples are also consistent with the properties of low metamorphic grade CO3 chondrites[5]. The above data of silicate and oxide indicate that Y-81020, Y-81025 and Y-74135 are considered to be the least metamorphosed CO3 chondrite, as ALH-77307.

Although it is considered that low metamorphic grade CO3 chondrites do not have necessarily cohenite grains, results of this work indicate that existence of cohenite is indeed one of the properties of the least metamorphosed CO3 chondrites. If cohenite were ubiquitously in primitive CO3 chondrites, it would suggest that how evolved the opaque phases in the nebular or asteroidal processes.

I do not know the details of formation of cohenite, however the occurrence of cohenite suggest that cohenite might form by crystallization from Fe-Ni-C melt during chondrule formation or before accretion on the parent body, not by reaction between Fe-Ni metal grains and CO or $CO_2$ gas. Because texture indicating shock melting and replacement texture suggesting solid-

gas reaction were not observed in cohenite-bearing samples.

References

[1] Sears, D.W.G., Batchelor, J.D., Lu, J. and Keck, B.D. (1991) Proc. NIPR Symp. Antarct. Meteorites, 4, 319-343. [2] Rubin, A.E., James, J.A., Keck, B.D., Weeks, K.S., Sears, D.W.G. and Jarosewich, E. (1985) Meteoritics, 20, 175-196. [3] Yanai, K. and Kojima, H. (1987): Photographic Catalog of the Antarctic Meteorites. NIPR, Tokyo, 298 p. [4] Scott, E.R.D. and Jones, R.H. (1990) Geochim. Cosmochim. Acta, 54, 2485-2502. [5] Johnson C. A. and Prinz M. (1991) Geochim. Cosmochim. Acta, 55, 893-904.

Table 1. Average compositions (wt.%) of cohenite in Y-81025 and Y-74135

| | Y-81025 | | Y-74135 | |
|---|---|---|---|---|
| No. of grains | 10 | | 11 | |
| Fe | 88.02 | *0.63* | 88.25 | *0.49* |
| Ni | 4.46 | *0.25* | 4.49 | *0.17* |
| Co | 0.10 | *0.07* | 0.31 | *0.08* |
| Cr | 0.20 | *0.19* | 0.10 | *0.20* |
| P | 0.05 | *0.06* | 0.01 | *0.01* |
| Total | 92.83 | | 93.16 | |

Italicized figures are standard deviations of the analyses.

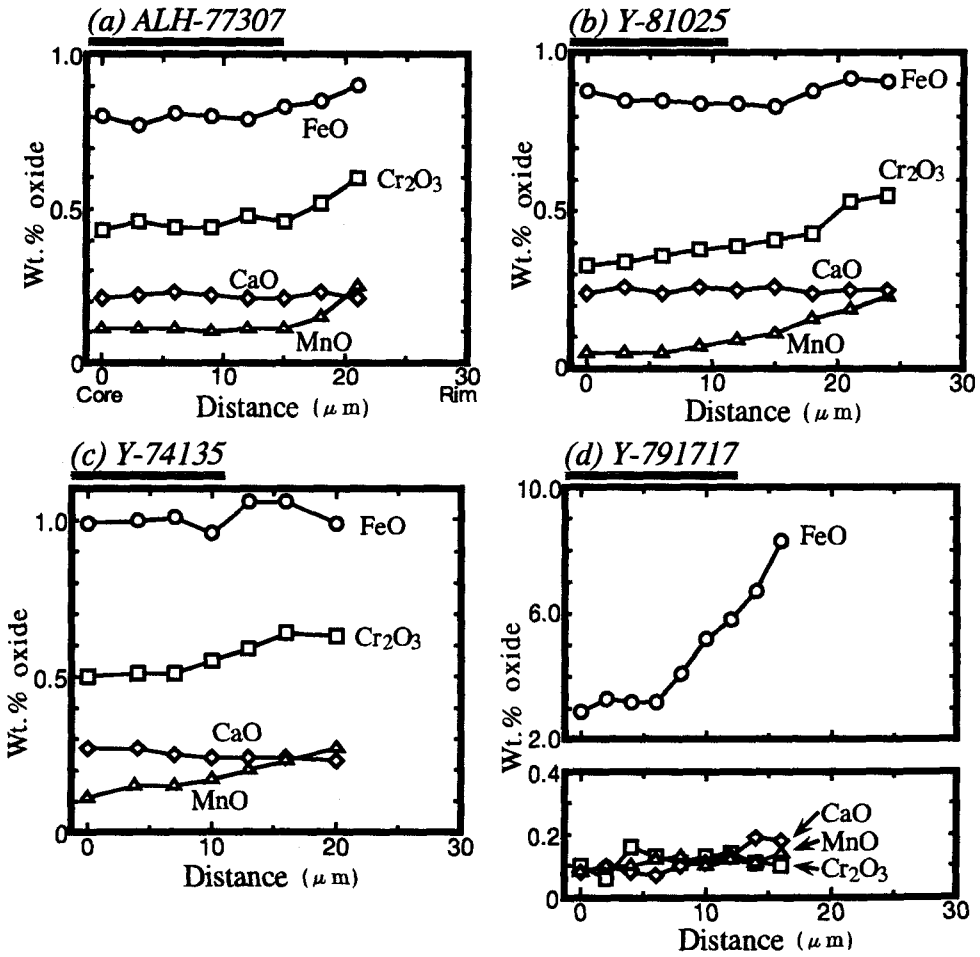


Fig. 1. Zoning profiles for FeO, $Cr_2O_3$, CaO and MnO taken from core to rim of olivine grains in type IA chondrules in ALH-77307, Y-81025, Y-74135 and Y-791717.

# Nitrogen isotopic compositions of some gas-rich chondrites

Naoji Sugiura , Kaoru Kiyota and Shigeo Zashu
Department of Earth and Planetary Physics, Univ. of Tokyo, Japan

## Introduction

Determination of isotopic compositions of volatile elements in the solar wind is quite important, because the solar wind is supposed to represent the bulk solar composition which in turn represents the whole solar system. The isotopic composition of nitrogen of the solar wind, detected in lunar soil samples is quite variable ranging from -200 permil to +200 permil (Kerridge,1993). The cause of the variation is not well known. Gas-rich meteorites are another valuable source of information on the solar wind compositions. We reported (Sugiura and Zashu, 1994) that a gas-rich chondrite (ALHA77216) has isotopically heavy nitrogen and suggested that it is solar nitrogen. It was recognized, however, that the heavy nitrogen was enriched in the magnetic fractions, and the abundance relative to solar rare gases is higher than that in the lunar soil samples. Thus, the nitrogen (and rare gases) in the ALHA77216 could not be unprocessed solar nitrogen, and there remained possibilities that the heavy nitrogen could be, e.g. presolar or indigenous nitrogen.

Here, we report the results of our new measurements of the isotopic compositions of nitrogen and rare gases on four gas-rich chondrites and comparison is made with the previous results on ALHA77216.

## Experimental Procedures

The chondrites we examined are Weston (H4), ALHA77278 (LL3.7), Yamato82133 (H3) and LEW86018 (L3.1). Nitrogen, neon and argon were extracted from samples of about 50 mg by a stepped combustion method. The details of the extraction and the mass-spectrometry have been published elsewhere (Hashizume and Sugiura, 1990; Sugiura and Hashizume,1992).

## Results

### Neon

Our results on solar neon in Y82133, ALHA77278 and LEW86018 are not of good quality mainly because the abundances of the solar Ne are small. In the case of Weston, solar Ne is the dominant component, and the isotopic composition and the abundance can be determined fairly precisely. In Fig.1 release patterns of the solar Ne are shown for the four chondrites and compared with the data for a bulk sample of ALHA77216. It can be seen that the abundance in Weston is by far the largest among the four samples although it is not as high as that in ALHA77216. The release patterns of the solar Ne from Weston and ALHA77216 are not grossly different although solar Ne is released in a

wider range of temperature from the ALHA77216. But the $^{20}Ne/^{22}Ne$ of the Weston is definitely higher than that of ALHA77216 (Fig.2). It has been suggested that the high isotopic ratio $^{22}Ne/^{20}Ne$ may mean that the Weston had been exposed to the solar wind long ago (Becker and Pepin, 1991).

## Argon

An interesting feature common to the present gas-rich chondrites (except for Y82133) is the release of $^{40}Ar$ at relatively low (600C) temperatures (Fig.3). Such early release of $^{40}Ar$ is also observed for other gas-rich chondrites, Feyetteville (Wieler et al., 1989) and PCA91002 (Sugiura and Zashu, 1995). Since K containing minerals are not oxidized at such low temperatures, the release is likely to be mainly due to diffusion. The dominance of low temperature release from gas-rich chondrites is probably attributed to the fine grain-size of these chondrites as a result of gardening processes on the parent bodies.

The release patterns of trapped $^{36}Ar$ are shown in Fig.4. The patterns are quite variable from one sample to another, but a couple of features can be recognized. If the abundances of solar Ne and solar Ar are proportional at a ratio (similar to that of solar abundances) observed in many gas rich meteorites, then the contribution of the solar Ar to the observed Ar contents can be considered to be negligible in the cases of Yamato82133, ALHA77278 and LEW86018 and the trapped Ar in these chondrites could be mostly primordial Ar. It is, however, possible that the solar Ne has been mostly lost but solar Ar has been retained due to slower diffusion. If this is the case, then a part of the trapped Ar could be solar Ar. The release pattern for the Yamato82133, which is characterized by a prominent peak at 800C with an additional peak at 1100C is quite similar to that from the ALHA77214 (Sugiura and Hashizume,1992) which is a non-gas-rich chondrite. The Ar in the ALHA77214 seems to be associated with isotopically anomalous nitrogen which was suggested to be possibly carried by presolar grains. The same pattern has been observed for several primitive ordinary chondrites (our unpublished data) and the carrier seems to be widespread among ordinary chondrites. Thus we consider that the peak of Y82133 is also due to this primordial (possibly presolar) Ar but not due to solar Ar. The 700-800C Ar release peaks of LEW86018 and of ALHA77278 are also considered to be due to the same primordial Ar but not due to solar Ar. The peaks at 1100C for these chondrites are higher than that of Y82133 and are not likely due entirely to primordial Ar. Since this is the temperature where ALHA77216 released Ar which is considered mostly due to SEP Ar (Sugiura and Zashu,1994), it is possible that these peaks in the release profiles of LEW86018 and ALHA77278 are also due mostly to SEP Ar.

In the case of Weston, solar Ar is considered to be the dominant component. The Ar release pattern is considered to be tri-modal. A

possible interpretation may be that the low temperature release peak is due to SW Ar, the peak at the intermediate temperature (about 900C) is due to solar (probably SEP) Ar, and the highest temperature (1200C) release peak is due to trapped Ar.

## Nitrogen

Release patterns of nitrogen are shown in Fig. 5, and the isotopic compositions are shown in Fig. 6. The nitrogen released below 600 C is dominated by terrestrial organic nitrogen whose delta$^{15}$N is about 15 permil. According to the previous study on ALHA77216, isotopically heavy nitrogen which is considered to be solar nitrogen is mainly released from 700C to 1100C. The release of these two components are somewhat overlapped. In Figs. 5 and 6 it is seen that the abundances of released nitrogen are rather small for ALHA77216 and Yamato82133 in this intermediate temperature range between 700 C and 1100C, and the maximum delta $^{15}$N values are higher than 100 permil. For the rest of the samples, in the same temperature range, the abundances of nitrogen are higher and the delta $^{15}$N values are less than 100 permil. The anti-correlation between the abundance and the delta $^{15}$N value can be explained as due to dilution of isotopically heavy (solar) nitrogen by isotopically nearly normal nitrogen which could be either indigenous or terrestrial contamination. At least qualitatively all the results (except for the Weston) in the intermediate temperature range are consistent with the above interpretation. We are not sure why Weston behaves differently from the other gas-rich chondrites. Figs. 5 and 6 show that Weston contains isotopically heavy (solar) nitrogen which is somehow released at 1100- 1200C.

## Conclusions

Nitrogen, neon and argon isotopic compositions of four gas-rich chondrites (one of which is only marginally gas rich) were measured. Together with a previously studied gas-rich chondrite, all gas-rich chondrites that we examined have isotopically heavy nitrogen. Thus, we suggest that the solar nitrogen is isotopically heavy. The abundance of the heavy nitrogen is, however, not proportional to that of the solar neon, suggesting complex processing on the surfaces of the parent bodies.

## References

R.Becker and R.O.Pepin (1991) Earth Planet. Sci. Lett. 103, 55-68.
J.F.Kerridge (1993) Rev. Geophysics, 31,, 423-437.
K.Hashizume and N.Sugiura (1990) Mass Spectrom. 38, 269-286.
R.Wieler, H.Baur, A.Pedroni, P.Signer and P.Pellas (1989) Geochim. Cosmochim. Acta, 53, 1449-1459.
N.Sugiura and K.Hashizume (1992) Earth Planet. Sci. Lett. 111, 444-454.
N.Sugiura and S.Zashu (1994) Earth Planet. Sci. Lett. 125, 323-339.
N.Sugiura and S.Zashu (1995) Proc. NIPR Symp. Antarctic Meteorites, No8, in press.

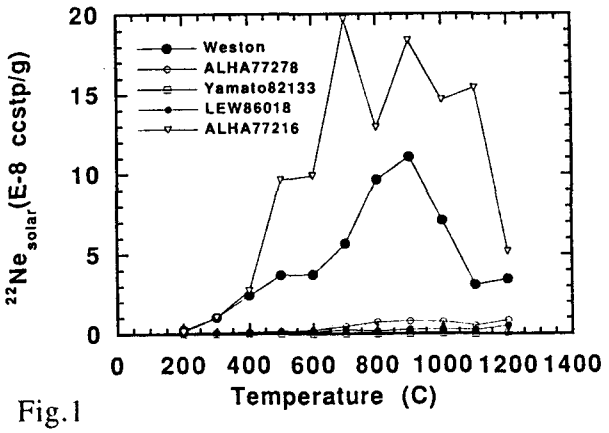


Fig.1

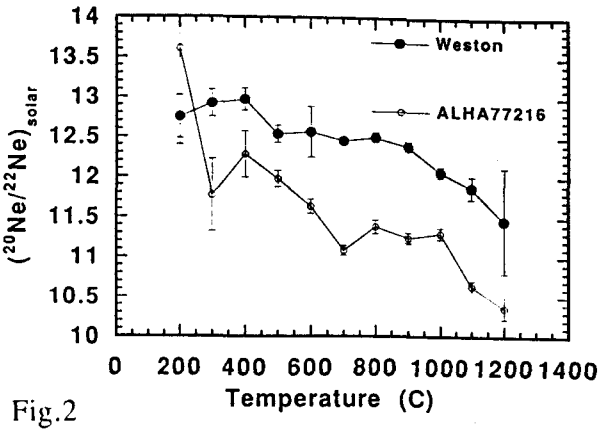


Fig.2

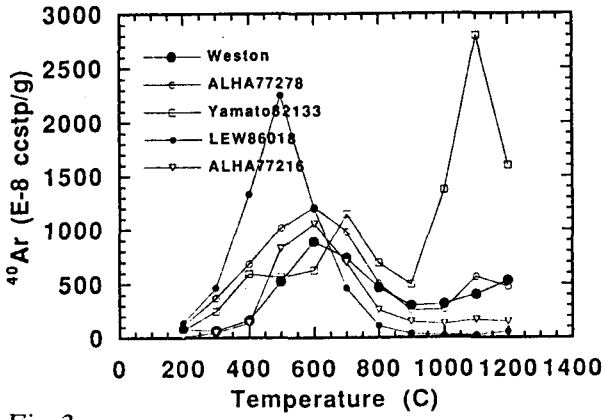


Fig.3

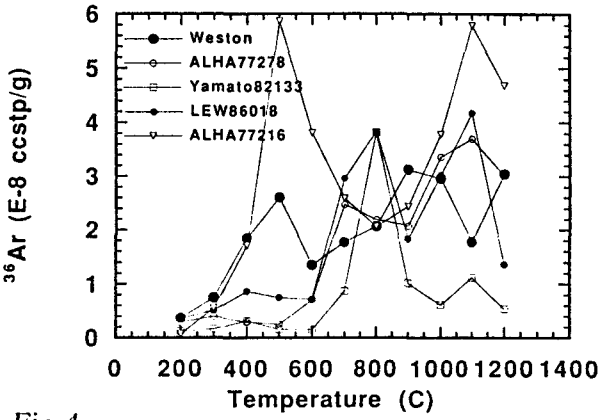


Fig.4

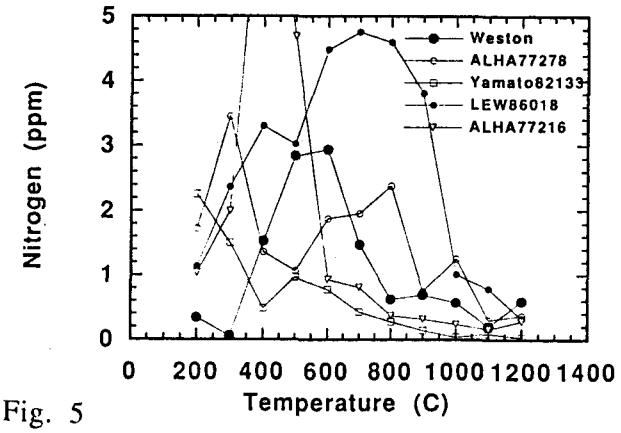


Fig. 5

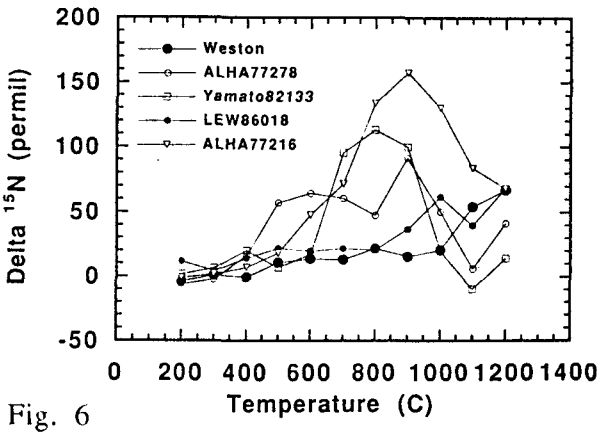


Fig. 6

SPHERULES IN THE LITTLE HUNGARIAN PLAIN

Szöőr, Gy. (Department of Miner. and Geol. Kossuth University, H-4olo. Debrecen, P.O.Box 4, Hungary).

A Microprobe system of Oxford Microbeams has been installed in the Institute of Nuclear Research of the Hungarian Academy of Sciences (ATOMKI), on one of the beamlines of the 5 MeV Van de Graaff accelerator. To identify and quantify the elements in the sample under investigation PIXYKLM programme package (Szabó et Borbély-Kiss, 1993) have been used.

Scanning proton microprobe, (SPM) as a complementary technique to electron probe microanalysis (SEM-EDAX) has been used for measuring elemental composition of spherules occuring in Upper Pannonian and Quaternary sediments.

By the continuous cores of borehole Nagylózs-1 (1325.2 m) Miocene, Pliocene and Quaternary sediments were uncovered in the western part of Little Hungarian Plain, NW Hungary.
In the Upper Pannonian layers which have accumulated continuously under moderate circumstances we have found tiny sphere and drop like, filament shape objects. They are amber to light brown smooth glassy objects of 3oo - 16oo um decorated with acicular vesicular or grains of crystal (chillcrystals), and they contain micro-bubbles of gas. On the basis of their normative composition, they are Ca rich ortho-silicate glasses bearing some accessories (Fe, Mn, Ti, Ba, K, Na, S, Ni, Nb, Zr, Sc, P, Cl).

The micro-bodies are supposed to be of extraterrestrial origin (Lunar impactite or Ca-rich micrometeorite?).

Magnetic spherules collected from the alluvial plain of Danube River in Hungary are very various in their morphology, chemical composition and their surface structure and texture. It is obvious because the natural enrichment of the materials from the surrounding area happened in this fluviatile basin.

On the basis of the researches three main genetic types were distinguished:

1. Meteoritic dust spherules and spheroids.
2. Impactite-globules.
3. Spheres of uncleared origin (igneous-metamorphic).

Reference.

Szabó, Gy. and I.Borbély-Kiss. 1993. PIXYKLM computer package for PIXE analysis. Nucl. Instr. Meth. in Phys. Res. B75. pp.123-126.

# Incongruent evaporation experiments on troilite (stoichiometric FeS)

TACHIBANA Shogo[1], TSUCHIYAMA Akira[1] and KITAMURA Masao[2]

[1]Department of Earth and Space Science, Osaka University, Toyonaka 560, JAPAN.
[2]Department of Geology and Mineralogy, Kyoto University, Kyoto 606, JAPAN

**Introduction.** Fe/S ratios of condritic meteorites are different from that of solar abundance. These differences indicate that Fe/S fractionation occurred in the primordial solar nebula. It is considered that such elemental fractionation is caused by evaporation or condensation processes. One of the possible processes for the Fe/S fractionation is incongruent evaporation of troilite in the primordial solar nebula. Tsuchiyama *et al.* [1] carried out incongruent evaporation experiments on pyrrhotite (non-stoichiometric FeS). However, experiments on troilite have not yet been done. In this study, incongruent evaporation experiments on troilite were carried out.

**Experiments.** It is difficult to obtain a large single crystal of troilite, which is common iron sulfide in the meteorites. To obtain troilite, pyrrhotite ($Fe_{0.886}S$, non-stoichiometric FeS) was heated with metallic iron powder at 950°C for 24 hours. The samples were about 3.0mm, 4.0mm, and 5.0mm thick. They were hung in a Pt-basket, and heated under $H_2$-rich conditions ($p(H_2)$=0.788-0.799atm) in a one atmosphere $H_2$-$CO_2$ mixing furnace at temperatures ranging 500°C-970°C for 1.0-67.25 hours. At 900°C, evaporation experiments on pyrrhotite ($Fe_{0.886}S$) were also carried out.

**Results.** Troilite evaporated incongruently to form iron residual layers on troilite crystals. The iron residue layer is spongy (generally a few μm) and porous (Figure 1(a)). There are roughly two types of the FeS surface (Figure 1(b)) ; one is the surface covered with metallic iron (type-(A)), and the other is the naked surface (type-(B)). It is seen from the BEI that the troilite near the type-(A) and -(B) surfaces are darker and brighter than bulk troilite, respectively.

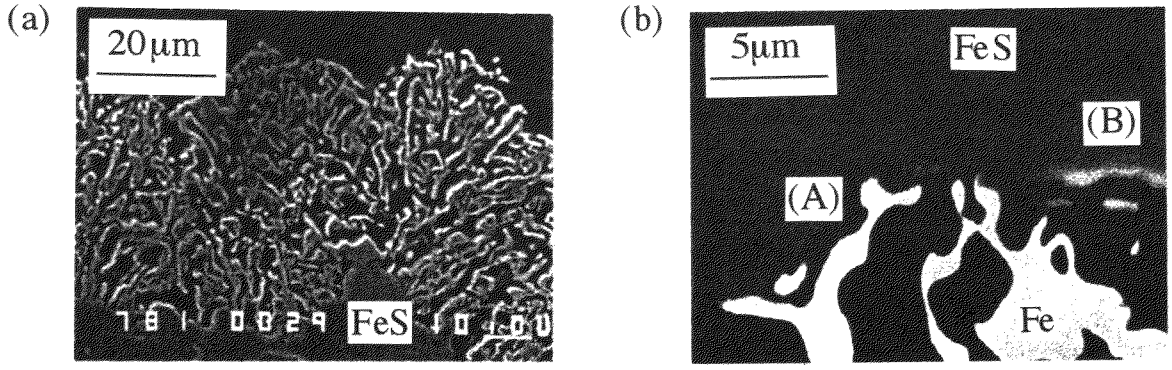


Figure 1. SEM micrographs of run products. (a) An SEM image of the iron residue layer at 600°C,16hr. (b) A BEI image of the Fe-FeS interface at 970°C, 2hr. Two patterns of the interface can be observed.

The thickness of the iron residual layer of run products, X(Fe), are plotted against time, t (Figure 1). It is reported that pyrrhotite evaporates incongruently to form metallic iron residue following a linear rate law ($X(Fe) = k_{FeS}t$) [1]. Similar results were observed in the present experiments. The linear rate constant, $k_{FeS}$, shows Arrhenius relation ; $k_{FeS}=1.94\pm0.18\times10^{-3}$[m/sec] exp (-106 ±1 [kJ/mol] /RT).

The present values of $k_{FeS}$ are larger than those of pyrrhotite [1] by two or three times. This difference is due to the difference of the experimental method. The samples were put into an alumina crucible in the previous experiments [1], while they were put into a Pt-basket to react directly with the gas in the present experiments. Indeed, the present experiments on pyrrhotite at 900°C show that the value of $k_{FeS}$ of troilite and that of pyrrhotite are almost same within an analytical error.

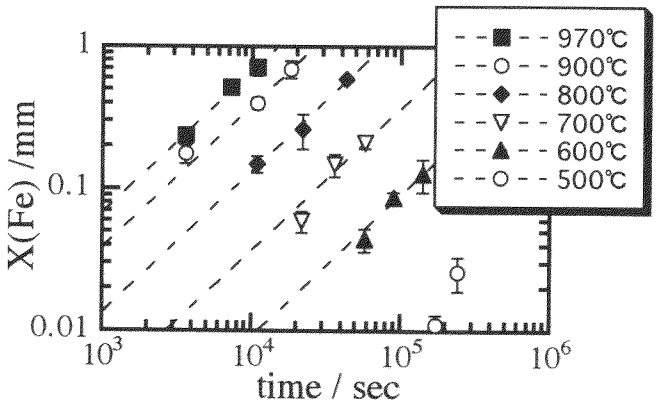


Figure 2. The thickness of the iron residual layer of run products, X(Fe), are plotted against time,t. X(Fe) increases in proportion to time at constant temperatures.

**Discussion.** Due to the formation of the porous Fe residues, incongruent evaporation of troilite is considered to obey a linear late law. In other words, the evaporation reaction is mainly controlled by the reaction at the Fe-FeS interface. The BEI shows that Fe is depleted or S is enriched near the type-(A) surface, while Fe is enriched or S is depleted near the type-(B) surface (Figure 1(b)). Incongruent evaporation on troilite to form porous Fe residues can be explained by the following mechanism. Sulfur near the type-(A) surface (S-rich) diffuses to the type-(B) surface (S-poor) and evaporates. By the evaporation of S from FeS, Fe is enriched near the type-(B) surface. Fe near the type-(B) surface (Fe-rich) diffuses to the type-(A) surface (Fe-poor), and the Fe residues grow. By the growth of Fe from FeS, S is enriched near the type-(A) surface and diffuses towards the type-(B) surface again.

The evaporation rate of sulfur from FeS, J(S/FeS), is expressed by using $k_{FeS}$ :

$$J(S/FeS) = \frac{N_A}{\Omega_{FeS}} k_{FeS} \quad , \tag{1}$$

where $\Omega_{FeS}$ is the molar volume of FeS, and $N_A$, the Avogadoro number. If we assume that $H_2S$ molecules are formed by the incongruent evaporation of FeS, J(S/FeS) can be calculated from Hertz-Knudsen equation :

$$J(S/FeS)_{calc.} = \frac{\alpha_{FeS} K_{FeS} p(H_2)}{\sqrt{2\pi m_{H_2S} kT}} \quad , \tag{2}$$

where $\alpha_{FeS}$ is the evaporation coefficient of FeS, $p(H_2)$, the partial pressure of $H_2$, $m_{H2S}$, the mass of the $H_2S$ molecule, and k, the Boltzmann constant. $K_{FeS}$ is the reaction constant of the reaction, $FeS(s) + H_2(g) \rightarrow Fe(s) + H_2S(g)$. The value of $K_{FeS}$ can be calculated by the thermochemical data [2]. When the value of $\alpha_{FeS}$ is equal unity, the evaporation process occurs under ideal conditions without any kinetic constrains. The measured J(S/FeS) were compared with the calculated J(S/FeS) with $\alpha_{FeS}$=1 (Figure 3). The values of $\alpha_{FeS}$ which were obtained in the present experiments are much smaller than unity ($3.88 \times 10^{-4}$ to $1.54 \times 10^{-5}$ at 970°C to 500°C). The small $\alpha_{FeS}$ values could be due to Fe-S interdiffusion near the FeS surfaces. As the present experiments were carried out at 1atm, transportation processes of $H_2S$ molecules in the surrounding gas phases may also reduce the values of $\alpha_{FeS}$.

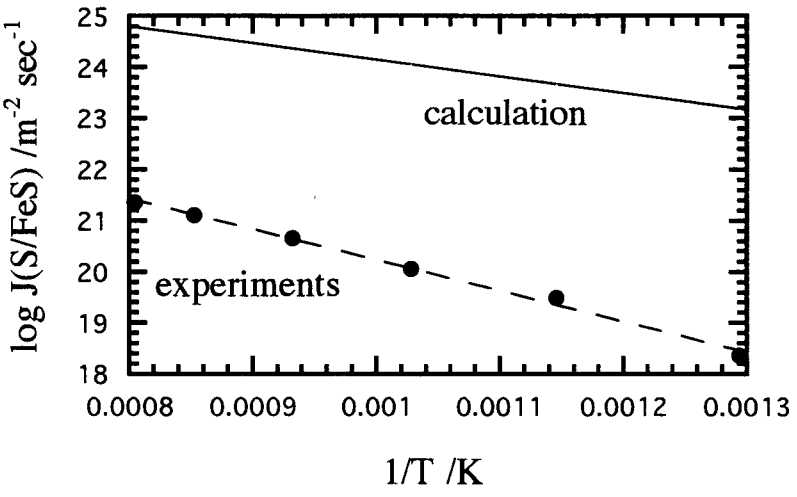


Figure 3. An Arrhenius plot of the evaporation rate of sulfur from FeS. J(S/FeS). The calculated $J(S/FeS)_{calc.}$ ,with $\alpha_{FeS}=1$, is shown as a solid line.

**References.**

[1] Tsuchiyama, A., C.Uyeda and Y.Makoshi, An experimental study of evaporation kinetics of FeS, and its cosmochemical significance,*18th Symp. Antarctic Meteorites (abstract)*, 121-124, 1993

[2] JANAF Thermochemical Tables, 2nd Ed., pp.1141, National Bureau of Standards, U.S.A., NSRDS-NBS37, 1971.

# Alteration of Coarse grained CAI in Allende meteorite

Hajime Takeda

Department of Polar Science, The Graduate University for Advanced Studies,

National Institute of Polar Research, Kaga 1-9-10, Itabashiku, Tokyo 173, Japan

CV chondrites have kept a lot of primary petrographic, chemical features because they are experienced little metamorphism and hydrous-alteration on their own parent bodies. Therefore, detailed study for this group is important to obtain information of early solar system. Especially, CAI's are considered to give us the knowledge in the earliest stage because they consist of minerals formed at the highest temperature, such as perovskite, spinel, and melilite. CAI's in carbonaceous chondrites are classified based on their mineral assemblages into three types; melilite rich type A's, fassaite and spinel rich type B's, and plagioclase rich type C's. Most CAI's, particularly type A's, were heavily altered in the latter stage, and alteration products such as nepheline, sodalite were observed in them.

We found a large CAI from Allende, and named this CAI "T4-CAI1". We present its petrographic, chemical feature, and discuss the alteration process.

The thin section "No. T-4" is 1.0cm × 1.5cm in size, and includes many chondrules relatively large in size (~2 mm) and a very large CAI (T4-CAI1). T4-CAI1 exists through across this thin section from end to end with 2-3 mm in width(Figure 1). Back-scattered electron (BSE) image shows that T4-CAI1 is composed of many brecciated fragments. Fine grained materials fill up interstice of these fragments. These fine grained materials are clearly distinguished into two kinds of components from their textures and mineral assemblages. One consists mainly of melilite, spinel, Al-rich pyroxene, and the other consists mainly of Fe-rich olivine. The former is considered to be the fragments derived from same large CAI because of their similarities in textures and mineralogy, while the latter seems to be matrix of the host meteorite.

Relatively larger fragments of T4-CAI1 are divided into three portions from the texture; core, mantle, and rim. The core consists of coarse grained melilite. In rare case, melilite crystals enclose amoeboidal spinel. The mantle consists of relatively fine grained minerals than those of the core. The mantle is subdivided into three types; type I consisting of melilite and spinel, type II consisting of melilite, Al-rich pyroxene, and

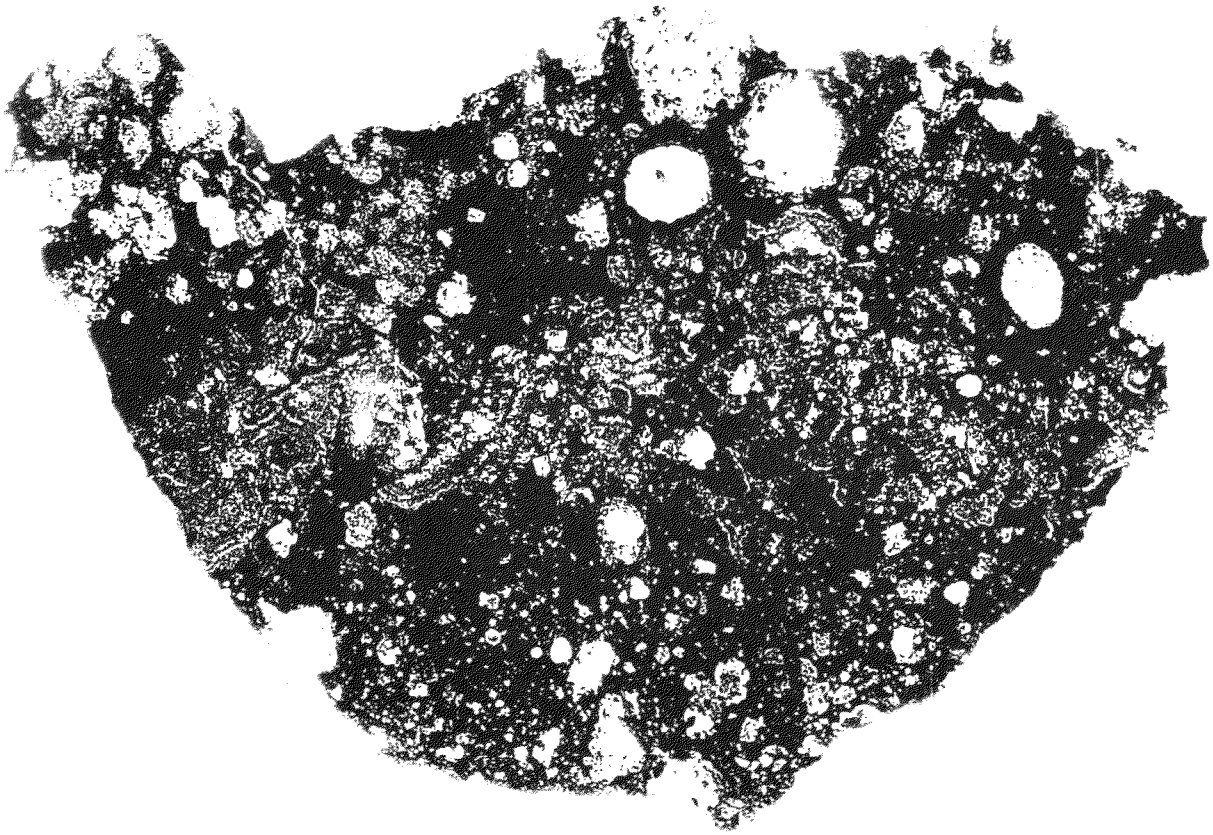

Figure 1 The photo of the thin section "T-4". T4-CAI1 exists through across the center of this thin section from right to left. 1cm×1,5cm in size.

spinel, type III consisting of Al-rich pyroxene and spinel. The rim is considered to be located along the original margin of pre-brecciation stage of the CAI and divided to inner rim and outer rim. The inner rim consists of Al-poor pyroxene (diopside), and the outer rim consists mostly of hedenbergite. In rare case, wollastonite is enclosed by hedenbergite. This rim texture is similar to an outer part of the rim sequence on type A CAI's in Allende described by Wark and Lovering (1977) in their mineral assemblages.

Melilite contain up to 20 mol% of akermanite component. Individual grain of melilite shows reverse zonation; the margin of the grain is richer in gehlenite component than the core of the same grain. However, there is no relationship between their occurrences and chemical compositions. These chemical features of melilite are resemble to those of melilite in fluffy type A CAI's (FTA's) in Allende meteorite mentioned by MacPherson and Grossman (1984).

Pyroxene in the mantle is usually rich in Al and Ti, on the other hand pyroxene in the rim is relatively poorer in these elements than in the mantle. The mantle's pyroxene contain 20~27wt.% of $Al_2O_3$ and 10~20wt.% of $TiO_2$. Ti in these pyroxenes is assumed to contain large amounts of $Ti^{3+}$. Most of rim's pyroxene contain up to 4wt.% of $Al_2O_3$ and 1wt.% of $TiO_2$.

Spinel in the core contain little amounts of Fe, though spinel in the mantle is relatively rich in Fe. Although MacPherson and Grossman (1984) have shown that some iron-rich spinels in FTA's contain up to 4.91wt% of $V_2O_3$, V-rich spinel is not found in this CAI (up to 0.27wt% of $V_2O_3$).

In this CAI, especially in the mantle, melilite is replaced by grossular, anorthite, and feldspathoids. Melilite in the fragments that contain the type I or II mantle are altered relatively weak, and the alteration products are usually grossular and anorthite. But in fragments that contain type III mantle have been heavily altered, and melilite is replaced by alteration products that are not only grossular and anorthite but also nepheline, in some cases also sodalite. These facts indicate two stages of alteration. Melilite was replaced by grossular and anorthite first. In the second stage, anorthite altered into nepheline and/or sodalite.

**Reference**; MacPherson G. J. and Grossman L. (1984) *Geochim. Cosmochim. Acta 48,* 29-46. Wark D. A. and Lovering J. F. (1977) *Proc. Lunar Sci. Conf. 8th,* 95-102.

# RECORDS OF CRUSTAL EVOLUTON IN SOME ANTARCTIC EUCRITES

Hiroshi Takeda, M. Otsuki, T. Mikouchi and M. Miyamoto
*Mineralogical Institute, Faculty of Science, University of Tokyo*
*Hongo, Tokyo 113, Japan.*

## Introduction

Among three calsses of the HED achondrites, eucrites are abundant and many of them are brecciated and metamorphosed products in their early history [1]. On the basis of the degree of homogenization of their pyroxenes, they are mostly type 5 and 6 eucrites [2], which have been called ordinary eurites [3]. The ordinary eucrtes are monomict breccias composed of pigeonites with exsolution and homogeneous Fe/Mg distribution and plagioclase with chemical zoning [3].

Nyquist et al. [4] proposed a hypothesis that these ordinary eucrites could have been produced at or near the floor of an impact crater. The recent dicovery of an asteroids having basaltic spectral signatures [5] supports the suggestion that this original parent body was the ~520 km diameter asteroid 4Vesta. Now, the information of the eucrites will be useful for a better understanding of the crustal evolution of the Vesta-like body.

During the studies of thermal and impact cratering history of the four Yamato Antarctic monomict eucrites, we found that Y74356 is a recrystallized clastic matrix similar to lunar granulitic breccias [6]. Y74356 was also compared with other typical monomict eucrites, Y792510 and Y791186. They reported that no granuritic area was detected, but pyroxene crystals at some grain boundaries and matrices are fractured to small granular grains without evidence of recrystallization.

In this paper, we reinvestigated these granular grains in new polished thin sections of Y792510 and compared them with granoblastic pyroxene (GP) areas of Juvinas by mineralogical techniques. we interprete the origin of the GP areas in conjunction with the crustal evolution of the eucritic protocrust in the early solar system, and propose that an importance of impact cratering techtonics for the crustal evolution of the HED parent body and 4Vesta.

## Samples and Analytical Techniques

We have studied four polished thin sections (PTS) , Y792510,62F3 and ,89-9 and Juvinas 40CL1 and 40E1a2. The presence of augite in Juvinas has been detected by the BEI (back scattered electron image) of JEOL 840A SEM of our Institute. The chemical analyses of minerals were made using JEOL 733 electron probe microanalyser (EPMA) at the Ocean Research Institute and JEOL 8600 Super Probe at Geological Institute, University of Tokyo. The augite lamella width and interval were measured by line analyses of the EPMA for 1-3 μm intervals.

## Results

*Y792510.*

PTS ,62F3 is 10.2 × 5.9 mm in size and shows a less brecciated texture of subophitic basalt than other previously studied PTSs (e.g. ,62F2). Lath-shaped plagioclase crystals (up to 1.5 × 3.7 mm in size) are set in pyroxene crystals or dark comminuted matrices. At some areas bounded by plagioclase lathes, a pyroxene

crystal is decomposed into small grains (ca. 0.1 mm in diameter) of different orientations. This texture is similar to that of GP areas of Juvinas as described below. The grain boundaries are more like fractures and a few dusty inclusions are still left.

PTS ,89-9 looks brecciated but the matrix with well difined fragments cannot be recognized. Therefore, it is difficult to find whether the matrix was recrystallized or annealed. A pyroxene crystal with coarser exsolution lamellae are found in a neighbor of the GP area bounded by two pyroxene lathes (Fig. 1a). The width of the lamellae in the core is thicker (up to 10 μm) than those of Juvinas and their spacings are wider (up to 50 μm) and the width is finer (1 to 3 μm) at the rims and the lamellae are closely spaced (less than 5 μm). The lamellae are slightly off set by a shock event. The bulk chemical composition of the core is $Ca_{8.6}Mg_{35.4}Fe_{56.0}$ and that of the rim is $Ca_{21.8}Mg_{33.5}Fe_{44.7}$, suggesting that the original crystal was chemically zoned. The clear GP crystals $Ca_{4.6}Mg_{35.9}Fe_{59.6}$ have lower contents of CaO 2.0, $Cr_2O_3$ 0.02, $Al_2O_3$ 0.2, $TiO_2$ 0.1 wt % than the bulk core pigeonite (CaO 3.9, $Cr_2O_3$ 0.4, $Al_2O_3$ 0.4, $TiO_2$ 0.37 wt %). The lamella augite $Ca_{44.4}Mg_{29.1}Fe_{26.6}$, is high in the Wo content. This feature is the same as that found in Y791186. Because parts of the host pigeonite are inverted to orthopyroxene optically, these eucrites were classified as a type 6 basalt [2]. The host composition of the exsolved pyroxene ($Ca_{1.8}Mg_{36.3}Fe_{61.9}$) is not much different from those of the granulitic one ($Ca_{1.7}Mg_{36.5}Fe_{61.8}$). One crystal in the GP area still have a remnant of the original coarse exsolution lamellae (Fig. 1b).

*Juvinas.*

The GP area of Juvinas consists of fine-grained polygonal clear crystals with fine exsolution lamellae of augite on (001). The width of the lamella is often coaser than those in the large pyroxenes and the clouding common in the Juvinas pyroxene are disappeared, but coarser opaque minerals (chromite and troilite) are found in the GP area. The GP area is generally found in a part of large single crystal bounded by lathes of plagioclase near the grain boundaries.

The presence of a few augite grains in the interstices of the granoblastic clear pigenites with fine augite exsolution lamellae has been deected in the GP area in the BEI of the SEM of sample 40CL1 (Fig.2a,b). The intervals of the lamellae and the bulk compositions of the paired pigeonite $Ca_{4.9}Mg_{39.6}Fe_{29.9}$ and augite $Ca_{40.2}Mg_{32.5}Fe_{27.3}$ were determined by EPMA.

Our new observation of the Juvinas texture includes two features. The area with acicular plagioclase and that with granoblastic texture were found in separate places in our previous studies. Now we found a pyroxene with the GP area at one end is penetrated by acicular plagioclase at another end. In another crystal, we found that a few fine pyroxene crystals in the GP area has the same orientation as that of the adjacent unaltered original single crystal, as judged from the same orientation of augite lamellae and the same extinction angle.

**Discussion**

The new observations of Y792510 and Juvinas show that the GP areas were produced in solid state from parts of the single crystal by a cratering event, because the original ophitic texture was preserved. The clear crystals in the GP area low in chromium etc. and the presence of coaser chromite crystals in the GP area are in agreement with this interpretation. However, the presence of the augite grains in the

GP area suggests that the temperature was high enough to grow such crystals and annealed after such event. The facts are in line with a picture in that the cratering event took place while the materials were hot.

Since all possible isotopic ages have been determined by Nyqust et al. [7] and Bogard et al. [in 7] , we are in a position to discuss a possible sequence of events recorded in the various textures observed in the PTSs of Y792510.

(1) Crystallization of coase-grained plagioclase and pigeonite.
(2) Thermal annealing to produce clouding and homogenization of Fe/Mg in pyroxene
(3) A shock event to make a monomict breccia and the GP area and the second stage cooling.
(4) Another shock event to produce the shock glassy veins in the matrix.

Event (1) took place at 4.64 Ga ($^{147}$Sm-$^{143}$Nd technique). Events (2) and (3) may be closer to 4.45 Ga ($^{146}$Sm-$^{142}$Nd). The Ar-out-gassing age of 3.45 Ga may represent event (4). The young Rb-Sr age (2.85 Ga) is an event difficult to explain.

The heat source which homogenized the type 5 and 6 eucrites has been a subject of contravercy. Internal heating is much easier heat source to covert a large mass of monomict breccia into a homogeneous rocks. However, we should not underevaluate the fact that the brecciation also took place in conjunction with the thermal homogenization. The present study also presents an evidence that the GP areas may have been produced by a shock event at high temperature.

Saiki [10] pointed out that the eucritic magma crystallizing diogenitic pyroxene at the bottom can be solidified as a scarf-like protocrust [11]. Hartman [12] pointed out that if a magma ocean existed, then its initial cooling was marked by a period of pre-lithospheric chaos in which impacts punched through the initially thin rocky skin, mixing rock fragments with splashed magma. Furthermore, his results show that intense brecciation and pulverization of rock materials must have occured to a depth of at least ten of kilometers in the first few hundred years of lunar history.

The bombardments into the eucritic protocrust were not as intense as in the lunar case, but it is possible to postulate that a cratering episode of the protocrust on the hot magma ocean [Fig. 1 in 11] is a good model compatible with the present observation. Such model should be investigated in future. The old recrystallization age of Juvinas [8,9] and Y792510 may be in line with such a hypothesis that the metamorphism took place by cratering of the protocrust on an evolving thin magma ocean as we invoked previously [11] and in this paper.

We thank NIPR and Paul Pellas in Paris for the samples and L. Nyquist for discussion.

**References:**

[1] Yamaguchi A., Takeda H., Bogard D. D., and Garrison D. H. (1994) *Meteoritics* 29, 237-245.
[2] Takeda H. and Graham A. L. (1991) *Meteoritics* 26, 129-134.
[3] Takeda H., Miyamoto M., Duke M. B., and Ishii T. (1978) *Proc. Lunar Sci. Conf. 9th*, 1157-1171.
[4] Nyquist L. E., Takeda H., Bansal B. M., Shih C.-Y., Wiesman H., and Wooden J. L. (1986) *J. Geophys. Res.* 91, 8137-8150.
[5] Binzel R. P. and Xu S. (1992) *Science* 260, 186-191.

[6] Yamaguchi A. and Takeda H. (1995) *Proc. NIPR Symp. Antarct. Meteorites* 8, in press.
[7] Nyquist L. E., Takeda H. Bogard D. D., Bansal B. M., Wiesmann H. and Shih C.-Y. (1995) *Lunar Planet. Sci.* 25, 1063-1064.
[8] Takeda H., Yamaguchi A., Kaneoka I. and Nagao K. (1995) in preparation.
[9] Kaneoka I., Nagao K., Yamaguchi A. and Takeda H. (1995) *Proc. NIPR Symp. Antarct. Meteorites* 8, in press.
[10] Saiki K. (1995) *Doctoral dessertation Univ. of Tokyo.*
[11] Takeda H. (1995) *Journ. of Geograph* (in Japanese) 104, 799-808.
[12] Hartman W. K. (1980) *Proc. Conf. Lunar Highland Crust*, Papike J. J. and Merrill R. B. eds. p. 155-171.

***(a)*** ***(b)***

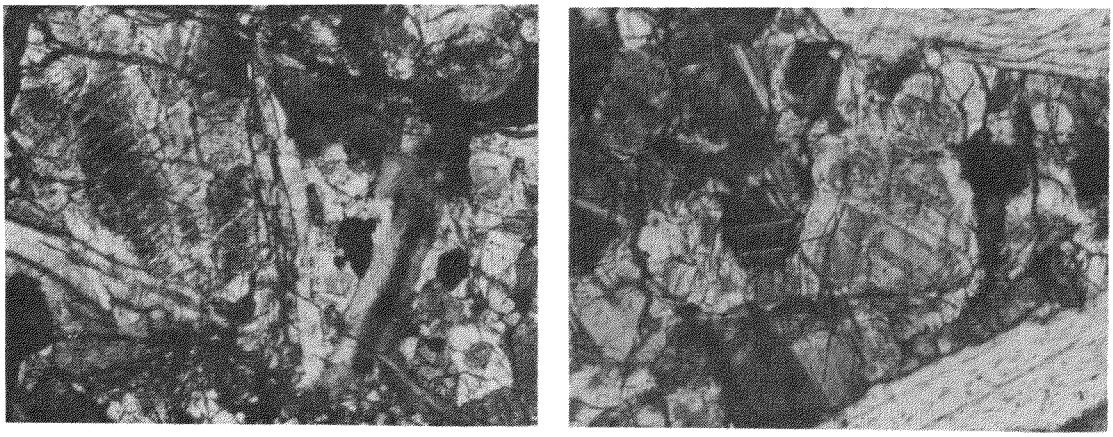

Fig. 1. Photomicrographs (cross polar) of Y792510 showing a pyroxene with thick exsolution lamellae and the granoblastic pyroxene (GP) area bounded by two plagioclase lathes. (a) Entire view. Width is 1.2 mm. (b) Enlarged portion of the GP area with a small pyroxene grain with thick exsolution lamellae. Width is 0.5 mm.

***(a)*** ***(b)***

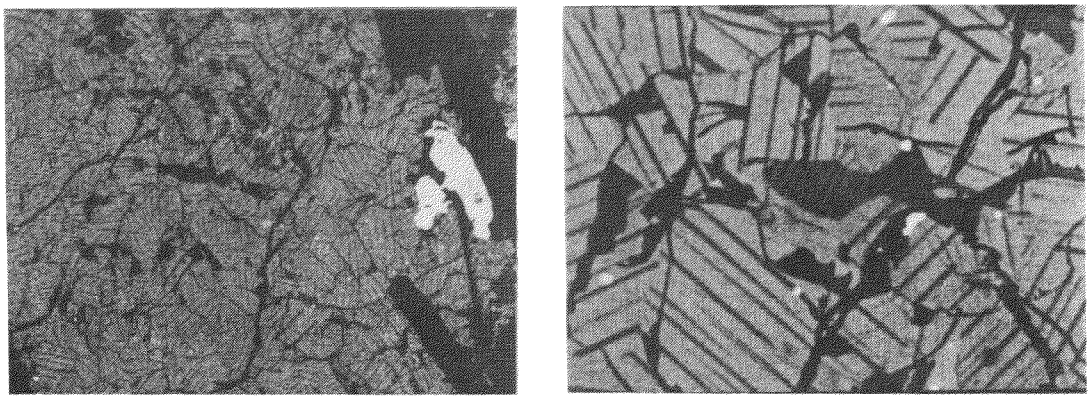

Fig. 2. BEI of the GP area of a pigeonite in Juvinas. (a) Entire view. (b) Enlarged portion with the augite grain. Gray area in the center is augite.

# EPMA AND TEM STUDY ON MATRIX MINERALOGY OF ALLENDE(CV3)

H.Tanaka* and J.Akai**

*:Department of Graduate School of Science and Technology Niigata University, Ikarashi 2-8050, Niigata 950-21, Japan

**:Department of Geological Science, Faculty of Science Niigata University, Ikarashi 2-8050, Niigata 950-21, Japan

In the matrix of Allende meteorite chondrules, and inclusions are contained. Isolated minerals in the matrix also occur. Many studies on matrix, and isolated and chondrule mineral grains of Allende(CV3) meteorite have been reported(J.A.Peck 1984, A.S.Kornacki and J.A.Wood 1984, J.A.Peck and Wood 1987, A.E.Rubin and J.T.Wasson 1987). The isolated minerals are regarded as fragments of chondrules and inclusions. Large isolated minerals can be observed under the polarizing microscope. However, small isolated minerals which can not be observed by polarizing microscope are also expect to occur as matrix constituent minerals. So, it is, in general, difficult to distinguish matrix minerals form isolated minerals and tentative classification is here applied.

In EPMA analyses, the followings were found : A typical olivine grain in the matrix is often acicular in shape and is about 3x15 μm in size although the shape depend on cutting direction. The chemical composition of the matrix olivine is homogeneous(Fo 50-55%). On the other hand, olivine grain of isolated mineral has variable size ranging from several μm to several hundreds μm and was irregular in shape. Most isolated olivine grain shows zoning pattern(core:Mg-rich, rim:Fe-rich). The chemical composition of olivine as isolated mineral has ranged from 100% to 50% in Fo component. Degree of zoning is various and core of the olivine reaches 50% in Fo component. Fig. 1 shows the compositions of matrix olivine grains and olivine grains as isolated minerals respectively although the distinction of the two types are not so strict but are tentative based only on shapes and sizes.

It was difficult to distinguish the matrix mineral grains from the other grains such as isolated minerals clearly. So we examined matrix materials by TEM-AEM method.

In TEM observation two type of olivine grains were observed ; The one is smaller olivine grains and the other is larger olivine crystal. The

former may be matrix olivine grains. The latter may be isolated mineral grains, inclusion grains or chondrule grains. The AEM results of the both types were consistent with the EPMA result. Olivine grains, especially the latter type olivine grains contains irrgular-sheped voids and is defective in its structure. Fig. 2 shows the TEM image of this latter type of olivine grains. Fig 3 shows the olivine grains of matrix which also shows a defective structure. On the other hand, enstatite grain which has stacking disorder of cpx and opx were also found. This grain was in contact with less defective olivine grain(Fig.4).

References

Kornacki ,A.S and Wood,J.A.(1984) GCA vol.48 pp.1663-1676
Peck,J.A.(1984) Lunar Planet Sci. XV, 635-636
Peck,J.A. and Wood,J.A.(1987) GCA vol.51 pp.1503-1510
Rubin,A.E. and Wasson,J.T.(1987) GCA vol.51 pp.1923-1937

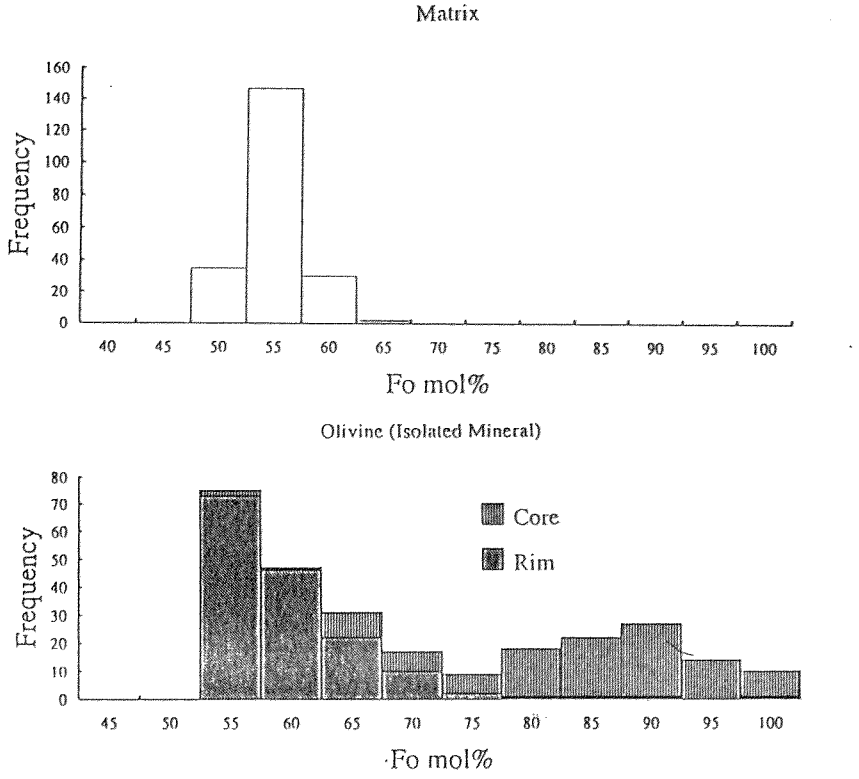


Fig. 1. Histogram of forsterite(Fo) content of olivine of (a)matrix grains and (b)isolated mineral grains.

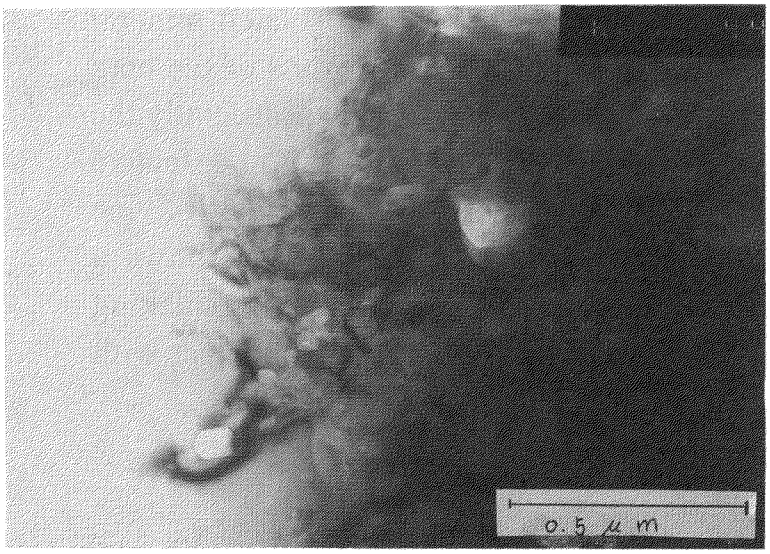


Fig.2 TEM image of larger olivine crystal. Characteristic void textures are often found.

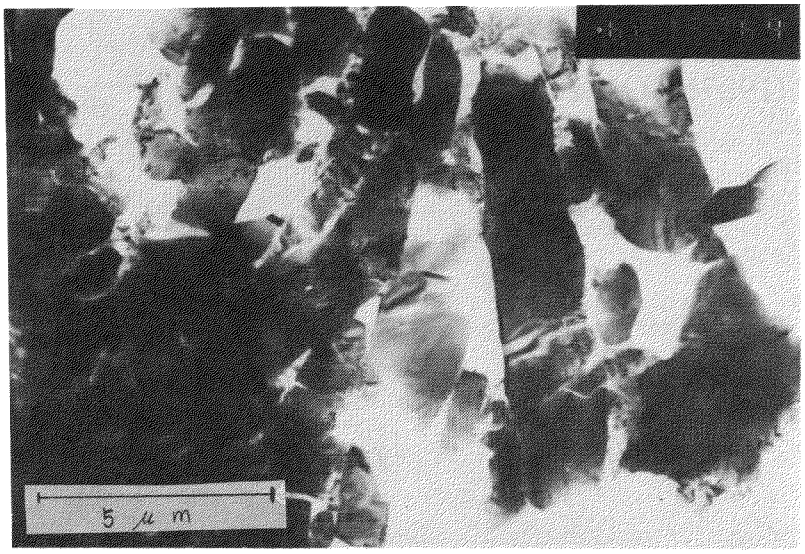


Fig.3 TEM image of smaller olivine grains in the matrix.

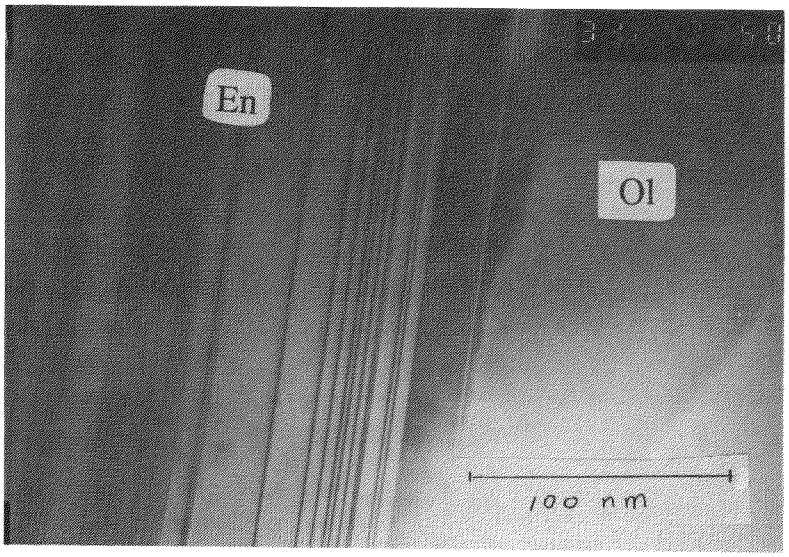


Fig.4 TEM image of stacking disorder in enstatite grains (En) and olivine grains (Ol) whose structure has not many defects.

# Possible cosmic spherules in the Mizuho ice core, Antarctica

Y.[1]Tazawa, T.[2]Fukuoka, E.[3]Yamanouchi, Y.[3]Miyano, K.[3]Endo, M.[4]Kohno, and Y.[5]Fujii
1:Grad. School. Phys. Astrophys., Kyoto Univ., 2:Dept. Chem. Gakushuin Univ., 3:Col. Human. Sci., Nihon Univ., 4:Inst. Study Earth's Int., Okayama Univ., and 5:Natl. Inst. Polar Res.

Introduction In the interplanetary space, not all the solid body has infinite life; the smaller one (e.g., dust grain) at a shorter distance from the Sun has the shorter lifetime. The grain is spiralled into the Sun via an increasingly circular orbit:i.e., Poynting-Robertson effect. Further, during the spiral orbiting the grain is reduced its size by space erosion/weathering. As a result, continuing dust sources are required: e.g., disintegration of comets, collisional destruction between asteroids, influx of interstellar dust grains, etc.. Therefore, dust grains fallen from the heaven to the Earth bring us new informations about the various origin and career of the cosmic matter.

More than $10^4$ tons/yr of the cosmic matter continuously fall on the Earth mostly as dust particles smaller than 1 mm [1]. Most of the particles larger than 10 $\mu$m have a round shape suggestive of melting by heating during the atmospheric entry [2]. In case of the entry of a larger meteoroid, e.g., meteorite, a large number of microparticles are derived and strewn, further, when a huge body happens to impact on the ground, extraordinary massive particles derived both from the body and the ground will be globally strewn [3].

The cosmic dust and the relatives are recovered from a wide variety of environment, e.g., polar ice/snow, stratosphere, deep-sea floor, etc.. Especially, the polar reagion is far from densely populated and/or arid continents, so that the dust concentration of the extraterrestrial component will be relatively high in the polar ice/snow. Moreover, there the dust has been frozen and preserved in strata in order of precipitation age ranging several $10^4$ years. Therefore, polar ice/snow is one of the optimal samples to study quantity and quality of secular infall of the cosmic dust and extraordinary events of dust accumulation (related to cosmic matter) for the past several $10^4$ years.

Recently, new sources of particulate cosmic matter were recovered in large quantity from the polar ice/ice lake [4,5] and glacial sediment [6]. Tazawa and Fujii also discovered several types of curious spherules from the melting and micro-filtering ice cores taken at the Mizuho station, Antarctica:e.g., CTS, FCN, ZST, etc. [7]. These types of spherules have chemical composition dissimilar to any of the previously reported cosmic spherules. They were inferred to be neither the artificial contaminations nor the steady-falling cosmic dust, but to be the droplets derived during an impact of large bolide on a metamorphic bedrock.

We have been studying another Mizuho ice core in order to clear the origin of the curious Mizuho spherules and also to search new population of cosmic dust and its relatives. We report here preliminary INAA/SEM/EDX result of 6 spherules collected from upper parts of a deep ice core down to a depth of 700 m. The par-

ticulate residues were taken from the melting ice by a microfiltering equipment. Spherules larger than ca. 10 $\mu$m were tweezed out under a view of stereomicroscope, and weighed by an electro-microbalance. Each of spherules and standards was irradiated by thermal neutron for 5 min in a pneumatic pipe of JRR-4 at a flux of $4\times10^{13}$n/cm$^3$·s to determine abundances of elements using short halflife nuclides. The $\gamma$-ray spectrometry of each sample was carried out for 400 sec after ca. 5 min cooling (Mg, Al, Ca, Ti, V), for 20~60 minafter 3~8 hrs (Na, Mn, K, etc.). After ca. 1 month, the samples were irradiated again for 98 hrs in JRR-3 at an flux of $1\times10^{14}$n/cm$^2$·s to determine abundances of elements using long half life nuclides:e.g., Na, K, Sc, Cr, Fe, Co, Ni, Zn, Rb, Sr, Zr, Cs, Ba, La, Ce, Nd, Sm, Eu, Tb, Yb, Lu, Hf, Ta, Ir, Au, Th, U, etc.. After ca. 1 week cooling, each sample was counted for 2 days to determine La, Nd, Sm, Yb, Lu, Ba, U, and finally after more than 1 month for 3 days to determine the rest elements. The observation of morphology and texture and quantitative chemical analysis of the spherules by SEM/EDX/XDP are in progress.

Preliminary results of the INAA are listed in Table and as follows: (1) the spherules seem to be stony types. (2) 3 spherules show mafic composition (magnetite and olivine ?). (3) 2 of them are especially rich in Fe (magnetite ?). (4) they are not composed of Ni, Ir, Au. These types of spherules have been usually seen in cosmic spherules but never seen in the types studied previously.

Table. Preliminary INAA results of spherules from Mizuho ice core

| | M23-1 | M13-1 | M3-1 | M6-3 | JB-1 | BHVO-1 |
|---|---|---|---|---|---|---|
| Wt($\mu$g) | 1.1 | 1.6 | 1.7 | 0.9 | 15.2 | 25.7 |
| $Al_2O_3$ % | - | - | 2.0 | - | [14.53] | 15.4 |
| FeO total | 28.5 | 40.9 | 45.2 | 26.4 | [ 8.11] | 11.5 |
| MgO | 16 | 15 | 11 | - | [ 7.73] | 8.34 |
| CaO | - | 20 | - | - | [ 9.29] | 15 |
| MnO | 0.44 | 0.10 | 0.17 | 0.20 | [ 0.16] | 0.19 |
| $Na_2O$ ppm | 80 | - | - | 32 | [ 2.79 %] | 2.22 |
| Cr | 87 | 57 | 71 | 55 | [414 ] | 290 |
| Lu | 0.021 | 0.013 | 0.073 | 0.027 | [ 0.37] | 0.31 |
| Sc | 0.03 | 0.08 | - | - | [28.9 ] | 33.2 |
| Co | 1.2 | 10.1 | 11.0 | 1.6 | [39.1 ] | 50.3 |

References

[1] Hughes, D. W. in Cosmic Dust, ed. J. A. M. McDonnell, pp.123-186, John Wiley & Sons, New York, 1978.
[2] e.g., Blanchard, M. B. et al., EPSL, 46, 178-190, 1982.
[3] e.g., Smit, J. & G. Klaver, Nature, 292, 47-49, 1981.
[4] Maurette, M. et al., Nature, 351, 44-46, 1991.
[5] Maurette, M. et al., Science, 233, 869-872, 1986.
[6] Hagen, E. H. et al., Contr. Antarctic Res. I, 50, 19-24, 1990.
[7] Tazawa, Y & Y. Fujii, Abst. 9th Symp. Antarctic Meteor., 1984; GRL, 14, 1199 - 1202, 1987.

# AQUEOUS ALTERATION OF THE ALLENDE CV3 CHONDRITE: A HYDROTHERMAL EXPERIMENT

Kazushige Tomeoka and Tomoko Kojima*
Department of Earth and Planetary Sciences, Faculty of Science, Kobe University, Nada, Kobe 657, Japan. * Also Mineralogical Institute, Faculty of Science, University of Tokyo, Hongo, Tokyo 113, Japan.

## INTRODUCTION

CI and CM types of carbonaceous chondrites consist in large part of phyllosilicates and show abundant textural evidence of aqueous alteration. Phyllosilicates have been also found in CV, CO chondrites [1-3] and unequilibrated ordinary chondrites [4], although in lesser amounts, indicating that these meteorites also have been affected by minor aqueous alteration. Recent studies of dark inclusions in CV chondrites [5,6] suggest that the CV chondrite parent body has been involved in extensive aqueous alteration. Therefore, aqueous alteration is an important process that prevailed in the early solar system. In order to better understand the alteration processes and conditions, we believe that experimental studies would be a promising approach. As a first step to experimentally simulate aqueous alteration in the carbonaceous chondrites, we embarked in hydrothermal alteration experiments of the Allende CV3 chondrite. We here present first results of our experiments. The goals of the present study are to reproduce aqueous alteration textures, thereby to investigate detailed mineralogical and chemical changes during alteration, and to compare texture, mineralogy and chemistry to those in the aqueously alterated chondrites.

## EXPERIMENTALS

We would like to note, at first, that the present study focused to reproduce the aqueous alteration textures in Allende, and not to reproduce the physico-chemical conditions in which the carbonaceous chondrites were altered. So we used considerably harsh conditions (high temperature and high pressure) compared to the real conditions in order to facilitate the alteration reactions. Samples of Allende were sealed in gold tubes with neutral water and 1-N HCl, then heated in a reactor vessel at 450 °C and 800 bars for 4 to 6 weeks. Thin sections were made from the run products, and they were observed and analyzed by a scanning electron microscope (JEOL JSM-5800) equipped with an EDS spectrometer.

## RESULTS AND DISCUSSION

***General petrography:*** Our experiments have produced remarkable alteration textures in the Allende chondrite. Alteration occurred in both runs performed with neutral and acidic water, but the extent of alteration is much higher in the products altered with acidic water than in the product altered with neutral water. So, most of the following descriptions are based on the observations of the products altered with acidic water. In the run products, small amounts of white and dark aggregates were produced as by-products. White aggregates are rich in Si, Mg, Ca, Fe, and Cl and appear to be related to phyllosilicate. Dark aggregates are composed of tiny dark

euhedral crystals (20 to 80 $\mu$m) which contain Fe, S and minor Ni; they may be pyrrhotite. The presence of these by-products means that the bulk Allende samples are considerably depleted in Si, Mg, Ca, Fe, S, and Ni.

Under an optical microscope, it is obvious that the Allende samples have been affected by aqueous alteration. The matrix of Allende samples turned to be brownish in color because of phyllosilicate formation. Parts of internal areas, especially mesostasis, of all the chondrules and aggregates are replaced by brownish-to-greenish phyllosilicate, exhibiting an appearance closely similar to altered ("spinach"-bearing) chondrules in CM chondrites [7]. Cracks and intersitices between chondrules and matrix, up to 20 $\mu$m in width and 1 mm in length, are filled with phyllosilicate, producing remarkable veins similar to those observed in CI chondrites.

SEM observations of phyllosilicates reveal characteristic fibrous-to-acicular morphologies. Mainly two kinds of phyllosilicates were produced. One contains major Mg and Fe and has compositions similar to Fe-rich saponite. This is the most common phyllosilicate that occurs in both chondrules and matrix, where it is primarily formed by replacing Fe-rich olivine and low-Ca pyroxene. The other kind of phyllosilicate contains major Mg, Fe, variable Al, and minor Na and K, which is possibly a mixture of two phases, so we tentatively call high-Al phyllosilicates (HAP). HAP occurs mainly in chondrule mesostasis and CAIs, where it is formed by replacing mesostasis glass and Ca-Al-rich minerals (melilite and anorthite). Of particular interest is that these phyllosilicates are very similar in composition to the phyllosilicates in the Mokoia CV3 chondrite, which were previously identified to be Fe-bearing saponite and an intergrowth of Na-rich phlogopite and serpentine [2].

***Chondrules and aggregates:*** Chondrules and aggregates are generally altered from their edges to inward. Olivine grains in outer areas of chondrules and aggregates are enriched in Fe, and most of individual olivine grains show strong Fe-Mg zoning, indicating substantial Fe was added from matrix to chondrules. Mesostasis in central areas is preferentially replaced by HAP, while that in outer areas is replaced by saponite, indicating that Al, Na and K in mesostasis leached out from the outer areas. Interstices and cracks in chondrules and aggregates are filled with saponite, forming a network of veins. There are remarkable differences in degree of alteration by phyllosilicates among the precursor minerals. Mesostasis glass and plagioclase are among the most susceptible to alteration. The resistance to alteration increases in the order, glass, anorthite, low-Ca pyroxene, olivine.

Interesting phenomina are observed in the alteration processes of olivine and low-Ca pyroxene. There seems to be a sequence in the alteration process of olivine to saponite. Olivine becomes Fe rich before being altered to saponite. At the same time, olivine produces numerous fine cracks and holes, being considerably disturbed in structure. It also includes microinclusions (<1 $\mu$m in diameter) rich in Fe and S. As the alteration advances, the Fe-rich olivine comes apart as small grains, forming a complex mixture with saponite. Alteration of low-Ca pyroxene produces intimate linear intergrowths of saponite and fine grains (<5 $\mu$m) of Fe-rich olivine and Fe-hydroxide. Saponite formed from low-Ca pyroxene is much poorer in Fe than that formed from olivine. Metal and Fe-sulfide globules are altered to saponite and Fe-hydroxide. Most of remaining suldfides are pentlandite.

***Matrix::*** Aggregates of Fe-rich saponite ranging in diameter from 10 to 50 $\mu$m are

produced in places in matrix. However, most of olivine grains in size less than 10 $\mu$m still remain, although their peripheries are replaced by saponite. This is surprising to us, taking into account the fact that chondrule internals were altered to the extent up to 200x200 $\mu m^2$ in area. This means that the alteration proceeds much faster in chondrule mesostasis than in the fine-grained matrix. Much of sulfide disappeared, probably due to leaching. Like in chondrules, most remaining sulfides in matrix are pentlandite.

By comparing mineralogies before and after alteration, it is evident that drastic chemical exchanges took place between chondrules and matrix and also between CAIs and matrix. Among major elements, Fe was added from matrix to chondrules mainly as an olivine component, whereas Mg, Al, Ca, Na and S were lost from chondrules. In the mesostasis of chondrules, Ca is almost completely lost, confirming that the mobility of Ca is particularly high. Despite the substantial migration of elements from chondrules, we could not find significant amounts of secondary phases expected to form from these elements in the matrix; most of the elements probably leached out of the samples and produced by-products as mentioned earlier. We analyzed the matrix by a defocused electron beam to compare bulk matrix compositions before and after alteration. The results show that Ca and S are much more depleted than other major elements, again indicating that these two elements are particularly mobile during aqueous alteration. As a result of these elemental exchanges and movements, it is evident that the meteorite became homogenized as a whole.

One of the most important findings of these experiments is that the texture and the phyllosilicate mineralogy produced in the altered Allende samples are closely similar to those observed in the Mokoia and Kaba CV3 chondrites [2,3], although the latter lacks the high-Al phyllosilicates. These similarities suggest that the alteration in Mokoia and Kaba occurred in conditions somewhat related to the present experimental condition, although the pressure and temperature should have been much lower in the real conditions. It has been controversial whether the aqueous alteration in these CV chondrites occurred in the solar nebula or in the meteorite parent body. The present study provides evidence supporting the interpretation that the alteration of these CV chondrites occurred after accretion on their parent body.

*Acknowledgments*- We thank Dr. K. Tsukimura, Japan Geological Survey, for helpful advices and discussion about hydrothermal experiments.

## REFERENCES

[1] Hashimoto, A. and Grossman, L. (1987) *Geochim. Cosmochim. Acta* 51, 1685-1704.
[2] Tomeoka, K. and Buseck, P.R. (1990) *Geochim. Cosmochim. Acta* 54, 1745-1754.
[3] Keller, L.P. and Buseck, P.R. (1990) *Geochim. Cosmochim. Acta* 54,1155-1163; *ibid.* 54, 2113-2120.
[4] Hutchison, R., Alexander, C.M.O.D. and Barber, D.J. (1987) *Geochim. Cosmochim. Acta* 51, 1875-1882.
[5] Kojima, T., Tomeoka, K. and Takeda, H. (1993) *Meteoritics* 28, 649-658.
[6] Kojima, T. and Tomeoka, K. (1994) *Meteoritics* 29, 484.
[7] Fuchs, L.H., Olsen, E. and Jensen, K.J. (1973) *Smithson. Contrib. Earth Sci.* 10, 1-39.

# EVAPORATION BEHAVIOR OF MINERAL DUST IN THE PRIMORDIAL SOLAR NEBULA.

TSUCHIYAMA Akira
*Department of Earth and Space Science, Osaka University, Toyonaka, Osaka 560*

**Introduction.** Evaporation is one of the most important processes to control chemical fractionation in the primordial solar nebula. When dust evaporates partially, the chemical compositions of residual solid and evaporated gas are generally different. Chemical fractionation takes place by separation of such solid and gas. Especially, when a mineral evaporates incongruently with a solid residue of different chemical composition, the fractionation can occur easily by evaporation of the mineral

If interplanetary dust, which had been incorporated into the nebula, falls towards the central star during the formation of protoplanetary disk, temperature of the dust increases with approaching the sun, and the dust evaporates by heating. Because solid and gas fall generally with different velocities, chemical fractionation is expected in this stage (active disk stage; Nakagawa and Watanabe, 1993). In the present paper, evaporation behavior of interplanetary dust of minerals in the active disk stage was examined based on a model for formation of protoplanetary disk (Nakagawa and Watanabe, 1993) and evaporation kinetics.

**Model.** In the present model, the following assumptions were made. (1) Dust of a single mineral phase is incorporated into protoplanetary nebula. (2) The dust immediately reaches the mid plane of the nebula, and falls towards the sun. (3) The dust is thermally in equilibrium with surrounding gas. (4) Evaporation of dust occurs in a gas of the solar H/O/C ratio without refractory elements, and accumulation of refractory elements in a gas by evaporation can be ignored. (5) Coagulation of dust occurs as well as evaporation.

Temperature in the mid plane, $T_c$, was obtained from the surface temperature;

$$T_c \approx 1200(r/1\mathrm{AU})^{9/8}{}_{[\mathrm{K}]}, \quad (1)$$

where $r$ is the heliocentric distance. Pressure in the mid plane, $p_c$, was obtained from the surface density of Hayashi model;

$$p_c \approx 8.8\times10^{-4}(r/1\mathrm{AU})^{-57/16}{}_{[\mathrm{bar}]}. \quad (2)$$

The velocity of dust falling towards the sun, $\dot{r}$, was obtained by considering coagulation of the dust. The time required for the coagulated dust to fall into the sun from 100AU was adopted to be $10^3$-$10^4$ yr;

$$\dot{r} \approx 1.3\times10^{-3}(r/1\mathrm{AU})^{9/8}{}_{[\mathrm{AU/s}]} \quad (3)$$

Amounts of evaporation of Mg-silicates (forsterite and enstatite) and Fe-S minerals (metallic iron and troilite) were calculated from the compiled data of Tsuchiyama and Uyeda (1995) together with Eqs.(1)-(3). The width of evaporation

of a mineral according to a linear rate law (forsterite and metallic iron), $X$, can be obtained from the linear rate constant, $k_L$;

$$X = \int_0^t k_L(T_c, p_c)dt. \quad (4)$$

The width of a residual layer formed by incongruent evaporation of a mineral according to a parabolic rate law (enstatite), $X^*$, can be obtained from the parabolic rate constant, $k_P$;

$$X^* = \int_0^t k_P(T_c, p_c)t^{1/2} d. \quad (5)$$

As incongruent evaporation of troilite obeys a linear rate law, $X^*$ for troilite was obtained from an equation similar to Eq.(4).

**Results and Discussion**. $X$ and $X^*$ are shown as a function of $r$ for the Mg-silicates (Fig.1a) and the Fe-S minerals (Fig.1b). The locations where the minerals evaporated completely if solid-gas equilibria are held with the solar composition are also shown in Fig.1. For example, forsterite disappears by evaporation at about 0.94AU in the equilibrium case (Fig.1a). On the other hand, $X_{Fo}$ is about 0.1-1 (0.01-0.1) μm when the evaporation coefficient of forsterite, $\alpha_V$, is 1 (0.1). This shows that forsterite of size larger than these $X_{Fo}$ values survives in an inner region from the equilibrium point. It is also seen from Fig.1a that the width of forsterite evaporated is much larger than the width of forsterite residue layer by incongruent evaporation of enstatite; that is, congruent evaporation of enstatite is expected in the nebula. Such congruent evaporation can be explained by kinetic effect that forsterite evaporation is enhanced under $H_2$-rich conditions in the nebula while formation of forsterite residue layer is still slow due to the diffusion controlled process. If the congruent evaporation of enstatite occurs, Mg/Si fractionation is not expected by evaporation of the Mg-silicate minerals. On the other hand, Mg/Si fractionation is expected by evaporation of Mg-silicate melts because Si is selectively evaporated from the melts and diffusion in melts is faster than that in solids. If a large grains of enstatite can survive against complete evaporation and begins to melt, Mg/Si fractionation is possible at high temperature regions above the melting point (Fig.1a). An alternative explanation for Mg/Si fractionation is that interplanetary dust evaporating in the nebula is an amorphous Mg-silicate.

Evaporation behavior of metallic iron is similar as that of forsterite (Fig.1b). Metal grain larger than 0.1 μm can survive in an inner region from the equilibrium point. Evaporation of troilite (FeS) is little before dust reaches the Fe-FeS eutectic point if the experimental results are adopted. When the eutectic is reached, eutectic melting between FeS and evaporation residue Fe should occur, and Fe/S fractionation takes place by evaporation of liquid Fe-S.

References: Nakagawa and Watanabe (1993) In "*Sciences for planets*" Ed. M.Shimizu, Asakura Pub. Co. (in Japanese). Tsuchiyama and Uyeda (1995) In "*The Earth's Central Part: Its Structure and Dynamics*", Ed. Y.Honkura, in press.

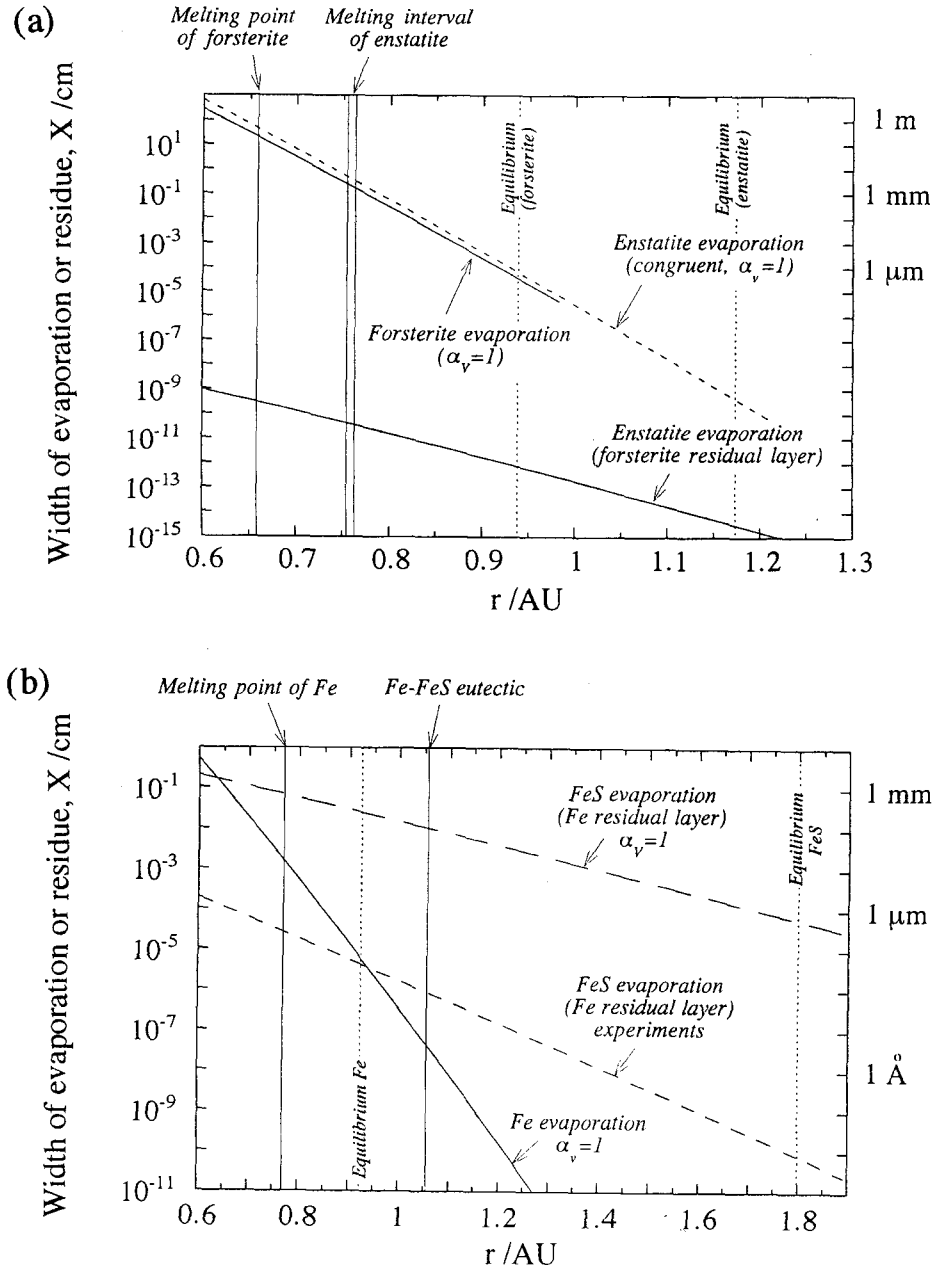


Fig.1 Evaporation behavior of minerals in the active disk stage of protoplanetary disk. The width of evaporation, $X$, and the width of a residual layer by incongruent evaporation of a mineral, $X^*$, are plotted against the heliocentric distance, $r$. (a) Mg-silicates (forsterite and enstatite). (b) Fe-S minerals (metallic iron and troilite).

# Consortium Investigation of the Asuka-881371 Angrite: Petrographic, Electron Microprobe, and Ion Microprobe Observations

Paul H. Warren[1,2] and Andrew M. Davis[3]

1: Mineralogical Institute, Graduate School of Science, University of Tokyo, Tokyo 113, Japan
2: Institute of Geophysics, University of California, Los Angeles, CA 90024, USA
3: Enrico Fermi Institute, University of Chicago, Chicago, IL 60637, USA

As a contribution to the Asuka-881371 consortium [1], we are using petrographic and microbeam techniques to study this unusual meteorite, which represents the fourth angrite, and only the third big enough to permit a wide range of investigations (the recovered mass of LEW87051 was only 0.6 g). As described by Yanai [2], A881371 is remarkably similar to LEW87051, both featuring distinctive extremely magnesian phenocrysts (or xenocrysts) of olivine scattered in a groundmass of fine-grained basaltic material with *mg* (= Mg/[Mg+Fe]) much too low for equilibrium with the coarse olivines. For simplicity, we employ the term phenocryst for the coarse, magnesian olivines in both A881371 and LEW87051 in most of the text below, but we use this term advisedly: there are reasons to doubt that these crystals were derived from the same asteroidal-interior region as the melt represented by the groundmass. The phenocryst olivines in LEW87 are <1.0 mm, and mostly <<0.5 mm, across [3; this work]. In A88, they are mostly 1-2 mm across [2; this work], and observations on the main mass during planning for the consortium revealed an exposed mass of olivine, with cleavage planes clearly visible (implying a single crystal), ~ 6.5 mm across, and also several 3-mm olivines (compare Fig. 3 in [2]). The groundmass is also about 2× more coarse-grained in A88. The smaller size of the LEW87 phenocrysts is more than offset by their greater abundance: Modal vol% of phenocrysts is roughly 25-30 vol% in LEW87, versus 5-10% in A88.

Another interesting observation on the main mass was the presence of two hemispherical (very smooth and regular in shape) depressions, on opposite sides of the stone, each ~ 1.5 mm across. One of these cavities is visible in Fig. 3 of [2], near the top center of the stone. Although these cavities strongly resemble vesicles, they did not necessarily form as gas bubbles. A881371 (like all angrites) is rather volatile-poor [1]. Conceivably the hemispherical depressions formed instead when olivine phenocrysts were removed by drag pressure during passage through Earth's atmosphere. Being much coarser and more refractory than the groundmass, the olivine phenocrysts may have been significantly more resistant to melting by atmospheric drag heating, and may have been largely removed as solids, instead of as melted (fusion crust) matter. No olivines noticeably protrude from the recovered stone (on the contrary, at least some appear to be exposed in depressions; compare Fig. 3 in [2]), but the fusion crust composition features remarkably low *mg* (38 mol%: Table) compared to the bulk rock (52 mol%: [2]). The phenocrysts are generally brecciated, so in most cases they probably would not break off as whole crystals. Assuming that a few of the least brecciated phenocrysts broke off in pieces extending ~ 2 mm into the stone, subsequent atmospheric heating (plus redistribution of preexisting melt coating) conceivably produced the final smooth, round appearance of the two depressions.

The general similarity between A881371 and LEW87051 extends to many, but not all, detailed characteristics. Our results for olivine and kirschsteinite major-element compositions (Fig. 1) strongly resemble the results of McKay et al. (1990) for LEW87. These authors found a few LEW87 olivines more magnesian ($Fo_{91}$) than the extreme found here ($Fo_{86}$), but Yanai [2] also reported rare $Fo_{89}$ olivine in A88. Phenocryst cores are compositionally uniform in A88, as in LEW87, and typical core compositions are similar: $Fo_{79\text{-}83}$ in LEW87 [3], $Fo_{83\text{-}85}$ in A88 [2; this work]. The zoned rims on the phenocryst olivines are wider and more complex in A88. Zonation in

the LEW87 phenocrysts is concentric, and confined to ~ 10 μm wide rims [3; this work]. In A88, the rims of the phenocrysts typically display a complex intergrowth (Fig. 7 in [2]) between fingers of mostly $Fo_{40-50}$ Ca-poor olivine, and fingers of mostly $Fo_{5-25}$ medium-Ca olivine (Fig. 1). The fingers (both types) are in general roughly 20×20 μm, and the interfingering zone occurs outward from a zone, mostly 20-40 μm thick, of simpler concentric zonation from the core ($Fo_{\sim 85}$) to the $Fo_{40-50}$ composition; and inward from a zone, mostly ~ 20 μm thick, of consistently low-*mg* olivine (and kirschsteinite). These structures presumably formed during a short-lived period of abortive equilibration between the high-*mg* core and the groundmass, as diffusion of MgO, FeO and CaO within the phenocryst was unable to keep pace with compositional alteration of the rim. Apparently, cooling of the groundmass was significantly slower in the case of A88, and as a result thicker, more complex rim structures developed.

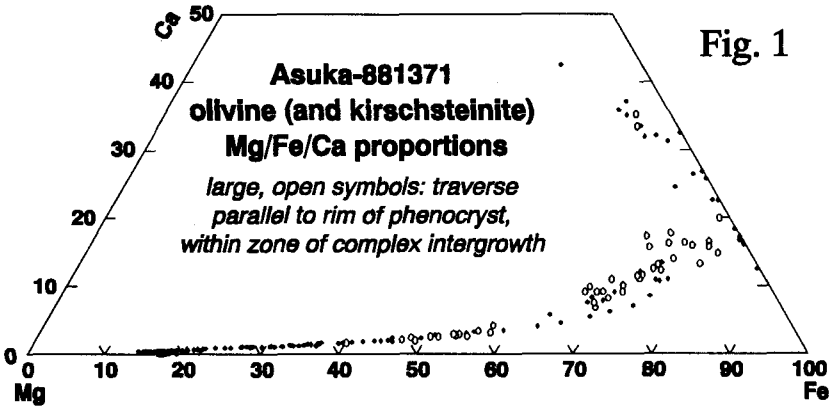


Fig. 1

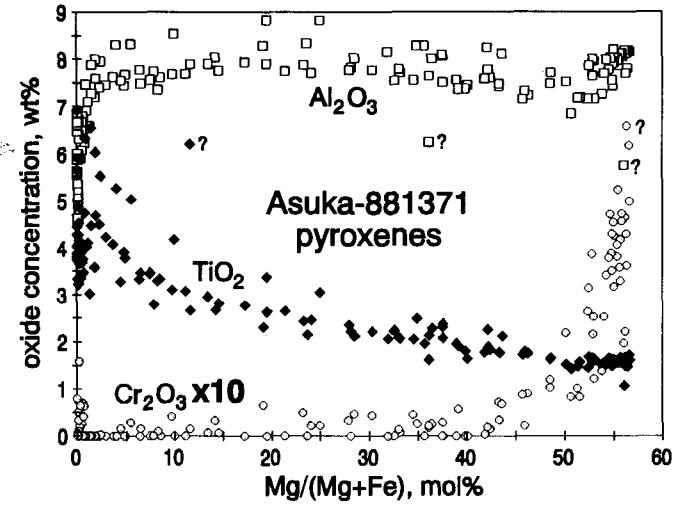


Fig. 2

Some A88 phenocryst cores are remarkably $Cr_2O_3$-rich: mostly ~ 0.3 wt%, but 0.6-0.9 wt% in two $Fo_{83}$ cores. For any given *mg*, LEW87 olivines are lower [3], and AdoR and LEW86010 are much lower, in $Cr_2O_3$. As in LEW87, A88 olivines show $Cr_2O_3$ zonation, with sharply falling $Cr_2O_3$ content between $Fo_{83}$ and $Fo_{70}$; nearly all analyses of $Fo_{<70}$ olivines show <0.08 wt% $Cr_2O_3$. Phenocryst-core CaO contents vary from grain to grain (the composition in the Table represents only a few of our highest-*mg* analyses), from 0.3 to <0.05 wt%. In most cores, $Cr_2O_3$/CaO is >>1. In contrast, LEW87 phenocryst cores typically contain 0.5-0.6 wt% CaO [4]. McKay et al. [3] report a shallow negative correlation between FeO/MnO and *mg* in LEW87 olivines, but thus far our data for A88 show only slight, probably insignificant scatter from the average olivine/kirschsteinite FeO/MnO of ~ 90 (more analyses are planned, however).

Fassaitic pyroxene $Al_2O_3$, $TiO_2$, and $Cr_2O_3$ contents are shown as a function of *mg* in Fig. 2. The $Al_2O_3$ variation is remarkably similar to the trend among LEW87 pyroxenes [3], except in A88 the overall trend is displaced to slightly higher $Al_2O_3$, by about 1 wt%, and the excursion toward high $Al_2O_3$ at *mg* ~ 55 does not reach the level (10 wt%) found by McKay et al. for a few rare grains in LEW87. In a paradoxical contrast to the situation with olivine, $Cr_2O_3$ contents in A88 pyroxene appear low in comparison to the levels reported by McKay et al. [3]: typically ~ 0.8 wt% in high-*mg* pyroxenes, and up to 1.3 wt%. As in LEW87, A88 pyroxene $TiO_2$ steadily increased during crystallization.

Our studies of opaques are far from complete, but we have detected an FeS phase; an Fe oxide, presumably magnetite (often Ti-rich — as in all three other angrites [4]); and ulvöspinel (Table). Yanai [2] reported another Fe-Ti oxide: ilmenite. The largest FeS (160 μm) shows a complexly intergrown rim that at least superficially resembles the olivine phenocryst rims. The two main intergrown phases in this case are FeS and MgO-free ($Fe_{83}Ca_{17}$) olivine, in fingers that average (dimensions are diverse) roughly 10×10 μm. In some cases, tiny fassaite and Ti-poor magnetite grains occur at the FeS end of the olivine finger. Another complex aspect of this FeS grain is the presence of several roughly ovoid cavities near its center. These cavities are lined with Fe oxide, and partly filled with a Fe,K-sulfide, probably a weathering product. The cavities, however, show little relationship to the brecciation within the FeS (as expected for weathering products), and thus are likely preterrestrial — adding credence to the vesicle hypothesis for the hemispherical surface cavities. The FeS/Fe,Ca-olivine intergrowth is surely preterrestrial, and may have formed at the same time as the olivine phenocryst rim intergrowths.

Less than 40 μm from this same FeS grain are four grains (apparently; three are conceivably parts of a single anhedral grain) of an unusual silicophosphate phase (Table), with cation proportions $Si_3FeCa_{12}P_6$ (or possibly $Si_9Fe_3TiCa_{36}P_{18}$). We are not aware of any previous description of this mineral. The stoichiometry is very consistent among about 19 good analyses. The sums range from 92.8 to 96.9 wt% (we have not yet analyzed for F, Cl, $H_2O$, REE oxides, etc.). The grains are up to 30 μm in max. dimension, and occur in various settings: surrounded by Fe,Ca-olivine; surrounded by fassaite; between fassaite, magnetite and Fe,Ca-olivine; and between fassaite, magnetite, Fe,Ca-olivine, and plagioclase. Possibly formation of this unusual phase was a byproduct of the same groundmass-FeS reaction that engendered the FeS-olivine intergrowth.

Our ion probe investigation is still at an early stage. Preliminary results for REE in plagioclase and fassaitic pyroxene are shown in Fig. 3. In a groundmass olivine, all REE are below detection limits (about 0.5×CI). Fig. 3 also shows for comparison data from McKay et al. [3] for LEW87. The A88 pyroxene data shown are from the most REE-poor (by a factor of about 1.5) among several analyses, but we have not yet carefully searched for the more REE-poor cores that would be most useful for inferring the composition of bulk-rock (or bulk-groundmass) parent melt. Nonetheless, Fig. 3 also shows REE contents of implied parent melts, based on the distribution coefficients derived for LEW86010-composition melts (i.e., similar, though not identical, to LEW87 and A88) by McKay et al. [5]. All of the plagioclase-rich angrites, including the clast in the North Haig ureilite analyzed by Davis et al. [6] (also described by Prinz et al. [4]),

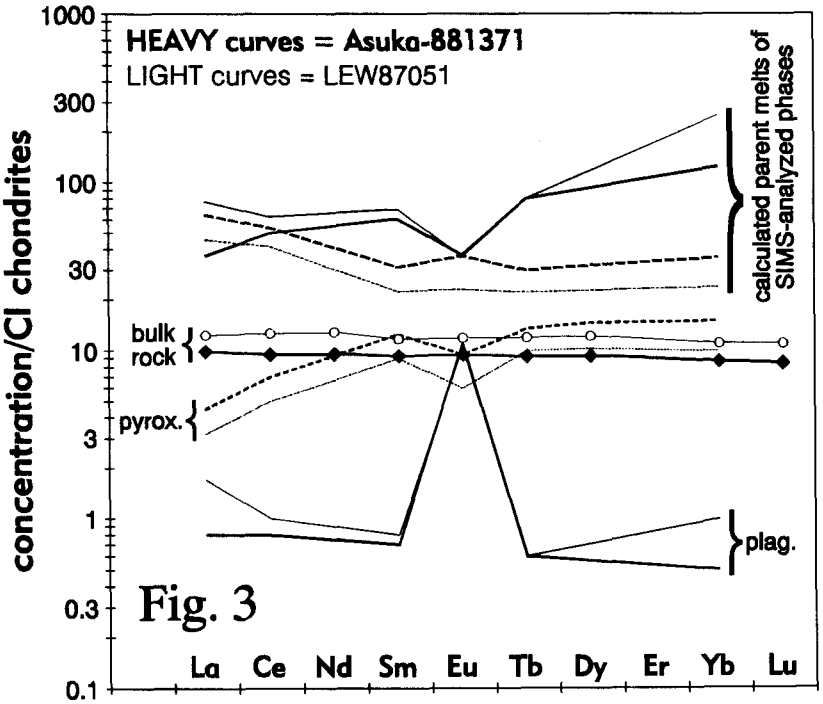

Fig. 3

have much lower pyroxene REE contents than the type angrite, Angra dos Reis [7]. For both A88 and LEW87, the match between the implied parent melt compositions, especially if based on plagioclase, and the measured bulk-rock compositions [1, and references therein], even if corrected for dilution by REE-poor olivine, is not close. Apparently the spots analyzed thus far do not preserve compositions from the earliest stage of crystallization. We plan many further analyses, however, including phosphates.

Are the large, high-*mg* olivines truly phenocrysts, or are they xenocrysts? Homogeneity within the cores of individual large olivines suggests that the range in core *mg*, CaO, and $Cr_2O_3$ among them is not simply an artifact (a uniform population of crystals with ~ $Fo_{90}$ cores having been sliced at diverse distances from their centers). Instead, it appears that a compositionally diverse population of high-*mg* olivines was mingled with a compositionally rather uniform (at least, similar between A88 and LEW87) groundmass material. The mingling process(es) probably occurred close to a cool surface of the asteroid, as both LEW87 and A88 have fine-grained groundmass that failed to equilibrate with the high-*mg* olivines. Assuming the olivines (say, within each meteorite) all came from a single source, the source would have to be cool and/or large enough to maintain a range of olivine compositions: $Fo_{73-91}$ in LEW87 [3,4], at least $Fo_{83-89}$ in A88. The mosaicized texture of the most magnesian olivine in A88 [2] suggests that the high-*mg* olivine cores did not form by fractional fusion of an original lower-*mg* ultramafite, similar to the moderate-*mg* material that must have been the source of the low-*mg* groundmass melt. During any fractional fusion process that involves compositionally homogeneous cores, mosaicism would probably be erased during extensive redistribution of the original crystal's FeO and MgO. We infer that the coarse olivines are probably xenocrysts, mingled with grossly dissimilar material, most likely by impact(s). The intergrown FeS may have been added together with the olivine. We doubt that the olivines are in any strict sense "chondritic relicts" [4], because addition of (at least) 25% of chondritic matter to LEW87 would have eliminated its extreme depletions of Na and other moderately volatile elements. Similarities in FeO/MnO and (at least for A88) O-isotopes [1] suggest (but do not prove) that the coarse olivines and groundmass had fundamentally similar ultimate provenance. Possibly the source of the coarse olivines was roughly brachinitic.

**References** [1] Warren P. H. et al. (1995) This volume. [2] Yanai K. (1994) *Proc. NIPR Symp. Antarctic Meteorites*, 7, 30-41. [3] McKay G. et al. (1990) *Lunar Planet. Sci.*, **XXI**, 771-772. [4] Prinz M. et al. (1990) *Lunar Planet. Sci.*, **XXI**, 979-980. [5] McKay G. et al. (1994) *Geoch. Cosmoch. Acta*, **58**, 2911-2919. [6] Davis A. M. et al. (1988) *Lunar Planet. Sci.*, **XIX**, 251-252. [7] Ma M-S. et al. (1977) *Earth Planet. Sci. Lett.*, **35**, 331-346.

**Table. Electron microprobe analyses.**

| phase | wt% $SiO_2$ | wt% MgO | wt% $Na_2O$ | wt% $Al_2O_3$ | wt% FeO | wt% MnO | wt% $Cr_2O_3$ | wt% $K_2O$ | wt% CaO | wt% $TiO_2$ | wt% NiO | wt% $P_2O_5$ | wt% sum | mol% X/(Mg+Fe+Ca) Mg | Fe | Ca | mol% *mg* |
|---|---|---|---|---|---|---|---|---|---|---|---|---|---|---|---|---|---|
| OlvP | 40.0 | 45.1 | 0.01 | 0.07 | 13.9 | 0.15 | *0.3?* | 0.00 | 0.34 | 0.01 | 0.03 | 0.00 | 99.9 | 84.9 | 14.7 | 0.46 | 85.2 |
| Kirs | 32.4 | 2.63 | 0.01 | 0.02 | 41.7 | 0.58 | 0.02 | 0.00 | 21.2 | 0.06 | 0.04 | 0.00 | 98.7 | 6.4 | 56.7 | 36.9 | 10.1 |
| Fass1 | 47.0 | 8.39 | 0.01 | 7.93 | 11.84 | 0.14 | *0.3?* | 0.00 | 22.9 | 1.58 | 0.02 | 0.00 | 100.3 | 26.7 | 21.1 | 52.2 | 55.8 |
| Fass2 | 40.7 | 0.00 | 0.12 | 5.67 | 25.8 | 0.17 | 0.01 | 0.01 | 21.2 | 4.40 | 0.02 | *1.05* | 99.1 | 0.0 | 48.7 | 51.3 | 0.03 |
| Fass3 | 43.8 | 3.80 | 0.03 | 7.32 | 19.0 | 0.17 | 0.11 | 0.01 | 22.2 | 2.87 | 0.02 | *0.17* | 99.5 | 12.5 | 35.1 | 52.4 | 26.3 |
| Ulvös | 0.2 | 0.02 | 0.00 | 2.60 | 66.9 | 0.26 | 0.00 | 0.01 | 0.21 | 27.0 | 0.01 | 0.01 | 97.2 | | | | 0.05 |
| Phos1 | 13.13 | 0.01 | 0.00 | 0.32 | 5.17 | 0.06 | 0.01 | 0.01 | 46.0 | 1.68 | 0.04 | 29.5 | 96.0 | | | | 0.4 |
| Phos2 | 2.91 | 0.02 | 0.16 | 0.13 | 5.95 | 0.01 | 0.00 | 0.04 | 46.3 | 0.08 | 0.00 | 42.6 | 98.2 | mol% X/(Ca+Na+K) | | | 0.5 |
| Fus. c | 38.1 | 9.24 | 0.01 | 8.53 | 26.8 | 0.28 | 0.07 | 0.01 | 13.7 | 0.99 | 0.02 | 0.18 | 97.9 | Ca | Na | K | 38.1 |
| Plag | 44.3 | 0.18 | 0.04 | 35.4 | 0.37 | 0.02 | 0.02 | 0.01 | 20.1 | 0.02 | 0.02 | 0.00 | 100.5 | 99.60 | 0.36 | 0.033 | 47 |

OlvP = olivine phenocryst cores (avg. 13 analyses), Kirs = kirschteinite (5 analyses), Fass1* = high-*mg* fassaite (19), Fass2 = low-*mg* fassaite (15), Fass3 = all fassaites (143), Ulvös = ulvöspinel (11), Phos1 = silicophosphate (19), Phos2 = merrillite (1), Fus. c = fusioncrust (9), Plag = plagioicase (44). *The Fass1 composition also includes detectable $V_2O_3$: 0.11 wt%.

# Consortium Investigation of the Asuka-881371 Angrite: Bulk-rock Geochemistry and Oxygen Isotopes

Paul H. Warren[1,2], Gregory W. Kallemeyn[1] and Tosh Mayeda[3]

1: Institute of Geophysics, University of California, Los Angeles, CA 90024, USA

2: Mineralogical Institute, Graduate School of Science, University of Tokyo, Tokyo 113, Japan

3: Enrico Fermi Institute, University of Chicago, Chicago, IL 60637, USA

The 11.3-gram Asuka-881371 angrite [1] is only the fourth meteorite of this distinctive type, and two of the others are even smaller (0.6-6.9 g). In order to derive maximum scientific benefit from this rare material, a consortium was organized under the leadership of (in alphabetical order) M. Miyamoto, P. Warren and K. Yanai. In addition to a sample sent earlier to Chicago for oxygen isotopic analysis, and samples used for Yanai's [1] initial petrologic study, a 1.2 g chip was generously allocated to the consortium by the NIPR. This chip was sent to UCLA, where it was split into smaller pieces, for allocation to consortium geochemists, and for production of four thin sections (three relatively large plus one smaller). Some early results from the consortium are being reported at this meeting.

As a contribution to this consortium, we are studying the meteorite's bulk-rock geochemistry and oxygen isotopic composition. Our oxygen-isotopic study is complete, but we have only analyzed about 2/3 of the elements that our study will eventually encompass. In order to derive maximum information from this rare material, we will later use the same powder analyzed by INAA for electron probe fused bead analysis (EPFBA) and for radiochemical NAA, but this approach has the drawback of requiring us to delay both EPFBA and RNAA by several months, at least. Even INAA is not quite complete, as of this writing.

Oxygen results for a whole-rock sample are: $\delta^{18}O = 3.91$, $\delta^{17}O = 1.94$. The $\Delta^{17}O$ ratio of –0.09 is within uncertainty identical to previous angrite results [e.g., 2]. Results for a sample of olivine phenocryst (or xenocryst) material are: $\delta^{18}O = 3.54$, $\delta^{17}O = 1.80$, $\Delta^{17}O = -0.04$. The cores of these coarse olivines have *mg* (= molar Mg/[Mg+Fe]) much too high to be in equilibrium with the groundmass, which raises the possibility that they might be xenocrysts [1, 3]. The similarity in $\Delta^{17}O$ (and also FeO/MnO) tends to suggest that despite their extreme *mg* contrast, the coarse olivines and the groundmass may have had fundamentally similar ultimate provenance.

Preliminary INAA results for A881371 are shown in the Table, along with some hitherto unpublished results for Angra dos Reis (AdoR) and the two LEW angrites. Ratios such as Na/Al, Ga/Al (Fig. 1), Fe/Mn, and Co/Cr confirm the angritic affinity of A881371. Mittlefehldt and Lindstrom [4] noted that the characteristically low alkali/Al ratios of angrites are presumably linked to the moderate volatility of alkali oxides. These authors inferred that alkalis were outgassed during primordial magmatism, and that outgassing was more intense on the angrite parent body compared to the eucrite parent asteroid, and/or that the angrite parent body was smaller.

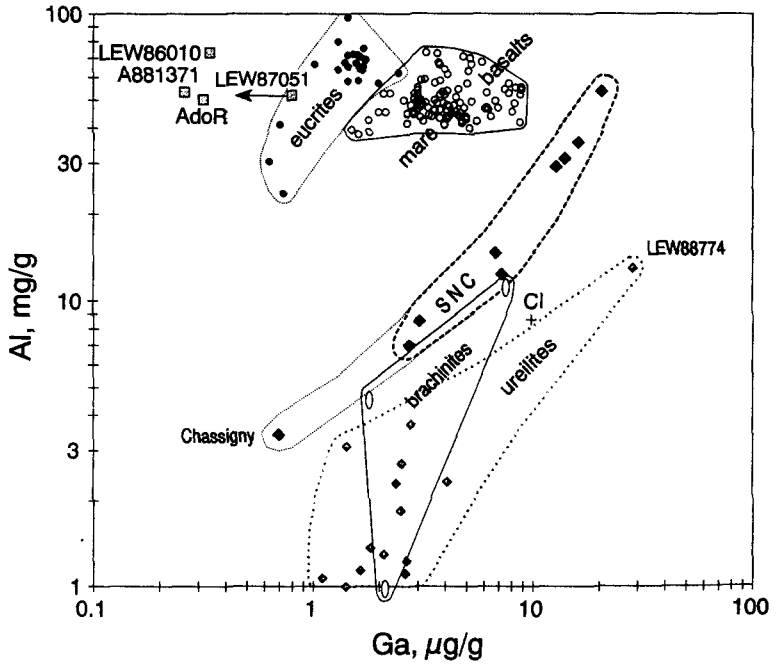

**Table. Bulk-rock compositional data for angrites (*italics* denote unusually high uncertainty).**

| | mass | Na | Mg | Al | Si | K | Ca | Sc | Ti | V | Cr | Mn | Fe | Co | *mg* |
|---|---|---|---|---|---|---|---|---|---|---|---|---|---|---|---|
| | mg | µg/g | mg/g | mg/g | mg/g | µg/g | mg/g | µg/g | mg/g | µg/g | mg/g | mg/g | mg/g | µg/g | mol% |
| *UCLA data: INAA, fused bead electron probe, and RNAA; analysis for A881371 incomplete and slightly preliminary* | | | | | | | | | | | | | | | |
| Asuka-881371 | 144 | 160 | -- | -- | -- | *51* | 73 | 32.9 | -- | -- | 0.95 | 1.79 | 171 | *51* | -- |
| LEW87051 | 27 | 223 | 94 | 55 | 189 | <113 | 86 | 42 | 5.1 | 113 | 1.10 | 1.89 | 163 | 28.5 | 57.0 |
| LEW86010 | 190 | 227 | 44.2 | 73 | 185 | 350 | 125 | 55 | 9.6 | 183 | 0.89 | 1.69 | 157 | 24.6 | 39.3 |
| AdoR #1 | 320 | 223 | 69.8 | 48.4 | 207 | *20* | 162 | 50 | 12.5 | -- | 1.49 | 0.91 | 81.2 | 22.4 | 66.4 |
| AdoR #2* | 340 | 223 | 69.7 | 48.5 | 206 | *27* | 162 | 51 | 11.8 | 176 | 1.49 | 0.99 | 80.2 | 15.7 | 66.6 |
| *Literature averages (including UCLA data)* | | | | | | | | | | | | | | | |
| Asuka-881371 | | 190 | 89.3 | 53.3 | 174.4 | *51* | 81 | 32.9 | 5.3 | -- | 0.92 | 1.67 | 179 | *51* | *53* |
| *A881371/L87051* | | *0.96* | *0.85* | *1.03* | *0.92* | -- | *1.01* | *0.85* | *1.11* | -- | *0.67* | *0.89* | *1.14* | *1.8* | -- |
| LEW87051 | | 198 | 105.5 | 51.8 | 188.9 | <113 | 80.3 | 38.9 | 4.7 | 113 | 1.38 | 1.87 | 157 | 28.0 | 60.7 |
| LEW86010 | | 192 | 43.2 | 73.7 | 184.9 | 350 | 128 | 55.9 | 8.2 | 183 | 0.83 | 1.62 | 149 | 23.2 | 40.0 |
| Angra dos Reis | | 250 | 66.8 | 50.3 | 205.6 | 30 | 168 | 50.7 | 13.6 | 173 | 1.63 | 0.79 | 73.4 | 17.0 | 67.7 |

| | mass | Ni | Zn | Ga | Ge | As | Se | Sr | Zr | Cd | Sb | Ba | La | Ce | Nd |
|---|---|---|---|---|---|---|---|---|---|---|---|---|---|---|---|
| | mg | µg/g | µg/g | µg/g | µg/g | µg/g | µg/g | µg/g | µg/g | ng/g | ng/g | µg/g | µg/g | µg/g | µg/g |
| *UCLA data: INAA, fused bead electron probe, and RNAA; analysis for A881371 incomplete and slightly preliminary* | | | | | | | | | | | | | | | |
| Asuka-881371 | 144 | *114* | *6* | *0.26* | -- | -- | *0.6* | --- | *34* | -- | --- | --- | 2.34 | 5.9 | *4.4* |
| LEW87051 | 27 | 45 | 0.89 | <0.8 | 0.027 | -- | -- | 92 | <61 | 6.2 | 145 | <60 | 3.51 | 9.4 | *5.9* |
| LEW86010 | 190 | 39 | 1.8 | 0.34 | 0.102 | <0.07 | 0.84 | 60 | 51 | 7.6 | <70 | 51 | 4.66 | 10.9 | 8.1 |
| AdoR #1 | 320 | 77 | 1.73 | *0.32* | 0.079 | 0.21 | 0.78 | 131 | 110 | 10.8 | 64 | *30* | 6.9 | 18.9 | 17.2 |
| AdoR #2* | 340 | 40 | *2.4* | *0.27* | *0.15* | 0.15 | 0.84 | 117 | 102 | 30 | *97* | <33 | 6.8 | 18.7 | 16.9 |
| *Literature averages (including UCLA data)* | | | | | | | | | | | | | | | |
| Asuka-881371 | | *114* | *6* | *0.26* | -- | -- | *0.6* | -- | *34* | -- | -- | -- | 2.34 | 5.9 | *4.4* |
| *A881371/L87051* | | 2.6 | *7* | -- | -- | -- | -- | -- | -- | -- | -- | -- | *0.80* | *0.75* | *0.75* |
| LEW87051 | | 45 | 0.89 | <0.8 | 0.027 | -- | -- | 80 | <61 | 6.2 | 145 | <60 | 2.92 | 7.8 | *5.9* |
| LEW86010 | | 39 | 1.80 | 0.34 | 0.102 | <0.07 | 0.84 | 60 | 51 | 7.6 | <70 | 49.5 | 4.02 | 10.5 | 8.1 |
| Angra dos Reis | | 64 | 1.92 | 0.32 | *0.079* | 0.18 | 0.81 | 112.1 | 118 | 20 | *64* | 28.4 | 7.13 | 19.5 | 18 |

| | mass | Sm | Eu | Tb | Dy | Yb | Lu | Hf | Ta | Re | Os | Ir | Au | Th | U |
|---|---|---|---|---|---|---|---|---|---|---|---|---|---|---|---|
| | mg | µg/g | µg/g | µg/g | µg/g | µg/g | µg/g | µg/g | µg/g | ng/g | ng/g | ng/g | ng/g | µg/g | µg/g |
| *UCLA data: INAA, fused bead electron probe, and RNAA; analysis for A881371 incomplete and slightly preliminary* | | | | | | | | | | | | | | | |
| Asuka-881371 | 144 | 1.39 | 0.53 | *0.33* | *2.3* | 1.38 | 0.21 | 1.03 | --- | -- | -- | 2.4 | <1 | *0.24* | --- |
| LEW87051 | 27 | 2.01 | 0.80 | 0.49 | *3.2* | 2.00 | 0.30 | 1.34 | 0.15 | 0.038 | <0.13 | 0.180 | <2.5 | 0.41 | <0.21 |
| LEW86010 | 190 | 2.6 | 0.97 | 0.61 | 4.4 | 2.61 | 0.38 | 1.87 | 0.29 | 0.148 | 2.44 | 7.1 | 0.37 | 0.40 | *0.15* |
| AdoR #1 | 320 | 5.8 | 1.9 | 1.32 | 8.7 | 5.0 | 0.74 | 2.37 | 0.36 | 2.8 | 0.020 | 0.07 | 5.0 | 0.55 | *0.14* |
| AdoR #2* | 340 | 5.7 | 1.9 | 1.32 | 8.6 | 4.9 | 0.72 | 2.43 | 0.37 | *5.9* | *0.047* | 0.07 | *150** | 0.55 | *0.11* |
| *Literature averages (including UCLA data)* | | | | | | | | | | | | | | | |
| Asuka-881371 | | 1.39 | 0.53 | *0.33* | *2.3* | 1.38 | 0.21 | 1.03 | -- | -- | -- | 2.4 | <1 | *0.24* | --- |
| *A881371/L87051* | | *0.80* | *0.79* | *0.78* | *0.77* | *0.78* | *0.77* | *0.82* | -- | -- | -- | *13* | -- | *0.75* | -- |
| LEW87051 | | 1.75 | 0.67 | 0.43 | *3* | 1.76 | 0.27 | 1.26 | 0.13 | 0.038 | <0.13 | 0.18 | <2.5 | 0.32 | <0.21 |
| LEW86010 | | 2.64 | 0.97 | 0.64 | 4.4 | 2.63 | 0.38 | 2.04 | 0.28 | 0.148 | 2.44 | 7.10 | 0.37 | 0.44 | *0.15* |
| Angra dos Reis | | 6.2 | 1.84 | 1.47 | 9.5 | 5.0 | 0.71 | 2.63 | 0.36 | *3* | *0.02* | 0.07 | *5* | 0.64 | 0.15 |

* Our Ador#2 sample seems to have been grossly contaminated with Au and probably other trace siderophile elements.

Probably based mainly on data for the readily-determined alkalis Na and K (assumed to be exemplary volatile elements) angrites have been characterized as "about 20× more depleted in volatiles than the eucrites" [5]. However, these alkali-based perspectives are oversimplified. Actually, more highly volatile elements such as Se, Zn and Cd are about equally or *less* depleted in the angrite average than in averages for (non-polymict) eucrites, or typical lunar basalts (Fig. 2). Our volatile results for A881371 are incomplete (the Zn datum, in particular, is near the INAA detection limit — RNAA should eventually yield a much more precise result), but even based only on AdoR and the two LEW angrites, this pattern seems firmly established.

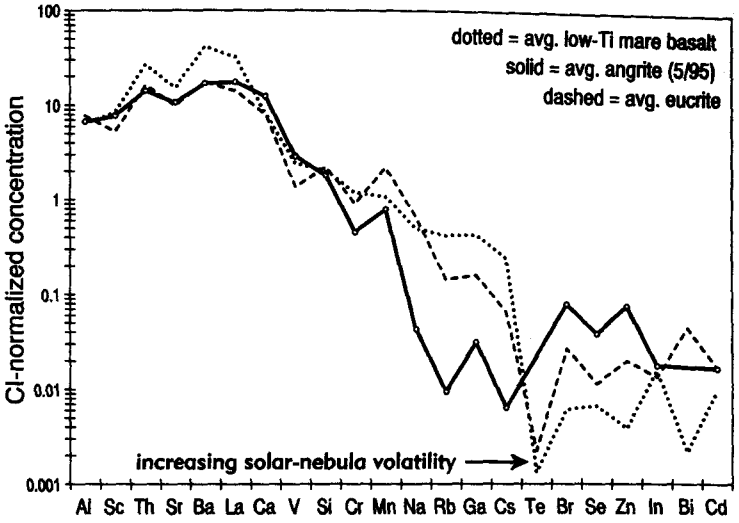


As far as we have been able to determine, the only volatile elements depleted by large, clearly significant factors in angrites versus eucrites (or versus lunar basalts) are alkalis plus gallium. Besides being moderately volatile, the most noteworthy characteristic shared among Ga and the alkalis (and not shared with elements such as Se, Zn and Cd) is that all these elements probably tend to strongly partition into crustal feldspar during gross differentiation of small, low-pressure asteroids. Angrites are often assumed to have been derived by differentiation starting from CAI-like, refractory-enriched material [e.g., 5], but except for a few elements in AdoR (most notably Ti, but AdoR may have formed as a cumulate from an igneously evolved magma), angrites are not significantly enriched in refractory elements (despite the high Ti and Al contents of their fassaitic pyroxenes) versus eucrites. In terms of oxygen-isotopic ratios, angrites resemble the eucrite parent body (probably Vesta), the Moon, the Earth, and the SNC parent body (probably Mars), much more closely than they resemble CAIs. If gallium + alkalis were depleted by a single process starting from "normal" chondritic (i.e., ordinary-chondrite-like or bulk-carbonaceous chondrite-like) material, that process would seem to require selective exposure of a feldspar-enriched region (i.e., an asteroidal crust) to extremely high temperature. The igneous crystallization of the angrites occurred when the solar system was still extremely young (4.54-4.56 Ga [6,7]). The peculiar volatile-depletion pattern of the angrites (Fig. 2) may be the product of heating by a short-lived but intense heat source that melted and partially vaporized an asteroidal crust, without much affecting the deep interior, which later (through impact-mixing and/or magmatism) significantly replenished the angritic materials in most volatiles, but not alkalis and Ga. The often-conjectured (but hard to test) hypothesis that a major early heat source was enhanced solar luminosity (as in FU-Orionis cycles) would seem to be required for this model, and even then it must be assumed that the cumulative effects of earlier excursions to high luminosity had already differentiated the asteroid into a crust/mantle structure. This scenario is admittedly speculative, but the peculiar volatile-depletion pattern (Fig. 2) is difficult to rationalize with any other model.

Data for refractory lithophile elements are shown in Fig. 3. The abundance pattern is equally as flat as, and even lower than, the pattern of LEW87051 — which also resembles A881371 petrographically, most notably in containing abundant phenocrysts (or xenocrysts) of olivine far too magnesian to be in equilibrium with the groundmass [1,3]. Literature data for angrites are nearly all from sources cited in Mittlefehldt and Lindstrom [4].

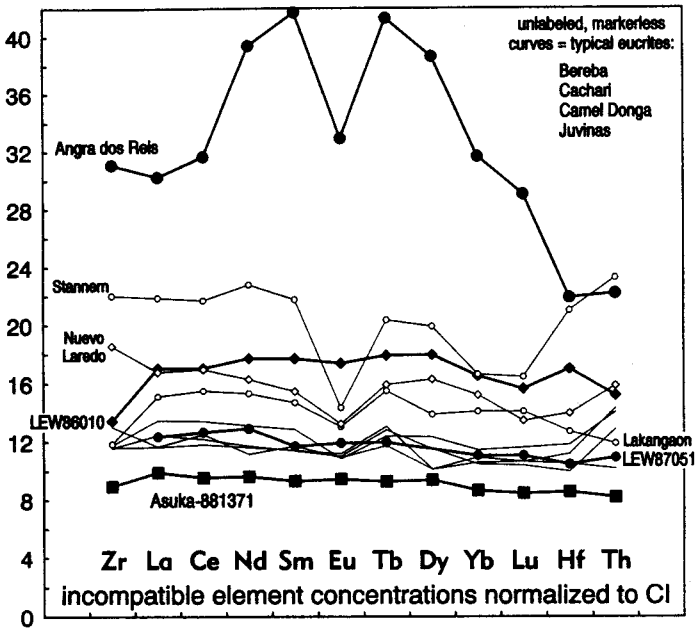


Average modal data [3] indicate that phenocrysts constitute only 5-10 vol% of A88, vs. 25-30 vol% of LEW87. However, the proportion of coarse olivine in our bulk-A88 sample appeared much higher (roughly 20 vol%), and the Co concentration is also surprisingly high. Until we acquire additional major-element data we cannot be sure the bulk-rock REE content of A88 is significantly lower than that of LEW87 (for which sample representativeness is also problematical). In any case, the groundmass materials in both A88 and LEW87 are no more enriched in REE than a typical eucrite. LEW86010 is more REE-rich, but still lower than Stannern for most REE, especially LREE. The weak development of Eu anomalies in these three angrites suggests that comparatively high oxygen fugacity prevailed in the angrite parent body [8].

The prototype angrite, AdoR, appears highly atypical. There has been some controversy as to whether AdoR is a cumulate [9] or a porphyry [10]. The contrast between AdoR and the other three angrites in Fig. 3 indicates that (assuming all were derived from the same starting material) AdoR formed from an extraordinarily evolved parent melt, at least in terms of incompatible trace elements. Assuming the parent melt probably was also evolved in terms of *mg*, the comparatively high bulk-rock *mg* (Table) tends to suggest that AdoR is largely cumulate in origin, the well-reasoned petrologic arguments of Treiman et al. [9] notwithstanding.

Fig. 4 shows siderophile data, which for A88 are strictly from INAA, and thus are very incomplete (and imprecise, in the case Ir, only marginally detected by INAA; note, too, that the INAA Au result for A88 is an upper limit). Angrite siderophile patterns are complex and diverse, but the general trend (again, AdoR is exceptional) is for the most intensely siderophile elements (Re-Os-Ir) to be less depleted in angrites than in eucrites or lunar basalts. The average angrite siderophile pattern is roughly similar to the average for SNC (martian) meteorites.

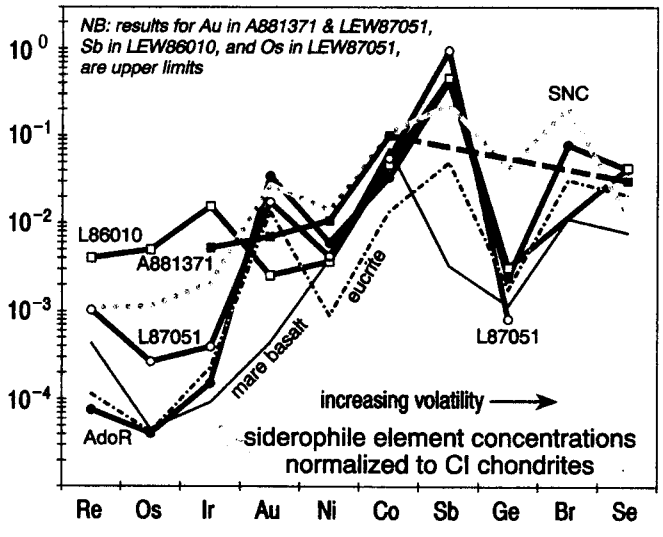


**References:** [1] Yanai K. (1994) *Proc. NIPR Symp. Antarctic Meteorites*, 7, 30-41. [2] Clayton, R. N. et al. (1976) *Earth Planet. Sci. Lett.*, **30**, 10-18. [3] Warren P. H. and Davis A. M. (1995) This volume. [4] Mittlefehldt D. W. and Lindstrom M. M. (1990) *Geoch. Cosmoch. Acta*, **54**, 3209-3218. [5] Prinz M. et al. (1990) *Lunar Planet. Sci.*, **XXI**, 979-980. [6] Jacobsen S. B. and Wasserburg G. J. (1984) *Earth Planet. Sci. Lett.*, **67**, 137-150. [7] Lugmair G. W. et al. (1989) *Lunar Planet. Sci.*, **XX**, 605-606. [8] Jurewicz A. J. G., Mittlefehldt D. W., and Jones J. H. (1990) *Geoch. Cosmoch. Acta*, **57**, 2123-2139. [9] Prinz M. et al. (1977) *Earth Planet. Sci. Lett.*, **35**, 317-330. [10] Treiman A. H. (1989) *Proc. Lunar Planet. Sci. Conf., 19th*, 443-450.

# OCCURRENCES OF HIGH-PRESSURE MINERAL POLYMORPHS IN TWO SHOCKED CHONDRITES

Xie Xiande and Chen Ming
Guangzhou Institute of Geochemistry, Chinese Academy of Science, Guangzhou 510640, China.

## Introduction

Ringwoodite, wadsleyite and majorite are three high-pressure mineral polymorphs which have been found in the shock-produced veins of some L6 chondrites. The presence of these high-pressure phases indicates that the shock pressures were more than 45 GPa [1]. Since the shock veins are not rare in ordinary chondrites and the high-pressure mineral polymorphs have not been observed in all these shocked chondrites, special conditions may be required for the formation of high-pressure phases. Our recent investigation indicated that the formation and survival of high-pressure phases intimately depend on shock pressures and subsequent cooling rates [2, 3]. Very high shock pressures (more than 80 GPa) which would induce higher post-shock temperatures, and subsequently slower cooling rates should result in extensive melting and recrystallization of chondritic minerals, as well as the back transformation of shock-produced high-pressure polymorphs. Here we report the occurrence characteristics of high-pressure mineral polymorphs in two heavily shocked Chinese chondrites, Sixiangkou (L6) and Yanzhuang (H6). The Yanzhuang chondrite is one of most heavily shocked ordinary chondrites [4], and it was more severely metamorphosed than the Sixiangkou chondrite. The different occurrence characteristics of high-pressure phases between the two chondrites have been identified.

## Sixiangkou (L6) chondrite

Most shock veins in this meteorite have the widths from 0.1 to 2 mm. In addition to shock-produced plagioclase glass and recrystallized metal-troilite eutectic intergrows, the shock veins consist of abundant high-pressure mineral polymorphs including ringwoodite, wadsleyite, majorite and "phase A" (a new high-pressure polymorph of chlorapatite). Figure 1 shows the occurrence of these minerals or phases in a vein.

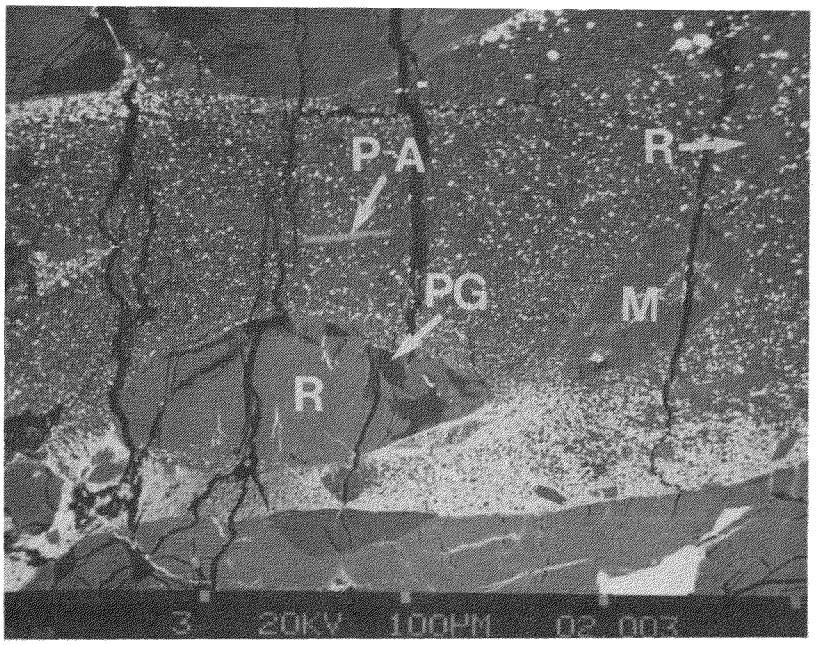


Fig.1. SEM photograph of the shock vein in the Sixiangkou chondrite. The vein contains abundant high-pressure mineral polymorphs ringwoodite (R), majorite (M) and phase A (P-A). The dark matrix of vein is mainly consists of microcrystal majorite rich in Al, Ca, Na and Cr, and silicate melt glass. Plagioclase glass is designated as PG.

(1) Ringwoodite and wadsleyite: They are the high-pressure polymorphs of olivine. Ringwoodite is with high degree of crystallinity and contains only a small percentage of the β-

phase (wadsleyite), which have been identified by Raman spectroscopy. Ringwoodite with minor wadsleyite occurs as isotropic and colorless grains up to 300 μm in length. The ringwoodite formed from a solid state transition from olivine. The wadsleyite formed from ringwoodite by retrograde metamorphism. Electron microprobe analyses indicate the ringwoodite and wadsleyite have same composition as the olivine in the neighbouring unmolten chondritic host [5].

(2) Majorite: Two compositional types of majorite are encountered. First one is colorless to yellowish brown and consists of isotropic polycrystalline grains in sizes ranging from 20 to 200 μm. This type majorite has the same composition as the low-Ca pyroxene of the chondritic host, and formed from a solid state transition of pyroxene. Second one is isolated yellowish brown microcrystals in sizes ranging from 1 to 3 μm. These majorite microcrystals occur as subhedral or euhedral crystals in the matrix of veins, and surrounded by troilite, metal and plagioclase glass. Electron microprobe analyses indicate this type of majorite is rich in Al, Ca, Na and Cr [5]. It is indicated that second type majorite must crystallized from shock-produced silicate melt at high pressure and high temperature.

(3) Phase A: Phase A is a newly found high-pressure polymorph of chlorapatite in the shock veins [2]. It is isotropic (or dark fist-order grey) grains ranging from 6 to 50 μm in lengths or diameters. Some grains contain minor amounts of metal inclusions, thus indicating that the grains were partially melted during the shock event. This high-pressure phase has a similar composition as the chlorapatite in neighbouring chondritic host, but its Cl and Na contents are lower than unshocked chlorapatite [2]. It is identified that the hexagonal structure of chlorapatite has been transformed to a more dense crystalline polymorph (phase A).

**Yanzhuang (H6) chondrite**

Widths of most shock melt veins in this meteorite are from 0.1 to 12 mm. A shock melt pocket is as big as 24 $cm^3$ in volume. The melt veins and pocket mainly consist of recrystallized olivine and pyroxene microcrystals, eutectic metal-troilite nodules and silicate melt glass (Fig. 2). Most of shock-produced ringwoodite, wadsleyite and majorite had been transformed back to their low-pressure polymorphs olivine and pyroxene, and only small amounts of them remained in the melt veins and pocket, as well as in the blackening and partial melting chondritic host neighbouring veins. All apatite and whitlockite in the melt veins and pocket decomposed.

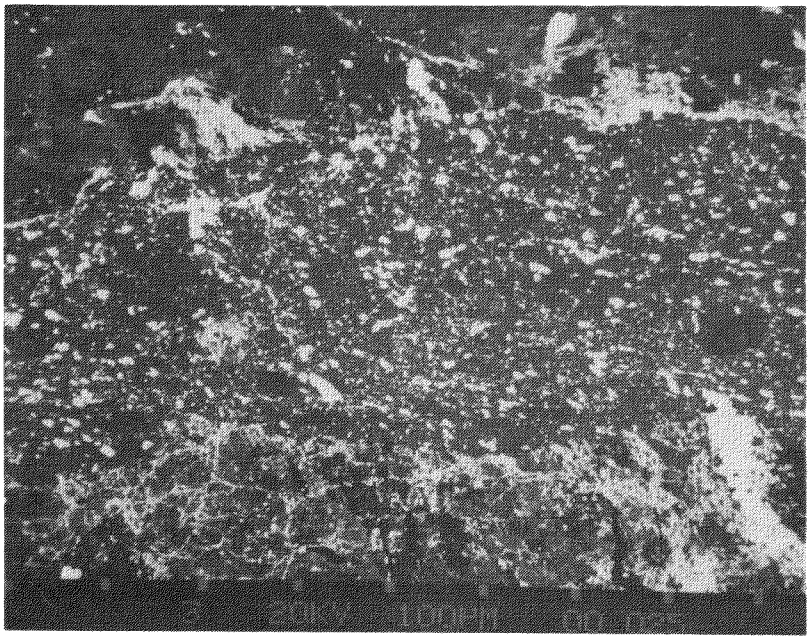

Fig.2. SEM photograph of the shock vein in the Yanzhuang chondrite. The vein consists of mainly recrystallized olivine and pyroxene microcrystals, metal, troilite and silicate melt glass. Small amounts of ringwoodite, wadsleyite and majorite were found remained in the vein.

(1) Ringwoodite and wadsleyite: Figure 3 is a TEM micrograph of a ringwoodite microcrystals in the matrix of melt veins. The ringwoodite contains abundant faults and the very fine antiphase domains within the plates, thus indicating the inversion of γ spinel to β modified spinel phase (wadsleyite). The subhedral and euhedral ringwoodite surrounded by silicate glass shows it crystallized from shock-produced melt. In addition, some big mineral fragments (0.1 - 0.2 mm) identified Raman to be the polyphase assemblage of α (olivine), γ (ringwoodite) and olivine glass were found in the veins, characteristic of shock-induced prograde and retrograde transformation of olivine.

(2) Majorite: Some remained majorite grains were found in the melt veins and pocket. Figure 4 shows a TEM micrograph of recrystallized low-Ca pyroxene containing a remained majorite grain, indicating low-pressure phase pyroxene replacing high pressure polymorph majorite upon the release of pressure.

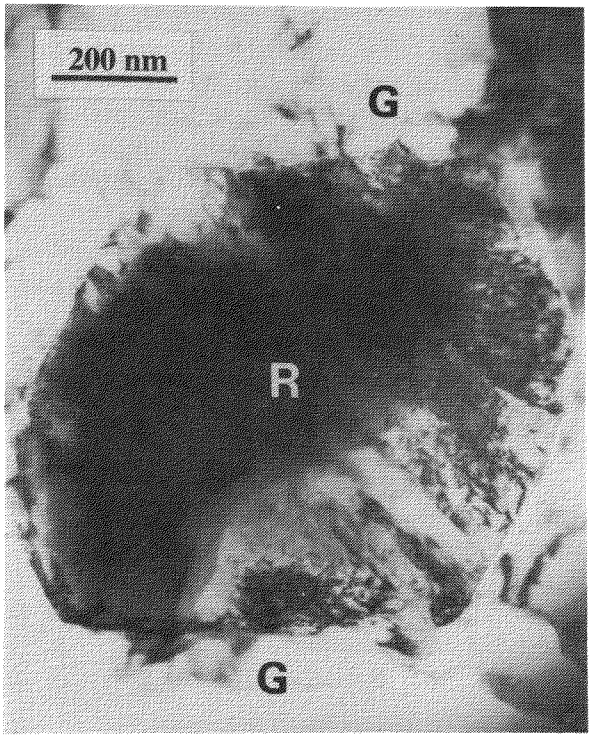


Fig.3. TEM micrograph of a ringwoodite microcrystals in the matrix of shock vein of the Yanzhuang chondrite. The ringwoodite (R) contains abundant faults and very fine antiphase domains within the plates, indicating the partial inversion of γ spinel to β modified spinel phase (wadsleyite). The ringwoodite is surrounded by silicate melt glass (G).

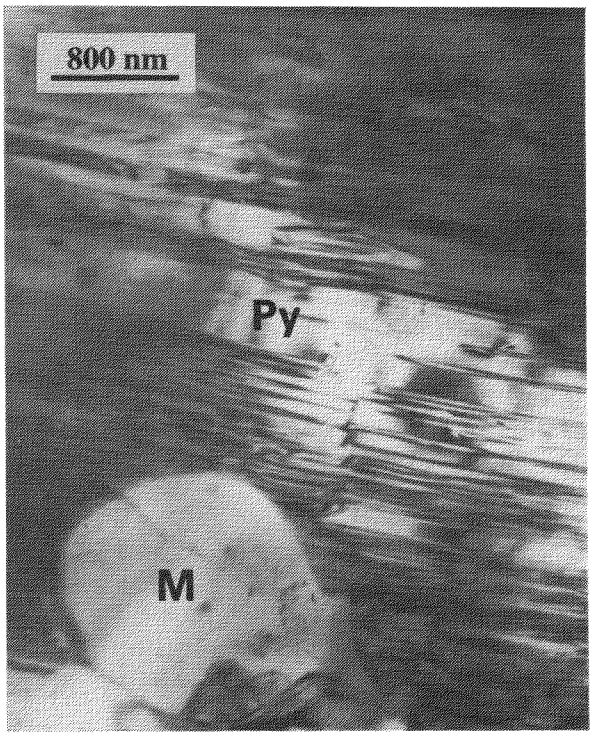


Fig.4. TEM micrograph of a remained majorite grain (M) surrounded by recrystallized low-Ca pyroxene (Py) in a shock vein of the Yanzhuang chondrite. It shows that majorite was replaced by recrystallizing pyroxene.

**Shock wave physical chemistry**

Based on the mineral occurrence characteristics in shock veins, we have estimated the peak shock pressures and post-shock temperatures experienced by the two chondrites: (1) More

than 45 GPa and 1000 °C were induced in the Sixiangkou chondrite, which resulted in extensive solid state transformation of minerals from low-pressure phases to high-pressure polymorphs; (2) More than 80 GPa and 1500 °C were produced in the Yanzhuang chondrite, which resulted in the formation of some high-pressure phases and extensive melting and recrystallization of minerals.

Cooling rates (in the interval of 950 to 1400 °C) of shock-induced melt veins and pocket of the two chondrites have been estimated: (1) about 7 X $10^4$ °C/s in the Sixiangkou chondrite [3]; (2) 6 - 400 °C/s in the Yanzhuang chondrite [6]. The cooling rate is an important condition for the survival and retrograde metamorphism of high-pressure mineral polymorphs. If cooling after high-pressure and high-temperature event is slow, high-pressure mineral polymorphs would easily transform to their low-pressure phases. In contrast, rapid cooling would lead to the quenching and survival of high-pressure phases. The different cooling rates in the shock veins of the Sixiangkou and Yanzhuang chondrites may correspond to the different occurrence and mineralogical characteristics of high-pressure phases in the two meteorites.

**Summary**

(1) The Sixiangkou chondrite contain abundant high-pressure mineral polymorphs, i.e. ringwoodite (with minor wadsleyite), two compositional types of majorite and "phase A"(high pressure polymorph of chlorapatite) in the shock-produced veins. The shock wave high-pressure (>45 GPa) and rapid cooling (7 X $10^4$ °C/s) following the shock-induced high temperature were due to the formation and survival of these high-pressure phases, especially the ringwoodite with high degree of crystallinity and high pressure polymorph of chlorapatite.

(2) The Yanzhuang chondrite experienced very high shock pressure (>80 GPa) and post-shock high-temperature (>1500 °C) in the veins. thus resulting in an extensive melting and recrystallization of minerals. Although ringwoodite and majorite had ever been formed in the melt veins and pocket at high-pressure and high-temperature, a subsequently slower cooling (6 - 400 °C/s) upon the release of pressure had led to the retrograde metamorphism of most high-pressure polymorphs to their low-pressure phases. Only minor amounts of ringwoodite, wadsleyite and majorite remained in the melt veins and pocket.

**Acknowledgements**

We would like to thank Wang Sichao of Purple Mountain Observatory of the Academia Sinica for providing the Sixiangkou meteorite sample used in this study. Drs. A. El Goresy of the Max-Planck-Institut für Kernphysik Germany and B. Wopenka of the Washington University USA are greatly thanked for their contributions in the study of the Sixiangkou chondrite.

**References**

[1] Price G.D. et al. (1979) Contrib. Mineral. Petrol. 71, 211-218.
[2] Chen, M. et al. (1995) Lunar Planet. Sci. XXVI.
[3] Chen, M. et al. (1995) Journal Annal. Geophy.(Abstract), Suppl. 13.
[4] Xie, X. et al. (1991) Meteoritics, 26, 411.
[5] Chen, M. and El Goresy, A. (1994) Meteoritics, 29, 456.
[6] Chen, M. et al. (1995) Meteoritics, 30, 28 - 32.

# THE BEHAVIOR OF METALLIC PHASE IN SHOCKED CHONDRITES

Xie Xiande 1,2,Chen Ming 1,Zhao Biqiang 2,Wang Weidun 2.

1. Guangzhou Institute of Geochemistry,Academia Sinica, Guangzhou 510640,China.

2 .Guangdong Academy of Sciences,Guangzhou 510070 ,China.

**INTRODUCTION** Metallic phase in shocked chondrites are relatively movable during the thermal event caused by shock process in space(Xie and Wang,1979,Xie,1986,Xie and Wang,1992).

Our recent investigates have revealed that during shock and thermal metamorphism of the Jilin H5(S3) and the Yanzhuang H6(S6)chondrites fine Fe-Ni metal particles migrated easily by diffision in solid state,or became molten,and subsequently aggregated into metal nodules about 5-30 mm in length,or recrystallized from melt together with FeS into metallic blobs of various sizes ranging from 0.1um to 7mm.

In this paper we present some results of our study concerning the migration and concentration of Fe-Ni metal in Jilin Chondrite, and the microstructure and distribution of Ni and P in metallic blobs of Yanzhuang chondrite on the basis of optical,SEM observations and shock loading experiments.

**Migration and Concentration of Fe-Ni Metal in the Jilin Chondrite.** It is found that Jilin chondrite contains large metal grains or nodules with the grain size ranging from 5-10mm to 30mm or more. In order to obtain the data on metal grain size,we manually crushed a specimen of Jilin No.2 meteorite weighing 1500g and separated by hand sorting ,sieve separation and magnet separation.Four groups of metal grains of different sizes are partially shown in Figure1.It can be seen that the metal grains in the Jilin chondrite are generally within the range of 0.2-0.8mm in grain size, and there also exist some large grains up to 8-10mm across.Separated from the specimen, weighing 1500g, are 37 metal grains larger than 5mm in size.Their mode of occurance is just like grape raisins embraced in fruit meat.

It is found from our futher studies that these large metal grains sometimes occur along the slicken side within the meteorite or where fractured planes and dark veinlets are well developed.. Some large metal nodules being root-hair shaped jointing with the microstructures developed in the meteorite.

The above facts show that during shock event and subsequent heat influence small Fe-Ni metal grains aggregate into larger grains in situ or after

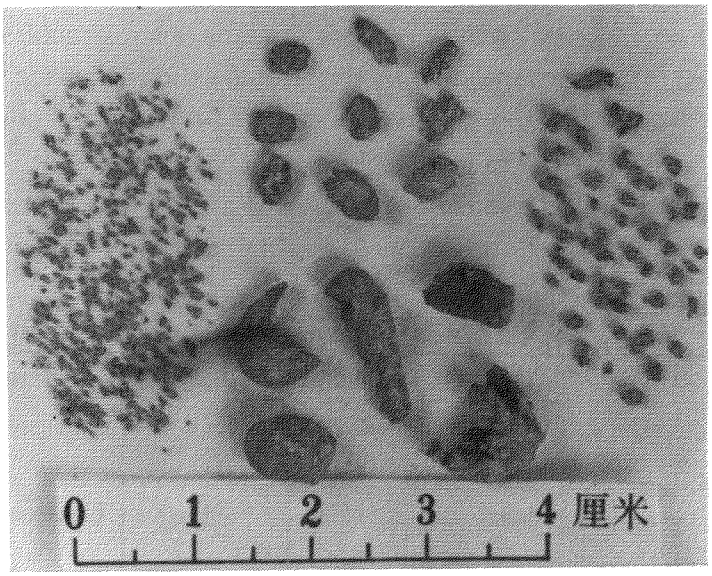


Fig.1 Some FeNi metal grains of different sizes in Jilin No.2 meteorite.

a short-distance migration and concentration, and their chemical composition still remains unchanged.

Shock-loading experiments on the Jilin chondrite were carried out at 4 to 30 Gpa. The results indicate that when the shock-loading pressure is equal to or less than 22 Gpa, metals in the meteorite show no remarkable change, and when the shock-loading pressure reaches 30 Gpa , a few metal grains may become elongated, but their chemical composition remains unchanged (6.50-6.75 Ni in kamacite;and 29.50%Ni in taenite ) or what it was pre-experimentally. It follows from this that shock-induced temperature (about 521°K at 30 Gpa)is so low that metal migration and concentration cannot take place.

**Microstructures of Metal Phase in the Shock-induced Melt of Yanzhuang Chondrite** The Yanzhuang chondrite was considered to be one of the most heavily shocked and severely reheated chondrite described so far (Xie et al,1991). Both shock-generated melt veins and melt pockets in Yanzhuang contain numerous metal-troilite spherules or blobs whose diameters vary from 0.1 to 10mm. These spherules display dendritic or cellular nickel-iron enclosed in troilite due to the fast cooling (Fig.2). Although the bulk composition of the dendrites in the melt veins and in the melt pocket are identical, they display diffecent structures with different compositions. The metal dendrites in the melt pocket have a typical crust-core microstructure, but those in the melt veins exhibit heterogeneous microstructures or three microstructural areas (Chen et al.1995),the cores(Area 1) Ni-rich rims(Area 3)and the martensite regions (Area 2)in between( Fig.3)

Figure 4.E-F shows Profiles of Ni and P concentrations across a metal particle in melt pocket . It demonstrates that the Ni-content in the martensite core is relatively homogeneous, the Ni-content steeply increases to the rim,the P-content decrease from the interior to the rim (about from 0.65 to 0.45wt%). Some P-poor regions were encountered in the martensite core.

Figure 4.A-B and 4.C-D depict microprobe profiles of Ni and P concentrations across a metal particle in a melt vein . It shows that both Ni and P concentrations increase from Area 1 to Area 2, while only Ni steeply increases in Area 3 along with a decrease in P .It is interesting that Area 1 and 2 have relatively constant Ni-and P-contents .Two composition steps are recognized in the Ni profile across Area 1 and 2. Based on the characteristics of the compositions and microstructures of the three metal areas in the dendrites, we conclude that the crystallization sequence was :Area 1 → Area 2 → Area 3.

The high phosphorus content (0.3-0.65 wt%) concerntrating in the metal dendrites in Yanzhuang indicates that phosphides may be present . However, none were encountered during optical microscopy , or SEM and EPMA.Therefore ,we consider that most of the phosphorus is present in the metal dendrites in solid solution or as submicroscopic phosphide grains , thus indicating fast cooling .

**Table 1.Characteristics of metal phase in chondrites**

| Chondrite | Occurence | Temp.℃ | Cooling rate | Structure | Ni-concentr. | P-concentr. |
|---|---|---|---|---|---|---|
| Jilin H5(S3) | Chondritic mass | <800 | 1℃ /Ma | Homogeneous | Uniform (6.55-8.39wt.%) | Uniform(0.12wt.%) |
| Yanzhuang H6(S6) | Melt Pocket | >1500 | 6-30℃/s | Crust-core | M-type(7.5-8.1,12.5-23.3wt.%) | V-type(0.45-0.65wt.%) |
| | Melt Veins | >1500 | 100-400℃/s | Three areas | Step-type(6.4-7.3,7.4-8.5,12.8-21.4wt.%) | W-type(0.35-0.7wt.%) |

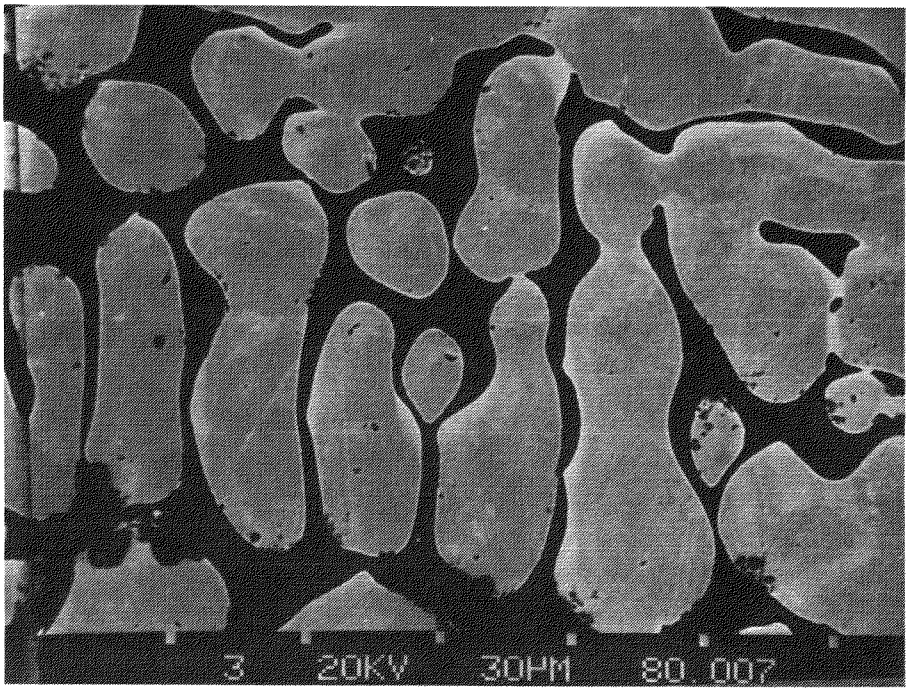


Fig.2. SEM image of the metal-troilite spherule in a melt vein of Yanzhuang

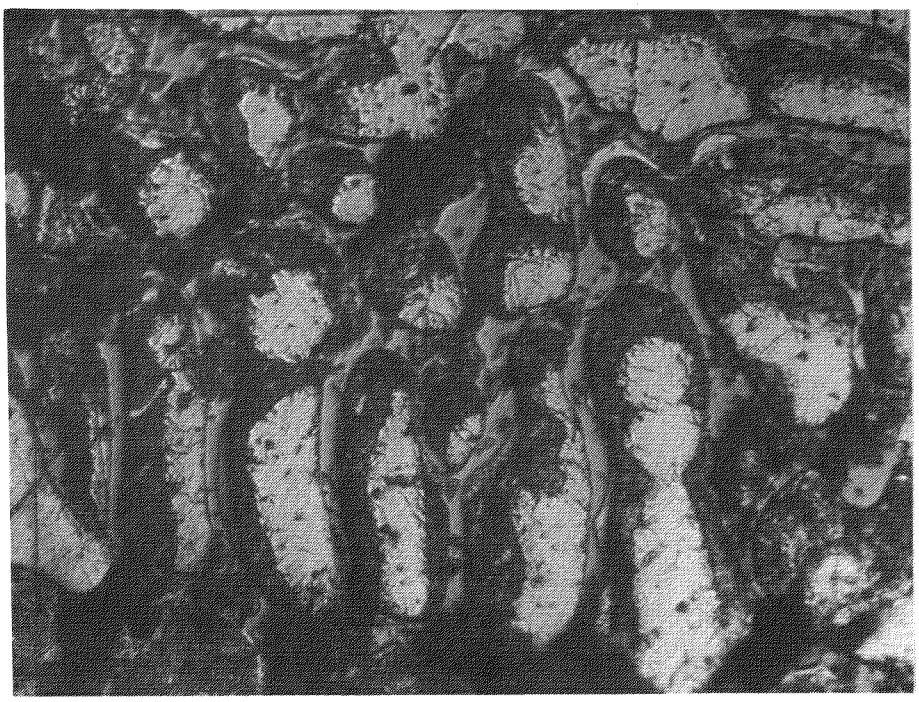

Fig.3. As Fig.2, etched surface,reflect light.

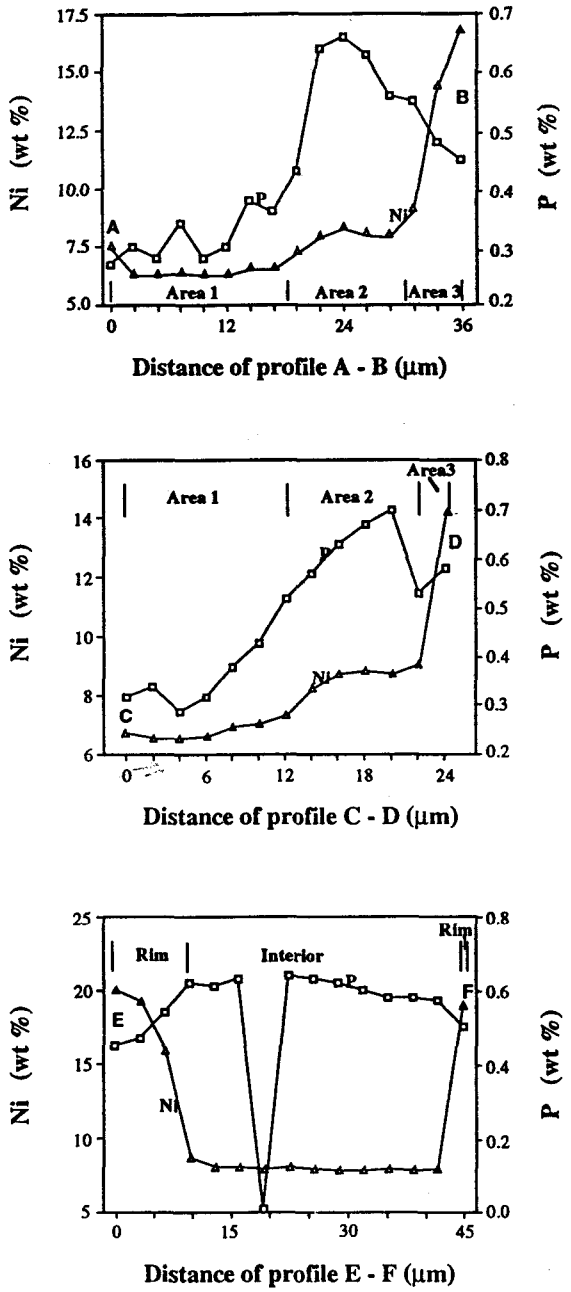


Fig.4. The Ni-and P-concentration profiles across metal particles.
A-B and C-D are profiles for particles in a melt vein.
E-D are profiles for the particle in a melt pocket.

**SUMMARY** We have shown three distinct kinds of behavior of metal phase in weakly shocked Jilin Chondrite and heavily shocked and severely reheated Yanzhuang chondrite.Their characteristics is summarized in Table 1.The different behavior of metal phase was caused by the different degree of shock and shock-induced temperature, and in cooling rates .

**REFERENCE**: (1) Xie Xiande and Wang Daode(1979) Compiled Data on the Jilin Meteorite Shower, Science Press, Beijing 184-191.(2)Xie Xiande(1986) Abstracts 14th GM of IMA,271.(3)Xie Xiande, Wang Daode (1992) Chinese Journal of Geochemistry Vol.11,No.1,23-31.(4)Chen Ming, Xie Xiande and. A.El Goresy (1995) Meteoritics.30,28-32.

**Formation process of magnetic spherules in deep-sea sediments**

T. Yada, T. Nakamura and N. Takaoka
Dept. Earth & Planet. Sci., Kyushu Univ., Fukuoka 812-81

## Introduction

Spherules in deep sea sediment have been long studied for extraterrestrial materials since 1884 [1]. They are grouped into I(Iron)-type, S(Stony)-type, and G(Glassy)-type [2].They are supposed to be ablation products of micrometeroids [2-4], which were melted and quenched in several seconds. But their formation process is still uncertain [3-8]. In order to make clear this problem, we studied spherules separated by magnet and handpicking from deep sea sediment dredged at offshore of Hawaii about 5800m depth. We analyzed about 100 spherules for morphology and surface chemistry by EPMA. Then we selected typical spherules from each morphological group and polished them to examine mineral chemistry in the interior.

## Morphology and internal structure

The morphology of S-type spherules are barred, microporphyritic and porphyritic structures. Usually they consist of olivine. The internal texture is matched with their morphology. In I-type spherules, their morphology is roughly devided into dendritic, relatively smooth and polygonal structures, but no relation between their morphology and internal texture is observed. On the chemical composition, they are grouped into Fe-oxide and Fe-Ni oxide. In addition, some Fe-Ni oxide spherules have a metallic core with magnetite mantle, while others don't have a metallic core and consist of relatively homogeneous Fe-Ni oxide.

## Cooling rate of S-type spherules containing relict grains [3]

Some S-type spherules contain relatively large forsterite grains (Fig.1). They usually have zonal structure. FeO and CaO in olivine decrease toward the center. This indicates that FeO and CaO might diffuse into relict forsterite grains from surrounding materials rich in Fe and Ca during heating of atmospheric entry. From the depth profile fitting [9], the cooling rate and peak temperature for one of the relict grains were calculated to be $3.0 \times 10^5$ ℃/hour and 1800℃, respectively.

## Formation model of I-type spherules

The structure of I-type spherules depends on their starting material and thermal history (peak temperature, heating time and cooling rate). As starting material, we suppose Fe-Ni metal (Ni: 6 wt%) with <1 wt% Co and minor elements common in the metal phase of meteorites, such as Pt group. Heating time is supposed to be several seconds and melting time must be shorter [4]. Fig. 2 shows standard free energy of formation ($\Delta G$) vs temperature (℃) graph for oxides. $\Delta G$ gives free energy difference from an oxide phase to a metallic one at a certain temperature. When an oxide phase is more stable than a metallic one, the former has smaller free energy than the latter, resulting in $\Delta G<0$. In the same way,

$\Delta G>0$ indicates a metallic phase is stable.

As shown in Fig. 2, $Fe_3O_4$ is more stable than FeO above 3360℃ and FeO is so below 3360℃, because $\Delta G$ of FeO is higher than that of $Fe_3O_4$ above 3360℃ and lower than it below 3360℃. $\Delta G$ of Ni is positive over 2300℃ and negative at lower temperature, so above 2300℃ Ni is stable in a metal phase and NiO is stable below 2300℃. Co is stable in a metal phase over 2800℃ and becomes oxide below 2800℃. Pt group keeps metal phase until they are solidified because of their excessive $\Delta G$ beyond NiO.

Based on these redox conditions, we propose a formation model of I-type spherules. If the peak temperature exceeds 2800℃, Fe is oxidized to form oxide mantle around a metallic core in which Ni, Co and Pt group are consequently concentrated (Fig. 2 (C) and (D)). In this case, the mantle is free from Ni because Ni is swept out into the core.

In contrast, below 2300℃, Fe, Ni, and Co are oxidized homogeneously, except for Pt group. Consequently, an I-type spherule with homogeneous Fe-Ni oxide and small Pt group nuggets (PGN) is formed, as Fig. 2 (A).

When the peak temperature rises above 2800℃, Fe-Ni core and magnetite mantle are formed. If it cools slowly, parts of Fe, Ni and Co in the core are oxidized and disperse homogeneously to the magnetite mantle. Therefore, the spherules is formed homogeneous Fe-Ni oxide mantle containing a Fe-Ni metallic core, just like Fig. 2 (B).

Fe-Ni grains entering the atmosphere are heated and oxidized at high altitude. When the grains' entry speed is 30 km/s, $P_{O2}$ that the grain head received is lower by $10^{-4}$ at 100 km altitude than the atmospheric $O_2$ pressure. It increases at low altitude, e.g., for a grain with 14 km/s at 50 km, the pressure comes approximately to the atmospheric one. We use this diagram to interpret the variety of I-type spherules for simplicity, although pressure dependency should be considered for quantitative discussion.

The size of spherule depends on surface tension of liquid alloy and wind pressure they experienced. When their entry speed are fast and deformation by wind pressure exceeds surface tension, they couldn't keep large size and fragment into small spheres. In the case of low entry speed and small wind pressure, the liquid alloy could keep a large sphere. Therefore, high entry speed gives small spherules experienced high peak temperature, and low entry speed forms large spherules at low peak temperature. In general, I-type spherules with metallic cores are usually in small size whereas homogeneously oxidized I-type spherules are in relatively large size [6]. This is consistent with our I-type spherule formation model.

**What we have to do next**

In order to confirm our model, we have to analyze Ni isotope of each iron spherules' type to observe intensity of mass fractionation as a result of evaporation of atmospheric entry [11] because evaporation might depend on peak temperature and heating time they experienced.

Peak temperature and heating time of micrometeoroids are supposed to depend on their entry speed and angle. With exact simulation and mineralogical study of spherules, we

could estimate limits of some orbital factors of micrometeoroid which result in spherules. It is important to simulate micrometeoroids' temperature with a better model and examine statistics of occurrence mode of iron spherules' mineralogical type.

We thank Prof. M. Miyamoto in Mineralogical Institute, University of Tokyo for calculation of the cooling rate of relict grains and late Prof. K. Yamakoshi in Institute of Cosmic Ray Research, University of Tokyo for giving us the sediment sample.

(Reference)

[1] J. Murray and A.F. Renard (1884), Proc. R. Soc. Edinb. , 12, 474-495
[2] D. E. Brownlee (1985), Ann. Rev. Earth Plant. Sci., 13, 147-173
[3] M. B. Blanchard, D. E. Brownlee, T. E. Bunch, P. W. Hodge and F. T. Kyte (1980), Earth Plant. Sci. Lett., 46, 178-190
[4] S. G. Love and D. E. Brownlee (1991), Icarus, 89, 26-43
[5] R. A. Schmidt and K. Keil (1966), Geochim. Cosmochim. Acta, 30, 471-478
[6] D. E. Brownlee, B. A. Bates and M. M. Wheelock (1984), Nature, 309, 693-695
[7] S. Tayler and D. E. Brownlee (1991), Meteoritics, 26, 203-211
[8] Dong Bi, R. D. Morton and Kun Wang (1993), Geochim. Cosmochim. Acta, 57, 4129-4136
[9] M. Miyamoto, D. S. Mckay, G. A. Mckay and M. B. Duke (1986), J. Geophys. Res., 91,12804-12816
[10] J. F. Elliott and M. Gleiser (1960), Addison-Wesley, Thermochemistry for Steelmaking, Vol. I
[11] G. F. Herzog, G. S. Hall and D. E. Brownlee (1994), Geochim. Cosmochim. Acta, 58, 5319-5323

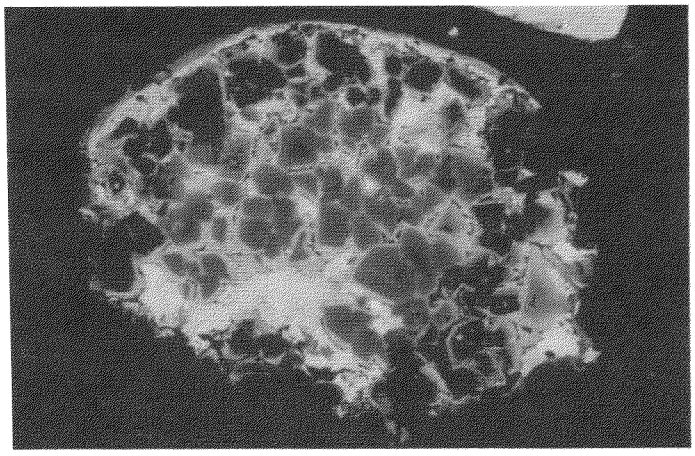

Fig. 1: A S-type spherule containing relict grains. Over 30 of relict forsterite grains (gray) distribute around the center. FeO content is $Fa_3$ in the center and increases toward the edge up to $Fa_{47}$. White area surrounding the grains is Fe-Ni sulfide. Black vesicles are grains etched away by sea water. The spherule's width is 164$\mu$m.

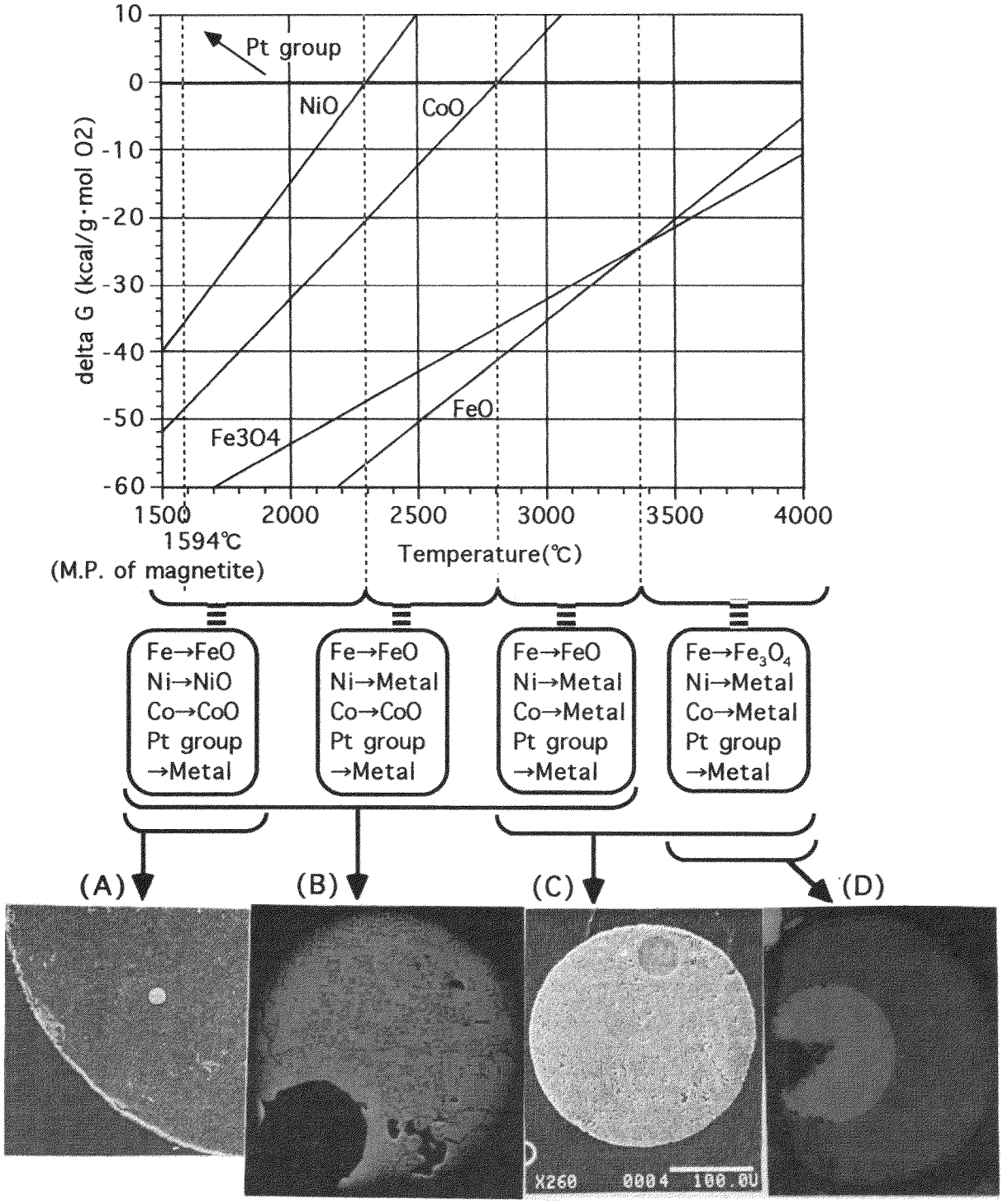


Fig. 2: A graph of temperature to standard free energy of formation which are extrapolated from [10] (upper), phases of elements classified on the basis of their temperature range in the graph (medium) and real spherules collected from deep sea sediment (lower). (A) A 8$\mu$m Pt group nugget (white) in a homogeneous Fe-Ni oxide spherule (black matrix), which size is over 300$\mu$m [6]. (B) A 88$\mu$m spherule consisting of Fe-Ni oxide mantle including >10wt% Ni and metal core omission, supposed to have existed at lower left vesicle. Light and gray texture results from Ni exsolution, during cooling. (this work) (C) A 270$\mu$m spherule with Fe-Ni metal core and mantle of magnetite and wüstite [7]. (D) A 92$\mu$m spherule of magnetite mantle and Fe-Ni metal core (Ni: 39wt%). (this work)

## EUCRITES: GLOBAL CRUSTAL METAMORPHISM BY BURIAL ON VESTA

A. Yamaguchi, G. J. Taylor, and K. Keil, Hawaii Institute of Geophysics and Planetology, SOEST, University of Hawaii, HI 96822, USA.

### Introduction

Eucrites are basalts that make up part of crust of asteroid 4 Vesta [1, 2]. They have Sm-Nd ages of 4.46-4.56 Ga [3]. Most of eucrites show petrographic, mineralogical, and radiometric evidence for complex metamorphism, brecciation, and shock. The rich diversity of igneous, metamorphic, and impact effects in eucrites allow us to develop a picture of the crustal history of Vesta. This is an important task because it will eventually allow us to compare crustal formation on a small body like Vesta to progressively larger bodies: the Moon, Mars, Venus, and Earth. The story is far from complete, but we present our preliminary conclusions here. We focus on the nature of the heat source that drove the metamorphism.

### Thermal and impact history of eucrites

Initial cooling rate of the basaltic eucrites near the melting point was relatively fast (on the order of 0.1 to 100 °C/hr [4]). As shown by Walker et al. [5], these cooling rates imply distances from a cooling surface of roughly 10 cm to a few meters, consistent with formation in lava flows or shallow dikes. Such thin flows cool too fast to be the sites of the extensive thermal metamorphism experienced by the eucrites. Even the centers of flows 5 meters thick cool to ambient temperatures (probably 0 °C on the surface of Vesta) in about a year, too little time to cause any metamorphic effects.

After eucritic basalts formed in lava flows, the minerals in them were undoubtedly chemically zoned. However, much of this zoning has been erased by subsequent thermal metamorphism, resulting in equilibrated eucrites [e.g. 6, 7]. Miyamoto et al. [8] suggested that equilibrated eucrites (e.g. Juvinas) formed by thermal annealing of unequilibrated eucrites, and the equilibration of the pyroxene grains occurred over < 1 Ma at 1000 °C. Thermal histories of the equilibrated eucrites are variable; many of them probably experienced more extended metamorphic histories [7, 9].

During the thermal metamorphism, the basaltic eucrites experienced repeated shock and brecciation events. Because of this, various recrystallization and melting textures are observed in the equilibrated eucrites [9, 10]. The breccia textures of the equilibrated eucrites look like 'genomict breccias' rather than 'monomict breccias'.

### Crustal evolution of Vesta

*Impact heating: inadequate*

Equilibrated eucrites are multistage breccias, so impact has certainly affected the eucrite parent body. The geologic setting for the formation of such breccias could be at the floors of

craters [11] but impact deposits cool faster than required for eucrite metamorphism. Nyquist et al. [3] suggested that the equilibrated eucrites could have been metamorphosed at the base of impact melt sheets. However, even large melt sheets cool too fast to provide the necessary $10^4$ - $10^6$ y needed to equilibrate eucrites. The temperatures in a melt sheet depend on the melt/clast ratio, and the cooling period depends largely on the total mass of the melt sheet [12]. For example, at the terrestrial Manicouagan crater (65 km in diameter, with a melt sheet 200 m thick), the melt sheet quenched to 1000°C in minutes, then cooled to ambient temperatures in only 1000 y [12]. It is unlikely that much larger impacts with much larger melt sheets occurred on Vesta, which is only 520 km in diameter. In addition, metamorphic effects in impact melt sheets and below them are minimal. Besides the thermal problem, impact melt rocks are very rare among eucrites. If impact melts provided most of the heat for the ubiquitous eucrite metamorphism, there ought to be large numbers of impact melt breccias of eucrite composition.

*Metamorphism by successive lava flows: inadequate*

In principle, rapid eruption of lava flows on top of one another could lead to autometamorphism of underlying hot lava flows. However, this requires an exceptional rate of lava eruption. As noted above, the plagioclase sizes in eucrite basalt clasts suggest cooling rates consistent with lava flows at most a few meters thick. These cool to ambient temperatures in about one year. For each flow to be held at a higher temperature subsequent lava flows would need to flow on top more frequently than once a year, and do so globally.

This is inconsistent with reasonable eruption rates on Vesta. If the basaltic crust is 25 km thick, as estimated by Delany [13], its volume would be $1.8 \times 10^7$ $km^3$. If all this basalt was erupted during a period of only 1 million years, and ignoring the portion of the basaltic magma that would be intrusive, the average mass effusion rate would be 18 $km^3/y$. For comparison, this is approximately equal to the total magma production on Earth today, and much more than typical active magmatic regions on Earth such as Kilauea Volcano, which produces 0.1 $km^3/y$. In spite of this impressive lava production rate, it results in a global average of 20 meters of lava per thousand years. This suggests that the interval between eruptions at any given site is almost always far greater than the cooling time of an individual lava flow. In other words, the basaltic crust grows too slowly to allow lavas to metamorphose the previous flows that they cover.

*Global crustal metamorphism by burial*

If eucrites formed by partial melting [14], the melts would migrate readily to the surface, producing a basaltic crust. The crust would grow with time as new lavas were added to the top, finally reaching a thickness of between 10 km [15] and 25 km [13]. The result is that flows initially at the top would be buried progressively deeper, eventually heating up to metamorphic temperatures, 800-1000 °C [9]. The metamorphism would be aided by heat added to lower crustal levels by intrusions of basaltic magma.

We envision that this crustal growth would take place rapidly, probably lasting about 1 My, certainly not longer than a few My. During crust formation and after the crust was in place, impacts would produce a regolith on it, providing insulation to aid in retaining remnant heat inside the body, and any additional generated heat. Assuming a thermal diffusivity of 0.01 $cm^2/s$, the heat would diffuse from the hot interior an average of 5 km in 1 My and about 15 km in 10 My. The temperature gradient in the crust, which would be most pronounced near the surface, and the thickness of the crust provide a range of metamorphic environments and are consistent with the roughly 100 My age differences among eucrites [16]. There would be regions of the crust where the temperature never exceeded 800 °C, but were held at almost that temperature for > 1 My, producing rocks like type 4 [7], which retain evidence of Ca zoning in pyroxenes but have 2-pyroxene temperatures of about 800 °C [9]. There could be others that reached 1000 °C and cooled slowly, producing rocks like type 6 [7] that have no remnant Ca zoning, equilibrated pyroxenes, and low 2-pyroxene temperatures [9].

Impact played an important role in the evolution of Vesta's crust. Besides the role of regolith in insulating the body, impacts would have produced a highly brecciated surface, thus accounting for the ubiquity of eucrite breccias. While magmatism was still active on Vesta, the breccias would have been buried by lava flows. Some impacts would be large, excavating deep into the crust. These would produce eucrites with more complicated brecciation and metamorphism histories, as recorded in many eucrites. Larger impacts would excavate hot rocks at a variety of times, accounting for the range in metamorphic temperatures and ages of eucrites.

**References:** [1] Binzel R. P. and Xu S. (1993) Science, 260, 186-191. [2] Gaffey M. J. and Hall W. (1995) Icarus, in press. [3] Nyquist L. E., et al. (1986) J. Geophys. Res., 91, 8137-8150. [4] Walker D. et al. (1978) Proc. Lunar Planet. Sci. Conf., 9, 1369-1391. [5] Walker D. et al. (1976) Proc. Lunar Sci. Conf. 8, 1489-1499. [6] Reid A. M. and Barnard B. M. (1979) Lunar Planet. Sci., 10, 1019-1022. [7] Takeda H. and Graham A. L. (1991) Meteoritics, 26, 129-134. [8] Miyamoto M. et al. (1985) Proc. Lunar Planet. Sci. Conf., 15, C629-C635. [9] Yamaguchi A. et al. (1995) Lunar Planet. Sci., 26, 1531-1532. [10] Metzler K. et al. (1994) Planet. Space. Sci., in press. [11] Stöffler D. et al. (1981) Workshop on Apollo 16, 132-141. LPI, Houston. [12] Onorato P. I. K. (1978) J. Geophys. Res., 83, 2789-2798. [13] Delaney J. S. (1995) Lunar Planet. Sci., 26, 329-330. [14] Stolper E. et al. (1977) Geochim. Cosmochim. Acta, 41, 587-611. [15] Miyamoto M. and Takeda H. (1994) Earth Planet. Sci. Lett., 122, 343-349. [16] Warren P. H. et al. (1991) J. Geophys. Res., 96, 5909-5923.

# Mineral distribution and the opaque grain shapes of primitive achondrites

Keiko Yugami, Hiroshi Takeda and Masamichi Miyamoto
Mineralogical Institute, Graduate School of Science, University of Tokyo,
Hongo, Tokyo 113, Japan.

**Introduction.**

Primitive achondrites include sub-groups: acapulcoites, lodranites, winonaites and silicate inclusions of iron meteorites. The oxygen isotopic compositions indicate that acapulcoites and lodranites (AL) are from the same parent body [1]. The AL group includes meteorites of various modal abundances of minerals and textures. Lodranites are distinguished from acapulcoites mainly by a criterion of that they are coarser grained and depleted in plagioclase. Their opaque minerals are FeNi metal, troilite and accessory chromite. They often coexist within one opaque grain. The opaque grains have interesting complicated shapes. The complexity of opaque mineral shapes varies from meteorites to meteorites.

The area and perimeter of the opaque grains of six meteorites in the AL group have been measured to represent the complexity of the shape of an opaque grain by numerical values [2]. We made two dimensional distribution modal maps of opaque grains and plagioclase of four acapulcoites and made a hypothetical map in a larger scale to examine the relationship between the textures and the mineral distributions of meteorites in the AL group.

**Samples and Methods.**

We studied polished thin sections (PTS) of six meteorites in the AL group, Acapulco, ALH77081, ALH78230, EET84302, Y791491 and MAC88177. These samples were supplied from Meteorite Working Group, National Institute of Polar Research, and Planetary Materials Database Collections of University of Tokyo. Acapulco, ALH77081 and ALH78230 are acapulcoites; Y791491 and MAC88177 are lodranites. EET84302 has acapulcoite-like modal abundances of silicate minerals and lodranite-like large grain size.

The opaque grains of EET84302 show extremely complex shapes. They often almost surround silicate grains. It is well known that EET84302 has heterogeneous distribution of minerals [3]. There are remarkable differenses between PTS,19 and PTS,28 in modal abundances of minerals and one area is a lodranite-like area with major orthopyroxene and chromite, and other areas are rich in metal and plagioclase [3]. Acapulco, ALH77081, ALH78230 and EET84302, 28 were studied by electron probe microanalyzer (EPMA) at Geological Institute, Graduate School of Science, University of Tokyo. Two dimensional chemicals mapping analysis (CMA) techniques of have been applied to Acapulco, ALH77081, ALH78230 and EET84302, 28. Modal abundances of minerals of Acapulco, ALH77081 and ALH78230 are obtained from CMA. Photomicrographs of polished thin sections of Y791791, MAC88177 and EET84302,19 were taken with transmitted light to make the hypothetical mineral distribution map.

**Results and discussion.**

The distribution of opaque minerals (FeNi metal, troilite, chromite and shreibersite) and plagioclase of Acapulco, ALH77081, ALH78230 and EET84302, 28 are shown in Fig.1.

Modal abundances of minerals of Acapulco, ALH77081, ALH78230 obtained by CMA are shown in Table 1.

The areas (S) and perimeters (L) of the opaque grains of six meteorites in the AL group have been measured [2]. The amounts of plagioclase and opaque minerals and the value of $L/\sqrt{(4\pi S)}$ of six samples are plotted in Fig. 2. The value of $L/\sqrt{(4\pi S)}$ indicates the complexity of the grain shape. EET84302 is much larger in the opaque grain size and in the total amount of opaque minerals and in $L/\sqrt{(4\pi S)}$ than other five samples. Acapulco has larger grain size and larger $L/\sqrt{(4\pi S)}$ value and slightly smaller amounts of plagioclase than other acapulcoites. The silicate grains of Acapulco are also larger than other acapulcoites. The meteorites which are similar to Acapulco [4] are called acapulcoites [e.g. 5], but Acapulco is not a very typical acapulcoite [6].

Plagioclase grains appear often next to opaque grains. EET84302 is the largest in grain size of plagioclase and Acapulco is the second. Some opaque grains seem to align to a line, or in circles that are the parts of big network. Opaque grains have shapes that fill the space between silicate grains in these six samples. If the spaces are large and big amounts of melt were supplied, the spaces are connected and large opaque grains with complex shapes like those in EET84302 can be formed. If the process goes one step further, an iron meteorite with silicate inclusions can be formed. The complexity of the opaque grain shapes may be resulted from the melting and migration of low-temperature melting materials such as the Fe-Ni-S eutectic melt and Ca-Al-rich melt.

We made a hypothetical map of the distribution of opaque minerals and plagioclase in a larger scale (Fig. 3) to show the idea that local heterogeneity of materials in AL parent body can explain the variability of abundances of minerals [3]. The fine grained region is acapulcoite and the region with coarse grained minerals and depleted in plagioclase is lodranite. Iron meteorites with silicate inclusions may also be formed in the same parent body if the Fe-Ni-S eutectic melt is concentrated at one region.

We thank the Meteorite Working Group, National Institute of Polar Research, and Planetary Materials Database Collections of University of Tokyo for samples and Mr. H. Yoshida for technical assistance.

**References:** [1] Clayton R. N. et al. (1992) *Lunar Planet. Sci.* **23**, 231-232. [2] Yugami K. et al. (1995) *Mineralogical Society of Japan 1995 Annual Meeting Abstract.* [3] Takeda H. et al. (1994) *Meteoritics* **29**, 830-842. [4] McCoy T. J. et al. (1993) *Lunar Planet. Sci.* **24**, 945-946. [5] Palme H. et al. (1981) *Geochim. Cosmochim Acta* **45**,727-752. [6] Yugami K. et al. (1995) *Proc. 27th ISAS Lunar and Planetary Symp.*, 129-123.

Table 1. Modal abundances of minerals of Acapulco, ALH77081, ALH78230 obtained by CMA. (volume %)

| | Acapulco | ALH77081 | ALH78230 |
|---|---|---|---|
| Orthopyroxene | 39.3 | 36.2 | 37.2 |
| Olivine | 30.7 | 32.2 | 29.1 |
| Augite | 3.9 | 7.7 | 11.5 |
| Plagioclace | 11.2 | 13.3 | 12.4 |
| Ca phosphate | 1.4 | 0.5 | 0.4 |
| FeNi Metal | 4.3 | 2.8 | 4.7 |
| troilite | 8.5 | 4.2 | 4.3 |
| chromite | 0.7 | 3.1 | 0.4 |

Fig. 1. Two dimensional distribution maps of plagioclase and opaque minerals of ALH77081, ALH78230, Acapulco and EET84302, 28. ■ = opaque minerals. ▨ = plagioclase.

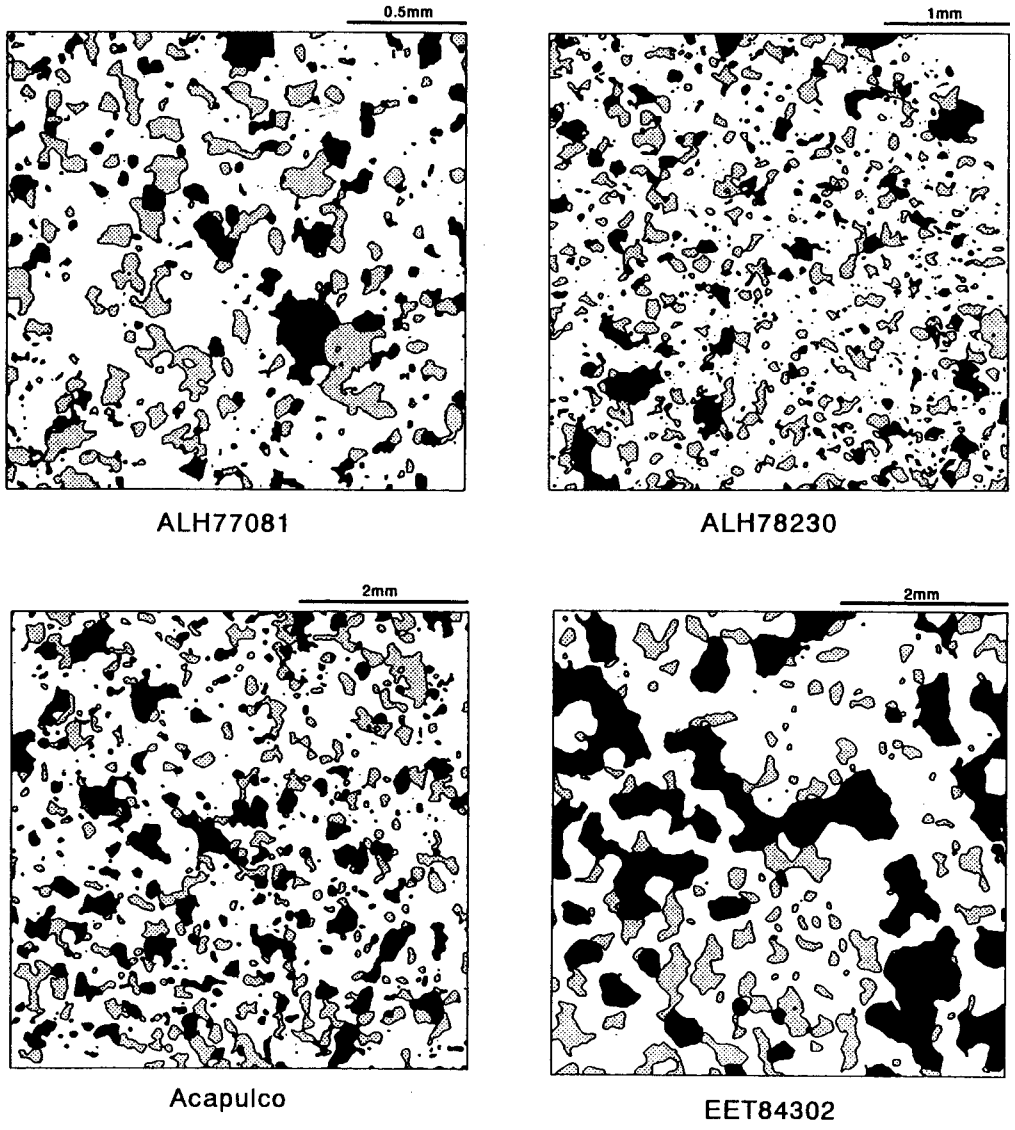

Fig. 2. Opaque grains and plagioclase volume percentage and $L\sqrt{(4\pi S)}$ are plotted in one figure. The volume percentage data of Y791491, MAC88177 and EET84302 are from Takeda et al (1994). Shape = $L\sqrt{(4\pi S)}$.
Aca = Acapulco. A081 = ALH77081.
A230 = ALH78230. Y = Y7891491.
M = MAC88177. E = EET84302, 28.

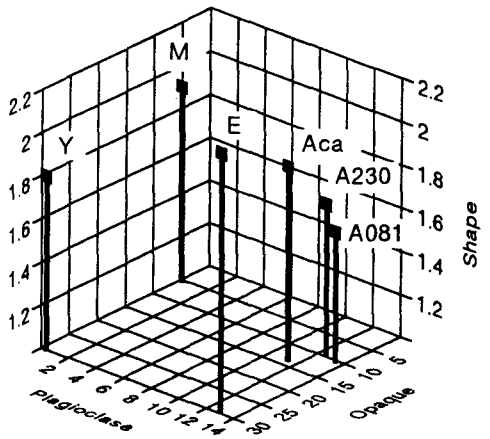


Fig. 3. The hypothetical map of the distribution of opaque minerals and plagioclase in a large scale. It does not indicate the true ratio of grain size and the distance because it is to show the idea of local heterogeneity of materials simply. ■ = opaque minerals. ▒ = plagioclase.

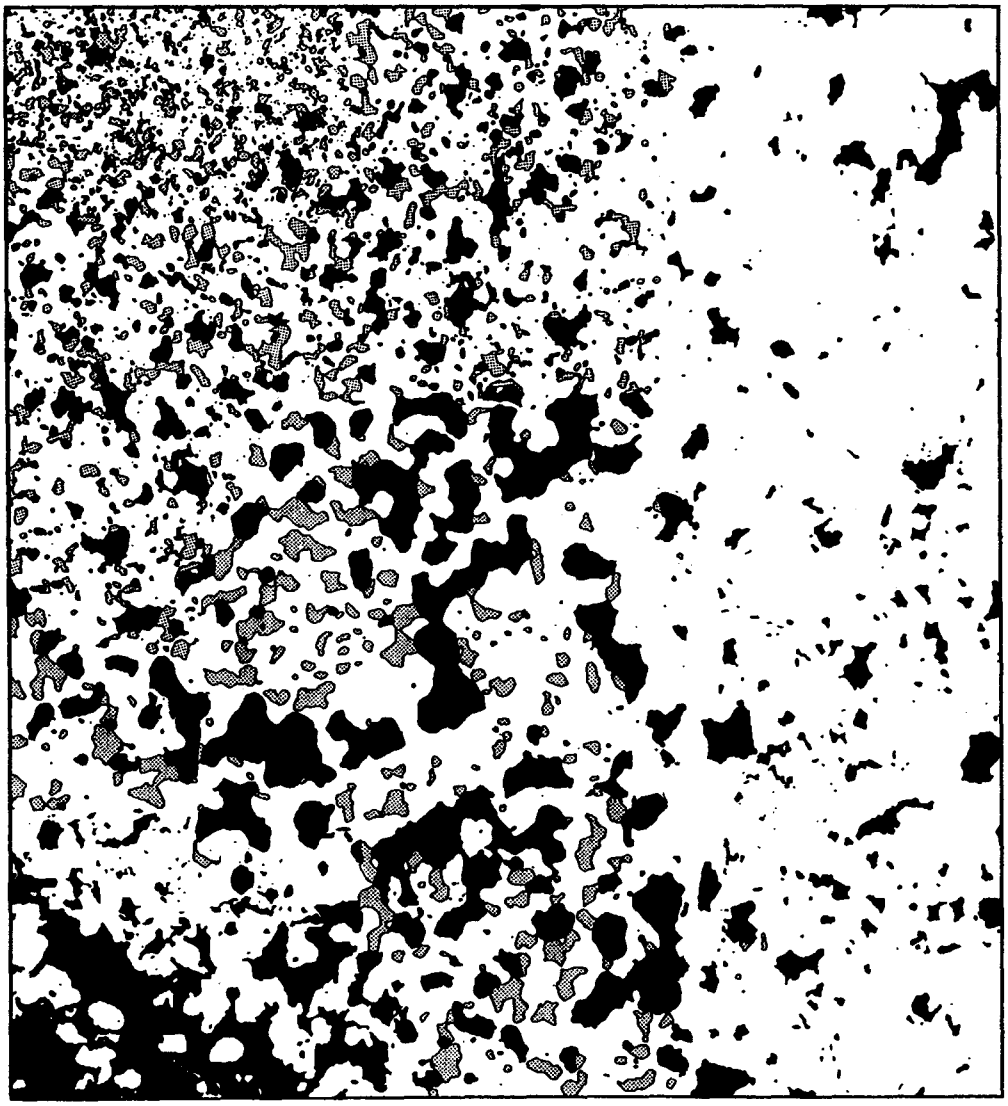

# Circumstellar Grains in Meteorites: A New Window to the Stars

Ernst Zinner

*McDonnell Center for the Space Sciences and the Physics Department*
*Washington University, Saint Louis, Missouri 63130-4899 USA*

Traditionally, information about the distant stars has been obtained by astronomical observation of visible light. In the recent past use of the wavelength range of the electromagnetic spectrum that carries information on stars has been vastly expanded, reaching from radio waves to gamma rays. In addition, cosmic rays are believed to reflect the elemental and isotopic compositions of stellar sources and neutrinos originating from our sun and a supernova source have been observed.

In the last few years a new source of information about stellar sources has become available in the form of circumstellar grains found in primitive meteorites [1-3]. These grains are believed to have condensed in stellar outflows and ejecta and thus reflect the elemental and isotopic composition of stellar sources. The isolation and identification of carbonaceous circumstellar grains has been greatly facilitated by the fact that they carry "exotic" (i.e., isotopically anomalous) noble gases. Carbonaceous grains identified to data are: **diamond**, carrier of Xe-HL [4], **silicon carbide**, carrier of Ne-E(H) and Xe-S [5, 6], and **graphite**, carrier of Ne-E(L) [7]. In addition, SiC and graphite were found to contain tiny subgrains of **Ti, Zr and Mo carbides** identified in the transmission electron microscope [8-10]. Interstellar **oxide** grains apparently do not carry any noble gases [11] and were found by ion microprobe isotopic analysis of single grains [12-15] as were **silicon nitride** grains [16]. The ion microprobe also played an important role for the anlysis of graphite and SiC grains since this instrument makes it possible to measure the isotopic compositions of individual grains down to sizes of less than 1μm (diamond grains are too small for single grain analysis).

Based on the isotopic compositions of the grains, two important stellar sources could be identified for meteoritic circumstellar grains: red giant stars, low to medium mass stars during late stages of their evolution, and supernovae, massive stars that exploded at the end of their evolution.

**Red Giant Stars.** – Most of the SiC grains are believed to originate from red giants, specifically from thermally pulsing AGB stars because [see 3]: 1) the distribution of $^{12}C/^{13}C$ ratios in single SiC grains is similar to that in carbon stars ; 2) AGB stars are the main contributor of carbonaceous dust to the interstellar medium; 3) there is evidence for SiC in the dusty envelopes of carbon stars from their 11.2 μm emission feature and 4) AGB stars are believed to be the main source of s-process elements and "bulk samples" (collections of many grains) of SiC grains carry the s-process signature in the isotopic compositions of Kr, Xe, Ba, Nd and Sm [see 1]. Most isotopic compositions measured in single SiC grains generally agree with the expectations for carbon stars. The mainstream and type Y grains have heavy to moderately light C and light N (Fig. 1). Such compositions can be explained by nucleosynthesis in the CNO cycle during H-burning and dredge-up of $^{12}C$ produced by He-burning during the AGB phase. The Si- and Ti-isotopic compositions of single grains [17] cannot be explained by nucleosynthesis taking place in a single star and indicate multiple stellar sources [18].

Corundum grains show a large range in their O-isotopic ratios (Fig. 2) and $^{26}Al/^{27}Al$ ratios [14, 19, 20]. Some must have formed in red giant atmospheres before the third dredge-up, most during the TP-AGB phase. Similarly to the Si-isotopic compositions of SiC grains, the O-isotopic compositions of individual corundum grains cannot be explained by nucleosynthetic processes taking place in a single star. Excesses in $^{17}O$ and moderate depletions in $^{18}O$ relative to the star's

original composition are believed to be due to mixing into the envelope of material processed in the star's interior during core H-burning (first dredge-up). However, the spread in O-isotopic compositions found in meteoritic oxide grains can only be explained by assuming that different stars with different masses (variations in $^{16}O/^{17}O$) and different initial isotopic compositions (variations in both $^{16}O/^{17}O$ and $^{16}O/^{18}O$, see Fig. 2) contributed oxide grains to the solar system [21]. Some grains with high $^{16}O/^{18}O$ ratios (Fig. 2) must have come from AGB stars of intermediate mass in which hot bottom burning, which destroys essentially all $^{18}O$, took place. Others have $^{18}O$ excesses (low $^{16}O/^{18}O$) that could have resulted from dredge-up of $^{18}O$ during the first few thermal pulses of AGB stars [22].

**Supernovae.** – Two types of circumstellar grains in meteorites are believed to come from supernovae: low density graphite grains and SiC grains of the rare type X. The C-, N-, O-, and Al-isotopic ratios of single grains from the low density graphite fraction KE3 (1.60 to 1.90 g $cm^{-3}$) from Murchison [23] are shown in Fig. 3, the Si-isotopic compositions in Fig. 4. Most grains have $^{15}N$ excesses and large $^{18}O$ (up to 100×, corresponding to $^{16}O/^{18}O = 5$) excesses, expected to be found in the He-burning zone of massive stars at the end of their evolution just before their explosion as supernovae [24]. The first are produced by explosive reactions, the latter by He-burning of $^{14}N$ during the hydrostatic evolution of the star. $^{26}Al$ is expected to be produced in the overlying He/N shell during H-burning. The large variations in Si-isotopic compositions and specifically excesses in $^{28}Si$ are interpreted as being due to the mixing of interior stellar layers, where O-burning took place, with the C-rich outer He zone during the supernova explosion [25]. Violent mixing has indeed ben observed during supernova explosions [e.g., 26].

SiC grains of type X [27] constitute only about 1% of all circumstellar SiC found in meteorites (they are over-represented in Fig. 1). Isotopically they are characterized by $^{15}N$ excesses (Fig. 1), $^{28}Si$ excesses (Fig. 4) and high $^{26}Al/^{27}Al$ ratios. In all three signatures they are similar to but more extreme than low density graphite grains (Figs. 3 and 4). A supernova origin of X grains is indicated by their Si-isotopic compositions ($^{28}Si$ as product of O-burning) and especially by $^{44}Ca$ excesses, apparently from the decay of short-lived $^{44}Ti$ ($\tau_{1/2}$ = 58 years), observed in a subset of SiC X grains [28]. $^{44}Ti$ is produced by Si- or statistical equilibrium burning and, similar to $^{28}Si$, has to be mixed into C-rich zones during the supernova explosion in order to present in carbonaceous grains. However, not all detailed isotopic compositions of SiC X grains agree with existing supernova models. Problems are the high $^{26}Al/^{27}Al$ ratios associated with large $^{15}N$ excesses in the same grains; $^{26}Al$ and $^{15}N$ are believed to be produced in different zones of supernovae [24].

**REFERENCES** [1] E. Anders and E. Zinner (1993) *Meteoritics* **28**, 490. [2] U. Ott (1993) *Nature* **364**, 25. [3] E. Zinner (1995) in: Nuclei in the Cosmos III, M. Busso, R. Gallino and C. M. Raiteri, eds., p. 546, AIP, New York. [4] R. S. Lewis, M. Tang, J. F. Wacker, E. Anders and E. Steel (1987) *Nature* **326**, 160. [5] M. Tang and E. Anders (1988) *Geochim. Cosmochim. Acta* **52**, 1235. [6] T. Bernatowicz, G. Fraundorf, M. Tang, E. Anders, B. Wopenka, E. Zinner and P. Fraundorf (1987) *Nature* **330**, 728. [7] S. Amari, E. Anders, A. Virag and E. Zinner (1990) *Nature* **345**, 238. [8] T. J. Bernatowicz, S. Amari, E. K. Zinner and R. S. Lewis (1991) *Astrophys. J.* **373**, L73. [9] T. J. Bernatowicz, S. Amari and R. S. Lewis (1992) *Lunar Planet. Sci.* XXIII, 91. [10] T. J. Bernatowicz, S. Amari and R. S. Lewis (1994) *Lunar Planet. Sci.* XXV, 103. [11] R. S. Lewis and B. Srinivasan (1993) *Lunar Planet. Sci.* XXIV, 873. [12] G. R. Huss, I. D. Hutcheon, G. J. Wasserburg and J. Stone (1992) *Lunar Planet. Sci.* XXIII, 563. [13] L. R. Nittler, S. Amari, R. M. Walker, E. K. Zinner and R. S. Lewis (1993) *Meteoritics* **28**, 413. [14] L. R. Nittler, C. M. O. D. Alexander, X. Gao, R. M. Walker and E. K. Zinner (1994) *Nature* **370**, 443. [15] I. D. Hutcheon, G. R. Huss, A. J. Fahey and G. J. Wasserburg (1994) *Astrophys. J.* **425**, L97. [16] L. Nittler, S. Amari, X. Gao, R. Walker, E. Zinner, P. Hoppe, R. Strebel, P. Eberhardt and R. Lewis (1995) *Astrophys. J.* submitted. [17] P. Hoppe, S. Amari, E. Zinner, T. Ireland and R. S. Lewis (1994) *Astrophys. J.* **430**,

870. [18] R. Gallino, C. M. Raiteri, M. Busso and F. Matteucci (1994) *Astrophys. J.* **430**, 858. [19] L. Nittler, C. Alexander, X. Gao, R. Walker and E. Zinner (1995), in: Nuclei in the Cosmos III, M. Busso, R. Gallino and C. M. Raiteri, eds., p. 563, AIP, New York. [20] G. R. Huss, A. J. Fahey, R. Gallino and G. J. Wasserburg (1994) *Astrophys. J.* **430**, L81. [21] A. I. Boothroyd, I.-J. Sackmann and G. J. Wasserburg (1994) *Astrophys. J.* **430**, L77. [22] N. Mowlavi, (1995), Pers. comm. [23] S. Amari, E. Zinner and R. Lewis (1995) *Astrophys. J.* in press. [24] S. E. Woosley and T. A. Weaver (1995) *Astrophys. J. Suppl.*, in press. [25] E. Zinner, S. Amari, C. Travaglio, R. Gallino, M. Busso and S. Woosley (1995) *Lunar Planet. Sci.* XXVI in press. [26] T. Ebisuzaki, T. Shigeyama and K. Nomoto (1989) *Astrophys. J.* **344**, L65. [27] S. Amari, P. Hoppe, E. Zinner and R. S. Lewis (1992) *Astrophys. J.* **394**, L43. [28] L. Nittler (1995) unpublished data.

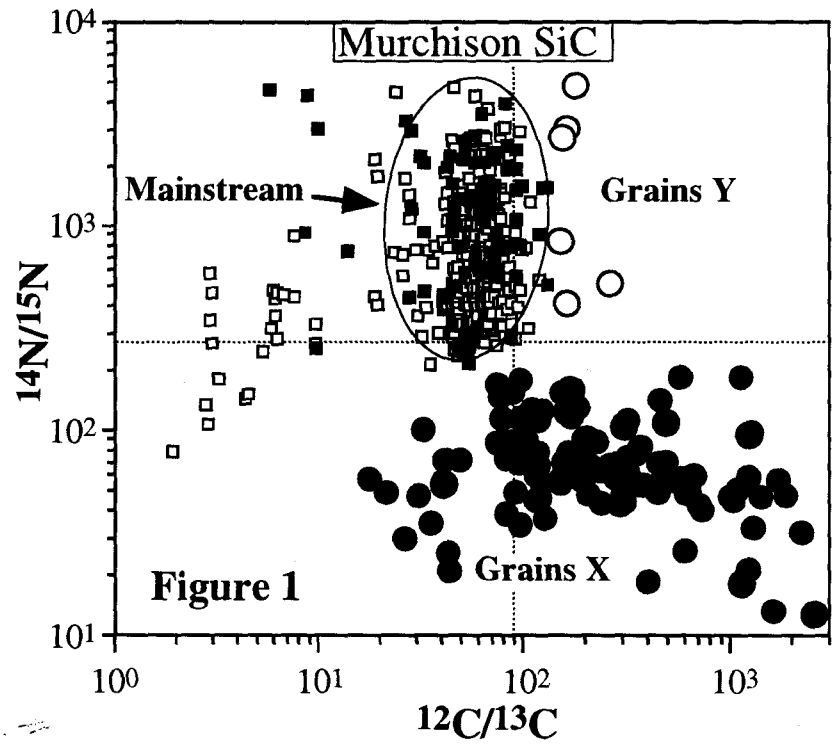


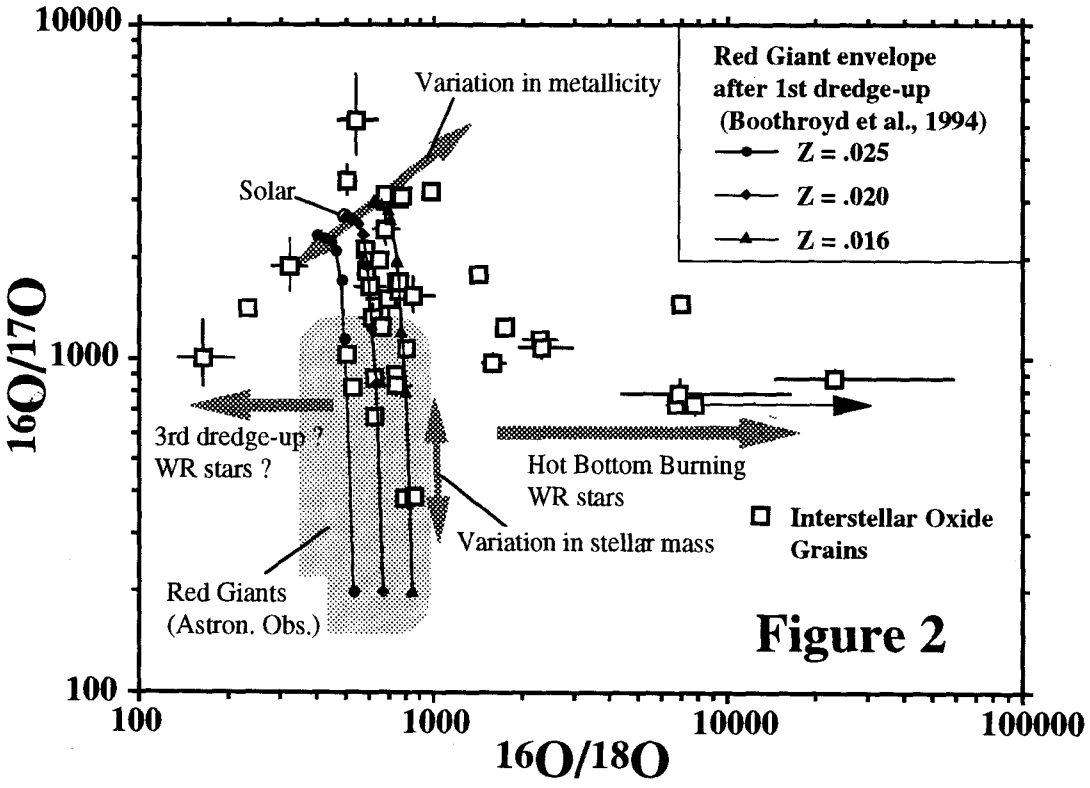

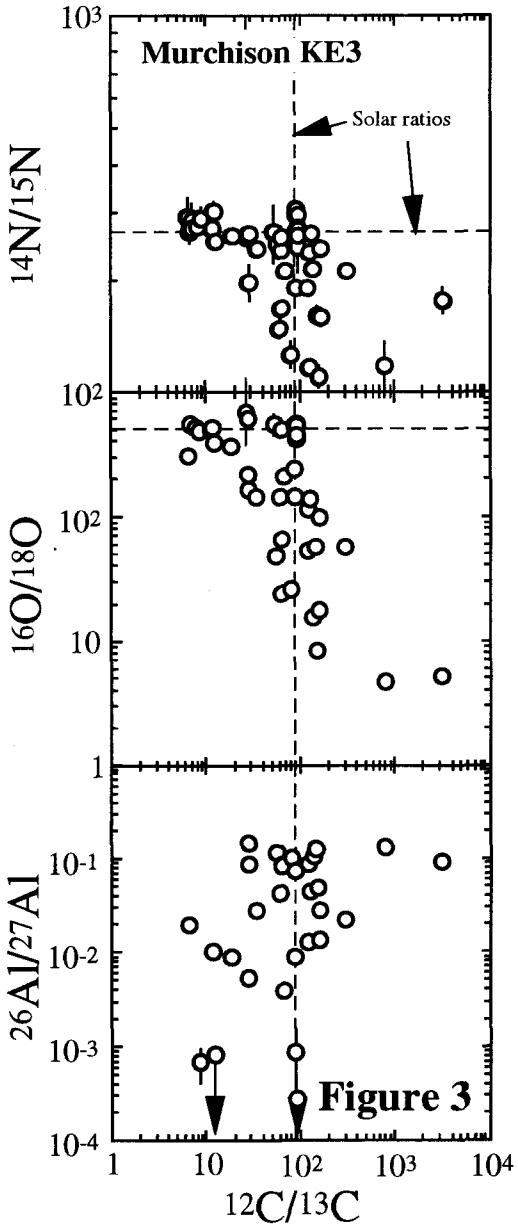
Murchison KE3
Solar ratios
14N/15N
16O/18O
26Al/27Al
12C/13C
10³
10²
10
1
10-1
10-2
10-3
10-4
1
10
10²
10³
10⁴

Figure 3

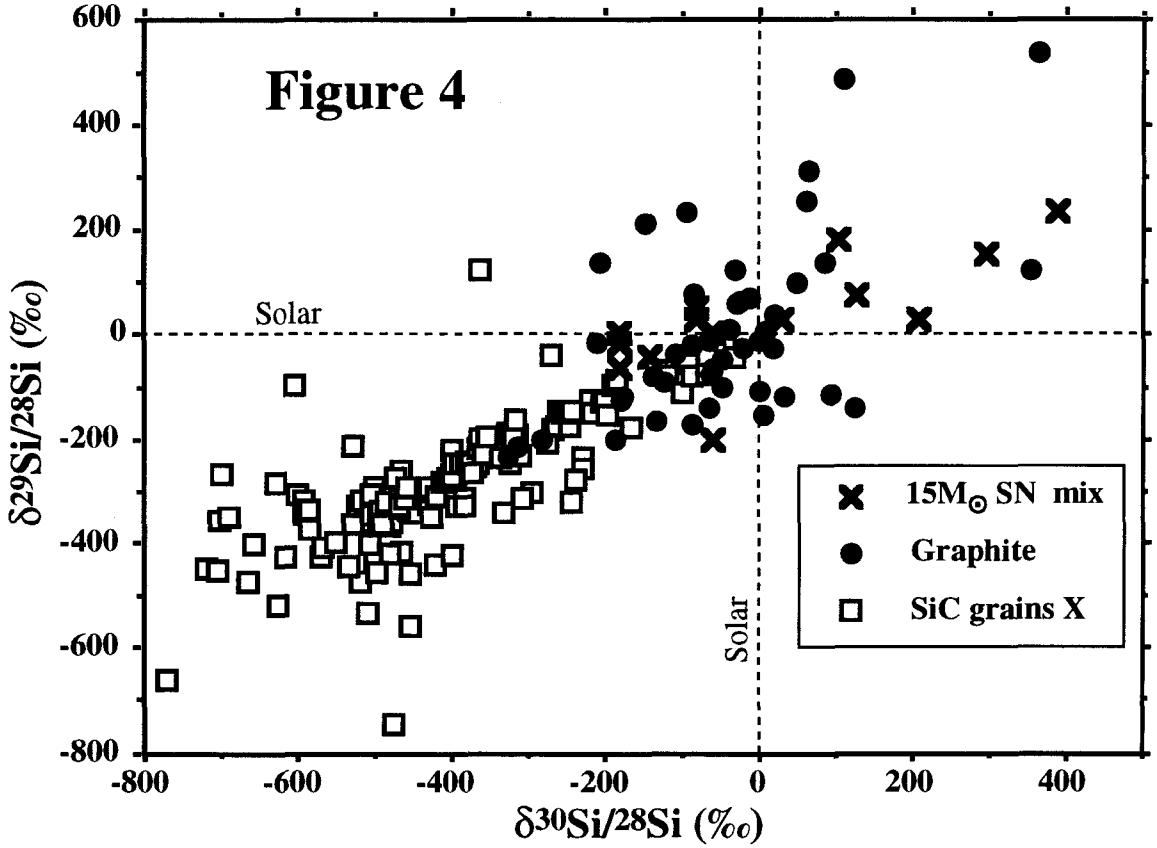
Figure 4
Solar
Solar
δ29Si/28Si (‰)
δ30Si/28Si (‰)
600
400
200
0
-200
-400
-600
-800
-800
-600
-400
-200
0
200
400
15M⊙ SN mix
Graphite
SiC grains X

# SPECIFIC PYROXENE-OLIVINE CHONDRULES OF THE YAMATO-82133 (H3) CHONDRITE: EVIDENCE OF THE EVOLUTION OF REDOX CONDITIONS DURING THE CHONDRULE FORMATION

**Nina G. Zinovieva, Olga B. Mitreikina, and Lev B. Granovsky**

Department of Petrology, Faculty of Geology, Moscow State University, Lenin Gory, Moscow 119899, Russia

The presence of olivine-pyroxene chondrules with high variations in Fe-contents of their minerals is typical of the Yamato-82133 (H3) ordinary chondrite. Most of the chondrules show a normal zoning of olivine and pyroxene but some of the chondrules may be of an earlier origin have a complicated (both normal and reverse) zoning of these minerals. Examination of such chondrules provided a deeper insight in their genetic conditions.

These chondrules consist on porphyritic olivine (Fa - 4-28) and pyroxene (En - 80-97, Fs - 2-19, Wol - 0-1), which are surrounded by clinopyroxene rims. Both olivine and pyroxene are cemented by plagioclase glass with acicular and tabular clinopyroxene crystals. Contrary to the usual porphyritic pyroxene-olivine chondrules with normal olivine and pyroxene zoning, the central parts of the studied chondrules contain large olivine grains, whose central parts consist on olivine (Fa - 9-10) with abundant microinclusions of native iron. The native iron does not contain nickel by contrast to kamacite from the matrix and usual chondrules. The central parts of olivine grains are surrounded by Mg-rich olivine (Fa - 7). The origin of the central part of the olivine grains can be described by the reaction of the pseudomorph replacement of more ferrous olivine (the bulk compositions of the $Ol_{10}$ + $Fe^0$ aggregates is equal to $Ol_{15}$) by magnesian olivine and native iron (Fig. 1):

$$1.92Mg_{1.7}Fe_{0.3}SiO_4 + 0.24H_2 = 1.7Mg_{1.8}Fe_{0.2}SiO_4 + 0.21MgSiO_3 + \\ + 0.24Fe^0 + 0.24H_2O$$

The enrichment of the residual chondrite melt in the enstatite end-member led to the formation of a poikilitic texture, where fine grains of the earlier ferrous olivine (Fa - 16-19) and pyroxene (En - 80, Fs - 19, Wol - 1) are present as poikilitic inclusions in large porphyritic pyroxene grains (Fig. 2). The latter form a paragenetic assemblage with Mg-rich olivine (Fa - 4-6). Pyroxene grains show the reverse zoning as well (core: En - 87, Fs - 13; rim: En - 92-97, Fs - 2-7, Wol - 1). Significantly, the metal phase occurs as small drop-like separations in grains of the Mg-rich olivine and the pyroxene contains on kamacite and, therefore, are captured from a chondrule melt during its crystallization. The crystallization ends with the formation of rims, tabular, and acicular grains of clinopyroxene cemented by a glass of plagioclase composition.

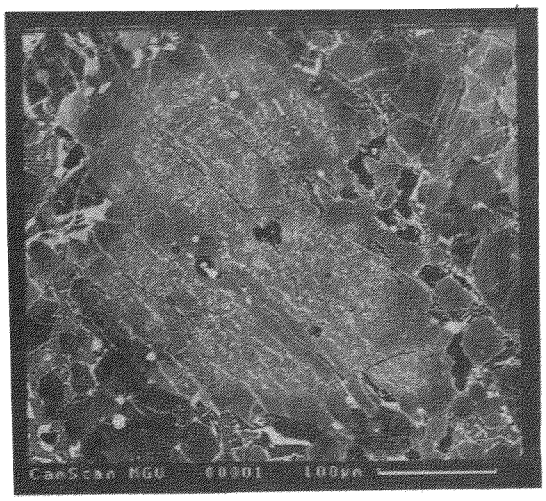

Fig. 1. Back-scattered electron image of porphyritic olivine grain (Fa - 15) replaced pseudomorphously by olivine (light gray, Fa - 10) and native iron (white). This grain is surrounded by a rim of Mg-rich olivine (gray).

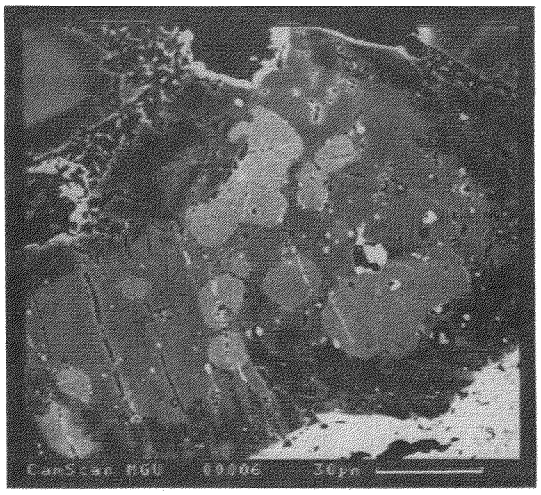

Fig. 2. Back-scattered electron image of poikilitic olivine grains (light gray, Fa - 16-19) in reversely zoned pyroxene (gray core: En - 87, Fs - 13; dark gray rim: En - 92-97, Fs - 2-7, Wol - 1).

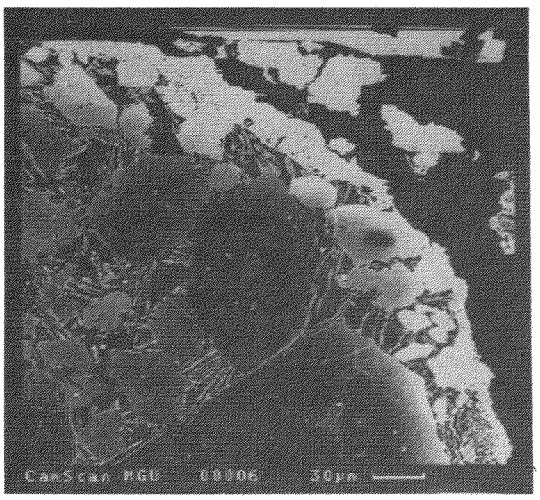

Fig. 3. Back-scattered electron image of recrystallized olivine and newly formed more ferrous olivine (Fa - 28) on the troilite-kamacite matrix boundary.

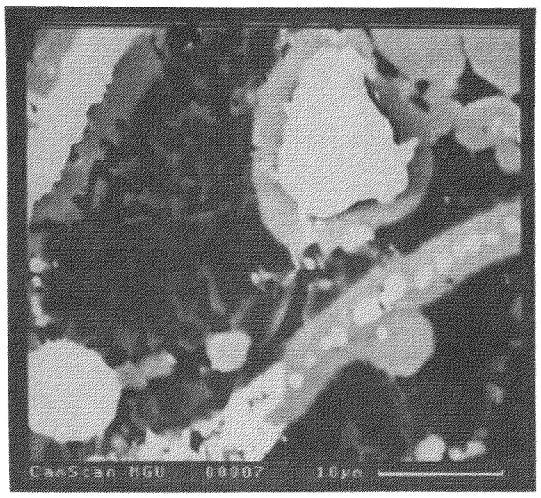

Fig. 4. Back-scattered electron image showing enstatite grains cut by troilite-kamacite veins (white), which are surrounded by olivine (Fa - 28) rims (light gray).

The formation of the reverse zoning of olivine grains was described earlier [1 and other] and explained by a shock reheating process. As was shown above, the formation of a reverse zoning cannot be explained solely by the reheating process. This reaction is accompanied by the reduction of $Fe^{2+}$ to $Fe^{o}$, the fact reflecting the increasing of reduced conditions during the initial stage of the chondrule formation. The external parts of the

completely crystallized chondrules underwent the intense influence of the matrix material. This process resulted in the olivine recrystallization accompanied by the formation of more ferrous olivine (Fa - 28) on the chondrule boundaries (Fig. 3) and troilite-kamacite veins crossing the chondrule material. The troilite-kamacite veins cutting pyroxene grains have olivine rims (Fa - 28), whereas the veins crossing olivine grains (Fa - 13) are accompanied only by recrystallization (Fig. 4) of the olivine and increase in its iron content (Fa - 20). This reaction is accompanied by an increase in the ferrous iron content as a result of kamacite oxidation. Thus, it was shown that the redox conditions evolved during the chondrule formation. First, the conditions became more reduced (the iron of the olivine reduced to the form of native iron, and the olivine and pyroxene acquired a reverse zoning). Then, the conditions sharply changed to oxidized and this lead to the recrystallization of Mg-rich olivine accompanied by the formation of more ferrous olivine.

**ACKNOWLEDGMENTS:** This research described in this contribution was made possible in part by Grant MU8300 from the International Science Foundation and Russian Goverment, and by Grant 94-05-16942 from Russian Foundation for Fundamental Researches.

**REFERENCES:** [1] Fujita T. and Kitamura M. (1993) Origin of a lithic fragment in the Moorabie (L3) chondrite. 18th Symp. Antarct. Meteorites (Abstr.), 15-18.

# AUTHOR INDEX

**Antarctic Meteorites XX**

ERRATA

Author Index

| | |
|---|---|
| Lukács B. | *Insert* 68 |
| Nakamura T. | *For* 268 *read* 273 |
| Takaoka N. | *For* 268 *read* 273 |
| Yada T. | *For* 268 *read* 273 |